

# Synthesis and Biological Evaluation of Anti-Cancer Platinum(IV) Glycoconjugates using CuAAC “Click” Chemistry



A thesis submitted to Maynooth University in fulfilment of the  
requirements for the degree of

**Doctor of Philosophy**

by

**Eoin Moynihan, B.Sc.**

Department of Chemistry,

Maynooth University,

Maynooth,

Co. Kildare,

Ireland

**October 2023**

**Research Supervisor: Dr Diego Montagner**

**Co-Supervisor: Dr Trinidad Velasco-Torrijos**

**Head of Department: Prof A. Denise Rooney**



# Table of Contents

|   |     |
|---|-----|
| Acknowledgements.....   | i   |
| Declaration.....  | iii |
| Abstract.....   | iv  |
| Abbreviations.....  | vi  |
| Chapter 1: Introduction.....  | 1   |
| 1.1 Global burden of Cancer.....  | 2   |
| 1.2 The Role of Platinum in Medicine.....   | 4   |
| 1.2.1 Platinum (II) Drugs.....  | 4   |
| 1.2.2 Platinum (IV) Drugs.....  | 8   |
| 1.3 Glycoconjugation for the targeted delivery of metallodrugs.....                             | 13  |
| 1.3.1 Tumour glycolysis.....  | 13  |
| 1.3.2 Targeting glucose transporters.....   | 15  |
| 1.4 Metal-Based Glycoconjugates.....  | 19  |
| 1.4.1 Platinum(II) glycoconjugates.....   | 19  |
| 1.4.2 Platinum(IV) glycoconjugates.....   | 23  |
| 1.4.3 Other glycoconjugated metallodrugs.....   | 26  |
| 1.5 Copper catalysed azide-alkyne cycloaddition (CuAAC) 'Click' chemistry and metallodrugs..... | 31  |
| 1.5.1 Click chemistry in platinum-based drugs.....  | 31  |
| 1.6 Research aims and thesis outline.....   | 34  |
| Chapter 2: C1 Platinum(IV) Acetylated Glycoconjugates.....                                      | 36  |
| 2.1 Introduction.....   | 37  |
| 2.1.1 Osteosarcoma.....   | 37  |
| 2.1.2 Acetylated carbohydrates as anticancer agents.....  | 39  |
| 2.2 Chapter Objective.....  | 41  |
| 2.3 Results and Discussion.....   | 43  |
| 2.3.1 Synthesis of acetylated Pt(IV) glycoconjugate prodrugs.....                               | 43  |
| 2.3.2 Synthesis of Sugar Azides (2.16, 2.17, 2.24 and 2.25).....                                | 44  |
| 2.3.3 Copper-catalysed azide-alkyne cycloaddition (CuAAC) reaction.....                         | 46  |
| 2.3.4 Synthesis of Click Carbohydrate ligands (2.18, 2.19, 2.26 and 2.27).....                  | 49  |
| 2.3.5 Synthesis of active <i>N</i> -hydroxysuccinimide esters (2.20, 2.21, 2.28, 2.29).....     | 51  |
| 2.3.6 EDCI coupling reagent.....  | 55  |
| 2.3.7 Synthesis of mono functionalised Pt(IV)-glycosides (1 – 4).....                           | 56  |
| 2.4 Biological Evaluation.....  | 59  |
| 2.4.1 <i>In vitro</i> cytotoxicity.....   | 59  |

|   |     |
|---|-----|
| 2.4.2 Cell Morphology evaluation .....  | 61  |
| 2.4.3 Anti-cancer potential against CSC-enriched cell lines .....             | 62  |
| 2.5 Conclusion.....   | 63  |
| 2.6 Materials and Methods.....  | 64  |
| 2.6.1 <i>In vitro</i> biological evaluation .....                             | 65  |
| 2.6.2 Cell culture .....  | 65  |
| 2.6.3 Enriched-CSCs culture .....   | 66  |
| 2.6.4 MTT cell viability assay.....   | 66  |
| 2.6.5 Cell morphology evaluation .....  | 67  |
| 2.6.6 Inductively coupled plasma-optical emission spectrometry (ICP-OES)..... | 67  |
| 2.6.7 Statistical Analysis .....  | 67  |
| 2.7 Experimental procedures.....  | 68  |
| Chapter 3: C1 Platinum(IV) Free Glycoconjugates.....                          | 87  |
| 3.1 Introduction .....  | 88  |
| 3.1.1 Free (deprotected) carbohydrates as anticancer agents .....             | 88  |
| 3.2 Chapter Objective .....   | 90  |
| 3.3 Results and Discussion .....  | 91  |
| 3.3.1 Synthesis of free carbohydrate Pt(IV) glycoconjugates.....              | 91  |
| 3.3.2 Synthesis of free sugar ligands (3.9, 3.10, 3.13, and 3.14).....        | 92  |
| 3.3.3 Synthesis of free sugar NHS esters (3.11, 3.12, 3.15, and 3.16).....    | 94  |
| 3.3.4 Synthesis of free sugar Pt(IV) complexes (1 – 4).....                   | 98  |
| 3.4 Reduction properties of free sugar complexes (1 and 3). .....             | 103 |
| 3.5 Biological Evaluation .....   | 105 |
| 3.5.1 <i>In vitro</i> cytotoxicity.....                                       | 105 |
| 3.5.2 3D scaffold-based OS model .....  | 108 |
| 3.6 Conclusions .....   | 110 |
| 3.7 Materials and Methods.....  | 111 |
| 3.7.1 Cyclic voltammetry.....   | 112 |
| 3.7.2 Reduction studies.....  | 112 |
| 3.7.3 <i>In vitro</i> biological evaluation .....                             | 112 |
| 3.7.4 Cell culture .....  | 113 |
| 3.7.5 Synthesis of bone mimetic scaffolds .....                               | 113 |
| 3.7.6 3D scaffold – based osteosarcoma models (3D OS model).....              | 114 |
| 3.7.7 MTT cell viability assay.....   | 115 |
| 3.7.8 Cell morphology evaluation .....  | 115 |
| 3.7.9 Statistical analysis.....   | 116 |



|   |     |
|---|-----|
| 3.8 Experimental procedures.....  | 116 |
| Chapter 4: C2 Platinum(IV) Glycoconjugates .....  | 128 |
| 4.1 Introduction .....  | 129 |
| 4.2 Chapter objective.....  | 131 |
| 4.3 Results and Discussion .....  | 133 |
| 4.3.1 Synthesis of C2-glycoconjugated Pt(IV) complexes.....                                       | 133 |
| 4.3.2 Synthesis of C2 sugar azides through diazo-transfer (4.8, 4.15) .....                       | 136 |
| 4.3.3 Synthesis of C2 sugar azide through substitution reaction (4.19).....                       | 139 |
| 4.3.4 Synthesis of acetylated C2 ligands using CuAAC “Click” chemistry (4.9, 4.16 and 4.20) ..... | 141 |
| 4.3.5 Synthesis of acetylated C2 active esters (4.10, 4.17 and 4.21) .....                        | 143 |
| 4.3.6 Synthesis of acetylated C2 Pt(IV) complexes (1, 2, and 3) .....                             | 146 |
| 4.3.7 Synthesis of free sugar C2 Pt(IV) Complex (4).....  | 150 |
| 4.3.8 Attempted synthesis of free sugar C2 Pt(IV) complexes (4.9.2 and 4.16.3).....               | 153 |
| 4.4 Reduction properties of C2 complexes (3 and 4).....   | 156 |
| 4.5 Biological Evaluation .....   | 157 |
| 4.5.1 <i>In vitro</i> cytotoxicity.....   | 157 |
| 4.5.2 Cell morphology evaluation .....  | 160 |
| 4.6 Conclusions .....   | 160 |
| 4.7 Materials and Methods.....  | 161 |
| 2.7.1 Reduction studies.....  | 162 |
| 2.7.2 <i>In vitro</i> biological evaluation .....   | 162 |
| 2.7.3 Cell culture .....  | 163 |
| 2.7.4 MTT cell viability assay.....   | 163 |
| 2.7.5 Cell morphology evaluation .....  | 164 |
| 2.7.6 Statistical analysis.....   | 164 |
| 4.8 Experimental procedures.....  | 165 |
| Chapter 5: Multivalent Platinum(IV) Glycoconjugates .....   | 189 |
| 5.1 Introduction .....  | 190 |
| 5.1.1 Hepatocellular carcinoma (HCC) .....  | 190 |
| 5.1.2 Asialoglycoprotein receptor (ASGPR).....  | 191 |
| 5.1.3 Multivalent effect for the targeting of ASGPR.....  | 193 |
| 5.2 Chapter objective.....  | 195 |
| 5.3 Results and Discussion .....  | 197 |
| 5.3.1 Synthesis of free amine scaffold (5.9) .....  | 197 |

|   |     |
|---|-----|
| 5.3.2 Cyclic derivatives through initial route to form multivalent Pt(IV) glycoconjugates ..... | 198 |
| 5.3.3 Synthesis of multivalent glycoconjugated Pt(IV) pro-drugs using alternative route .....   | 201 |
| 5.3.4 Synthesis of acetylated multivalent ligand using CuAAC “Click” chemistry (5.18) .....     | 203 |
| 5.3.4 Synthesis of free multivalent ligand (5.20).....  | 204 |
| 5.3.5 Synthesis of multivalent active esters (5.19 and 5.21).....                               | 205 |
| 5.3.6 Attempted synthesis of multivalent Pt(IV) glycoconjugates (5.19.1 and 5.21.1)             | 208 |
| 5.4 Conclusions .....   | 212 |
| 5.5 Materials and methods .....   | 213 |
| 5.6 Experimental procedures.....  | 214 |
| Chapter 6: Conclusion .....   | 226 |
| 6.1 Conclusion.....   | 227 |
| Bibliography .....  | 231 |
| Appendix .....  | 258 |

## Acknowledgements

Completing this thesis wouldn't have been possible without the help of a few people that deserve muchos, muchos praise. Firstly, I'd like to thank my two supervisors Dr. Diego Montagner and Dr. Trinidad Velasco-Torrijos, both of whom have been incredibly kind and supportive throughout my time here in the lab. In particular I'd like to thank Diego for always pushing me to get the work done, especially around the time it came to write the thesis, and for sending me to all the lovely conferences (Holidays). I'd also like to thank Trini for the mammoth amount of support she gave me throughout each aspect of the project (and in particular for the coffee mill visits). I couldn't have asked for better supervisors.

I'd like to thank Maynooth University for awarding me the esteemed scholarship: Maynooth University Teaching Studentship (MUTS), which allowed me to complete my PhD and gave me so many opportunities to teach undergraduate students which I've found a great love for. I'd also like to thank the current and previous heads of the chemistry department. A big thank you to Prof. Jennifer McManus and her PhD student, Alessandro Strofaldi, who encouraged me to pursue a PhD. I'd like to give a special thanks to the admin staff, Donna and Carol and the technical staff, Noel, Ria, Karen, Anne, Orla, Walter and Carmel for all the help with demonstrating undergraduate labs and making my time here a lot easier, and the previous postgrads in the department – Harlei, Luke M, Stephen B, Amanda and Jason for all the help they gave when I first started the PhD, in particular, Harlei, who I plagued with questions. They all made me feel welcome when I started which I really appreciate.

Good luck to the lads on the right-hand side of the lab as well, Gero and Conor W who started with me. Stephen H (Yu-Gi-OH enthusiast), Luke B, Farhad, Sinead and all the new guys starting, best of luck in the future. I'd also like to acknowledge Alessio for the endless good times we had when he was in our lab, and most importantly for introducing me to Grá pizza.

To Darren (1:12 baby), I can't thank you enough for all the chemistry knowledge you've shared, all the anime talks we've had and the small rooms we've shared at conferences. You're a great chemist and a great friend, even if you try to steal my

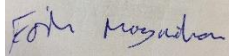
ideas from time to time (TSTU). Adam (my “average height” friend) thanks for all the laughs and for igniting my passion for ball. Don’t forget to talk to the new guys about street fighting. Keela, try not to behead Adam in your remaining two years. If the vapes don’t run out, I’m sure you’ll get through the rest of the PhD in one piece. The time you guys have left here will fly by so try to enjoy it.

To Kyle (Doho), I’ve had a great four years of exchanging quotes from stepbrothers (Like Kobayashi, aghaghaghagh), Breaking bad (Tight! Tight! Tight!/Breathe into his mouth..), American psycho (I am simply not there) and Django (Po’ lil squirrels). It’s made my time here a lot more entertaining, especially when we’d talk about steak and food in general. Thanks for putting up with my constant whinging and only sometimes making fun of me for cyberpunk/german manga/freestyle coke. Inshallah you have a good time in SK Biotek amigo.

A big thank you to my family who have supported me throughout the PhD and in particular my parents, Mick and Katie, who paid my way through the undergraduate degree, kept me fed and for not kicking me out of the house during these four years. Finally, thank you to Maia for being so supportive of me, and for making the time outside of the lab so enjoyable. You’ve helped me more than you know.

## Declaration

I declare that the work presented in this thesis was carried out in accordance with the regulations of Maynooth University. The work is original, except where indicated by reference, and has not been submitted before, in whole or in part, to this or any other university for any other degree.

Signed: 

Date: 23/10/2023

Eoin Moynihan, B.Sc

## Abstract

Cisplatin is the most widely used chemotherapeutic drug worldwide. Unfortunately, its use is hampered by severe dose-limiting side effects, intrinsic and acquired resistance and high toxicity. Furthermore, a major drawback associated with cisplatin therapy is its lack of selectivity for cancer cells with respect to healthy tissues.

One method to circumvent these side effects is to modify the chemical structure of the drug with selective targeting vectors whose receptors are overexpressed on the cell membrane of cancer cells. One example of this are sugars which are recognised by glucose transporters (GLUT). In this thesis, a series of glyco-functionalised platinum(IV) anticancer pro-drugs (where the sugar is glucose or galactose) are described, which were synthesised and characterised with the aim to create a library of novel selective metal-based chemotherapeutics. These complexes contain the Platinum metal centre in the +4 oxidation state, which have been shown to be more stable with respect to the classical Pt(II) complexes such as cisplatin. Our ligands consist of a combination of protected and deprotected glucose and galactose moieties conjugated to the axial positions of platinum(IV) complexes centre through the anomeric C1, and C2 positions, using CuAAC “click” chemistry. This thesis is divided in five chapters, with **Chapter 1** containing an introduction outlining the aims and objectives of this thesis, together with a literature review which summarises the novelty of this research topic.

**Chapter 2** reports the synthesis, characterisation and biological evaluation of a series of C1-acetylated Pt(IV) complexes which show similar activity to cisplatin against OS cell lines (SAOS-2, U-2 OS, MG63), but lack selectivity for cancer cells. This is probably due to the presence of the acetyl protecting groups that hamper the complexes' ability to be internalised into the tumoral cells through GLUTs.

In **Chapter 3**, a novel series of C1 de-acetylated (free sugar) Pt(IV) pro-drug derivatives are described. Like their acetylated counterparts, these complexes show similar cytotoxicity to cancer cells (MG63 and SAOS-2) as the reference drug cisplatin but, when incubated with healthy cells (hFOBs), they show a reduced cytotoxicity, ascribable to the uptake through GLUTs.

**Chapter 4** outlines our efforts to enhance the selectivity for cancer cells by functionalising the carbohydrate moiety in the C2 position, which has been shown to improve the drug uptake by GLUTs when compared to its C1 isomers. This series of complexes were found to display superior activity in comparison to cisplatin against cancer cells (SAOS-2, U-2 OS, MG63, MDA-MB-468, U-87 MG).

Finally, **Chapter 5** details the synthesis and characterisation of multivalent galactose ligands which were intended to be coupled to our Pt(IV) scaffold. These ligands target the asialo-glycoprotein receptor (ASGPR), rather than GLUT, for the treatment of hepatocellular carcinoma (HCC), the most common type of liver cancer in Asia and Africa. Synthetic problems are encountered during the experimental work which prevent the formation of the final complexes pure enough for biological studies. However, future work and perspectives are discussed in this chapter that may result in the successful formation of these complexes.

## Abbreviations

°C = Degrees Celsius

ACN = acetonitrile

Ac = Acetyl

Ac<sub>2</sub>O = Acetic anhydride

Aq = Aqueous

Ar = Aromatic

Atm = Atmospheric pressure

ATR = Attenuated Total Reflection

Boc = *t*-butyloxycarbonyl

Cbz = Benzyl chloroformate

CDCl<sub>3</sub> = Deuterated chloroform

COSY = Correlation Spectroscopy

CuAAC = Copper(I) catalysed azide-alkyne cycloaddition

CSC = Cancer stem cell

d<sub>5</sub>-Pyridine = Deuterated pyridine

DCC = *N,N'*-Dicyclohexylcarbodiimide

DCM = Dichloromethane

DCU = Dicyclohexylurea

DEPT = Distortionless enhancement by polarisation transfer

DMF = Dimethylformamide

DMSO = Dimethylsulfoxide

DMSO-d<sub>6</sub> = Deuterated Dimethylsulfoxide

DNA = Deoxyribonucleic acid

EDCI = *N*-(3-Dimethylaminopropyl)-*N'*-ethylcarbodiimide hydrochloride

e.g. = Exempli gratia (Latin for 'for example')

Equiv. = Equivalentents

ESI = Electrospray ionisation

Et<sub>2</sub>O = Diethyl ether



EtOAc = Ethyl acetate  
EtOH = Ethanol  
Gal = Galactose  
GalNAc = *N*-Acetylgalactosamine  
Glc = Glucose  
GLUT = Glucose transporter  
h = Hours  
HCl = Hydrochloric acid  
HMBC = Heteronuclear Multiple Bond Correlation  
HPLC = High Performance Liquid Chromatography  
HR-MS = High Resolution Mass Spectrometry  
HSQC = Heteronuclear Single Quantum Coherence  
IC<sub>50</sub> = Half maximal inhibitory concentration  
i.e. = Id est (Latin for 'that is')  
IR = Infrared spectroscopy  
IBCF = Isobutyl chloroformate  
MeOD = Deuterated methanol  
MeOH = Methanol  
mg = Milligram  
min = Minutes  
mL = Millilitre  
mm = Millimetre  
μm = Micrometre  
NaASC = Sodium ascorbate  
NEt<sub>3</sub> = Triethylamine  
NHS = *N*-Hydroxysuccinimide  
nm = Nanometre  
NMR = Nuclear Magnetic Resonance  
OAc = Acetoxy group

OH = Hydroxy group

OS = Osteosarcoma

Pd/C = Palladium on activated carbon

Pet Ether = Petroleum ether

R<sub>f</sub> = Retention Factor

rt = Room temperature

SAR = Structure Activity Relationship

sat. = Saturated

sec = Seconds

TBTU = *O*-(Benzotriazol-1-yl)-*N,N,N',N'*-tetramethyluronium tetrafluoroborate

*t*-BuOH = Tertiary-Butyl alcohol

TBAPF<sub>6</sub> = tetrabutylammonium hexafluorophosphate

TFA = Trifluoroacetic acid

Tf<sub>2</sub>O = Trifluoromethanesulfonic anhydride

TfN<sub>3</sub> = trifluoromethanesulfonyl azide

THF = Tetrahydrofuran

TLC = Thin Layer Chromatography

TMSN<sub>3</sub> = Trimethylsilyl azide

TSTU = *N,N,N',N'*-Tetramethyl-*O*-(*N*-succinimidyl)uronium tetrafluoroborate

# Chapter 1: Introduction

## 1.1 Global burden of Cancer

Cancer is a generic term for a large group of diseases which can affect any part of the body. A defining feature of cancer is the rapid growth and proliferation of abnormal cells, which can invade adjoining parts of the body and spread to other organs. The process of spreading to other organs is referred to as metastasis, which is the primary cause of death from cancer [1]. Cancer was responsible for nearly 10 million deaths worldwide in 2020 [2].

Typically, non-cancerous cells will only proliferate when supplied with appropriate mitogenic factors such as growth signals, which are transmitted by transmembrane receptors that bind different signalling molecules; examples being diffusible growth factors, extracellular matrix components and cell-to-cell adhesion/interaction molecules. Such reliance on these growth signals is not apparent in cancer cells, which lead researchers to the conclusion that tumour cells must generate their own growth signals, liberating cancer cells from their dependence on exogenously derived signals [3]. To fulfil the biosynthetic needs associated with rapid proliferation and growth, cancer cells must increase their intake of nutrients in the form of glucose and glutamine. These nutrients are transformed into useful building blocks for important macromolecules and are used for their reducing ability in the form of NADH and FADH<sub>2</sub> to fuel ATP generation [4]. The increased uptake of glucose in cancer cells through glucose transporters (GLUTs) in comparison to healthy cells was first described by Otto Warburg [5] in 1927. For this reason, it was termed the Warburg Effect [6], and it will be discussed in more depth in a later section. Glutamine, a second growth-supporting substrate, is used to produce purine and pyrimidine nucleotides and plays a role in the uptake of essential amino acids (e.g., leucine, isoleucine, valine, methionine, tyrosine, tryptophan and phenylalanine) through L-type amino acid transporter 1 (LAT1) [7,8].

While the causes of cancer development are not entirely understood, factors such as tobacco and inactivity are known to increase the risk of developing tumours. In the United States in 2022, ~42% of cancers were potentially avoidable, including the 19% caused by smoking and 18% caused by a combination of excess body weight, poor

nutrition and alcohol consumption. Around 5 million skin cancers are also diagnosed annually due to inadequate skin protection from excessive sun exposure and the use of indoor tanning devices. The 5-year relative survival rate for all cancers has substantially increased since the 1960s, from 39% to 68%, due to advances in treatment and early diagnosis [9,10]. Other known causes of cancer are due to mutations in the p53 transcription factor (encoded by the human gene *TP53*), a gene that is a key tumour suppressor responsible for inducing cell cycle arrest, DNA repair and apoptosis. Mutations of this gene were reported in almost every type of cancer from rates of 10% to almost 100% and mutations in p53 are also able to actively promote tumour development. These mutations can occur from exposure to carcinogens such as dietary aflatoxin B1, tobacco smoke and exposure to sunlight and UV radiation [11].

It is estimated that one in five cancer cases are caused by infection, with most caused by viruses [12]. Cancer development is a multistep process and viruses can exert effects on different stages of tumour formation, depending on the virus. These can act in the early stages of oncogenesis or in later stages by effecting signalling pathways involved in regulation of cell proliferation, apoptosis and tumour promotion [13]. There is now evidence of carcinogenicity in humans for human T-cell lymphotropic virus (HTLV), human immunodeficiency virus (HIV), hepatitis B, hepatitis C, human papillomavirus (HPV), Epstein-Barr virus (EBV) and human herpes virus 8 (HHV-8) [14].

Chemotherapy, surgery and radiotherapy are the most common forms of treatment for cancer available today. Modern surgery has changed significantly since the 1960s, with more non-invasive procedures replacing aggressive surgeries. Surgery alone, however, can be ineffective due to tumour metastasis [15]. Radiation therapy is an important and highly cost-effective mode of cancer treatment, accounting for only 5% of the overall cost of cancer care and it is administered to approximately 50% of all cancer patients [16]. Radiation (given in the form of X-rays or  $\gamma$ -rays) or charged particles ( $\alpha$ ,  $\beta^+$ ,  $\beta^-$ ) are administered in small doses to limit damage to healthy tissue due to their longer proliferation time, which gives healthy tissue time to repair the damage before replication. Tumour tissue on the other hand, replicates much

quicker and has less time to repair the damaged genetic information [17]. Chemotherapy is considered the most effective and commonly used treatment in most types of cancers. The main drawback of this form of therapy is the lack of selectivity for cancerous cells and the harm they cause to ordinary cells, resulting in dose-dependent side effects such as fatigue, nausea, hair loss, vomiting and death in extreme cases [18]. Cancer therapy in the form of combination therapy, uses targeted strategies which incorporate radiotherapy, surgery, treatments to target cancer-inducing or cell-sustaining pathways and “traditional” chemotherapeutics (i.e., taxanes and platinum complexes) have shown synergistic effects. Conventional mono-therapeutic agents are still common in many forms of cancer treatment; however, this method is generally deemed less effective than combination therapy as it works synergistically, requiring lower doses of each drug and reducing the dose-dependent side effects associated with them [19,20].

## 1.2 The Role of Platinum in Medicine

### 1.2.1 Platinum (II) Drugs

Metals have been used in a medicinal setting as far back as 2500 BC in China, where gold was employed to treat illnesses [21]. Ancient cultures in India and Egypt also treated illnesses with metals. Egypt, in particular used copper for the sterilisation of wounds, which was detailed in the Edwin Smith papyrus, an ancient Egyptian medical text which dates back to 1501 BC [22,23].

At the beginning of the 20<sup>th</sup> century, the German Nobel laureate Paul Ehrlich introduced the compound 3-amino-4-hydroxyphenylarsenic(I) (Salvarsan) as a cure to syphilis in early 1910 [24]. While this treatment was inevitably phased out by the use of antibiotics in the 1940s, this was a significant milestone in medicinal inorganic chemistry. It was not until the 1960s that the discovery of the anticancer properties of *cis*-diamminedichloroplatinum(II) (cisplatin), initially synthesised by Michele Peyrone in 1844 with its structure later elucidated by Alfred Werner in 1892, which led to an explosion in research of metal chemotherapeutics [25,26].

Cisplatin [27] was later approved globally for the treatment of advanced pancreatic cancer, breast cancer, non-small lung cell cancer, advanced bladder cancer and other

tumours in 1978, followed by the approval of carboplatin [28] in 1989 and oxaliplatin [29] in 2002 (**Figure 1.1**), that are considered “second generation of Pt(II) chemotherapeutics”. Other platinum drugs were also developed with their approval limited to certain countries, examples being Nedaplatin [30] which was approved for use in Japan in 1995, Heptaplatin [31] which was approved in Korea in 1999 and Lobaplatin [32] which was approved in China in 2010 (**Figure 1.1**).

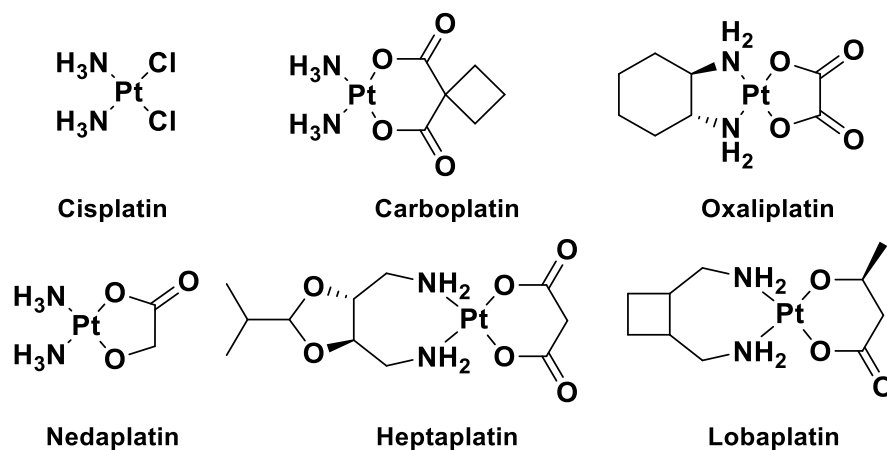


**Figure 1.1:** Structures of approved Pt anticancer drugs for treatment of various types of cancer.

In the years following the approval of cisplatin, much research was conducted to elucidate the mechanism by which cisplatin acts on cancer cells. Four main steps were identified: cellular uptake, aquation/activation, DNA platination and cellular processing of Pt-DNA adducts [33].

Cellular uptake was originally thought to occur through passive diffusion [34] however, more research has shown that active transport through copper transporter 1 (CTR1) [35] and organic cation transporter 2 (OCT2) [36] are also responsible for the cellular accumulation of cisplatin, carboplatin and oxaliplatin (**Figure 1.2**). Inhibition of CTR1 leads to a decreased uptake of these platinum anticancer drugs in mammalian and yeast cells, while an overexpression of CTR1 leads to cells becoming resistant to the drugs anticancer effects [37]. However, conflicting reports have questioned whether varying CTR1 levels affects sensitivity to platinum based anticancer drugs. Reports from Bompiani et al. [38] and Akerfeldt et al. [39] have

shown that removing or overexpressing CTR1, led to little impact on cisplatin sensitivity or increased platinum accumulation in certain cell lines respectively [40].

Once inside the cellular cytoplasm, cisplatin is hydrolysed, and this process is facilitated by a lower chloride ion concentration (3-20 mM) within the cell than in the extracellular fluid (100 mM) [33]. The hydrolysed products  $cis\text{-}[\text{Pt}(\text{NH}_3)_2\text{Cl}(\text{OH}_2)]^+$  and  $cis\text{-}[\text{Pt}(\text{NH}_3)_2(\text{OH}_2)_2]^{2+}$  are strong electrophiles which can react with a variety of nucleophiles, including thiol groups on proteins and nitrogen donor atoms on nucleic acids (**Figure 1.2**). Aquated cisplatin binds to the N7 reactive centre on purine residues causing 1,2-intrastrand guanine-platinum-guanine (d(GpG)) adducts, which represent 90% of adducts and 1,2-intrastrand adenine-platinum-guanine (d(ApG)) adducts which is about 10% of adducts. 1,3-intrastrand guanine-platinum-guanine adducts, inter-strand crosslinks and other non-functional adducts also contribute to cisplatin's mechanism of action [41,42]. These DNA-platinum adducts are recognised by DNA mismatch repair proteins and some damage recognition proteins [43]; if these adducts are not repaired this can cause DNA damage in cancer cells. This in turn blocks cell division and results in apoptotic cell death (**Figure 1.2**).

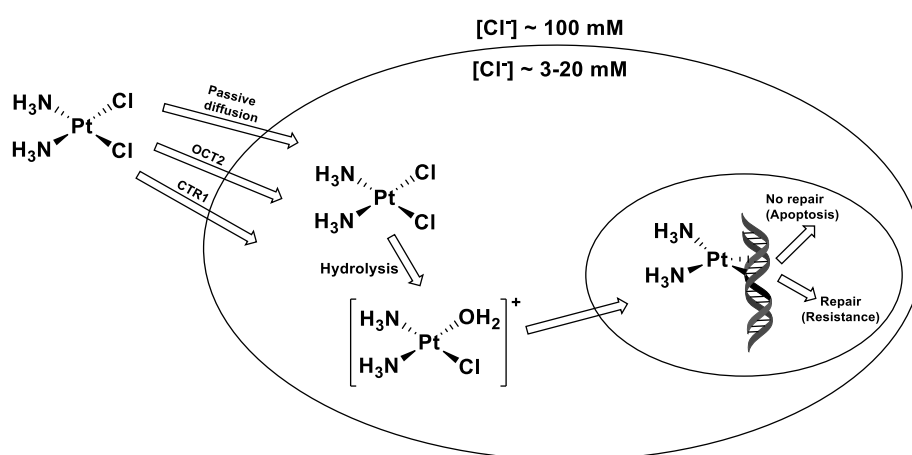


**Figure 1.2:** Cisplatin mechanism of action, adapted from Browning *et al.* [44].

It is a common belief that attempts to repair cisplatin-DNA adducts play a key role in the cytotoxicity of platinum drugs and a loss of mismatch repair activity can lead to cisplatin resistance [45]. While cisplatin is a potent anticancer agent, chemoresistance can develop through chronic drug exposure or can present itself as an intrinsic phenomenon [46]. Tissue culture studies have suggested that resistance



can result from epigenetic changes at molecular and cellular levels, including reducing platinum accumulation by active efflux [47]/sequestration [48]/secretion [49] or by hampering its influx [50,51].

One of the major drawbacks in the use of cisplatin is that it lacks specificity for cancer cells and causes damage to healthy cells. It also has poor oral bioavailability which means the drug must be administered intravenously [52]. Specific side effects of cisplatin include nephrotoxicity [53], ototoxicity [54], neurotoxicity [55], cardiotoxicity [56], haematological toxicity [57], hepatotoxicity [58] and gastrointestinal toxicity [59]. While some of these side effects can be treated during the course of chemotherapy (nephrotoxicity for instance, can be alleviated by hyperhydration with saline up to 12 hours before and up to three days after treatment [60]), there has been a push to eliminate these side effects by creating cisplatin analogues which are less toxic to healthy cells and more selective for cancer cells. Second generation Pt(II) chemotherapeutics, carboplatin and oxaliplatin are two worldwide approved drugs which overcome some of the drawbacks and limitations of cisplatin. Carboplatin (**Figure 1.1**) [28] has a lower hydration rate due to its bidentate cyclobutene dicarboxylic acid ligand which reduces its unfavourable side effects when compared to cisplatin. Due to its lower toxicity, carboplatin can be used in higher doses to treat more aggressive tumours [61]. However, while there are benefits for the use of carboplatin, the issue of chemoresistance and a variety of side effects still remain. Oxaliplatin (**Figure 1.1**) [29], which features the bidentate 1,2-diaminocyclohexane (DACH) ligand instead of cisplatin's monodentate amine ligand, was found to be active in some cisplatin-resistant tumours and is currently employed against colorectal cancer accompanied by 5-fluorouracil and folic acid (FOLFOX) and lung cancer [62]. Oxaliplatin, like cisplatin, exhibits its cytotoxic effects mainly through the formation of DNA adducts and apoptosis. A major difference between the two is that oxaliplatin also triggers immunogenic cell death (ICD) through interactions with RNA and proteins. This leads to T cell activation and proliferation to kill cancer cells through four damage associated molecular patterns (DAMP): (1) Calreticulin (CRT) exposure, (2) adenosine-5'-triphosphate (ATP) secretion, (3) release of non-histone chromatin-binding protein high mobility group

box 1 (HMGB1) and (4) interferon (IFN) type I and II production by malignant cells or immune effectors [63].

Other platinum anticancer drugs, without global approval, are still used in clinical settings in Japan, Korea and China (**Figure 1.1**). Nedaplatin [30] acts under the same mechanism as cisplatin but is more water-soluble and has lower gastrointestinal side effects and renal toxicity [64]. Heptaplatin [31] shows similar antitumour activity and less toxicity compared to cisplatin, while also being effective against cisplatin resistant L1210 leukemia cells, possibly due to its unique chelating ligand. It does, however, still cause dose-limiting side effects, such as nephrotoxicity due to its poor water solubility. Lobaplatin [32] is used in China to treat metastatic breast cancer, chronic myelogenous leukemia and small-cell lung cancer. It has also showed lower renal toxicity when compared to cisplatin and incomplete cross-resistance with other platinum anticancer agents. Thrombocytopenia is a commonly observed dose-limiting side effect for lobaplatin, however, there has not been much work done to research synergistic treatments which may reduce this side effect [65,66]. Patients receiving lobaplatin as treatment also commonly experience relapses, greatly reducing the drug's efficacy [67].

### 1.2.2 Platinum (IV) Drugs

All of the above complexes show the Platinum metallic centre in the +2 oxidation state, all are square planar  $d^8$  complexes typically functionalised through amine non-leaving ligands and forms active DNA adducts through anionic labile ligands, chlorides or carboxylates [68,69]. In recent decades, scientists have developed new anticancer complexes based on Platinum in the +4 oxidation state that form stable octahedral low spin  $d^6$  complexes. It is accepted that platinum(II) is essential for anticancer activity while platinum(IV) must be reduced inside the cell by glutathione and ascorbate, or under hypoxic conditions to form toxic DNA adducts which classifies them as prodrugs [70]. These reducing agents are found in higher concentrations within cancer cells compared to healthy cells, allowing for the intracellular reduction of Pt(IV) to Pt(II) [71]. Upon reduction, one or both of the axial ligands are released from the complex and the active Pt(II) is free to bind to cellular DNA (**Figure 1.3**).

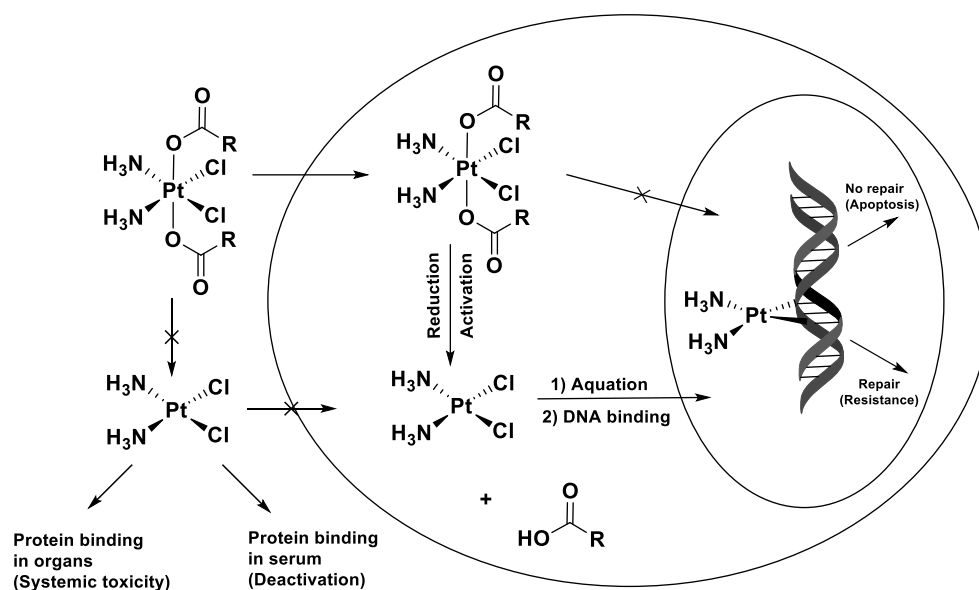


**Figure 1.3:** Mechanism of Pt(IV) entry and activation within the cell, releasing axial ligands and forming DNA adducts. Figure adapted from [72].

Axial substituents of the Pt(IV) species can be bioactive ligands which, when released, carry out their own functions within the cell. For example, multi-action drugs targeting histone deacetylase (HDAC), thioredoxin reductase (TrxR), and cyclooxygenase-2 (COX-2) by functionalising the platinum centre with HDAC and TrxR inhibitors [73], and non-steroidal anti-inflammatory drugs (NSAIDs) [74,75] have been employed to target a variety of cellular entities to improve cytotoxicity, drug uptake, and to circumvent chemoresistance (**Figure 1.4**).

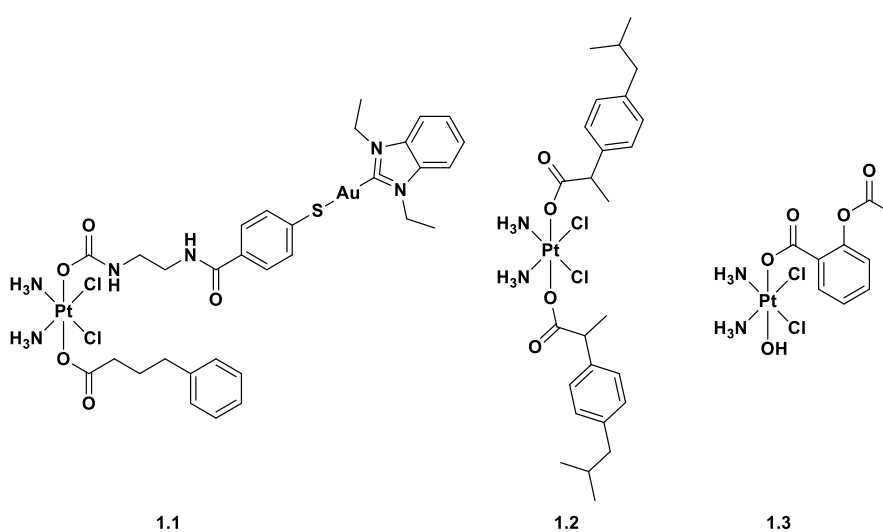


**Figure 1.4:** Structures of multi-action platinum drugs containing HDAC inhibitors (**1.1**) [73], NSAIDs (**1.2** [74], **1.3** [75]).

Studies have been focused on the influence the axial ligands have on the cellular uptake, biodistribution and the rate of reductive activation [76]. The reduction potential of Pt(IV) prodrugs is an important pharmacological parameter for estimating their activity. Pt(IV) complexes with a more positive reduction potential can easily undergo reduction, risking the possibility of the drug being reduced in the blood to its active form before reaching its target. In this regard, a positive reduction potential may be detrimental when trying to overcome Pt(II) associated side effects. Alternatively, Pt(IV) complexes with a negative reduction potential might take too long to reduce, resulting in excretion from the body without completing its function, effectively decreasing the drug's efficacy [77,78].

To date, only four Pt(IV) complexes have undergone clinical trials (**Figure 1.5**). Satraplatin or *trans,cis,cis*-bis(acetato)aminecyclohexylaminodichloroplatinum(IV) [79] was the first oral candidate for treatment of cisplatin resistant tumours with a carboplatin-like toxicity profile. Its mechanism of action is similar to that of cisplatin, however, its asymmetry from its amine ligands alters its DNA-adduct profile, increasing its efficiency to inhibit translational DNA synthesis and decreasing the likelihood of being recognised by DNA-mismatch repair proteins [80]. Ormaplatin or tetrachloro(*trans*-1,2-diaminocyclohexane)platinum(IV) [81,82] (**Figure 1.5**) was one of the first Pt(IV) agents to undergo clinical trials, however, it induced strong neurotoxicity at its maximum tolerated dose. This is thought to occur from fast reduction to its active Pt(II) species due to its axial chloride ligands [83]. Iproplatin or *cis,trans,cis*-dichlorodihydroxobis(isopropylamine)platinum(IV) [84] (**Figure 1.5**) was similar to ormaplatin in terms of its mechanism of action but had an increased water solubility and was less prone to reduction and deactivation by biological reducing agents, most likely due to its axial hydroxide ligands [83,85]. Clinical trials were ultimately discontinued due to the response rate of iproplatin being not vastly different to cisplatin [86]. LA-12 or *cis,trans,cis*-bis(acetato)(1-adamantylamine)aminodichloroplatinum(IV) [87] is a derivative of satraplatin which contains 1-adamantylamine instead of cyclohexylamine as its non-leaving amino ligand. LA-12 has shown higher cytotoxicity than cisplatin and satraplatin. While its

mechanism of action is not fully understood, there is some evidence that LA-12 can disrupt cell proliferation and induce apoptosis more efficiently than cisplatin [88].

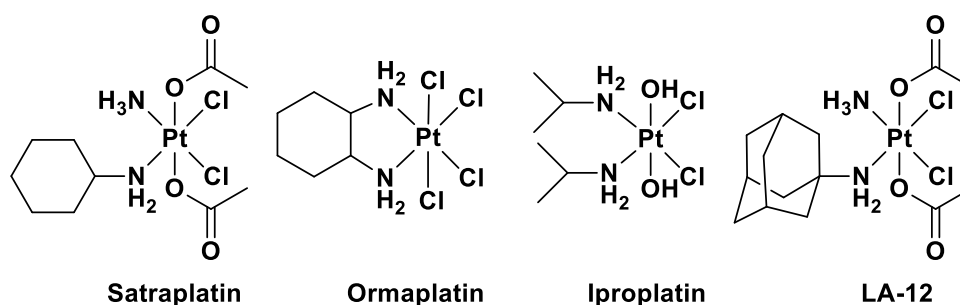


**Figure 1.5:** Structures of four platinum(IV) pro-drugs which have undergone clinical trials.

While the above complexes have been designed to reduce the inherent toxic side effects of cisplatin, few of them are capable of addressing the drawback of the toxicity towards healthy cells. For this reason, much research has been conducted into functionalising various platinum drugs with moieties to target specific cellular features or by incorporating ligands with distinct biological functions [89]. The aim of this “multitargeted” approach is to improve drug uptake [90], improve cytotoxicity [83], reduce side effects [91] and enhance drug specificity [92]. Strategies to target tumour cells typically include modifying the metal coordination sphere with ligands (**Figure 1.6**) such as carbohydrates [93–96], peptides [97,98], steroids [99,100], antibodies [101] and enzyme inhibitors [102] to target receptors which tumours overexpress for growth. In particular, **1.4**, a Pt(IV) tumour penetrating peptide (TPP) conjugate, is designed to target the 70-kDa heat shock protein (HSP70) which is a stress-inducible chaperone responsible for protecting cells against apoptosis during a stress response [103] and is overexpressed on cancer cells. This membrane bound chaperone was found to be present on 50% of tumours of the 1000 patients tested and was not expressed on healthy cells, making it an attractive target for selective chemotherapy [104].

Inhibition of enzymes associated with T-cell suppression is also a viable route for increasing anticancer activity through a synergistic effect with the active Pt(II) drug. Complex **1.5** specifically targets the indoleamine 2,3-dioxygenase (IDO) enzyme, which metabolises the amino acid tryptophan [105]. These metabolites are shown to

induce the differentiation of regulatory T cells and cause apoptosis of effector T cells, giving rise to immunosuppression. The presence of these metabolites can be used as a prognostic marker to measure cancer invasiveness and progression, alternatively, overexpression of the IDO enzyme can be used to target cancer cells due to their overexpression on tumour cell membranes [106].

Steroid-tethered Pt(IV) complexes have also been developed to target cellular entities associated with cancer and acquired or intrinsic resistance. Complex **1.6** is conjugated to estrogen, which has been shown to sensitise cells to cisplatin through inducing the overexpression of high mobility group box 1 protein (HMGB1). This protein shields cisplatin-DNA adducts from DNA repair proteins, which can serve as a viable route to overcome cisplatin resistance [107].

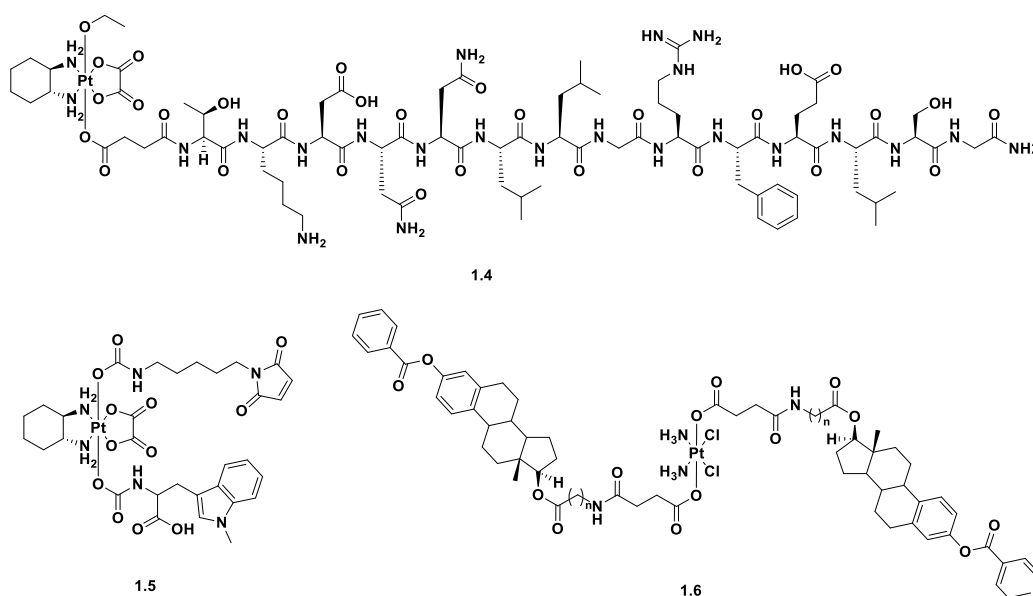


**Figure 1.6:** Structures of targeted Pt(IV) prodrugs using peptides [98], enzyme inhibitors [105], and steroids [107].

It is now recognised that a lack of cancer cell selectivity is a serious drawback of small molecule anticancer drugs, which stymies their therapeutic potential and has become a focus of many research groups [108].

## 1.3 Glycoconjugation for the targeted delivery of metallodrugs

### 1.3.1 Tumour glycolysis

Glycolysis is a universal pathway for catabolism of glucose in animals and plants. The process of glycolysis converts one molecule of glucose into two molecules of pyruvic acid. The energy released is preserved in the form of ATP and NADH and the main function of glycolysis is to provide energy and intermediates for other metabolic pathways (**Figure 1.7**). Glycolysis is provided with glucose through two major routes, carbohydrate consumption and cellular glycogen. Glucose undergoes glycolysis by a sequence of ten reactions, the first five reactions are referred to as the “investment” phase since ATP is consumed in these reactions. The last five reactions constitute the “pay off” phase and yield 2 ATP, 2 NADH and 2 pyruvates. The two pyruvates are converted to two acetyl-CoA molecules using the pyruvate dehydrogenase complex. Then, each acetyl-CoA molecule enters the tricarboxylic acid cycle (TCA) under aerobic conditions [109]. The products of the TCA cycle finally enter the electron transport system (ETS), also known as oxidative phosphorylation (OXPHOS), where ATP production is very efficient and can produce between 32 to 36 ATP molecules per molecule of glucose [110].

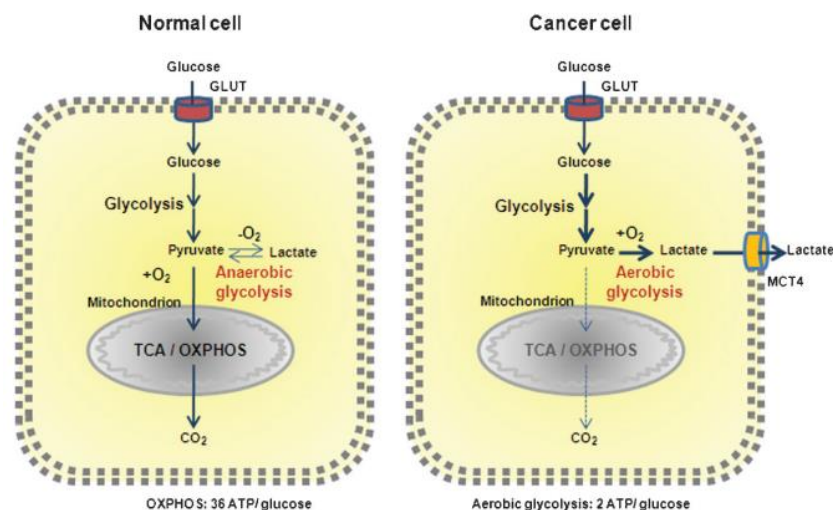


**Figure 1.7:** Glycolysis pathway for healthy cells (left) and cancerous cells (right) [111].

Tumour cells deviate from the typical cycle of ATP production because cells switch from OXPHOS to glycolysis for the synthesis of ATP which is a key event in tumorigenesis. The typical fate of pyruvate is avoided in cancer cells and through

aerobic glycolysis, it is converted into lactate even in the presence of oxygen [112]. This observation was first noted by Otto Warburg in the 1920s and was coined “The Warburg Effect” [5]. Much research was focused on determining why the Warburg effect was advantageous for tumour growth. The first proposed explanation was that with increased glycolysis, intermediates can funnel into side pathways to support the synthesis of nucleotides, lipids and amino acids which are needed to facilitate cell proliferation. The TCA cycle has also been identified as a key facilitator of tumour growth due to pyruvate carboxylase which generates oxaloacetate, a TCA cycle metabolite from pyruvate, being necessary for primary and metastatic tumour growth [113].

The benefits of this method of ATP production have been investigated and while they are still unknown, it has been postulated that cancer cells use this mechanism to proliferate in hypoxic environments, an example being the conditions of solid tumours. Another hypothesis is that the reduction in oxidative metabolism could help the cells escape from apoptosis [114]. Evaluations of metabolic flux have demonstrated that glycolysis is increased in a number of cancer cell lines and one explanation is that there is an overexpression of close to all enzymes of the glycolytic pathway. Hypoxia-inducible factor 1 (HIF-1) has been identified as a key regulator for aerobic glycolysis in tumours as it controls the expression of glycolysis enzymes (hexokinase 1 and 2 (HK1 and HK2), enolase 1, phosphoglycerate kinase 1 (PGK-1), pyruvate kinase M2 (PKM2) and pyruvate dehydrogenase kinase 1 (PDK-1)), lactate dehydrogenase (LDHA), glucose transporters (GLUT1 and GLUT3) and several other tumour related genes. In cancer cells, PDK-1 deactivates the pyruvate dehydrogenase complex (PDH), stopping conversion from pyruvate to acetyl-CoA. This reduces delivery of NADH and FADH<sub>2</sub> to the ETS, stimulating the production of lactate to stabilise HIF-1. This is characteristic of cancer cells shift from OXPHOS to aerobic glycolysis [115–117]. Research has been done to synthesise drugs which target HIFs or its subunits HIF-1 $\alpha$  and HIF-1 $\beta$ . Several drugs have been proposed which modulate the levels of HIF-1 $\alpha$ , which influences HIF-1 without directly targeting it: examples being Digoxin [118,119], ganetespib [120,121], Baicalein [122], methylalpinumisoflavone [123], oroxylin A [124], EGCG [125] and resveratrol



[126,127]. Synthesizing compounds to target HIFs is difficult due to the lack of selectivity for the HIF-1 $\alpha$  subunit.

### 1.3.2 Targeting glucose transporters

As previously discussed, the Warburg effect leads to cells producing ATP through aerobic glycolysis, rather than OXPHOS. An important manifestation of the Warburg effect is the overexpression of glucose transporters (GLUTs) on the membranes of cancer cells which are encoded by the solute carrier family 2 (SLC2) gene. To date, fourteen human GLUTs have been identified and sorted into three classes based on sequence similarity: Class 1 (GLUTs 1-4, 14), class 2 (GLUTs 5, 7, 9 and 11) and class 3 (GLUTs 6, 8, 10, 12 and 13 (HMIT)) [128]. GLUTs 1-4 are among the most meticulously characterised, with GLUT1 being one of the first characterised and crystallised [129]. This was accomplished by inducing point mutations in the structure (N45T and E329Q) and binding nonyl- $\beta$ -D-glucoside. As a result, its mechanism of binding and release of its substrate was elucidated (**Figure 1.8**). The substrate is bound at the primary site on the extracellular C-domain, with extra contacts by the N-domain. This induces closure of the extracellular domain, rearranging interactions on both sides of the bound substrate. The protein may then switch from an outward-open conformation to an inward-open conformation, exposing the substrate to a low concentration environment, where the substrate is then dissociated [129].

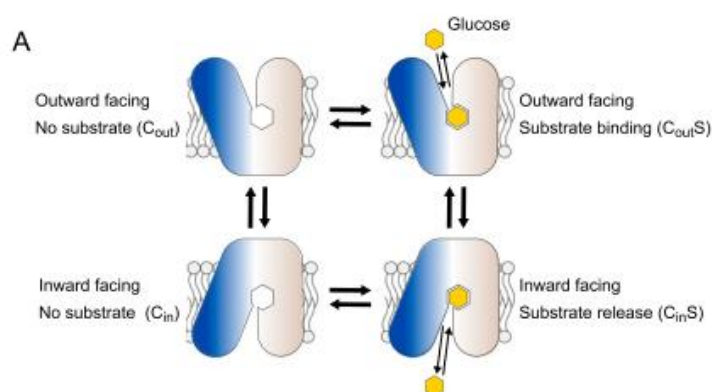


**Figure 1.8:** Mechanism for transport of glucose by GLUTs [130].

GLUT1 is present in high amounts in human erythrocytes and deficiency in this transporter can lead to a variety of issues, ranging from mild to severe developmental

and metabolic perturbation [131]. The specificity and transport kinetic features of the GLUT proteins for carbohydrates and transport inhibitors have been extensively studied for class 1 GLUTs and GLUT5 and reviewed in great detail by Holman [132]. Interactions of GLUTs with substrates is an important consideration for designing drugs which target cancer cells through glucose transporters. Differences in the amino acid side chains present in the binding pocket for different GLUTs result in drastic changes in substrate preference and interaction.

With respect to GLUT1, hydroxyl groups at C1, C3, C4, C6 (**Figure 1.9**) and the ring oxygen are all important for hexose binding. C4, when switched to the axial position in galactose led to a strong decrease in binding affinity in comparison to when the hydroxyl is in the equatorial position in glucose [132,133]. The hydrogen bond donor and acceptor ability of each of these hydroxyl groups is also important for substrate recognition. Hydrogen bond acceptor positions being C1, C3 and C6, while C4 is the only hydrogen bond donor. The hydroxyl at C2 does not seem to participate in hydrogen bonding, proven by the fact that 2-deoxyglucose is transported by all class 1 GLUTs, making C2 an attractive position for drug conjugation [132].

The preference of GLUTs for the  $\alpha$ - and  $\beta$ - anomers of glucose has also been studied. In particular, it was found that the  $\beta$  anomer binds more strongly than the  $\alpha$  anomer and is transported more rapidly by GLUT1, but in the crystal structure of GLUT3, both the  $\alpha$  and  $\beta$  anomers are present even if the  $\alpha$  anomer is more abundant [132,134]. An example of this being shown by the group of Lippard [135] which found that functionalisation of their platinum(II) anticancer drugs with carbohydrates at C2 and C1 $\alpha$  both improved intracellular accumulation of platinum drugs as well as their cytotoxicity profiles.

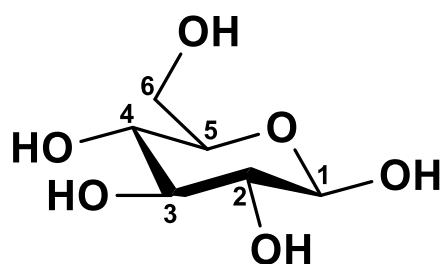


**Figure 1.9:** Structure of  $\beta$ -D-glucose with carbon atoms labelled.

Carbohydrates other than glucose can also be used to target glucose transporters. 2-deoxy-D-glucose, D-mannose, D-galactose, D-xylose, 2-deoxy-D-galactose, L-arabinose, D-ribose, D-fructose and D-lyxose, in order of decreasing affinity, were all found to be transported through a transporter-mediated manner [136]. For example, GLUT3 and GLUT4 show a similar affinity for galactose and glucose [132].

Glucose transporters can also serve as targets for tumour imaging by using 2- $^{18}\text{F}$ -fluoro-2-deoxy-D-glucose (FDG) (**Figure 1.10**) in positron emission tomography (PET) which is used for the detection and staging of cancer [137]. As the C2 position is not important for transport through GLUT1, fluorodeoxyglucose is transported into the cell in the same way as glucose. In the cytosol, it is phosphorylated into fluorodeoxyglucose 6-phosphate by hexokinase enzymes. Once in this form, further glycolysis is prevented as it cannot be converted to deoxyfructose 6-phosphate, leaving fluorodeoxyglucose 6-phosphate trapped inside the cell [138]. This accumulation can then serve as a contrast agent for imaging by detection of high energy gamma rays emitted from the decaying  $^{18}\text{F}$  atoms. The detection of these gamma rays shows the distribution of FDG in the body and can be used to locate metabolically active tissues in three dimensions [139].

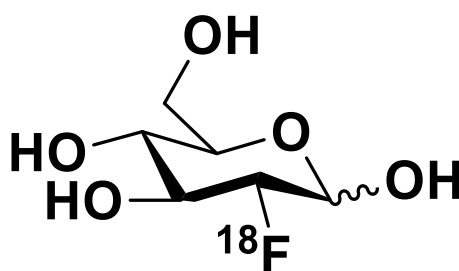


**Figure 1.10:** Structure of 2- $^{18}\text{F}$ -fluoro-2-deoxy-D-glucose (FDG).

Finally, targeting glucose transporters with the goal of inhibiting their function has also been explored. Cytochalasin B (**Figure 1.11**) is a natural product identified to inhibit cytoplasmic division [140,141], phagocytosis [142], pinocytosis [143], secretion of thyroid and growth hormone [144] and the inhibition of morphogenesis [145]. It was also shown to inhibit the uptake of deoxyglucose and glucose by tracking

the metabolites formed from 2-deoxy-D-[<sup>14</sup>C]-glucose and D-[<sup>14</sup>C]-glucose in samples of cell culture fluid [145]. Inhibitors inspired by this natural product, GLUT-i1 and GLUT-i2 (**Figure 1.11**) were synthesised based on a phe-amide core scaffold and used to compete with glucose at the binding site on GLUT1 [146]. Other natural products, such as the flavonoids curcumin [147] and silybin [148] were shown to directly inhibit GLUT1 and GLUT4 respectively. While the exact mechanism is not fully understood, researchers have hypothesised that, like cytochalasin, the inhibitors compete with glucose binding to the protein and inhibits its uptake. Chalcones, such as phloretin [149] were shown to target GLUT1 and GLUT2 by acting in the same way as the previously mentioned inhibitors. Interestingly, phlorizin [150], a chalcone containing glucose in its structure, does not affect GLUTs (1-12) but only acts on sodium linked glucose transporters (SGLTs). The study of this inhibitor led to the identification of these SGLTs, which are involved in a separate energy-dependent uptake mechanism to the energy-independent GLUT-mediated mechanism [151]. Forskolin, pentobarbital and dipyridamole have also been identified as potent GLUT1 and GLUT4 inhibitors (**Figure 1.11**) [152].

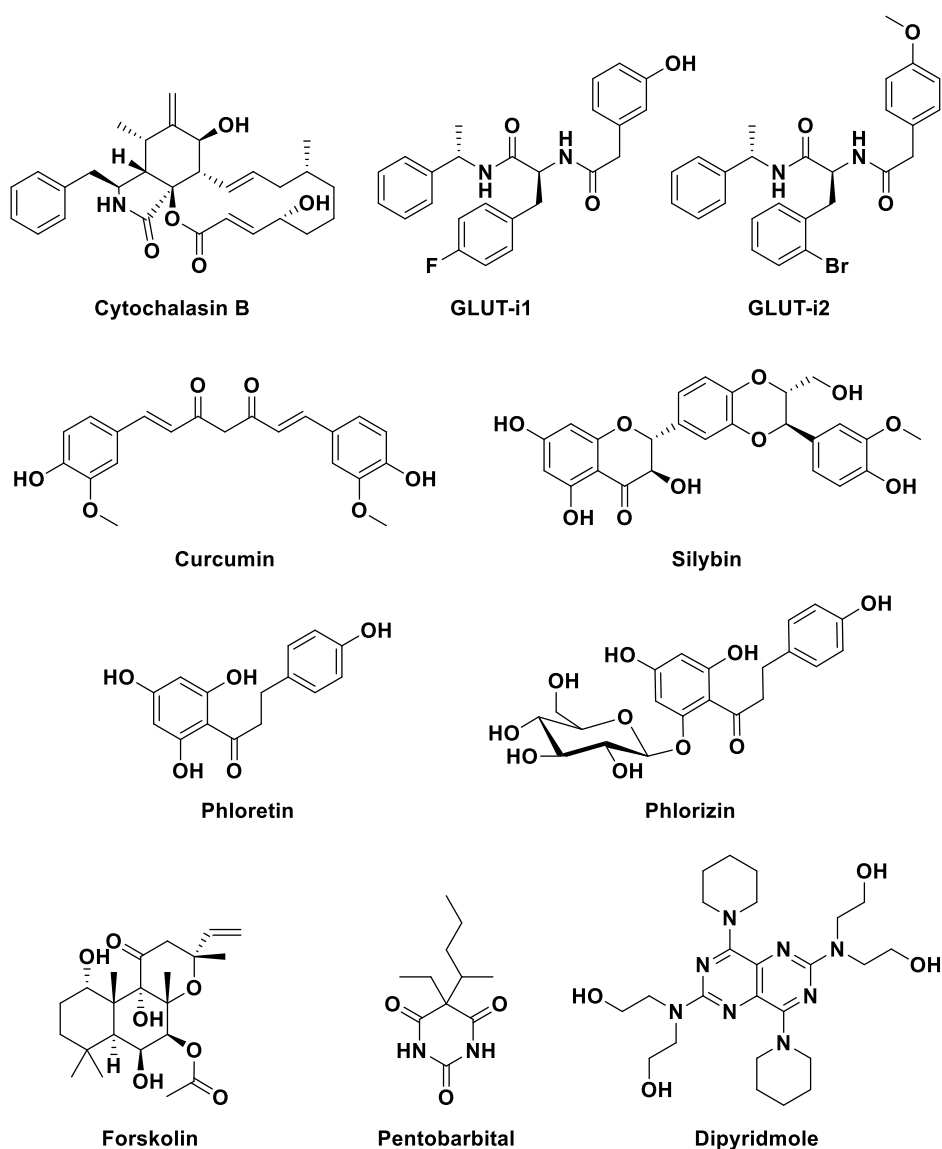


**Figure 1.11:** Structures of potent GLUT inhibitors and SGLT inhibitor phlorizin.

## 1.4 Metal-Based Glycoconjugates

### 1.4.1 Platinum(II) glycoconjugates

The first carbohydrate-based chemotherapeutic agent, glufosfamide [153,154], an ifosfamide mustard serving as a DNA alkylating agent, was developed to exploit the Warburg effect and was published in 1995. Much research has been conducted since then to target GLUTs and exploit the Warburg effect through glycoconjugation. Many metal complexes and, in particular platinum-based complexes, have been developed for this purpose, which will be discussed throughout this section (**Section 1.4**). Platinum(II) glycoconjugates were among the first complexes to be studied with the

intent of targeting glucose transporters and early work in this area of research was reviewed by Hartinger in 2008 [155]. In the last ten years, the groups of Gao and Lippard have developed many Pt(II) glycoconjugates using oxaliplatin [29] as the active therapeutic Pt(II) scaffold. Oxaliplatin is likely chosen as a good candidate for conjugation due to its altered toxicity profile when compared to cisplatin as well the use of a bidentate *O,O*-malonate leaving ligand, which allows for functionalisation with a variety of compounds. This leaving ligand is important because, when functionalised with carbohydrates and other targeting vectors, essentially creates a Pt(II) prodrug capable of targeting cellular entities while still providing anticancer activity [89].

Since 2013, the group of Gao have been interested in synthesising oxaliplatin derivatives conjugated to carbohydrates (**Figure 1.12**) to increase their water solubility (reducing renal toxicity) and improving their tumour selectivity. Complexes **1.7 – 1.9** were first synthesised containing glucose conjugated in the C1 position to a malonate leaving ligand. While the sugar itself helped to improve water solubility, the addition of halides (Cl or F) in the 2-position of malonic acid further increased water solubility, an example being oxaliplatin in comparison to Complex **1.9**, which displayed an enhanced water solubility from 6.0 mg/ml to 946.8 mg/ml, respectively. **1.9** was found to exert the highest cytotoxic effect, likely due to its superior solubility through the addition of a fluoro-substituent. The dependency between the cytotoxicity of Complex **1.9** and its interaction with glucose transporters was evaluated using phlorizin to inhibit SGLTs and it was found that the cell-killing ability of **1.9** was reduced in the presence of the inhibitor. The same assay conducted with oxaliplatin had no effect on its potency, meaning the toxicity of **1.9** was dependent on SGLTs for drug uptake [156]. Further tests were also conducted with **1.9** to see if combination therapy with this oxaliplatin glyco-derivative, folic acid (FA) and 5-fluorouracil (5-FU) would improve the efficacy of oxaliplatin combination therapy (FOLFOX). Comparisons between the two combination therapies (both in a ratio of 1:5:10, Pt:FA:5-FU) showed that Complex **1.9** exhibited better overall cytotoxicity against the cell lines HT29, SKOV3, DU146, MCF7, and H460. In particular, the glycoconjugate combination therapy displayed statistically significant activity against

the SKOV3 cell line (0.17  $\mu\text{M}$ ) as opposed to FOLFOX (0.73  $\mu\text{M}$ ). These results suggest that this complex could be used as a suitable replacement for oxaliplatin while also improving the maximum tolerated dose (MTD) for the drug [157].

Later studies from the same group also looked at the use of galactose and mannose glycoconjugates (**1.7**, **1.10**, **1.11**) against cell lines which overexpressed GLUT1 [158]. They observed that cell lines sensitive to glucose, which had a high expression of GLUT1, were also sensitive to mannose and galactose derivatives. They remarked that the galactose derivative **1.10** was much less potent in some of their testing as opposed to the glucose derivative **1.7**, particularly against HT29 (**1.10** = 1.7  $\mu\text{M}$  and **1.7** = 0.53  $\mu\text{M}$ ), A549 (**1.10** = 4.90  $\mu\text{M}$  and **1.7** = 0.35  $\mu\text{M}$ ), and MCF7 (**1.10** = 9.82  $\mu\text{M}$  and **1.7** = 0.61  $\mu\text{M}$ ) cell lines and hypothesised that different GLUT subtypes may be present in these cell lines. Interestingly, platinum uptake was measured in one cell line for the glucose derivative **1.7** but not for **1.10**, which might have provided more information on the lack of activity of this complex. The use of 2-deoxyglucose (2-DG) (**1.23** – **1.25**) was also analysed as it is transported through GLUT1 at much higher rates than glucose and has a greater binding affinity [159]. Again, these complexes showed cytotoxicity greater than oxaliplatin and with the addition of halides, showed improved water solubility and also showed GLUT1 dependent uptake [160].

Later publications looked at varying the linker length from the sugar targeting moiety to the platinum core. This variable has been shown to affect the translocation efficiency of GLUTs and subsequently affect the cellular accumulation of the glycoconjugates [161]. Complexes **1.12** – **1.22** all showed great potential as anticancer agents, however, **1.22** was two to three times less effective than its counterpart **1.21** and when incubated with the lung cancer cell line (A549) was fourteen times less cytotoxic [162]. Through the use of a linker differing by one carbon atom shows such a drastic change in anticancer activity.

Gao and coworkers also developed different Pt(II)-glyco conjugated with conjugation to different positions of the sugar (Glu, Gal and Man) (**1.26** – **1.28**), in particular at C6. As discussed in **Section 1.3.2**, functionalisation at this position should be tolerated as long as the hydrogen bond donor ability of the sugar is conserved. This group accomplishes this aspect by using amide bonds to link the sugar with malonic

acid. In assays against various cancer cell lines (HT29, H460, DU145, A549, SKOV3, MCF7), Complex **1.26**, a glucose conjugate, was the most potent, and was particularly active against H460 cells (1.08  $\mu\text{M}$  vs 22  $\mu\text{M}$  (Oxaliplatin and mannose/galactose derivatives)). This indicates that, while all complexes had good activity against the cell lines tested, the glucose conjugated complex had a stronger affinity for the glucose transporters present in the cells [163].

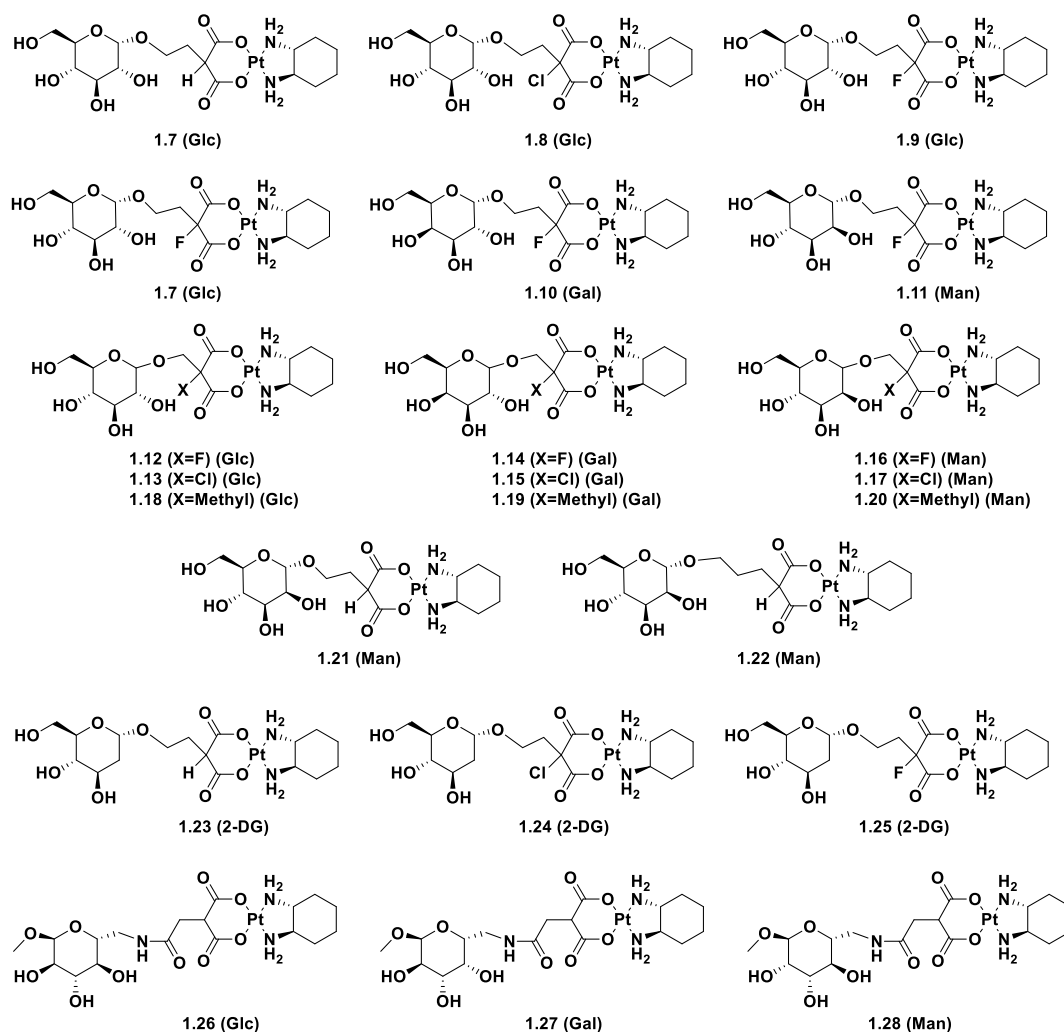


**Figure 1.12:** Structures of oxaliplatin glycoconjugates synthesised by Gao *et al.* (**1.7 – 1.9** [156]) (**1.10 – 1.11** [158]) (**1.12 – 1.17** [164]) (**1.18 – 1.20** [165]) (**1.21, 1.22** [162]) (**1.23 – 1.25** [160]) (**1.26 – 1.28** [163])

Similarly, the group of Lippard developed novel Pt(II) glycoconjugates to target the overexpression of glucose transporters. In particular, the group looked at developing complexes conjugated at every position of the glucose ring [135] (this aspect will be further discussed in **Chapter 3**). Importantly, other than the position of conjugation



to the glucose molecule, the distance of the sugar to the metal centre is vital for tuning anticancer activity, and this was investigated by this group through the synthesis of complexes **1.29** – **1.31** (**Figure 1.13**). They hypothesised that steric hindrance, caused by an overly long substrate would block the conformational change needed for the transport of substrates through GLUTs. This hypothesis is supported by the observed decrease in cellular uptake (**1.29**>**1.30**>**1.31**) in ovarian (A2780), prostate (DU145), and lung cancer (A549) cells. To further support this, docking studies were carried out with complexes **1.29** and **1.31** which showed significant steric clashes occurring with **1.31** but not **1.29**. The group concluded that the translocation efficiency and subsequent cellular accumulation were reduced with increasing linker length [161].

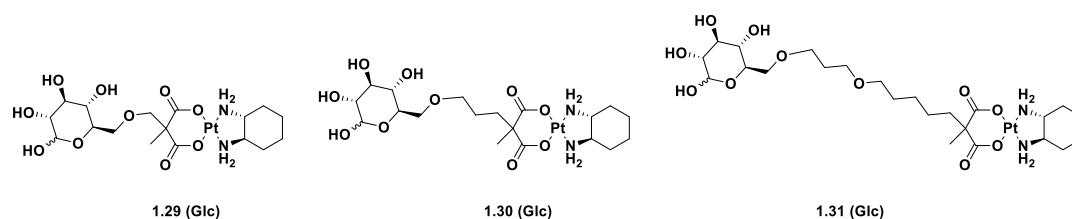


**Figure 1.13:** Structures of oxaliplatin glycoconjugates synthesised by Lippard *et al.* (**1.29** – **1.31** [161]).

#### 1.4.2 Platinum(IV) glycoconjugates

Pt(IV) glycoconjugates have also gained attention as suitable substrates for targeting glucose transporters. Octahedral Pt(IV) complexes, as discussed in **Section 1.2**, are considered inert prodrugs that can be administered orally and are activated by the reduction inside the cell to their active Pt(II) counterparts [166]. Examples of complexes employing these methods of targeting can be seen from the group of Wang. This group explores the use of acetylated and deacetylated Pt(IV) glycoconjugates of glucose, galactose, mannose and rhamnose (**Figure 1.14**).

**Figure 1.14** show the structures of amide linked, mono- and bis-functionalised acetylated Pt(IV) glycoconjugates. A major aspect of this work was the evaluation of the reduction properties present in mono- and bis-functionalised Pt(IV) complexes. The overarching hypothesis was that altering the axial ligands will alter the Pt(IV) to Pt(II) reduction potential, allowing for reduction in cancer cells but not in healthy cells

[167]. The reduction potentials of complexes **1.32** – **1.46** were analysed using cyclic voltammetry at a pH of 6.4 to mimic the pH of the cancer microenvironment [168]. Normal physiological pH of 7.4 was also analysed to determine if functionalisation allows for the selective reduction within the tumour rather than the bloodstream. With lower pH, the reduction potential of a redox couple will increase [169]. Bis-functionalised complexes **1.32** – **1.36** did not show much of a difference in reduction potentials between pH 6.4 and 7.4 [167] while the mono-functionalised complexes **1.37** – **1.46** displayed a more positive shift in reduction properties at pH 6.4 than the bis-functionalised prodrugs. It is believed that mono-functionalisation of the Pt(IV) prodrugs should be a mainstay in drug design due to its favourable reduction properties. Wang *et al.* also concluded that a cisplatin core, as seen in complexes **1.37** – **1.41** should be employed because of their superior activity compared to their oxaliplatin derivatives [170].

The group also varied the distance of the carbohydrate to the platinum centre by using two and three carbon chains bound through amide bonds. Interestingly, the only sugar whose linker was not varied was the glucose derivative, and while the cytotoxicity of Complex **1.32** was not spectacular, varying the linker and evaluation against healthy cells could still hold some value. Mannose derivatives (**1.33**, **1.34**) and their mono-functionalised counterparts (**1.38**, **1.39**) were chosen to evaluate their selectivity for healthy cells. Complex **1.33** had an IC<sub>50</sub> of 84 µM and **1.34** showed cytotoxicity at 169 µM. **1.38** and **1.39** had comparable IC<sub>50</sub> values and when compared to their activity against cancerous cells, showed a highly significant reduction in cell killing ability. Unfortunately, these complexes were not tested in the presence of GLUT inhibitors, meaning their method of uptake into the cell cannot be concluded. What is interesting however, is their lack of activity against the healthy cell line, even with their highly lipophilic protecting groups.

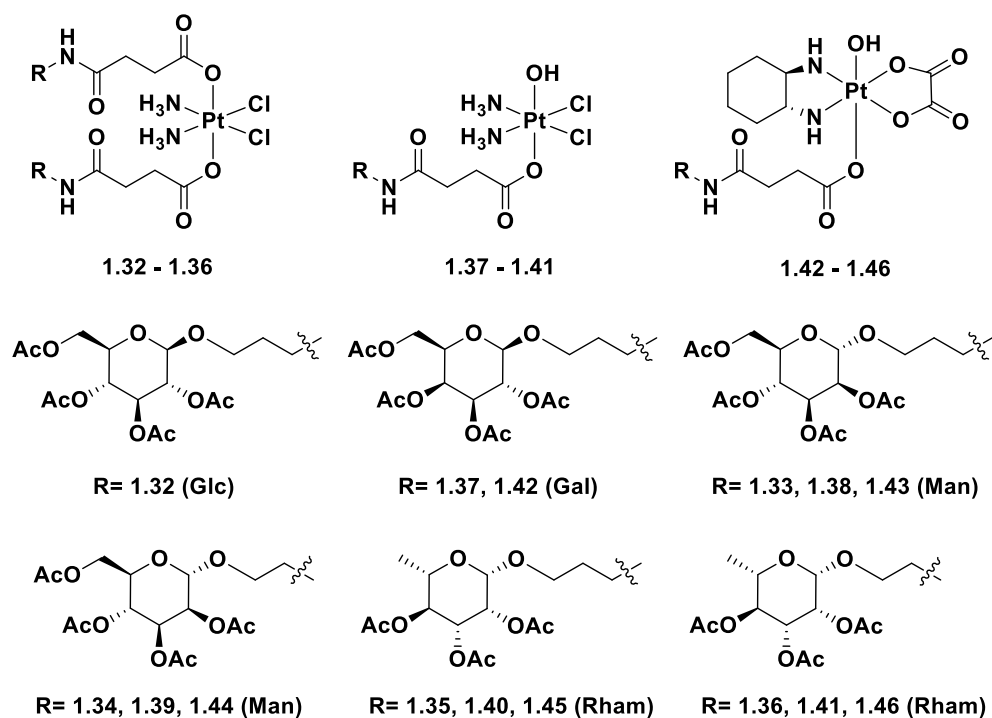


**Figure 1.14:** Structures of acetylated mono- and bis-Pt(IV) glycoconjugates of glucose, galactose, mannose and rhamnose with varying linker lengths and platinum cores [167,170].

Wang *et al.* also synthesised a library of mono-functionalised, acetylated and deacetylated Pt(IV) prodrugs (**Figure 1.15**), based on their previous findings [171]. Specifically, the group attempted to improve the GLUT1 targeting ability of their complexes, through the variation of their carbohydrate targeting vectors by incorporating the disaccharides maltose and lactose and also through the use of deprotected sugars which should have a greater affinity for GLUTs. As expected, free sugar derivatives showed greater activity against the majority of cell lines tested compared to their per-acetylated counterparts. In particular, the deprotected mannose Complex (**1.53**) showed a far improved cytotoxicity (thirty-times more effective against HeLa cells) when compared to the acetylated mannose Complex (**1.50**). Importantly, lactose conjugates (**1.48**, **1.57**) were particularly effective at overcoming the chemoresistance of the A549R cell line (4.26  $\mu\text{M}$  and 8.37  $\mu\text{M}$ , respectively).

Incubation of **1.55** with phloretin shows a large decrease in activity, with  $\text{IC}_{50}$  increasing from 0.89  $\mu\text{M}$  to 31.80  $\mu\text{M}$ . This shows that transport of the free sugar complexes is mediated by GLUTs and with inhibition, drug cytotoxicity dramatically

decreases [171]. Interestingly, **1.55** is functionalised in the C6 position, suggesting that while isomers of C1 and C2 might be more suitable for drug conjugation, there is a need for further exploration of the use of different positional isomers. Interestingly, the results of the docking studies for **1.55** shows an interaction between proteins in the GLUT1 binding site and the oxygen of C6, whereas no such interaction is seen in the C2 position. Also notably, **1.55** employs an oxaliplatin core, which is thought to be sub-optimal in terms of activity and reduction potential. It is clear that more research is needed into this field to optimise the three fundamental aspects of these complexes: (i) the carbohydrate vector used and which position to functionalise; (ii) the type and length of linker used and (iii) the active therapeutic agent used.

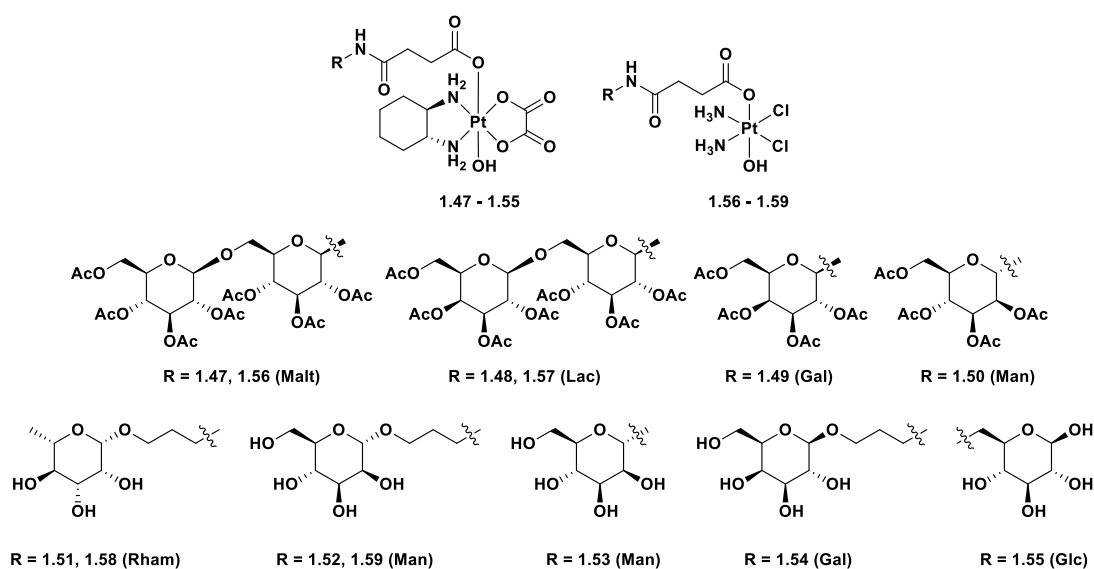


**Figure 1.15:** Structures of mono-functionalised acetylated and deacetylated Pt(IV) glycoconjugates of maltose, lactose, glucose, galactose, mannose and rhamnose. Complexes are synthesised on cisplatin or oxaliplatin scaffolds [171].

### 1.4.3 Other glycoconjugated metallodrugs

While platinum-based glycoconjugates have been studied extensively as potential alternatives to cisplatin, other metallodrugs of Ru, Pd, Au, Cu, Fe, Sn and Co have been studied as potential chemotherapeutics [172]. In the case of Ru-based complexes, many are considered to be less toxic than Pt-based drugs and more selective for cancer cells which could allow them to overcome the limitations and resistances of platinum-based drugs. This is potentially due to the ability of Ru to

mimic iron in binding to biomolecules; transferrin receptors, for example, may transport Ru rather than iron to cancer cells [173].

Ru bipyridyl (bpy) complexes display luminescent properties which make them attractive candidates for fluorescent sensors and photodynamic-therapeutic applications [174]. Complexes **1.60** – **1.62** (**Figure 1.16**) show an enhanced cellular uptake in cancer cells, with respect to their unconjugated counterparts, while retaining their luminescent properties. *S*-glycosylation is also employed to resist intracellular hydrolysis. Although uptake through GLUTs could not be confirmed, the addition of the carbohydrate moieties improved both water solubility and drug accumulation, while **1.60** showed the highest accumulation [175].

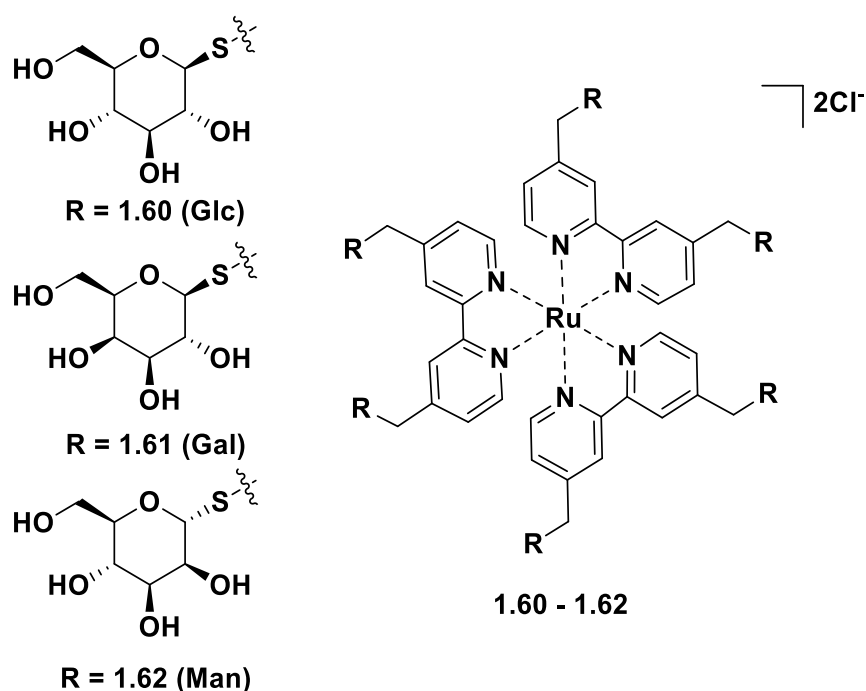


**Figure 1.16:** Ru(bpy)<sub>3</sub> glycoconjugates of *S*-glycosylated glucose, galactose and mannose [175].

Gottschaldt *et al.* have also used carbohydrates for the functionalisation of Ru(bpy)<sub>2</sub> curcumin conjugates (**Figure 1.17**). Fructose (**1.64**) has also been employed as a targeting group to take advantage of GLUT5 which is overexpressed in the small intestine, kidney cells and breast cancer cells and has a preference for fructose [176]. Curcumin is used as a *O,O*-bidentate chelating ligand in this complex for its reported antimicrobial, anti-inflammatory and antitumour effects [177]. A drawback of

curcumin as a chemotherapeutic is its rapid metabolism in the body and poor water solubility. Conjugation of this ligand to a metal centre has been shown to increase water solubility; the addition of carbohydrates to these complexes has the added benefit of further improving their water solubility [178]. The complexes showed varying levels of anticancer activity; however, the authors suggest the high lipophilicity of the bipyridyl ligands may hamper its targeted anticancer effects. Importantly, there was a noticeable increase in the toxicity of the glycoconjugated curcumin complexes, which is in line with the authors expectations.

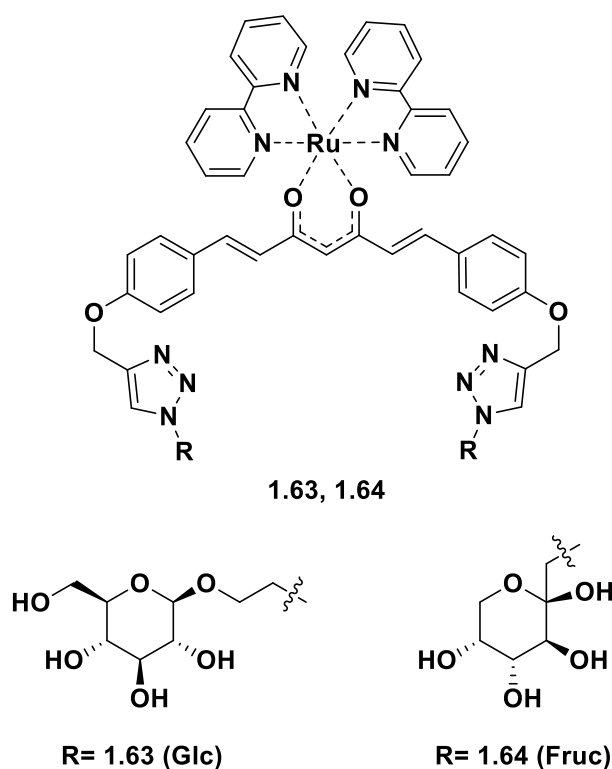


**Figure 1.17:** Ru(II) curcumin glycoconjugate of glucose and fructose [178].

Palladium(II) shares structural and thermodynamic features with Pt(II), in particular its square planar geometry. Pd however, is much less kinetically stable than Pt(II) but it can be used for anticancer treatments with mechanisms different to cisplatin [179]. Photodynamic therapy (PDT) using Pd is also utilised as an anticancer therapy by photo-irradiating nontoxic photosensitisers with visible light. This generates reactive oxygen species (ROS) to kill malignant cells. For successful PDT treatment, a photosensitiser must meet several conditions: (1) no cytotoxicity without photoirradiation, (2) reasonable cytotoxic ROS generation upon photoirradiation, (3)

availability of longer wavelength light, (4) reasonable water solubility, (5) selective accumulation at the tumour site [180]. In order to meet the requirements of (4) and (5), carbohydrates are incorporated to both improve water solubility and improve selectivity through the Warburg effect (**Figure 1.18**). Experimentally, uptake of **1.65** and **1.66** was shown to be almost four-times higher than that of the un-glycosylated standard.

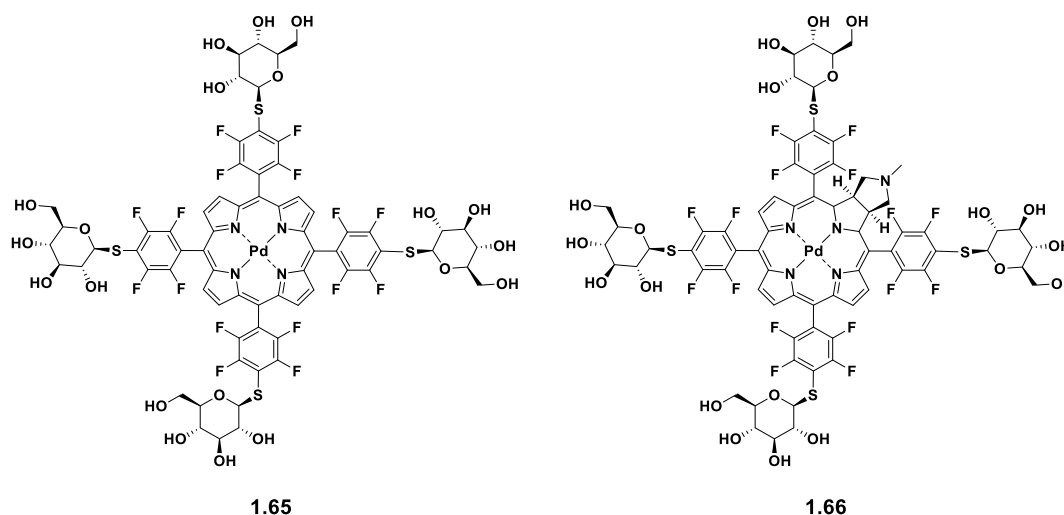
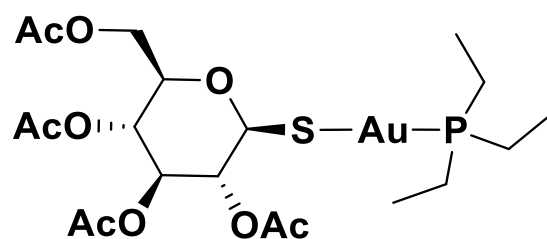


**Figure 1.18:** Porphyrin and chlorin palladium glycoconjugates [180].

Gold has also gained much attention as a new class of potential chemotherapeutics, with the ability to inhibit tumour cell growth through non-cisplatin-like mechanisms of action. Gold complexes have seen applications in both the +1 and +3 oxidation states. Gold(III) shares cisplatin's square-planar geometry while gold(I) has a linear geometry which has seen more success in terms of clinical applications [181].

Auranofin (**Figure 1.19**) is a linear gold(I) complex containing triethylphosphine and thio-glucose tetraacetate as ligands. Auranofin has been used clinically since 1985 for the treatment of rheumatoid arthritis and has shown excellent anti-inflammatory and anticancer activity *in vivo* [182]. Auranofin acts as an inhibitor of thioredoxin reductase, altering the redox state of the cell and increasing the production of hydrogen peroxide. This peroxide oxidises components of the thioredoxin system and creates the conditions needed for apoptosis [183].



### Auranofin

**Figure 1.19:** Structure of gold(I) glycoconjugate, auranofin [182].

Complexes of gold(III) have also been researched extensively, however, the issue of instability and reactivity of the Au(III) ion, such as the reduction of Au(III) to Au(I) or Au(0) have hampered its therapeutic potential [184]. Stabilisation with the use of carbon deprotonated bidentate ( $C^{\wedge}N$ ) and tridentate ( $C^{\wedge}N^{\wedge}C$  or  $C^{\wedge}N^{\wedge}N$ ) ligands has been shown to increase stability to reduction in the presence of common biological reductants [185]. These ligands, however, have not aided in increasing drug targeting or selectivity. Functionalisation with carbohydrates is attractive in this regard and has appeared in many examples, reviewed by the group of Ronconi *et al.* [181].

Au(III) glycoconjugates with positional isomers of glucose and glucosamine (**1.67** – **1.70**) are shown in **Figure 1.20**. *In vitro* antiproliferative assays against four human cell lines (A2780, A2780cis, HT29 and HeLa) showed that the glycosylated complexes only showed activity against A2780 cells. It was also shown that cell internalisation was not GLUT mediated but incubation with GLUT inhibitor 4,6-*O*-ethylidene- $\alpha$ -D-glucose (EDG) actually improved cytotoxic activity of **1.67** – **1.70**. The group speculates that an alternative facilitated diffusion method is responsible for uptake [186]. Potentially, steric bulk is responsible for the poor uptake through GLUTs.



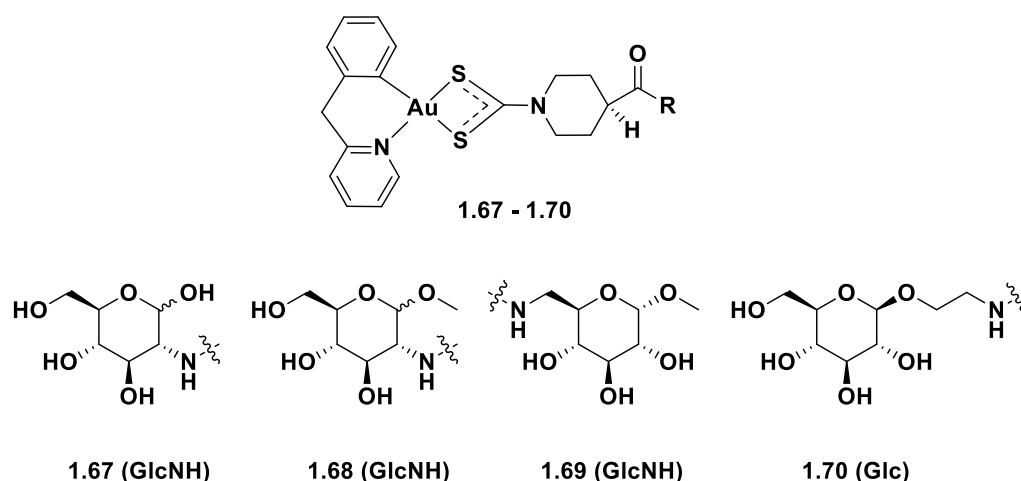


**Figure 1.20:** Structure of gold(III) glycoconjugates functionalised in the C2 position (**1.67** – **1.68**), C6 position (**1.69**) and anomeric position (**1.70**) [186].

The complexes discussed in this section have been primarily synthesised by linking the carbohydrate moiety to the metal centre through amide bonding or glycosylation reactions. One drawback of these methods of conjugation is their relative instability *in vivo* through hydrolysis [187]. Earlier in this section, examples can be seen of the use of thiol linkages to overcome the chemical/enzymatic degradation of glycosidic bonds (**Figure 1.19**). In the literature, amide bond degradation is avoided through the use of peptide bonds mimics, the most common mimics being *N*-methylated amide bonds, reduced amide bonds, semicarbazides, peptoids, and alkenes [188]. 1,4-disubstituted 1,2,3-triazoles have also been identified as suitable bioisostere for amide bonds and has seen widespread use in the field of carbohydrate chemistry for its enhanced stability and mild reaction conditions in comparison to glycosidic bonds [189].

## 1.5 Copper catalysed azide-alkyne cycloaddition (CuAAC) ‘Click’ chemistry

### 1.5.1 Click chemistry in platinum-based drugs

As described later in the aim and scope section, sugar moieties and the Pt metallic centre are conjugated with linkers featuring a triazole group obtained through “click” chemistry. Copper catalysed azide-alkyne cycloaddition (CuAAC) or ‘Click’ reactions are catalysed variations of Huisgens 1,3-dipolar cycloaddition reaction [190]. Classically, these reactions converted organic azides and terminal alkynes using high

temperatures into a mixture of 1,4- and 1,5-triazole regio-isomers [191]. More recently, research by Meldal [192] and Sharpless [193] introduced copper(I) as a catalyst for the regiospecific formation of 1,4-disubstituted 1,2,3-triazoles (**Figure 1.21**) [194]. This reaction will be discussed in greater detail in **Chapter 2**.

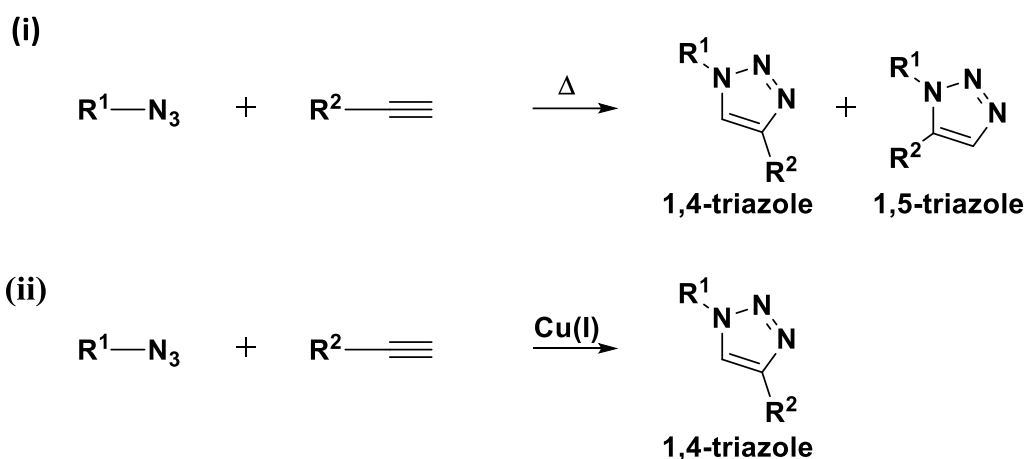


**Figure 1.21:** Synthesis of 1,2,3-triazoles using (i) Huisgen 1,3-dipolar cycloaddition conditions, yielding a mixture of 1,4- and 1,5-regioisomers; (ii) CuAAC conditions, yielding 1,4-disubstituted 1,2,3-triazoles only.

Click chemistry has seen a wide variety of applications in organic synthesis and the fields of biology, biochemistry and biotechnology. The resulting heterocycle is stable against oxidation, reduction and hydrolysis under acidic or basic conditions and can participate in hydrogen bond formation, dipole-dipole and  $\pi$  stacking interactions, making it an attractive mimetic for amide bonds [195,196].

Examples of this type of linkage include conjugation of classical cancer targeting ligands to platinum (**Figure 1.22**) [197]. These complexes were synthesised by the click reaction of ethynylestradiol and di-*tert*-butyl (2-azidopropane-1,3-diyl)dicarbamate, and the subsequent *N*-Boc deprotection of the diamine groups for coupling to cisplatin and carboplatin derivatives. The cytotoxicity of both estrogen linked complexes was analysed against a panel of cervical, breast, ovarian and colon cancer cell lines. Both complexes (**1.71** and **1.72**) exhibited far superior cytotoxicity compared to the reference cisplatin and carboplatin.

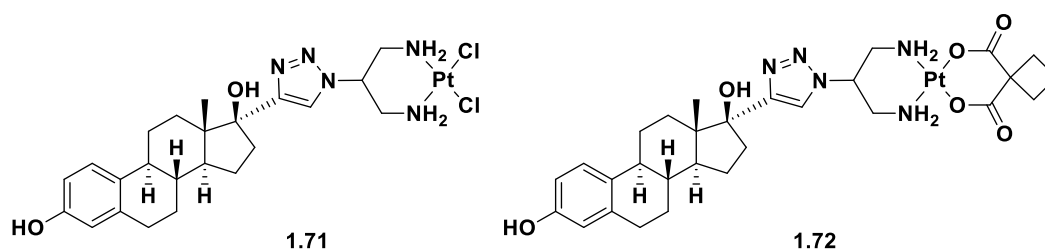


**Figure 1.22:** Structures of estrogen Pt(II) complexes linked *via* CuAAC chemistry, complexes contain cisplatin (**1.71**) and carboplatin (**1.72**) cores [197].

The example shown in **Figure 1.22**, is more representative of the type of click chemistry that will be employed in later chapters, however the scope of click chemistry is much larger than that of functionalising ligands for conjugation to platinum drugs. In particular, groups have used strain-promoted azide-alkyne cycloaddition (SPAAC) to exploit the reactivity of cyclooctynes (due to ring strain) for coupling to azides directly coordinated to the metal centre [198]. Farrer *et al.* synthesised a di-nuclear Pt(IV) complex (**Figure 1.23**), coupled through SPAAC click chemistry, which is capable of photoreduction to Pt(II) through azido groups [199].

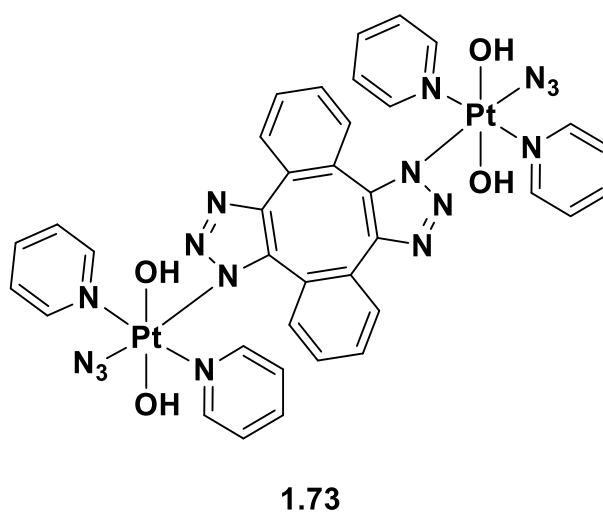


**Figure 1.23:** Structure of Pt(IV) triazolato azido complex [199].

Functionalisation of the metal centre with fluorescent agents using click chemistry has also been explored to investigate the cellular transport and cytoplasmic localisation of Pt-based chemotherapeutics [200]. Click chemistry has also been employed for the functionalisation of Pt-based drugs with secondary chemotherapeutics, biomarkers for post-treatment analysis and for tracking Pt drugs

within cells, all of which have been previously reviewed by Griffith and Farrer in 2020 [201].

## 1.6 Research aims and thesis outline

The aim of the research described in this thesis is to develop different series of novel Pt(IV)-glycoconjugated prodrugs to enhance the selectivity for osteosarcoma (OS) cancer cells (the importance of targeting osteosarcoma will be discussed in detail in **Chapter 2**). With this in mind, the complexes designed in later chapters were designed with the following requirements (**Figure 1.25**):

- A targeting vector (glucose or galactose) whose receptor is overexpressed on cancer cell membranes, yielding a complex which higher selectivity for cancer cells (Red).
- A linker (blue) which allows the targeting vector to couple to the metal centre, preferably one prepared with mild reaction conditions and relatively high yields. This linker is versatile and allows for various modifications, supporting the synthesis of derivatives of different targeting moieties and linker lengths.
- The active therapeutic agent (yellow) which is inert in the bloodstream and is reduced to its active form intracellularly. This strategy is called the prodrug approach.

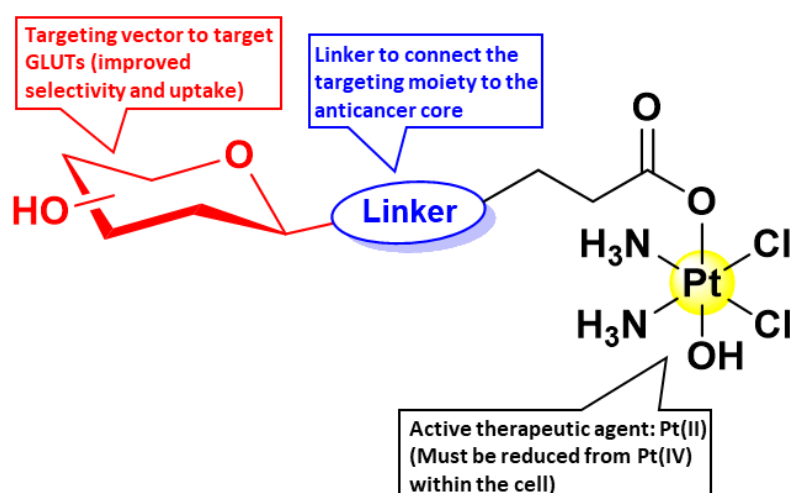


**Figure 1.25:** Schematic structure of the complexes designed and synthesised in this research project.

A general outline of the chapters contained in this thesis is summarised here, explaining the evolution of my research project which will be discussed in depth in the chapters to follow:

- 1) Synthesis, characterisation, and *in vitro* evaluation of four acetylated Pt(IV) glycoconjugates against a panel of OS cell lines. Anticancer activity and cellular uptake are analysed for three different OS cell lines (MG63, SAOS-2, and U-2OS) as well as an enriched-cancer stem cell (CSC) culture (**Chapter 2**).
- 2) Synthesis, characterisation, reduction properties and *in vitro* evaluation (2D and 3D) of four free sugar Pt(IV) glyco-conjugated prodrugs against two OS cell lines (SAOS-2 and MG63) and a healthy osteoblast cell line (hFOB5) (**Chapter 3**).
- 3) Synthesis, characterisation and preliminary biological evaluation of a library of C2 functionalised Pt(IV) glycoconjugates with the aim of improving cytotoxicity and uptake through substitution of the sugar at a position other than C1 (**Chapter 4**).
- 4) Synthesis, and characterisation of multivalent galactose Pt(IV) glycoconjugates to target the asialoglycoprotein receptor (ASGPR) overexpressed in hepatic carcinoma cells (**Chapter 5**).

## **Chapter 2: C1 Platinum(IV) Acetylated Glycoconjugates**

## 2.1 Introduction

### 2.1.1 Osteosarcoma

Osteosarcoma (OS) is a primary malignant bone tumour which affects 3.4 million people per year. Before the 1970s, the five-year survival rate of patients affected was only 20%, however, with the introduction of chemotherapy, this rate has increased to >65%. OS is most common in adolescents between the ages of five and fifteen (5.6 cases per million children) and young adults over the age of twenty [202]. OS is classified based on its location, involved cell type, and tumour grade and is divided into five groups: central [203,204], multifocal [205], gnathic [206], surface OS [207,208], and secondary OS [209,210].

Before the 1970s, treatment options were limited to surgery, making OS a universally fatal disease due to its tendency to form pulmonary metastases. With the introduction of chemotherapeutics in conjunction with surgery, long-term survival rates in young patients rose dramatically. Current treatments use a combination of doxorubicin, cisplatin, ifosfamide, and methotrexate (**Figure 2.1**), with the most commonly used combination being the “MAP” regimen of methotrexate (M), doxorubicin (A (anthracycline)) and cisplatin (P) [211].

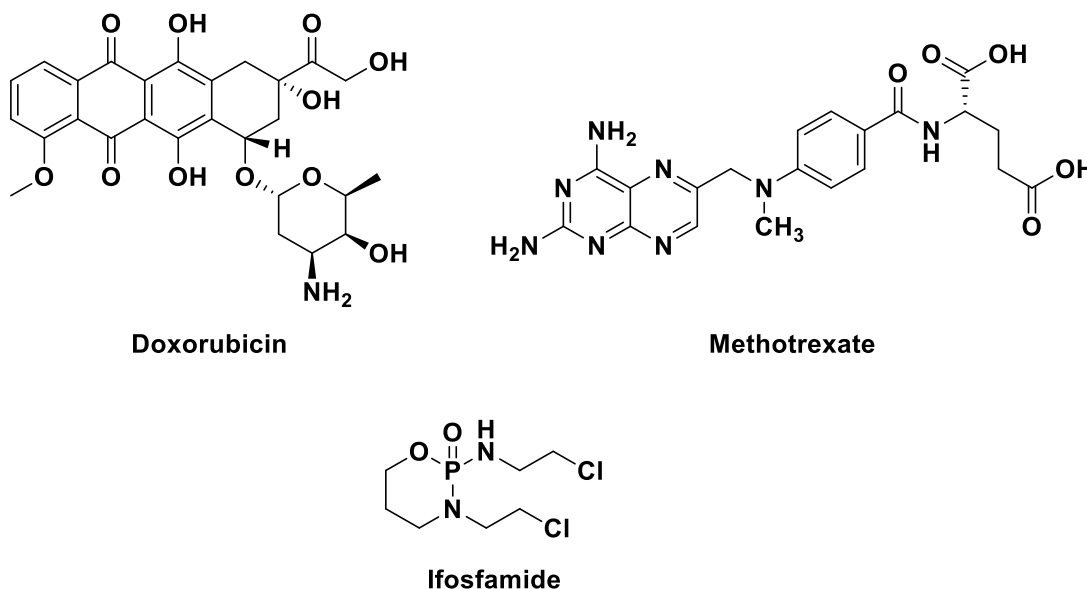


**Figure 2.1:** Structures of clinically approved drugs to treat OS, all of which may be used in combination with cisplatin (**Figure 1.1**) [211].

While the survival rate of patients with OS has significantly improved, no major advances have been made in the last 10 plus years which has led to poor prognosis due to chemoresistance and early metastasis [212]. A major issue in the treatment of this disease is the lack of targeted therapies, and while some drugs have been developed to target specific pathways and growth factors (DNA damage repair and cell cycle, vascular endothelial growth factor, platelet – derived growth factor, insulin – like growth factor, PI3K/mTOR pathway, and the avian myelocytomatosis viral oncogene homolog), further exploration is needed to provide targeted drugs with better effects [213]. Photodynamic therapy [214] and nanodelivery [215] of the above described “MAP” regimen have also been developed as methods to increase drug uptake in specific tumours, however, the volume of research in these fields is low, and until now, there has been no targeted metallo-drugs developed to treat osteosarcoma.

As discussed in **chapter 1**, we hope to overcome this chemoresistance and lack of targeted treatments by targeting glucose transporters overexpressed on the cell surface. GLUT1 is positively overexpressed in OS and its downregulation can inhibit the formation, growth, and invasion of OS cells *in vitro* and *in vivo* [216]. GLUT3 is also overexpressed due to the ELK1/miR-134/PTBP1 signalling cascade, which enhances aerobic glycolysis and promotes chemoresistance [217,218]. GLUT1 and GLUT3 are selective for glucose and galactose, respectively, and these two sugars are functionalised for coordination to platinum anticancer drugs, which will be discussed later in this chapter. The three main OS cell lines tested in this chapter are MG-63 [219] (an osteoblast-derived cell line), SAOS-2 [220] (a non-transformed osteoblast-like cell line), and U-2 OS [221] (derived from a moderately differentiated tibia sarcoma): these are three of the most widely used cell lines for bone biology and drug testing research [222].

Lack of selectivity for Cancer Stem Cells (CSCs) has also been identified as an issue in OS treatment. Mesenchymal stem cells (MSCs) are defined as fibroblast-colony forming units which can renew themselves through cell division and can differentiate themselves into osteoblasts, adipocytes, and chondrocytes after exposure to specific soluble factors in the microenvironment [223]. OS contains distinct and defined cell



populations of MSCs, which have a stem-like phenotype and form spherical colonies, called sarsospheres. These sarsospheres are involved in tumour progression, metastasis and tumour recurrence which is often seen in patients with OS [224].

Targeting these cancer cells and CSCs is important for the future treatment of the disease; so far, drugs targeting CSC-associated surface markers and the CSC microenvironment have been developed and some are undergoing clinical trials [225]. However, drugs to specifically target the OS CSC microenvironment have not been identified [226]. As discussed above, targeting the GLUT overexpression present on these cancer cells is a route for targeted therapy.

### 2.1.2 Acetylated carbohydrates as anticancer agents

**Section 1.4** discussed the use of metal-based glycoconjugates for targeted chemotherapy, taking advantage of glucose transporters for drug uptake and selectivity. Notably, the majority of the complexes discussed contained carbohydrates with free hydroxyl moieties, and these were confirmed to be taken up through GLUTs. However, certain complexes functionalised with sugars containing the *O*-acetyl protecting group showed good cytotoxicity without the use of glucose transporters. Wang et al [227] reported the synthesis, characterisation and discussed the cytotoxicity, cellular uptake and reduction properties of the complexes shown in **Figure 2.2**. In general, complexes containing the cisplatin scaffold (**2.1 – 2.3**) possessed higher antitumour activity than those with the oxaliplatin scaffold (**2.4 – 2.6**). It was observed that the linkages between the active therapeutic agent and the sugar have a large influence on anticancer activity. This effect can be seen in complexes **2.7**, **2.11** and **2.12**, in which the linker is exchanged with butyryl and valeryl groups. The resulting cytotoxicity of **2.11** and **2.12** were reduced by two-to-three times in most cell lines and in the case of the A549 carcinoma cell line, there was a fivefold reduction in activity.

Interestingly, galactose derivatives (**2.2**, **2.5**) showed the most promising anticancer activity when compared to their glucose derivatives and showed comparable activity to both cisplatin and oxaliplatin. These complexes also displayed the ability to overcome drug resistance of A549R cells, most likely due to the higher cellular uptake and increased DNA platination. *In vivo* studies of **2.2** show that the increased

cytotoxicity seen *in vitro*, does not carry over to animal models, however, the addition of this galactose moiety does significantly reduce the weight loss associated with cisplatin treatment, thus reducing toxic side effects of classical platinum drugs.

Finally, the effect of the GLUT inhibitor phlorizin on the anticancer activity of **2.2**, **2.5** and **2.9** was investigated however, it had no remarkable influence on the IC<sub>50</sub> values of the tested complexes. A conclusion can be drawn that these complexes are not transported by GLUTs, possibly due to the acetyl protecting groups of the sugars. A possible explanation of the good activity observed for these complexes may be related to the increased lipophilicity caused by the acetyl groups. Enzymatic hydrolysis takes place when these esters enter the bloodstream, allowing the carbohydrates to act as prodrugs with esters increasing the drugs overall bioavailability [228].

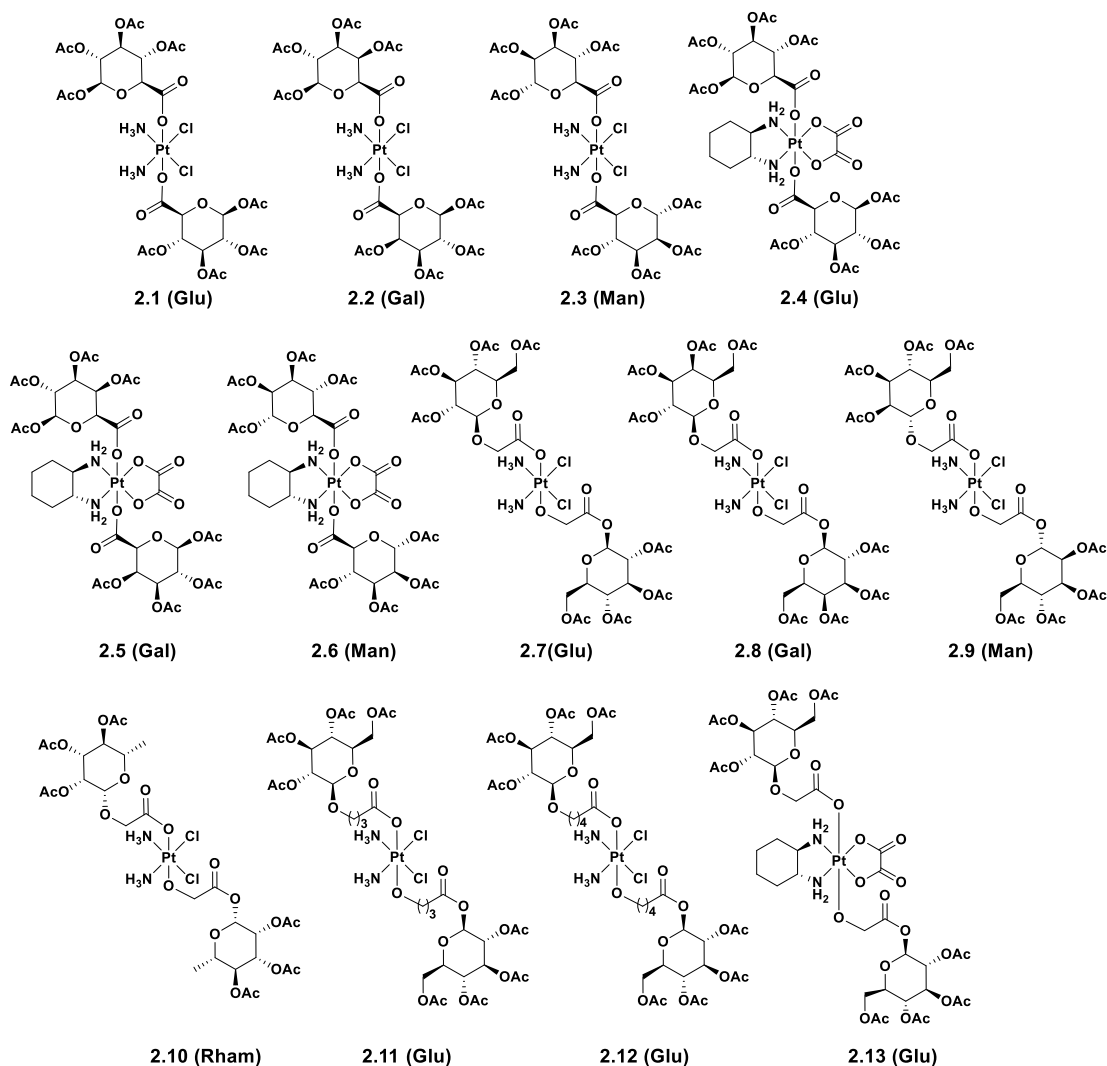


**Figure 2.2:** Structures of Pt(IV) glycoconjugates with glycuronic acid functionalised complexes **2.1 – 2.6** and glucose, galactose, mannose, rhamnose functionalised complexes **2.7 – 2.13** (Peng G. Wang et al. [227]).

## 2.2 Chapter Objective

This chapter discusses the synthesis of acetylated Pt(IV)-C1-Glycoconjugates as potential anticancer agents against OS. The selectivity of anticancer drugs has long been an issue; cisplatin (one of the most important drugs for the treatment of many types of tumours) shows little to no selectivity for cancer cells and resistance to the treatment has often developed by many types of cancers after prolonged use. Platinum(IV) prodrugs containing carbohydrate (Glucose/Galactose) targeting vectors have been synthesised for their ability to exploit the Warburg effect and overcome the drawbacks of classical cisplatin based chemotherapy. In this chapter an investigation on a series of Pt(IV) complexes synthesised with acetylated sugars in

order to compare their anticancer activity to their free sugar counterparts was investigated, which is discussed further in **Chapter 3**. This chapter describes the synthesis of a library of acetylated Pt(IV)-C1-glycoconjugates and their subsequent evaluation as anticancer agents against OS.

Our complexes were designed based on a variety of factors, intended to provide structural diversity to analyse their anticancer activity. GLUT3/4 have similar binding affinities for both glucose and galactose which allows us to vary the carbohydrate moiety. The anomeric position was also functionalised with *N*-glycosides and *O*-glycosides to investigate any differences in cell uptake or cytotoxicity. CuAAC “click” chemistry was used due to its versatility, mild reaction conditions and ability of the triazole linker to act as bioisosteres for amide bonds with increased metabolic stability. Anomeric triazoles were formed, which are shown to have increased stability when compared to *O*-glycosides [229]. Finally, the distance of the sugar from the Platinum core was varied using two linkers. This variation has been shown to have an effect on anticancer activity where complexes that differed by a single CH<sub>2</sub> showed significantly different levels of toxicity [167,227].

Importantly, these complexes are functionalised in the anomeric position (C1). As discussed in **Chapter 1**, functionalisation at this position is suitable as long as the H-bond acceptor ability of the position is conserved. The hydrogen bonding ability of the triazole group is vital in this regard, as it is a capable H-bond acceptor. The *O*-glycosidic linkage is also suitable as this oxygen can accept H-bonds as well [132,135]. While these theoretical aspects are important to consider, a synthetically viable route is just as important. In this regard, functionalisation in the C1 position can be done with relative ease when compared to other positions of a carbohydrate. The combination of these two aspects is what led us to synthesise the complexes whose general structure is shown in **Figure 2.3**.

Finally, as discussed in **Section 1.4**, mono- or bis-functionalisation of the target complexes should be considered. The group of Wang stressed the importance of the more positive reduction potential associated with mono-functionalisation when compared to the bis-adducts. This was taken into account when synthesising our target complexes in this chapter, with the hope that a quicker reduction within the

cell results in a more active prodrug. With this modular approach, a library of Pt(IV) pro-drugs were assembled with sufficient structural diversity to initially analyse the anticancer activity of our complexes (**Figure 2.3**). The results discussed in this chapter were published in *Frontiers in Chemistry* (doi: 10.3389/fchem.2021.795997) [230] attached at the end of the thesis.

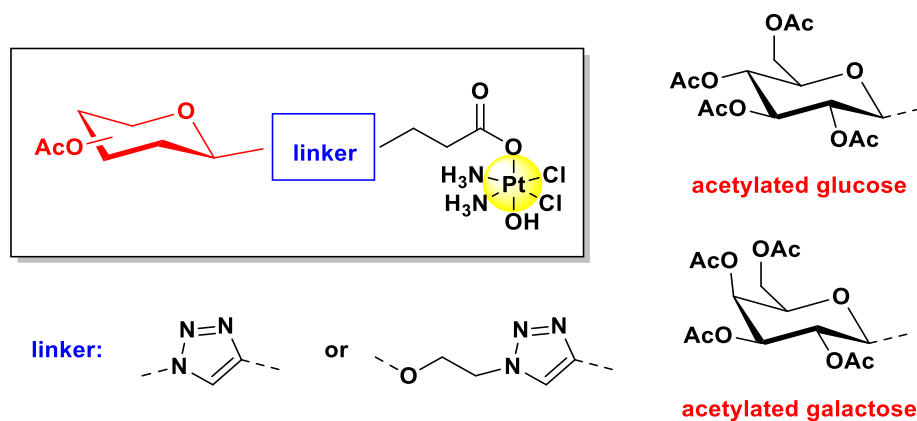


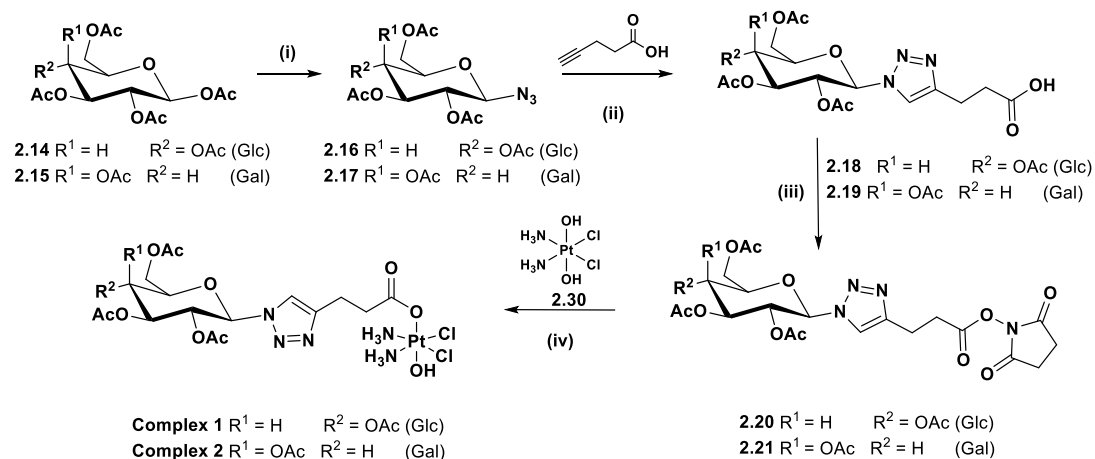
**Figure 2.3:** General structure of the novel Pt(IV) complexes based on cisplatin scaffold and functionalised with acetylated C1-glucose and galactose.

## 2.3 Results and Discussion

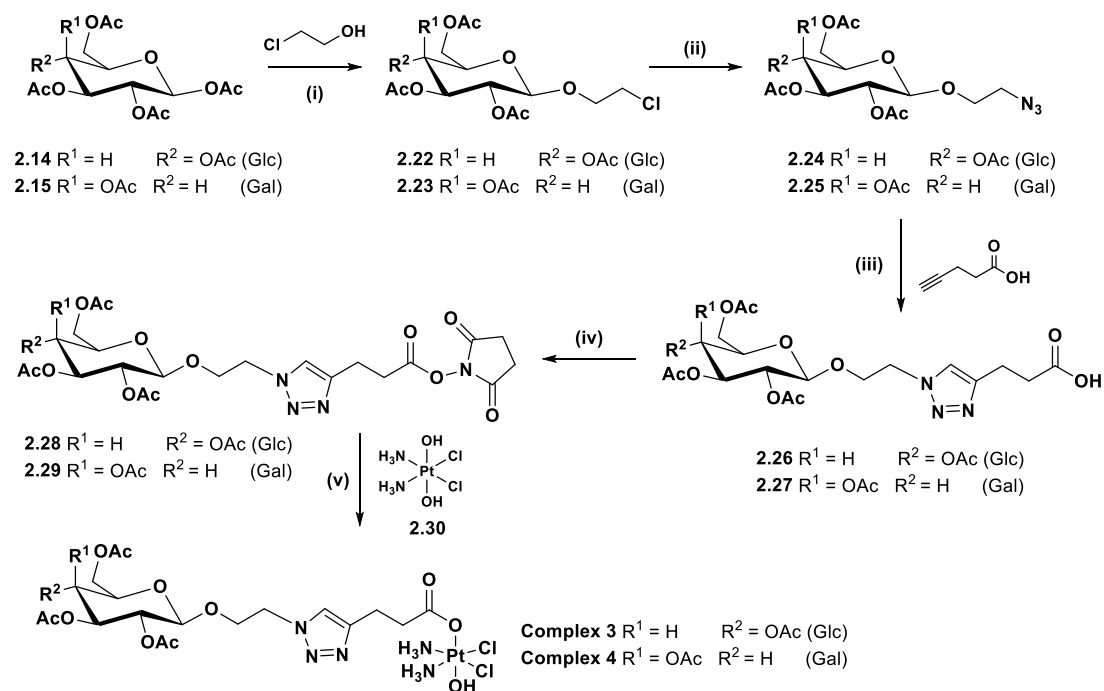
### 2.3.1 Synthesis of acetylated Pt(IV) glycoconjugate prodrugs

**Schemes 2.1** and **2.2** show the synthetic route for the production of complexes **1** – **4**. The following novel complexes were synthesised using four main reactions.

First, commercially available peracetylated sugars (glucose and galactose, **2.14** and **2.15**) are reacted to introduce an azide group through *N*-/*O*-glycosylation reactions (**2.16**, **2.17**, **2.24** and **2.25**). Secondly, the CuAAC 'click' reaction is used to react these azides with 4-pentynoic acid to give the corresponding carboxylic acids (**2.18**, **2.19**, **2.26** and **2.27**). Third, esterification is used to synthesise the active NHS esters through the use of a coupling reagent, EDCI (**2.20**, **2.21**, **2.28** and **2.29**). Finally, a transesterification is used to afford the final platinum complexes **1** – **4** through reaction with the active ester. Every single reaction will be discussed in detail later in this section.



**Scheme 2.1:** Synthetic route for the complexes **1** and **2**: (i) TMSN<sub>3</sub>, SnCl<sub>4</sub>, DCM, rt, 16 h, 94% (**2.16**), 97% (**2.17**); (ii) CuSO<sub>4</sub>, sodium ascorbate, *t*-BuOH, THF, H<sub>2</sub>O, rt, 16 h, 64% (**2.18**), 74% (**2.19**); (iii) EDCI, NHS, DCM, rt, 16 h, 77% (**2.20**), 54% (**2.21**); (iv) DMSO, 60°C, 16 h, 43% (**1**), 36% (**2**).



**Scheme 2.2:** Synthetic route for complexes **3** and **4**: (i) BF<sub>3</sub>·OEt<sub>2</sub>, 3 Å MS, 0°C to rt, DCM, 16 h, 22% (**2.22**), 25% (**2.23**); (ii) NaN<sub>3</sub>, DMF, 80°C, 16 h, 62% (**2.24**), 60% (**2.25**); (iii) CuSO<sub>4</sub>, sodium ascorbate, *t*-BuOH, THF, H<sub>2</sub>O, rt, 16 h, 44% (**2.26**), 47% (**2.27**); (iv) EDCI, NHS, DCM, rt, 16 h, 87.5% (**2.28**), 79% (**2.29**); (v) DMSO, 60°C, 16 h, 29% (**3**), 38% (**4**).

### 2.3.2 Synthesis of Sugar Azides (**2.16**, **2.17**, **2.24** and **2.25**)

The sugar azides (**2.16**, **2.17**) were synthesised following previously reported procedures [231,232]. Glucose and galactose derivatives were synthesised from commercially available peracetylated starting materials. **Figure 2.4** depicts the *N*-glycosylation reaction mechanism for the synthesis of anomeric sugar azides.

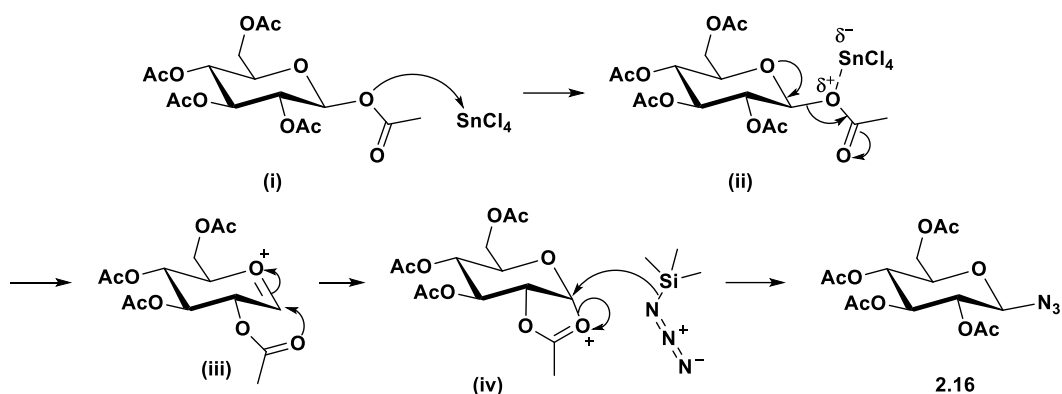
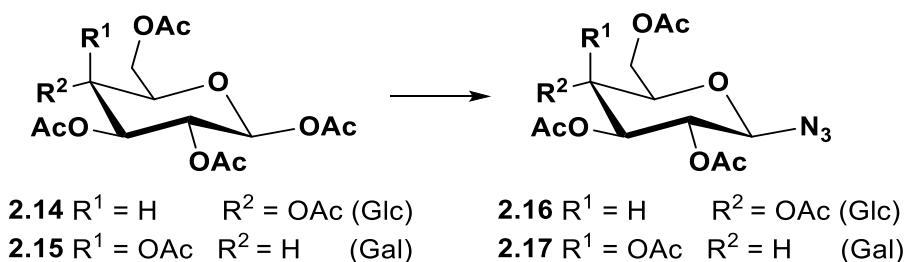
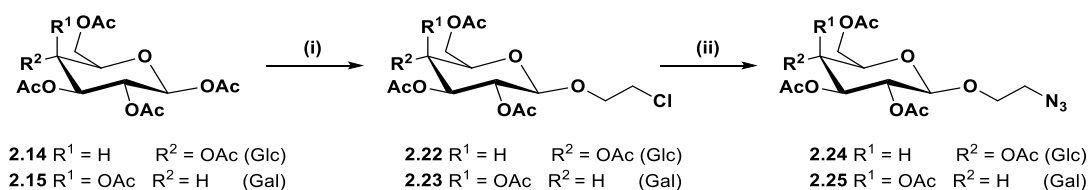


**Figure 2.4:** *N*-glycosylation reaction mechanism for the synthesis of sugar azides, using  $\text{SnCl}_4$  and  $\text{TMSN}_3$ .

The anomeric position was functionalised with the azide using  $\text{TMSN}_3$  and  $\text{SnCl}_4$ .  $\text{SnCl}_4$  is a Lewis acid used to activate the anomeric acetate protecting group forming a good leaving group. The anomeric acetyl tin complex **(ii)** is removed and the resulting glycosyl cation **(iii)** is stabilised by the neighbouring group participation of the carbonyl oxygen of the C-2 acetyl protecting group, which also prevents attack from the bottom face **(iv)** [233]. The resulting  $\text{S}_{\text{N}}2$  reaction with  $\text{TMSN}_3$  yields the  $\beta$ -anomer of the sugar azide. **Scheme 2.3** shows the synthesis of the D-sugar azides [231].



**Scheme 2.3:** Synthesis of  $\beta$ -D-sugar azides. Reagents and conditions:  $\text{TMSN}_3$ ,  $\text{SnCl}_4$ , anhydrous DCM,  $\text{N}_2$ , 16 h, 94% (**2.16**), 97% (**2.17**).



**Scheme 2.4:** Synthesis of 2-Azidoethyl 2,3,4,6-tetra-*O*-acetyl- $\beta$ -D-glucopyranoside and 2-Azidoethyl 2,3,4,6-tetra-*O*-acetyl- $\beta$ -D-galactopyranoside. Reagents and conditions: (i)  $\text{BF}_3 \cdot \text{OEt}_2$ , 2-Chloroethanol, dry DCM, rt, 16 h, 22% (**2.22**), 25% (**2.23**); (ii)  $\text{NaN}_3$ , DMF,  $80^\circ\text{C}$ , 16 h, 62% (**2.24**), 60% (**2.25**).

2-Azidoethyl 2,3,4,6-tetra-*O*-acetyl- $\beta$ -D-glucopyranoside (**2.24**) and 2-Azidoethyl 2,3,4,6-tetra-*O*-acetyl- $\beta$ -D-galactopyranoside (**2.25**) were prepared from commercially available peracetylated sugars (**Scheme 2.4**). The peracetylated starting materials underwent an *O*-glycosylation reaction with 2-chloroethanol in the presence of  $\text{BF}_3 \cdot \text{OEt}_2$  at low temperatures (**Scheme 2.4**).  $\text{BF}_3 \cdot \text{OEt}_2$  acts as the Lewis acid in a similar fashion to the Lewis acid in **Figure 2.4** and facilitates the removal of the anomeric acetate protecting group. Nucleophilic attack from the hydroxyl of 2-chloroethanol to the glycosyl cation results in the formation of mainly  $\beta$ -anomer. This product was purified through recrystallisation in ethanol and then reacted with  $\text{NaN}_3$  in DMF at high temperatures (**ii**). The reaction follows an  $\text{S}_{\text{N}}2$  mechanism in which the chloride is substituted for the azide of the sodium azide yielding the products **2.24** and **2.25** which are used for the following steps without further purification[232].

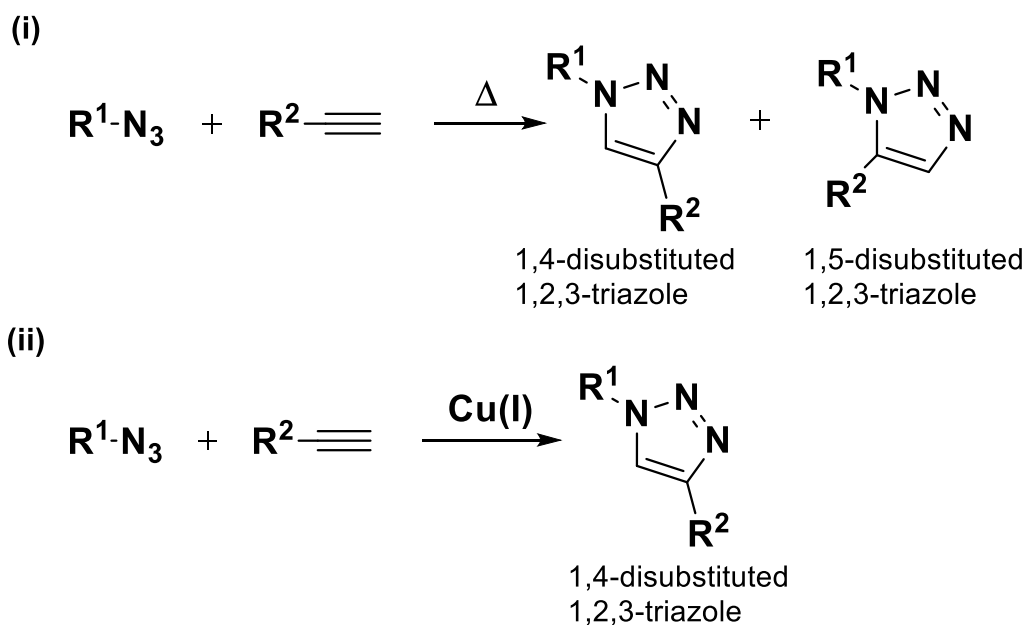
### 2.3.3 Copper-catalysed azide-alkyne cycloaddition (CuAAC) reaction

Copper-catalysed azide-alkyne cycloaddition or “Click” chemistry, is a method of selectively forming 1,4-disubstituted 1,2,3-triazoles. This reaction has seen widespread use in medicinal chemistry and chemical biology as the 1,2,3-triazoles are formed from very mild reaction conditions and have excellent yields, while also being chemically inert to oxidation, reduction and hydrolysis [234]. 1,2,3-triazoles also mimic the atom placement and electronic properties of amide bonds, while possessing a stronger dipole moment which enhances the hydrogen bond donor and acceptor properties of the heterocycle [235].

The reaction was developed from the Huisgen 1,3-dipolar cycloaddition and was improved by Tornøe and Meldal in 2001 with the addition of Cu(I) catalysis for the development of peptidotriazoles on solid state resins. The use of a Cu(I) catalyst resulted in the 1,4-disubstituted 1,2,3-triazole product only and a qualitative conversion with very high purity. In comparison, the uncatalyzed reaction yields a mixture of 1,4-disubstituted and 1,5-disubstituted regioisomers, as well as the need for higher temperatures and longer reaction times [192], as shown in **Scheme 2.5 (i)**. In the same year, the groups of Folkin and Sharpless developed the protocol for the

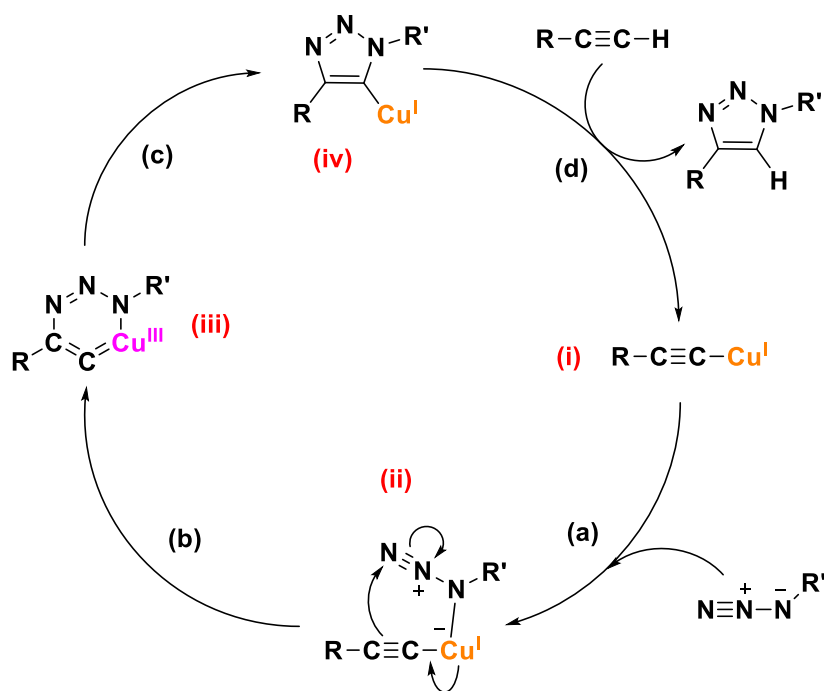


synthesis of 1,4-disubstituted 1,2,3-triazoles using a copper catalyst prepared *in situ*, by the reduction of Cu(II) to Cu(I) using sodium ascorbate [236]. The huge importance of the development of this kind of mechanisms and applications in biorthogonal chemistry are demonstrated by the Nobel price award for chemistry in 2022 assigned to C. R. Bertozzi, M. Meldal, and K. B. Sharpless. The same synthetic procedure is utilised later in this chapter (**Scheme 2.5 (ii)**).



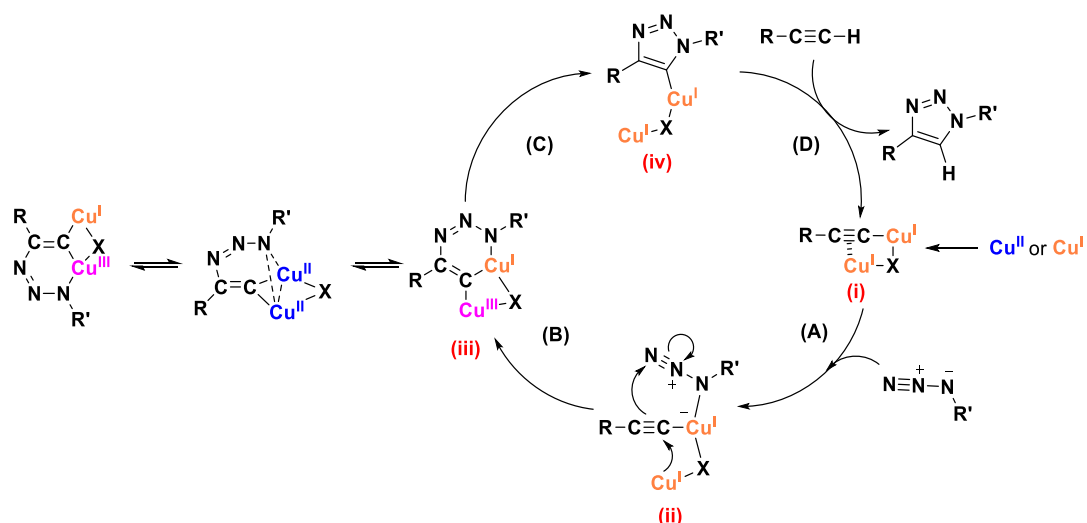
**Scheme 2.5:** Synthesis of 1,2,3-Triazoles *via* (i) Huisgen 1,3-dipolar cycloaddition of azides and alkynes; (ii) Copper-Catalysed Azide-Alkyne Cycloaddition (CuAAC).

**Scheme 2.6** shows an outdated catalytic cycle for the CuAAC “click” reaction. The initial model, proposed by Folkin and Sharpless [236] involved the formation of a mononuclear Copper(I) acetylide complex **(i)** and through two steps led to the transformation into the copper metallacycle **(iii)** from the formation of the first C-N bond. This intermediate was found to constrain the sp-hybridised carbon in the metallacycle and required a high activation energy, leading researchers to believe that the reaction proceeded through an alternative mechanism. The addition of an extra copper(I) ion in the **(i)** intermediate helped to alleviate the ring strain of the **(iii)** metallacycle, reducing the activation energy, this is seen in the now accepted catalytic cycle (**Scheme 2.7**).



**Scheme 2.6:** Initial mononuclear mechanism of Copper(I)-Catalysed Azide-Alkyne Cycloaddition proposed by Folkin and Sharpless [236,237].

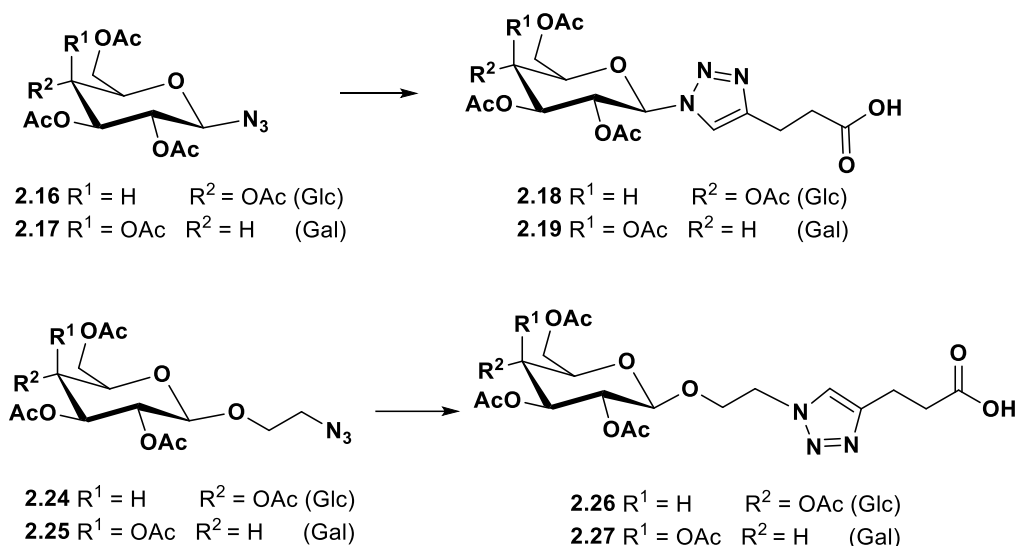
**Scheme 2.7** describes the dinuclear catalytic cycle of the CuAAC “click” reaction. The reaction is initiated by the formation of a  $\sigma$ ,  $\pi$ -di(copper) acetylide complex **(i)**. The acetylide engages in both  $\sigma$  and  $\pi$  bonding with copper(I) and with the addition of the azido group (**Step A**), forms an azide/alkyne/copper(I) ternary complex **(ii)**. The metallacycle **(iii)** is formed in **step B**, accompanied by the oxidation of one copper ion from Cu(I) to Cu(III). **Step C** involves reductive ring contraction of the metallacycle to yield a Cu(I) triazolide **(iv)**. The Cu(I) triazolide then deprotonates an alkyne in the final step (**Step D**) to complete the catalytic cycle. Evidence supporting this proposed cycle comes in the form of characterisation of **(i)** [238] and **(iv)** [239] which proves them to be viable intermediates for the CuAAC reaction. **(ii)** and **(iii)** are the only intermediates yet to be isolated, which has garnered much attention. **(ii)** has only been detected once by using an ion-tagged electron spray ionisation mass spectrometric method [240]. Finally, **(iii)** was determined by Folkin et al. to be involved in rapid internal rearrangement equilibrium to scramble the two copper centres [241].



**Scheme 2.7:** Proposed dinuclear mechanism of Copper(I)-Catalysed Azide-Alkyne Cycloaddition [237].

### 2.3.4 Synthesis of Click Carbohydrate ligands (2.18, 2.19, 2.26 and 2.27)

*N*-(2,3,4,6-tetra-*O*-acetyl- $\beta$ -D-glucopyranosyl-1,2,3-triazol-4-yl)-propanoic acid (**2.18**), *N*-(2,3,4,6-tetra-*O*-acetyl- $\beta$ -D-galactopyranosyl-1,2,3-triazol-4-yl)-propanoic acid (**2.19**), *N*-[2-*O*-(2,3,4,6-tetra-*O*-acetyl- $\beta$ -D-glucopyranosyl)-ethyl-1,2,3-triazol-4-yl]-propanoic acid (**2.26**) and *N*-[2-*O*-(2,3,4,6-tetra-*O*-acetyl- $\beta$ -D-galactopyranosyl)-ethyl-1,2,3-triazol-4-yl]-propanoic acid (**2.27**) were synthesised from the previously discussed sugar azides (**2.16**, **2.17**, **2.24** and **2.25**), using a procedure reported by Mangunuru *et al* [242]. 4-pentynoic acid was reacted with the sugar azides at room temperature under click conditions to yield the free ligands. **2.18** and **2.19** had yields of 64% and 74% respectively. Lower yields were obtained for **2.26** and **2.27** (44% and 47% respectively (**Scheme 2.8**)). Notably, the yields for **2.26** and **2.27** were relatively low due to the difficulties found with the purification. The polar carboxylic acid group is strongly retained on the silica powder used for chromatography, meaning that even when using a strongly polar mobile phase, streaking occurs and causes the ligand to elute over a long period of time [243].



**Scheme 2.8:** Synthesis of click carbohydrate ligands (OAc); 4-pentynoic acid, CuSO<sub>4</sub>, sodium ascorbate, *t*-BuOH, THF, H<sub>2</sub>O, rt, 16 h, 64% (**2.18**), 74% (**2.19**), 44% (**2.26**), 47% (**2.27**).

**Figure 2.5** shows the <sup>1</sup>H NMR spectrum of the free ligand **2.18** with the triazole proton at  $\delta = 7.62$  ppm (blue spot) and the CH<sub>2</sub>'s at  $\delta = 3.1$  ppm (purple spot) corresponding to the carboxylic acid linker. These two signals are important for comparing the carboxylic acid starting material to the active ester, whose synthesis is discussed in the following sections.

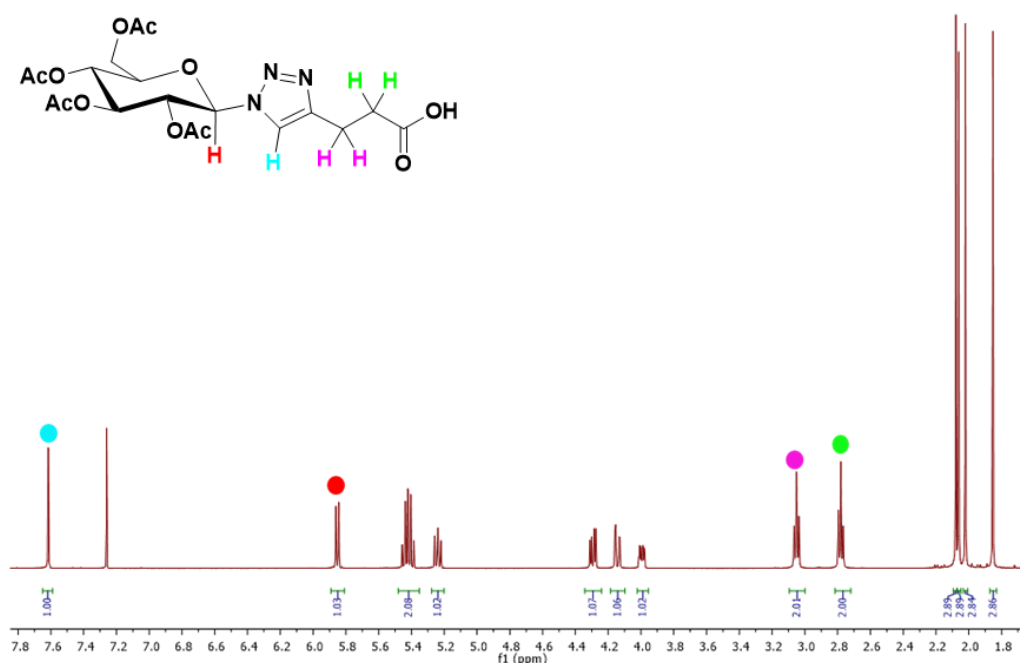


**Figure 2.5:** <sup>1</sup>H NMR spectrum of **2.18** in CDCl<sub>3</sub>, characteristic signals highlighted.

### 2.3.5 Synthesis of active *N*-hydroxysuccinimide esters (2.20, 2.21, 2.28, 2.29)

Various methods exist to functionalise Platinum(IV) with axial ligands for targeting and multi-action purposes. In particular, oxoplatin (2.30 in **Figure 2.6**), the oxidised form of cisplatin containing two axial nucleophilic hydroxyl ligands, is used as a scaffold to add various functionalities. A major method used in literature for the conjugation of ligands in the axial position of Pt(IV) involves the use of activated carboxylic acids. The activation can be achieved *via* NHS esters (a), acid anhydrides (b) and acyl chlorides (c), or through direct coupling of the carboxylic acid (d) in the presence of coupling reagents such as DCC or TBTU (**Figure 2.6**) [244].

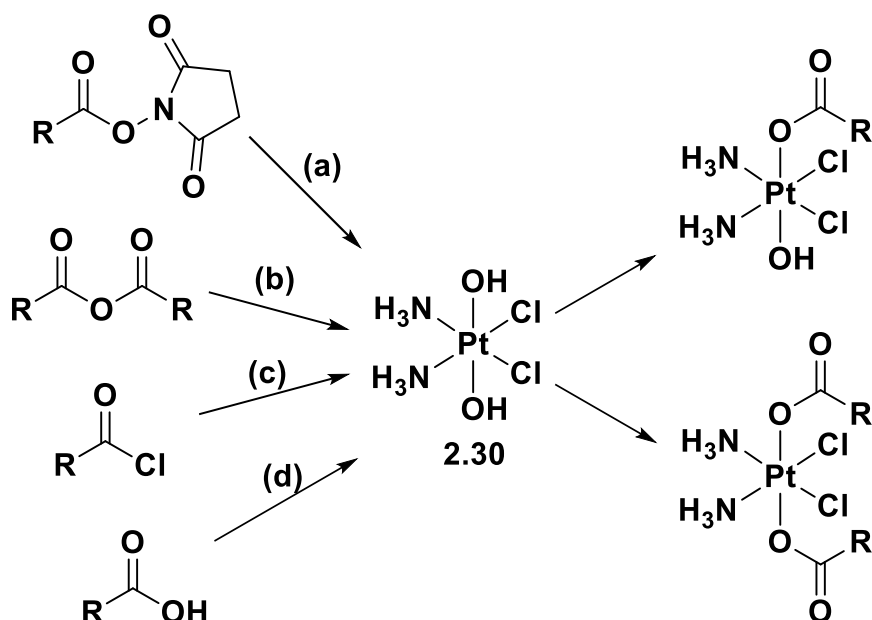


**Figure 2.6:** Methods to synthesise Pt(IV) prodrugs with ester linkages.

Other than acids, carbamates [245,246] and carbonates [247,248] can also be used to link the platinum centre with ligands. The advantage of these functional groups for coupling is the fact that some FDA approved drugs do not naturally have carboxylic acid functional groups available for activation, therefore, when the ligands are released, they contain the non FDA approved drug. Using the coupling agent *N,N'*-Disuccinimidyl carbonate (DSC) (**Figure 2.7**) amines and hydroxyls can be activated and coupled to oxoplatin. Rapid decarboxylation of the

carbamate/carbonate occurs upon reduction from Pt(IV) to Pt(II), yielding the free amine or hydroxyl respectively.

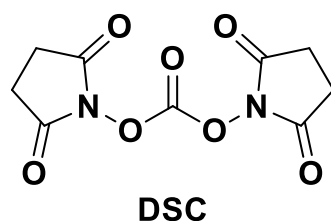
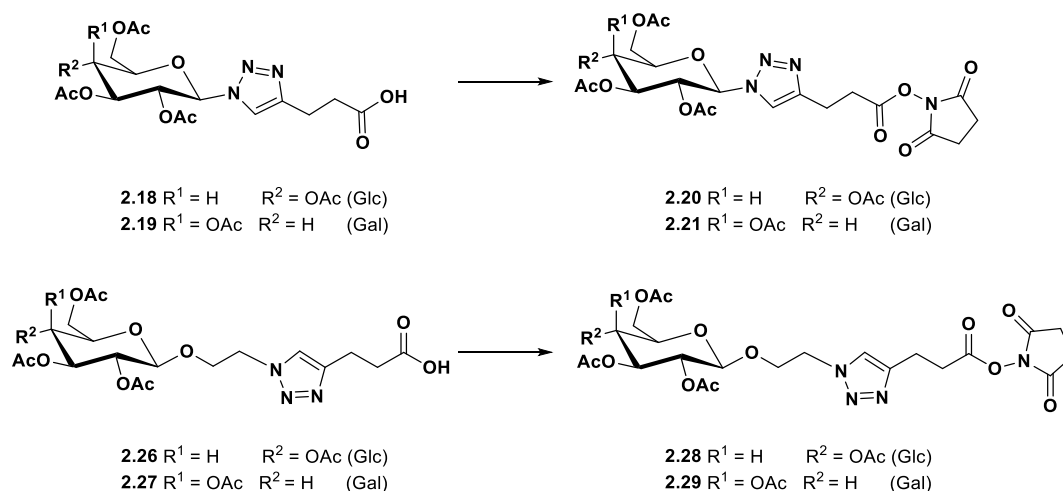


**Figure 2.7:** Structure of DSC used for the synthesis of carbonates and carbamates.

NHS esters are used in the synthesis of our complexes due to the NHS excellent leaving group ability and relative stability in acidic media [249,250]. The active esters shown in **Scheme 2.9** were synthesised by the addition of EDCI in DCM to a solution of a carboxylic acid and NHS under a nitrogen atmosphere. The mixture was stirred overnight at room temperature and treated with HCl and brine to yield the corresponding NHS ester as a white solid, which is used without further purification. The esters **2.20** and **2.21** were isolated with a yield of 77% and 54%, and the esters **2.28** and **2.29** had yields of 87.5% and 79%.



**Scheme 2.9:** Synthesis of Carbohydrate NHS esters(OAc); EDCI, *N*-hydroxysuccinimide, DCM, rt, 16 h, 77% (**2.20**), 54% (**2.21**), 87.5% (**2.28**), 79% (**2.29**).

The characterisation of these esters was carried out using one- and two-dimensional NMR spectroscopic methods and HR-MS. The signal highlighted in orange corresponds to the four protons of the succinimide (**Figure 2.8**).

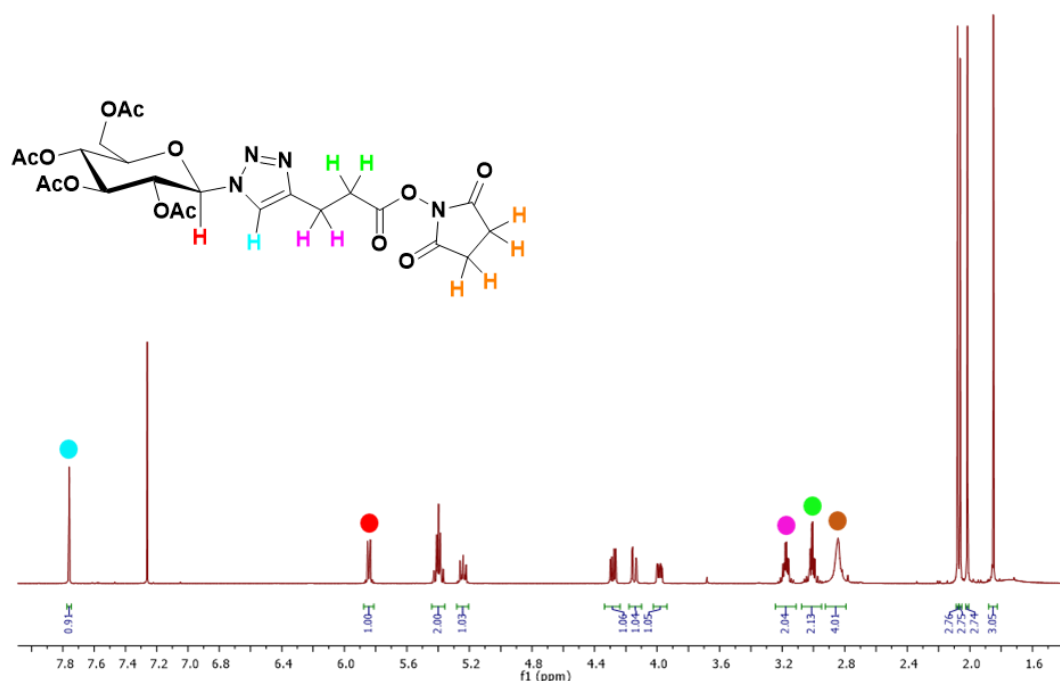


**Figure 2.8:**  $^1\text{H}$  NMR spectrum of **2.20** in  $\text{CDCl}_3$ , characteristic signals highlighted.

The coupling of NHS to the free ligand (**2.18**) is accompanied by the downfield shift ( $\Delta\delta = 0.13$  ppm) of the purple and ( $\Delta\delta = 0.23$  ppm) green signals, as seen in **Figure 2.9**, and ( $\Delta\delta = 0.06$  ppm) for purple and ( $\Delta\delta = 0.19$  ppm) for the green signals of ester (**2.28**) and carboxylic acid ligand (**2.26**) (**Figure 2.10**). Notably, **Figure 2.9** and **Figure 2.10**, also show a distinct difference in the splitting pattern of the  $\text{CH}_2$ 's of esters **2.20** and **2.28**, when compared to their carboxylic acid counterparts. These signals are changed from triplets to triplet of doublets (**Figure 2.9** and **Figure 2.10**). A possible explanation for this change is that through the addition of the ester, the chemical environment around the  $\text{CH}_2$ 's changes, making the protons inequivalent. In this case, the purple protons (**Figure 2.8**) are split by two inequivalent green protons, forming a triplet of doublets.

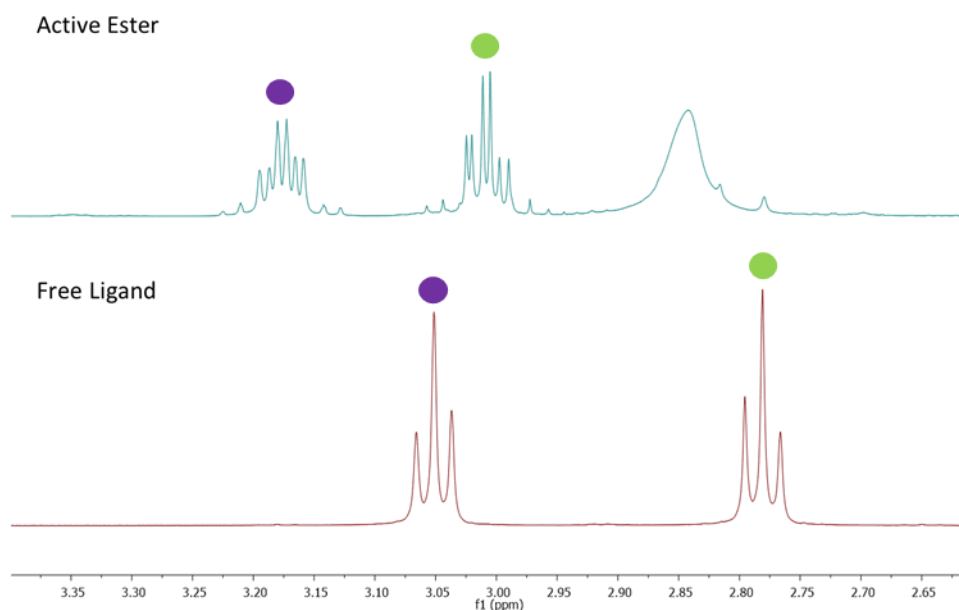


**Figure 2.9:**  $^1\text{H}$  NMR spectrum comparing the two  $\text{CH}_2$  signals of the free ligand (**2.18**) and active ester (**2.20**).

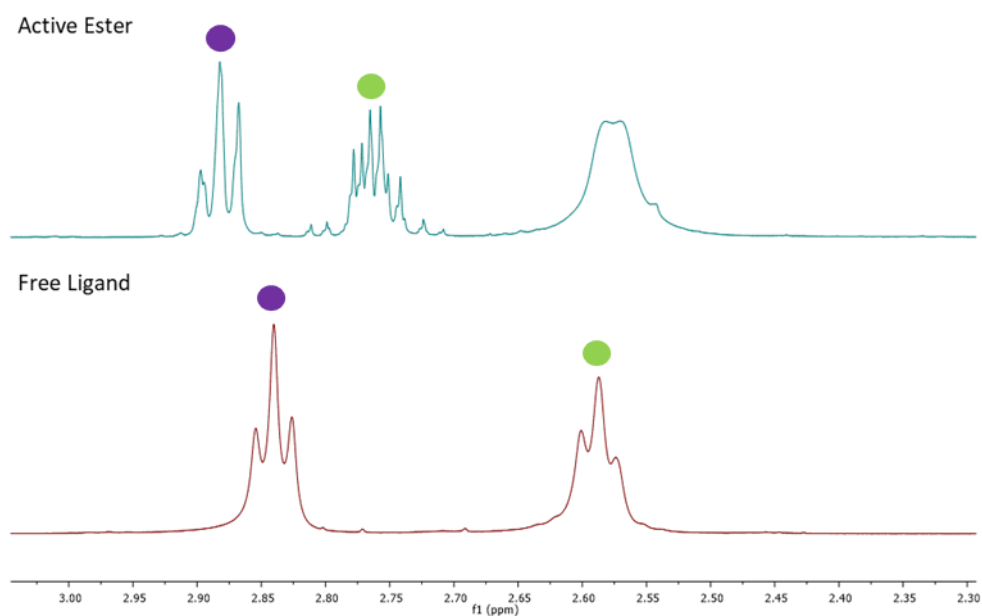
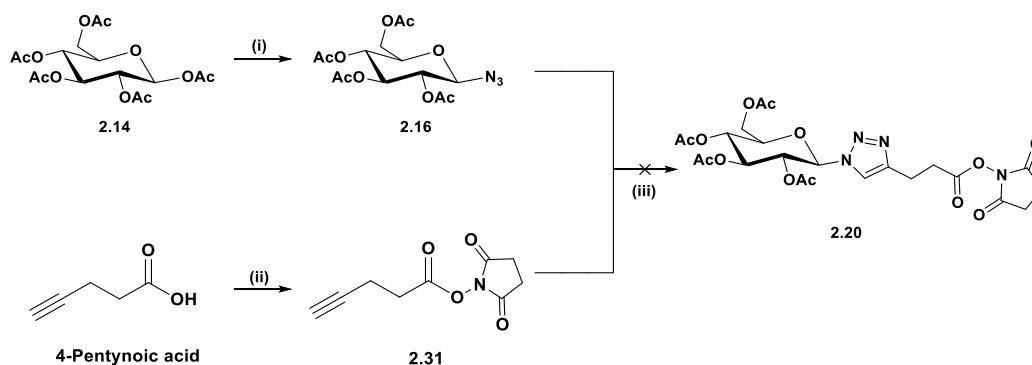


**Figure 2.10:**  $^1\text{H}$  NMR spectrum comparing the two  $\text{CH}_2$  signals of the free ligand (**2.26**) and active ester (**2.28**).

Initially, our planned route to form the active esters was to react 4-pentynoic acid with *N*-hydroxysuccinimide using *N,N'*-dicyclohexylcarbodiimide (DCC) as a coupling



reagent (**Scheme 2.10**). This coupling reaction undergoes the same reaction mechanism when using EDCI, however, the resulting by-product (dicyclohexylurea, DCU) is both insoluble in organic solvent and water. Through filtration of DCU the resulting ester was isolated and reacted with peracetylated glucose azide. Our reasoning for abandoning this route, in favour of the reaction in **Scheme 2.9**, is the instability of the active ester (**2.31**). The following click reaction was carried out using microwave irradiation at 30°C followed by stirring at room temperature overnight, the crude product was extracted with DCM and purified through column chromatography. However, the resulting yield of the reaction was much lower than anticipated. We hypothesise that through heating during the reaction, or potentially during the purification, hydrolysis of the ester occurs, reducing the yield to a mere 23%. In comparison to the yield obtained using **Scheme 2.9** of 87.5%, this route was unsustainable due to the large waste of starting materials, leading us to search for alternative routes like the one discussed earlier.



**Scheme 2.10:** Initial synthetic route for the formation of the esters **2.20** and **2.21**. (i) TMSN<sub>3</sub>, SnCl<sub>4</sub>, DCM, rt, 16 h, 91%; (ii) DCC, NHS, THF, rt, 3 h, 98%; (iii) NaAsc, CuSO<sub>4</sub>, MeCN, H<sub>2</sub>O, 30°C MW, 30 min, rt, 14 h, 23%.

### 2.3.6 EDCI coupling reagent.

EDCI is a carbodiimide coupling agent, first introduced in 1960 as a water- and acid-soluble carbodiimide for the use in peptide synthesis to allow for easier purification steps in the synthesis of amide bonds. The corresponding by-products can be easily removed by simple water or acid washes [251,252]. In our case EDCI was used to synthesise active esters, by the reaction of a carboxylic acid and an alcohol.

The initial step of the reaction is the deprotonation of the carboxylic acid (**2.18**) as shown in **Figure 2.11**, which allows for the attack of the carboxylate anion to the electrophilic carbon of the carbodiimide **EDCI**. The N=C bond is then cleaved, and a neutral charge is returned to the nucleophilic nitrogen. The electrophilic carbon of active ester (**i**) undergoes nucleophilic attack by the NHS hydroxide. This results in the elimination of the urea by-product (**ii**) and formation of NHS ester **2.20**.

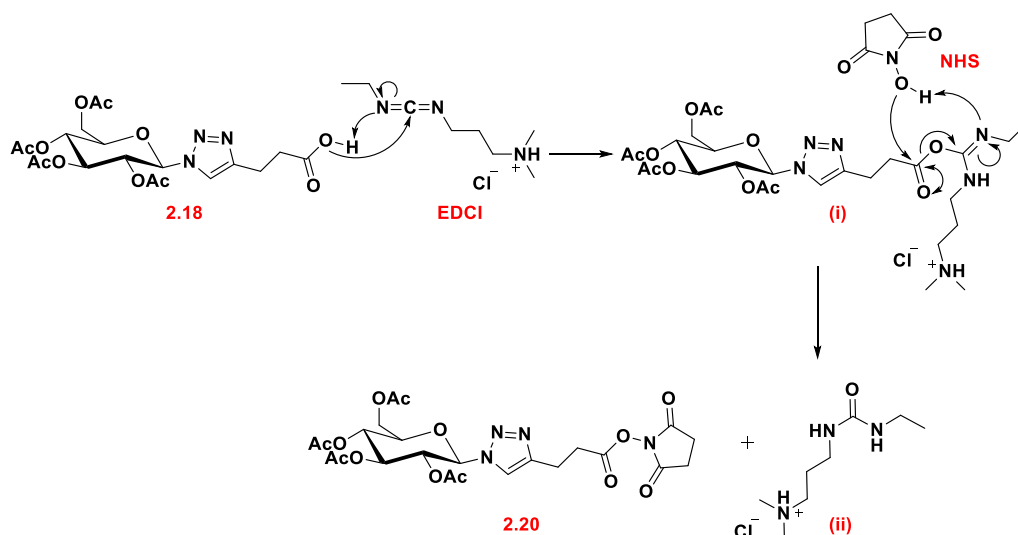
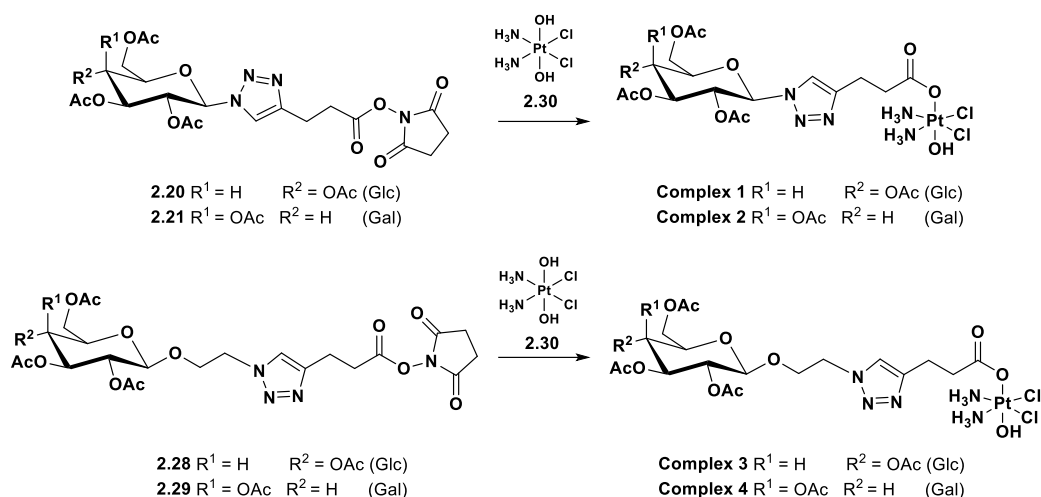


**Figure 2.11:** Mechanism of reaction to form NHS esters using EDCI as a coupling agent.

### 2.3.7 Synthesis of mono functionalised Pt(IV)-glycosides (**1 – 4**)

The complexes **1 – 4** shown in **Scheme 2.11** were synthesised by the substitution of a single axial hydroxyl ligand bound to the Pt(IV) centre (**2.30**). Oxoplatin and the activated NHS ester are mixed in DMSO and the suspension is heated at 60°C overnight. A slight excess of oxoplatin is used in order to avoid the formation of bis-adducts where both axial ligands are substituted. The complexes were isolated by filtering off the excess oxoplatin, evaporating the remaining DMSO and treating the residue with acetone and diethyl ether.



**Scheme 2.11:** Synthetic route for Pt(IV)-glycosides(OAc); Oxoplatin, DMSO, 60°C, 16 h, 43% (1), 36% (2), 29% (3), 38% (4).

**Figure 2.12** shows the <sup>1</sup>H NMR spectrum of **Complex 1** with the characteristic signals highlighted. A characteristic signal to prove the mono functionalisation of the platinum complex is the broad triplet amine peak at δ = 6.00 ppm. This arises due to the quadrupolar nuclei of <sup>14</sup>N, where the three equivalent protons form a triplet from their coupling to the Nitrogen nuclei [253]. Further characterisation was carried out with <sup>13</sup>C NMR, two-dimensional NMR, <sup>195</sup>Pt NMR and HR-MS.

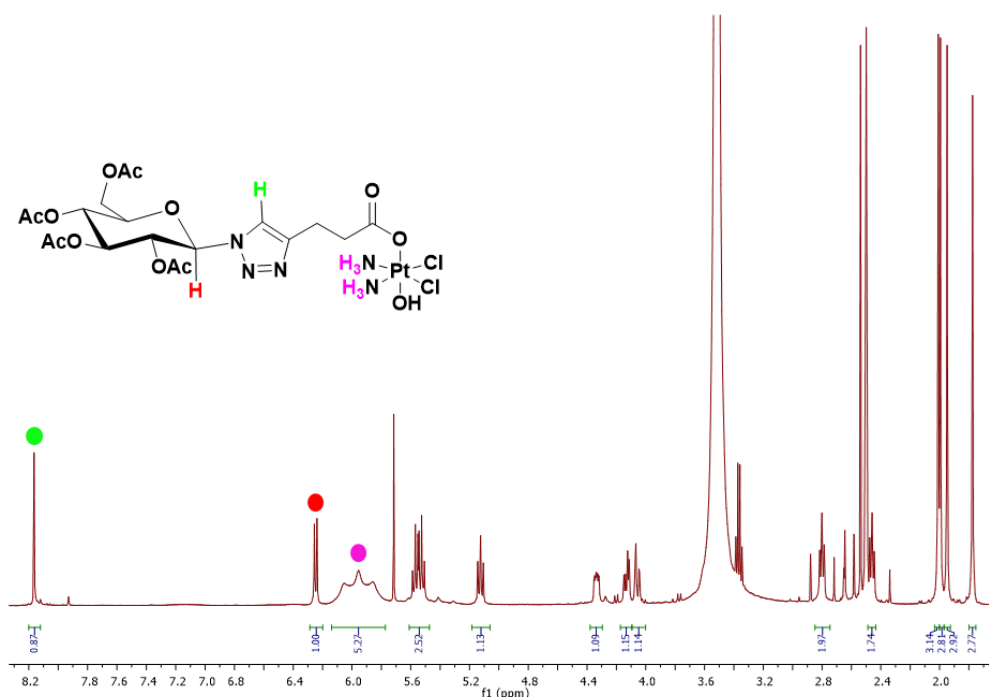


**Figure 2.12:** <sup>1</sup>H NMR spectrum of **Complex 1** in DMSO-d<sub>6</sub>. Characteristic signals highlighted.

**Figure 2.13** depicts the  $^{195}\text{Pt}$ -NMR with one signal in the region of  $\delta = +1040$  ppm, typical of platinum(IV) species, whereas platinum(II) would appear in the region of  $\delta -1000$  [254]. This spectroscopic method is important validation for the synthesis of our complexes as it shows only one signal, meaning that there is only one platinum species, as well as showing that our complex is in the correct oxidation state.

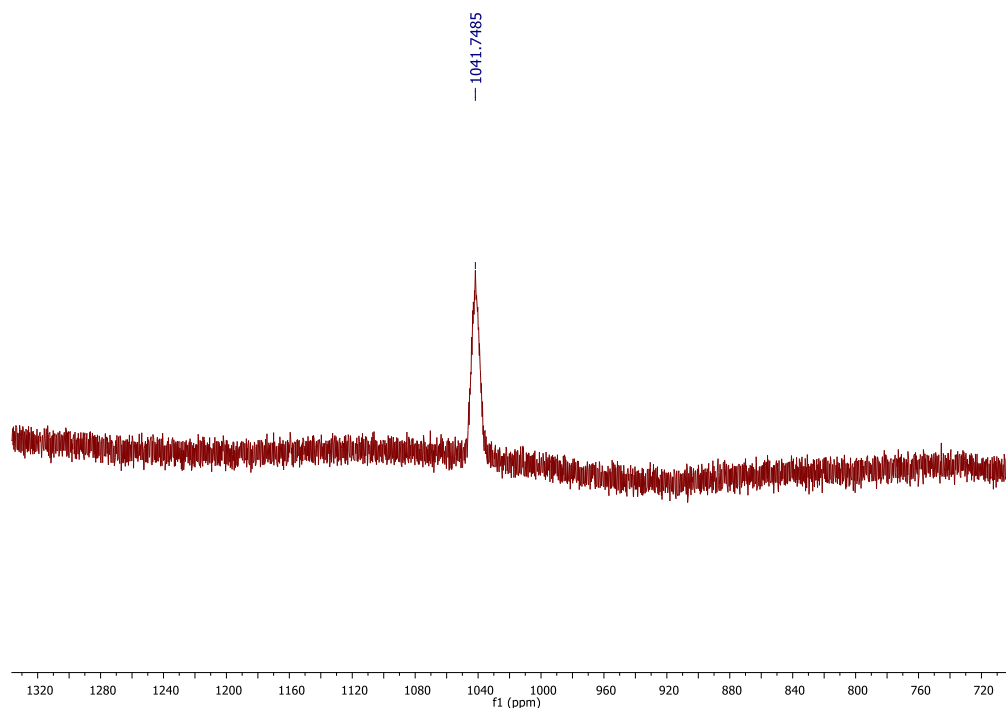


**Figure 2.13:**  $^{195}\text{Pt}$  NMR spectrum of **Complex 1** in  $\text{DMSO-d}_6$ .

**Figure 2.14** shows the HR-MS spectrum (negative mode) of **Complex 1** with a central peak found at  $m/z$  786.0898 related to the  $[\text{M} - \text{H}]^-$  mass of the most abundant isotope of Pt, being 195. The spectrum below shows the characteristic isotopic pattern for Platinum.

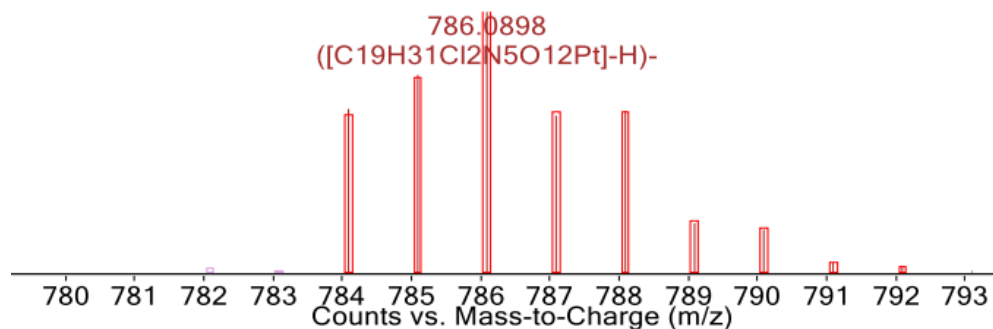


**Figure 2.14:** HR-MS of **Complex 1**, shows the characteristic isotopic pattern of Platinum.

The physiological stability of the drugs has been evaluated with HPLC in DMSO/HEPES at pH 6.8 buffer (**Figure 2.15**). This experiment showed that the complexes were stable, however, a small amount of decomposition (8%) was observed after 1 week at r.t. This is important to evaluate since a poor physiological stability significantly reduces anticancer activity. This can occur due to degradation of the complex through the premature removal of its axial ligands.

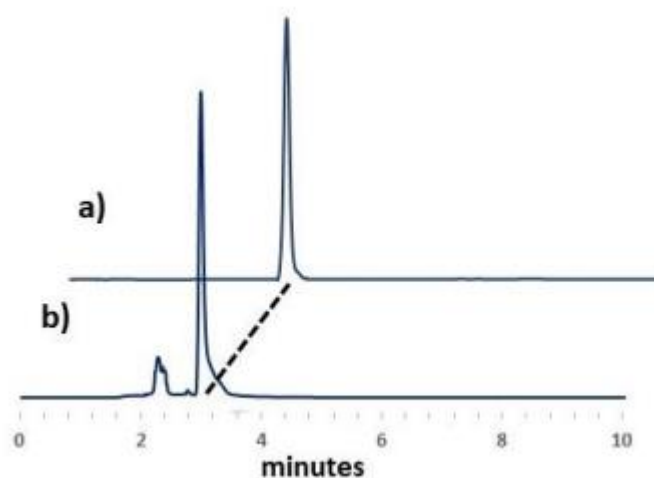


**Figure 2.15:** HPLC chromatogram of **Complex 4** in DMSO/HEPES (pH 6.8): **a)**  $t = 0$  minutes; **b)** after one week at r.t.

## 2.4 Biological Evaluation

### 2.4.1 *In vitro* cytotoxicity

In order to evaluate the anti-cancer potential of the above Pt(IV)-glycosides, their antitumor potential was assessed in collaboration with Dr. Silvia Panseri and Dr.

Monica Montesi at the ISTE-CNR of Faenza (Italy) against a panel of OS cell lines, SAOS-2, U-2 OS and MG63. In comparison to cisplatin, all drugs showed a dose dependent anti-cancer effect (**Figure 2.16**) in all tested cell lines.

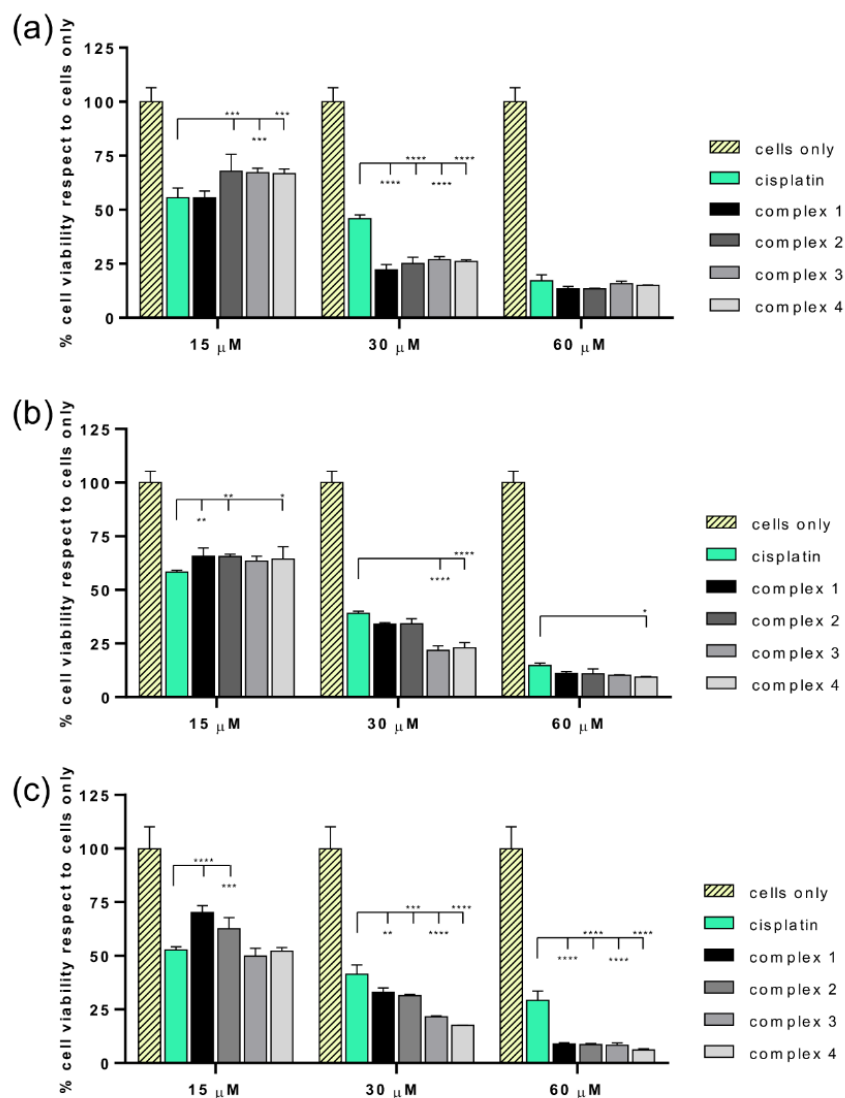


**Figure 2.16:** MTT assay of SAOS-2, U-2 OS and MG63. Percentage of cell viability (mean ± SEM) respect to cells only is reported in the graphs for SAOS-2 (a), U-2 OS (b) and MG63 (c) after 72 hours of drug exposure. Statistically significant differences respect to cisplatin are reported in the graphs (\* p value ≤0.05, \*\* p value ≤0.01, \*\*\* p value ≤0.001, \*\*\*\* p value ≤0.0001).

Looking at the cell lines in detail, it is possible to observe phenotypic-dependent behaviours in response to different complexes. The viability of SAOS-2 (a) was decreased significantly in the presence of the 4 complexes, compared to cisplatin, at 30 μM (p value ≤0.0001); conversely, the viability of U-2 OS (b) was reduced in the

presence of the long chain complexes **3** and **4**, only at 30  $\mu\text{M}$  when compared to cisplatin ( $p$  value  $\leq 0.0001$ ) and only in the presence of the galactose long chain Complex **4** at 60  $\mu\text{M}$  ( $p$  value  $\leq 0.05$ ). All the complexes seem to be more effective with respect to cisplatin in MG63 cell line (**c**), starting from 30  $\mu\text{M}$  and at higher concentration the anticancer effect greatly increases ( $p$  value  $\leq 0.0001$ ).

The  $\text{IC}_{50}$  values reported in **Table 2.1** confirm this phenotypic-dependent effect of the complexes and highlight some standout complexes as well, in terms of activity. In SAOS-2, **Complex 1** is the most effective, showing an  $\text{IC}_{50}$  of 16.48 (-1.84; +2.08)  $\mu\text{M}$ , while in U-2 OS and MG63, **Complex 3** had the best  $\text{IC}_{50}$  values of 18.57 (-1.3; +1.4)  $\mu\text{M}$  and 14.88 (-0.91; +0.98)  $\mu\text{M}$ , respectively.

**Table 2.1:**  $\text{IC}_{50}$  ( $\mu\text{M}$ ) values of Cisplatin and complexes **1-4** on OS cell lines.

| Complex              | Cisplatin                             |                 | 1                                     |                 | 2                                     |                 | 3                                     |                 | 4                                     |                 |
|----------------------|---------------------------------------|-----------------|---------------------------------------|-----------------|---------------------------------------|-----------------|---------------------------------------|-----------------|---------------------------------------|-----------------|
|                      | $\text{IC}_{50}$<br>( $\mu\text{M}$ ) | 95%<br>CI       | $\text{IC}_{50}$<br>( $\mu\text{M}$ ) | 95%<br>CI       | $\text{IC}_{50}$<br>( $\mu\text{M}$ ) | 95%<br>CI       | $\text{IC}_{50}$<br>( $\mu\text{M}$ ) | 95%<br>CI       | $\text{IC}_{50}$<br>( $\mu\text{M}$ ) | 95%<br>CI       |
| OS<br>Cancer<br>cell |                                       |                 |                                       |                 |                                       |                 |                                       |                 |                                       |                 |
| SAOS-2               | 20.42                                 | -4.13;<br>+5.17 | 16.48                                 | -1.84;<br>+2.08 | 20.18                                 | -2.38;<br>+2.7  | 20.39                                 | -2.12;<br>+2.37 | 20.1                                  | -1.99;<br>+2.21 |
| U-2 OS               | 19.85                                 | -1.64;<br>+1.8  | 21.09                                 | -0.98;<br>+1.02 | 21.09                                 | -0.86;<br>+0.89 | 18.57                                 | -1.3;<br>+1.4   | 18.91                                 | -1.5;<br>+1.63  |
| MG63                 | 17.8                                  | -3.34;<br>+4.13 | 21.9                                  | -0.86;<br>+0.89 | 19.68                                 | -1.27;<br>+1.36 | 14.88                                 | -0.91;<br>+0.98 | 15.5                                  | -0.54;<br>+0.55 |

#### 2.4.2 Cell Morphology evaluation

The qualitative analysis of cell morphology confirmed the cytotoxicity results. As shown in **Figure 2.17**, the number of cells treated with cisplatin and complexes **1 – 4** drastically decreased compared to cells only which, on the contrary, showed a higher cell density. The different behaviours observed among the osteosarcoma cell lines, induced by the different drugs, are ascribable to the well-known different degrees of genetic complexity of each cell line, inducing cell-specific biological behaviours (e.g.,

tumorigenicity, colony-forming ability, invasive/migratory potential, metabolism and proliferation capacity) [255,256].

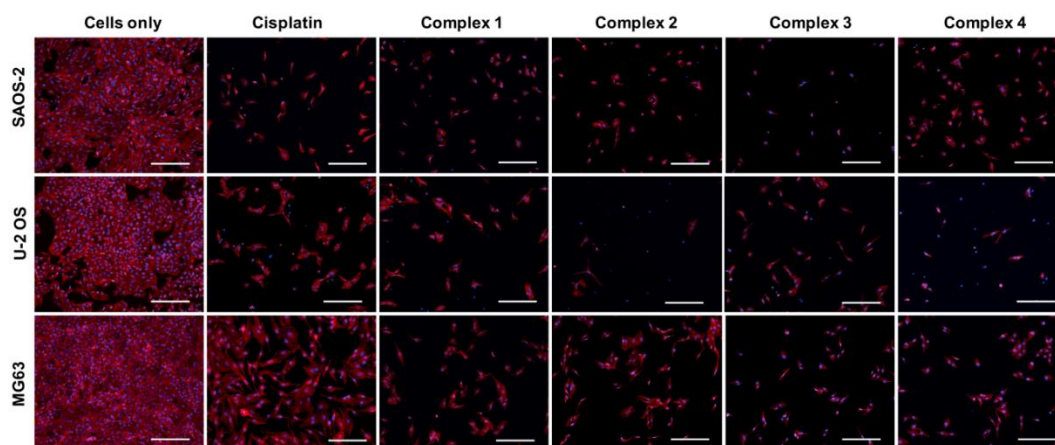


**Figure 2.17:** Cell morphology evaluation on SAOS-2, U-2 OS and MG63. Actin & DAPI staining of osteosarcoma cell lines treated with and without drugs (30 $\mu$ M) for 72 hours. F-actin filaments in red; cell nuclei in blue. Scale bars 200  $\mu$ m.

### 2.4.3 Anti-cancer potential against CSC-enriched cell lines

Cancer Stem Cells (CSCs), unipotent cell population present within the tumour microenvironment, can alter their metabolism in order to respond to specific bio-energetic and biosynthetic requirements [257,258]. CSCs are key tumour initiating cells that play an integral role in metastatic process, and tumour recurrence even after chemotherapy. It is easily understood why CSCs, in the last years, have gained intense interest as specific target for new therapeutic strategies. Based on this evidence, a preliminary *in vitro* study of the drugs effects on enriched osteosarcoma stem cell viability and on the drug-uptake has been performed.



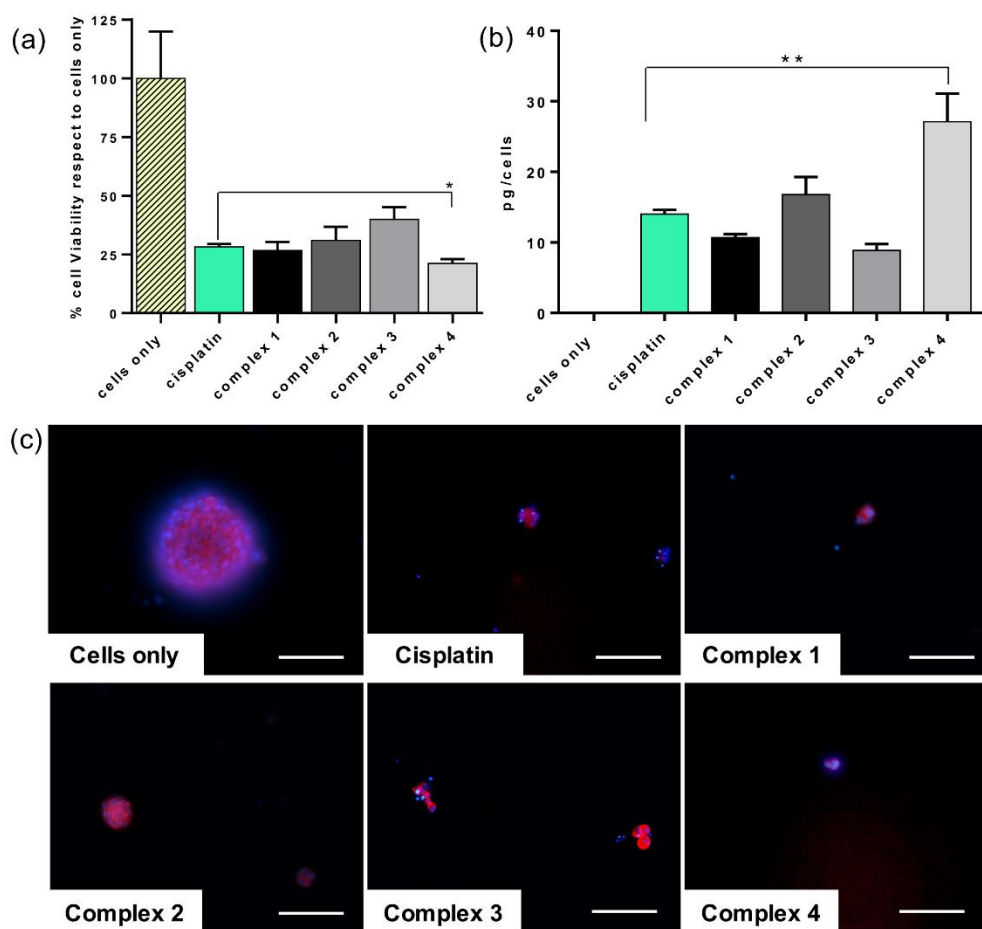


**Figure 2.18:** Cisplatin and complexes 1-4 effect on CSCs. CSCs treated for 72h with 30  $\mu$ M of drugs. (a) MTT assay. Mean  $\pm$  SEM of the percentage of cell viability respect to cells only (\* p value  $\leq 0.05$ ). (b) ICP-OES analysis. Cellular uptake of picograms of platinum ions (mean  $\pm$  SEM) per cell are expressed in the graph (\*\* p value  $\leq 0.01$ ). (c) Actin & DAPI staining of CSCs. F-actin filaments in red; cell nuclei in blue. Scale bars 100  $\mu$ m.

An unexpected outcome from these tests showed that **Complex 4** significantly decreased cell viability when compared to cisplatin and the other three complexes tested, p value  $\leq 0.05$  (a). This coincides with the increased quantity of platinum inside the cells when treated with **Complex 4** (27.1 pg/cells, p value  $\leq 0.01$ ), compared to cisplatin (b). The cells morphological evaluation showed a reduction in the spheres dimension, which is a typical morphological marker of CSCs, confirming the cytotoxicity results (c) [259].

## 2.5 Conclusion

In conclusion, four novel mono-functionalised Pt(IV)-glycosides, based on the cisplatin scaffold, were synthesised, linking the sugar moiety and the metal centre

*via* CuAAC “click” chemistry. The complexes were screened against a panel of different OS cell lines and showed promising activity, when compared to the reference cisplatin. The complexes were also particularly active towards CSCs with the most promising activity shown by **Complex 4**, a galactose derivative. Interestingly, galactose has attracted a lot of attention for its role in the metabolism of CSCs, due to its diagnostic and therapeutic possibilities [260,261]. It should be noted that no assays were conducted which suppressed or blocked the overexpression of GLUTs, so the drugs activity without its target was not assessed. However, this preliminary study did show that with the sugar ligand, the anticancer activity as well as the drug internalisation, was higher when compared to cisplatin (demonstrated by the uptake experiments in CSCs); allowing us to move onto the next chapter of this thesis where free sugar derivatives were synthesised to test their anticancer activity. It is possible that the increased activity could be due to the protected sugar ligands, leading to an increase in lipophilicity from the acetyl groups. This could mean the movement of the complex into the cell, occurs by passive diffusion rather than transport *via* the GLUTs. An inhibition assay would need to be conducted to determine if this is the case. This chapter was published in *Frontiers in Chemistry* (doi: 10.3389/fchem.2021.795997) attached at the end of the thesis.

## 2.6 Materials and Methods

All reagents and reactants were purchased from commercial sources. The two sources used were Sigma-Aldrich and Fluorochem. All solvents were used without further purification. Cisplatin and oxoplatin were synthesised as previously reported [262,263].

The elemental analysis studies (carbon, hydrogen, and nitrogen) were performed by means of a PerkinElmer 2400 series II analyzer. ESI Mass Spectra were recorded with a Waters LCT Premier XE Spectrometer. NMR:  $^1\text{H}$ ,  $^{13}\text{C}$  and  $^{195}\text{Pt}$  NMR spectra were obtained in a solution of  $\text{CDCl}_3$  or  $\text{DMSO-}d_6$  at 300 K, in 5-mm sample tubes, with a premium shielded Agilent Varian 500 MHz (operating at 500.13, 125.75, and 107.49 MHz, respectively). The  $^1\text{H}$  and  $^{13}\text{C}$  chemical shift was referenced to the residual impurity of the solvent. The external reference was  $\text{Na}_2\text{PtCl}_4$  in  $\text{D}_2\text{O}$  (adjusted to  $\delta = -1628$  ppm from  $\text{Na}_2\text{PtCl}_6$ ) for  $^{195}\text{Pt}$ . The stability was followed using high-

performance liquid chromatography (HPLC) with a Phenomenex Luna C18 (5  $\mu$ M, 100 Å, 250mm  $\times$  4.60 mm i.d.) column at room temperature at a flow rate of 1.0 mL/min with 254 nm UV detection. Mobile phase containing 80:20 acetonitrile (0.1% trifluoroacetic acid): water (0.1% trifluoroacetic acid): the complexes were dissolved in DMF (0.5 ml) and diluted to a final concentration of 0.5 mM using acetonitrile and water solution (1/1) and 2 mM 4-(2-hydroxyethyl)piperazine-1-ethanesulfonic acid (HEPES) buffer (pH 6.8). Infrared (IR) spectra were recorded in the region 4000–400  $\text{cm}^{-1}$  on a Perkin Elmer precisely spectrum 100 FT/IR spectrometer. The solid samples were run using ATR.

### 2.6.1 *In vitro* biological evaluation

*In vitro* tests of cisplatin-based drugs were performed to evaluate the cellular behaviours in response to the different complexes (**1** – **4**) compared to cisplatin. All the drugs were reconstituted in Dimethyl Sulfoxide (DMSO) at 1 mg/ml final concentration, and then dissolved in the culture media at different concentrations: 15, 30 and 60  $\mu$ M. Three different osteosarcoma cells lines (MG63, SAOS-2, U-2OS) and an *in vitro* model of osteosarcoma stem cells (enriched-CSCs) were maintained in culture with and without the drugs for 72 hours.

### 2.6.2 Cell culture

Human Osteosarcoma cell lines MG63 (ATCC® CRL1427™), U-2OS (ATCC® HTB-96™) and SAOS-2 (ATCC® HTB-85™), purchased from American Type Culture Collection (ATCC), were used. MG63 cell line was cultured in DMEM F12-GlutaMAX™ Modified Medium (Gibco) supplemented with 10% Foetal Bovine Serum (FBS) (Gibco) and 1% of penicillin/streptomycin mixture (pen/strep) (100 U/ml - 100  $\mu$ g/mL, Gibco). SAOS-2 and U-2OS cell lines were cultured in McCoy's 5A Modified Medium (Gibco) supplemented with 15% and 10% FBS, respectively, and 1% pen/strep. Cells were kept in an incubator at 37°C under controlled humidity and 5% CO<sub>2</sub> atmosphere conditions. Cells were detached from culture flasks by trypsinisation and centrifuged. The cell number and viability were determined by Trypan Blue Dye Exclusion test and all cell handling procedures were performed under laminar flow hood in sterility conditions. For the experiment, all cell lines were seeded 5.0  $\times$  10<sup>3</sup> cells/well in 96 well-plates and 5.0  $\times$  10<sup>4</sup> cells/well in 6 well-plates.

### 2.6.3 Enriched-CSCs culture

Enriched-Cancer Stem Cells (CSCs) were obtained under specific culture conditions as reported in literature [257,264] as sarcospheres forming method starting from human MG63 osteosarcoma cell line. MG63 cell line was seeded in Ultra-Low Attachment T25 flasks (Corning Inc., NY) with a density of  $2.0 \times 10^3$  cells/cm<sup>2</sup> in serum-free DMEM F12-GlutaMAX™ Modified Medium supplemented with a specific cocktail of factors: 10 µl/ml N2 (Gibco), 20 µl/ml B27 (Gibco), 0.1 µl/ml human Basic-Fibroblast Growth Factor (bFGF) (Invitrogen) and 0.01 µl/ml human Epidermal Growth Factor (EGF) (PeproTech). The cocktail was added to each flask every 2/3 days for a total of 10 days of culture. After their formation, the CSCs were collected and centrifugated for 10 minutes at 130 x g; the pellet was resuspended in the same medium conditions, well mixed, and directly seeded in Ultra-Low Attachment 96 well-plate and Ultra-Low Attachment 6 well-plate with 200 µL/well and 1.5 mL/well volume of cell culture medium, respectively. The factors' cocktail was added every 2/3 days during the experiment following the above-reported manufacturer's instructions.

### 2.6.4 MTT cell viability assay

A quantitative analysis of cell viability and proliferation was carried out by MTT assay on cell cultures, by using the cells only as the negative control. At 72 hours, the MTT assay was performed according to manufacturer's instructions. Briefly, MTT reagent [3-(4,5-dimethylthiazol-2-yl)-2,5-diphenyltetrazolium bromide] (5 mg/mL) was dissolved in Phosphate Saline Buffer 1X (PBS 1X). At 72 hours, the cells were incubated with 10% media volume MTT solution for 2 hours at 37 °C, 5% CO<sub>2</sub> and controlled humidity conditions. The cell culture media was removed and substituted with DMSO (Sigma) dissolving formazan crystals derived from MTT conversion by metabolically active cells. For CSCs, the total media was centrifugated and the deposited crystals were directly resuspended in DMSO. After 15-minutes incubation under slight stirring conditions, the absorbance of formazan was read at 570 nm by using a Multiskan FC Microplate Photometer (Thermo Scientific). The values of absorbance are directly proportional to the number of metabolic active cells in each

well. One experiment was carried out and a biological triplicate for each condition was performed.

### **2.6.5 Cell morphology evaluation**

Cells treated with and without the drugs (30  $\mu$ M) were fixed in 4% buffered Paraformaldehyde (PFA) following the manufacturer's instructions. The fixed cells were permeabilised in PBS 1X with 0.1% (v/v) Triton X-100 (Sigma) for 5 minutes at room temperature and F-actin filaments were highlighted with red fluorescent solution of Rhodamine Phalloidin (Actin Red 555 Ready Probes™ Reagent, Invitrogen), following the company indications, for 30 minutes at room temperature. DAPI (600 nM) counterstaining was performed for cell nuclei identification, following the manufacturer's instructions. The images were acquired by using an Inverted Ti-E Fluorescent Microscope.

### **2.6.6 Inductively coupled plasma-optical emission spectrometry (ICP-OES)**

The ICP-OES (Agilent Technologies 5100 ICP-OES, Santa Clara, USA) was performed on Enriched-CSCs culture to quantify cellular internalisation of drugs, following the manufacturer's instructions. At 72 hours, cells were mechanically by 50-100 times p200 pipetting to disaggregate spheroid, counted by Trypan Blue Dye Exclusion Test and collected in 400  $\mu$ L PBS 1X. ICP-OES was used for the quantitative determination of platinum ions content per cell derived by cisplatin-based drugs, by using cells only as negative control. Briefly, the samples were dissolved in 500  $\mu$ L nitric acid (65 wt.%) and 2.1 mL of milliQ water followed by 30 minutes of sonication in a ultrasonicator bath. The analytical wavelength of Pt was 265.945 nm. One experiment was carried out and for each condition the amount of drug per cell was quantified in biological triplicate. Data are represented in the graph.

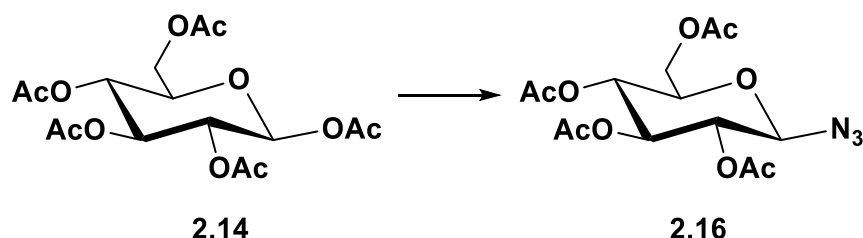
### **2.6.7 Statistical Analysis**

Statistical analysis was performed by using GraphPad Prism Software (8.0.1 version). The results of MTT assay are reported in the graphs as mean percentage of cell viability respect to cells only  $\pm$  standard deviation and they were analysed by Two-way analysis of variance (Two-way ANOVA) and Tukey's multiple comparisons test. IC<sub>50</sub> values were calculated as Log(inhibitor) versus mean percentage of dead cells respect to cells only and the obtained values are reported in the graphs  $\pm$  95%

confidence interval (CI) for each cell line. The results of MTT assay on CSCs are reported in the graph as mean percentage of cell viability respect to cells only  $\pm$  standard error of the mean and they were analysed by Unpaired t-test setting a p value  $\leq 0.05$  to determine statistically significant differences. The ICP-OES data were elaborated as picograms of iron ions per cell and reported in the graph  $\pm$  standard error of the mean. The results were analysed by One-way analysis of variance (One-way ANOVA) and Dunnett's multiple comparisons test (\* p value  $\leq 0.05$ , \*\* p value  $\leq 0.01$ , \*\*\* p value  $\leq 0.001$ , \*\*\*\* p value  $\leq 0.0001$ ).

## 2.7 Experimental procedures

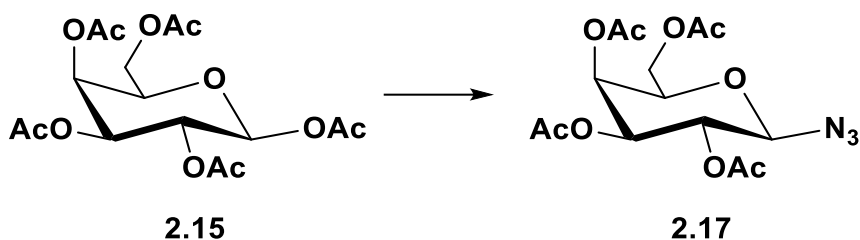
### 2,3,4,6-tetra-O-acetyl-1- $\beta$ -azido-D-glucopyranoside (2.16)



TMSN<sub>3</sub> (1.68 mL, 12.80 mmol, 2.5 equiv.) was added to a solution of  $\beta$ -D-glucose pentaacetate **2.14** (2 g, 5.12 mmol) in anhydrous DCM (20 mL). SnCl<sub>4</sub> (0.3 mL, 2.56 mmol, 0.5 equiv) was added to this solution and the reaction mixture was stirred at rt for 18 h. Sat. NaHCO<sub>3</sub> solution (30 mL) was added, and the suspension was extracted with DCM (2 x 30 mL). The combined organic layers were dried over MgSO<sub>4</sub>, filtered and concentrated *in vacuo*. The crude product was obtained as a white solid, which was recrystallised from EtOH giving the pure product **2.16** as white crystals (1.79 g, 4.79 mmol, 94 %).

<sup>1</sup>H NMR (500 MHz, CDCl<sub>3</sub>)  $\delta$  5.21 (appt,  $J = 9.5$ , 1H, H-3), 5.09 (appt,  $J = 9.7$  Hz, 1H, H-4), 4.94 (appt,  $J = 9.2$  Hz, 1H, H-2), 4.64 (d,  $J = 8.9$  Hz, 1H, H-1), 4.26 (dd,  $J = 12.5, 4.8$  Hz, 1H, H-6), 4.16 (dd,  $J = 12.4, 2.1$  Hz, 1H, H-6'), 3.79 (ddd,  $J = 10.1, 4.7, 2.2$  Hz, 1H, H-5), 2.09 (s, 3H, OAc), 2.07 (s, 3H, OAc), 2.02 (s, 3H, OAc), 2.00 (s, 3H, OAc).

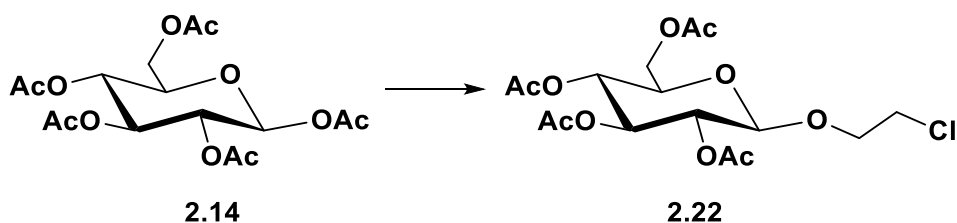
The NMR data is in agreement with the data reported in the literature [231].

**2,3,4,6-tetra-O-acetyl-1- $\beta$ -azido-D-galactopyranoside (2.17)**

TMSN<sub>3</sub> (1.68 mL, 12.80 mmol, 2.5 equiv) was added to a solution of  $\beta$ -D-galactose pentaacetate **2.15** (2 g, 5.12 mmol) in anhydrous DCM (20 mL). SnCl<sub>4</sub> (0.3 mL, 2.56 mmol, 0.5 equiv) was added to this solution and the reaction mixture was stirred at rt for 18 h. Sat. NaHCO<sub>3</sub> solution (30 mL) was added, and the suspension was extracted with DCM (2 x 30 mL). The combined organic layers were dried over MgSO<sub>4</sub>, filtered and concentrated *in vacuo* to afford **2.17** as a white solid which was recrystallised from EtOH giving the pure product **2.17** as white crystals (1.86 g, 4.98 mmol, 97 %).

<sup>1</sup>H NMR (500 MHz, CDCl<sub>3</sub>)  $\delta$  5.42 (appd,  $J$  = 3.3 Hz, 1H, H-4), 5.18 – 5.13 (m, 1H, H-2), 5.03 (dd,  $J$  = 10.3, 3.4 Hz, 1H, H-3), 4.59 (d,  $J$  = 8.8 Hz, 1H, H-1), 4.20 – 4.13 (m, 2H, H-6 and H-6'), 4.01 (appt,  $J$  = 6.6 Hz, 1H, H-5), 2.16 (s, 3H, OAc), 2.09 (s, 3H, OAc), 2.06 (s, 3H, OAc), 1.98 (s, 3H, OAc).

The NMR data is in agreement with the data reported in the literature [231].

**2-Chloroethyl 2,3,4,6-tetra-O-acetyl- $\beta$ -D-glucopyranoside (2.22)**

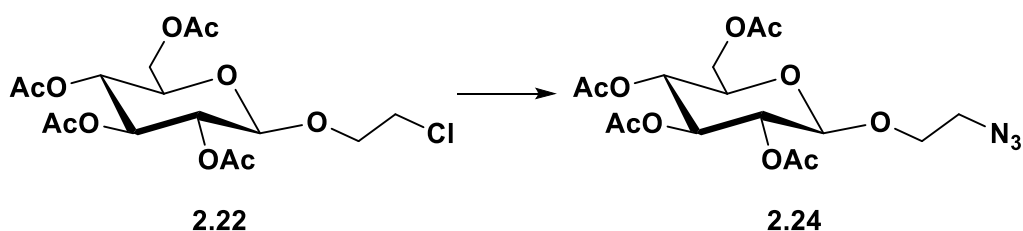
A solution of  $\beta$ -D-glucose pentaacetate **2.14** (2 g, 5.12 mmol) and 2-chloroethanol (0.45 mL, 6.66 mmol, 1.3 equiv) in anhydrous DCM (20 mL) with 3 Å molecular sieves (3 g) was stirred under N<sub>2</sub> in an ice bath for 15 min. A freshly prepared solution of BF<sub>3</sub>·OEt<sub>2</sub> (1.2 mL, 9.73 mmol, 1.9 equiv) in anhydrous DCM (2 mL) was added

dropwise over a period of 30 min via cannula. When addition was complete, the mixture was allowed to reach rt and stirred overnight. The molecular sieves were filtered using fluted filter paper, the solids were washed with DCM (10 mL) and the filtrate was washed with a sat. NaHCO<sub>3</sub> solution (2 x 20 mL). The combined aqueous layers were extracted with DCM (20 mL), the combined organic layers were washed with brine (20 mL) and distilled water (20 mL), dried over MgSO<sub>4</sub>, filtered and concentrated *in vacuo*. The crude product was obtained as a white solid, which was recrystallised from EtOH giving the pure product **2.22** as white crystals (0.480 g, 1.16 mmol, 22 %).

<sup>1</sup>H NMR (500 MHz, CDCl<sub>3</sub>) δ 5.22 (appt, *J* = 9.5 Hz, 1H, H-3), 5.09 (appt, *J* = 9.7 Hz, 1H, H-4), 5.02 (dd, *J* = 9.6, 8.0 Hz, 1H, H-2), 4.58 (d, *J* = 8.0 Hz, 1H, H-1), 4.26 (dd, *J* = 12.3, 4.8 Hz, 1H, H-6), 4.15 (dd, *J* = 12.3, 2.4 Hz, 1H, H-6'), 4.13 – 4.06 (m, 1H, OCH), 3.80 – 3.73 (m, 1H, OCH'), 3.71 (ddd, *J* = 9.9, 4.7, 2.4 Hz, 1H, H-5), 3.62 (t, *J* = 5.7 Hz, 2H, CH<sub>2</sub>Cl), 2.09 (s, 3H, OAc), 2.06 (s, 3H, OAc), 2.03 (s, 3H, OAc), 2.01 (s, 3H, OAc).

The NMR data is in agreement with the data reported in the literature [232].

### 2-Azidoethyl 2,3,4,6-tetra-*O*-acetyl-β-D-glucopyranoside (**2.24**)



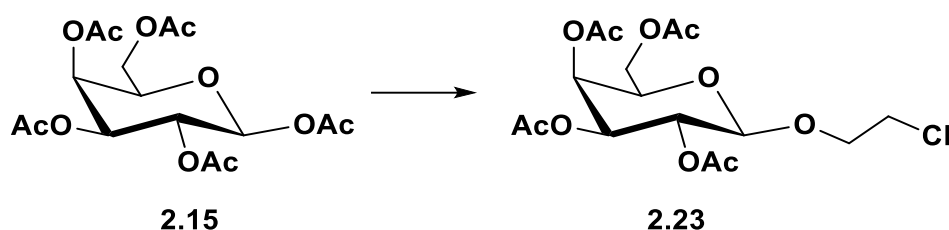
A solution of 2-chloroethyl 2,3,4,6-tetra-*O*-acetyl-β-D-glucopyranoside **2.22** (0.850 g, 2.069 mmol) and NaN<sub>3</sub> (0.269 g, 4.138 mmol, 2 equiv) in anhydrous DMF (30 mL) was stirred at 80°C in a round bottomed flask equipped with a condenser and a CaCl<sub>2</sub> drying tube. After 16 h, the solvent was removed under reduced pressure. The crude product was dissolved in DCM (30 mL) and washed with brine (3 x 20 mL). The organic phases were combined, dried over MgSO<sub>4</sub> and concentrated *in vacuo* to give a clear syrup that turned into a white solid **2.24** upon exposure to high vacuum, which was reacted without further purification (0.540 g, 1.29 mmol, 62 %).



$^1\text{H NMR}$  (500 MHz,  $\text{CDCl}_3$ )  $\delta$  5.21 (appt,  $J = 9.5$  Hz, 1H, H-3), 5.09 (appt,  $J = 9.7$  Hz, 1H, H-4), 5.02 (dd,  $J = 9.5, 8.1$  Hz, 1H, H-2), 4.59 (d,  $J = 8.0$  Hz, 1H, H-1), 4.25 (dd,  $J = 12.3, 4.7$  Hz, 1H, H-6), 4.16 (dd,  $J = 12.3, 2.4$  Hz, 1H, H-6'), 4.03 – 4.01 (m, 1H, OCH), 3.78 – 3.60 (m, 2H, H-5, OCH'), 3.54 – 3.38 (m, 1H, CHN<sub>3</sub>), 3.33 – 3.21 (m, 1H, CH'N<sub>3</sub>), 2.08 (s, 3H, OAc), 2.04 (s, 3H, OAc), 2.02 (s, 3H, OAc), 2.00 (s, 3H, OAc).

The NMR data is in agreement with the data reported in the literature [232].

### 2-Chloroethyl 2,3,4,6-tetra-*O*-acetyl- $\beta$ -D-galactopyranoside (**2.23**)



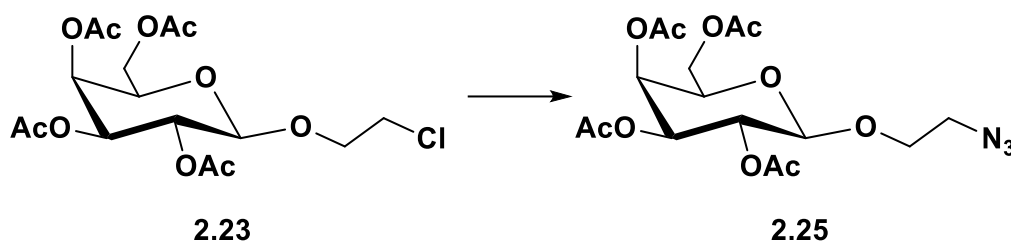
A solution of  $\beta$ -D-galactose pentaacetate **2.15** (2 g, 5.12 mmol) and 2-chloroethanol (0.45 mL, 6.66 mmol, 1.3 equiv) in anhydrous DCM (20 mL) with 3 Å molecular sieves (3 g) was stirred under  $\text{N}_2$  in an ice bath for 15 min. A freshly prepared solution of  $\text{BF}_3 \cdot \text{OEt}_2$  (1.2 mL, 9.73 mmol, 1.9 equiv) in anhydrous DCM (2 mL) was added dropwise over a period of 30 min via cannula. When addition was complete, the mixture was allowed to reach rt and stirred overnight. The molecular sieves were filtered using fluted filter paper, the solids were washed with DCM (10 mL) and the filtrate was washed with a sat.  $\text{NaHCO}_3$  solution (2 x 20 mL). The combined aqueous layers were extracted with DCM (20 mL), the combined organic layers were washed with brine (20 mL) and distilled water (20 mL), dried over  $\text{MgSO}_4$ , filtered and concentrated *in vacuo*. The crude product was obtained as a white solid, which was recrystallised from EtOH giving the pure product **2.23** as white crystals (0.540 g, 1.31 mmol, 25 %).

$^1\text{H NMR}$  (500 MHz,  $\text{CDCl}_3$ )  $\delta$  5.39 (appd,  $J = 2.7$  Hz, 1H, H-4), 5.22 (dd,  $J = 10.4, 8.0$  Hz, 1H, H-2), 5.02 (dd,  $J = 10.5, 3.4$  Hz, 1H, H-3), 4.53 (d,  $J = 7.9$  Hz, 1H, H-1), 4.20 – 4.08 (m, 3H, H-6, H-6' and OCH), 3.91 (appt,  $J = 6.4$  Hz, 1H, H-5), 3.76 (dt,  $J = 11.2, 6.6$  Hz,

1H, OCH), 3.62 (dd,  $J = 6.3, 5.2$  Hz, 2H, CH<sub>2</sub>Cl), 2.15 (s, 3H, OAc), 2.07 (s, 3H, OAc), 2.05 (s, 3H, OAc), 1.98 (s, 3H, OAc).

The NMR data is in agreement with the data reported in the literature [232].

### 2-Azidoethyl 2,3,4,6-tetra-*O*-acetyl- $\beta$ -D-galactopyranoside (**2.25**)

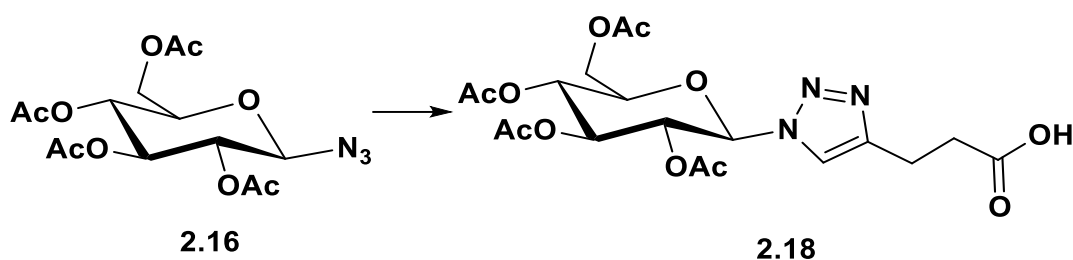


A solution of 2-chloroethyl 2,3,4,6-tetra-*O*-acetyl- $\beta$ -D-galactopyranoside **2.23** (0.850 g, 2.069 mmol) and NaN<sub>3</sub> (0.269 g, 4.138 mmol, 2 equiv) in anhydrous DMF (30 mL) was stirred at 80 °C in a round bottomed flask equipped with a condenser and a CaCl<sub>2</sub> drying tube. After 16 h, the solvent was removed under reduced pressure. The crude product was dissolved in DCM (30 mL) and washed with brine (3 x 20 mL). The organic phases were combined, dried over MgSO<sub>4</sub> and concentrated *in vacuo* to give a clear syrup that turned into a white solid **2.25** upon exposure to high vacuum, which was reacted without further purification (0.518 g, 1.24 mmol, 60 %).

<sup>1</sup>H NMR (500 MHz, CDCl<sub>3</sub>)  $\delta$  5.33 (dd,  $J = 3.4, 1.1$  Hz, 1H, H-4), 5.17 (dd,  $J = 10.5, 8.0$  Hz, 1H, H-2), 4.97 (dd,  $J = 10.5, 3.4$  Hz, 1H, H-3), 4.51 (d,  $J = 8.0$  Hz, 1H, H-1), 4.15-4.04 (m, 2H, H-6 and H-6'), 3.98 (ddd,  $J = 10.7, 4.8, 3.5$  Hz, 1H, OCH), 3.88 (td,  $J = 6.6, 1.1$  Hz, 1H, H-5), 3.64 (ddd,  $J = 10.8, 8.4, 3.4$  Hz, 1H, OCH), 3.44 (ddd,  $J = 13.3, 8.4, 3.5$  Hz, 1H, CHN<sub>3</sub>), 3.25 (ddd,  $J = 13.4, 4.8, 3.4$  Hz, 1H, CHN<sub>3</sub>), 2.09 (s, 3H, OAc), 2.00 (s, 3H, OAc), 1.98 (s, 3H, OAc), 1.92 (s, 3H, OAc).

The NMR data is in agreement with the data reported in the literature [232].

***N*-(2,3,4,6-tetra-*O*-acetyl- $\beta$ -D-glucopyranosyl-1,2,3-triazol-4-yl)-propanoic acid (2.18)**



**2.16** (0.98 g, 2.650 mmol, 1.3 equiv) and 4-pentynoic acid (0.2 g, 2.038 mmol) were dissolved in a mixture of tetrahydrofuran (6 ml), tert-Butanol (6 mL) and deionised water (4 mL). Separately, copper(II) sulphate pentahydrate (0.1 g, 0.407 mmol, 0.2 equiv) and sodium ascorbate (0.161 g, 0.815 mmol, 0.4 equiv) were dissolved in deionised water (2 mL), added to reaction flask and allowed to stir at r.t. overnight (16 h). The solvent was removed *in vacuo* and the residue was dissolved in DCM (15 mL) and washed with brine (2 x 20 mL). The organic phase was dried with MgSO<sub>4</sub>, filtered and the solvent was evaporated. The crude product was purified by column chromatography (1:1, pet. ether:EtOAc) to yield a white solid (0.615 g, 1.304 mmol, 64%).

$R_f$  = 0.92 (90:10 DCM:MeOH).

**<sup>1</sup>H NMR** (500 MHz, CDCl<sub>3</sub>)  $\delta$  7.62 (s, 1H, triaz-H), 5.85 (d,  $J$  = 9.0 Hz, 1H, H-1), 5.46 – 5.37 (m, 2H, H-2, H-3), 5.24 (t,  $J$  = 9.9 Hz, 1H, H-4), 4.29 (dd,  $J$  = 12.6, 5.0 Hz, 1H, H-6), 4.14 (dd,  $J$  = 12.6, 2.1 Hz, 1H, H-6'), 3.99 (ddd,  $J$  = 10.1, 5.0, 2.1 Hz, 1H, H-5), 3.05 (t,  $J$  = 7.3 Hz, 2H, triaz-CH<sub>2</sub>), 2.78 (t,  $J$  = 7.3 Hz, 2H, CH<sub>2</sub>CO), 2.08 (s, 3H, CH<sub>3</sub> of OAc), 2.06 (s, 3H, CH<sub>3</sub> of OAc), 2.02 (s, 3H, CH<sub>3</sub> of OAc), 1.85 (s, 3H, CH<sub>3</sub> of OAc) ppm.

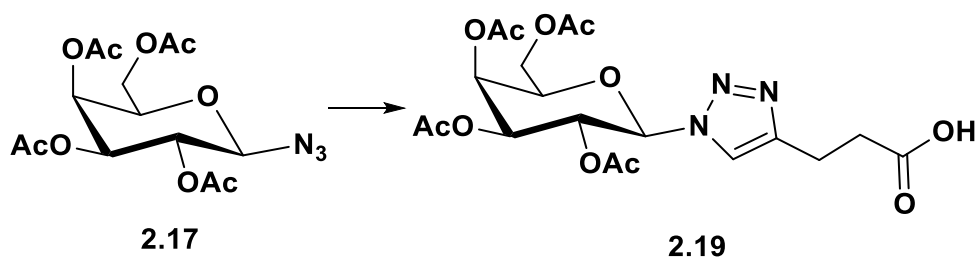
**<sup>13</sup>C NMR** (125 MHz, CDCl<sub>3</sub>)  $\delta$  176.9 (COOH), 170.7 (CO of OAc), 170.1 (CO of OAc), 169.5 (CO of OAc), 169.1 (CO of OAc), 147.0 (triaz-C), 119.8 (triaz-CH), 85.8 (C-1), 75.2 (C-5), 72.8 (C-3), 70.3 (C-2), 67.9 (C-4), 61.7 (C-6), 33.2 (CH<sub>2</sub>COOH), 20.8 (2 x CH<sub>3</sub> of OAc), 20.7 (2 x CH<sub>3</sub> of OAc), 20.2 (triaz-CH<sub>2</sub>) ppm.

**IR (ATR)** 2966.47, 1738.08, 1701.08, 1429.63, 1369.28, 1218.46, 1096.44, 1037.86, 918.27, 838.17 cm<sup>-1</sup>.

**HR-MS (+):**  $m/z$  calcd for  $C_{19}H_{25}N_3O_{11} + Na^+ [M+Na]^+$  494.1489, found 494.1383. **HR-**

**MS (+):**  $m/z$  calcd for  $C_{19}H_{25}N_3O_{11} + H^+ [M+H]^+$  472.1489, found 472.1564.

***N*-(2,3,4,6-tetra-*O*-acetyl- $\beta$ -D-galactopyranosyl-1,2,3-triazol-4-yl)-propanoic acid (2.19)**



**2.17** (0.98 g, 2.650 mmol, 1.3 equiv) and 4-pentynoic acid (0.2 g, 2.038 mmol) were dissolved in a mixture of tetrahydrofuran (6 ml), tert-Butanol (6 mL) and deionised water (4 mL). Separately, copper(II) sulphate pentahydrate (0.1 g, 0.407 mmol, 0.2 equiv) and sodium ascorbate (0.161 g, 0.815 mmol, 0.4 equiv) were dissolved in deionised water (2 mL), added to reaction flask and allowed to stir at r.t. overnight (16 h). The solvent was removed *in vacuo* and the residue was dissolved in DCM (15 mL) and washed with brine (2 x 20 mL). The organic phase was dried with  $MgSO_4$ , filtered and the solvent was evaporated. The crude product was purified by column chromatography (1:1, pet. ether:EtOAc) to yield a white solid (Yield 0.713 g, 1.512 mmol, 74%).

$R_f = 0.33$  (95:5 DCM:MeOH).

**$^1H$  NMR** (500 MHz,  $CDCl_3$ )  $\delta$  7.65 (s, 1H, triaz-H), 5.81 (d,  $J = 9.4$  Hz, 1H, H-1), 5.57 – 5.50 (m, 2H, H-2, H-3), 5.23 (dd,  $J = 10.3, 3.4$  Hz, 1H, H-4), 4.24 – 4.10 (m, 3H, H-5, H-6, H-6'), 3.05 (t,  $J = 7.4$  Hz, 2H, triaz- $CH_2$ ), 2.79 (t,  $J = 7.4$  Hz, 2H,  $CH_2CO$ ), 2.21 (s, 3H,  $CH_3$  of OAc), 2.03 (s, 3H,  $CH_3$  of OAc), 1.99 (s, 3H,  $CH_3$  of OAc), 1.86 (s, 3H,  $CH_3$  of OAc) ppm.

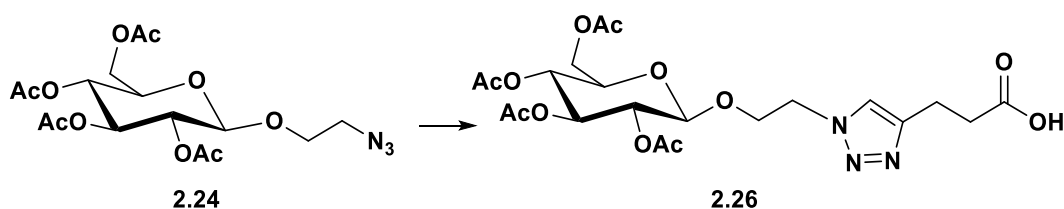
**$^{13}C$  NMR** (125 MHz,  $CDCl_3$ )  $\delta$  177.1 (COOH), 170.5 (CO of OAc), 170.1 (CO of OAc), 169.9 (CO of OAc), 169.2 (CO of OAc), 146.9 (triaz-C), 119.9 (triaz-CH), 86.3 (C-1), 74.1 (C-5), 70.9 (C-4), 67.9 (C-2), 67.0 (C-3), 61.31 (C-6), 33.27 ( $CH_2COOH$ ), 20.81 (triaz-

CH<sub>2</sub>), 20.78 (CH<sub>3</sub> of OAc), 20.76 (CH<sub>3</sub> of OAc), 20.6 (CH<sub>3</sub> of OAc), 20.3 (CH<sub>3</sub> of OAc) ppm.

**IR (ATR)** 3087.65, 1734.80, 1715.92, 1436.51, 1366.99, 1216.01, 1045.12, 923.00, 850.50, 717.78 cm<sup>-1</sup>.

**HR-MS (+):** m/z calcd for C<sub>19</sub>H<sub>25</sub>N<sub>3</sub>O<sub>11</sub> + H<sup>+</sup> [M+H]<sup>+</sup> 472.1489, found 472.1564. **HR-MS (+):** m/z calcd for C<sub>19</sub>H<sub>25</sub>N<sub>3</sub>O<sub>11</sub> + Na<sup>+</sup> [M+Na]<sup>+</sup> 494.1489, found 494.1384.

***N*-[2-*O*-(2,3,4,6-tetra-*O*-acetyl-β-*D*-glucopyranosyl)-ethyl-1,2,3-triazol-4-yl]-propanoic acid (2.26)**



**2.24** (0.35 g, 0.838 mmol, 1.3 equiv) and 4-pentynoic acid (0.063 g, 0.642 mmol) were dissolved in a mixture of tetrahydrofuran (6 ml), tert-Butanol (6 mL) and deionised water (4 mL). Separately, copper(II) sulphate pentahydrate (0.032 g, 0.128 mmol, 0.2 equiv) and sodium ascorbate (0.050 g, 0.256 mmol, 0.4 equiv) were dissolved in deionised water (2 mL), added to reaction flask and allowed to stir at r.t. overnight (16 h). The solvent was removed *in vacuo* and the residue was dissolved in DCM (15 mL) and washed with brine (2 x 20 mL). The organic phase was dried with MgSO<sub>4</sub>, filtered and the solvent was evaporated. The crude product was purified by column chromatography (1:1, pet. ether:EtOAc) to yield a white solid (Yield 0.147 g, 0.285 mmol, 44%).

**R<sub>f</sub>** = 0.35 (DCM:MeOH 95:5).

**<sup>1</sup>H NMR** (500 MHz, CDCl<sub>3</sub>) δ 7.44 (s, 1H, triaz-*H*), 5.19 (t, *J* = 9.5 Hz, 1H, H-3), 5.06 (t, *J* = 9.7 Hz, 1H, H-4), 4.97 (dd, *J* = 9.6, 8.0 Hz, 1H, H-2), 4.55 (dt, *J* = 14.4, 3.8 Hz, 1H, *CH*-triaz), 4.50 – 4.44 (m, 1H, *CH'*-triaz), 4.43 (d, *J* = 7.9 Hz, 1H, H-1), 4.24 (dd, *J* = 12.4, 4.7 Hz, 1H, H-6), 4.19 (dt, *J* = 10.6, 4.0 Hz, 1H, OCH), 4.11 (dd, *J* = 12.4, 2.2 Hz, 1H, H-6'), 3.95 – 3.87 (m, 1H, OCH'), 3.68 (ddd, *J* = 10.0, 4.6, 2.3 Hz, 1H, H-5), 3.02 (t, *J* = 7.0

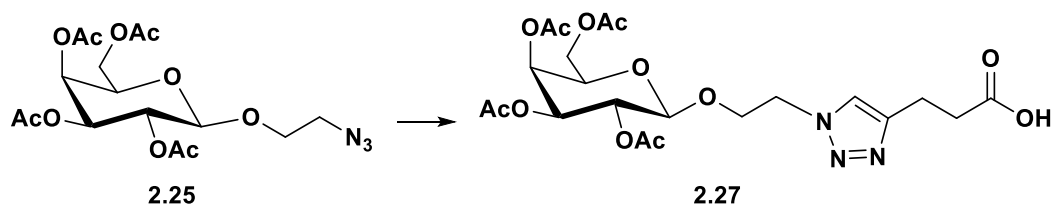
Hz, 2H, triaz-CH<sub>2</sub>), 2.77 (t, *J* = 6.7 Hz, 2H, CH<sub>2</sub>CO), 2.07 (s, 3H, OAc), 2.01 (s, 3H, OAc), 1.99 (s, 3H, OAc), 1.96 (s, 3H, OAc) ppm.

<sup>13</sup>C NMR (125 MHz, CDCl<sub>3</sub>) δ 176.4 (COOH), 170.8 (CO of OAc), 170.5 (CO of OAc), 169.6 (CO of OAc), 169.5 (CO of OAc), 146.2 (C-triaz), 122.8 (CH-triaz), 100.7 (C-1), 72.7 (C-3), 72.0 (C-5), 71.2 (C-2), 68.3 (C-4), 67.9 (OCH<sub>2</sub>), 61.9 (C-6), 50.2 (CH<sub>2</sub>-triaz), 33.5 (CH<sub>2</sub>COOH), 20.9 (triaz-CH<sub>2</sub>), 20.8 (CH<sub>3</sub> of OAc), 20.70 (2 x CH<sub>3</sub> of OAc), 20.68 (CH<sub>3</sub> of OAc) ppm.

IR (ATR) 3136.33, 2954.03, 1753.42, 1742.06, 1720.47, 1428.59, 1367.14, 1251.30, 1221.16, 1167.23, 1046.93, 1031.50, 910.47, 826.13 cm<sup>-1</sup>.

HR-MS (+): *m/z* calcd for C<sub>21</sub>H<sub>29</sub>N<sub>3</sub>O<sub>12</sub> +H<sup>+</sup> [M+H]<sup>+</sup> 516.1751, found 516.1826. HR-MS (+): *m/z* calcd for C<sub>21</sub>H<sub>29</sub>N<sub>3</sub>O<sub>12</sub> +Na<sup>+</sup> [M+Na]<sup>+</sup> 538.1781, found 538.1644.

***N*-[2-*O*-(2,3,4,6-tetra-*O*-acetyl-β-*D*-galactopyranosyl)-ethyl-1,2,3-triazol-4-yl]-propanoic acid (2.27)**



**2.25** (1.105 g, 2.649 mmol, 1.3 equiv) and 4-pentynoic acid (0.2 g, 2.038 mmol) were dissolved in a mixture of tetrahydrofuran (6 ml), tert-Butanol (6 mL) and deionised water (4 mL). Separately, copper(II) sulphate pentahydrate (0.101 g, 0.407 mmol, 0.2 equiv) and sodium ascorbate (0.161 g, 0.815 mmol, 0.4 equiv) were dissolved in deionised water (2 mL), added to reaction flask and allowed to stir at r.t. overnight (16 h). The solvent was removed *in vacuo* and the residue was dissolved in DCM (15 mL) and washed with brine (2 x 20 mL). The organic phase was dried with MgSO<sub>4</sub>, filtered and the solvent was evaporated. The crude product was purified by column chromatography (1:1, pet. ether:EtOAc) to yield a white solid (Yield 0.500 g, 0.969 mmol, 47%).

*R<sub>f</sub>* = 0.41 (DCM:MeOH 95:5).

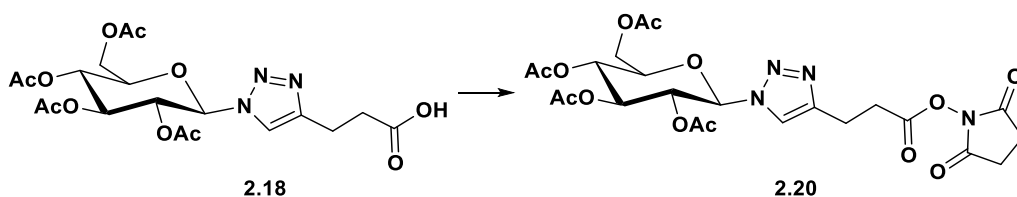
**<sup>1</sup>H NMR** (500 MHz, CDCl<sub>3</sub>) δ 7.46 (s, 1H, triaz-H), 5.38 (dd, *J* = 3.4, 0.9 Hz, 1H, H-4), 5.17 (dd, *J* = 10.5, 7.9 Hz, 1H, H-2), 5.01 (dd, *J* = 10.5, 3.4 Hz, 1H, H-3), 4.57 (dt, *J* = 7.7, 3.4 Hz, 1H, CH-triaz), 4.49 (ddd, *J* = 14.5, 8.8, 3.4 Hz, 1H, CH'-triaz), 4.41 (d, *J* = 7.9 Hz, 1H, H-1), 4.21 (dt, *J* = 10.6, 3.9 Hz, 1H, OCH), 4.13 (qd, *J* = 11.3, 6.7 Hz, 2H, H-6, H-6'), 3.95 – 3.87 (m, 2H, H-5, OCH'), 3.04 (t, *J* = 7.1 Hz, 2H, triaz-CH<sub>2</sub>), 2.79 (t, *J* = 7.1 Hz, 2H, CH<sub>2</sub>CO), 2.16 (s, 3H, CH<sub>3</sub> of OAc), 2.04 (s, *J* = 3.6 Hz, 3H, CH<sub>3</sub> of OAc), 1.97 (d, *J* = 2.1 Hz, 6H, 2 x CH<sub>3</sub> of OAc).

**<sup>13</sup>C NMR** (125 MHz, CDCl<sub>3</sub>) δ 176.3 (COOH), 170.6 (CO of OAc), 170.3 (2 x CO of OAc), 169.8 (CO of OAc), 146.2 (C-triaz), 122.9 (CH-triaz), 101.1 (C-1), 71.0 (C-5), 70.7 (C-3), 68.8 (C-2), 67.8 (OCH<sub>2</sub>), 67.0 (C-4), 61.3 (C-6), 50.2 (CH<sub>2</sub>-triaz), 33.5 (CH<sub>2</sub>COOH), 20.9 (triaz-CH<sub>2</sub>), 20.82 (CH<sub>3</sub> of OAc), 20.80 (CH<sub>3</sub> of OAc), 20.77 (CH<sub>3</sub> of OAc), 20.69 (CH<sub>3</sub> of OAc).

**IR (ATR)** 2940.25, 1739.44, 1430.24, 1367.99, 1214.32, 1043.51, 955.29, 916.32, 859.50, 827.84, 734.98 cm<sup>-1</sup>.

**HR-MS (+):** *m/z* calcd for C<sub>21</sub>H<sub>29</sub>N<sub>3</sub>O<sub>12</sub> + H<sup>+</sup> [M+H]<sup>+</sup> 516.1751, found 516.1826. **HR-MS (+):** *m/z* calcd for C<sub>21</sub>H<sub>29</sub>N<sub>3</sub>O<sub>12</sub> + Na<sup>+</sup> [M+Na]<sup>+</sup> 538.1781, found 538.1664.

***N*-(2,3,4,6-tetra-*O*-acetyl-β-*D*-glucopyranosyl-1,2,3-triazol-4-yl)-(3-oxopropyl-(oxy(2,5-dioxopyrrolidin-1-yl))) (2.20)**



**2.18** (0.2 g, 0.424 mmol) and *N*-hydroxysuccinimide (0.058 g, 0.509 mmol, 1.2 equiv) were dissolved in anhydrous DCM (7 mL) and purged with N<sub>2</sub>. A solution of EDCI (0.097 g, 0.509 mmol, 1.2 equiv) in anhydrous DCM (2 mL) was added *via* cannula over ice bath and the solution was stirred for 45 min. The reaction was warmed to r.t. and stirred for further 16 h. The organic layer was washed with 0.1M HCl (2 x 10 mL) and dried with MgSO<sub>4</sub>, filtered and concentrated *in vacuo*. The product was

obtained as a white solid which was reacted on without further purification (0.185 g, 0.325 mmol, 77%).

$R_f = 0.72$  (DCM:MeOH 95:5).

$^1\text{H NMR}$  (500 MHz,  $\text{CDCl}_3$ )  $\delta$  7.74 (s, 1H, CH-triaz), 5.83 (d,  $J = 9.2$  Hz, 1H, H-1), 5.40 – 5.35 (m, 2H, H-2 and H-3), 5.24 – 5.18 (m, 1H, H-4), 4.25 (dd,  $J = 12.6, 5.1$  Hz, 1H, H-6), 4.11 (dd,  $J = 12.6, 2.1$  Hz, 1H, H-6'), 4.01 – 3.94 (m, 1H, H-5), 3.14 (td,  $J = 7.1, 3.2$  Hz, 2H, triaz- $\text{CH}_2$ ), 3.00 – 2.95 (m, 2H,  $\text{CH}_2\text{CO}$ ), 2.81 (s, 4H,  $\text{CH}_2\text{CH}_2$ -succ), 2.03 (s, 3H,  $\text{CH}_3$  of OAc), 2.02 (s, 3H,  $\text{CH}_3$  of OAc), 1.98 (s, 3H,  $\text{CH}_3$  of OAc), 1.81 (s, 3H,  $\text{CH}_3$  of OAc) ppm.

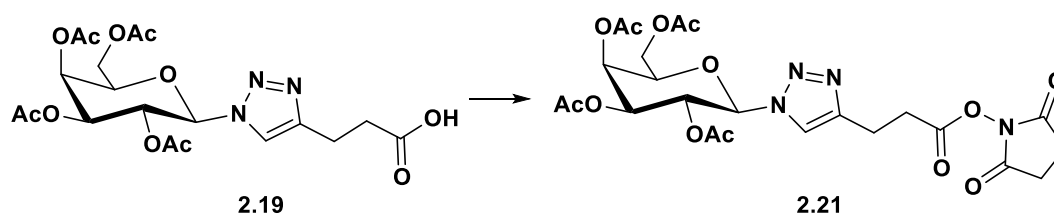
$^{13}\text{C NMR}$  (125 MHz,  $\text{CDCl}_3$ )  $\delta$  170.7 (CO of OAc), 170.1 (CO of OAc), 169.5 (CO of OAc), 169.2 (CO succ x2), 169.1 (CO of OAc), 167.8 (CO), 145.8 (C-triaz), 120.3 (CH-triaz), 85.8 (C-1), 75.2 (C-5), 72.9 (C-3), 70.4 (C-2), 67.9 (C-4), 61.8 (C-6), 31.0 ( $\text{CH}_2\text{CO}$ ), 25.7 ( $\text{CH}_2\text{CH}_2$ -succ), 21.1 ( $\text{CH}_2$ -triaz), 20.8 ( $\text{CH}_3$  of OAc), 20.69 ( $\text{CH}_3$  of OAc), 20.66 ( $\text{CH}_3$  of OAc), 20.3 ( $\text{CH}_3$  of OAc) ppm.

**IR (ATR)** 2945.90, 1732.16, 1430.40, 1367.42, 1203.35, 1064.13, 1035.83, 924.03, 813.55, 736.68  $\text{cm}^{-1}$ .

**HR-MS (+):**  $m/z$  calcd for  $\text{C}_{23}\text{H}_{28}\text{N}_4\text{O}_{13} + \text{H}^+$   $[\text{M}+\text{H}]^+$  569.1653, found 569.1727. **HR-MS**

**(+):**  $m/z$  calcd for  $\text{C}_{23}\text{H}_{28}\text{N}_4\text{O}_{13} + \text{Na}^+$   $[\text{M}+\text{Na}]^+$  591.1653, found 591.1554.

***N*-(2,3,4,6-tetra-*O*-acetyl- $\beta$ -D-galactopyranosyl-1,2,3-triazol-4-yl)-(3-oxopropyl-(oxy(2,5-dioxopyrrolidin-1-yl))) (2.21)**



**2.19** (0.2 g, 0.424 mmol) and *N*-hydroxysuccinimide (0.058 g, 0.509 mmol, 1.2 equiv) were dissolved in anhydrous DCM (7 mL) and purged with  $\text{N}_2$ . A solution of EDCI (0.097 g, 0.509 mmol, 1.2 equiv) in anhydrous DCM (2 mL) was added *via* cannula



over ice bath and the solution was stirred for 45 min. The reaction was warmed to r.t. and stirred for further 16 h. The organic layer was washed with 0.1M HCl (2 x 10 mL) and dried with MgSO<sub>4</sub>, filtered and concentrated *in vacuo*. The product was obtained as a white solid which was reacted on without further purification (Yield 0.131 g, 0.230 mmol, 54%).

$R_f$  = 0.15 (pet. ether: EtOAc 1:1).

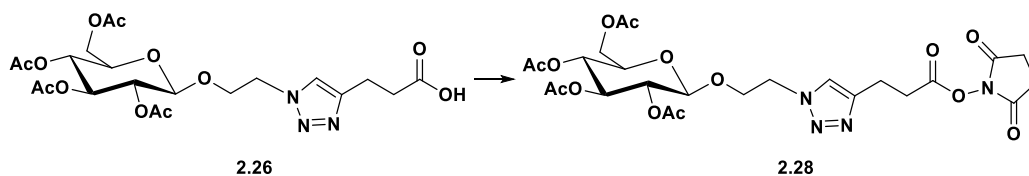
**<sup>1</sup>H NMR** (500 MHz, CDCl<sub>3</sub>) δ 7.79 (s, 1H, CH-triaz), 5.81 (d,  $J$  = 9.3 Hz, 1H, H-1), 5.55 (dd,  $J$  = 12.5, 7.0 Hz, 2H, H-2 and H-4), 5.22 (dd,  $J$  = 10.3, 3.3 Hz, 1H, H-3), 4.23 – 4.12 (m, 3H, H-5, H-6 and H-6'), 3.18 (t,  $J$  = 7.1 Hz, 2H, triaz-CH<sub>2</sub>), 3.04 (t,  $J$  = 7.1 Hz, 2H, CH<sub>2</sub>CO), 2.84 (s, 4H, CH<sub>2</sub>CH<sub>2</sub>-succ), 2.23 (s, 3H, CH<sub>3</sub> of OAc), 2.05 (s, 3H, CH<sub>3</sub> of OAc), 2.01 (s, 3H, CH<sub>3</sub> of OAc), 1.88 (s, 3H, CH<sub>3</sub> of OAc) ppm.

**<sup>13</sup>C NMR** (125 MHz, CDCl<sub>3</sub>) δ 170.5 (CO of OAc), 170.2 (CO of OAc), 170.0 (CO of OAc), 169.2 (CO of OAc), 169.1 (CO Succ x2), 167.8 (CO), 145.8 (C-triaz), 120.3 (CH-triaz), 86.4 (C-1), 74.1 (C-5), 71.1 (C-3), 68.0 (C-2), 67.0 (C-4), 61.4 (C-6), 30.9 (triaz-CH<sub>2</sub>), 25.7 (CH<sub>2</sub>CH<sub>2</sub>-succ), 21.0 (CH<sub>2</sub>CO), 20.8 (CH<sub>3</sub> of OAc), 20.8 (CH<sub>3</sub> of OAc), 20.7 (CH<sub>3</sub> of OAc), 20.4 (CH<sub>3</sub> of OAc) ppm.

**IR (ATR)** 2944.04, 1731.92, 1430.13, 1368.12, 1205.23, 1045.44, 923.03, 812.54, 744.66 cm<sup>-1</sup>.

**HR-MS (+):**  $m/z$  calcd for C<sub>23</sub>H<sub>28</sub>N<sub>4</sub>O<sub>13</sub> + H<sup>+</sup> [M+H]<sup>+</sup> 569.1653, found 569.1726. **HR-MS (+):**  $m/z$  calcd for C<sub>23</sub>H<sub>28</sub>N<sub>4</sub>O<sub>13</sub> + Na<sup>+</sup> [M+Na]<sup>+</sup> 591.1653, found 591.1547.

***N*-[2-*O*-(2,3,4,6-tetra-*O*-acetyl-β-*D*-glucopyranosyl)-ethyl-1,2,3-triazol-4-yl]-(3-oxopropyl-(oxy(2,5-dioxopyrrolidin-1-yl))) (2.28)**



**2.26** (0.121 g, 0.234 mmol) and *N*-hydroxysuccinimide (0.032 g, 0.280 mmol, 1.2 equiv) were dissolved in anhydrous DCM (7 mL) and purged with N<sub>2</sub>. A solution of

EDCI (0.053 g, 0.280 mmol, 1.2 equiv) in anhydrous DCM (2 mL) was added *via* cannula over ice bath and the solution was stirred for 45 min. The reaction was warmed to r.t. and stirred for further 16 h. The organic layer was washed with 0.1M HCl (2 x 10 mL) and dried with MgSO<sub>4</sub>, filtered and concentrated *in vacuo*. The product was obtained as a white solid which was reacted on without further purification (0.126 g, 0.205 mmol, 87.5%).

$R_f = 0.75$  (DCM:MeOH 95:5).

**<sup>1</sup>H NMR** (500 MHz, CDCl<sub>3</sub>)  $\delta$  7.49 (s, 1H, triaz-*H*), 5.11 (t,  $J = 9.5$  Hz, 1H, H-3), 5.02 (t,  $J = 9.7$  Hz, 1H, H-4), 4.92 (dd,  $J = 9.6, 7.9$  Hz, 1H, H-2), 4.51 (ddd,  $J = 14.5, 4.6, 3.7$  Hz, 1H, CH-triaz), 4.48 – 4.43 (m, 2H, H-1 and CH'-triaz), 4.21 – 4.11 (m, 2H, H-6' and OCH), 4.06 (dd,  $J = 12.3, 2.3$  Hz, 1H, H-6), 3.88 (ddd,  $J = 10.7, 8.4, 3.6$  Hz, 1H, OCH'), 3.66 (ddd,  $J = 10.0, 4.8, 2.4$  Hz, 1H, H-5), 3.09 (dd,  $J = 10.7, 4.1$  Hz, 2H, triaz-CH<sub>2</sub>), 3.00 – 2.95 (m, 2H, CH<sub>2</sub>CO), 2.80 (d,  $J = 5.7$  Hz, 4H, CH<sub>2</sub>CH<sub>2</sub>-succ), 2.02 (s, 3H, CH<sub>3</sub> of OAc), 1.96 (s, 3H, CH<sub>3</sub> of OAc), 1.93 (s, 3H, CH<sub>3</sub> of OAc), 1.90 (s, 3H, CH<sub>3</sub> of OAc) ppm.

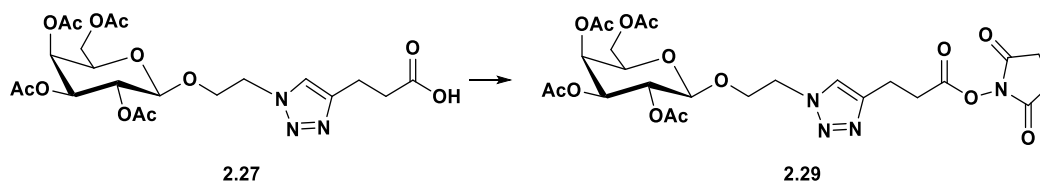
**<sup>13</sup>C NMR** (125 MHz, CDCl<sub>3</sub>)  $\delta$  170.8 (CO of OAc), 170.3 (CO of OAc), 169.5 (CO of OAc), 169.4 (CO of OAc), 169.2 (CO succ x2), 168.1 (CO), 145.0 (C-triaz), 123.0 (CH-triaz), 100.7 (C-1), 72.69 (C-3), 72.1 (C-5), 71.1 (C-2), 68.4 (C-4), 68.0 (OCH<sub>2</sub>), 61.9 (C-6), 50.1 (CH<sub>2</sub>-triaz), 31.0 (CH<sub>2</sub>CO), 25.7 (CH<sub>2</sub>CH<sub>2</sub>-succ), 21.0 (triaz-CH<sub>2</sub>), 20.9 (CH<sub>3</sub> of OAc), 20.7 (3xCH<sub>3</sub> of OAc) ppm.

**IR (ATR)** 2955.80, 1733.40, 1430.16, 1366.33, 1208.17, 1033.60, 907.61, 812.61, 733.58, 700.28 cm<sup>-1</sup>.

**HR-MS (ESI+):**  $m/z$  calcd for C<sub>25</sub>H<sub>32</sub>N<sub>4</sub>O<sub>14</sub> +H<sup>+</sup> [M+H]<sup>+</sup> 613.1915, found 613.1985. **HR-**

**MS (ESI+):**  $m/z$  calcd for C<sub>25</sub>H<sub>32</sub>N<sub>4</sub>O<sub>14</sub> +Na<sup>+</sup> [M+Na]<sup>+</sup> 635.1915, found 635.1806.

***N*-[2-*O*-(2,3,4,6-tetra-*O*-acetyl- $\beta$ -D-galactopyranosyl)-ethyl-1,2,3-triazol-4-yl]-(3-oxopropyl-(oxy(2,5-dioxopyrrolidin-1-yl))) (2.29)**



**2.27** (0.112 g, 0.217 mmol) and *N*-hydroxysuccinimide (0.030 g, 0.260 mmol, 1.2 equiv) were dissolved in anhydrous DCM (7 mL) and purged with N<sub>2</sub>. A solution of EDCI (0.049 g, 0.260 mmol, 1.2 equiv) in anhydrous DCM (2 mL) was added *via* cannula over ice bath and the solution was stirred for 45 min. The reaction was warmed to r.t. and stirred for further 16 h. The organic layer was washed with 0.1M HCl (2 x 10 mL) and dried with MgSO<sub>4</sub>, filtered and concentrated *in vacuo*. The product was obtained as a white solid which was reacted on without further purification (Yield 0.106 g, 0.173 mmol, 79%).

$R_f = 0.69$  (DCM:MeOH 95:5).  $[\alpha]_D^{21.6} = -1.49$  (c 0.67, DCM).

**<sup>1</sup>H NMR** (500 MHz, CDCl<sub>3</sub>)  $\delta$  7.48 (s, 1H, triaz-*H*), 5.33 (d,  $J = 2.7$  Hz, 1H, H-4), 5.12 (dd,  $J = 10.5, 7.9$  Hz, 1H, H-2), 4.93 (dd,  $J = 10.5, 3.4$  Hz, 1H, H-3), 4.53 (dt,  $J = 14.4, 3.9$  Hz, 1H, *CH*-triaz), 4.49 – 4.42 (m, 1H, *CH'*-triaz), 4.40 (d,  $J = 7.9$  Hz, 1H, H-1), 4.19 (dt,  $J = 10.4, 4.1$  Hz, 1H, *OCH'*), 4.08 (ddd,  $J = 25.0, 11.3, 6.6$  Hz, 2H, H-6, H-6'), 3.93 – 3.85 (m, 2H, H-5, *OCH*), 3.11 (t,  $J = 6.8$  Hz, 2H, triaz-CH<sub>2</sub>), 3.03 – 2.97 (m, 2H, CH<sub>2</sub>CO), 2.80 (s,  $J = 12.2$  Hz, 4H, CH<sub>2</sub>CH<sub>2</sub>-succ), 2.11 (s, 3H, CH<sub>3</sub> of OAc), 2.00 (s, 3H, CH<sub>3</sub> of OAc), 1.92 (s, 3H, CH<sub>3</sub> of OAc), 1.91 (s, 3H, CH<sub>3</sub> of OAc).

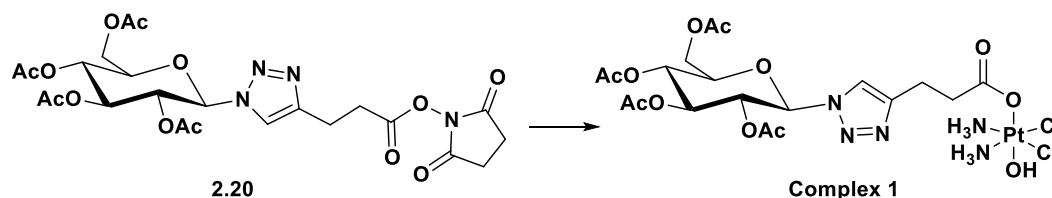
**<sup>13</sup>C NMR** (125 MHz, CDCl<sub>3</sub>)  $\delta$  170.5 (CO of OAc), 170.3 (CO of OAc), 170.2 (CO of OAc), 169.6 (CO of OAc), 169.2 (CO succ x2), 168.1 (CO), 145.0 (C-triaz), 123.0 (CH-triaz), 101.1 (C-1), 71.0 (C-5), 70.8 (C-3), 68.7 (C-2), 67.8 (*OCH*<sub>2</sub>), 67.0 (C-4), 61.3 (C-6), 50.1 (CH<sub>2</sub>-triaz), 30.9 (CH<sub>2</sub>CO), 25.7 (CH<sub>2</sub>CH<sub>2</sub>-succ), 21.0 (triaz-CH<sub>2</sub>), 20.82 (2xCH<sub>3</sub> of OAc), 20.81 (CH<sub>3</sub> of OAc), 20.7 (CH<sub>3</sub> of OAc).

**IR (ATR)** 2959.63, 1732.72, 1429.93, 1367.59, 1211.91, 1045.63, 915.63, 812.19, 731.78 cm<sup>-1</sup>.

**HR-MS (+):**  $m/z$  calcd for  $C_{25}H_{32}N_4O_{14} + H^+$   $[M+H]^+$  613.1915, found 613.1983. **HR-MS**

**(+):**  $m/z$  calcd for  $C_{25}H_{32}N_4O_{14} + H^+$   $[M+H]^+$  635.1915, found 635.1804.

***Cis,cis,trans*-[Pt<sup>IV</sup>(NH<sub>3</sub>)<sub>2</sub>(**2.18**)(OH)Cl<sub>2</sub>] (**1**)**



**2.20** (0.140 g, 0.246 mmol) was added to a suspension of oxoplatin (**2.30**) (0.086 g, 0.258 mmol, 1.05 equiv) in DMSO (5 mL) and stirred at 60°C for 16 hr. Residual oxoplatin was filtered through cotton wool and the solvent was removed by lyophilisation. The oily residue was dissolved in acetone and the product was precipitated with diethyl ether and collected by centrifugation. The yellow-white solid was washed with diethyl ether and dried *in vacuo* (0.083 g, 0.105 mmol, 43 %).

**<sup>1</sup>H NMR** (500 MHz, DMSO)  $\delta$  8.16 (s, 1H, triaz-CH), 6.25 (d,  $J = 8.8$  Hz, 1H, H-1), 5.96 (br. t, 6H, 2 x NH<sub>3</sub>), 5.60 – 5.49 (m, 2H, H-2,H-3), 5.12 (t,  $J = 9.6$  Hz, 1H, H-4), 4.34 (ddd,  $J = 10.0, 5.2, 2.2$  Hz, 1H, H-5), 4.13 (dd,  $J = 12.5, 5.4$  Hz, 1H, H-6), 4.08 – 4.03 (m, 1H, H-6'), 2.80 (t,  $J = 7.6$  Hz, 2H, triaz-CH<sub>2</sub>), 2.46 (t,  $J = 7.7$  Hz, 2H, CH<sub>2</sub>CO), 2.01 (s, 3H, CH<sub>3</sub> of OAc), 1.99 (s, 3H, CH<sub>3</sub> of OAc), 1.95 (s, 3H, CH<sub>3</sub> of OAc), 1.78 (s, 3H, CH<sub>3</sub> of OAc) ppm.

**<sup>13</sup>C NMR** (125 MHz, DMSO)  $\delta$  179.9 (COOPt), 170.3 (CO of OAc), 169.8 (CO of OAc), 169.6 (CO of OAc), 168.8 (CO of OAc), 147.3 (triaz-C), 121.4 (triaz-CH), 83.9 (C-1), 73.4 (C-5), 72.3 (C-3), 70.3 (C-2), 67.7 (H-4), 61.9 (C-6), 35.9 (CH<sub>2</sub>CO), 22.0 (triaz-CH<sub>2</sub>), 20.7 (CH<sub>3</sub> of OAc), 20.5 (CH<sub>3</sub> of OAc), 20.4 (CH<sub>3</sub> of OAc), 20.1 (CH<sub>3</sub> of OAc) ppm.

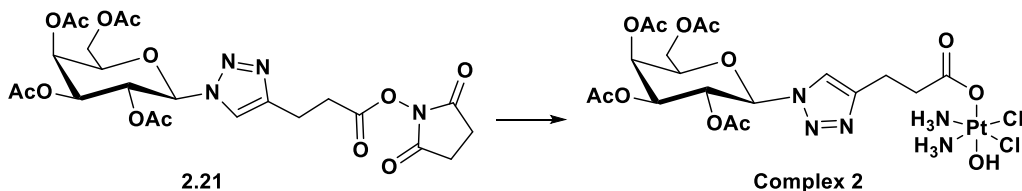
**<sup>195</sup>Pt{<sup>1</sup>H} NMR** (108 MHz, DMSO)  $\delta$  1041.75 ppm.

**IR (ATR)** 3212.46, 1746.40, 1627.32, 1367.46, 1215.23, 1035.51, 924.48, 822.96 cm<sup>-1</sup>.

**HR-MS (-):**  $m/z$  calcd for  $C_{19}H_{31}Cl_2N_5O_{12}Pt - H^-$   $[M-H]^-$  786.4640, found 786.0898.

**El. Anal.** Calcd. for  $C_{19}H_{31}Cl_2N_5O_{12}Pt$ : % C = 28.29; H = 3.97; N = 8.89; found: % C = 28.88; H = 4.18; N = 8.52.

***Cis,cis,trans*-[Pt<sup>IV</sup>(NH<sub>3</sub>)<sub>2</sub>(2.19)(OH)Cl<sub>2</sub>] (2)**



**2.21** (0.130 g, 0.228 mmol) was added to a suspension of oxoplatin (**2.30**) (0.080 g, 0.240 mmol, 1.05 equiv) in DMSO (5 mL) and stirred at 60°C for 16 hr. Residual oxoplatin was filtered through cotton wool and the solvent was removed by lyophilisation. The oily residue was dissolved in acetone and the product was precipitated with diethyl ether and collected by centrifugation. The yellow-white solid was washed with diethyl ether and dried *in vacuo* (Yield 0.065 g, 0.082 mmol, 36%).

**<sup>1</sup>H NMR** (500 MHz, DMSO)  $\delta$  8.12 (s, 1H, triaz-CH), 6.18 (d,  $J$  = 9.2 Hz, 1H, H-1), 5.95 (br. t., 6H, 2 x NH<sub>3</sub>), 5.58 (t,  $J$  = 10.1 Hz, 1H, H-2), 5.45 (dd,  $J$  = 10.1, 3.5 Hz, 1H, H-3), 5.40 (dd,  $J$  = 3.4, 1.0 Hz, 1H, H-4), 4.59 – 4.56 (t,  $J$  = 6.75 Hz, 1H, H-5), 4.13 (dd,  $J$  = 11.6, 5.1 Hz, 1H, H-6), 4.01 (dd,  $J$  = 11.5, 7.3 Hz, 1H, H-6'), 2.82 (t,  $J$  = 7.25 Hz, 2H, triaz-CH<sub>2</sub>), 2.47 – 2.46 (m, 2H, CH<sub>2</sub>CO), 2.19 (s, 3H, CH<sub>3</sub> of OAc), 1.99 (s, 3H, CH<sub>3</sub> of OAc), 1.94 (s, 3H, CH<sub>3</sub> of OAc), 1.82 (s, 3H, CH<sub>3</sub> of OAc) ppm.

**<sup>13</sup>C NMR** (125 MHz, DMSO)  $\delta$  179.7 (COOPt), 170.0 (CO of OAc), 169.9 (CO of OAc), 169.5 (CO of OAc), 168.6 (CO of OAc), 147.1 (triaz-C), 121.4 (triaz-CH), 84.2 (C-1), 72.8 (C-5), 70.4 (C-3), 67.8 (C-2), 67.3 (C-4), 61.6 (C-6), 36.0 (CH<sub>2</sub>CO), 21.8 (triaz-CH<sub>2</sub>), 20.5 (CH<sub>3</sub> of OAc), 20.5 (CH<sub>3</sub> of OAc), 20.3 (CH<sub>3</sub> of OAc), 20.0 (CH<sub>3</sub> of OAc) ppm.

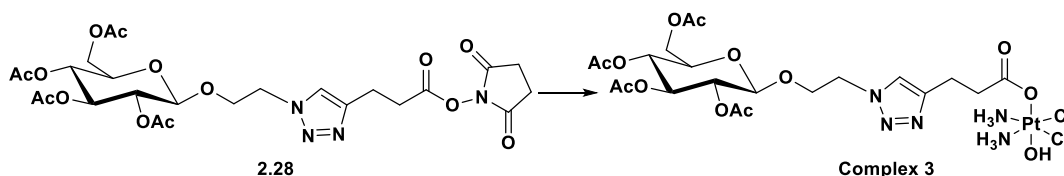
**<sup>195</sup>Pt{<sup>1</sup>H} NMR** (108 MHz, DMSO)  $\delta$  1044.64 ppm.

**IR (ATR)** 3207.92, 1746.25, 1625.63, 1368.09, 1214.56, 1050.93, 922.78 cm<sup>-1</sup>.

**HR-MS (+):**  $m/z$  calcd for  $C_{19}H_{31}Cl_2N_5O_{12}Pt + H^+$  [M+H]<sup>+</sup> 786.4640, found 786.1041.

**El. Anal.** Calcd. for  $C_{19}H_{31}Cl_2N_5O_{12}Pt$ : % C = 28.98; H = 3.97; N = 8.89; found: % C = 28.48; H = 4.18; N = 8.52.

***Cis,cis,trans*-[Pt<sup>IV</sup>(NH<sub>3</sub>)<sub>2</sub>(2.26)(OH)Cl<sub>2</sub>] (3)**



**2.28** (0.126 g, 0.205 mmol) was added to a suspension of oxoplatin (**2.30**) (0.072 g, 0.215 mmol, 1.05 equiv) in DMSO (5 mL) and stirred at 60°C for 16 hr. Residual oxoplatin was filtered through cotton wool and the solvent was removed by lyophilisation. The oily residue was dissolved in acetone and the product was precipitated with diethyl ether and collected by centrifugation. The yellow-white solid was washed with diethyl ether and dried *in vacuo* (0.050 g, 0.060 mmol, 29%).

**<sup>1</sup>H NMR** (500 MHz, CDCl<sub>3</sub>)  $\delta$  7.76 (s, 1H, triaz-CH), 5.87 (br t, 6H, 2x NH<sub>3</sub>), 5.23 (t,  $J$  = 9.6 Hz, 1H, H-3), 4.89 (t,  $J$  = 9.7 Hz, 1H, H-4), 4.81 (d,  $J$  = 8.0 Hz, 1H, H-1), 4.75 – 4.69 (m, 1H, H-2), 4.53 – 4.40 (m, 2H, CH<sub>2</sub>-triaz), 4.18 (dd,  $J$  = 12.3, 5.0 Hz, 1H, H-6), 4.08 (dt,  $J$  = 8.9, 4.1 Hz, 1H, OCH), 4.02 (dd,  $J$  = 12.2, 2.1 Hz, 1H, H-6'), 3.98 (ddd,  $J$  = 9.9, 4.9, 2.4 Hz, 1H, H-5), 3.89 (ddd,  $J$  = 11.4, 7.8, 4.0 Hz, 1H, OCH'), 2.81 – 2.77 (m, 2H, triaz-CH<sub>2</sub>), 2.48 – 2.43 (m, 2H, CH<sub>2</sub>CO), 2.02 (s, 3H, CH<sub>3</sub> of OAc), 1.97 (s, 3H, CH<sub>3</sub> of OAc), 1.92 (s, 3H, CH<sub>3</sub> of OAc), 1.88 (s, 3H, CH<sub>3</sub> of OAc) ppm.

**<sup>13</sup>C NMR** (125 MHz, CDCl<sub>3</sub>)  $\delta$  179.9 (COOPt), 170.1 (CO of OAc), 169.5 (CO of OAc), 169.3 (CO of OAc), 169.0 (CO of OAc), 146.1 (triaz-C), 122.5 (triaz-CH), 99.2 (C-1), 71.9 (C-3), 70.64 (C-2), 70.59 (C-5), 68.1 (C-4), 67.5 (OCH<sub>2</sub>), 61.6 (C-6), 49.1 (CH<sub>2</sub>-triaz), 36.2 (CH<sub>2</sub>CO), 22.0 (triaz-CH<sub>2</sub>), 20.5 (CH<sub>3</sub> of OAc), 20.4 (CH<sub>3</sub> of OAc), 20.29 (CH<sub>3</sub> of OAc), 20.27 (CH<sub>3</sub> of OAc) ppm.

**<sup>195</sup>Pt{<sup>1</sup>H} NMR** (108 MHz, DMSO)  $\delta$  1047.09 ppm.

**IR (ATR)** 3214.82, 1745.13, 1626.73, 1430.32, 1365.92, 1217.35, 1034.85, 908.82 cm<sup>-1</sup>.

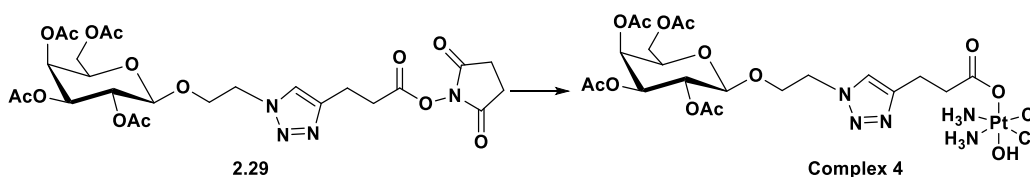
1.

**HR-MS (+):**  $m/z$  calcd for  $C_{21}H_{35}Cl_2N_5O_{13}Pt + H^+$   $[M+H]^+$  832.5170, found 832.1316.

**HR-MS (+):**  $m/z$  calcd for  $C_{21}H_{35}Cl_2N_5O_{13}Pt + Na^+$   $[M+H]^+$  854.5170, found 854.1134.

**El. Anal.** Calcd. for  $C_{21}H_{35}Cl_2N_5O_{13}Pt$ : % C = 30.33; H = 4.24; N = 8.42; found: % C = 30.79; H = 4.61; N = 8.90.

***Cis,cis,trans*-[Pt<sup>IV</sup>(NH<sub>3</sub>)<sub>2</sub>(2.27)(OH)Cl<sub>2</sub>] (4)**



**2.29** (0.133 g, 0.217 mmol) was added to a suspension of oxoplatin (**2.30**) (0.076 g, 0.227 mmol, 1.05 equiv) in DMSO (6 mL) and stirred at 60°C for 16 hr. Residual oxoplatin was filtered through cotton wool and the solvent was removed by lyophilisation. The oily residue was dissolved in acetone and the product was precipitated with diethyl ether and collected by centrifugation. The yellow-white solid was washed with diethyl ether and dried *in vacuo* (0.070 g, 0.084 mmol, 38%).

**<sup>1</sup>H NMR** (500 MHz, DMSO)  $\delta$  7.75 (s, 1H, triaz-CH), 5.82 (br t, 6H, 2x NH<sub>3</sub>), 5.24 (dd,  $J$  = 3.5, 0.8 Hz, 1H, H-4), 5.12 (dd,  $J$  = 10.4, 3.6 Hz, 1H, H-3), 4.88 (dd,  $J$  = 10.4, 8.0 Hz, 1H, H-2), 4.71 (d,  $J$  = 8.0 Hz, 1H, H-1), 4.52 – 4.40 (m, 2H, CH<sub>2</sub>-triaz), 4.19 (dd,  $J$  = 7.2, 6.3 Hz, 1H, H-5), 4.12 – 4.00 (m, 3H, H-6, H-6', OCH), 3.93 – 3.86 (m, 1H, OCH'), 2.82 – 2.78 (t,  $J$  = 7.25 Hz, 2H, triaz-CH<sub>2</sub>), 2.47 (dd,  $J$  = 8.6, 6.9 Hz, 2H, CH<sub>2</sub>CO), 2.11 (s, 3H, CH<sub>3</sub> of OAc), 2.01 (s, 3H, CH<sub>3</sub> of OAc), 1.90 (s, 3H, CH<sub>3</sub> of OAc), 1.89 (s, 3H, CH<sub>3</sub> of OAc) ppm.

**<sup>13</sup>C NMR** (125 MHz, DMSO)  $\delta$  179.9 (COOPt), 169.93 (CO of OAc), 169.91 (CO of OAc), 169.5 (CO of OAc), 169.0 (CO of OAc), 146.1 (triaz-C), 122.4 (triaz-CH), 99.7 (C-1), 70.1 (C-5), 69.9 (C-3), 68.3 (C-2), 67.30 (C-4), 67.26 (OCH<sub>2</sub>), 61.2 (C-6), 49.09 (CH<sub>2</sub>-triaz), 36.1 (CH<sub>2</sub>CO), 22.0 (triaz-CH<sub>2</sub>), 20.5 (CH<sub>3</sub> of OAc), 20.4 (CH<sub>3</sub> of OAc), 20.3 (2x CH<sub>3</sub> of OAc) ppm.

**<sup>195</sup>Pt{<sup>1</sup>H} NMR** (108 MHz, DMSO)  $\delta$  1047.15 ppm.

**IR (ATR)** 3214.92, 1740.41, 1631.39, 1429.52, 1367.30, 1217.81, 1173.03, 1045.52, 952.53  $\text{cm}^{-1}$ .

**HR-MS (+):** m/z calcd for  $\text{C}_{21}\text{H}_{35}\text{Cl}_2\text{N}_5\text{O}_{13}\text{Pt} + \text{H}^+$   $[\text{M}+\text{H}]^+$  832.5170, found 854.1139.

**HR-MS (+):** m/z calcd for  $\text{C}_{21}\text{H}_{35}\text{Cl}_2\text{N}_5\text{O}_{13}\text{Pt} + \text{H}^+$   $[\text{M}+\text{Na}]^+$  854.5170, found 854.1315.

**El. Anal.** Calcd. for  $\text{C}_{21}\text{H}_{35}\text{Cl}_2\text{N}_5\text{O}_{13}\text{Pt}$ : % C = 30.33; H = 4.24; N = 8.42; found: % C = 29.98; H = 4.69; N = 8.01.



# **Chapter 3: C1 Platinum(IV) Free Glycoconjugates**

## 3.1 Introduction

### 3.1.1 Free (deprotected) carbohydrates as anticancer agents

In **Chapters 1** and **2**, we have shown that protected sugars are not well suited for transport into the cell through glucose transporters and this is the reason why, of all the compounds tested in the presence of GLUT inhibitors, many complexes with acetylated sugars showed little dependence on GLUTs for anticancer activity [89]. Other factors such as lipophilicity or steric hindrance may be the cause for this GLUT-independent uptake, however, to effectively target glucose transporters, it is seemingly imperative to use deprotected sugars as targeting vectors [89].

In 2017, the group of Wang produced examples of the first deprotected Pt(IV) glycoconjugates (**Figure 3.1**), with the aim of targeting GLUTs [265]. In this pioneering work, oxaliplatin derivatives were functionalised with glucose, galactose and mannose moieties (**3.4 – 3.8**) as well as glycuronic acid derivatives (**3.1 – 3.3**). Secondly, hexadecanoic acid was coupled to the second free axial hydroxyl of the Pt(IV) core with the goal of improving drug uptake through interaction between hexadecanoic acid and human serum albumin (HSA) [266]. As a result, Wang *et al.* describe these complexes as dual-targeted glycosylated Pt(IV) complexes. Interestingly, complexes functionalised in the C1 position (**3.4 – 3.8**) show greater cytotoxicity against the cell lines tested than their C6 counterparts (**3.1 – 3.3**). This correlates to what Lippard *et al.* observed from their study of the effect glucose positional isomers have on anticancer activity, where it was found that C1 and C2 were the more viable substitution positions [135]. Glucose (**3.4**) and mannose (**3.7, 3.8**) complexes were found to accumulate readily inside the cell; mannose is a C2 epimer of glucose where the hydroxyl group is axial rather than equatorial. As discussed in **Section 1.3.2**, the C2 position of the hexose ring does not interact in the binding site of GLUT1, suggesting that mannose could be used as a substitute for glucose in complexes of this nature.

Experiments to determine the dependency of complexes **3.1 – 3.8** on GLUTs were also conducted. The GLUT inhibitor, phloretin was co-incubated with Complex **3.4** against the breast cancer cell line, MCF-7. The group observed a slight decrease in

activity when **3.4** was incubated with the inhibitor ( $IC_{50} = 0.57 \mu\text{M}$ ) *versus* without the inhibitor ( $IC_{50} = 0.19 \mu\text{M}$ ). This small difference could indicate that GLUTs participate in the transport of complexes across the cell membrane. However, due to the presence of the long lipophilic linker, it cannot be said for certain that GLUTs mediate a large portion of drug uptake. In the case of the C6 functionalised complexes (**3.1 – 3.3**) it was clear that the presence of a GLUT inhibitor did not affect the activity of these complexes. A conclusion which can be drawn is that the interaction of the hexadecyl ligand with HSA, in tandem with the increased lipophilicity allows access through the cell membrane. In fact, the presence of this ligand may also block the uptake of the drug *via* GLUTs as described in **Section 1.4.1**.

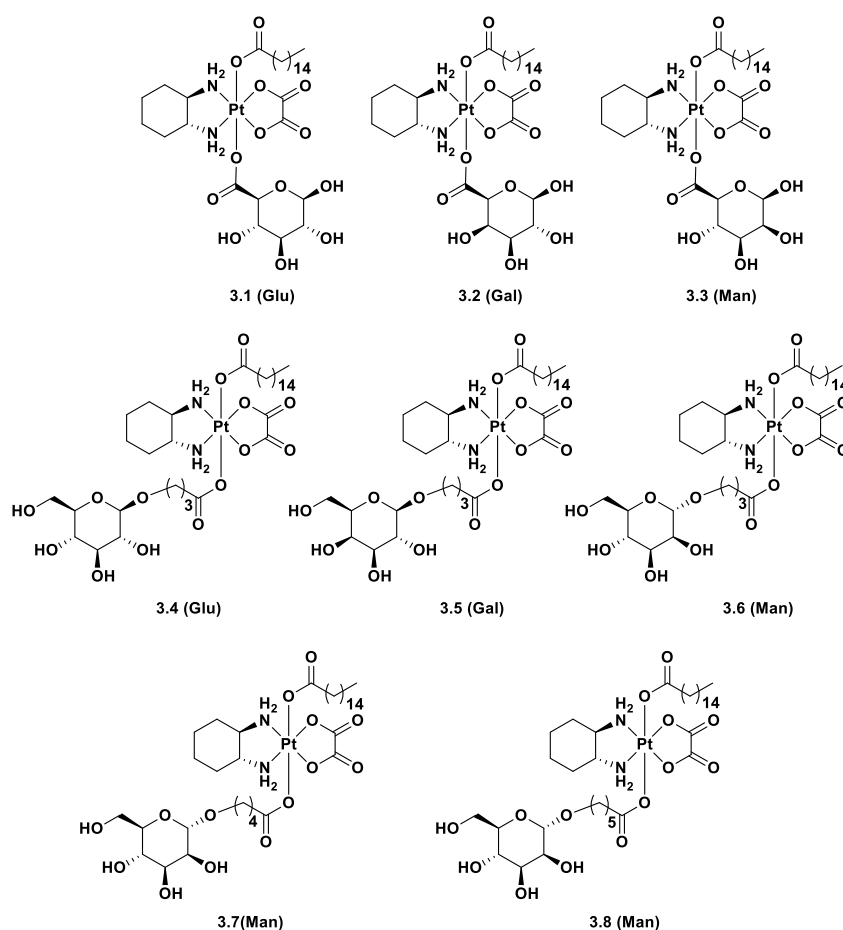


**Figure 3.1:** Structures of asymmetric bis-Pt(IV) glycoconjugates with glycuronic acid functionalised complexes **3.1 – 3.3** and glucose, galactose and mannose functionalised complexes **3.4 – 3.8**, containing hexadecanoic acid and varying aliphatic linkers between the carbohydrates [265].

Further discussion on relevant topics for this chapter have been made in **Chapter 1** and **2**, including other examples of the benefits of using deprotected sugars as targeting vectors compared to protected sugars.

### 3.2 Chapter Objective

This chapter discusses the synthesis, characterisation, physiological stability of free sugar Pt(IV) glycoconjugates, analogues of the complexes synthesised in **Chapter 2**, and their potential as anticancer agents (**Figure 3.2**). These octahedral Pt(IV) complexes are based on a cisplatin scaffold and are functionalised in the axial position with free glucose and galactose derivatives conjugated to the metallic centre *via* linkers of different length and chemical structure using CuAAC “click” reaction. These complexes are characterised using several spectroscopic techniques, including multinuclear 1D and 2D NMR ( $^1\text{H}$ ,  $^{13}\text{C}$ ,  $^{195}\text{Pt}$ , COSY, HSQC, HMBC), IR, HR-MS, Elemental analysis and cyclic voltammetry.

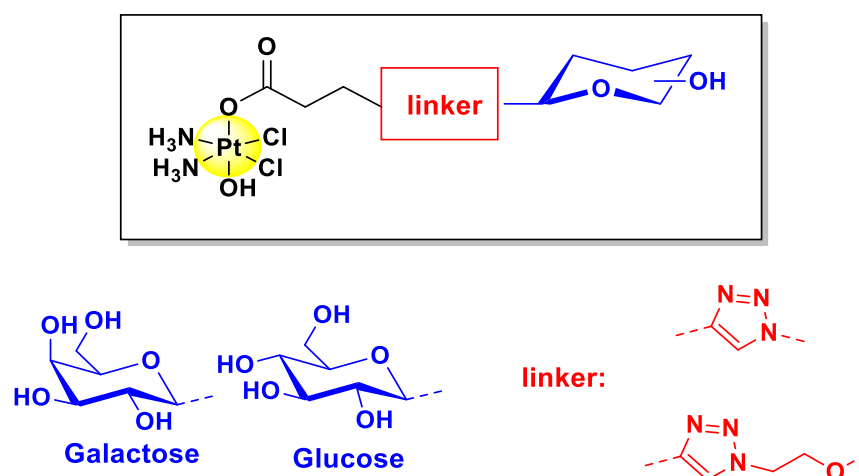


**Figure 3.2:** General structure for the novel Pt(IV) complexes based on the cisplatin scaffold and functionalised with glucose and galactose.

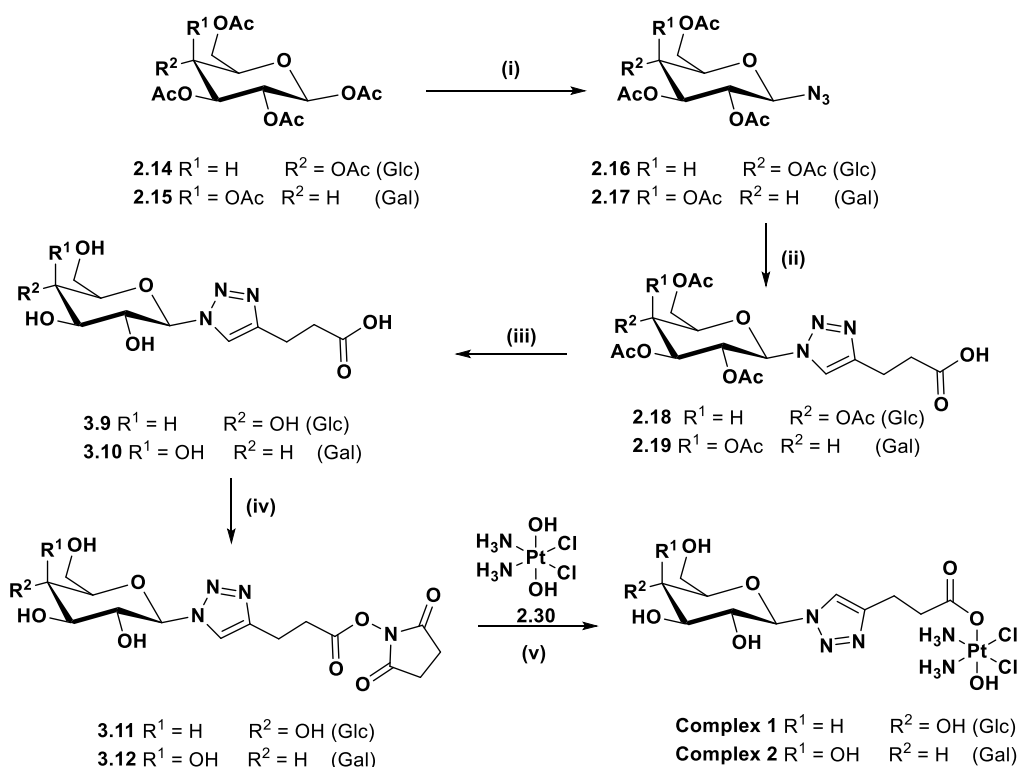
To synthesise this series of C1-free Pt(IV) glycoconjugates, our initial approach was to remove the acetyl protecting groups in complexes **1 – 4** reported in **Chapter 2** and form the free sugar derivatives. Unfortunately, this method was unsuccessful, and an alternative synthetic route was required. This chapter comprises of the reaction optimisation for the preparation of the free sugar NHS esters, and the following

coordination of these esters to the Pt(IV) scaffold. The reduction properties of the complexes was also analysed *via* NMR spectroscopy using sodium ascorbate (to mimic the cellular environment) and by cyclic voltammetry. The results of this chapter have been published in the International Journal of Molecular Science (doi: 10.3390/ijms24076028) [267].

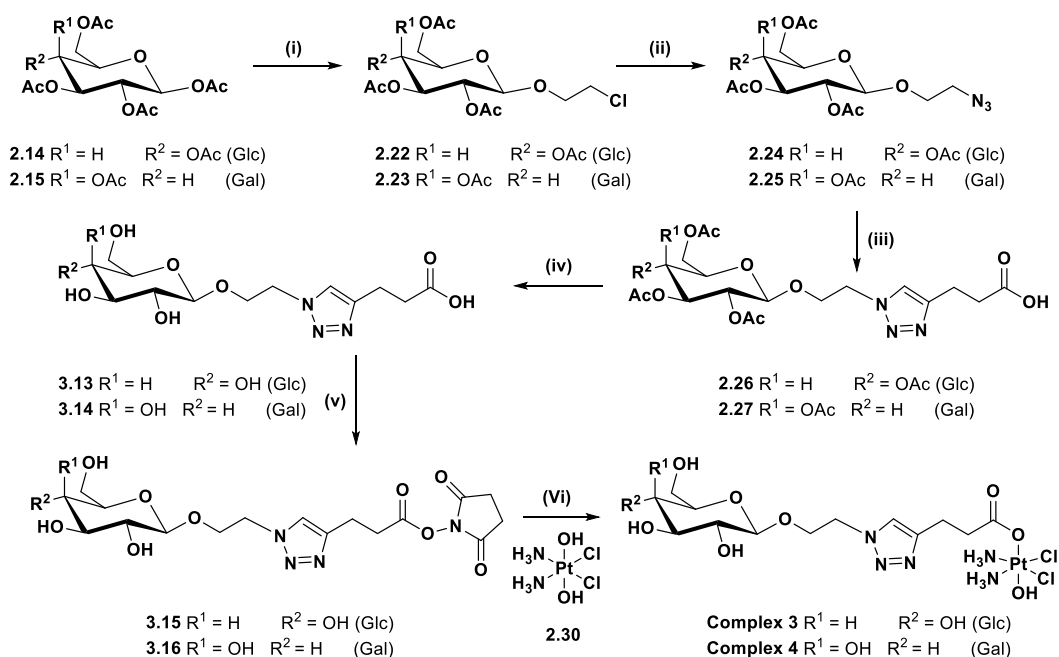
### 3.3 Results and Discussion

#### 3.3.1 Synthesis of free carbohydrate Pt(IV) glycoconjugates

**Schemes 3.1** (short chain linker) and **3.2** (long chain linker) show the synthetic routes for the preparation of the complexes **1 – 4**. Steps (i) – (ii) (**Scheme 3.1**) and (i) – (iii) (**Scheme 3.2**) were already discussed in detail in **Chapter 2**. The reactions after these steps consist of base-catalysed hydrolysis to deacetylate compounds (**2.18**, **2.19**) and (**2.26**, **2.27**); esterification with TSTU to form the NHS active esters (**3.11**, **3.12**, **3.15** and **3.16**) and finally a transesterification to form free sugar complexes **1 – 4**.



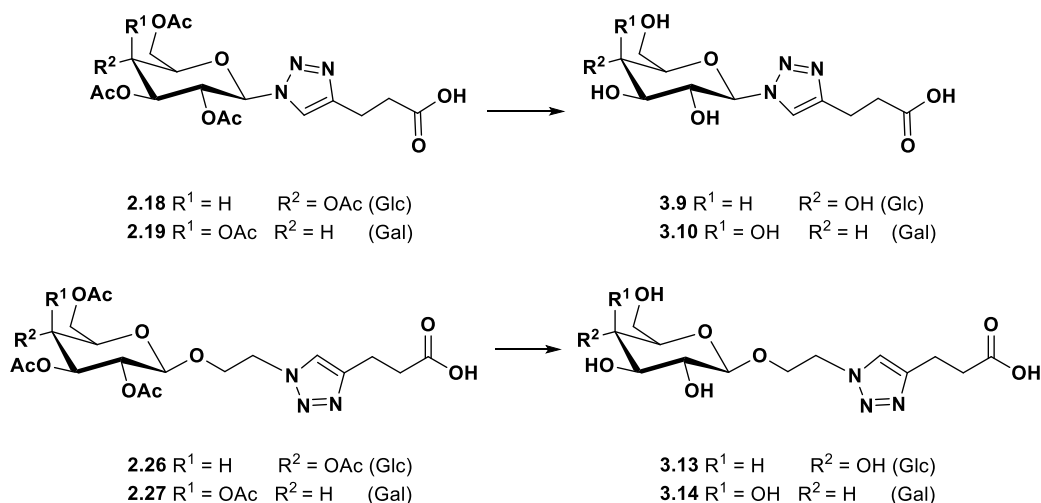
**Scheme 3.1:** Synthetic pathway for complexes **1** and **2**: (i) TMSN<sub>3</sub>, SnCl<sub>4</sub>, DCM, rt, 16 h, 94% (**2.16**), 97% (**2.17**); (ii) 4-pentynoic acid, CuSO<sub>4</sub>, sodium ascorbate, *t*-BuOH, THF, H<sub>2</sub>O, rt, 16 h, 64% (**2.18**), 74% (**2.19**); (iii) TEA, MeOH, H<sub>2</sub>O, 45°C, 16 h, 95% (**3.9**), 97% (**3.10**); (iv) TSTU, TEA, DMF, rt, 20min, 68% (**3.11**), 68% (**3.12**); (v) DMSO, 40°C, 48 h, 59% (**1**), 35% (**2**).



**Scheme 3.2:** Synthetic pathway for complexes **3** and **4**: (i) 2-Chloroethanol,  $\text{BF}_3 \cdot \text{OEt}_2$ , 3 Å MS, 0°C to rt, DCM, 16 h, 22% (**2.22**), 25% (**2.23**); (ii)  $\text{NaN}_3$ , DMF, 80°C, 16 h, 62% (**2.24**), 60% (**2.25**); (iii)  $\text{CuSO}_4$ , sodium ascorbate, *t*-BuOH, THF,  $\text{H}_2\text{O}$ , rt, 16 h, 44% (**2.26**), 47% (**2.27**); (iv) TEA, MeOH,  $\text{H}_2\text{O}$ , 45°C, 16 h, 86% (**3.13**), 96% (**3.14**); (v) TSTU, TEA, DMF, 20 mins, rt, 60% (**3.15**), 75% (**3.16**); (vi) DMSO, 40°C, 48 h, 47% (**3**), 61% (**4**).

### 3.3.2 Synthesis of free sugar ligands (**3.9**, **3.10**, **3.13**, and **3.14**)

The ligands containing the free sugars derivatives of glucose (**3.9** and **3.13**) and galactose (**3.10** and **3.14**) were synthesised from their acetylated analogues (**2.18**, **2.19**, **2.26** and **2.27**) through the removal of the acetyl protecting groups using catalytic triethylamine in aqueous methanol, as shown in **Scheme 3.3** [268].



**Scheme 3.3:** Deacetylation of acetylated ligands using  $\text{Net}_3$ , MeOH, and  $\text{H}_2\text{O}$ , 45°C, 16 h, 95% (**3.9**), 97% (**3.10**), 86% (**3.13**), 96% (**3.14**).

These ligands were characterised using  $^1\text{H}$  NMR,  $^{13}\text{C}$  NMR, COSY, HSQC, and HMBC 2D NMR. These compounds are water-soluble, and the NMR (**Figure 3.3**) was obtained in  $\text{D}_2\text{O}$ . Interestingly, the anomeric proton at  $\delta = 5.67$  (red spot) appears as one doublet due to the coupling with the proton in the C2 position ( $^3J = 9.2$  Hz). The triazole proton (purple spot) signal is at  $\delta = 8.0$  ppm. The quartet at  $\delta = 3.2$  ppm belongs to the triethylammonium salt, the presence of which did not interfere with further reactions.

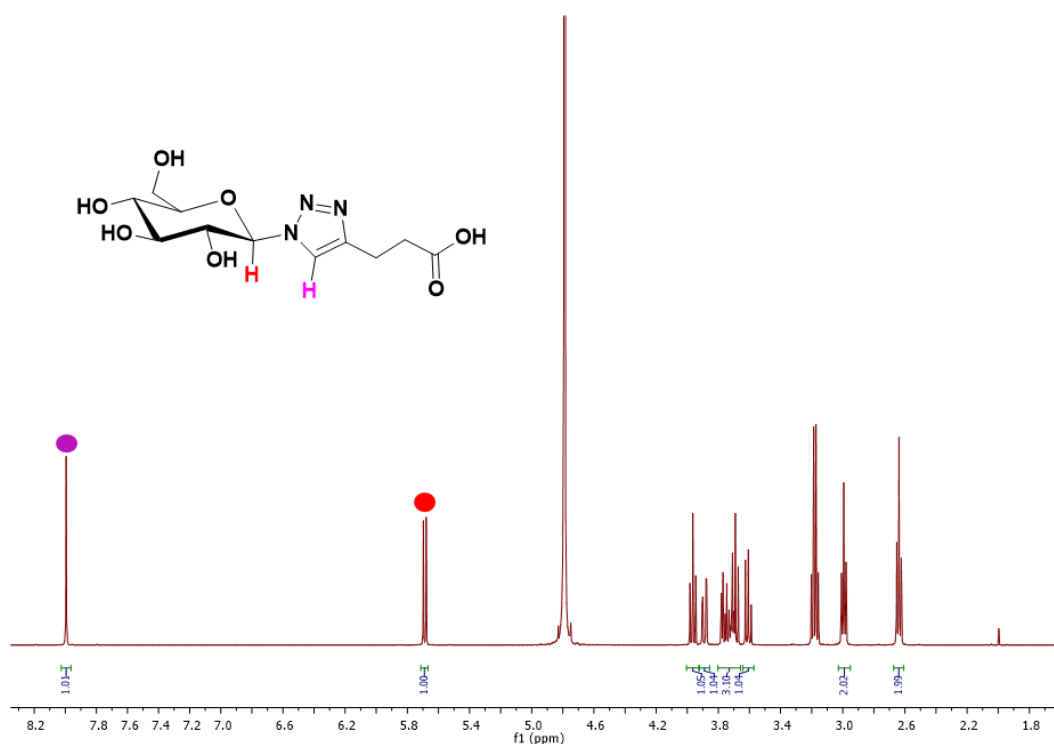


**Figure 3.3:**  $^1\text{H}$  NMR spectrum of free ligand (**3.9**) in  $\text{D}_2\text{O}$ , with important signals emphasised.

The most important method for determining if the correct product has been formed, is the comparison between the acetylated ligand and the free deprotected ligand using  $^1\text{H}$  NMR (**Figure 3.4**). The free deprotected ligand (**3.9**) will lack the four singlets, found in the acetylated ligand (**2.18**), which correspond to the four methyl groups of the acetyl protecting groups.

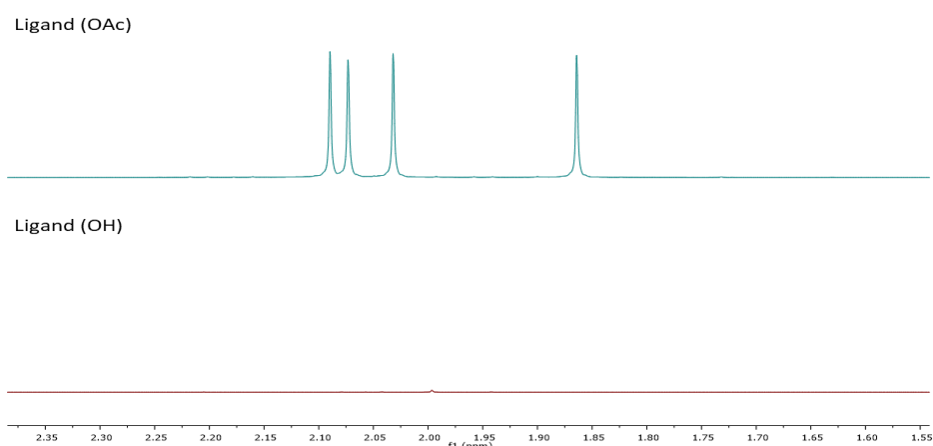
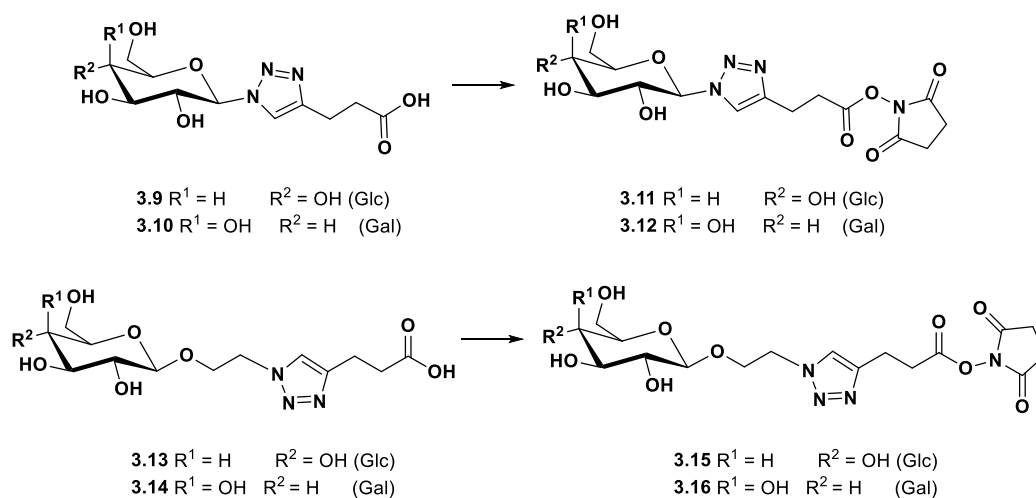


**Figure 3.4:** Comparison of acetylated ligand (**2.18**) versus free ligand (**3.9**).

### 3.3.3 Synthesis of free sugar NHS esters (**3.11**, **3.12**, **3.15**, and **3.16**)

The NHS esters (**3.11**, **3.12**, **3.15** and **3.16**) were synthesised from their corresponding carboxylic acids (**3.9**, **3.10**, **3.13** and **3.14**). This reaction required extensive optimisation of a variety of parameters including coupling reagent, base, solvent and reaction duration (**Table 3.1**). In addition, the reaction conditions had to be finely tuned to avoid competing reactions of the nucleophilic hydroxyls of the free sugars. Finally, using the coupling reagent *N,N,N',N'*-Tetramethyl-*O*-(*N*-succinimidyl)uronium tetrafluoroborate (TSTU) (**Scheme 3.4**), a method was achieved to yield free sugar NHS esters in relatively high yields with high purity, suitable for further reactions.



**Scheme 3.4:** Synthesis of free sugar NHS esters using TSTU, NEt<sub>3</sub>, and DMF, under N<sub>2</sub> for 20 mins, 68% (**3.11**), 68% (**3.12**), 60% (**3.15**), 75% (**3.16**).



**Table 3.1:** Reaction optimisation for the synthesis of free sugar NHS esters.

| Reaction Attempt | Solvent      | Reaction Time (Hr) | Coupling Agent +(Equiv.) | Base +(Equiv.)       | NHS (Equiv.) | Additive  | Yield (%)   |
|------------------|--------------|--------------------|--------------------------|----------------------|--------------|-----------|-------------|
| 1                | DMF          | 3                  | DCC (1.5)                | -                    | 1.25         | -         | 10          |
| 2                | DMF          | 16                 | DCC (1.5)                | -                    | 1.25         | -         | No reaction |
| 3                | DMF          | 16                 | DCC (2)                  | -                    | 2            | -         | No reaction |
| 4                | DMF/THF      | 16                 | DCC (1.5)                | -                    | 1.25         | -         | No reaction |
| 5                | DMF          | 3                  | DCC (1.5)                | -                    | 1.25         | 3Å Sieves | No reaction |
| 6                | DMF          | 16                 | DCC (5)                  | -                    | 5            | 3Å Sieves | No reaction |
| 7                | DMF          | 16                 | DCC (5)                  | NEt <sub>3</sub> (3) | 5            | -         | No reaction |
| 8                | DMF          | 16                 | DIC (1.5)                | NEt <sub>3</sub> (3) | 1.25         | -         | No reaction |
| 9                | DMF          | 16                 | DIC (1.5)                | NEt <sub>3</sub> (3) | 5            | 3Å Sieves | No reaction |
| 10               | DMF          | 5                  | IBCF (5)                 | NEt <sub>3</sub> (3) | 5            | 3Å Sieves | No reaction |
| 11               | Pyridine     | 3                  | DCC (1.5)                | -                    | 1.25         | 3Å Sieves | No reaction |
| 12               | DMF(min)/THF | 3                  | DCC (1)                  | -                    | 1            | -         | 14          |
| 13               | DMF(min)/THF | 3                  | DCC (1.5)                | -                    | 1.25         | -         | 13          |
| 14               | DMF(min)/THF | 7                  | DCC (1.5)                | -                    | 1.25         | -         | 8           |
| 15               | DMF(min)/THF | 16                 | DCC (1.5)                | -                    | 1.25         | -         | 2           |

The coupling reagent used ideally would form water-insoluble byproducts, this is imperative due to the water-solubility of the ligand as a whole and the fact that purification through column chromatography would be impossible (due to the high polarity of the carbohydrate moiety). Hence, the coupling reagent investigated was DCC as the reaction by-product (dicyclohexylurea) tends to precipitate out of the reaction solvent and can be removed by filtration. Reactions with DIC (entries 8 and 9) and *iso*-butyl chloroformate (IBCF, entry 10) were also attempted. Short reaction

times were also vital. Through NMR spectroscopy analysis of the different reaction crudes, it was clear that longer reaction times caused degradation of the product. This was overcome partially with the use of solvents other than DMF, but complete conversion still was not achieved. Entries 1, 12 and 13 were all carried out over 3 hour reaction time, using DCC as the coupling reagent and NHS with molar equivalents of 1.25, 1, and 1.25 respectively. Entries 12 and 13 produced crude products with similar conversion, however, entry 1 produced much less ester. Using the minimum amount of DMF for solubility and diluting with dry THF helped to improve the yield.

In an effort to reduce reaction times with the hope of improving conversion rates, the coupling agent TSTU (**Figure 3.5**) was used. TSTU, a uronium-based coupling reagent which can be used in aqueous media, is typically used for amide coupling reactions as it forms a transient NHS ester prior to amine nucleophilic attack [269].

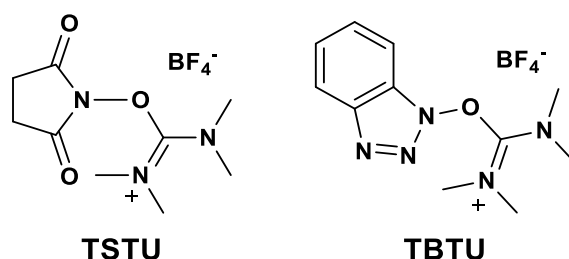


**Figure 3.5:** Structures of uronium-based coupling agents TSTU and TBTU.

Much like 2-(1H-Benzotriazole-1-yl)-1,1,3,3-tetramethylaminium tetrafluoroborate (TBTU), treatment of the carboxylic acid with a base in the presence of the coupling reagent leads to the formation of a good leaving group. Upon reaction with NHS from TSTU or hydroxybenzotriazole (HOBT) from TBTU, yields the respective active ester product (**Figure 3.6**). For typical coupling reactions using TSTU or TBTU, this activation occurs within the first 20 minutes and then an amine is added to form amide bonds [270]. For our purposes however, it was only necessary to do the initial activation step and isolate the resulting ester. Through evaporation of the reaction solvent and treatment with DCM and acetonitrile, excess NHS, coupling reagent and reaction by-products were removed. The final NHS esters were used without further

purification with moderate yields of 68% (**3.11**), 68% (**3.12**), 60% (**3.15**), and 75% (**3.16**).

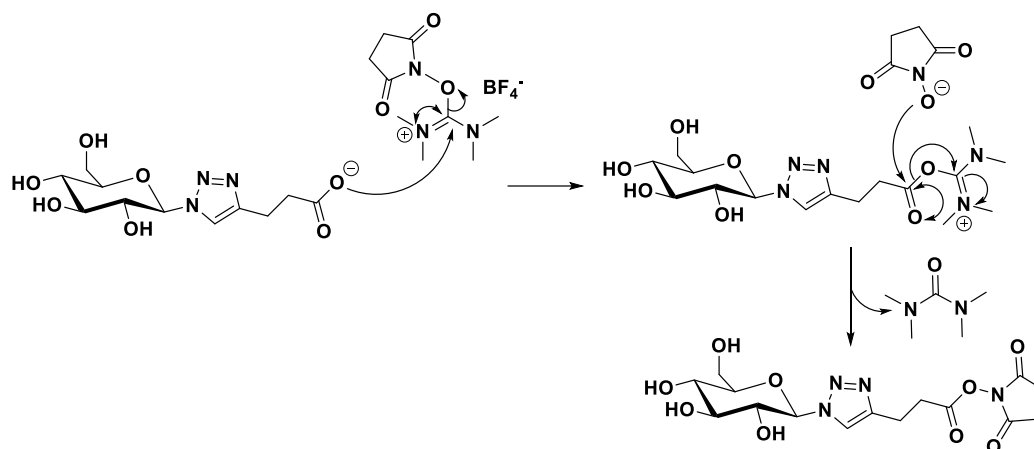


**Figure 3.6:** Reaction mechanism for the synthesis of active NHS esters **3.11** using TSTU.

These compounds were characterised using 1D and 2D NMR, IR and HR-MS. **Figure 3.7** shows the  $^1\text{H}$  NMR spectrum in  $\text{DMSO-d}_6$  of compound **3.11** with the characteristic peaks highlighted. The protons of the free hydroxyl groups of the sugar moiety are seen at  $\delta = 5.32, 5.26, 5.14$  and  $4.62$  ppm, confirmed by the fact that these protons do not show coupling to any carbon on the HSQC spectrum (Appendix, pg. 291). It is also notable that the signals highlighted in red, green and purple are all doublets whereas the blue highlighted signal is a broad triplet. This is due to the coupling with the  $\text{CH}_2$  adjacent to the hydroxyl group. The presence of the NHS protons with an integral of four at  $\delta = 2.8$  ppm ( $\text{H}_5$ ) also confirms the formation of **3.11**.

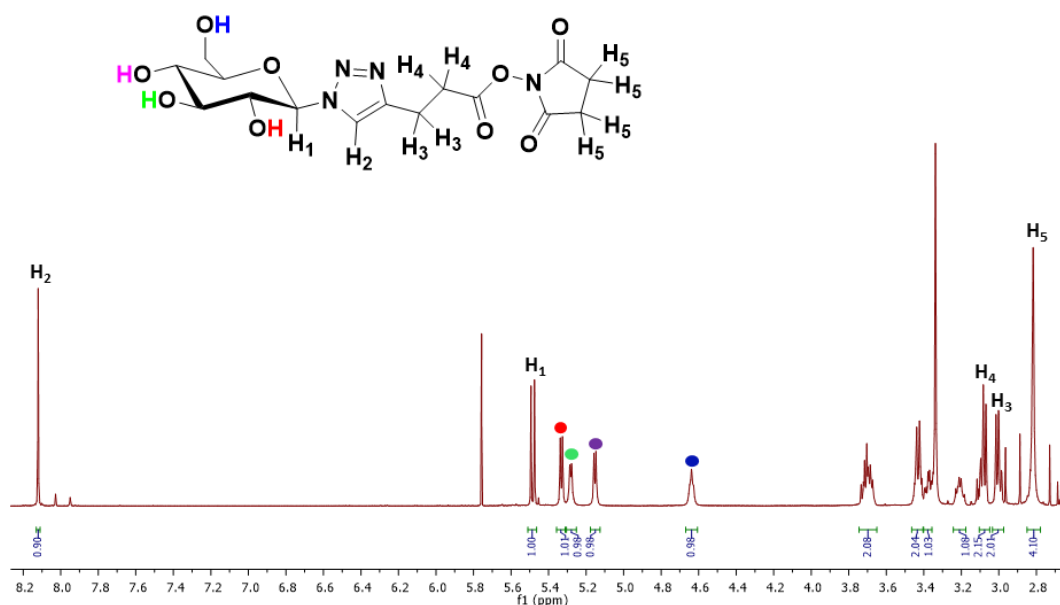
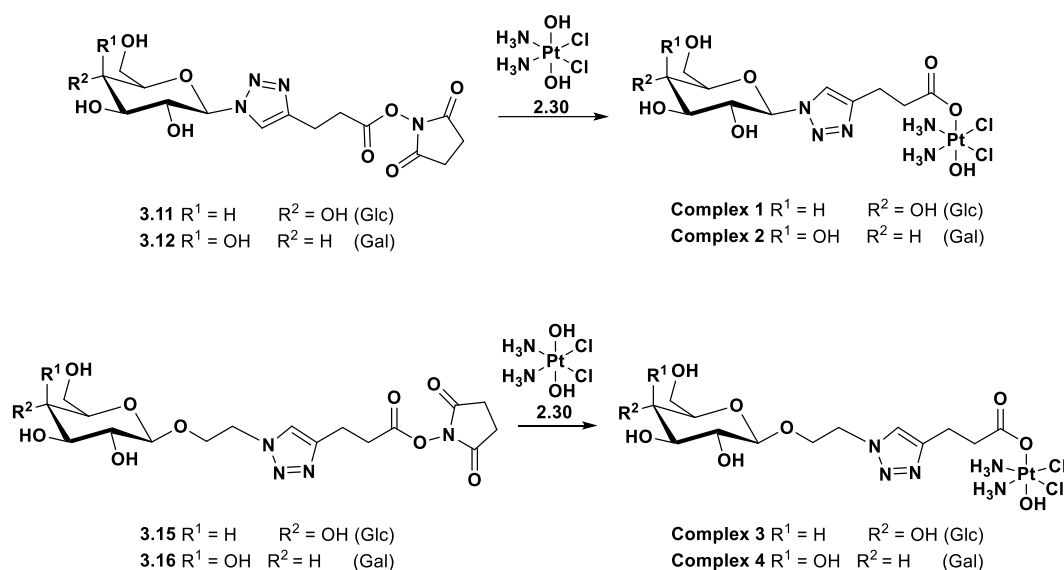


**Figure 3.7:**  $^1\text{H}$  NMR spectrum of **3.11** in  $\text{DMSO-d}_6$  with characteristic peaks highlighted.

### 3.3.4 Synthesis of free sugar Pt(IV) complexes (1 – 4)

Much like the complexes formed in **Chapter 2**, the reaction of the active esters (**3.11**, **3.12**, **3.15** and **3.16**) in DMSO with a slight excess of oxoplatin yields the free sugar derivatives of the complexes previously developed (**Scheme 3.5**). The difficulty with these derivatives, however, is that when heated at the same temperature of  $60^\circ\text{C}$  as their acetylated counterparts, degradation of the ester occurs with the resulting product containing a mixture of free ligand and a small portion of complex. This mixture proved impossible to be separated with trituration or column chromatography due to the similar solubility and the high polarity of both the complexes and the ligands. Optimisation of this reaction was required, in which parameters such as temperature, reaction time and dropwise addition of a solution of the ligand were important for reaction progression.



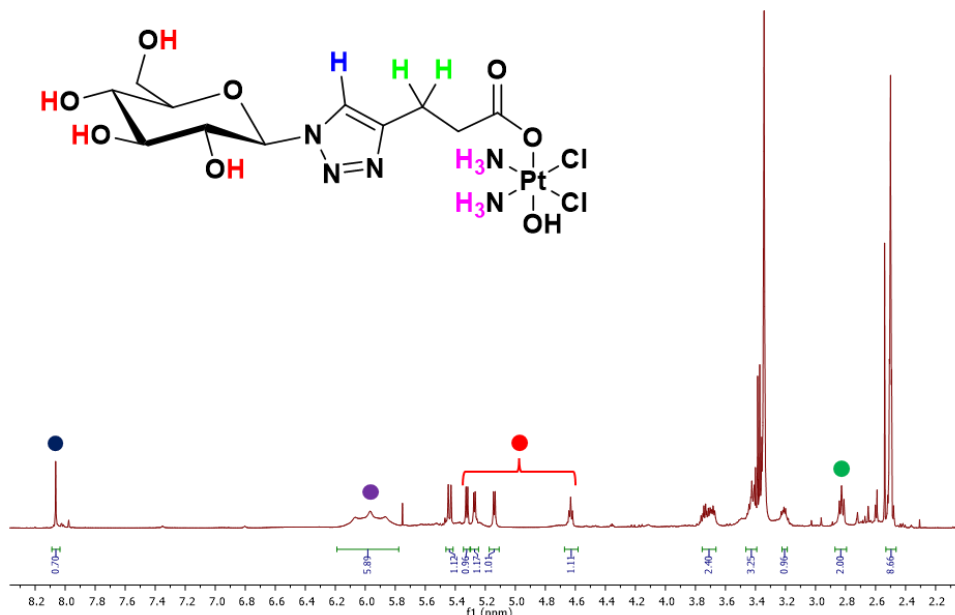
**Scheme 3.5:** Synthesis of free sugar Pt(IV) complexes using oxoplatin and NHS esters in DMSO.

**Table 3.2** shows the different attempts to synthesise complexes **1 – 4** while changing the previously stated variables. The most important parameter was seemingly the reaction temperature. It was seen through <sup>1</sup>H NMR that a 5°C change in temperature resulted in a large difference in purity. The importance of the reaction temperature on the purity of the resulting Complex was observed and from entry 5 onward, the majority of reactions were carried out at 40°C. Another parameter that could influence reaction progression was the use of dried DMSO, even if this proved to have a negligible effect while the final two parameters (dropwise addition and reaction time) had a much greater effect. A solution of the ester in DMSO was added dropwise to a suspension of oxoplatin in DMSO. The idea here was to add the ester to the complex slowly so it would be in a much higher excess of platinum, pushing the reaction forward and avoiding the degradation of the starting material. Once this method was attempted, the quality of the crude product was vastly improved compared to the attempts where the ester was added initially in its entirety. Finally, attempt 6 in the table below shows a reaction time of 72 hours. Reacting for three days at 40°C with dropwise addition of the ester produced a pure product. Allowing the reaction to proceed for only 48 hours yielded the pure complex and the same procedure was used to synthesise complexes **1 – 4**.

**Table 3.2:** Reaction optimisation for the synthesis of free sugar Pt(IV) complexes **1-4**.

| Reaction Attempt | Temp (°C) | Vol. DMSO (ml) | Dried DMSO | Dropwise addition | Reaction time (h) | Yield (%) |
|------------------|-----------|----------------|------------|-------------------|-------------------|-----------|
| 1                | 60        | 6              | No         | No                | 16                | N/A       |
| 2                | 55        | 6              | No         | No                | 16                | N/A       |
| 3                | 40        | 7              | No         | No                | 16                | 11        |
| 4                | 45        | 10             | Yes        | No                | 16                | 10        |
| 5                | 40        | 10             | Yes        | Yes               | 16                | 26        |
| 6                | 40        | 10             | Yes        | Yes               | 72                | 19        |
| 7                | 70        | 10             | No         | No                | 16                | N/A       |
| 8                | 40        | 20             | No         | Yes               | 16                | 44        |
| 9                | 40        | 20             | No         | Yes               | 48                | 53        |

The  $^1\text{H}$  NMR spectrum of Complex **1** is shown in **Figure 3.8**. Similarly, to what was described in **Section 3.3.3**, the presence of the free hydroxyl peaks with integrals of one demonstrates that throughout the two day reaction, heating of the ligand and complex did not result in any dimerisation of the ligand.

**Figure 3.8:**  $^1\text{H}$  NMR of Complex **1** in  $\text{DMSO-d}_6$ .

These complexes were further characterised using  $^{13}\text{C}$  and 2D NMR experiments (Appendix, pg, 297). Much like the complexes in **Chapter 2**,  $^{195}\text{Pt}$  NMR was important for the

characterisation of these complexes and a single peak in the region of +1000 ppm confirms that the complex is in the +4 oxidation state.

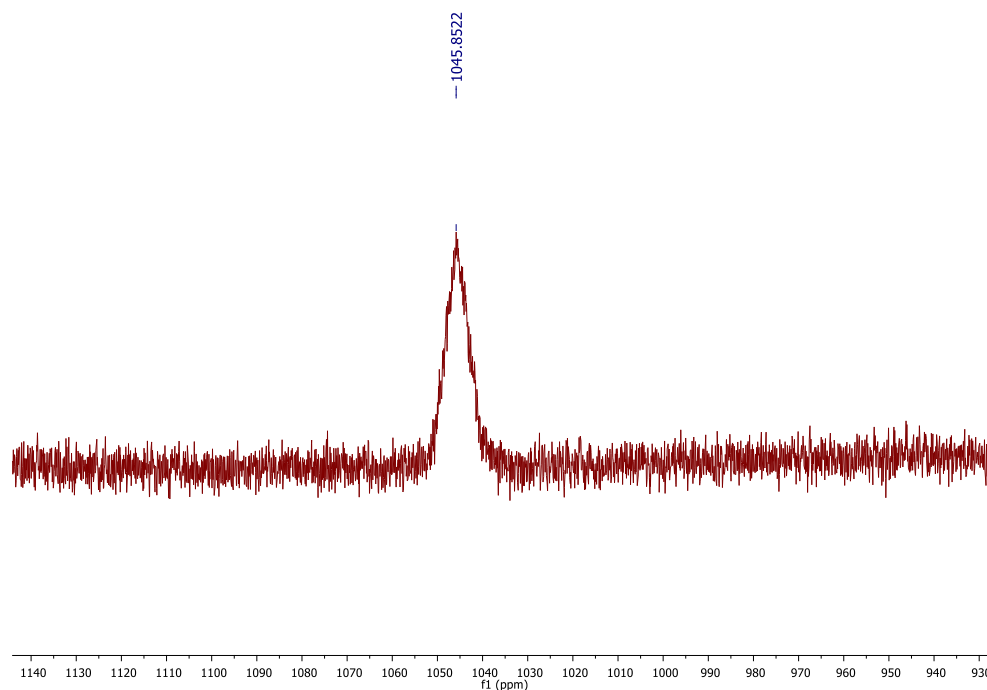
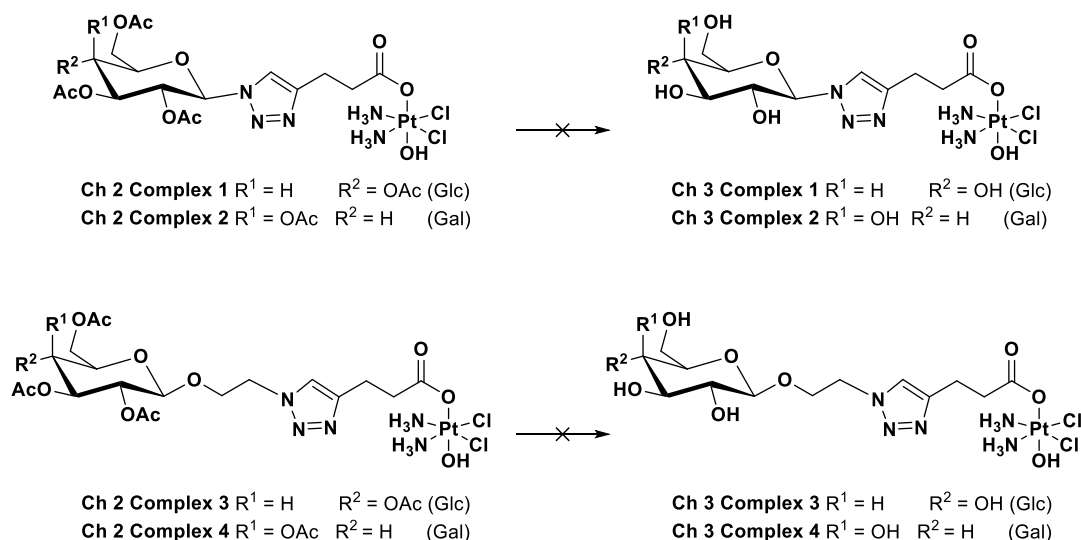


**Figure 3.9:**  $^{195}\text{Pt}$  NMR of Complex **1** in  $\text{DMSO-d}_6$ .

As discussed in the chapter objectives, ideally, these complexes would have been synthesised through the hydrolysis of the acetyl protecting groups present on the analogous complexes **1** – **4** synthesised in **Chapter 2 (Scheme 3.6)**. Alongside the synthesis of the complexes through the route described above, a variety of different deprotection methods of the **Chapter 2** acetylated complexes were investigated, however, none of these yielded the desired product.



**Scheme 3.6:** Original route to the synthesis of complexes **1 – 4**.

**Table 3.3** shows the procedures attempted for the deprotection of **Chapter 2** complexes **1 – 4**. Of the reactions attempted, only entry 1 had any effect on the starting material, however, the reaction brought degradation of the complex. **Figure 3.10** shows the  $^1\text{H}$  NMR spectrum of pure **Complex 1** and the crude product obtained from the reaction conditions used in entry 1. We suggest that while these conditions are suitable for the hydrolysis of acetyl esters, the ligand bound to the complex is itself an ester which would account for the signals on the  $^1\text{H}$  NMR corresponding to the carbohydrate but not the complex. It is possible that these conditions cleave the ligand from the complex and the highly insoluble oxoplatin remains as a byproduct.

**Table 3.3:** Reaction conditions to deprotect acetylated complexes

| Reaction Attempt | Solvent   | Conditions                        | Result                       |
|------------------|-----------|-----------------------------------|------------------------------|
| <b>1</b>         | DMSO/MeOH | $\text{NEt}_3/\text{H}_2\text{O}$ | No $\text{NH}_3$ peak on NMR |
| <b>2</b>         | DMSO/ACN  | Amberlite ( $\text{H}^+$ )        | No reaction                  |
| <b>3</b>         | DMSO/MeOH | $\text{NaOMe}$                    | No reaction                  |
| <b>4</b>         | DMSO/MeOH | $\text{KOH}$ 5%                   | No reaction                  |



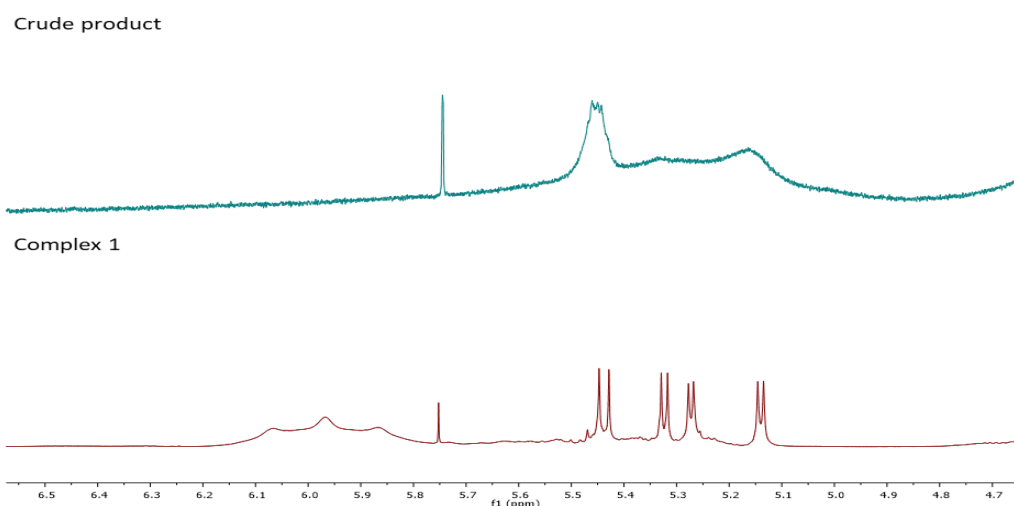


**Figure 3.10:** <sup>1</sup>H NMR spectrum of **1** compared to the crude product obtained from reaction attempt 1 (Table 3.3).

### 3.4 Reduction properties of free sugar complexes (**1** and **3**).

The redox behaviour of free sugar complexes **1** and **3** as well as their corresponding free ligands **3.9** and **3.13** (cathodic processes  $E_p^c$  (I),  $E_p^c$  (II), Figure 3.11) was studied *via* cyclic voltammetry with  $E_{Pt(IV)/Pt(II)}^0 = -1.034$  V and  $-1.002$  V found for **1** and **3**, respectively. The electrochemical reduction was irreversible, in line with previous reported Pt(IV) species based on cisplatin [271], and no major difference was observed according to the type of linker used to connect the carbohydrate moiety and the Pt centre.

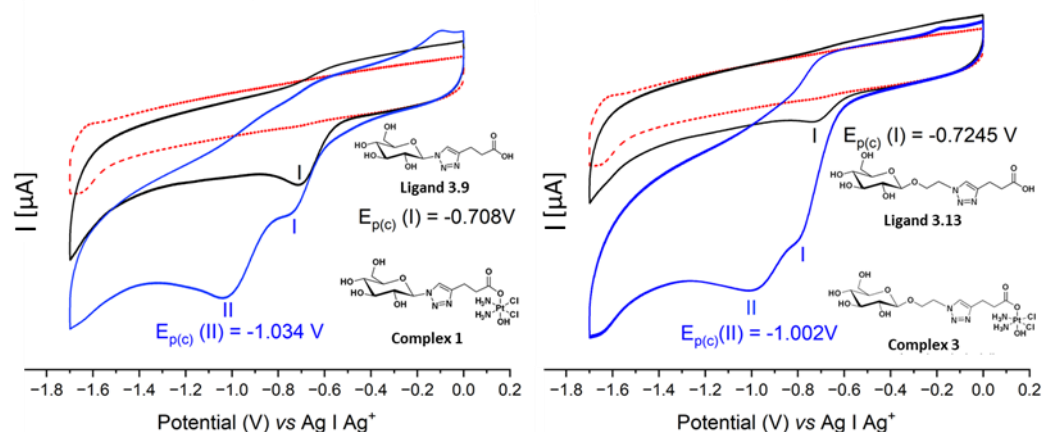


**Figure 3.11:** Cyclic voltammograms of complexes **1** and **3** (blue), with evidence of irreversible cathodic processes I and II and axial ligands **3.9** and **3.13** (black), showing process I only, with the background supporting electrolyte (red). All experiments were performed at the same concentration ( $[\text{compound}] = 2\text{ mM}$ ) in deuterated  $0.1\text{ M DMSO-}[n\text{-Bu}_4\text{N}][\text{PF}_6]$  at a scan rate of  $0.1\text{ Vs}^{-1}$ , using a non-aqueous  $\text{Ag} | \text{Ag}^+$  reference electrode.

To confirm that activation through intracellular reduction occurs in the Pt(IV) species, the behaviour of the Pt(IV) pro-drugs was studied by means of the addition of a ten-fold excess of ascorbic acid into a solution of Complex **3**, mimicking the intracellular environment [272]. The reduction process was followed by  $^1\text{H-NMR}$  (Figure 3.12) with complete release of the carbohydrate axial ligand observed after 48 h, as seen by the disappearance of the triazole proton at  $\delta = 7.93\text{ ppm}$  of Complex **3** and the concomitant formation of the corresponding peak at  $\delta = 7.91\text{ ppm}$  of the free carboxylic acid **3.13**.

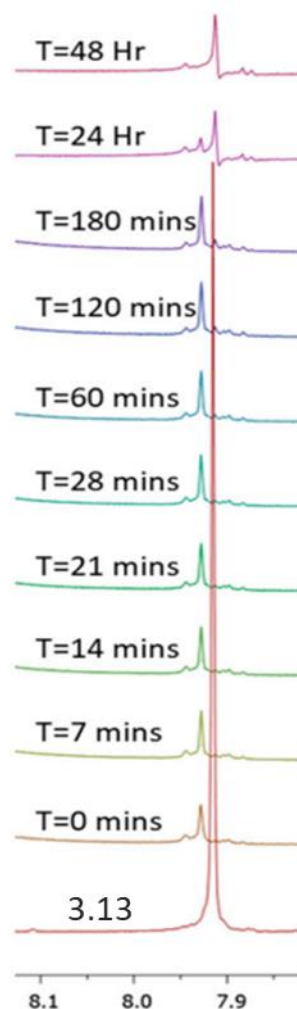


**Figure 3.12:** Reduction of **Complex 3** by a 10-fold excess of ascorbic acid.  $^1\text{H}$  NMR spectra over 48 hours in  $\text{DMSO-d}_6$ .

## 3.5 Biological Evaluation

### 3.5.1 *In vitro* cytotoxicity

The anticancer activity of the four complexes were tested *in vitro* in 2D and 3D models against two osteosarcoma cancer cell lines (SAOS-2 and MG63) and also in a 2D model against a healthy osteoblast cell line (hFOB5), to evaluate if the strategic use of glucose and galactose as vectors is enhancing the selectivity. These studies were done in collaboration with Dr. Monica Montesi and Dr. Silvia Panseri at the CNR-ISTEC of Faenza (Italy).

The evaluation of cell viability demonstrates a dose-dependent cancer cell toxicity exerted by all the drugs (**Figure 3.13**). Although no significant differences in the  $\text{IC}_{50}$

were detected in the four complexes compared to cisplatin, at high concentrations the complexes showed better performance with respect to cisplatin. In MG63 cells the mean effect of the complexes **1-4** showed ~ 3 fold-reduction of the cell viability with respect to cisplatin and ~ 1.5 fold-reduction for SAOS-2 (**Figure 3.13**). The higher anticancer activity of all the complexes **1-4** with respect to cisplatin, is statistically significant at 30  $\mu\text{M}$  for SAOS-2 and 60  $\mu\text{M}$  for MG63. The different cellular behaviour between the cell lines can be attributable to the intrinsic biological differences of the two osteosarcoma cell lines [273].

Most importantly, in the healthy cells hFOBs, the cisplatin begins to be extremely toxic at very low concentration, 1.5  $\mu\text{M}$  ( $p \leq 0.001$  with respect to cells only), while all the complexes **1-4** showed a cytotoxic effect at much higher concentrations,  $\geq 15$   $\mu\text{M}$  (Complex 1  $p \leq 0.05$ ; 2  $p \leq 0.001$ ; 3  $p \leq 0.0001$ ; 4  $p \leq 0.001$  with respect to cells only). The evaluation of the  $\text{IC}_{50}$  values confirms the cell viability results; in fact, in the hFOBs the  $\text{IC}_{50}$  of the cisplatin (i.e., 4.1  $\mu\text{M}$ ) was far lower compared to the  $\text{IC}_{50}$  values of the complexes **1-4** which are  $> 16$   $\mu\text{M}$  (**Table 3.4**). Moreover, it was shown that the toxic effect of the complexes is statistically significantly lower, with respect to the effect of cisplatin at 1.5  $\mu\text{M}$ , 5  $\mu\text{M}$ , 15  $\mu\text{M}$  and 30  $\mu\text{M}$  (**Figure 3.13**). The cell behaviours observed by cell viability assay were also confirmed using morphological analysis, where a reduction in cell density directly relates to the increase of drug concentration was detected.

These results demonstrated that all complexes **1-4** have high selectivity for cancer cells and a lower toxic effect on healthy hFOBs. We believe that this selectivity could be ascribable to the overexpression of the GLUT family members, specifically GLUT-1, observed in cancer cells leading to an increased glycolytic activity [274,275]. The higher toxicity of all complexes with respect to the cisplatin observed in both MG63 and SAOS-2 at 30  $\mu\text{M}$  and 60  $\mu\text{M}$ , strengthens the hypothesis of the role of the GLUT receptor overexpression in the uptake, induced by the presence of sugar moieties connected to the drug, and consequently in the increased anticancer effect.

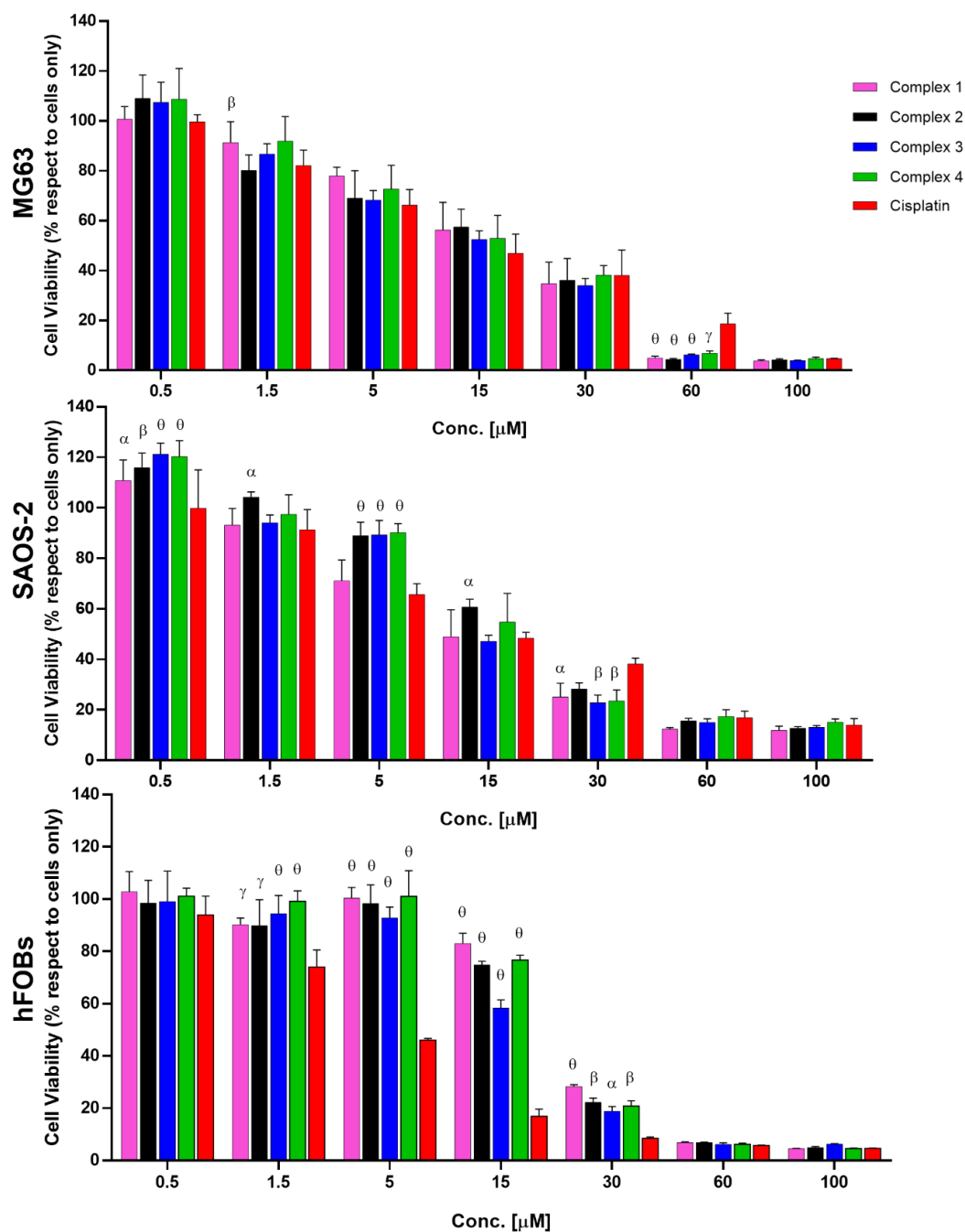


**Figure 3.13:** 2D drug screening of complexes 1–4 by MTT assay. Cell viability evaluation after 72 h incubation with complexes. Data is reported in the graph as a percentage (%) mean  $\pm$  standard error of the mean. Statistical analysis with respect to cisplatin is reported in the graph, p value is  $\alpha \leq 0.05$ ,  $\beta \leq 0.01$ ,  $\gamma \leq 0.001$  and  $\theta \leq 0.0001$ .

**Table 3.4:** IC<sub>50</sub> (μM) values of the complexes **1 – 4** and cisplatin against MG63, SAOS-2 and hFOBs cells.

| Complex<br>OS Cancer<br>cell | Cisplatin                |      | 1                        |      | 2                        |      | 3                        |      | 4                        |      |
|------------------------------|--------------------------|------|--------------------------|------|--------------------------|------|--------------------------|------|--------------------------|------|
|                              | IC <sub>50</sub><br>(μM) | SI   | IC <sub>50</sub><br>(μM) | SI   | IC <sub>50</sub><br>(μM) | SI   | IC <sub>50</sub><br>(μM) | SI   | IC <sub>50</sub><br>(μM) | SI   |
| MG63                         | 12.20<br>±2.85           | 0.33 | 15.90<br>±3.1            | 1.46 | 13.60<br>±4.6            | 1.53 | 13.0<br>±2.95            | 1.29 | 14.90<br>±3.85           | 1.4  |
| SAOS-2                       | 13.70<br>±2.95           | 0.29 | 12.94<br>±3.2            | 1.8  | 19.09<br>±3.2            | 1.09 | 15.18<br>±3.4            | 1.11 | 17.22<br>±4.1            | 1.21 |
| hFOBs                        | 4.109<br>±0.44           | 1    | 23.36<br>±1.77           | 1    | 20.85<br>±2.01           | 1    | 16.88<br>±1.72           | 1    | 20.91<br>±0.44           | 1    |

### 3.5.2 3D scaffold-based OS model

In order to confirm these promising results, a proof of concept *in vitro* was performed using more relevant cancer models. In fact, it is well known that the use of conventional 2D approaches showed some limitations because they fail to mimic the real tumour complexity leading to a low predictivity of preclinical results [276,277]. To overcome this limitation and to strengthen the results obtained in the previous 2D study, MG63 cell line was cultured on a 3D scaffold that mimics the feature of the bone extracellular matrix (**Figure 3.14c**) by the physical, chemical and nanostructure point of view, as previously demonstrated [278,279].

After the seeding of the MG63 cell line, the cells were able to interact and colonise the scaffold providing a more mimetic 3D scaffold-based osteosarcoma model (3D OS model) that is then used to test the effect of the proposed drugs. As shown in **Figure 3.14a** and **b**, MG63 cells easily adhered to the nanostructure of the biomimetic scaffolds and, 48 hours after seeding, the scaffolds were nearly completely covered by the cells exhibiting their characteristic morphology and high level of cell/material interactions.

It is well known that the behaviour of the cells cultured in 3D is different with respect to the standard 2D model [280]. For this reason, before testing the complexes in the 3D OS mode, a preliminary evaluation of the cisplatin effective concentration was

performed by comparing the toxicity of cisplatin 15  $\mu\text{M}$  in 2D and in 3D OS model. 15  $\mu\text{M}$  of cisplatin did not compromise the cell viability in 3D OS model, while significantly reduced the viable cells grown in 2D standard culture conditions (p-value  $\leq 0.0001$ ).

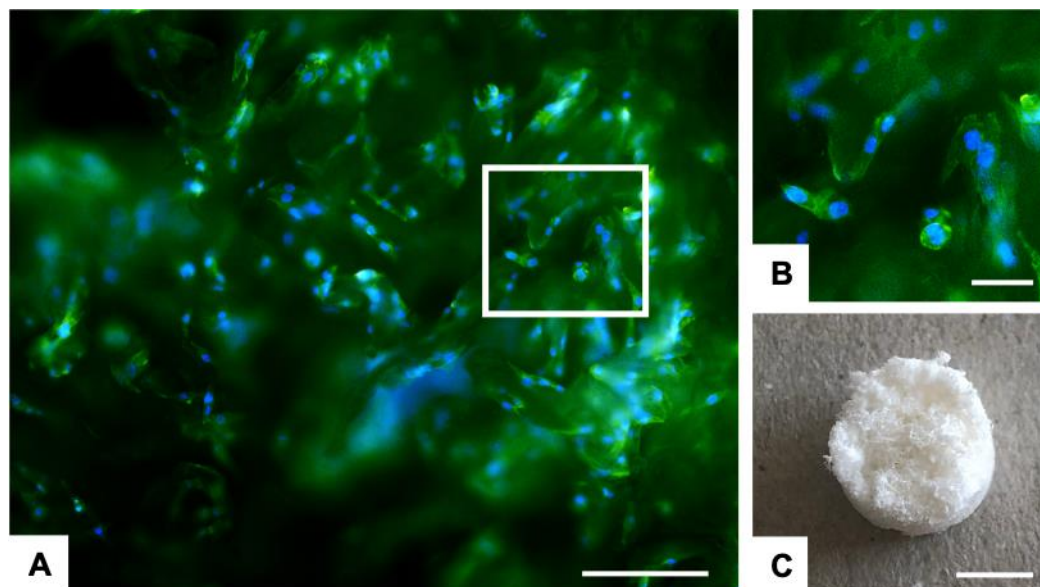


**Figure 3.14:** 3D scaffold-based osteosarcoma model (3D OS model). (A) Analysis of cell morphology of 3D MG63 culture on bone-mimetic scaffold 48 h after seeding. F-Actin filaments in green (FITC) and cell nuclei in blue (DAPI); scale bars 200  $\mu\text{m}$ . (B) Image enlargement (white square) of the cell morphology details; scale bars 50  $\mu\text{m}$ . (C) Representative image of the 3D bone-mimetic scaffold; scale bars 4 mm

Based on these results, complexes **1-4** and cisplatin were tested at 30 and 60  $\mu\text{M}$  in the 3D tumour model. At 60  $\mu\text{M}$  all of the complexes showed higher toxic effect with respect to cisplatin, and these differences are statistically significant for the complex **2** and **4** with p value  $\leq 0.05$  (**Figure 3.15**). Morphological analysis confirms the cell viability results.

This proof of concept highlights the cancer cells selectivity of the complexes for the considered OS cells, compared to cisplatin, and reinforces the data obtained in the 2D *in vitro* study, demonstrating the better performance of complexes **1-4** as anticancer drugs.

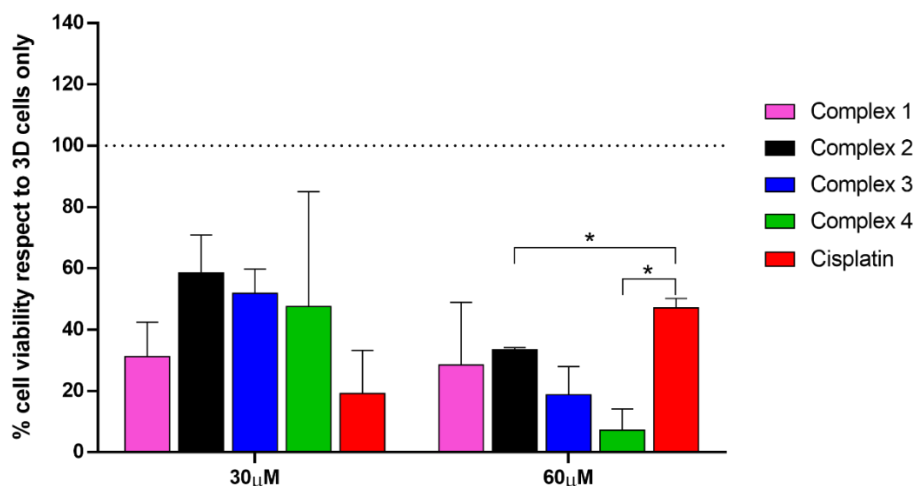


**Figure 3.15:** Anti-cancerous effect of complexes 1 – 4 on 3D OS model. Cell viability evaluation after 72 h of incubation with complexes using MTT assay. Data is reported on the graph as percentage (%) mean  $\pm$  standard error of the mean. Statistical analyses with respect to cisplatin is reported in the graph, \* p value  $\leq$  0.05.

### 3.6 Conclusions

Four novel Pt(IV) pro-drugs, based on cisplatin scaffold with carbohydrate vectors in axial positions were synthesised, linking the sugar moiety and the metal centre *via* CuAAC “click” chemistry. These prodrugs are functionalised with deprotected glyco-moieties that act as real vectors to selectively target cancer cells. Most of the carbohydrate-functionalised Pt-based complexes reported in literature contain protected acetylated sugars, due to an easy synthetic and purification procedure. The complexes were tested on a panel of two 2D and 3D OS (Osteosarcoma) cell lines as well as on healthy OS cells. All the complexes showed very promising activity, comparable to the reference cisplatin, demonstrating that the presence of a monosaccharide does not hamper the anticancer effect. Notably, the complexes are much less active against the healthy lines, showing a promising selectivity for these OS cell lines, with respect to cisplatin. The complexes were also particularly active in the 3D model, a more reliable system compared to 2D, with the most promising activity shown by complexes 2 and 4 with a galactose substituent. The role of galactose in the metabolism of cancer cells is attracting high attention because of potential diagnostic and therapeutic possibilities [260,261]. While the role of the free sugars as targeting vectors is not completely confirmed yet, the selectivity showed in



2D studies is a solid base to hypothesise that the carbohydrate moieties play an important role in targeted therapies. More specific biological studies (beyond the scope of this thesis) should be conducted (i.e., inhibition the GLUTs receptors), but this selectivity was not observed in the protected-Pt(IV) analogues, as discussed in **chapter 2**. While all the complexes showed very promising activity, the discrimination between the two linkers is not observed. In ongoing studies in the Montagner group, these complexes have been conjugated to graphene oxide nanoparticles that act as delivering agents to further enhance the selectivity. The results of this chapter have been published in the International Journal of Molecular Science in 2023, volume 24, issue 7, special issue: Metal-Based complexes in Cancer 2.0 (doi: 10.3390/ijms24076028) [267].

### 3.7 Materials and Methods

All reagents and reactants were purchased from commercial sources. The two sources used were Sigma-Aldrich and Fluorochem. All solvents were used without further purification. Cisplatin and oxoplatin were synthesised as previously reported [262,263]. Compounds **2.16** – **2.19** and **2.22** – **2.27** were synthesised as per the previous chapter.

The elemental analysis studies (carbon, hydrogen, and nitrogen) were performed by means of a PerkinElmer 2400 series II analyzer. HR-Mass Spectra were recorded with a Waters LCT Premier XE Spectrometer. NMR:  $^1\text{H}$ ,  $^{13}\text{C}$  and  $^{195}\text{Pt}$  NMR spectra were obtained in a solution of  $\text{D}_2\text{O}$  or  $\text{DMSO-}d_6$  at 300 K, in 5-mm sample tubes, with a premium shielded Agilent Varian 500 MHz (operating at 500.13, 125.75, and 107.49 MHz, respectively). The  $^1\text{H}$  and  $^{13}\text{C}$  chemical shift was referenced to the residual impurity of the solvent. The external reference was  $\text{Na}_2\text{PtCl}_4$  in  $\text{D}_2\text{O}$  (adjusted to  $\delta = -1628$  ppm from  $\text{Na}_2\text{PtCl}_6$ ) for  $^{195}\text{Pt}$ . The stability was followed using high-performance liquid chromatography (HPLC) with a Phenomenex Luna C18 (5  $\mu\text{M}$ , 100 Å, 250mm  $\times$  4.60 mm i.d.) column at room temperature at a flow rate of 1.0 mL/min with 254 nm UV detection. Mobile phase containing 80:20 acetonitrile (0.1% trifluoroacetic acid): water (0.1% trifluoroacetic acid): the complexes were dissolved in DMF (0.5 ml) and diluted to a final concentration of 0.5 mM using acetonitrile and

water solution (1/1) and 2 mM 4-(2-hydroxyethyl)piperazine-1-ethanesulfonic acid (HEPES) buffer (pH 6.8). Infrared (IR) spectra were recorded in the region 4000–400  $\text{cm}^{-1}$  on a Perkin Elmer precisely spectrum 100 FT/IR spectrometer. The solid samples were run using ATR. An extensive biological evaluation of the activity of all the compounds was performed in human osteosarcoma cell line *in vitro* models as reported below.

### 3.7.1 Cyclic voltammetry

Measurements were made using a Solartron SI2187 Electrochemical Potentiostat/Galvanostat and a CHI Instruments 1200 Potentiostat. Non-aqueous voltammetry of 2 mM of each of **3.9**, **3.13**, **1**, and **3** was carried out at a glassy carbon working electrode ( $0.07 \text{ cm}^2$ ) in a three-electrode configuration with Pt wire counter and non-aqueous  $\text{Ag}|\text{Ag}^+$  reference electrode in 0.1 M tetrabutylammonium hexafluorophosphate ( $\text{TBAPF}_6$ ) supporting electrolyte in DMSO as solvent. The working electrodes were prepared polishing with 1  $\mu\text{m}$  microcrystalline diamond suspension on a micro-cloth followed by rinsing in deionised water. Voltammograms were generated over the range 0.2 to -1.7 V vs.  $\text{Ag}/\text{Ag}^+$  in a deaerated solution ( $\text{N}_2$  bubbling 10 min), with a cathodic scan direction at  $100 \text{ mV} \cdot \text{s}^{-1}$  in all cases.

### 3.7.2 Reduction studies

Measurements were obtained in a solution of  $\text{DMSO-}d_6$  at 300 K, in 5-mm sample tubes, with a premium shielded Agilent Varian 500 MHz (operating at 500.13 MHz). Complex **3** (5 mg, 7.53  $\mu\text{mol}$ ) was dissolved in 500  $\mu\text{L}$  of  $\text{DMSO-}d_6$ . Ascorbic acid (13 mg, 10 Equiv.) was added and a  $^1\text{H}$  NMR spectrum was recorded every 7 minutes for 30 minutes. After no reduction had taken place initially, the  $^1\text{H}$  NMR spectrum was recorded every hour for three hours, and finally every 24 hours until full reduction of  $\text{Pt(IV)}$  to  $\text{Pt(II)}$  and cleavage of the axial ligand was observed after 48 hours.

### 3.7.3 *In vitro* biological evaluation

*In vitro* tests of the four  $\text{Pt(IV)}$ -Carbohydrate derivatives complexes (**1** – **4**) were performed to evaluate their biological activity towards two osteosarcoma cell lines (MG63 and SAOS-2) and a non-cancerous cell line of human foetal osteoblasts (hFOBs), compared to cisplatin. The drugs were reconstituted in Dimethyl Sulfoxide

(DMSO) at 1 mg/mL concentration before being diluted in culture media at the required concentration. A 2D *in vitro* screening of all the drugs was performed at 72 hours in a wide concentration range (0.5, 1.5, 5, 15, 30, 60, and 100  $\mu$ M) on the three different cell lines in terms of cell viability and the IC<sub>50</sub> was calculated. The cell morphology in the presence of the complexes was evaluated at 15 and 30  $\mu$ M concentrations for MG63 and SAOS-2, and for hFOBs cells, respectively, according to the IC<sub>50</sub> at 72 hours. Moreover, as more predictive *in vitro* cell culture systems, 3D tumour scaffold-based models of osteosarcoma were developed and the anticancer activity of cisplatin and complexes **1 – 4** on MG63 cells was investigated at 30 and 60  $\mu$ M concentrations after 72 hours of culture. For the models, a composite hydroxyapatite-based scaffold (MgHA/Coll) as bone-like matrix was used in combination with MG63 cells. For both 2D and 3D *in vitro* cell cultures, cisplatin was used as a control group and cells only were used as a negative control.

#### 3.7.4 Cell culture

Human Osteosarcoma cell lines MG63 (ATCC<sup>®</sup> CRL1427<sup>™</sup>), SAOS-2 (ATCC<sup>®</sup> HTB-85<sup>™</sup>), and Human Foetal Osteoblasts (hFOBs 1.19) (ATCC<sup>®</sup> CRL-11372<sup>™</sup>) were purchased from American Type Culture Collection (ATCC) and used for this study. MG63 cell line was cultured in DMEM F12-GlutaMAX<sup>™</sup> Modified Medium (Gibco) supplemented with 10% Foetal Bovine Serum (FBS) (Gibco) and 1% of penicillin/streptomycin mixture (pen/strep) (100 U/ml - 100  $\mu$ g/mL, Gibco). The SAOS-2 cell line was cultured in McCoy's 5A Modified Medium (Gibco) supplemented with 15% and 10% FBS, respectively, and 1% pen/strep. The hFOBs cell line was cultured in DMEM F12 no phenol red with L-glutamine supplemented with 10% FBS and 0.3 mg/mL Geneticin (G418, Gibco). Cells were kept in an incubator at 37°C under controlled humidity and 5% CO<sub>2</sub> atmospheric conditions. Cells were detached from culture flasks by trypsinisation and centrifuged. The cell number and viability were determined by Trypan Blue Dye Exclusion test and all cell handling procedures were performed under laminar flow hood in sterile conditions.

#### 3.7.5 Synthesis of bone mimetic scaffolds

The Mg-doped hydroxyapatite collagen composite scaffolds were designed and synthesised at ISSMC of CNR of Italy [278]. Briefly, 150 g of Collagen gel (1 wt%,

Opocrin SpA, MO, Italy) was diluted into a phosphoric acid solution (2.4 g in 500 mL; H<sub>3</sub>PO<sub>4</sub>, 85 wt.%, Sigma) at room temperature to obtain an acidic aqueous homogenous suspension. Separately, a basic aqueous suspension was obtained by mixing 2.7 g of calcium hydroxide (Ca(OH)<sub>2</sub>, 95 wt.%, Sigma) and 0.35 g of magnesium chloride (MgCl<sub>2</sub>·6H<sub>2</sub>O, 99 wt.%, Sigma) in 500 ml of milli-Q water at room temperature to obtain a basic aqueous homogenous suspension. The acidic suspension was dripped into the basic one at 25 ± 2°C under continuous stirring condition and matured for 2 hours. Later, the slurry solution was rinsed thrice in milli-Q water and filtered through metallic sieve (150 m) to exclude unreacted counter ions. The recovered slurry solution was cross-linked with 2 wt.% BDDGE (with respect to Collagen) at 25 ± 2°C for 24 hours and at 4°C for another 24 h. Later, the solution was rinsed thrice in milli-Q water to remove any residue and freeze-dried (–40 °C and +25 °C) for 48 hours under 0.086 mbar vacuum conditions (LIO 3000 PLT, SPASCAL, Italy). The obtained scaffolds (8 x 4 mm) named bone mimetic scaffolds were sterilised by 25 kGy  $\gamma$ -ray irradiation before the use.

### **3.7.6 3D scaffold – based osteosarcoma models (3D OS model)**

For the development of the in vitro 3D scaffold-based osteosarcoma model, bone-mimetic scaffolds were used as bone-like matrix in combination with MG63 cells. The scaffolds were conditioned in culture media for 24 h before the cell seeding. The MG63 cell line was seeded with a density of  $3.0 \times 10^4$  per scaffold by dropping the cellular suspension on the material upper surface followed by 30 min pre-adhesion at 37°C before cell media addition. The 3D OS model has been grown in the incubator under standard culture medium conditions for 48 h to allow cell colonisation of the scaffold, then the medium was changed, and the drugs were added. The in vitro 3D OS models were cultured in the presence of the drugs for 72 h at 37°C under controlled humidity and 5% CO<sub>2</sub> atmospheric conditions; the cells grown in 3D in standard condition, without the drugs, were used as control group (3D cells only). All cell handling procedures were performed under a laminar flow hood in sterile conditions.

### 3.7.7 MTT cell viability assay

A quantitative analysis of cell viability was carried out by MTT assay, following the manufacturer's instructions. For the *in vitro* 2D cell cultures, all cell lines were seeded at a density of  $5.0 \times 10^3$  cells/well in 96 well-plates, and for the *in vitro* 3D cell cultures, see section 3.7.6. The MTT reagent [3-(4,5-dimethylthiazol-2-yl)-2,5-diphenyltetrazolium bromide] (5 mg/mL) was dissolved in Phosphate Saline Buffer 1X (PBS 1X). At 72 hours, the cells were incubated with 10% media volume MTT solution for 2 hours at 37 °C, 5% CO<sub>2</sub> and controlled humidity conditions. The cell culture media was removed and substituted with DMSO (Merck) dissolving formazan crystals derived from MTT conversion by metabolically active cells. For 3D scaffold-based models of osteosarcoma, each scaffold was transferred into a 2 mL Eppendorf and completely broken using pestles after DMSO addition. After 15 minutes of incubation with slight stirring, the absorbance of formazan was read at 570 nm by using a Multiskan FC Microplate Photometer (Thermo Fisher Scientific). The values of absorbance are directly proportional to the number of metabolic active cells in each well. One experiment was carried out and a biological triplicate for each condition was performed. For the 3D tumour models, one biological experiment was performed, two scaffolds for each condition were used.

### 3.7.8 Cell morphology evaluation

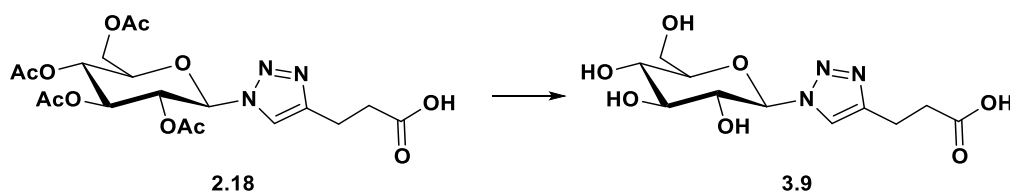
For the *in vitro* 2D cell cultures, all cell lines were seeded at a density of  $5.0 \times 10^3$  cells/well in 96 well-plates, for the *in vitro* 3D cell cultures cells were treated as previously described. Both the 2D and 3D cell cultures were fixed in 4% buffered Paraformaldehyde (PFA) following the manufacturer's instructions. The fixed samples were permeabilised in PBS 1X with 0.1% (v/v) Triton X-100 (Merck) for 5 minutes at room temperature and F-actin filaments were highlighted with Alexa Fluor 488 Phalloidin (Invitrogen) for 20 minutes at room temperature in the dark. DAPI (600 nM) counterstaining was performed for cell nuclei identification, following the manufacturer's instructions. The images were acquired by using an Inverted Ti-E Fluorescent Microscope.

### 3.7.9 Statistical analysis

Statistical analysis was performed by using GraphPad Prism Software (8.0.1 version). The results of MTT assay of the *in vitro* 2D drug screening are reported in the graphs as mean percentage of cell viability with respect to cells only  $\pm$  standard deviation and they were analysed using Two-way analysis of variance (Two-way ANOVA) and Dunnett's multiple comparisons test. The MTT results were further analysed by One-way analysis of variance (One-way ANOVA) and Dunnett's multiple comparisons test. IC<sub>50</sub> values were calculated as Log(inhibitor) versus mean percentage of dead cells with respect to cells only and the obtained values are reported in the graphs  $\pm$  95% confidence interval (CI) for each cell line. The MTT results of 3D tumour engineered models of osteosarcoma were reported in the graph as percentage mean  $\pm$  standard error of the mean and they were analysed by Two-way ANOVA and Dunnett's multiple comparisons test. A further analysis was performed by unpaired *t*-test on all drugs with respect to cisplatin.

## 3.8 Experimental procedures

### *N*-( $\beta$ -D-glucopyranosyl-1,2,3-triazol-4-yl)-propanoic acid (3.9)



**2.18** (0.612 g, 1.29 mmol) was suspended in a mixture of methanol (6 mL) and water (3 mL) and heated at 45°C. NEt<sub>3</sub> (0.2 mL) was added, and the reaction was allowed to stir overnight. The progress was checked using TLC (95:5 DCM:MeOH). The solvent was removed under vacuum and the residue was redissolved in H<sub>2</sub>O and stirred with Amberlite H<sup>+</sup> resin for 40 minutes. The Amberlite was filtered, and the residue was dried by lyophilisation and reacted in the following step without further purification (0.375 g, 1.23 mmol, 95%).

R<sub>f</sub> = 0.40 (DCM:MeOH:H<sub>2</sub>O 60:35:5).

<sup>1</sup>H NMR (500 MHz, D<sub>2</sub>O)  $\delta$  7.97 (s, 1H, triaz-CH), 5.67 (d, *J* = 9.2 Hz, 1H, H-1), 3.95 (t, *J* = 9.2 Hz, 1H, H-2), 3.87 (dd, *J* = 12.4, 2.0 Hz, 1H, H-6), 3.77 – 3.64 (m, 3H, H-3, H-6'),

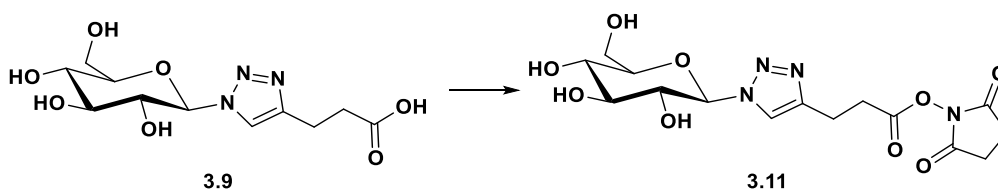
H-5), 3.62 – 3.56 (m, 1H, H-4), 2.96 (t,  $J = 7.4$  Hz, 2H, triaz-CH<sub>2</sub>), 2.55 (t,  $J = 7.4$  Hz, 2H, CH<sub>2</sub>CO) ppm.

<sup>13</sup>C NMR (125 MHz, D<sub>2</sub>O)  $\delta$  180.9 (CO), 147.9 (triaz-C), 122.2 (triaz-CH), 87.4 (C-1), 78.8 (C-5), 75.9 (C-3), 72.2 (C-2), 68.9 (C-4), 60.4 (C-6), 36.2 (CH<sub>2</sub>CO), 21.5 (triaz-CH<sub>2</sub>) ppm.

IR (ATR) 3256.84, 2915.58, 1567.38, 1396.39, 1042.54, 898.47, 599.49 cm<sup>-1</sup>.

HR-MS (+):  $m/z$  calcd for C<sub>11</sub>H<sub>17</sub>N<sub>3</sub>O<sub>7</sub> + H<sup>+</sup> [M+H]<sup>+</sup> 304.1145, found 304.1140. HR-MS (+):  $m/z$  calcd for C<sub>11</sub>H<sub>17</sub>N<sub>3</sub>O<sub>7</sub> + Na<sup>+</sup> [M+Na]<sup>+</sup> 326.0964, found 326.0958.

***N*-( $\beta$ -D-glucopyranosyl-1,2,3-triazol-4-yl)-(3-oxopropyl-(oxy(2,5-dioxopyrrolidin-1-yl))) (3.11)**



**3.9** (0.2 g, 0.659 mmol) was added to a flask containing TSTU (0.218 g, 0.725 mmol, 1.1 equiv.) and placed under N<sub>2</sub>. Anhydrous DMF (10 mL) and anhydrous Triethylamine (0.101 mL, 0.725 mmol, 1.1 equiv.) were added. The reaction was stirred for 20 minutes, and reaction progress was monitored by TLC (60:35:5 DCM:MeOH:H<sub>2</sub>O). The solvent was removed in vacuo and the residue was washed with DCM. The precipitate was collected by centrifugation and dried, yielding a light pink powder (Yield 0.182 g, 0.454 mmol, 68%).

R<sub>f</sub> = 0.92 (DCM:MeOH:H<sub>2</sub>O 60:35:5).

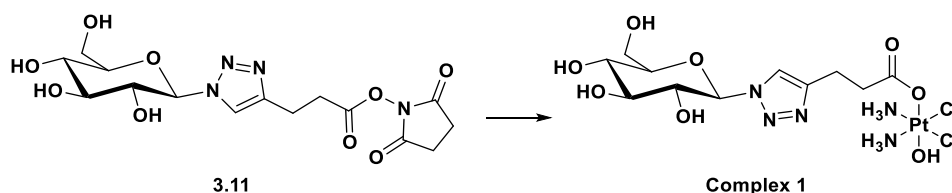
<sup>1</sup>H NMR (500 MHz, DMSO)  $\delta$  8.11 (s, 1H, triaz-CH), 5.48 (d,  $J = 9.3$  Hz, 1H, H-1), 5.32 (d,  $J = 6.0$  Hz, 1H, OH of C-2), 5.26 (d,  $J = 4.6$  Hz, 1H, OH of C-3), 5.14 (d,  $J = 5.4$  Hz, 1H, OH of C-4), 4.62 (s, 1H, OH of C-6), 3.74 – 3.66 (m, 2H, H-2, H-6), 3.43 (d,  $J = 7.6$  Hz, 2H, H-6', H-5), 3.39 (dd,  $J = 8.9, 3.9$  Hz, 1H, H-3), 3.21 (dt,  $J = 13.9, 7.0$  Hz, 1H, H-4), 3.10 – 3.05 (m, 2H, CH<sub>2</sub>CO), 3.02 – 2.98 (m, 2H, triaz-CH<sub>2</sub>), 2.82 (s, 4H, CH<sub>2</sub>CH<sub>2</sub>-succ) ppm.

**<sup>13</sup>C NMR** (125 MHz, DMSO)  $\delta$  170.3 (CO succ x2), 168.4 (CO), 144.4 (triaz-C), 121.4 (triaz-CH), 87.4 (C-1), 79.9 (C-5), 77.0 (C-3), 72.2 (C-2), 69.6 (C-4), 60.7 (C-6), 29.58 (CH<sub>2</sub>CO), 25.5 (CH<sub>2</sub>CH<sub>2</sub>-succ), 20.3 (triaz-CH<sub>2</sub>) ppm.

**IR (ATR)** 3298.62, 2917.68, 1731.73, 1708.88, 1406.06, 1367.70, 1206.78, 1019.20, 818.67, 647.68 cm<sup>-1</sup>.

**HR-MS (+):** m/z calcd for C<sub>15</sub>H<sub>20</sub>N<sub>4</sub>O<sub>9</sub> + H<sup>+</sup> [M+H]<sup>+</sup> 401.1309, found 401.1300. **HR-MS (+):** m/z calcd for C<sub>15</sub>H<sub>20</sub>N<sub>4</sub>O<sub>9</sub> + Na<sup>+</sup> [M+Na]<sup>+</sup> 423.1128, found 423.1119.

***Cis,cis,trans*-[Pt<sup>IV</sup>(NH<sub>3</sub>)<sub>2</sub>(3.9)(OH)Cl<sub>2</sub>] (1)**



**3.11** (0.321 g, 0.801 mmol) dissolved in DMSO (15 mL) was added dropwise overnight to a suspension of Oxoplatin (0.280 g, 0.841 mmol, 1.05 equiv.) in DMSO (5 mL) and stirred in the dark at 40°C for 48 hours. The yellow suspension was filtered and the DMSO was evaporated by lyophilisation. The remaining oil was treated with methanol (10mL) and the white/yellow precipitate that was formed was washed with DCM and diethyl ether. The product was dried under reduced pressure (Yield 0.293 g, 0.473 mmol, 59%).

**<sup>1</sup>H NMR** (500 MHz, DMSO)  $\delta$  8.06 (s, 1H, triaz-CH), 6.17 – 5.79 (m, 6H, 2x NH<sub>3</sub>), 5.44 (d,  $J$  = 9.3 Hz, 1H, H-1), 5.32 (d,  $J$  = 6.0 Hz, 1H, OH of C-2), 5.27 (d,  $J$  = 4.8 Hz, 1H, OH of C-3), 5.14 (d,  $J$  = 5.4 Hz, 1H, OH of C-4), 4.63 (t,  $J$  = 5.6 Hz, 1H, OH of C-6), 3.77 – 3.65 (m, 2H, H-2, H-6), 3.43 (dt,  $J$  = 11.9, 4.9 Hz, 3H, H-6', H-3, H-5), 3.21 (dd,  $J$  = 8.9, 5.2 Hz, 1H, H-4), 2.83 (t,  $J$  = 7.6 Hz, 2H, triaz-CH<sub>2</sub>), 2.49 (m, 2H, CH<sub>2</sub>CO) ppm.

**<sup>13</sup>C NMR** (125 MHz, DMSO)  $\delta$  179.9 (CO), 146.3 (triaz-C), 121.2 (triaz-CH), 87.4 (C-1), 79.9 (C-5), 77.0 (C-3), 72.0 (C-2), 69.6 (C-4), 60.8 (C-6), 36.0 (CH<sub>2</sub>CO), 21.9 (triaz-CH<sub>2</sub>) ppm.

**<sup>195</sup>Pt{<sup>1</sup>H} NMR** (108 MHz, DMSO)  $\delta$  1047.07 ppm.

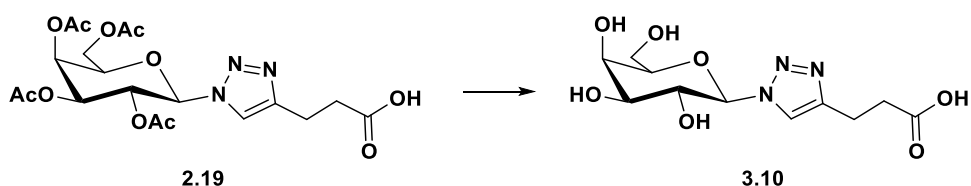


**IR (ATR)** 3221.35, 1619.15, 1351.11, 1094.74, 579.32, 438.05  $\text{cm}^{-1}$ .

**HR-MS (+):**  $m/z$  calcd for  $\text{C}_{11}\text{H}_{23}\text{Cl}_2\text{N}_5\text{O}_8\text{Pt} + \text{H}^+$   $[\text{M}+\text{H}]^+$  619.0644, found 620.0639.

**El. Anal.** Calcd. for  $\text{C}_{11}\text{H}_{23}\text{Cl}_2\text{N}_5\text{O}_8\text{Pt}$ : % C = 21.33; H = 3.74; N = 11.31; found: % C = 21.85; H = 3.39; N = 11.82.

***N*-( $\beta$ -D-galactopyranosyl-1,2,3-triazol-4-yl)-propanoic acid (3.10)**



**2.19** (0.156 g, 0.332 mmol) was suspended in a mixture of methanol (4 mL) and water (2 mL) and heated at 45°C.  $\text{NEt}_3$  (0.1 mL) was added, and the reaction was allowed to stir overnight. The progress was checked using TLC (95:5 DCM:MeOH). The solvent was removed under vacuum and the residue was redissolved in  $\text{H}_2\text{O}$  and stirred with Amberlite  $\text{H}^+$  resin for 40 minutes. The Amberlite was filtered, and the residue was dried by lyophilisation and reacted in the following step without further purification (Yield 0.098 g, 0.323 mmol, 97%).

$R_f = 0.51$  (DCM:MeOH: $\text{H}_2\text{O}$  60:35:5).

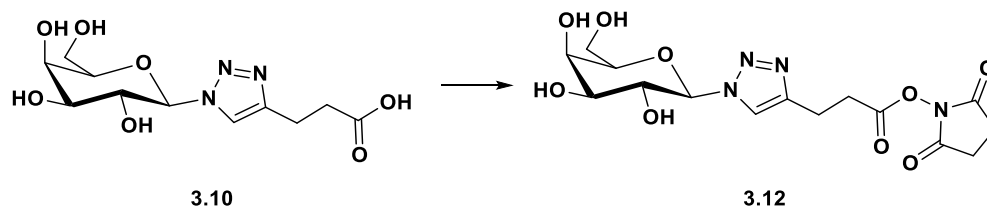
**$^1\text{H}$  NMR** (500 MHz,  $\text{D}_2\text{O}$ )  $\delta$  7.96 (s, 1H, triaz-CH), 5.55 (d,  $J = 9.2$  Hz, 1H, H-1), 4.11 (t,  $J = 9.5$  Hz, 1H, H-2), 3.99 (dd,  $J = 3.3, 0.7$  Hz, 1H, H-4), 3.89 (td,  $J = 6.0, 0.8$  Hz, 1H, H-5), 3.78 (dd,  $J = 9.8, 3.3$  Hz, 1H, H-3), 3.69 (d,  $J = 6.2$  Hz, 2H, H-6, H-6'), 2.89 (t,  $J = 7.4$  Hz, 2H, triaz- $\text{CH}_2$ ), 2.52 (t,  $J = 7.4$  Hz, 2H,  $\text{CH}_2\text{CO}$ ) ppm.

**$^{13}\text{C}$  NMR** (125 MHz,  $\text{D}_2\text{O}$ )  $\delta$  180.0 (CO), 147.6 (triaz-C), 121.9 (triaz-CH), 87.9 (C-1), 78.2 (C-5), 72.9 (C-3), 69.6 (C-2), 68.5 (C-4), 60.8 (C-6), 35.5 ( $\text{CH}_2\text{CO}$ ), 21.2 (triaz- $\text{CH}_2$ ) ppm.

**IR (ATR)** 3247.67, 1565.21, 1399.66, 1053.32, 883.22, 553.54  $\text{cm}^{-1}$ .

**HR-MS (+):**  $m/z$  calcd for  $\text{C}_{11}\text{H}_{17}\text{N}_3\text{O}_7 + \text{H}^+$   $[\text{M}+\text{H}]^+$  304.1145, found 304.1138. **HR-MS (+):**  $m/z$  calcd for  $\text{C}_{11}\text{H}_{17}\text{N}_3\text{O}_7 + \text{Na}^+$   $[\text{M}+\text{Na}]^+$  326.0964, found 326.0956.

***N*-(β-D-galactopyranosyl-1,2,3-triazol-4-yl)-(3-oxopropyl-(oxy(2,5-dioxopyrrolidin-1-yl))) (3.12)**



**3.10** (0.226 g, 0.748 mmol) was added to a flask containing TSTU (0.247 g, 0.822 mmol, 1.1 equiv.) and placed under N<sub>2</sub>. Anhydrous DMF (10 mL) and anhydrous Triethylamine (0.114 mL, 0.822 mmol, 1.1 equiv.) were added. The reaction was stirred for 20 minutes, and reaction progress was monitored by TLC (60:35:5 DCM:MeOH:H<sub>2</sub>O). The solvent was removed in vacuo and the residue was washed with DCM. The precipitate was collected by centrifugation and dried, yielding a light pink powder (Yield 0.204 g, 0.509 mmol, 68%).

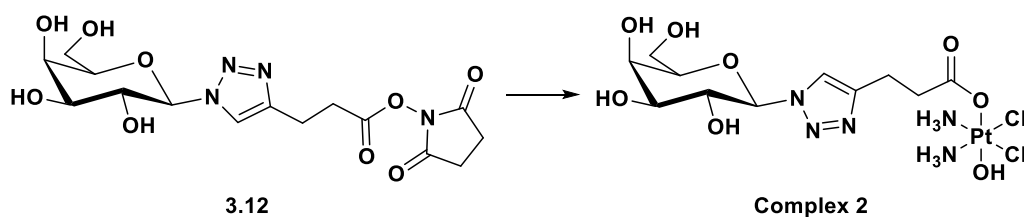
R<sub>f</sub> = 0.9 (DCM:MeOH:H<sub>2</sub>O 60:35:5).

<sup>1</sup>H NMR (500 MHz, DMSO) δ 8.07 (s, 1H, triaz-CH), 5.44 (d, *J* = 9.2 Hz, 1H, H-1), 5.16 (d, *J* = 6.0 Hz, 1H, OH of C-2), 5.03 (d, *J* = 5.7 Hz, 1H, OH of C-3), 4.70 (t, *J* = 5.7 Hz, 1H, OH of C-6), 4.66 (d, *J* = 4.9 Hz, 1H, OH of C-4), 4.03 – 3.96 (m, 1H, H-2), 3.76 (t, *J* = 3.75 Hz, 1H, H-4), 3.70 (t, *J* = 6.1 Hz, 1H, H-5), 3.56 – 3.44 (m, 3H, H-3, H-6, H-6'), 3.09 (t, *J* = 7.0 Hz, 2H, CH<sub>2</sub>CO), 3.02 – 2.99 (m, 2H, triaz-CH<sub>2</sub>), 2.82 (s, 2H, CH<sub>2</sub>CH<sub>2</sub>-succ) ppm.

<sup>13</sup>C NMR (125 MHz, DMSO) δ 170.2 (CO succ x2), 168.4 (CO), 144.4 (triaz-C), 121.1 (triaz-CH), 88.1 (C-1), 78.4 (C-5), 73.7 (C-3), 69.3 (C-2), 68.4 (C-4), 60.5 (C-6), 29.6 (CH<sub>2</sub>CO), 25.5 (CH<sub>2</sub>CH<sub>2</sub>-succ), 20.3 (triaz-CH<sub>2</sub>) ppm.

IR (ATR) 3309.24, 2917.95, 1731.99, 1368.41, 1205.61, 1020.46, 891.00, 820.54, 647.48 cm<sup>-1</sup>.

HR-MS (+): *m/z* calcd for C<sub>15</sub>H<sub>20</sub>N<sub>4</sub>O<sub>9</sub> + H<sup>+</sup> [M+H]<sup>+</sup> 401.1309, found 401.1305. HR-MS (+): *m/z* calcd for C<sub>15</sub>H<sub>20</sub>N<sub>4</sub>O<sub>9</sub> + Na<sup>+</sup> [M+Na]<sup>+</sup> 423.1128, found 423.1127.

***Cis,cis,trans*-[Pt<sup>IV</sup>(NH<sub>3</sub>)<sub>2</sub>(3.10)(OH)Cl<sub>2</sub>] (2)**

**3.12** (0.204 g, 0.509 mmol) was dissolved in DMSO (15mL) and added dropwise to a suspension of Oxoplatin (0.255 g, 0.764 mmol, 1.5 equiv.) in DMSO (5 mL) at 40°C and stirred for 48 hours. The unreacted Oxoplatin was removed by filtration and the DMSO was evaporated by lyophilisation. The remaining oil was treated with DCM, MeOH and Diethyl Ether. The remaining solid was dried under reduced pressure to yield a white/yellow powder (Yield 0.111 g, 0.179 mmol, 35%).

<sup>1</sup>H NMR (500 MHz, DMSO) δ 8.00 (s, 1H, triaz-CH), 6.11 – 5.80 (br. t, 6H, 2x NH<sub>3</sub>), 5.39 (d, *J* = 9.2 Hz, 1H, H-1), 5.18 (d, *J* = 5.9 Hz, 1H, OH of C-2), 5.03 (d, *J* = 5.6 Hz, 1H, OH of C-3), 4.70 (t, *J* = 5.6 Hz, 1H, OH of C-6), 4.64 (d, *J* = 5.1 Hz, 1H, OH of C-4), 4.05 – 3.98 (m, 1H, H-2), 3.75 (t, *J* = 3.6 Hz, 1H, H-4), 3.68 (t, *J* = 5.9 Hz, 1H, H-5), 3.56 – 3.47 (m, 3H, H-3, H-6, H-6'), 2.83 (t, *J* = 7.45 Hz, 2H, triaz-CH<sub>2</sub>), 2.53 – 2.51 (m, 2H, CH<sub>2</sub>CO, overlaps with DMSO) ppm.

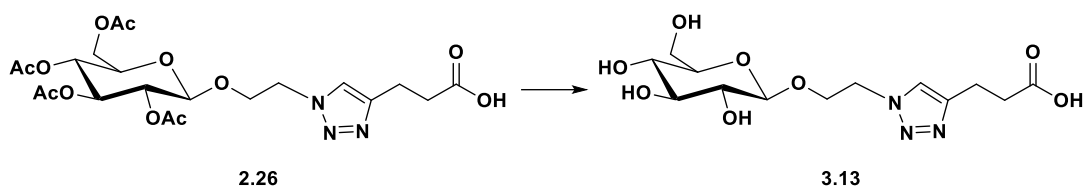
<sup>13</sup>C NMR (125 MHz, DMSO) δ 179.9 (CO), 146.4 (triaz-C), 121.0 (triaz-CH), 88.0 (C-1), 78.4 (C-5), 73.7 (C-3), 69.2 (C-2), 68.5 (C-4), 60.5 (C-6), 36.0 (CH<sub>2</sub>CO), 21.9 (triaz-CH<sub>2</sub>) ppm.

<sup>195</sup>Pt{<sup>1</sup>H} NMR (108 MHz, DMSO) δ 1045.09 ppm.

IR (ATR) 3224.69, 1617.95, 1352.08, 1090.21, 890.51, 563.88, 437.95 cm<sup>-1</sup>.

HR-MS (+): *m/z* calcd for C<sub>11</sub>H<sub>23</sub>Cl<sub>2</sub>N<sub>5</sub>O<sub>8</sub>Pt + H<sup>+</sup> [M+H]<sup>+</sup> 619.0644, found 620.0634.

El. Anal. Calcd. for C<sub>11</sub>H<sub>23</sub>Cl<sub>2</sub>N<sub>5</sub>O<sub>8</sub>Pt: % C = 21.33; H = 3.74; N = 11.31; found: % C = 21.64; H = 3.82; N = 11.72.

***N*-[2-*O*-( $\beta$ -D-glucopyranosyl)-ethyl-1,2,3-triazol-4-yl]-propanoic acid (3.13)**

**2.26** (0.088 g, 0.170 mmol) was suspended in a mixture of methanol (4 mL) and water (2 mL) and heated at 45°C. NEt<sub>3</sub> (0.1 mL) was added, and the reaction was allowed to stir overnight. The progress was checked using TLC (95:5 DCM:MeOH). The solvent was removed under vacuum and the residue was redissolved in H<sub>2</sub>O and stirred with Amberlite H<sup>+</sup> resin for 40 minutes. The Amberlite was filtered, and the residue was dried by lyophilisation and reacted in the following step without further purification (Yield 0.053 g, 0.152 mmol, 89%).

**R<sub>f</sub>** = 0.56 (DCM:MeOH:H<sub>2</sub>O 60:35:5).

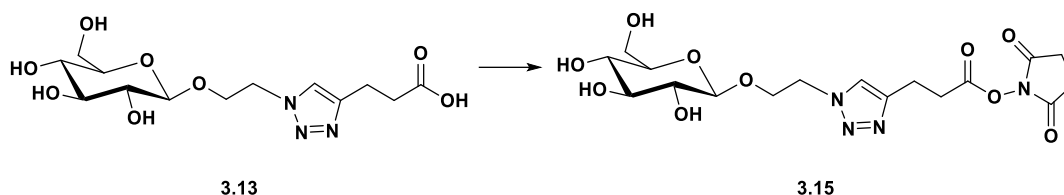
**<sup>1</sup>H NMR** (500 MHz, D<sub>2</sub>O)  $\delta$  7.80 (s, 1H, triaz-CH), 4.57 (dd,  $J$  = 14.3, 3.5 Hz, 2H, CH<sub>2</sub>-triaz), 4.35 (d,  $J$  = 6.8 Hz, 1H, H-1), 4.27 – 4.20 (m, 1H, OCH), 4.05 (dt,  $J$  = 6.2, 4.1 Hz, 1H, OCH'), 3.84 (d,  $J$  = 12.3 Hz, 1H, H-6), 3.67 – 3.60 (m, 1H, H-6'), 3.43 – 3.27 (m, 3H, H-3, H-4, H-5), 3.21 – 3.18 (m, 1H, H-2), 2.92 (td,  $J$  = 7.3, 1.3 Hz, 2H, triaz-CH<sub>2</sub>), 2.53 (t,  $J$  = 7.4 Hz, 2H, CH<sub>2</sub>CO) ppm.

**<sup>13</sup>C NMR** (125 MHz, D<sub>2</sub>O)  $\delta$  180.8 (CO), 147.4 (triaz-C), 123.7 (triaz-CH), 102.4 (C-1), 75.9 (C-3), 75.6 (C-5), 72.9 (C-2), 69.5 (C-4), 68.1 (OCH<sub>2</sub>), 60.7 (C-6), 50.1 (CH<sub>2</sub>-triaz), 36.0 (CH<sub>2</sub>CO), 21.4 (triaz-CH<sub>2</sub>) ppm.

**IR (ATR)** 3334.48, 2885.68, 1711.54, 1553.96, 1358.20, 1219.58, 1030.84, 828.66, 494.93 cm<sup>-1</sup>.

**HR-MS (+):**  $m/z$  calcd for C<sub>13</sub>H<sub>21</sub>N<sub>3</sub>O<sub>8</sub> + H<sup>+</sup> [M+H]<sup>+</sup> 348.1407, found 348.1402. **HR-MS (+):**  $m/z$  calcd for C<sub>13</sub>H<sub>21</sub>N<sub>3</sub>O<sub>8</sub> + Na<sup>+</sup> [M+Na]<sup>+</sup> 370.1226, found 370.1218.

***N*-[2-*O*-( $\beta$ -D-glucopyranosyl)-ethyl-1,2,3-triazol-4-yl]-[3-oxopropyl-(oxy(2,5-dioxopyrrolidin-1-yl))] (3.15)**



**3.13** (0.371 g, 1.068 mmol) was added to a flask containing TSTU (0.353 g, 1.174 mmol, 1.1 equiv.) and placed under  $N_2$ . Anhydrous DMF (10 mL) and anhydrous Triethylamine (0.163 mL, 1.174 mmol, 1.1 equiv.) were added. The reaction was stirred for 20 minutes, and reaction progress was monitored by TLC (60:35:5 DCM:MeOH:H<sub>2</sub>O). The solvent was removed in vacuo and the residue was washed with DCM. The precipitate was collected by centrifugation and dried, yielding a light pink powder (Yield 0.380 g, 0.855 mmol, 80%).

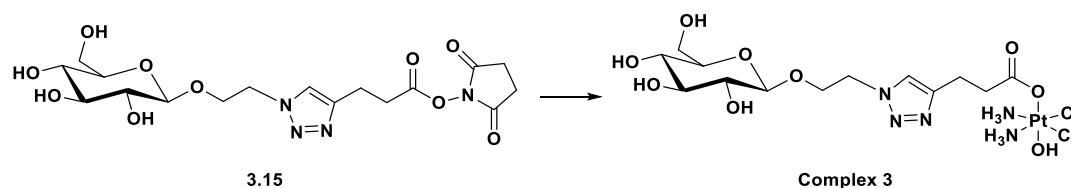
$R_f$  = 0.86 (DCM:MeOH:H<sub>2</sub>O 60:35:5).

**<sup>1</sup>H NMR** (500 MHz, DMSO)  $\delta$  7.99 (s, 1H, triaz-CH), 5.10 (d,  $J$  = 5.0 Hz, 1H, OH of C-2), 4.99 (d,  $J$  = 4.8 Hz, 1H, OH of C-3), 4.94 (d,  $J$  = 5.3 Hz, 1H, OH of C-4), 4.52 (dt,  $J$  = 6.8, 4.2 Hz, 3H, CH<sub>2</sub>-triaz, OH of C-6), 4.21 (d,  $J$  = 7.8 Hz, 1H, H-1), 4.06 (ddd,  $J$  = 10.6, 5.9, 4.4 Hz, 1H, OCH), 3.86 (ddd,  $J$  = 11.2, 6.7, 4.4 Hz, 1H, OCH'), 3.67 (ddd,  $J$  = 11.5, 5.9, 1.8 Hz, 1H, H-6), 3.43 (dt,  $J$  = 11.7, 5.9 Hz, 1H, H-6'), 3.16 – 3.08 (m, 2H, H-3, H-5), 3.08 – 3.01 (m, 3H, CH<sub>2</sub>CO, H-4), 3.00 – 2.93 (m, 3H, H-2, triaz-CH<sub>2</sub>), 2.81 (s, 4H, CH<sub>2</sub>CH<sub>2</sub>-succ) ppm.

**<sup>13</sup>C NMR** (125 MHz, DMSO)  $\delta$  170.2 (CO succ x2), 168.3 (CO), 144.2 (triaz-C), 123.2 (triaz-CH), 102.9 (C-1), 77.0 (C-3), 76.6 (C-5), 73.3 (C-2), 70.0 (C-4), 67.3 (OCH<sub>2</sub>), 61.1 (C-6), 49.5 (CH<sub>2</sub>-triaz), 29.8 (CH<sub>2</sub>CO), 25.5 (CH<sub>2</sub>CH<sub>2</sub>-succ), 20.4 (triaz-CH<sub>2</sub>) ppm.

**IR (ATR)** 3369.66, 2886.72, 1728.66, 1366.57, 1206.12, 1033.96, 813.22, 645.50 cm<sup>-1</sup>.

**HR-MS (+):**  $m/z$  calcd for C<sub>17</sub>H<sub>24</sub>N<sub>4</sub>O<sub>10</sub> + H<sup>+</sup> [M+H]<sup>+</sup> 445.1571, found 445.1561. **HR-MS (+):**  $m/z$  calcd for C<sub>17</sub>H<sub>24</sub>N<sub>4</sub>O<sub>10</sub> + Na<sup>+</sup> [M+Na]<sup>+</sup> 467.1390, found 467.1384.

***Cis,cis,trans*-[Pt<sup>IV</sup>(NH<sub>3</sub>)<sub>2</sub>(3.13)(OH)Cl<sub>2</sub>] (3)**

**3.15** (0.310 g, 0.697 mmol) was dissolved in DMSO (20 mL) and added dropwise to a suspension of Oxoplatin (0.349 g, 1.045 mmol, 1.5 equiv.) in DMSO (5 mL) at 40°C and stirred for 48 hours. The unreacted Oxoplatin was removed by filtration and the DMSO was evaporated by lyophilisation. The remaining oil was treated with DCM, MeOH and Diethyl Ether. The remaining solid was dried under reduced pressure to yield a white/yellow powder (Yield 0.218 g, 0.328 mmol, 47%).

<sup>1</sup>H NMR (500 MHz, DMSO) δ 7.93 (s, 1H, triaz-CH), 5.98 (t, *J* = 48.2 Hz, 6H, 2x NH<sub>3</sub>), 5.10 (d, *J* = 4.9 Hz, 1H, OH of C-2), 4.98 (d, *J* = 4.7 Hz, 1H, OH of C-3), 4.93 (d, *J* = 5.2 Hz, 1H, OH of C-4), 4.57 – 4.46 (m, 3H, CH<sub>2</sub>-triaz, OH of C-6), 4.21 (d, *J* = 7.8 Hz, 1H, H-1), 4.10 – 4.03 (m, 1H, OCH), 3.89 – 3.83 (m, 1H, OCH'), 3.67 (dd, *J* = 10.7, 4.4 Hz, 1H, H-6), 3.43 (dd, *J* = 11.4, 5.6 Hz, 1H, H-6'), 3.16 – 3.09 (m, 2H, H-3, H-5), 3.03 (dd, *J* = 9.0, 4.0 Hz, 1H, H-4), 2.98 – 2.93 (m, 1H, H-2), 2.80 (t, *J* = 7.2 Hz, 2H, triaz-CH<sub>2</sub>), 2.46 (d, *J* = 7.3 Hz, 2H, CH<sub>2</sub>CO) ppm.

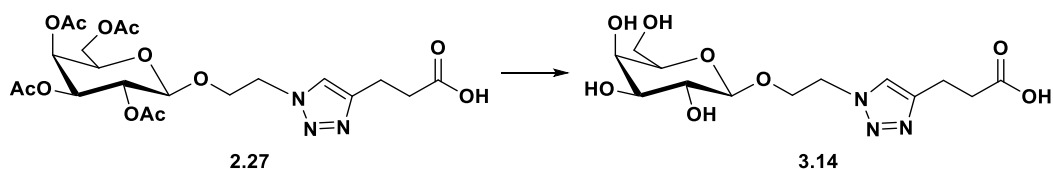
<sup>13</sup>C NMR (125 MHz, DMSO) δ 179.9 (CO), 146.2 (triaz-C), 122.9 (triaz-CH), 102.8 (C-1), 77.0 (C-3), 76.5 (C-5), 73.3 (C-2), 70.0 (C-4), 67.3 (OCH<sub>2</sub>), 61.1 (C-6), 49.4 (CH<sub>2</sub>-triaz), 36.1 (CH<sub>2</sub>CO), 22.0 (triaz-CH<sub>2</sub>) ppm.

<sup>195</sup>Pt{<sup>1</sup>H} NMR (108 MHz, DMSO) δ 1047.34 ppm.

IR (ATR) 3247.15, 1623.71, 1356.54, 1035.26, 578.92, 426.46 cm<sup>-1</sup>.

HR-MS (+): *m/z* calcd for C<sub>13</sub>H<sub>27</sub>Cl<sub>2</sub>N<sub>5</sub>O<sub>9</sub>Pt + H<sup>+</sup> [M+H]<sup>+</sup> 663.0907, found 664.0904.

El. Anal. Calcd. for C<sub>13</sub>H<sub>27</sub>Cl<sub>2</sub>N<sub>5</sub>O<sub>9</sub>Pt: % C = 23.54; H = 4.10; N = 10.56; found: % C = 23.27; H = 4.91; N = 10.11.

***N*-[2-*O*-( $\beta$ -D-galactopyranosyl)-ethyl-1,2,3-triazol-4-yl]-propanoic acid (3.14)**

**2.27** (0.357 g, 0.692 mmol) was suspended in a mixture of methanol (6 mL) and water (3 mL) and heated at 45°C. NEt<sub>3</sub> (0.2 mL) was added, and the reaction was allowed to stir overnight. The progress was checked using TLC (95:5 DCM:MeOH). The solvent was removed under vacuum and the residue was redissolved in H<sub>2</sub>O and stirred with Amberlite H<sup>+</sup> resin for 40 minutes. The Amberlite was filtered, and the residue was dried by lyophilisation and reacted in the following step without further purification (Yield 0.231 g, 0.665 mmol, 96%).

R<sub>f</sub> = 0.30 (DCM:MeOH:H<sub>2</sub>O 60:35:5).

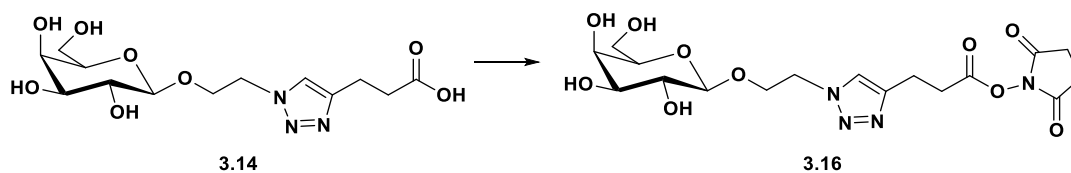
<sup>1</sup>H NMR (500 MHz, D<sub>2</sub>O)  $\delta$  7.85 (s, 1H, triaz-CH), 4.61 (t, *J* = 5.1 Hz, 2H, CH<sub>2</sub>-triaz), 4.31 (d, *J* = 7.9 Hz, 1H, H-1), 4.26 (dt, *J* = 11.5, 4.7 Hz, 1H, OCH), 4.09 – 4.04 (m, 1H, OCH'), 3.87 (d, *J* = 3.4 Hz, 1H, H-4), 3.75 – 3.67 (m, 2H, H-6, H-6'), 3.62 (dd, *J* = 7.7, 4.6 Hz, 1H, H-5), 3.58 (dd, *J* = 9.9, 3.5 Hz, 1H, H-3), 3.45 (dd, *J* = 9.9, 7.9 Hz, 1H, H-2), 2.96 (t, *J* = 7.3 Hz, 2H, triaz-CH<sub>2</sub>), 2.65 (t, *J* = 7.3 Hz, 2H, CH<sub>2</sub>CO) ppm.

<sup>13</sup>C NMR (125 MHz, D<sub>2</sub>O)  $\delta$  178.9 (CO), 146.9 (triaz-C), 123.9 (triaz-CH), 103.0 (C-1), 75.1 (C-5), 72.6 (C-3), 70.6 (C-2), 68.5 (C-4), 68.0 (OCH<sub>2</sub>), 60.9 (C-6), 50.2 (CH<sub>2</sub>-triaz), 34.5 (CH<sub>2</sub>CO), 20.7 (triaz-CH<sub>2</sub>) ppm.

IR (ATR) 3282.63, 2926.54, 1568.45, 1398.02, 1044.17, 781.51, 533.03 cm<sup>-1</sup>.

HR-MS (+): *m/z* calcd for C<sub>13</sub>H<sub>21</sub>N<sub>3</sub>O<sub>8</sub> + H<sup>+</sup> [M+H]<sup>+</sup> 348.1407, found 348.1403. HR-MS (+): *m/z* calcd for C<sub>13</sub>H<sub>21</sub>N<sub>3</sub>O<sub>8</sub> + Na<sup>+</sup> [M+Na]<sup>+</sup> 370.1226, found 370.1221.

***N*-[2-*O*-( $\beta$ -D-galactopyranosyl)-ethyl-1,2,3-triazol-4-yl]-(3-oxopropyl-(oxy(2,5-dioxopyrrolidin-1-yl))) (3.16)**



**3.14** (0.376 g, 1.082 mmol) was added to a flask containing TSTU (0.358 g, 1.190 mmol, 1.1 equiv.) and placed under N<sub>2</sub>. Anhydrous DMF (10 mL) and anhydrous Triethylamine (0.165 mL, 1.190 mmol, 1.1 equiv.) were added. The reaction was stirred for 20 minutes, and reaction progress was monitored by TLC (60:35:5 DCM:MeOH:H<sub>2</sub>O). The solvent was removed in vacuo and the residue was washed with DCM. The precipitate was collected by centrifugation and dried, yielding a light pink powder (Yield 0.360 g, 0.810 mmol, 75%).

R<sub>f</sub> = 0.84 (DCM:MeOH:H<sub>2</sub>O 60:35:5).

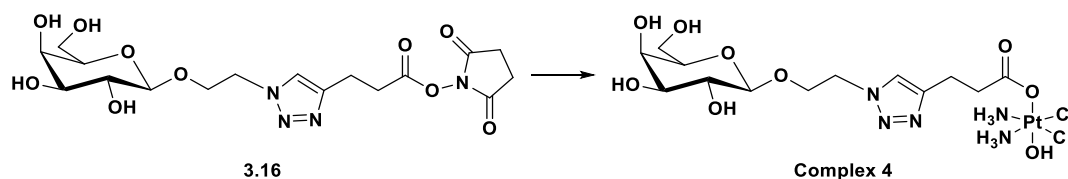
**<sup>1</sup>H NMR** (500 MHz, DMSO)  $\delta$  7.99 (s, 1H, triaz-CH), 4.95 (d, *J* = 4.6 Hz, 1H, OH of C-2), 4.76 (d, *J* = 5.3 Hz, 1H, OH of C-3), 4.59 (t, *J* = 5.7 Hz, 1H, OH of C-6), 4.51 (qdd, *J* = 14.3, 6.4, 4.2 Hz, 2H, CH<sub>2</sub>-triaz), 4.39 (d, *J* = 4.6 Hz, 1H, OH of C-4), 4.15 (d, *J* = 7.3 Hz, 1H, H-1), 4.05 (ddd, *J* = 10.7, 6.2, 4.3 Hz, 1H, OCH), 3.83 (ddd, *J* = 11.1, 6.7, 4.3 Hz, 1H, OCH'), 3.63 – 3.60 (m, 1H, H-4), 3.55 – 3.44 (m, 2H, H-6, H-6'), 3.34 – 3.24 (m, 3H, H-2, H-5, H-3), 3.07 – 3.03 (m, 2H, CH<sub>2</sub>CO), 3.00 – 2.95 (m, 2H, triaz-CH<sub>2</sub>), 2.81 (s, 4H, CH<sub>2</sub>CH<sub>2</sub>-succ) ppm.

**<sup>13</sup>C NMR** (125 MHz, DMSO)  $\delta$  170.2 (CO succ x2), 168.4 (CO), 144.2 (triaz-C), 123.2 (triaz-CH), 103.5 (C-1), 75.4 (C-5), 73.3 (C-3), 70.4 (C-2), 68.2 (C-4), 67.2 (OCH<sub>2</sub>), 60.5 (C-6), 49.6 (CH<sub>2</sub>-triaz), 29.8 (CH<sub>2</sub>CO), 25.5 (CH<sub>2</sub>CH<sub>2</sub>-succ), 20.4 (triaz-CH<sub>2</sub>) ppm.

**IR (ATR)** 3378.02, 2939.53, 1728.86, 1366.45, 1206.01, 1046.41, 648.73 cm<sup>-1</sup>.

**HR-MS (+):** *m/z* calcd for C<sub>17</sub>H<sub>24</sub>N<sub>4</sub>O<sub>10</sub> + H<sup>+</sup> [M+H]<sup>+</sup> 445.1571, found 445.1559. **HR-MS (+):** *m/z* calcd for C<sub>17</sub>H<sub>24</sub>N<sub>4</sub>O<sub>10</sub> + Na<sup>+</sup> [M+Na]<sup>+</sup> 467.1390, found 467.1385.



***Cis,cis,trans*-[Pt<sup>IV</sup>(NH<sub>3</sub>)<sub>2</sub>(3.16)(OH)Cl<sub>2</sub>] (4)**

**3.16** (0.322 g, 0.724 mmol) was dissolved in DMSO (15 mL) and added dropwise to a suspension of Oxoplatin (0.254 g, 0.760 mmol, 1.5 equiv.) in DMSO (5 mL) at 40°C and stirred for 48 hours. The unreacted Oxoplatin was removed by filtration and the DMSO was evaporated by lyophilisation. The remaining oil was treated with DCM, MeOH and Diethyl Ether. The remaining solid was dried under reduced pressure to yield a white/yellow powder (Yield 0.296 g, 0.446 mmol, 61%).

<sup>1</sup>H NMR (500 MHz, DMSO) δ 7.93 (s, 1H, triaz-CH), 5.98 (t, *J* = 48.4 Hz, 6H, 2x NH<sub>3</sub>), 4.96 (d, *J* = 4.3 Hz, 1H, OH of C-3), 4.77 (d, *J* = 4.4 Hz, 1H, OH of C-2), 4.59 (d, *J* = 5.1 Hz, 1H, OH of C-6), 4.55 – 4.41 (m, 2H, CH<sub>2</sub>-triaz), 4.40 (d, *J* = 4.4 Hz, 1H, OH of C-4), 4.15 (d, *J* = 7.1 Hz, 1H, H-1), 4.05 (ddd, *J* = 14.4, 9.4, 6.4 Hz, 1H, OCH), 3.84 (ddd, *J* = 11.0, 6.5, 4.6 Hz, 1H, OCH'), 3.62 (s, 1H, H-4), 3.50 (dd, *J* = 12.2, 6.4 Hz, 2H, H-6, H-6'), 3.35 (s, 1H, H-5 overlaps with H<sub>2</sub>O), 3.30 – 3.27 (m, 2H, H-2, H-3), 2.82 – 2.77 (m, 2H, triaz-CH<sub>2</sub>), 2.46 (d, *J* = 7.3 Hz, 2H, CH<sub>2</sub>CO) ppm.

<sup>13</sup>C NMR (125 MHz, DMSO) δ 179.9 (CO), 146.2 (triaz-C), 122.9 (triaz-CH), 103.5 (C-1), 75.4 (C-5), 73.3 (C-3), 70.4 (C-2), 68.2 (C-4), 67.2 (OCH<sub>2</sub>), 60.5 (C-6), 49.5 (CH<sub>2</sub>-triaz), 36.1 (CH<sub>2</sub>CO), 22.0 (triaz-CH<sub>2</sub>) ppm.

<sup>195</sup>Pt{<sup>1</sup>H} NMR (108 MHz, DMSO) δ 1046.82 ppm.

IR (ATR) 3215.30, 1618.19, 1358.28, 1061.49, 575.94 cm<sup>-1</sup>.

HR-MS (+): *m/z* calcd for C<sub>13</sub>H<sub>27</sub>Cl<sub>2</sub>N<sub>5</sub>O<sub>9</sub>Pt + H<sup>+</sup> [M+H]<sup>+</sup> 663.0907, found 664.0902.

El. Anal. Calcd. for C<sub>13</sub>H<sub>27</sub>Cl<sub>2</sub>N<sub>5</sub>O<sub>9</sub>Pt: % C = 23.54; H = 4.10; N = 10.56; found: % C = 23.18; H = 4.75; N = 10.06.

## **Chapter 4: C2 Platinum(IV) Glycoconjugates**

## 4.1 Introduction

In **Chapter 1** the important contribution of Gao and coworkers, who mainly investigated oxaliplatin analogues with different carbohydrate targeting moieties with the aim of improving their water solubility was discussed. The group of Lippard, on the other hand, focused on examining fundamental drug design of Pt(II) glycoconjugates. An important focus of this work was studying the effect of positional isomers of glucose-platinum conjugates on cell uptake and cytotoxicity, and this represents the first SAR (Structure Activity Relationship) study reported in literature with platinum-based glycoconjugates. The difference in cellular uptake between 2-NBDG (C2 4-nitrobenzofurazan) and 6-NBDG (C6 4-nitrobenzofurazan) (**Figure 4.1**) rationalises this study, as the C6-substituted conjugate was shown to bind GLUT1 with a 300-times greater affinity than 2-NBDG but had a much slower cellular uptake, whereas 2-NBDG has a much greater rate of accumulation [281].

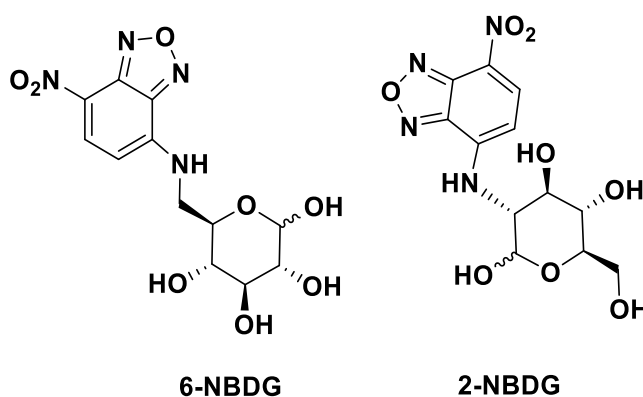


**Figure 4.1:** Structures of 6-NBDG and 2-NBDG.

The potency of the six complexes (**4.1 – 4.6** in **Figure 4.2**) was evaluated against prostate, ovarian and lung cancer cells and also against a non-cancerous cell line. The group concluded that after 72 hours, the substitution position did not have a significant influence on cytotoxicity, possibly because protein-mediated transport becomes saturated at longer time scales [161], resulting in a tight distribution of values, leading them to analyse the prostate cell line (DU145) after 7.5 hours (**Table 4.1**).

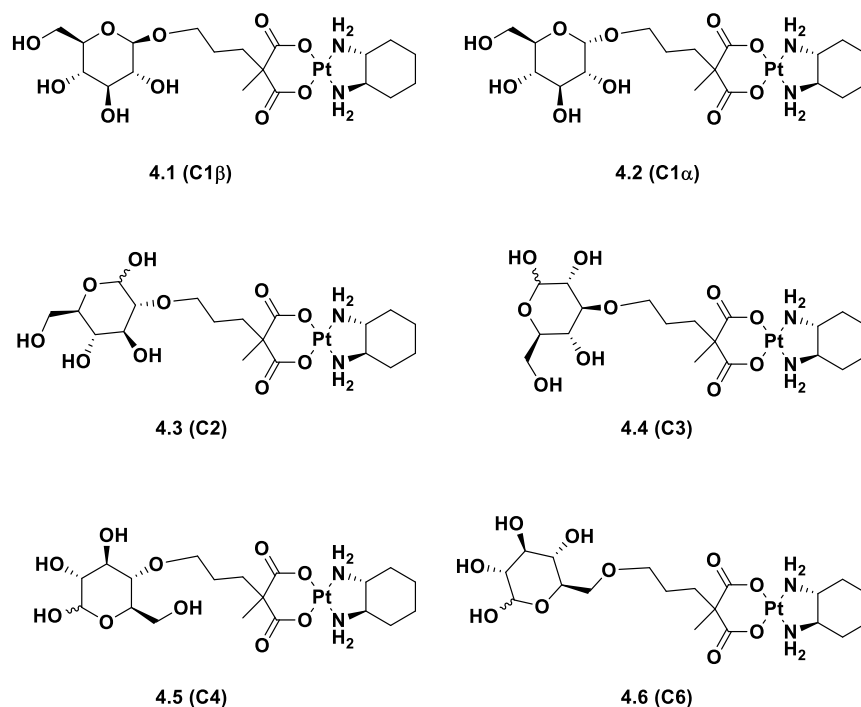


**Figure 4.2:** Structures of positional isomers of oxaliplatin glycoconjugates synthesised by Lippard et al. (4.1 – 4.6 [135]).

**Table 4.1:** IC<sub>50</sub> values ( $\mu\text{M}$ ) for complexes 4.1 – 4.6 against DU145 prostate cancer (7.5 and 72 h assays) and MRC5 non-cancerous lung epithelial cells (72 h assay). Adapted from [135].

| Cell line | Incubation time (h) | 4.1            | 4.2            | 4.3            | 4.4            | 4.5            | 4.6            |
|-----------|---------------------|----------------|----------------|----------------|----------------|----------------|----------------|
| DU145     | 7.5                 | 12 $\pm$ 2     | 11 $\pm$ 1     | 9 $\pm$ 0.5    | 26 $\pm$ 4     | 18 $\pm$ 2     | 19 $\pm$ 1     |
| DU145     | 72                  | 2.6 $\pm$ 0.08 | 3.7 $\pm$ 0.07 | 2.8 $\pm$ 0.27 | 3.4 $\pm$ 0.21 | 2.4 $\pm$ 0.14 | 2.4 $\pm$ 0.35 |
| MRC5      | 72                  | 13 $\pm$ 6.2   | >100           | >100           | 93.6 $\pm$ 15  | 72.3 $\pm$ 5.8 | 95.5 $\pm$ 19  |

4.3 displayed the greatest potency of the glycoconjugates tested with 4.1 and 4.2 sharing similar cytotoxicity. The group concluded that, in terms of conveying cytotoxicity in cancer cells, functionalisation at C1 or C2 is preferred over the other positions. Cellular uptake of the six complexes was also analysed (Figure 4.3), with 4.1 and 4.3 having the highest uptake in cancer cells.

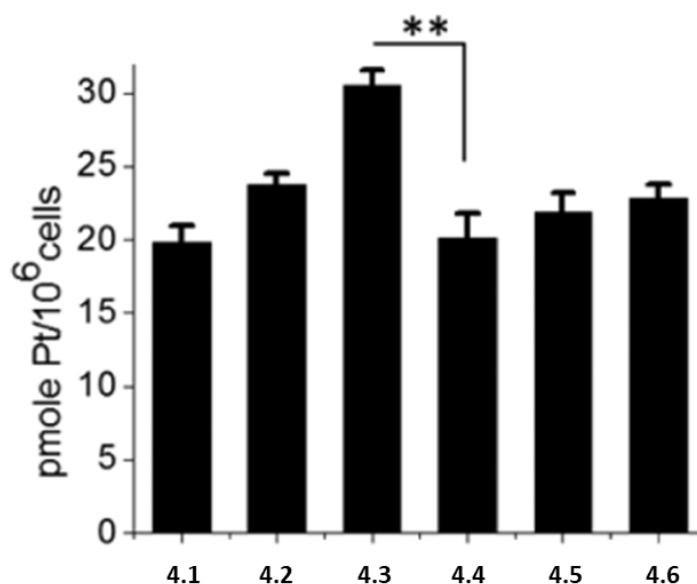


**Figure 4.3:** Whole cell uptake of complexes **4.1** – **4.6** in A549 lung epithelial cells, asterisks denote differences that are statistically significant (\*P < 0.01, \*\*P < 0.001). Adapted from [135].

Uptake studies which inhibit GLUT1 also showed that **4.3** had the highest dependency on GLUT1 for cellular uptake. These results suggest that C2 is the most preferential site for carbohydrate functionalisation, at least when coupled to an oxaliplatin scaffold [135].

To date, no other Pt(II) or Pt(IV) complexes have been synthesised using the results of this study and very few other metal-based glycoconjugates drugs have been developed which take advantage of substitution at the C2 position. The majority of anticancer complexes developed have been functionalised in the C1 or C6 positions, and while C1 has been shown to have good potency when compared to C2, C2's lack of interaction in the binding site of GLUT1 is too important to be ignored. Interestingly, the C2 position has been functionalised in a variety of metal complexes for cancer diagnostic purposes, but apart from Complex **4.3** in **Figure 4.2**, none have been employed as anticancer agents [282,283]. This gap in the research has led our group to develop four C2-functionalised Pt(IV) pro-drugs for the treatment of OS.

## 4.2 Chapter objective

This chapter discusses the synthesis of C2 Pt(IV) glycoconjugates, both protected and deprotected, with the aim of improving the cellular uptake and anticancer activity

when compared to their C1 counterparts. These novel complexes, reported in **Figure 4.4**, are characterised using multinuclear 1D and 2D NMR ( $^1\text{H}$ ,  $^{13}\text{C}$ ,  $^{195}\text{Pt}$ , COSY, HSQC, HMBC), IR, HR-MS, and Elemental analysis.

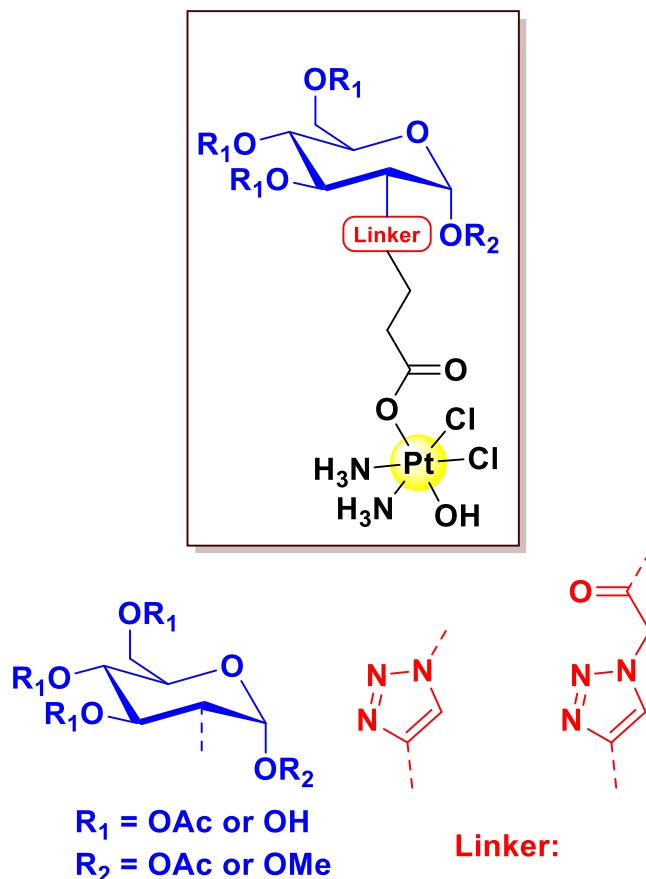


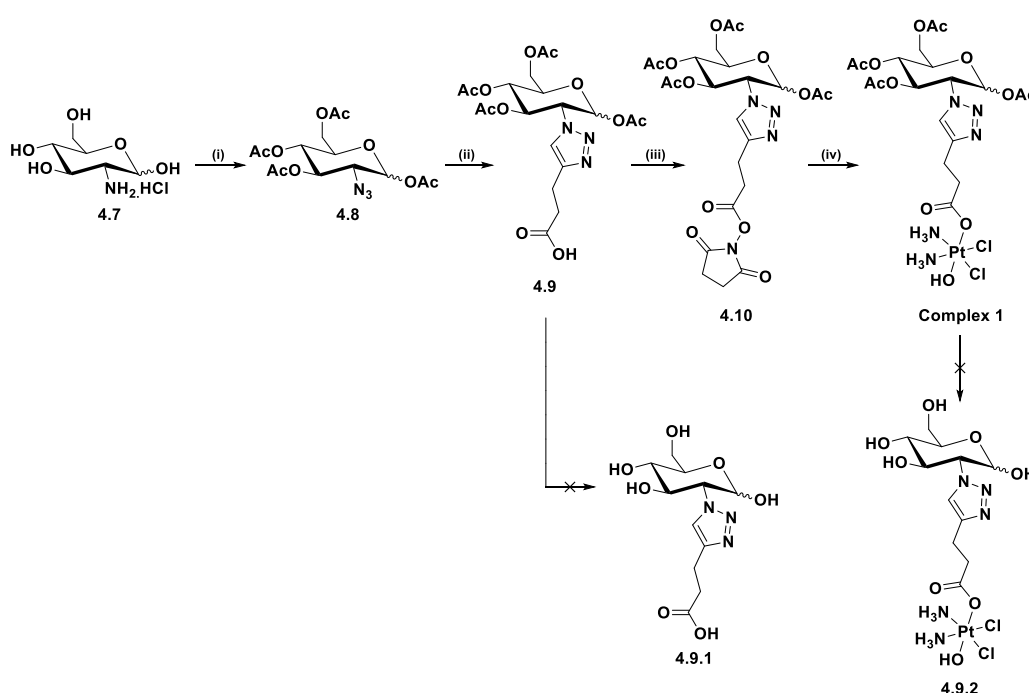
**Figure 4.4:** General structure for novel C2 Pt(IV) complexes based on the cisplatin scaffold, functionalised with glucose, and linked through click chemistry.

The complexes are synthesised using a combination of synthetic procedures described in the previous chapters as well as a variety of new reactions. Much like **Chapter 3**, a major portion of this chapter involved optimisation of different steps of the synthesis, in particular click reactions and coupling reactions to the metal centre. These complexes were then analysed against a panel of osteosarcoma cells, triple negative breast cancer, and glioblastoma cells.

## 4.3 Results and Discussion

### 4.3.1 Synthesis of C2-glycoconjugated Pt(IV) complexes

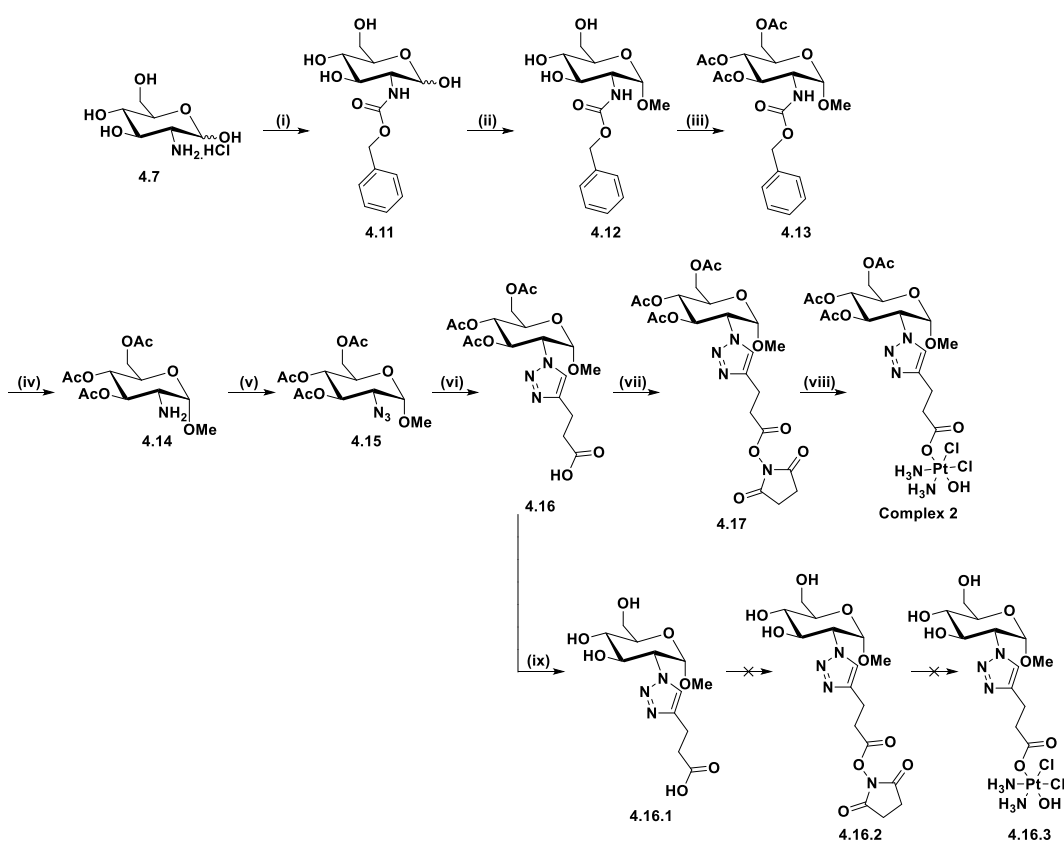
**Schemes 4.1, 4.2** and **4.3** depict the synthetic routes to obtain complexes **1 – 4**, as well as the attempted routes for complexes **4.9.2** and **4.16.3**. **Scheme 4.1** shows the steps to synthesise **Complex 1**, which is obtained through a diazo transfer reaction with D-glucosamine hydrochloride, which is followed by an acetylation of the free glucose azide (**i**). A CuAAC “click” reaction is then used to conjugate the resulting azide to 4-pentynoic acid (**ii**), the carboxylic acid product of this click reaction is then converted to its corresponding active ester using EDCI and NHS (**iii**). Finally, a transesterification reaction is used to form **Complex 1** with a mixture of  $\alpha$ -, and  $\beta$ -anomers (**iv**). This route also explores the attempted reactions to form the free sugar derivative of **Complex 1**. The first attempt being the deprotection of **Complex 1**, and the second attempt the deprotection of compound **4.9**.



**Scheme 4.1:** Synthetic route for **Complex 1** and the attempted route for its free sugar derivative: (i)  $\text{Tf}_2\text{O}$ ,  $\text{NaN}_3$ ,  $\text{H}_2\text{O}$ ,  $\text{DCM}$ ,  $\text{K}_2\text{CO}_3$ ,  $\text{MeOH}$ ,  $\text{CuSO}_4$ ; then  $\text{Ac}_2\text{O}$ , Pyridine, rt, 16 h, 74% for the two steps; (ii) 4-pentynoic acid,  $\text{CuSO}_4$ ,  $\text{NaAsc}$ ,  $t\text{-BuOH}$ ,  $\text{THF}$ ,  $\text{H}_2\text{O}$ , rt, 16 h, 59%; (iii) EDCI, NHS,  $\text{DCM}$ , rt, 16 h, 89%; (iv)  $\text{DMSO}$ ,  $60^\circ\text{C}$ , 16 h, 67%.

**Scheme 4.2** shows the synthetic route to **Complex 2**, a derivative of **Complex 1** which contains only the methyl-*O*-glucoside  $\alpha$ -anomer, and also shows the attempt to

synthesise the free sugar derivative of **Complex 2** (**4.16.3**). The synthesis begins with the protection of D-glucosamine hydrochloride using benzyl chloroformate (Cbz) to give **4.11** (**i**), and in two steps, the anomeric position is glycosylated (**ii**), and subsequent acetylation of the remaining hydroxyl groups (**iii**) gives the *O*-methyl glucoside (**4.13**), isolated by column chromatography. The C2 amine is reformed by removal of the *N*-Cbz protecting group using Pd-catalyzed hydrogenation to give **4.14** (**iv**) and much like in **scheme 4.1**, a diazo-transfer reaction is used in step (**v**) to give the resulting azide (**4.15**). The click reaction of said azide with 4-pentynoic acid gives **4.16** (**vi**), followed by NHS ester formation through reaction with EDCI (**vii**) to give NHS ester **4.17**. Finally, transesterification reaction (**viii**) produced the acetylated **Complex 2**. The click reaction in this scheme and **Scheme 4.3** required optimisation and the best reaction condition was when 4-pentynoic acid was used in excess with a solvent system of *t*-BuOH and H<sub>2</sub>O. Finally, the synthesis of the deprotected derivative of this complex (**4.16.3**) was attempted, but we were unable to isolate a pure product.

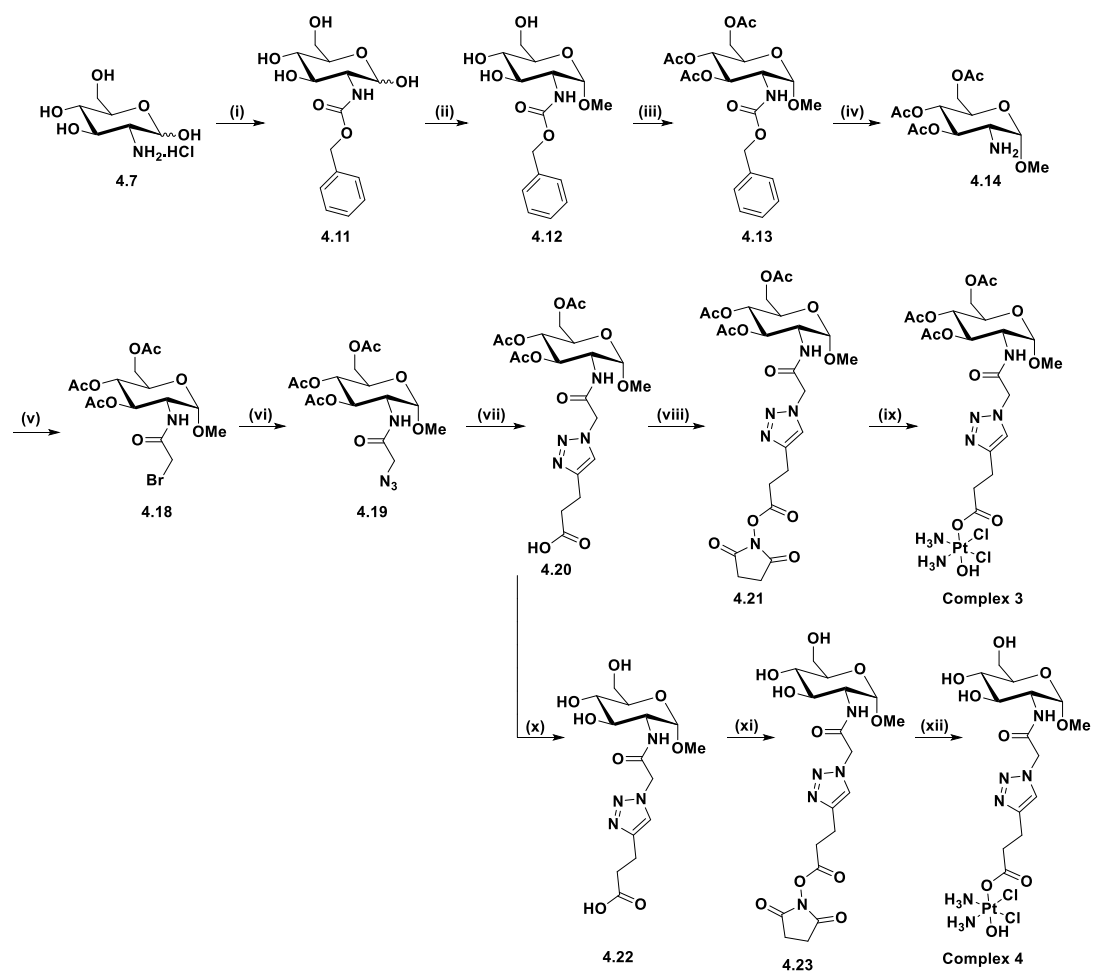


**Scheme 4.2:** Synthetic route for **Complex 2** and the attempted route to **Complex 4.16.3**: (i) NaHCO<sub>3</sub>, Benzyl chloroformate, H<sub>2</sub>O, 16 h, rt, 92%; (ii) HCl/MeOH soln. 1.25 M, 80°C, 18 h;



(iii) Pyridine, Ac<sub>2</sub>O, rt, 16 h, 73%; (iv) Pd/C, H<sub>2</sub>, DCM, rt, 16 h; (v) NaN<sub>3</sub>, Tf<sub>2</sub>O, K<sub>2</sub>CO<sub>3</sub>, CuSO<sub>4</sub>·5H<sub>2</sub>O, DCM, MeOH, H<sub>2</sub>O, rt, 16 h, 35%; (vi) 4-pentynoic acid, CuSO<sub>4</sub>·5H<sub>2</sub>O, NaAsc, t-BuOH, H<sub>2</sub>O, rt, 16 h, 65%; (vii) NHS, EDCI, DCM, rt, 16 h, 91%; (viii) Oxoplatin, DMSO, 60°C, 16 h, 86%; (ix) NEt<sub>3</sub>, MeOH, H<sub>2</sub>O, 40°C, 16 h, 96%.

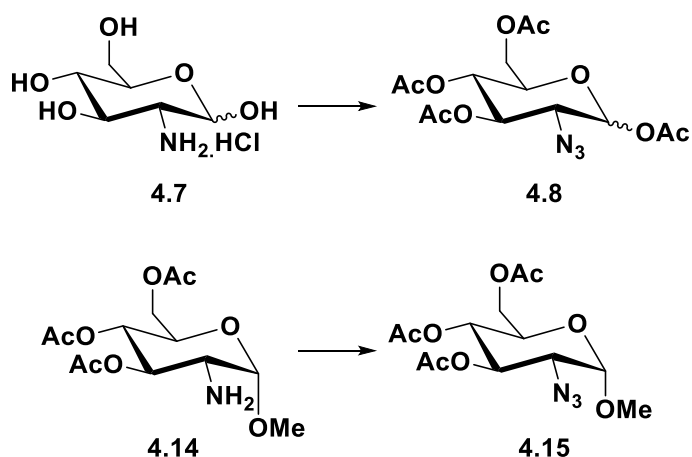
**Scheme 4.3** shows the synthesis of **Complex 3** and its free sugar derivative, **Complex 4**. This route connects the azide derivative (**4.19**) through an amide bond to the carbohydrate targeting moiety, differing from **complexes 1** and **2** which feature the azido group (**4.8**, **4.15**) directly attached on the sugar. Steps **(i)**, **(ii)**, **(iii)**, and **(iv)** followed the same procedures used in **Scheme 4.2**, but in the following step, the free amine **4.14** is converted to an amide through reaction with bromoacetyl bromide to give **4.18 (v)**; this bromide **4.18** is then converted to the corresponding azide (**4.19 (vi)**). Steps **(vii)**, **(viii)**, and **(ix)** follow the same procedures as for **scheme 4.2** to yield **Complex 3**. However, in this case it was possible to isolate the free sugar derivative (**Complex 4**). The synthesis of this complex begins with a deprotection of the carboxylic acid (**4.20**) to give **4.22 (x)** and the corresponding ester **4.23** is formed using TSTU **(xi)**. This was then reacted with oxoplatin to yield **Complex 4 (xii)**.



**Scheme 4.3:** Synthetic route for **complexes 3** and **4**: (i)  $\text{NaHCO}_3$ , Benzyl chloroformate,  $\text{H}_2\text{O}$ , 16 h, rt, 92%; (ii)  $\text{HCl}/\text{MeOH}$  soln. 1.25 M,  $80^\circ\text{C}$ , 18 h; (iii) Pyridine,  $\text{Ac}_2\text{O}$ , rt, 16 h, 73%; (iv)  $\text{Pd}/\text{C}$ ,  $\text{H}_2$ ,  $\text{DCM}$ , rt, 16 h; (v) Bromoacetyl bromide,  $\text{NEt}_3$ ,  $\text{DCM}$ ,  $\text{N}_2$ , rt, 16 h, 71%; (vi)  $\text{NaN}_3$ ,  $\text{DMF}$ ,  $\text{N}_2$ ,  $80^\circ\text{C}$ , 16 h, 98%; (vii) 4-pentynoic acid,  $\text{NaAsc}$ ,  $\text{CuSO}_4 \cdot 5\text{H}_2\text{O}$ ,  $t\text{-BuOH}$ ,  $\text{H}_2\text{O}$ , rt, 16 h, 41%; (viii)  $\text{EDCI}$ ,  $\text{NHS}$ ,  $\text{DCM}$ , rt, 16 h, 82%; (ix) Oxoplatin,  $\text{DMSO}$ ,  $60^\circ\text{C}$ , 16 h, 82%; (x)  $\text{NEt}_3$ ,  $\text{MeOH}$ ,  $\text{H}_2\text{O}$ ,  $40^\circ\text{C}$ , 16 h, 98%; (xi)  $\text{TSTU}$ ,  $\text{NEt}_3$ ,  $\text{DMF}$ , rt, 20 min, 79%; (xii) Oxoplatin, dry  $\text{DMSO}$ ,  $40^\circ\text{C}$ , 5 days, 39%.

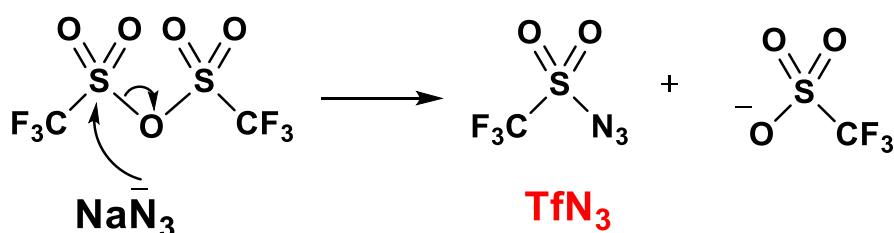
#### 4.3.2 Synthesis of C2 sugar azides through diazo-transfer (4.8, 4.15)

The following C2 sugar azides were synthesised using the diazo-transfer reaction (**Scheme 4.4**), first by synthesizing the diazo-transfer reagent trifluoromethanesulfonyl azide ( $\text{TfN}_3$ ), which is then reacted with D-glucosamine in the presence of a base and the copper catalyst to produce the desired product.



**Scheme 4.4:** Diazo-transfer reaction to form C2 glucose azides **4.8** (74%) and **4.15** (35%). Compound **4.8** is acetylated directly after the reaction takes place. The method to synthesise **4.14** is discussed in section 4.3.3.

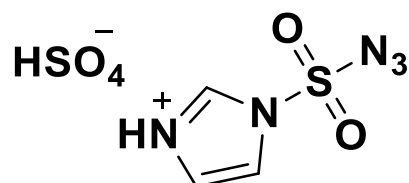
This reaction occurs when a diazo group ( $-N_2$ ) is transferred to an amine to form an azide while maintaining the stereochemistry of the starting material and producing no side products. Azides are important functional groups which show applications either in protecting group chemistry and, of course, in click chemistry reactions. Indeed, the diazo-transfer reaction is a convenient method to synthesise azides from their corresponding amines [284]. These reactions require diazo-transfer reagents which are typically synthesised immediately prior carrying out the reaction. As mentioned earlier, our group used  $TfN_3$ , which is synthesised from a reaction between trifluoromethanesulfonic anhydride ( $Tf_2O$ ) and  $NaN_3$  (Scheme 4.5).



**Scheme 4.5:** Mechanism for the synthesis of diazo transfer reagent  $TfN_3$ .

This compound is reacted immediately in the following step [285], however, due to the various hazards during its synthesis and storage, other groups have designed diazo-transfer reagents which are shelf stable and much less hazardous. In particular, imidazole-1-sulfonyl azide (Figure 4.5) was designed to be a diazo-transfer source

with similar reactivity to TfN<sub>3</sub>, but with a longer shelf life, lower cost to prepare, and lower electrostatic discharge and friction sensitivities than TfN<sub>3</sub> [286].

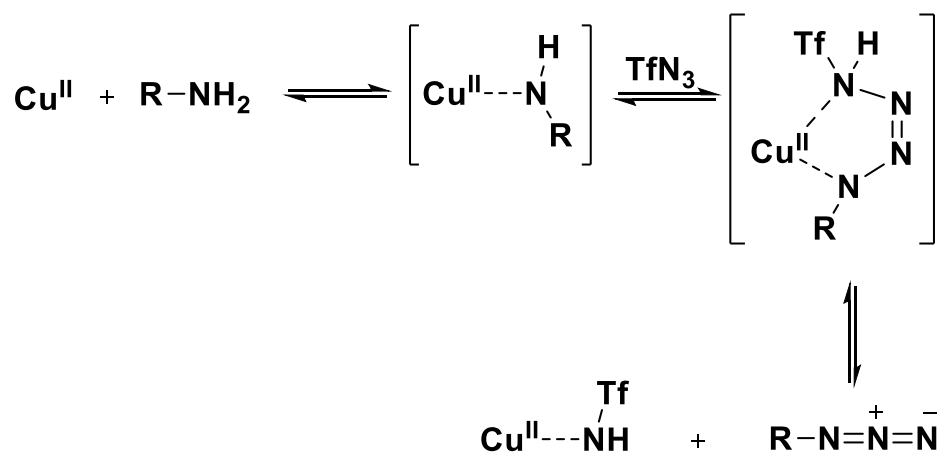


**Imidazole-1-sulfonyl azide**

**Figure 4.5:** Structure of diazo transfer reagent Imidazole-1-sulfonyl azide [286].

Our initial attempt was to use the above reagent due to its reported safety and ease of production, however, the isolation of this product was unsuccessful. After several attempts at optimizing the reaction conditions, including use of dry solvents or different reagent batches, we opted to synthesise TfN<sub>3</sub>, which proved to be a much more reliable method and allowed us to proceed with the synthesis of **4.8** and **4.15**.

The mechanism of this reaction has not been fully elucidated, however experimental evidence by Samuelson *et al.* [284] shows that the coordination of the amino group to the copper (II) catalyst facilitates the formation of cycloaddition-like intermediate through nucleophilic attack of the terminal nitrogen of the azide group; This species then collapses to liberate the azido-transfer product and the copper-amino triflate adduct that can re-enter the catalytic cycle (**Scheme 4.6**).

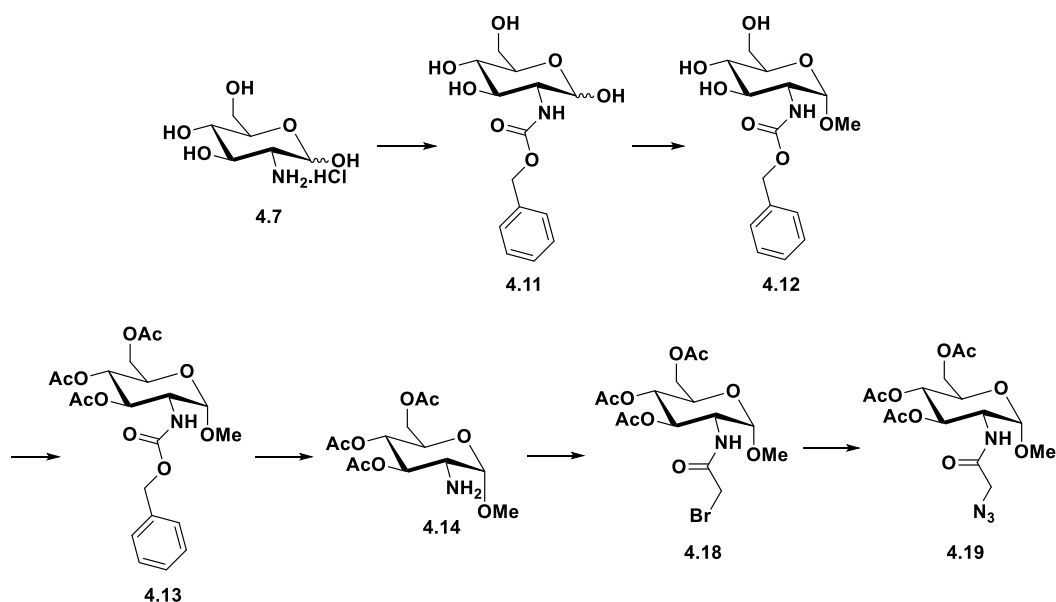


**Scheme 4.6:** Proposed mechanism for the copper catalysed diazo-transfer reaction [284,287].

In the case of compound **4.8**, the D-glucosamine hydrochloride starting material was dissolved in water and treated with  $K_2CO_3$  and  $CuSO_4 \cdot 5H_2O$ . The base functions to deprotonate the amine salt and aid coordination to the copper catalyst, and the corresponding conjugate acid donates protons to produce  $TfNH_2$ , which is removed during the workup. The free sugar azide is then acetylated using pyridine and acetic anhydride to produce the C2 azide with a mixture of  $\alpha$ - and  $\beta$ -anomers. **4.15** is produced in a similar reaction, however the starting material is already acetylated which means that DCM must be used as solvent due to the water-insolubility of the acetylated starting material **4.14**. Both **4.8** and **4.15** were purified using flash column chromatography and characterised using proton NMR, where the data matched reported literature values [285,288].

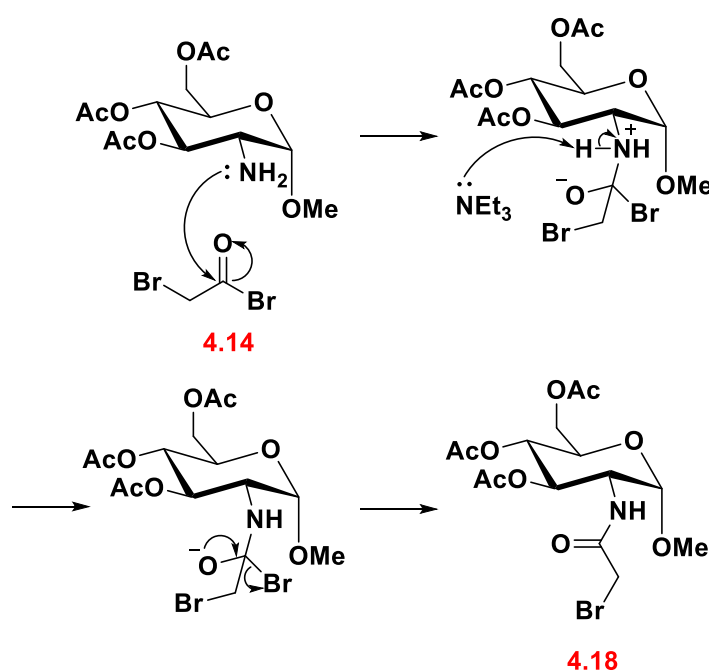
### 4.3.3 Synthesis of C2 sugar azide through substitution reaction (4.19)

**4.19** was synthesised through a 6-steps route to produce an azide with an increased linker length (**Scheme 4.7**). The purpose is to compare between the previously discussed azides and to see whether the different distance between the sugar and the platinum centre will affect the biological properties such as cellular uptake and cytotoxicity, as discussed in the previous chapters.



**Scheme 4.7:** Synthetic route to form the C2 azide (**4.19**), from **4.18** at 80°C for 16 hours, 98%.

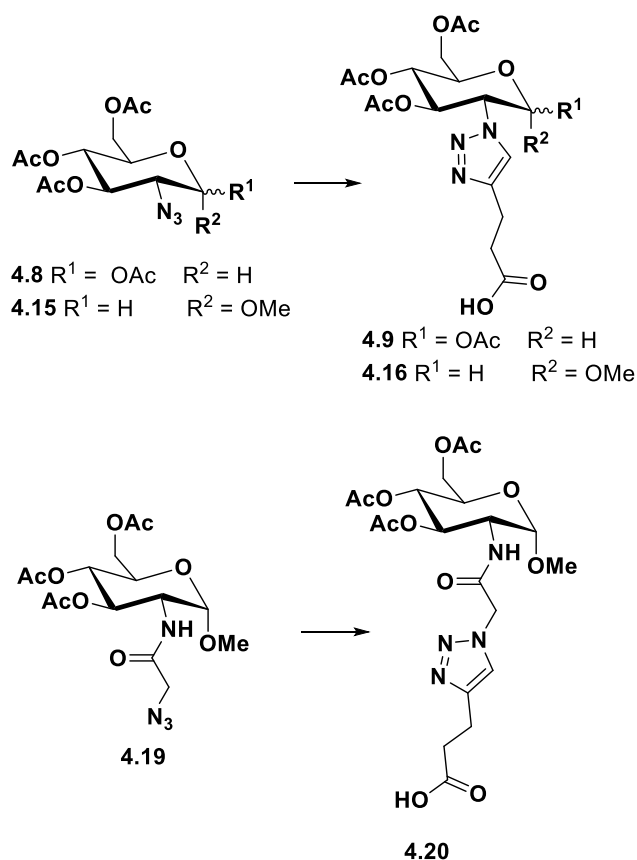
The route to form **4.19** begins with the protection of the C2 amine using benzyl chloroformate (Cbz) under basic conditions. This was isolated as a white solid (**4.11**) which was then dissolved in a solution of HCl in methanol (1.25 M) and refluxed overnight (**4.12**) [289]. The remaining hydroxyl groups were protected using pyridine and acetic anhydride to yield compound **4.13** which was purified by flash chromatography [290]. **4.14** was synthesised through the hydrogenative deprotection of the carbamate protecting group bubbling H<sub>2</sub> gas through a suspension of 10% w/w of palladium on activated charcoal in a solution of **4.13** in DCM. This product was used in the next reaction without further purification. The formation of **4.18** was achieved through adaptation of a previously reported procedure by Martin *et al.* [291], in which bromoacetyl bromide is reacted with the free amine in the presence of a base. The reaction proceeds by the nucleophilic attack of the amine at C2 to the carbonyl carbon of bromoacetyl bromide, resulting in the formation of a tetrahedral intermediate. The base (triethylamine in this case) deprotonates the ammonium, leaving the bromide as the best leaving group and thus resulting in the formation of the amide **4.18** (Scheme 4.8). Through an S<sub>N</sub>2 type mechanism this bromide is substituted by the azido group through reaction with NaN<sub>3</sub> at 80°C, forming the C2 azide **4.19**.



**Scheme 4.8:** Reaction mechanism for the formation of compound **4.18** through reaction with bromoacetyl bromide and NEt<sub>3</sub>.

### 4.3.4 Synthesis of acetylated C2 ligands using CuAAC “Click” chemistry (4.9, 4.16 and 4.20)

The **4.9**, **4.16** and **4.20** ligands were synthesised using CuAAC “click” chemistry (Scheme 4.9), with a similar method originally used to synthesise the ligands of Chapter 2, 3 and the compound **4.9**. However, for the C2 ligands containing the methoxy group in the anomeric position, different conditions were required to increase the overall yield of the product.



**Scheme 4.9:** Synthetic route to form free C2 ligands (**4.9** (59%), **4.16** (65%), and **4.20** (41%)) through copper catalysed reaction with 4-pentynoic acid in t-BuOH and H<sub>2</sub>O.

The synthesis of compound **4.20** was first attempted using the conditions described in the previous chapters, however the crude yield obtained was only 41% and after purification, became only 10%. To remedy this drawback, the sugar starting material (**4.19**) which was originally in excess, was made the limiting reagent and the alkyne (4-pentynoic acid) was used in excess. Ideally, the product obtained from this reaction should be suitable for use without column chromatography, as the alkyne is

removed in the workup through treatment with water. This should occur provided there is full conversion of the limiting reagents (**4.8**, **4.15**, and **4.19**). In practice, water/brine treatment during the workup yields a crude product with minimal impurities and purification through flash chromatography is still required. The removal of THF as a reaction solvent also improved yields and with these changes, an overall yield of 55% after purification was achieved. These ligands were characterised using NMR ( $^1\text{H}$ ,  $^{13}\text{C}$ , COSY, HSQC, and HMBC), IR spectroscopy and HR-MS.

The  $^1\text{H}$  NMR spectra of compounds **4.9** and **4.20** are shown below where the characteristic peaks are highlighted. Importantly, **4.9** exists as a mixture of the  $\alpha$ - and  $\beta$ -anomers (0.51:1.00 ratio), which can be seen from the purple and green highlighted signals in the  $^1\text{H}$  NMR (**Figure 4.6**).

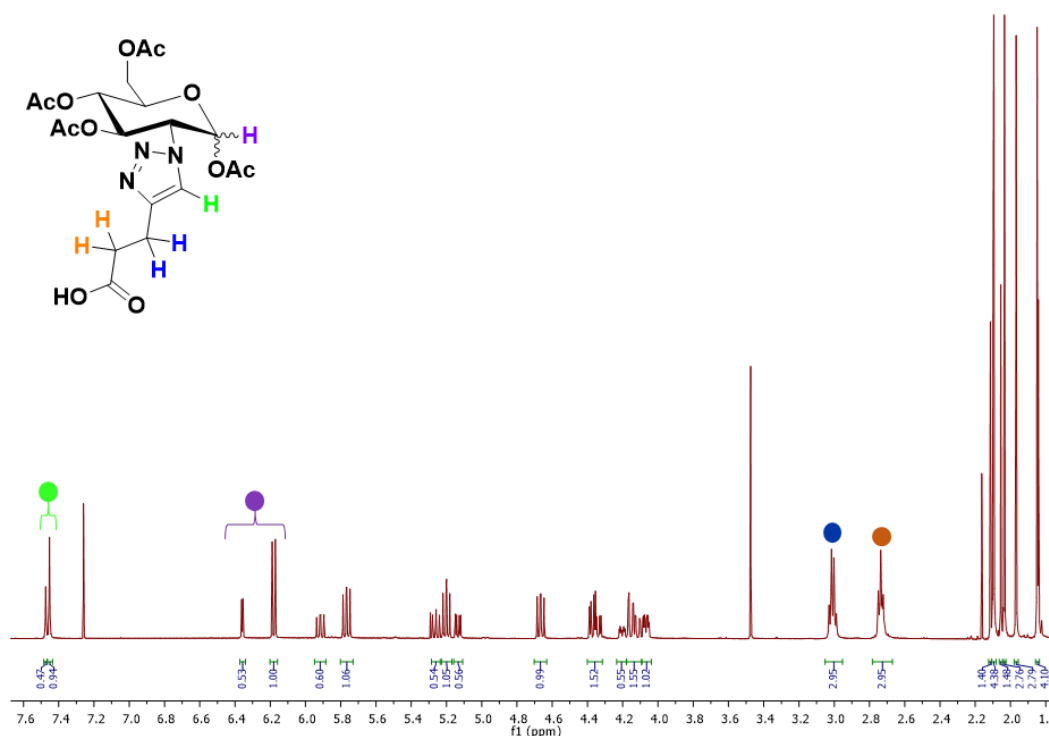


**Figure 4.6:**  $^1\text{H}$  NMR spectrum of the ligand **4.9**, in  $\text{CDCl}_3$ .

The ligands **4.16** and **4.20** are then synthesised, with an *O*-methyl group at the anomeric position, that allowed for the isolation of its precursor **4.12** as a single anomer ( $\alpha$ -anomer). The  $^1\text{H}$  NMR spectrum of **4.20** is reported below (**Figure 4.7**), with its characteristic peaks highlighted. The presence of the amide proton (red) at  $\delta = 6.75$  ppm demonstrates that the linker is preserved throughout the click reaction.



Finally, the two CH<sub>2</sub> signals (burgundy and orange) as well as the presence of the triazole (blue), confirmed the presence of the carboxylic acid (**4.20**).

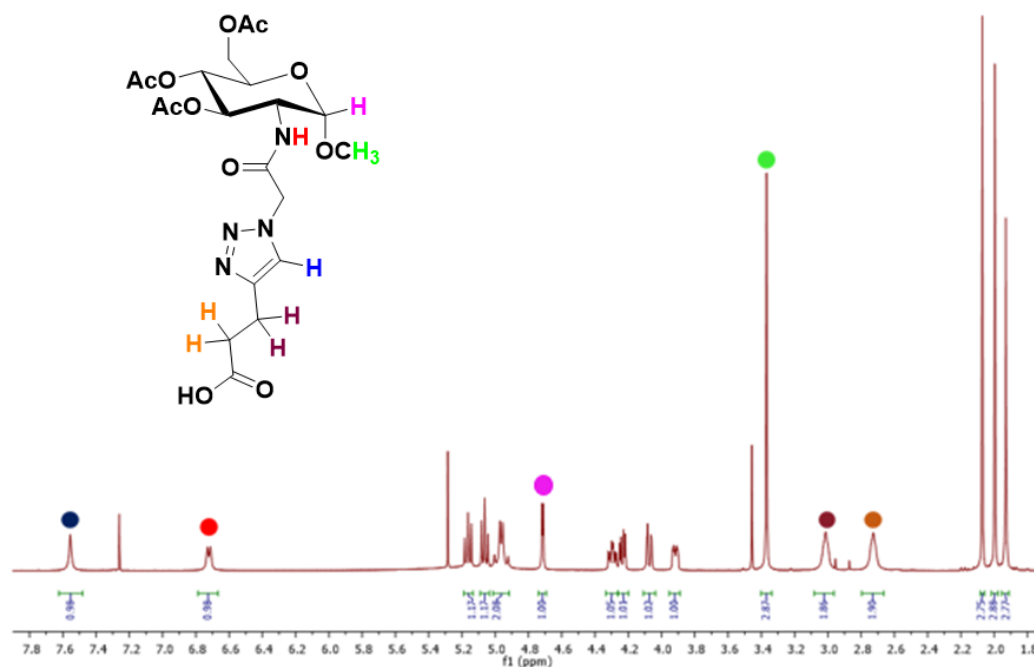
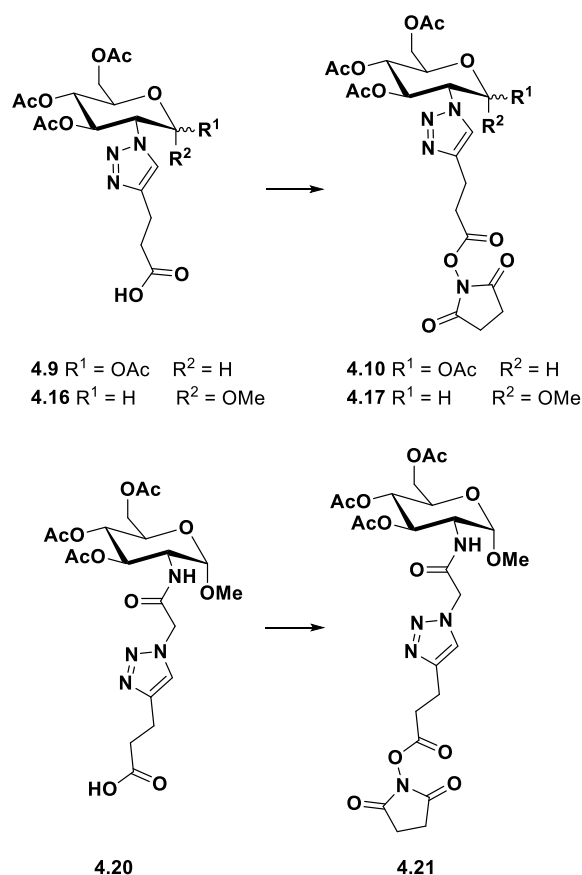


**Figure 4.7:** <sup>1</sup>H NMR spectrum of the ligand **4.20**, in CDCl<sub>3</sub>.

#### 4.3.5 Synthesis of acetylated C2 active esters (**4.10**, **4.17** and **4.21**)

The active esters **4.10**, **4.17** and **4.21** (**Scheme 4.10**) are synthesised from their carboxylic acids (**4.9**, **4.16**, and **4.20**) in the same manner as the active esters discussed in **Chapter 2**, using EDCI as a coupling reagent and NHS. The products are washed with 0.1M HCl and reacted without further purification.



**Scheme 4.10:** Synthetic route to form acetylated C2 active esters using EDCI as a coupling reagent, the reaction was carried out at room temperature for 16 hours with the following yields: **4.10** (89%), **4.17** (91%), **4.21** (82%).

The  $^1\text{H}$  NMR spectrum of compound **4.10** is shown below (**Figure 4.8**). Similar to the free ligand (**4.9**), this compound exists as a mixture of  $\alpha$ - and  $\beta$ -anomers, with a ratio of (0.81:1.00). The identification of the  $\alpha$ - and  $\beta$ -anomers are determined analysing the coupling constant of the anomeric proton. According to the Karplus equation, which describes the relationship between the coupling constant and the dihedral angle between vicinal hydrogens, axial substituents at the anomeric carbon in D-glucose (the  $\alpha$ -anomers) will have a smaller coupling constant than the  $\beta$ -anomers, with equatorial substituents.

The formation of the NHS ester is confirmed by the appearance of a singlet at  $\delta = 2.8$  ppm (orange) accompanied by a downfield shift of the blue ( $\Delta\delta = 0.10$  ppm) and purple ( $\Delta\delta = 0.20$  ppm) signals corresponding to the  $\text{CH}_2$ 's protons.

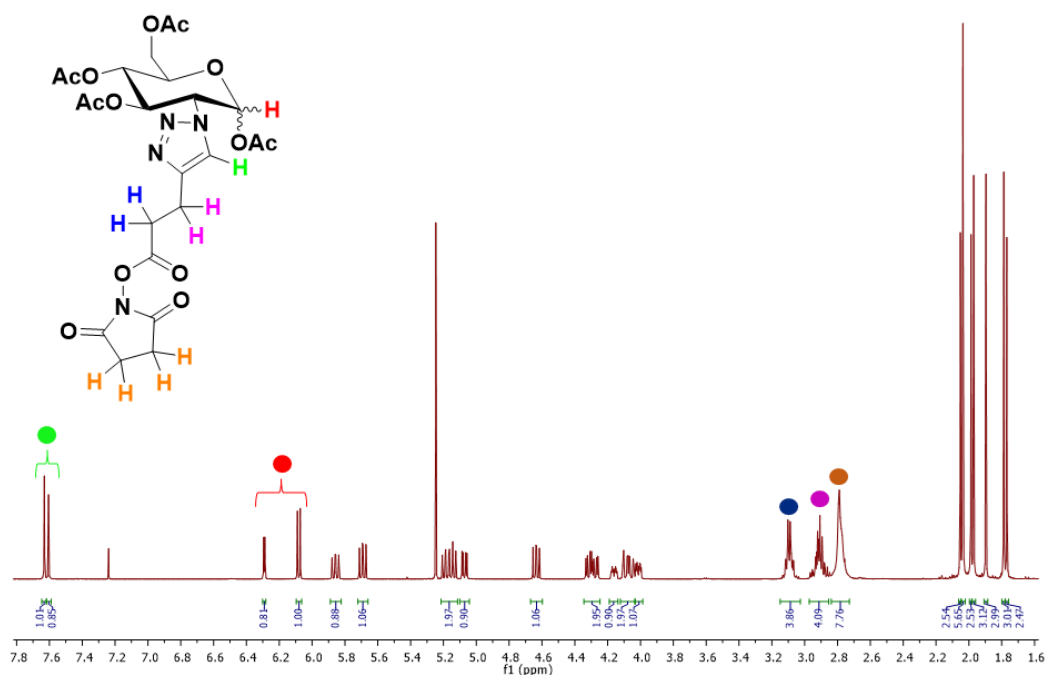


**Figure 4.8:** <sup>1</sup>H NMR spectrum of active ester **4.10**, in CDCl<sub>3</sub>.

Compound **4.21** (**Figure 4.9**) is synthesised under the same conditions and differs from **4.10** in the α-O-methyl group in the anomeric position (red) as well as the increased linker length through the addition of an amide bond (green). The single anomeric proton at δ = 4.7 ppm (blue) and the presence of the succinimido protons at δ = 2.85 ppm (burgundy) confirm the formation of the product.

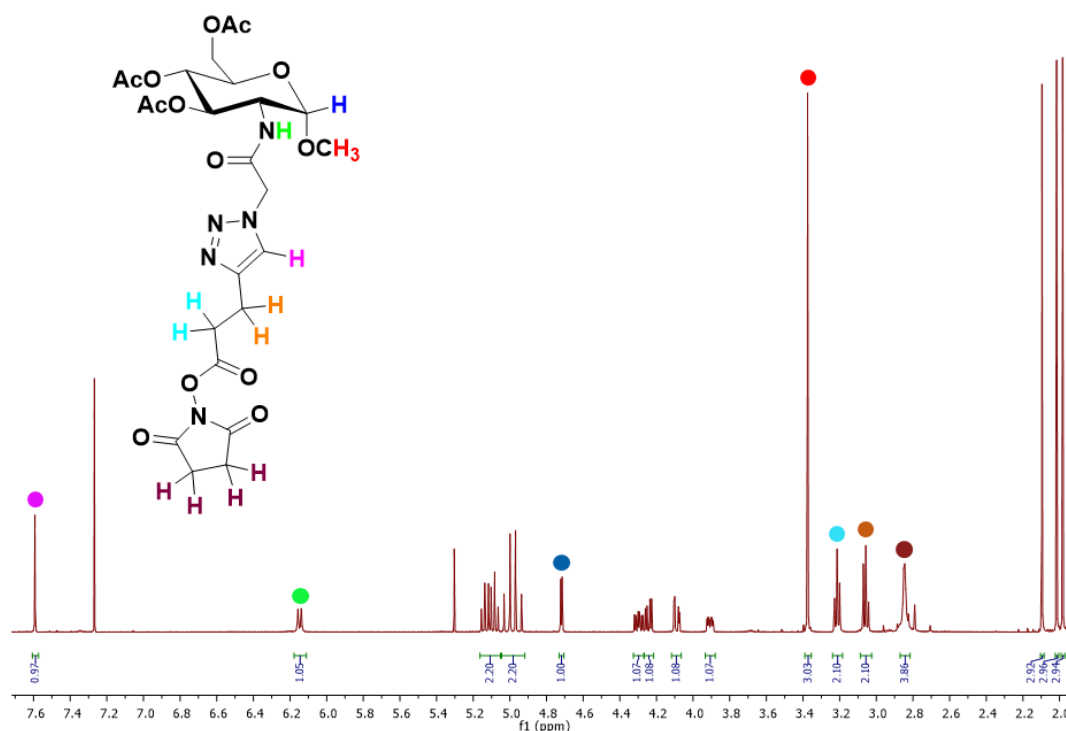
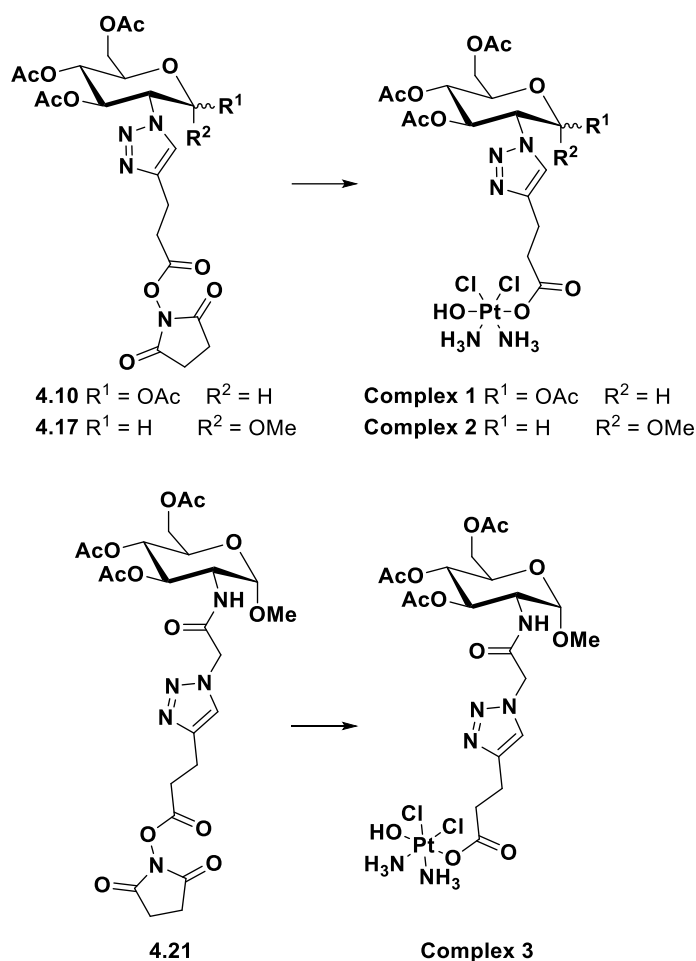


**Figure 4.9:**  $^1\text{H}$  NMR spectrum of active ester **4.21**, in  $\text{CDCl}_3$ .

#### 4.3.6 Synthesis of acetylated C2 Pt(IV) complexes (**1**, **2**, and **3**)

The acetylated complexes **1**, **2** and **3** (Scheme 4.11) were synthesised following previously reported procedures [230], in which the active ester is stirred in a suspension of oxoplatin and DMSO at  $60^\circ\text{C}$  for 16 h. The solution was then filtered to remove excess oxoplatin and the DMSO was evaporated. The treatment of the oily residues with diethyl ether afforded the target complexes (**1**, **2**, and **3**) with moderate to excellent yields, 67%, 86%, and 82% respectively. Unlike their free sugar derivatives, the synthesis of these complexes (which is discussed later) is relatively straightforward and they are characterised by 1D, and 2D NMR ( $^1\text{H}$ ,  $^{13}\text{C}$ , COSY, HSQC, HMBC,  $^{195}\text{Pt}$ ), HR-MS, and IR spectroscopy.



**Scheme 4.11:** Synthetic route to form acetylated C2 Pt(IV) complexes through reaction of active esters with oxoplatin at 60°C, 16 hours, **1** (67%), **2** (86%), **3** (82%).

The  $^1\text{H}$  NMR spectrum of Complex **1** is shown in **Figure 4.10**. Similarly for the free ligand (**4.9**) and the NHS ester ligand (**4.10**), this complex was prepared as a mixture of  $\alpha$ - and  $\beta$ -anomers (0.51:1.00), which can be seen from the two anomeric proton signals, highlighted in red in the  $^1\text{H}$  NMR spectrum (**Figure 4.10**). The triazole protons from the two anomers is highlighted in green, sharing the same ratio of  $\alpha$ : $\beta$ . The broad triplet seen at  $\delta = 6.00$  ppm (purple signal) corresponds to the amino ligands on the platinum scaffold. As seen on the  $^1\text{H}$  NMR spectrum, this triplet is overlapping with the H-3 proton of the carbohydrate, determined by 2D NMR spectroscopic methods.

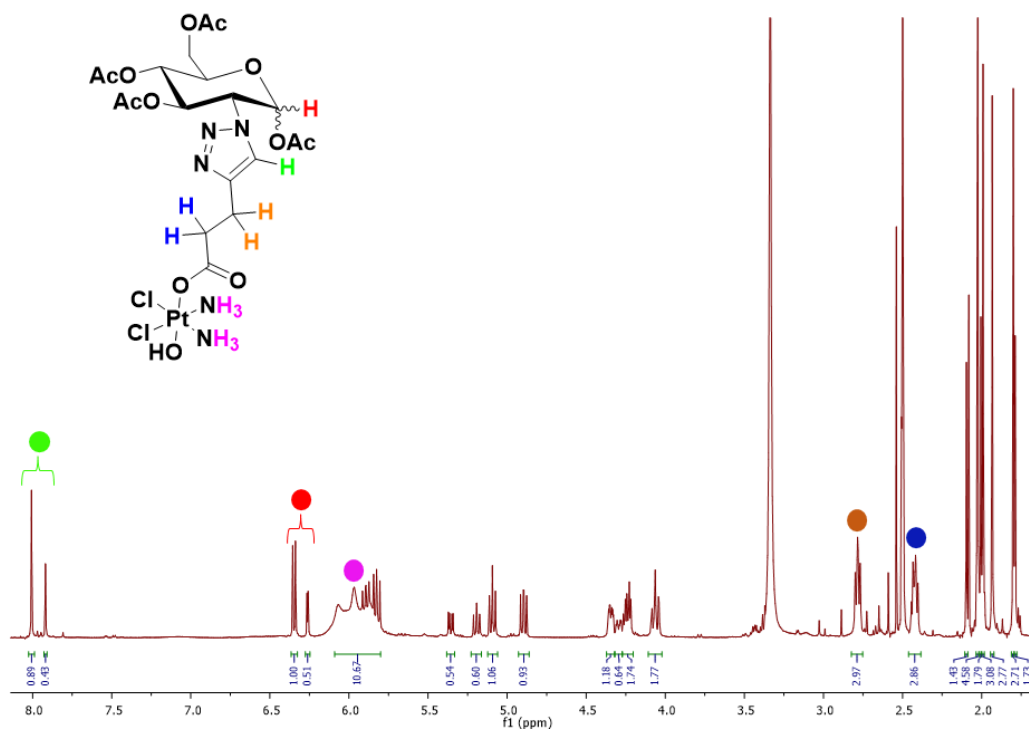


**Figure 4.10:**  $^1\text{H}$  NMR spectrum of **Complex 1**, in  $\text{DMSO-d}_6$ .

This complex is further characterised by  $^{13}\text{C}$  NMR, where the two anomers can be accounted for (Appendix, pg. 331), and  $^{195}\text{Pt}$  NMR (**Figure 4.11**) with a broad peak at  $\delta = 1045$  ppm.

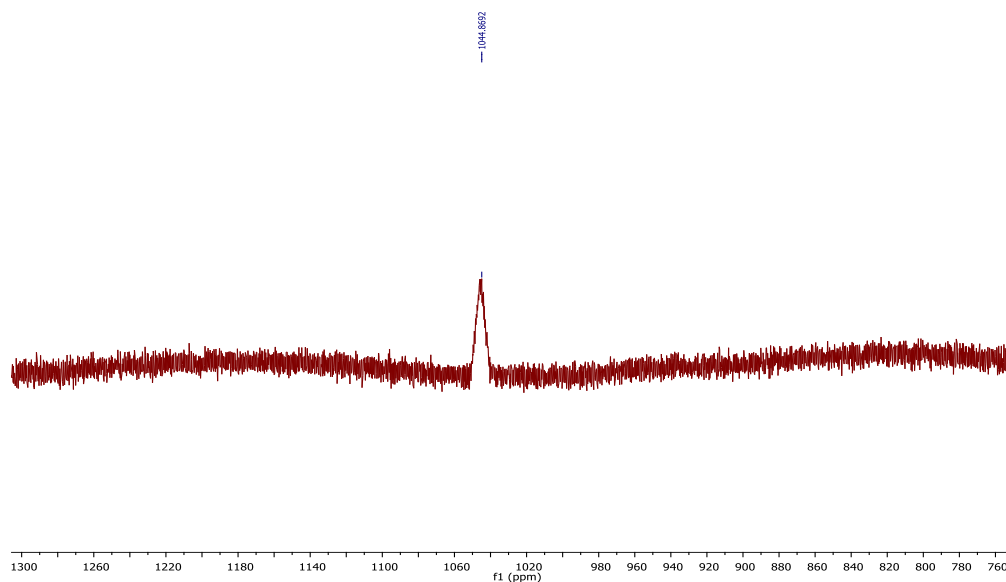


**Figure 4.11:**  $^{195}\text{Pt}$  NMR spectrum of **Complex 1**, in  $\text{DMSO-d}_6$ .

The  $^1\text{H}$  NMR of Complex **3** is shown in **Figure 4.12**, where the characteristic peaks are highlighted in colour. The amide proton (green) is seen at  $\delta = 8.52$  ppm, as well as the triazole proton (orange) at  $\delta = 7.80$  ppm. The purple highlighted peak represents the characteristic amino ligands of the platinum scaffold at  $\delta = 5.97$  ppm which has an integral of 6 protons. The  $\text{OCH}_3$  signal (red) is below the peak for water  $\delta = 3.33$  ppm, the presence of these protons is confirmed through the use of HSQC, and HMBC, where the carbon of the methyl group correlates with the methyl protons (red) and H-1 (turquoise) respectively.

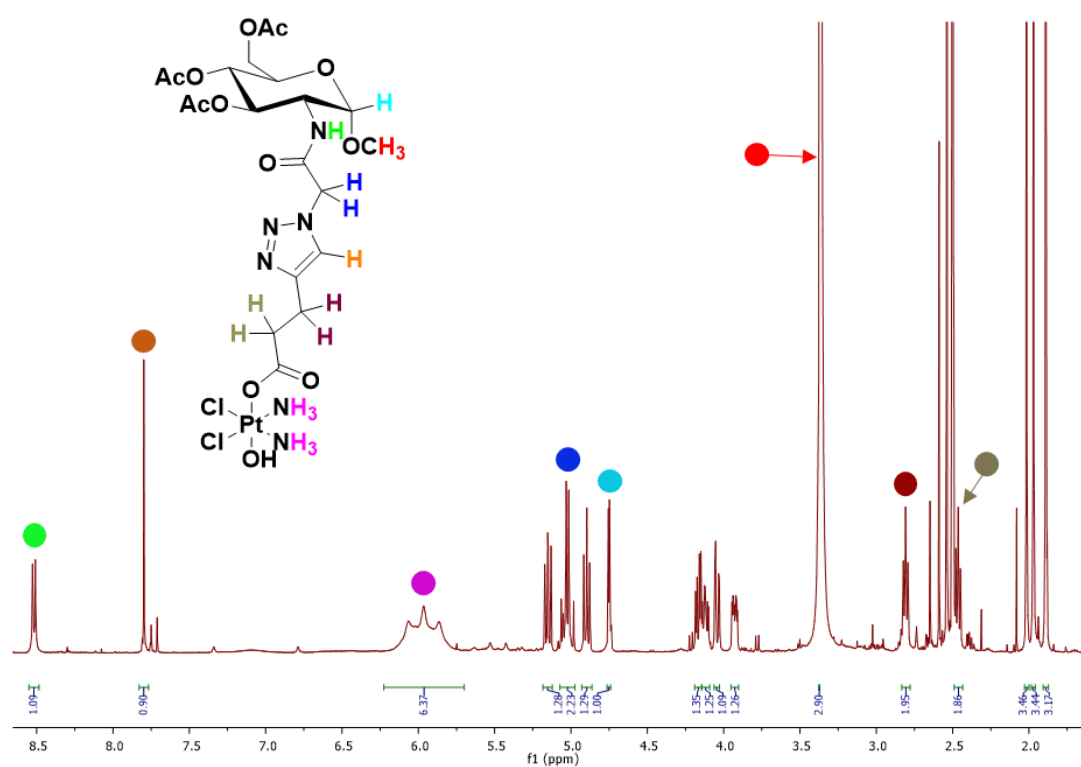


**Figure 4.12:**  $^1\text{H}$  NMR spectrum of **Complex 3** in  $\text{DMSO-d}_6$

Like Complex **1**,  $^{195}\text{Pt}$  NMR (**Figure 4.13**) was used to determine the oxidation state of the platinum centre and a peak appearing in the region of  $\delta = +1000$  ppm, confirmed that the complex is in the +4 oxidation state. The full characterisation of complexes **1** – **3** can be found in the appendix (pg. 331 – 336) as well as the experimental section at the end of this chapter.

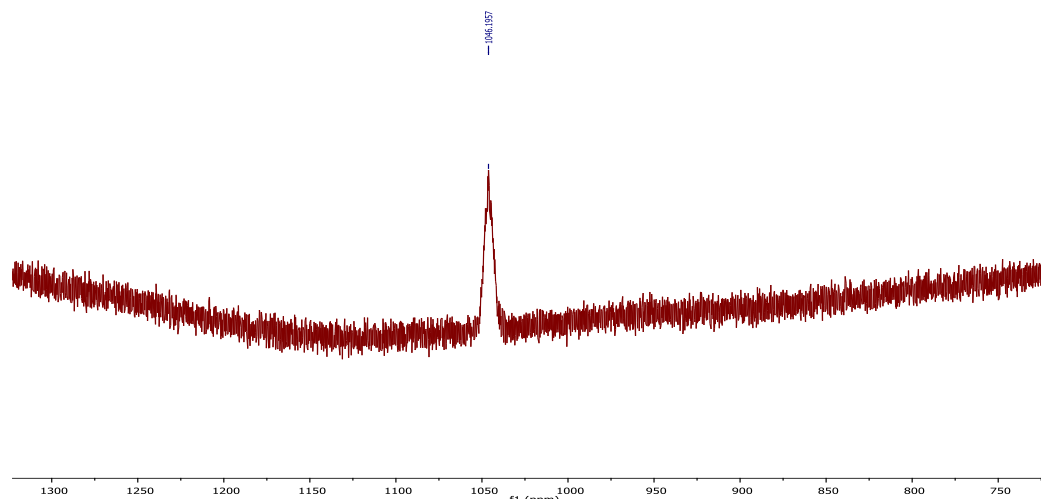
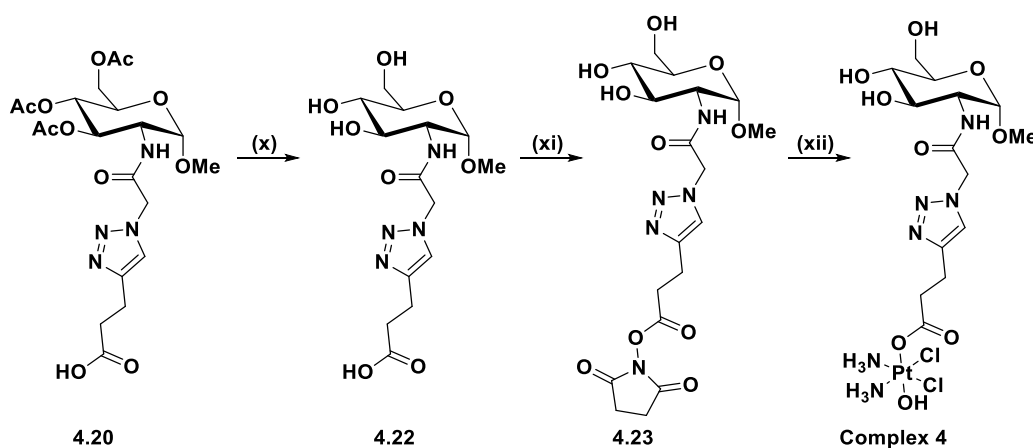


Figure 4.13:  $^{195}\text{Pt}$  NMR of **Complex 3** in  $\text{DMSO-d}_6$

#### 4.3.7 Synthesis of free sugar C2 Pt(IV) Complex (**4**)

The free sugar complex (**4**) was synthesised according to the scheme shown below (**Scheme 4.12**), in which the acetylated ligand **4.20** was deprotected using the same conditions reported in **Chapter 3** and then the carboxylic acid was activated with TSTU to yield the active ester **4.23**. This was then conjugated to the platinum scaffold through slow addition of a solution of **4.23** to a suspension of oxoplatin in dry DMSO at  $40^\circ\text{C}$  and reacted for 5 days.



**Scheme 4.12:** Synthetic route to form free sugar C2 Pt(IV) Complex (**4**): (x)  $\text{NEt}_3$ ,  $\text{MeOH}$ ,  $\text{H}_2\text{O}$ ,  $40^\circ\text{C}$ , 16 h, 98%; (xi) TSTU,  $\text{NEt}_3$ ,  $\text{DMF}$ , rt, 20 min, 79%; (xii) Oxoplatin, dry  $\text{DMSO}$ ,  $40^\circ\text{C}$ , 5 days, 39%.

The  $^1\text{H}$  NMR of **Complex 4** is shown in **Figure 4.14** where the characteristic signals are highlighted: the amide proton at  $\delta = 8.35$  ppm (green), the triazole at  $\delta = 7.8$  ppm



(blue) and the amino ligands of the platinum centre at  $\delta = 6.0$  ppm (pink). The C3, C4 and C5-OH protons are seen at  $\delta$  5.1, 4.95, and 4.6 ppm (turquoise) and two of these hydroxyl protons overlap with H-1 at  $\delta = 4.6$  ppm (purple) and the CH<sub>2</sub> of the amide linker (olive) at  $\delta = 5.1$  ppm, (the assignment was made using COSY, and HSQC NMR).

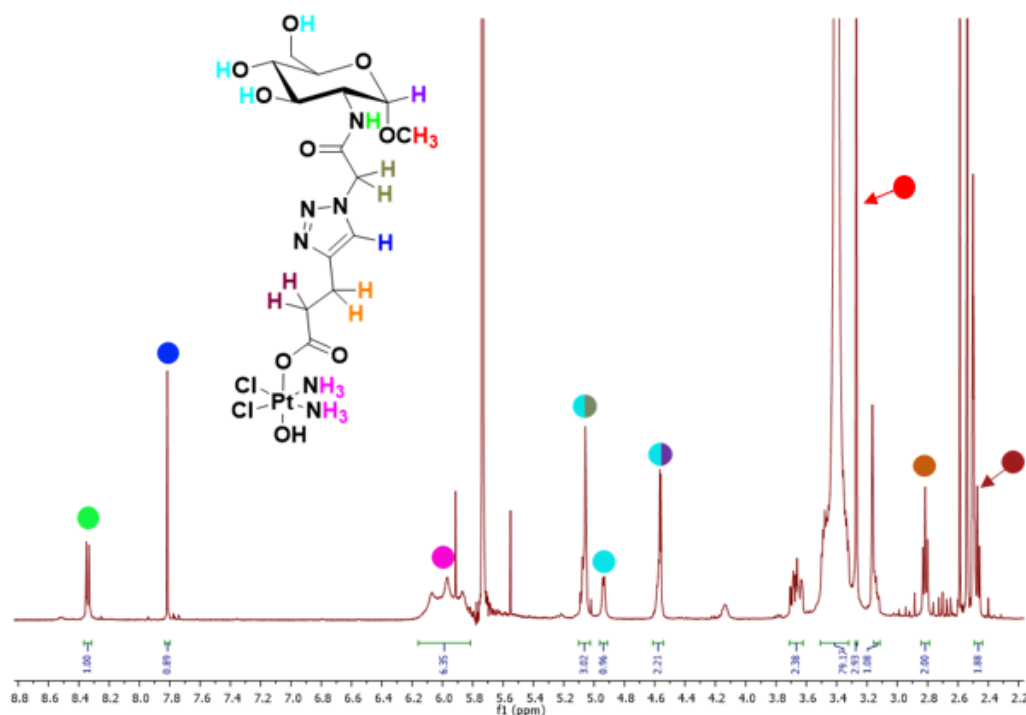


**Figure 4.14:** <sup>1</sup>H NMR spectrum of **Complex 3** in DMSO-d<sub>6</sub>

While this complex was eventually isolated with high purity, the procedure to achieve this result required a lot of optimisations. Initially, we attempted to use the procedure developed for the C1 free sugar complexes in **Chapter 3**. **Table 4.2** depicts the different reaction conditions attempted to yield **Complex 4**.

**Table 4.2:** Reaction optimisation for the synthesis of free sugar C2 Pt(IV) Complex 4.

| Entry | Temp (°C) | Reaction time | Dry DMSO | Equiv. of Pt |
|-------|-----------|---------------|----------|--------------|
| 1     | 40        | 24            | No       | 1.05         |
| 2     | 40        | 48            | No       | 1.05         |
| 3     | 50        | 24            | No       | 1.05         |
| 4     | 60        | 24            | No       | 1.05         |
| 5     | 40        | 120           | Yes      | 1.05         |
| 6     | 40        | 96            | Yes      | 1.05         |
| 7     | 40        | 120           | Yes      | 2            |

Entries **1** to **4** involved the use of the same method used for the synthesis of complexes **1** – **4** in **Chapter 3**. The ligand was added dropwise over the course of 8 – 16 hours with an addition funnel; from entry **5** we used a syringe pump to add the solution of ligand more accurately over 24 hours. The  $^1\text{H}$  NMR spectrum below (**Figure 4.15**) shows the comparison between entries **1** – **4**.

The stacked  $^1\text{H}$  NMR spectra shows a broad signal at  $\delta = 8.5$  ppm, and while we were not able to identify this new impurity, it is likely that it is the formation of a side product containing an amide bond, due to its proximity to the amide signal of the product. Interestingly, at higher temperatures (entries **3** and **4**), this peak appears to broaden and show two separate, more defined signals. Whereas at lower temperatures (entries **1** and **2**) this impurity is a single broad peak, and after 24 hours, reduces in intensity. For this reason, we decided to maintain a temperature of  $40^\circ\text{C}$  for further reactions.

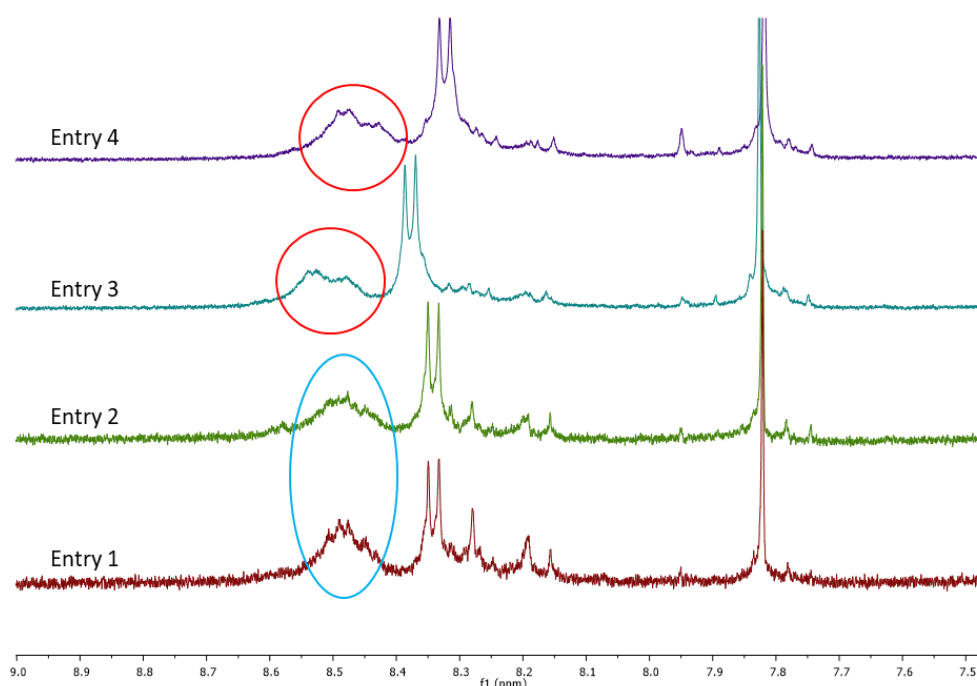


**Figure 4.15:** Comparison of  $^1\text{H}$  NMR spectra for the reaction conditions of entries **1** – **4** from **table 4.2**.

**Figure 4.16** shows the stacked NMR spectra of entries **5** and **6**. Entry **5** was our first success in synthesizing the pure complex. Interestingly, this success was through sheer serendipity; the reaction had taken place through the dropwise addition of the

ligand to a suspension of oxoplatin in dry DMSO. This addition was meant to take place over 24 hours and stir at 40°C for a further 4 days, however during the addition, the syringe dislodged from the pump after 16 hours resulting in a much larger excess of oxoplatin in the reaction. Initially we thought the cause of the success was the longer reaction time, however entry **6** disproved this, as seen from the  $^1\text{H}$  NMR where the impurities reappear. The number of equivalents of oxoplatin for entry **7**, whose spectrum is seen in **Figure 4.14**, was increased. The reaction mixture was filtered and treated with the minimum amount of methanol and diethyl ether to yield **Complex 4** in a yield of 39%. While this yield is quite low, it is entirely possible that the reaction will go to completion over a smaller period of time.

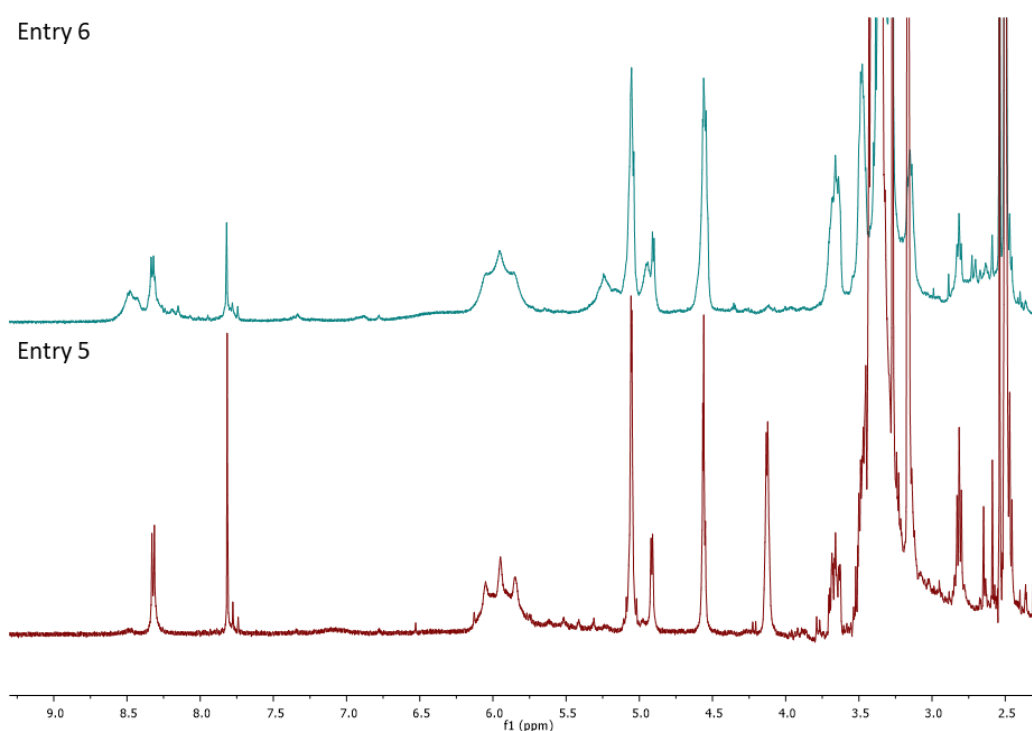
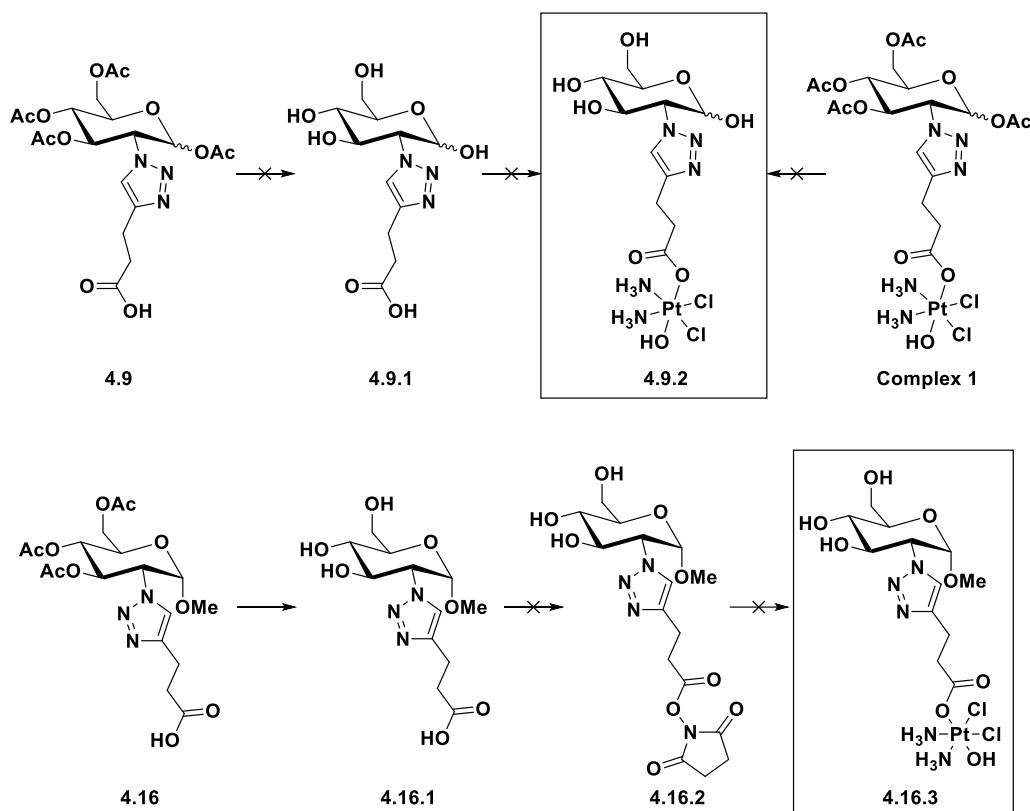


**Figure 4.16:** Comparison of  $^1\text{H}$  NMR spectra for the reaction conditions of entries **5** and **6** from **table 4.1**.

#### 4.3.8 Attempted synthesis of free sugar C2 Pt(IV) complexes (4.9.2 and 4.16.3)

The synthesis and isolation of free sugar derivatives of complexes **1** and **2** (**Scheme 4.13**) were attempted, however a variety of issues were encountered. We first wanted to synthesise Complex **4.9.2**, where the anomeric position was deprotected, a strategy also performed by Lippard and coworkers [135]. Importantly, Lippard *et al.* protected their carbohydrate moieties with benzyl (OBn) protecting groups and

the deprotection method was hydrogenation with Pd/C. In our case we used acetyl protecting groups on the starting material (**Complex 1**); as discussed in **Chapter 3**, the conditions to deprotect this starting material resulted in the degradation of **Complex 1**, which can be seen in **Figure 4.17**.



**Scheme 4.13:** Attempted routes to synthesise complexes **4.9.2** and **4.16.3**, free sugar derivatives of complexes **1** and **2**.

**Figure 4.17** shows a comparison between the crude samples of **Complex 4.9.2** and **Complex 4**. This reaction was attempted using the acetyl deprotection conditions described in **Chapter 3**, however this reaction did not result in the formation of a pure complex. The three singlets highlighted in red correspond to the formation of free ammonia which is characteristic of the degradation of cisplatin-based complexes [292]. A crude NMR of **Complex 4** was included here as there is a complete removal of the triplet ammine ligand peak at  $\delta = 6.00$  ppm, whereas **Complex 4.9.2** has only partially reacted.

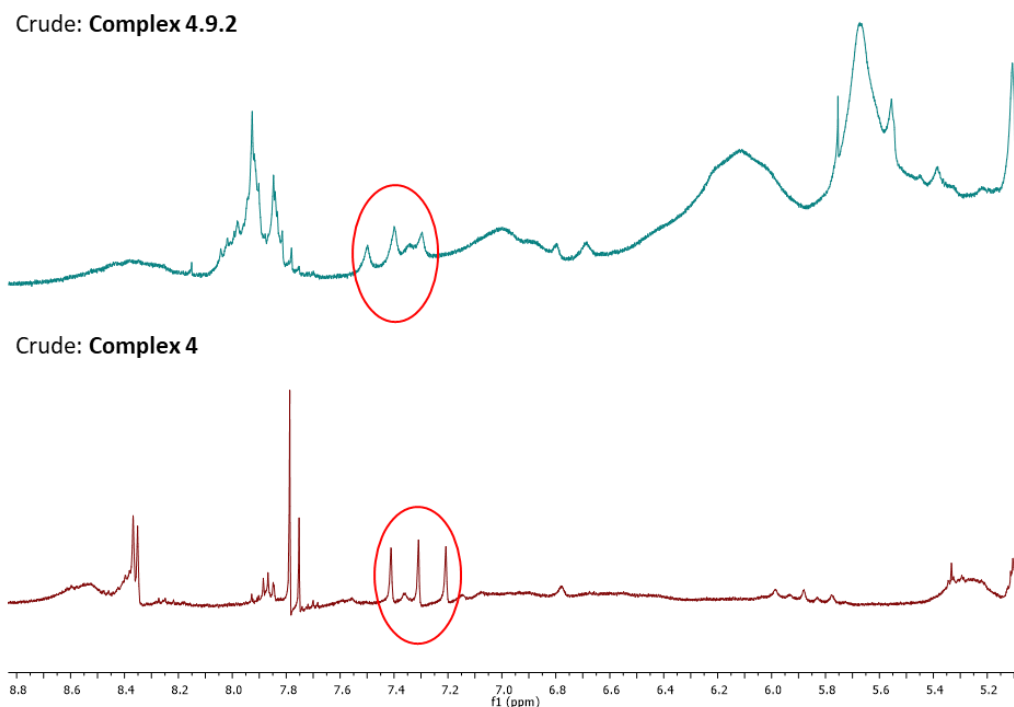


**Figure 4.17:**  $^1\text{H}$  NMR spectra comparing the crude **Complex 4.9.2** to a crude sample of **Complex 4**. This synthesis was attempted through deprotection of the acetylated complexes with  $\text{NEt}_3$ , MeOH,  $\text{H}_2\text{O}$  and DCM.

An alternative route we attempted to reach the desired complex was through the deacetylation of the free ligand (**4.9**), in a similar route to the synthesis of **complexes 1 – 4** used in **Chapter 3**. This also proved to be not achievable; while TLC analysis showed the reaction had gone to completion, the  $^1\text{H}$  NMR still displayed several impurities.

We also attempted to synthesise **Complex 4.16.3 (Scheme 4.13)**, the free sugar derivative of **Complex 2**. This reaction was unusual as the conditions we used to synthesise **Complex 4** did not seem to work for this complex. The only explanation we can give is that potentially the shorter chain length causes steric hindrance, where the ligand is more constrained and therefore, cannot optimally react with the complex. The  $^1\text{H}$  NMR spectrum of the crude product is shown below (**Figure 4.18**).

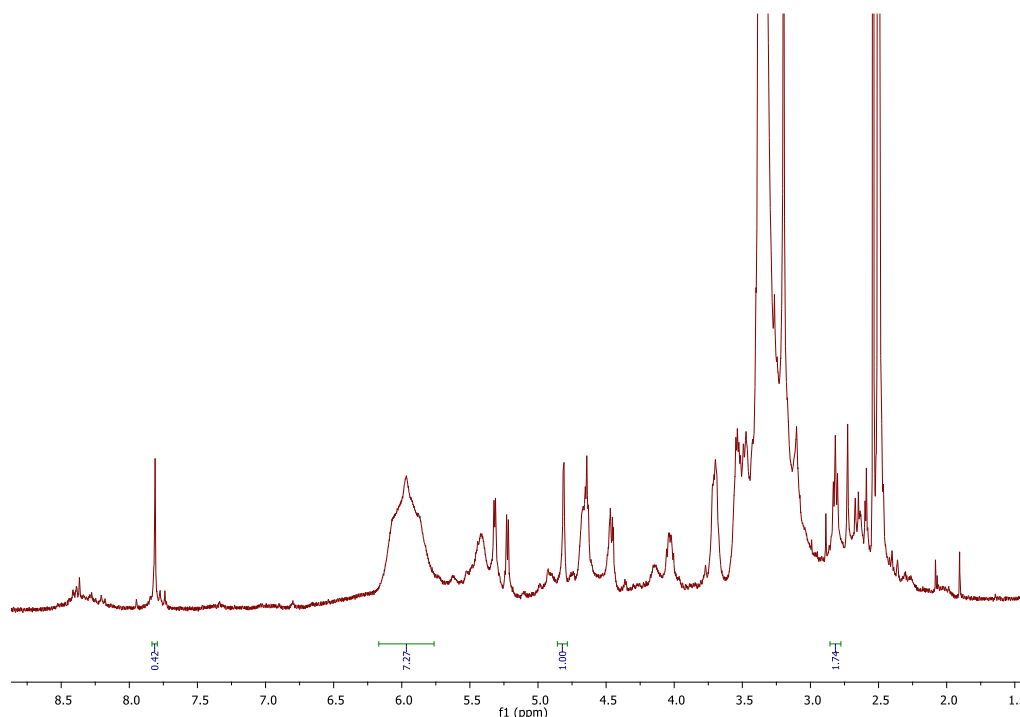


**Figure 4.18:**  $^1\text{H}$  NMR spectrum of **Complex 4.16.3** in  $\text{DMSO-d}_6$ .

Noticeably, the formation of the impurity at  $\delta = 8.5$  ppm was avoided in the synthesis of **Complex 4**, using the conditions described in **section 4.6.7**; however, it is present here using the same procedure. It is also important to see that the integration for the peaks corresponding to the triazole ( $\delta = 7.8$  ppm) and the triplet ammine ligand signal ( $\delta = 6.00$  ppm) are not consistent with the structure of the complex. Finally, the yield of this crude was only 4% which was not acceptable due to the length of the synthesis of the ligand. Due to time constraints, we were unable to make any more attempts at this complex, however a possibility to form both complexes **4.9.2** and **4.16.3** would be to protect the carbohydrate with OBn groups and remove them by hydrogenation once the complex has been formed, as done by Lippard and coworker [135].

#### 4.4 Reduction properties of C2 complexes (3 and 4)

To confirm the pro-drug nature of these series of complexes, they were incubated with an excess of ascorbic acid (a typical reductive compound present in the cytoplasm) to mimic the cellular environment and the response was studied via  $^1\text{H}$  NMR [272]. Complexes **3** and **4** were selected for this study representing a protected and free glycoconjugate complexes. **Figure 4.19** shows that there is complete release

of the carbohydrate axial ligand (and the concomitant reduction with the formation of cisplatin) after 72 h (Complex **3**) and 24 h (Complex **4**), as seen by the disappearance of the triazole proton at  $\delta = 7.80$  ppm (**3**) and at  $\delta = 7.82$  ppm (**4**). It is also observed that the triazole protons of the carboxylic acid ligands (**4.20** and **4.22**) reemerge at  $\delta = 7.75$  ppm and  $\delta = 7.78$  ppm respectively, proving that the reduction of the complexes from Pt(IV) to Pt(II) is accompanied by the release of the axial ligands.

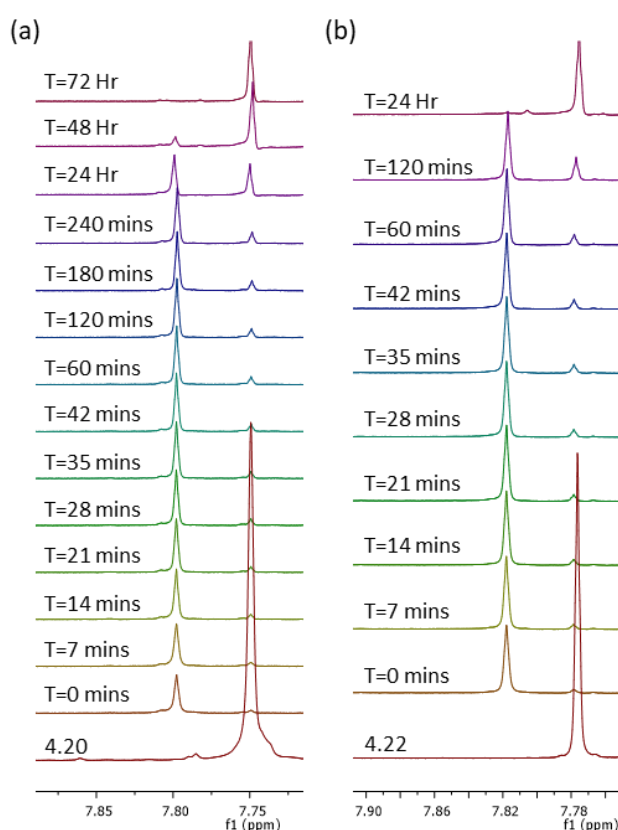


**Figure 4.19:** Reduction of complexes **3** and **4** by a 10-fold excess of ascorbic acid. <sup>1</sup>H NMR spectra over 72 h (a) and 24 h (b) in DMSO-d<sub>6</sub>.

## 4.5 Biological Evaluation

### 4.5.1 *In vitro* cytotoxicity

In order to evaluate the anti-cancer potential of the above C2 Pt(IV)-glycosides, their antitumor potential was assessed in collaboration with Dr. Silvia Panseri, Dr. Monica Montesi and Dr. María Galiana Cameo at the ISTECCNR of Faenza (Italy) against a panel of OS cell lines, SAOS-2, U-2 OS and MG63, a triple negative breast cancer cell

line, MDA-MB-468 and a glioblastoma cell line, U-87 MG. All drugs showed a dose/concentration dependent anti-cancer effect (**Figure 4.20**) in all tested cell lines.

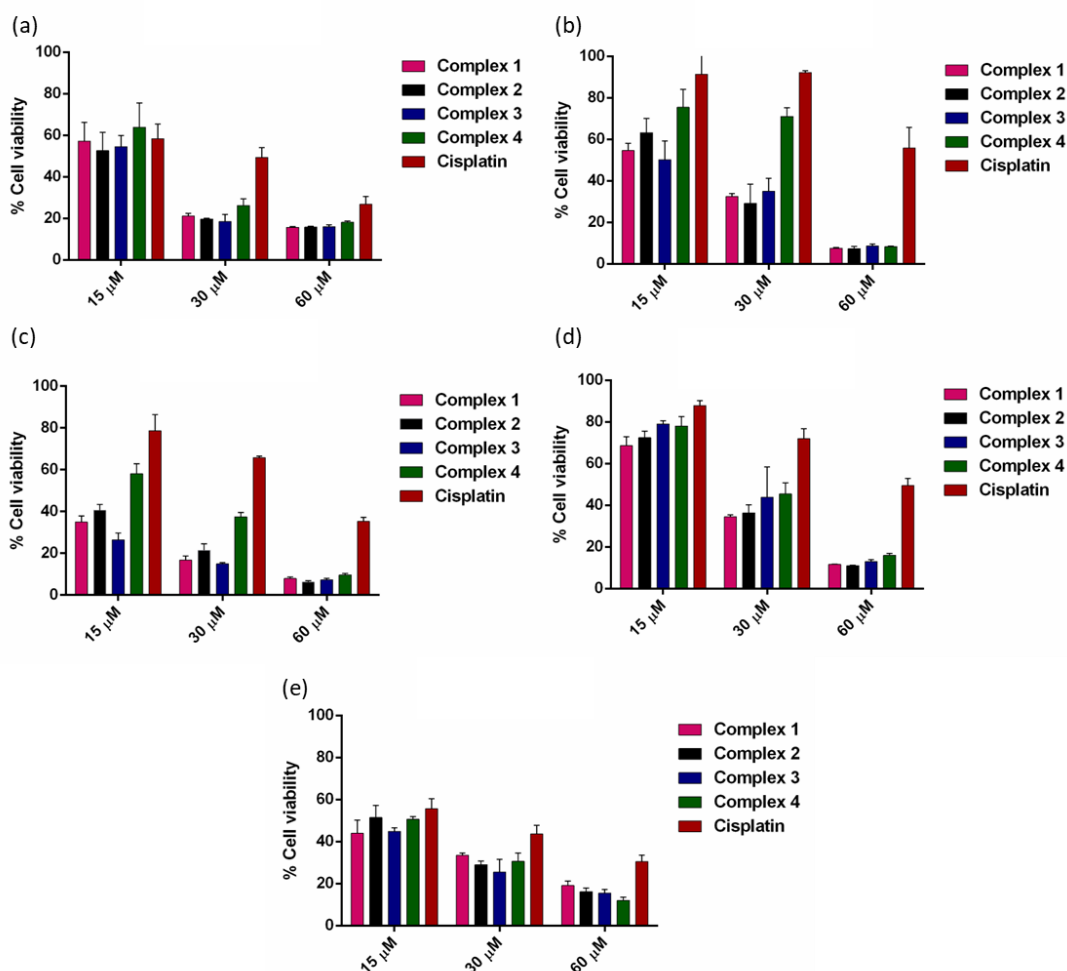


**Figure 4.20:** MTT assay of SAOS-2, U-2 OS, MG63, MDA-MB-468, and U-87 MG. Percentage of cell viability (mean  $\pm$  SEM) respect to cells only is reported in the graphs for SAOS-2 (a), U-2 OS (b), MG63 (c), MDA-MB-468 (d), and U-87 MG (e) after 72 hours of drug exposure.

At the concentrations of 30 μM, all complexes showed a statistically significant difference in cytotoxicity with respect to cisplatin against most of the cell lines tested and even at low concentrations of 15 μM, complexes **1 – 4** were particularly effective against the U-2 OS (**b**) and MG63 (**c**) cell lines. On average, acetylated complexes **1 – 3** showed an almost 5-fold decrease in cell viability when compared to the reference cisplatin against the U2-OS (**b**) and MG63 cell lines (**c**) at a concentration of 30 μM (**Table 4.3**). However, the deacetylated complex, **4**, had vastly reduced activity in both cell lines when compared to its protected counterparts, while still being



significantly more cytotoxic in comparison to cisplatin. Potentially, like we saw with the acetylated C1 derivatives in **chapter 1**, the addition of the lipophilic protecting groups may contribute to the cytotoxicity of complexes **1 – 3** due to a higher cellular uptake.

All of these complexes were particularly effective against the triple negative breast cancer cell line (**d**), which has been shown previously to intensely overexpress GLUT1 [293]. Interestingly, there was no significant difference in the cytotoxicity of this series of complexes against these cells, which may support the observation of Patra *et al.*, who suggests that protein-mediated transport becomes saturated over long time scales [161]. These complexes will be incubated with healthy cells to see if there is a difference in activity with respect to cisplatin, however at the time of writing, these tests have yet to be conducted. It is likely however, that Complex **4** will be much less cytotoxic to healthy cells than **1 – 3** and cisplatin, due to the presence of the free glucose moiety.

**Table 4.3:** IC<sub>50</sub> (μM) values of complexes **1 – 4** and cisplatin against SAOS-2, U-2 OS, MG63, MDA-MB-468, and U-87 MG cells

|                  | SAOS-2           |               | U-2 OS           |                 | MG63             |               | MDA-MB-468       |               | U-87 MG          |               |
|------------------|------------------|---------------|------------------|-----------------|------------------|---------------|------------------|---------------|------------------|---------------|
|                  | IC <sub>50</sub> | 95% CI        | IC <sub>50</sub> | 95% CI          | IC <sub>50</sub> | 95% CI        | IC <sub>50</sub> | 95% CI        | IC <sub>50</sub> | 95% CI        |
| <b>Complex 1</b> | 16.8             | +3.2;<br>-3.9 | 17.4             | +2.0;<br>-2.1   | 9.5              | +1.3;<br>-1.5 | 22.0             | +1.1;<br>-1.8 | 11.7             | +3.3;<br>-4.2 |
| <b>Complex 2</b> | 15.2             | +3.3;<br>-4.6 | 19.5             | +2.6;<br>-2.6   | 11.8             | +1.4;<br>-1.7 | 23.3             | +1.3;<br>-1.2 | 15.5             | +2.1;<br>-2.4 |
| <b>Complex 3</b> | 15.8             | +3.0;<br>-4.1 | 16.1             | +4.2;<br>-5.2   | 5.7              | +1.6;<br>-1.8 | 26.8             | +4.2;<br>-3.7 | 12.2             | +2.4;<br>-3.0 |
| <b>Complex 4</b> | 19.5             | +4.2;<br>-4.5 | 30.3             | +5.7;<br>-5.6   | 19.4             | +2.6;<br>-2.7 | 27.4             | +2.1;<br>-2.0 | 15.6             | +1.6;<br>-1.7 |
| <b>Cisplatin</b> | 23.9             | +6.1;<br>-6.1 | 78.4             | +13.2;<br>-12.9 | 41.9             | +7.4;<br>-5.5 | 58.9             | +9.1;<br>-6.2 | 20.6             | +4.0;<br>-4.4 |

We believe that the greater activity of the complexes **1 – 4** with respect to cisplatin is due to the combined effect of increased lipophilicity (complexes **1 – 3**) and overexpression of GLUT1, (Complex **4**) where the recognition of the carbohydrate moieties attached to the complexes enhances the drug uptake and improves the anticancer effect. Cellular uptake studies are underway to confirm this hypothesis.

### 4.5.2 Cell morphology evaluation

The qualitative analysis of the cell morphology confirmed the cytotoxicity results. As shown in **Figure 4.21**, the number of cells treated with cisplatin and complexes **1 – 4** drastically decreased compared to cells only, which showed a higher cell density.

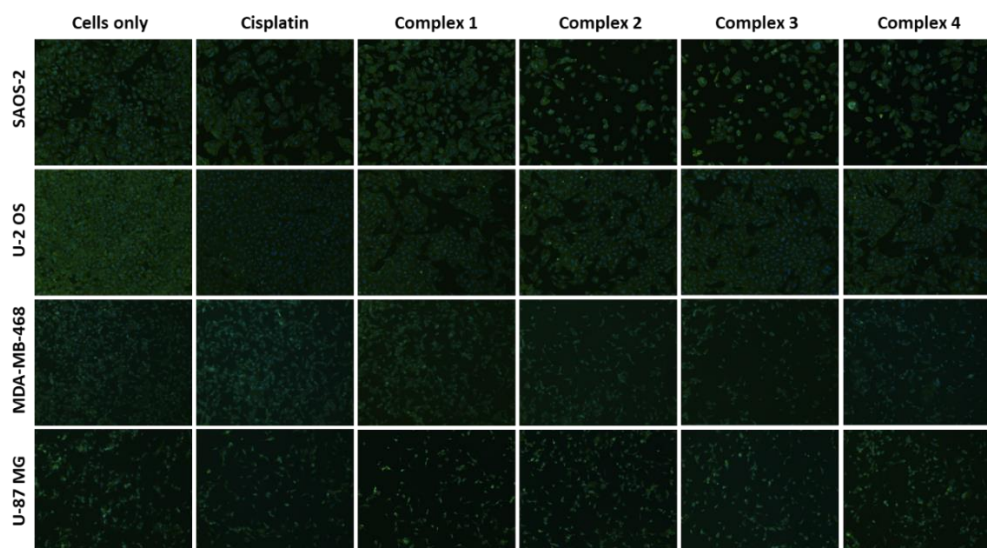


**Figure 4.21:** Cell morphology evaluation on SAOS-2, U-2 OS, MDA-MB-468, and U-87 MG. Actin and DAPI staining of cell lines treated with and without drugs (30 $\mu$ M) for 72 hours. F-actin filaments in green; cell nuclei in blue.

### 4.6 Conclusions

Four novel Pt(IV) pro-drugs, based on cisplatin with C2 functionalised carbohydrate moieties in the axial position were synthesised, characterised and screened as anticancer agents against different tumoral cell lines. In this series, the sugar targeting vector is linked to the platinum core at the C2 position *via* CuAAC “click” chemistry. These pro-drugs contain both protected and deprotected sugar moieties, whose function is to improve drug selectivity, cellular uptake and cytotoxicity. This is the first time in literature that these kind of glycoconjugated Pt(IV) prodrugs containing carbohydrates conjugated at this position have been reported. The complexes were tested against a panel of OS cells, a triple negative breast cancer cell line and a glioblastoma cell line, where their cytotoxicity was analysed, and all complexes showed excellent activity in comparison to cisplatin. These complexes were particularly effective against U-2 OS, MG63, and triple negative breast cancer cell line, MDA-MB-468. In comparison to the complexes reported in previous

chapters, it seems that the C2 functionalised complexes were more effective targeting vectors than carbohydrates modified in the anomeric position. This is in line with what was reported by Patra *et al.* [135]. While the results of the MTT assays show good cytotoxic activity from complexes **1** – **4**, it is important to note that healthy cell lines were not used yet in these assays and for the moment the selectivity of these drugs for cancer cells is not assessed. At the time of writing, no cell uptake or GLUT inhibition experiments have been conducted either, but all these studies are planned. Interestingly, the activity of the free sugar complex (**4**) was lower compared to the acetylated derivatives **1** – **3**. This could be rationalised by the presence of the acetyl protecting groups that increase the lipophilicity allowing a higher cellular internalisation by passive diffusion. Furthermore, based on the results of the  $^1\text{H}$  NMR reduction studies with ascorbic acid, Complex **4** displayed a much quicker reduction rate (fully reduced after 24 h) than Complex **3** (fully reduced after 72 h), indicating that cisplatin is produced faster, and this will hamper its activity that is studied at 72h in the MTT test (**Figure 4.20**) [78].

#### 4.7 Materials and Methods

All reagents and reactants were purchased from commercial sources. The two sources used were Sigma-Aldrich and Fluorochem. All solvents were used without further purification. Cisplatin and oxoplatin were synthesised as previously reported [262,263].

The elemental analysis studies (carbon, hydrogen, and nitrogen) were performed by means of a PerkinElmer 2400 series II analyzer. HR-Mass Spectra were recorded with a Waters LCT Premier XE Spectrometer. NMR:  $^1\text{H}$ ,  $^{13}\text{C}$  and  $^{195}\text{Pt}$  NMR spectra were obtained in a solution of  $\text{D}_2\text{O}$  or  $\text{DMSO-}d_6$  at 300 K, in 5-mm sample tubes, with a premium shielded Agilent Varian 500 MHz (operating at 500.13, 125.75, and 107.49 MHz, respectively). The  $^1\text{H}$  and  $^{13}\text{C}$  chemical shift was referenced to the residual impurity of the solvent. The external reference was  $\text{Na}_2\text{PtCl}_4$  in  $\text{D}_2\text{O}$  (adjusted to  $\delta = -1628$  ppm from  $\text{Na}_2\text{PtCl}_6$ ) for  $^{195}\text{Pt}$ . The stability was followed using high-performance liquid chromatography (HPLC) with a Phenomenex Luna C18 (5  $\mu\text{M}$ , 100 Å, 250mm  $\times$  4.60 mm i.d.) column at room temperature at a flow rate of 1.0 mL/min

with 254 nm UV detection. Mobile phase containing 80:20 acetonitrile (0.1% trifluoroacetic acid): water (0.1% trifluoroacetic acid): the complexes were dissolved in DMF (0.5 ml) and diluted to a final concentration of 0.5 mM using acetonitrile and water solution (1/1) and 2 mM 4-(2-hydroxyethyl)piperazine-1-ethanesulfonic acid (HEPES) buffer (pH 6.8). Infrared (IR) spectra were recorded in the region 4000–400  $\text{cm}^{-1}$  on a Perkin Elmer precisely spectrum 100 FT/IR spectrometer. The solid samples were run using ATR. An extensive biological evaluation of the activity of all the compounds was performed in human osteosarcoma cell line in vitro models as reported below.

### 2.7.1 Reduction studies

Measurements were obtained in a solution of DMSO- $d_6$  at 300 K, in 5-mm sample tubes, with a premium shielded Agilent Varian 500 MHz (operating at 500.13 MHz). Complex **3** (5 mg, 6.12  $\mu\text{mol}$ ) was dissolved in 500  $\mu\text{L}$  of DMSO- $d_6$ . Ascorbic acid (10 mg, 10 Equiv.) was added and a  $^1\text{H}$  NMR spectrum was recorded every 7 minutes for 1 hour. After no reduction had taken place initially, the  $^1\text{H}$  NMR spectrum was recorded every hour for four hours, and finally every 24 hours until full reduction of Pt(IV) to Pt(II) and cleavage of the axial ligand was observed after 72 hours. Complex **4** (5 mg, 7.19  $\mu\text{mol}$ ) was dissolved in 500  $\mu\text{L}$  of DMSO- $d_6$ . Ascorbic acid (12 mg, 10 Equiv.) was added and a  $^1\text{H}$  NMR spectrum was recorded every 7 minutes for 1 hour. After no reduction had taken place initially, the  $^1\text{H}$  NMR spectrum was recorded every hour for two hours, and finally every 24 hours until full reduction of Pt(IV) to Pt(II) and cleavage of the axial ligand was observed after 24 hours.

### 2.7.2 *In vitro* biological evaluation

*In vitro* tests of cisplatin-based drugs were performed to evaluate the cellular behaviours in response to the different complexes (**1** – **4**) compared to cisplatin. All the drugs were reconstituted in Dimethyl Sulfoxide (DMSO) at 1 mg/ml final concentration, and then dissolved in the culture media at different concentrations: 15, 30 and 60  $\mu\text{M}$ . Three different osteosarcoma cells lines (MG63, SAOS-2, U-2 OS), a triple negative breast cancer cell line (MDA-MB-468) and a glioblastoma cell line (U-87 MG) were maintained in culture with and without the drugs for 72 hours.

### 2.7.3 Cell culture

Human Osteosarcoma cell lines MG63 (ATCC® CRL1427™), U-2OS (ATCC® HTB-96™), SAOS-2 (ATCC® HTB-85™), triple negative breast cancer cell line MDA-MB-468 (ATCC® HTB-132™), and glioblastoma cell line U-87 MG (ATCC® HTB-14™), purchased from American Type Culture Collection (ATCC), were used. MG63 cell line was cultured in DMEM F12-GlutaMAX™ Modified Medium (Gibco) supplemented with 10% Foetal Bovine Serum (FBS) (Gibco) and 1% of penicillin/streptomycin mixture (pen/strep) (100 U/ml - 100 µg/mL, Gibco). SAOS-2 and U-2OS cell lines were cultured in McCoy's 5A Modified Medium (Gibco) supplemented with 15% and 10% FBS, respectively, and 1% pen/strep. MDA-MB-468 cell line was cultured in Leibovitz's L-15™ medium supplemented with 10% FBS and 1% pen/strep. U-87 MG cell line was cultured in Eagle's Minimum Essential™ medium supplemented with 10% FBS and 1% pen/strep. Cells were kept in an incubator at 37°C under controlled humidity and 5% CO<sub>2</sub> atmosphere conditions. Cells were detached from culture flasks by trypsinisation and centrifuged. The cell number and viability were determined by Trypan Blue Dye Exclusion test and all cell handling procedures were performed under laminar flow hood in sterility conditions. For the experiment, all cell lines were seeded  $5.0 \times 10^3$  cells/well in 96 well-plates and  $5.0 \times 10^4$  cells/well in 6 well-plates.

### 2.7.4 MTT cell viability assay

A quantitative analysis of cell viability and proliferation was carried out by MTT assay on cell cultures, by using the cells only as the negative control. At 72 hours, the MTT assay was performed according to manufacturer's instructions. Briefly, MTT reagent [3-(4,5-dimethylthiazol-2-yl)-2,5-diphenyltetrazolium bromide] (5 mg/mL) was dissolved in Phosphate Saline Buffer 1X (PBS 1X). At 72 hours, the cells were incubated with 10% media volume MTT solution for 2 hours at 37 °C, 5% CO<sub>2</sub> and controlled humidity conditions. The cell culture media was removed and substituted with DMSO (Sigma) dissolving formazan crystals derived from MTT conversion by metabolically active cells. After 15-minutes incubation under slight stirring conditions, the absorbance of formazan was read at 570 nm by using a Multiskan FC Microplate Photometer (Thermo Scientific). The values of absorbance are directly

proportional to the number of metabolic active cells in each well. One experiment was carried out and a biological triplicate for each condition was performed.

### 2.7.5 Cell morphology evaluation

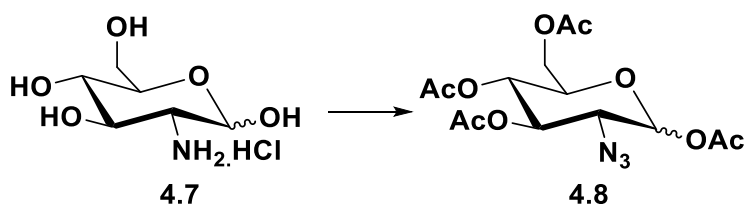
For the *in vitro* 2D cell cultures, all cell lines were seeded at a density of  $5.0 \times 10^3$  cells/well in 96 well-plates, for the *in vitro* 3D cell cultures cells were treated as previously described. Both the 2D and 3D cell cultures were fixed in 4% buffered Paraformaldehyde (PFA) following the manufacturer's instructions. The fixed samples were permeabilised in PBS 1X with 0.1% (v/v) Triton X-100 (Merck) for 5 minutes at room temperature and F-actin filaments were highlighted with Alexa Fluor 488 Phalloidin (Invitrogen) for 20 minutes at room temperature in the dark. DAPI (600 nM) counterstaining was performed for cell nuclei identification, following the manufacturer's instructions. The images were acquired by using an Inverted Ti-E Fluorescent Microscope.

### 2.7.6 Statistical analysis

Statistical analysis was performed by using GraphPad Prism Software (8.0.1 version). The results of MTT assay of the *in vitro* 2D drug screening are reported in the graphs as mean percentage of cell viability with respect to cells only  $\pm$  standard deviation and they were analysed using Two-way analysis of variance (Two-way ANOVA) and Dunnett's multiple comparisons test. The MTT results were further analysed by One-way analysis of variance (One-way ANOVA) and Dunnett's multiple comparisons test.  $IC_{50}$  values were calculated as Log(inhibitor) versus mean percentage of dead cells with respect to cells only and the obtained values are reported in the graphs  $\pm$  95% confidence interval (CI) for each cell line. The MTT results of 3D tumour engineered models of osteosarcoma were reported in the graph as percentage mean  $\pm$  standard error of the mean and they were analysed by Two-way ANOVA and Dunnett's multiple comparisons test. A further analysis was performed by unpaired *t*-test on all drugs with respect to cisplatin.

## 4.8 Experimental procedures

### 1,3,4,6-Tetra-*O*-acetyl-2-azido-2-deoxy-D-glucopyranoside (4.8)



A solution of  $\text{NaN}_3$  (8.94 g, 137 mmol) in  $\text{H}_2\text{O}$  (22 mL) was cooled to  $0^\circ\text{C}$  and stirred for 5 mins and DCM (40 mL) was added. The mixture was stirred vigorously and  $\text{Tf}_2\text{O}$  (4.68 mL, 27.90 mmol) added over a period of 5 mins, and the reaction stirred at  $0^\circ\text{C}$  for 2 h.

The organic phase was separated, and the aqueous phase was washed with DCM (35 mL). The combined organic phases were washed with saturated sodium carbonate solution. The total volume of  $\text{TfN}_3$  in DCM was 75 mL, and this reagent solution was used immediately without further purification (This reagent must not be evaporated to dryness as it is potentially explosive). **4.7** (3.0 g, 13.95 mmol) was dissolved in  $\text{H}_2\text{O}$  (45 mL) and treated with solid  $\text{K}_2\text{CO}_3$  (2.88 g, 20.93 mmol) and  $\text{CuSO}_4$  (21 mg, 132 mmol). Methanol (90 mL) was added followed by the dropwise addition of the freshly prepared  $\text{TfN}_3$  solution. Methanol was added until the solution was homogeneous, and the reaction was then stirred overnight at room temperature.

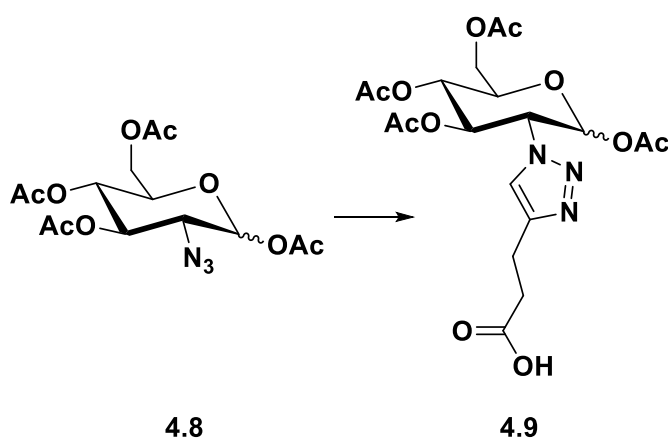
The solvent was removed under vacuum and the residue was redissolved in pyridine (75 mL). This solution was then cooled to  $0^\circ\text{C}$  and  $\text{Ac}_2\text{O}$  (45 mL) was added, and the mixture was allowed to stir at room temperature overnight.

Solvent was removed under vacuum and the residue was redissolved in EtOAc (300 mL) the organic phase was washed with saturated  $\text{CuSO}_4$  solution (200 mL $\times$ 2) and saturated  $\text{NaHCO}_3$  solution (200 mL) and the organic phase was dried with  $\text{Na}_2\text{SO}_4$  and filtered. The solvent was removed under vacuum to give a residue which was purified by column chromatography (EtOAc: Petroleum ether=3:7) to give the product as a colourless syrup (3.848 g, 10.307 mmol, 74%).

$^1\text{H NMR}$  (500 MHz,  $\text{CDCl}_3$ )  $\delta$  6.27 (d,  $J = 3.7$  Hz, 0.37H, H-1 $\alpha$ ), 5.54 (d,  $J = 8.6$  Hz, 0.59H, H-1 $\beta$ ), 5.43 (dd,  $J = 10.4, 9.5$  Hz, 0.39H, H-3 $\alpha$ ), 5.12 – 4.99 (m, 1.6H, H-3 $\beta$ , H-4), 4.27 (dt,  $J = 12.6, 4.5$  Hz, 1H, H-6), 4.08 – 4.00 (m, 1.38H, H-5 $\alpha$ , H-6'), 3.79 (ddd,  $J = 9.7, 4.5, 2.1$  Hz, 0.61H, H-5 $\beta$ ), 3.65 (ddd,  $J = 8.6, 5.8, 2.1$  Hz, 0.98H, H-2), 2.18 – 1.99 (m, 12H, 4 x  $\text{CH}_3$  of OAc) ppm.

NMR data is in agreement with the data reported in the literature [294].

***N*-(1,3,4,6-Tetra-*O*-acetyl-2-deoxy-D-glucopyranosyl-1,2,3-triazol-4-yl)-propanoic acid (4.9)**



**4.8** (0.989 g, 2.649 mmol, 1.3 equiv.) and 4-pentynoic acid (0.2 g, 2.03 mmol) were dissolved in a mixture of tetrahydrofuran (6 ml), tert-Butanol (6 mL) and deionised water (4 mL). Separately, copper(II) sulphate pentahydrate (0.1 g, 0.40 mmol) and sodium ascorbate (0.161 g, 0.815 mmol) were dissolved in deionised water (2 mL), added to reaction flask and allowed to stir at r.t. overnight (16 h). The solvent was removed *in vacuo* and the residue was dissolved in DCM (15 mL) and washed with brine (2 x 20 mL). The organic phase was dried with  $\text{MgSO}_4$ , filtered and the solvent was evaporated. The crude product was purified by column chromatography (1:1, petroleum ether : ethyl acetate) to yield a white solid (0.566 g, 1.20 mmol, 59%).

$R_f = 0.18$  (95:5 DCM : MeOH).

$^1\text{H NMR}$  (500 MHz,  $\text{CDCl}_3$ )  $\delta$  7.47 (s, 0.52H, triaz-H $\alpha$ ), 7.45 (s, 1H, triaz-H $\beta$ ), 6.36 (d,  $J = 3.6$  Hz, 0.51H, H-1 $\alpha$ ), 6.18 (d,  $J = 8.8$  Hz, 1H, H-1 $\beta$ ), 5.92 (dd,  $J = 11.4, 9.2$  Hz, 0.61H,



H-3 $\alpha$ ), 5.77 (dd,  $J = 10.8, 9.2$  Hz, 1H, H-3 $\beta$ ), 5.26 (dd,  $J = 10.2, 9.3$  Hz, 0.64H, H-4 $\alpha$ ), 5.20 (dd,  $J = 10.1, 9.3$  Hz, 1H, H-4 $\beta$ ), 5.13 (dd,  $J = 11.4, 3.6$  Hz, 0.55H, H-2 $\alpha$ ), 4.67 (dd,  $J = 10.8, 8.8$  Hz, 1H, H-2 $\beta$ ), 4.40 – 4.32 (m, 1.51H, H-6 $\alpha$ , H-6 $\beta$ ), 4.20 (ddd,  $J = 10.3, 4.0, 2.3$  Hz, 0.55H, H-5 $\alpha$ ), 4.13 (ddd,  $J = 19.2, 12.5, 2.2$  Hz, 1.54H, H-6' $\alpha$ , H-6' $\beta$ ), 4.07 (ddd,  $J = 10.1, 4.4, 2.2$  Hz, 1H, H-5 $\beta$ ), 3.01 (q,  $J = 6.9$  Hz, 3H,  $\alpha/\beta$  triaz-CH<sub>2</sub>), 2.74 (t,  $J = 6.9$  Hz, 3H,  $\alpha/\beta$  CH<sub>2</sub>CO), 2.11 (s, 1.5H,  $\alpha$  CH<sub>3</sub> of OAc), 2.10 (d,  $J = 2.2$  Hz, 4.5H,  $\alpha$  CH<sub>3</sub> of OAc,  $\beta$  CH<sub>3</sub> of OAc), 2.06 (s, 1.5H,  $\alpha$  CH<sub>3</sub> of OAc), 2.03 (s, 3H,  $\beta$  CH<sub>3</sub> of OAc), 1.97 (s, 3H,  $\beta$  CH<sub>3</sub> of OAc), 1.85 (d,  $J = 3.5$  Hz, 4.5H,  $\beta$  CH<sub>3</sub> of OAc,  $\alpha$  CH<sub>3</sub> of OAc) ppm.

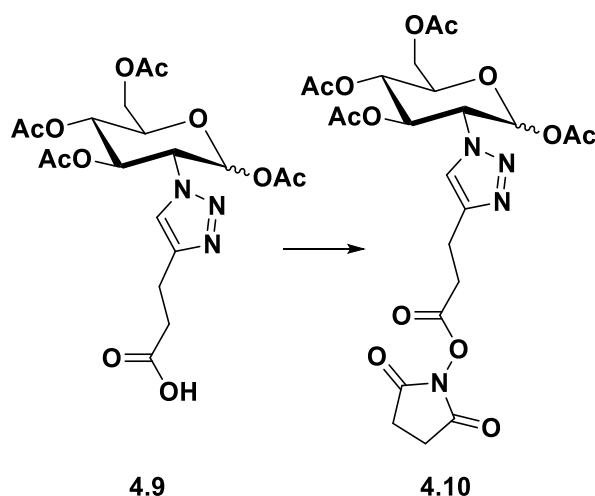
**<sup>13</sup>C NMR** (125 MHz, CDCl<sub>3</sub>)  $\delta$  176.7 (COOH), 170.75 ( $\alpha$  CO of OAc), 170.74 ( $\beta$  CO of OAc), 170.2 ( $\alpha$  CO of OAc), 169.8 ( $\beta$  CO of OAc), 169.48 ( $\alpha$  CO of OAc), 169.44 ( $\beta$  CO of OAc), 168.4 ( $\beta$  CO of OAc), 168.1 ( $\alpha$  CO of OAc), 146.7 (triaz-C $\alpha$ ), 146.5 (triaz-C $\beta$ ), 121.7 (triaz-CH $\beta$ ), 120.7 (triaz-CH $\alpha$ ), 91.7 (C-1 $\beta$ ), 90.2 (C-1 $\alpha$ ), 73.0 (C-5 $\beta$ ), 72.1 (C-3 $\beta$ ), 70.0 (C-5 $\alpha$ ), 68.9 (C-3 $\alpha$ ), 68.3 (C-4 $\beta$ ), 68.2 (C-4 $\alpha$ ), 62.8 (C-2 $\beta$ ), 61.54 (C-6 $\beta$ ), 61.47 (C-6 $\alpha$ ), 61.1 (C-2 $\alpha$ ), 33.4 ( $\alpha/\beta$  CH<sub>2</sub>CO), 20.83 (CH<sub>3</sub> of OAc), 20.80 (2 x CH<sub>3</sub> of OAc), 20.78 (CH<sub>3</sub> of OAc), 20.68 (CH<sub>3</sub> of OAc), 20.65 (CH<sub>3</sub> of OAc), 20.60 ( $\alpha/\beta$  triaz-CH<sub>2</sub>), 20.4 (CH<sub>3</sub> of OAc), 20.3 (CH<sub>3</sub> of OAc) ppm.

**IR (ATR)** 3141.55, 1753.04, 1736.47, 1367.40, 1207.16, 1026.92, 897.06 cm<sup>-1</sup>.

**HR-MS (+):** m/z calcd for C<sub>19</sub>H<sub>25</sub>N<sub>3</sub>O<sub>11</sub> + H<sup>+</sup> [M+H]<sup>+</sup> 472.1567, found 472.1607. **HR-MS**

**(+):** m/z calcd for C<sub>19</sub>H<sub>25</sub>N<sub>3</sub>O<sub>11</sub> + Na<sup>+</sup> [M+Na]<sup>+</sup> 494.1387, found 494.1431.

***N*-(1,3,4,6-Tetra-*O*-acetyl-2-deoxy-D-glucopyranosyl-1,2,3-triazol-4-yl)-(3-oxopropyl-(oxy(2,5-dioxopyrrolidin-1-yl))) (4.10)**



**4.9** (0.120 g, 0.254 mmol) was added to a flask with NHS (0.035 g, 0.305 mmol, 1.2 equiv.), purged with N<sub>2</sub> and dissolved in dry DCM. EDCI (0.058 g, 0.305 mmol, 1.2 equiv.) was dissolved in DCM and added *via* cannula. The reaction was stirred overnight at room temperature. The DCM was washed with 0.1M HCl, brine and dried with Na<sub>2</sub>SO<sub>4</sub>. The solvent was filtered and evaporated to yield a white solid which was used without further purification (0.130 g, 0.228 mmol, 89%) (The ratio of alpha:beta was 1:0.51)

R<sub>f</sub> = 0.69 (95:5 DCM : MeOH).

<sup>1</sup>H NMR (500 MHz, CDCl<sub>3</sub>) δ 7.65 (s, 1H, triaz-*H*β), 7.63 (s, 0.84H, triaz-*H*α), 6.31 (d, *J* = 3.5 Hz, 0.81H, H-1α), 6.10 (d, *J* = 8.8 Hz, 1H, H-1β), 5.88 (dd, *J* = 11.4, 9.2 Hz, 0.86H, H-3α), 5.71 (dd, *J* = 10.8, 9.2 Hz, 1H, H-3β), 5.19 (ddd, *J* = 21.6, 10.1, 9.3 Hz, 1.93H, H-4β, H-4α), 5.09 (dd, *J* = 11.4, 3.6 Hz, 0.88H, H-2α), 4.66 (dd, *J* = 10.8, 8.8 Hz, 1H, H-2β), 4.32 (ddd, *J* = 19.6, 12.5, 4.2 Hz, 1.9H, H-6α, H-6β), 4.18 (ddd, *J* = 10.3, 3.9, 2.3 Hz, 0.89H, H-5α), 4.09 (ddd, *J* = 18.8, 12.5, 2.2 Hz, 1.91H, H-6'α, H-6'β), 4.03 (ddd, *J* = 10.2, 4.3, 2.2 Hz, 1H, H-5β), 3.16 – 3.07 (m, 3.67H, α/β triaz-CH<sub>2</sub>), 3.00 – 2.89 (m, 3.76H, α/β CH<sub>2</sub>CO), 2.81 (s, 7.52H, α/β CH<sub>2</sub>CH<sub>2</sub>-Succ), 2.07 (s, 2.57H, α CH<sub>3</sub> of OAc), 2.06 (s, 5.43H, α/β CH<sub>3</sub> of OAc), 2.01 (s, 2.54H, α CH<sub>3</sub> of OAc), 1.99 (s, 3H, β CH<sub>3</sub> of OAc), 1.92 (s, 3H, β CH<sub>3</sub> of OAc), 1.81 (s, 3H, β CH<sub>3</sub> of OAc), 1.79 (s, 2.35H, α CH<sub>3</sub> of OAc) ppm.

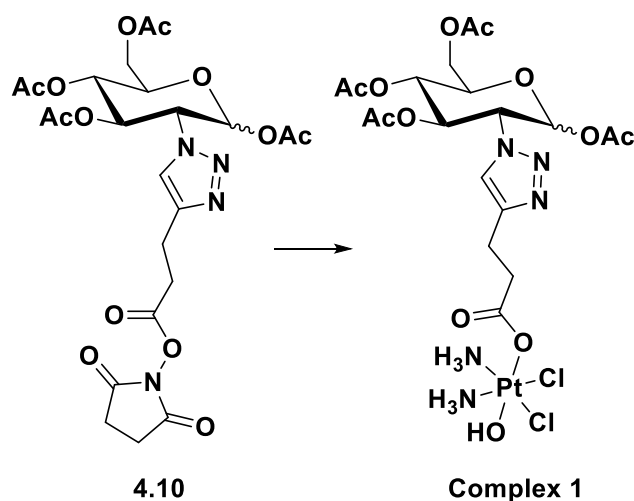
**$^{13}\text{C}$  NMR** (125 MHz,  $\text{CDCl}_3$ )  $\delta$  170.61 ( $\alpha$  CO of OAc), 170.59 ( $\beta$  CO of OAc), 169.9 ( $\alpha$  CO of OAc), 169.6 ( $\beta$  CO of OAc), 169.4 ( $\alpha$  CO of OAc), 169.32 ( $\beta$  CO of OAc), 169.27 ( $\alpha/\beta$  CO-Succ), 168.3 ( $\beta$  CO of OAc), 168.0 ( $\alpha$  CO of OAc), 167.72 (CO  $\beta$ ), 167.68 (CO  $\alpha$ ), 145.20 (triaz-C $\alpha$ ), 145.16 (triaz-C $\beta$ ), 121.9 (triaz-CH $\beta$ ), 121.2 (triaz-CH $\alpha$ ), 91.6 (C-1 $\beta$ ), 90.1 (C-1 $\alpha$ ), 72.8 (C-5 $\beta$ ), 72.0 (C-3 $\beta$ ), 69.8 (C-5 $\alpha$ ), 68.9 (C-3 $\alpha$ ), 68.4 (C-4 $\alpha$ ), 68.1 (C-4 $\beta$ ), 62.6 (C-2 $\beta$ ), 61.42 (C-6 $\beta$ ), 61.40 (C-6 $\alpha$ ), 61.0 (C-2 $\alpha$ ), 31.2 ( $\beta$   $\text{CH}_2\text{CO}$ ), 31.1 ( $\alpha$   $\text{CH}_2\text{CO}$ ), 25.64 ( $\beta$   $\text{CH}_2\text{CH}_2\text{-Succ}$ ), 25.63 ( $\alpha$   $\text{CH}_2\text{CH}_2\text{-Succ}$ ), 21.10 ( $\alpha$  triaz- $\text{CH}_2$ ), 21.05 ( $\beta$  triaz- $\text{CH}_2$ ), 20.73 ( $\beta$   $\text{CH}_3$  of OAc), 20.71 ( $\alpha$   $\text{CH}_3$  of OAc), 20.69 ( $\alpha$   $\text{CH}_3$  of OAc), 20.59 ( $\beta$   $\text{CH}_3$  of OAc), 20.57 ( $\alpha$   $\text{CH}_3$  of OAc), 20.50 ( $\beta$   $\text{CH}_3$  of OAc), 20.3 ( $\alpha$   $\text{CH}_3$  of OAc), 20.2 ( $\beta$   $\text{CH}_3$  of OAc) ppm.

**IR (ATR)** 2959.88, 1731.79, 1366.73, 1201.79, 1067.81, 1043.20, 813.86  $\text{cm}^{-1}$ .

**HR-MS (+):**  $m/z$  calcd for  $\text{C}_{23}\text{H}_{28}\text{N}_4\text{O}_{13} + \text{H}^+$   $[\text{M}+\text{H}]^+$  569.1731, found 569.1800. **HR-MS**

**(+):**  $m/z$  calcd for  $\text{C}_{23}\text{H}_{28}\text{N}_4\text{O}_{13} + \text{Na}^+$   $[\text{M}+\text{Na}]^+$  591.1551, found 591.1631.

***Cis,cis,trans*-[Pt<sub>IV</sub>(NH<sub>3</sub>)<sub>2</sub>(4.9)(OH)Cl<sub>2</sub>] (1)**



**4.10** (0.130 g, 0.2286 mmol) was added to a round bottom flask containing a suspension of oxoplatin (0.080 g, 0.239 mmol) in DMSO (6 mL) and stirred overnight at 60°C in the dark. the next morning, excess oxoplatin was filtered through cotton and the DMSO was evaporated by lyophilisation. The oily residue was redissolved in acetone and the product was precipitated using diethyl ether. The residual solvent

was then removed *in vacuo* yielding a yellow solid (0.122 g, 0.154 mmol, 67%). (The ratio of alpha:beta was 1:0.51)

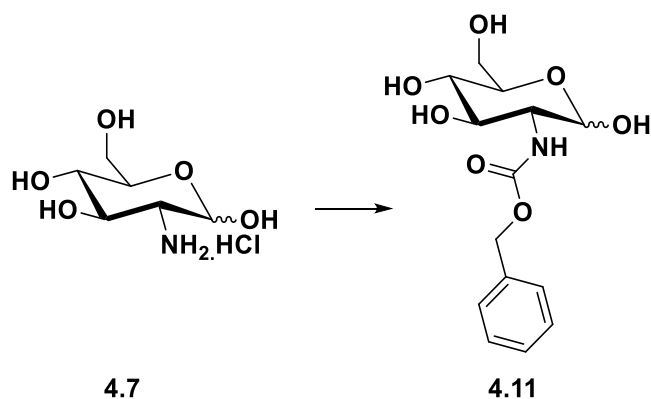
**<sup>1</sup>H NMR** (500 MHz, DMSO)  $\delta$  8.01 (s, 1H, triaz-CH $\beta$ ), 7.92 (s, 0.54H, triaz-CH $\alpha$ ), 6.35 (d,  $J$  = 8.7 Hz, 1H, H-1 $\beta$ ), 6.26 (d,  $J$  = 3.5 Hz, 0.51H, H-1 $\alpha$ ), 6.14 – 5.78 (m, 10.5H,  $\alpha/\beta$  NH $_3$ , H-3 $\beta$ , H-3 $\alpha$ ), 5.36 (dd,  $J$  = 11.2, 3.5 Hz, 0.54H, H-2 $\alpha$ ), 5.19 (t,  $J$  = 9.85, 0.60H, H-4 $\alpha$ ), 5.09 (t,  $J$  = 9.7 Hz, 1H, H-4 $\beta$ ), 4.90 (dd,  $J$  = 10.7, 8.7 Hz, 1H, H-2 $\beta$ ), 4.35 (ddd,  $J$  = 10.1, 4.6, 2.3 Hz, 1H, H-5 $\beta$ ), 4.32 – 4.27 (m, 0.64H, H-5 $\alpha$ ), 4.24 (m, 1.74H, H-6 $\alpha$ , H-6 $\beta$ ), 4.10 – 4.02 (m, 1.77H, H-6' $\alpha$ , H-6' $\beta$ ), 2.78 (t,  $J$  = 7.8, 3H,  $\alpha/\beta$  triaz-CH $_2$ ), 2.45 – 2.39 (m, 3H,  $\alpha/\beta$  CH $_2$ CO), 2.10 (s, 1.5H,  $\alpha$  CH $_3$  of OAc), 2.03 (d,  $J$  = 1.6 Hz, 4.5H,  $\alpha/\beta$  CH $_3$  of OAc), 2.00 (s, 1.5H,  $\alpha$  CH $_3$  of OAc), 1.99 (s, 3H,  $\beta$  CH $_3$  of OAc), 1.93 (s, 3H,  $\beta$  CH $_3$  of OAc), 1.80 (s, 3H,  $\beta$  CH $_3$  of OAc), 1.79 (s, 3H,  $\alpha$  CH $_3$  of OAc) ppm.

**<sup>13</sup>C NMR** (125 MHz, DMSO)  $\delta$  179.73 (COOPt  $\alpha$ ), 179.70 (COOPt  $\beta$ ), 170.1 (2x CO of OAc), 169.4 (CO of OAc), 169.3 (CO of OAc), 169.2 (CO of OAc), 168.9 (CO of OAc), 168.5 (CO of OAc), 168.3 (CO of OAc), 146.7 (triaz-C $\alpha$ ), 146.6 (triaz-C $\beta$ ), 122.1 (triaz-CH $\beta$ ), 121.9 (triaz-CH $\alpha$ ), 91.0 (C-1 $\beta$ ), 89.5 (C-1 $\alpha$ ), 71.7 (C-5 $\beta$ ), 71.5 (C-3 $\beta$ ), 69.3 (C-5 $\alpha$ ), 68.8 (C-3 $\alpha$ ), 68.0 (C-4 $\alpha$ ), 67.9 (C-4 $\beta$ ), 61.7 (C-2 $\beta$ ), 61.4 (C-6 $\beta$ ), 61.2 (C-6 $\alpha$ ), 59.7 (C-2 $\alpha$ ), 36.2 ( $\alpha$  CH $_2$ CO), 36.1 ( $\beta$  CH $_2$ CO), 21.9 ( $\alpha/\beta$  triaz-CH $_2$ ), 20.6 (3x CH $_3$  of OAc), 20.39 (CH $_3$  of OAc), 20.37 (CH $_3$  of OAc), 20.3 (CH $_3$  of OAc), 20.1 (CH $_3$  of OAc), 20.0 (CH $_3$  of OAc) ppm.

**<sup>195</sup>Pt{<sup>1</sup>H} NMR** (108 MHz, DMSO)  $\delta$  1045.54 ppm.

**IR (ATR)** 3220.55, 1747.64, 1623.98, 1367.12, 1212.66, 1043.50, 906.86 cm $^{-1}$ .

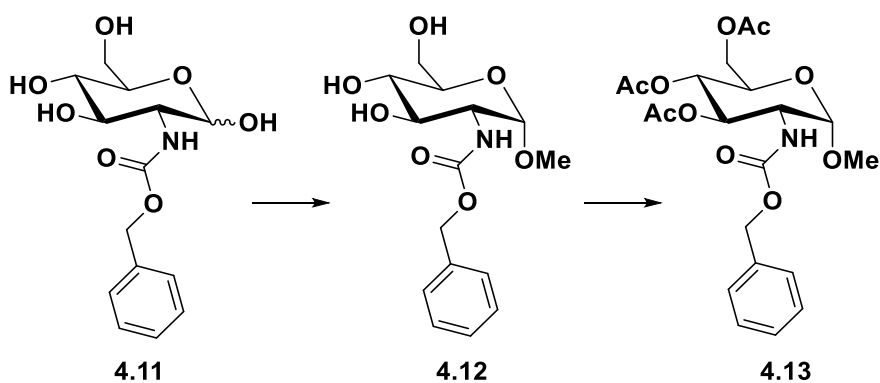
**HR-MS (-):** m/z calcd for C $_{19}$ H $_{31}$ Cl $_2$ N $_5$ O $_{12}$ Pt – H $^-$  [M-H] $^-$  786.4560, found 786.0913.

**2-(Benzyloxycarbonyl)amino-2-deoxy-D-glucopyranoside (4.11)**

NaHCO<sub>3</sub> (4.65 g, 55.3 mmol, 3 eq.) was added to a solution of **4.7** (3.85 g, 17.8 mmol) in H<sub>2</sub>O (115 mL). Benzyl chloroformate (2.8 mL, 19.6 mmol, 1.1 eq.) was added dropwise over 30 min and the mixture was stirred at room temperature for 18 h. A white precipitate was formed, and it was filtered and dried in vacuo to give the product as a white solid (4.67 g, 83%).

<sup>1</sup>H NMR (500 MHz, MeOD) δ 7.40 – 7.25 (m, 5H, H-Ar), 5.12 (d, *J* = 3.4 Hz, 0.83H, H-1α), 5.09 (s, 2H, CH<sub>2</sub>Ph), 4.58 (d, *J* = 8.1 Hz, 0.26H, H-1β), 3.86 (dd, *J* = 11.9, 2.2 Hz, 0.31H, C-6β), 3.81 – 3.75 (m, 1.79H, C-6α', C-4), 3.73 – 3.62 (m, 2.06H, C-3, C-6α, C-6β'), 3.57 (dd, *J* = 10.6, 3.4 Hz, 1H, C-2), 3.36 (t, *J* = 9.1 Hz, 1H, C-5) ppm.

NMR data is in agreement with the data reported in the literature [295].

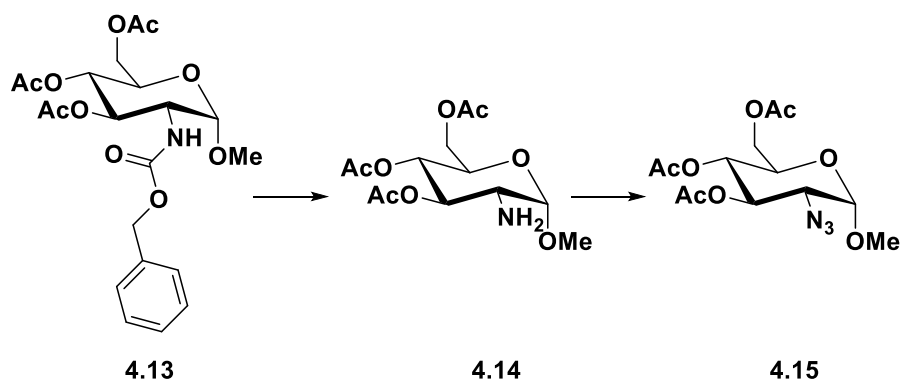
**Methyl-3,4,6-tri-*O*-acetyl-2-(benzyloxycarbonyl)amino-2-deoxy-α-D-glucopyranoside (4.13)**

**4.11** (1.2 g, 3.83 mmol) was added to a 1.25 M solution of HCl in methanol (10mL) and heated to 80°C and stirred overnight. The following day, the solvent was evaporated and dried *in vacuo* to yield a yellow/white solid. This was reacted without further purification. The crude product was dissolved in pyridine (10 mL) and stirred on ice. Acetic anhydride (0.67 mL, 7.16 mmol, 10 equiv.) was added and stirred overnight. The solvent was evaporated, and the residue was redissolved in EtOAc. The organic phase was washed with sat. CuSO<sub>4</sub> solution and NaHCO<sub>3</sub> solution. The organic phase was dried with Na<sub>2</sub>SO<sub>4</sub>, filtered and evaporated. The crude product was purified by column chromatography (1:1 Petroleum ether:Ethyl acetate) yielding a white solid (1.26 g, 2.77 mmol, 73%).

<sup>1</sup>H NMR (500 MHz, CDCl<sub>3</sub>) δ 7.34 – 7.26 (m, 5H, H-Ar), 5.18 – 5.14 (m, 1H, H-4), 5.11 – 5.03 (m, 2H, CHPh, H-3), 5.00 (t, *J* = 11.9 Hz, 1H, CH'Ph), 4.72 (d, *J* = 3.6 Hz, 1H, H-1), 4.21 (dd, *J* = 12.3, 4.7 Hz, 1H, H-6), 4.09 – 3.98 (m, 2H, H-6', H-2), 3.89 (ddd, *J* = 10.1, 4.6, 2.3 Hz, 1H, H-5), 3.35 (s, 3H, OCH<sub>3</sub>), 2.05 (s, 3H, CH<sub>3</sub> of OAc), 1.97 (s, 3H, CH<sub>3</sub> of OAc), 1.84 (s, 3H, CH<sub>3</sub> of OAc) ppm.

NMR data is in agreement with the data reported in the literature [296].

#### Methyl-3,4,6-tri-*O*-acetyl-2-azido-2-deoxy- $\alpha$ -D-glucopyranoside (**4.15**)



H<sub>2</sub> gas was bubbled through a suspension of **4.13** (3.826 g, 8.437 mmol) and Pd/C (0.382 g, 10 % w/w) in DCM (20 mL). It was left to stir for 18 hr at rt. The mixture was filtered through celite (washed with DCM); and dried *in vacuo*. The final product was reacted without further purification.

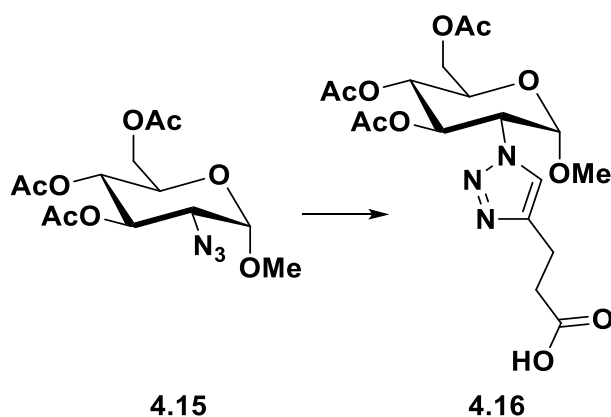
NaN<sub>3</sub> (4.47 g, 68.7 mmol, 4.9 equiv.) was dissolved in H<sub>2</sub>O (11mL) and cooled to 0°C for 5 minutes. DCM (20mL) was added and stirred vigorously while Tf<sub>2</sub>O (2.34 mL, 13.9 mmol) was added over 5 minutes. This was stirred at 0°C for 2 hours. The organic phase was separated, and the aqueous phase was washed with DCM (17.5mL) for a total volume of 37.5mL of DCM containing the TfN<sub>3</sub> product.

**4.14** (1.525 g, 4.77 mmol) was dissolved in DCM (22.5mL). K<sub>2</sub>CO<sub>3</sub> (1.44 g, 10.4 mmol, 1.5 equiv.) and CuSO<sub>4</sub> (10.5 mg) was dissolved separately in water (10 mL) and added so the solution of sugar in DCM. MeOH (45mL) was added, followed by the dropwise addition of the TfN<sub>3</sub> solution. More water was added to ensure the K<sub>2</sub>CO<sub>3</sub> and CuSO<sub>4</sub> remained in solution. Additional MeOH was added to make the solution homogeneous, this was allowed to stir overnight at room temperature. DCM and MeOH were evaporated *in vacuo* and the remaining water was washed with DCM. The organic phase was washed with NaHCO<sub>3</sub>, brine, dried with Na<sub>2</sub>SO<sub>4</sub> and the DCM was evaporated. The resulting oil was purified through column chromatography (Petroleum ether:Ethyl acetate. 7:3). (0.582 g, 1.68 mmol, 35%).

**<sup>1</sup>H NMR** (500 MHz, CDCl<sub>3</sub>) δ 5.43 (dd, *J* = 10.6, 9.2 Hz, 1H, H-3), 5.00 (dd, *J* = 10.2, 9.3 Hz, 1H, H-4), 4.84 (d, *J* = 3.5 Hz, 1H, H-1), 4.24 (dd, *J* = 12.4, 4.7 Hz, 1H, H-6), 4.08 – 4.04 (m, 1H, H-6'), 3.97 (ddd, *J* = 10.2, 4.6, 2.3 Hz, 1H, H-5), 3.43 (s, 3H, OCH<sub>3</sub>), 3.34 (dd, *J* = 10.6, 3.5 Hz, 1H, H-2), 2.05 (s, 3H, CH<sub>3</sub> of OAc), 2.05 (s, 3H, CH<sub>3</sub> of OAc), 2.00 (s, 3H, CH<sub>3</sub> of OAc) ppm.

NMR data is in agreement with the data reported in the literature [288].

**Methyl-*N*-(3,4,6-tri-*O*-acetyl-2-deoxy- $\alpha$ -D-glucopyranosyl-1,2,3-triazol-4-yl)-propanoic acid (4.16)**



**4.15** (0.469 g, 1.35 mmol) and 4-pentynoic acid (0.264 g, 2.7 mmol, 2 equiv.) were dissolved in *t*-BuOH (12mL), H<sub>2</sub>O (12mL) and THF (12mL). CuSO<sub>4</sub> (195 mg) and NaAsc (275 mg) were added and allowed to stir overnight. Completion of the reaction was followed by TLC (DCM:MeOH. 9:1). The solvent was then removed *in vacuo* and the resulting residue was redissolved in DCM and washed with brine. The organic layer was dried and filtered, and the crude product was purified by column chromatography (DCM:MeOH. 95:5). The pure product was obtained as a colourless oil (0.394 g, 0.888 mmol, 65%).

$R_f$  = 0.37 (95:5 DCM:MeOH).

**<sup>1</sup>H NMR** (500 MHz, CDCl<sub>3</sub>)  $\delta$  7.57 (s, 1H, triaz-CH), 5.75 (dd,  $J$  = 11.2, 9.1 Hz, 1H, H-3), 5.18 (dd,  $J$  = 10.1, 9.2 Hz, 1H, H-4), 5.01 (dd,  $J$  = 11.3, 3.4 Hz, 1H, H-2), 4.96 (d,  $J$  = 3.4 Hz, 1H, H-1), 4.31 (dd,  $J$  = 12.4, 4.7 Hz, 1H, H-6), 4.16 (dd,  $J$  = 12.3, 2.4 Hz, 1H, H-6'), 4.11 (ddd,  $J$  = 10.2, 4.7, 2.3 Hz, 1H, H-5), 3.39 (s, 3H, OCH<sub>3</sub>), 3.02 (t,  $J$  = 7.3 Hz, 2H, triaz-CH<sub>2</sub>), 2.75 (t,  $J$  = 7.4 Hz, 2H, CH<sub>2</sub>CO), 2.12 (s, 3H, CH<sub>3</sub> of OAc), 2.04 (s, 3H, CH<sub>3</sub> of OAc), 1.80 (s, 3H, CH<sub>3</sub> of OAc) ppm.

**<sup>13</sup>C NMR** (125 MHz, CDCl<sub>3</sub>)  $\delta$  177.0 (CO), 170.8 (CO of OAc), 170.2 (CO of OAc), 169.6 (CO of OAc), 146.3 (triaz-C), 121.1 (triaz-CH), 98.1 (C-1), 69.4 (C-3), 68.8 (C-4), 67.9 (C-5), 62.3 (C-2), 61.9 (C-6), 55.8 (OCH<sub>3</sub>), 33.5 (CH<sub>2</sub>CO), 20.91 (triaz-CH<sub>2</sub>), 20.85 (CH<sub>3</sub> of OAc), 20.7 (CH<sub>3</sub> of OAc), 20.4 (CH<sub>3</sub> of OAc) ppm.

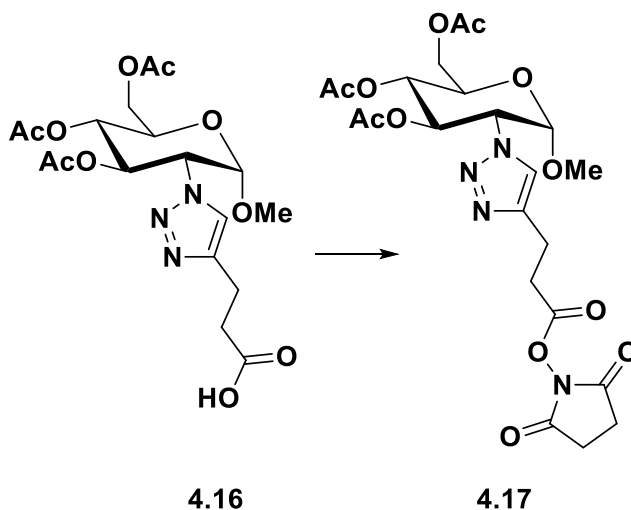
**IR (ATR)** 2943.14, 1739.49, 1367.31, 1217.89, 1032.28, 927.19, 733.50, 601.37 cm<sup>-1</sup>.



**HR-MS (+):**  $m/z$  calcd for  $C_{18}H_{25}N_3O_{10} + H^+$   $[M+H]^+$  444.1618, found 444.1616. **HR-MS**

**(+):**  $m/z$  calcd for  $C_{18}H_{25}N_3O_{10} + Na^+$   $[M+Na]^+$  466.1438, found 466.1433.

**Methyl-*N*-(3,4,6-tri-*O*-acetyl-2-deoxy- $\alpha$ -D-glucopyranosyl-1,2,3-triazol-4-yl)-(3-oxopropyl-(oxy(2,5-dioxopyrrolidin-1-yl))) (4.17)**



**4.16** (0.240 g, 0.541 mmol) and NHS (0.074 g, 0.649 mmol, 1.2 equiv.) were purged with  $N_2$  and dissolved in anhydrous DCM (10 mL). A separate flask containing EDCI (0.124 g, 0.649 mmol, 1.2 equiv.) was also purged with  $N_2$  and dissolved in anhydrous DCM (4 mL). This was added to the solution of **4.16** and NHS via cannula addition and the reaction was allowed to stir overnight at room temperature. The organic phase was washed with 0.1M HCl, dried, filtered and the solvent was evaporated and isolated as a white powder (0.267 g, 0.494 mmol, 91%).

$R_f = 0.77$  (95:5 DCM:MeOH).

$^1H$  NMR (500 MHz,  $CDCl_3$ )  $\delta$  7.68 (s, 1H, triaz-CH), 5.74 (dd,  $J = 11.2, 9.1$  Hz, 1H, H-3), 5.18 (dd,  $J = 10.1, 9.2$  Hz, 1H, H-4), 5.02 (dd,  $J = 11.2, 3.4$  Hz, 1H, H-2), 4.98 (d,  $J = 3.4$  Hz, 1H, H-1), 4.32 (dd,  $J = 12.3, 4.6$  Hz, 1H, H-6), 4.17 (dd,  $J = 12.3, 2.4$  Hz, 1H, H-6'), 4.13 (ddd,  $J = 10.3, 4.6, 2.4$  Hz, 1H, H-5), 3.40 (s, 3H,  $OCH_3$ ), 3.15 (td,  $J = 7.2, 2.4$  Hz, 2H, triaz- $CH_2$ ), 3.01 (td,  $J = 7.2, 2.4$  Hz, 2H,  $CH_2CO$ ), 2.83 (s, 4H,  $CH_2CH_2$ -succ), 2.12 (s, 3H,  $CH_3$  of OAc), 2.04 (s, 3H,  $CH_3$  of OAc), 1.81 (s, 3H,  $CH_3$  of OAc) ppm.

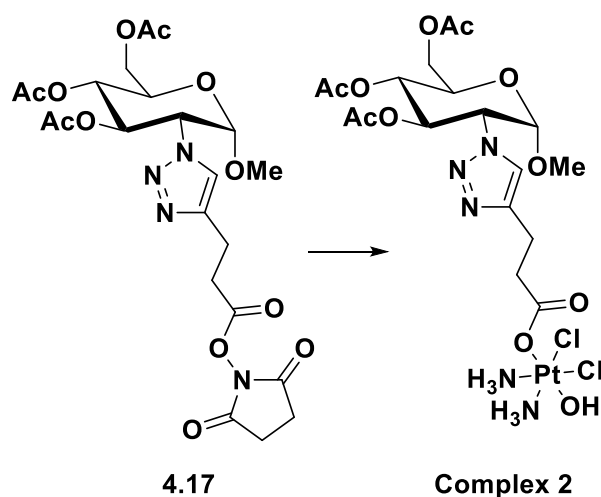
**$^{13}\text{C}$  NMR** (125 MHz,  $\text{CDCl}_3$ )  $\delta$  170.8 (CO of OAc), 170.1 (CO of OAc), 169.6 (CO of OAc), 169.2 (CO succ x2), 167.8 (CO), 145.2 (triaz-C), 121.5 (triaz-CH), 98.1 (C-1), 69.5 (C-3), 68.9 (C-4), 67.8 (C-5), 62.3 (C-2), 62.0 (C-6), 55.8 ( $\text{OCH}_3$ ), 31.1 ( $\text{CH}_2\text{CO}$ ), 25.7 ( $\text{CH}_2\text{CH}_2\text{-succ}$ ), 21.1 (triaz- $\text{CH}_2$ ), 20.9 ( $\text{CH}_3$  of OAc), 20.7 ( $\text{CH}_3$  of OAc), 20.4 ( $\text{CH}_3$  of OAc) ppm.

**IR (ATR)** 2962.23, 1731.98, 1366.80, 1204.22, 1029.25, 799.23  $\text{cm}^{-1}$ .

**HR-MS (+):**  $m/z$  calcd for  $\text{C}_{22}\text{H}_{28}\text{N}_4\text{O}_{12} + \text{H}^+$   $[\text{M}+\text{H}]^+$  541.1782, found 541.1817. **HR-MS**

**(+):**  $m/z$  calcd for  $\text{C}_{22}\text{H}_{28}\text{N}_4\text{O}_{12} + \text{Na}^+$   $[\text{M}+\text{Na}]^+$  563.1601, found 563.1641.

***Cis,cis,trans*-[Pt<sup>IV</sup>(NH<sub>3</sub>)<sub>2</sub>(4.16)(OH)Cl<sub>2</sub>] (2)**



**4.17** (0.236 g, 0.436 mmol) was added to a suspension of oxoplatin (0.153 g, 0.458 mmol, 1.05 equiv.) in DMSO (15 mL) and stirred at 55°C overnight. The resulting suspension was filtered, and the filtrate was lyophilised to remove the DMSO. The oily residue was washed then dissolved in acetone and precipitated with diethyl ether to yield a yellow-white powder (0.285 g, 0.375 mmol, 86%).

**$^1\text{H}$  NMR** (500 MHz, DMSO)  $\delta$  7.81 (s, 1H, triaz-CH), 6.13 – 5.81 (br t,  $J = 51.65$  Hz, 6H, 2x  $\text{NH}_3$ ), 5.73 – 5.67 (m, 1H, H-3), 5.14 – 5.06 (m, 3H, H-4, H-1, H-2), 4.22 (dd,  $J = 12.3$ , 5.0 Hz, 1H, H-6), 4.11 (dd,  $J = 12.3$ , 2.4 Hz, 1H, H-6'), 4.06 (ddd,  $J = 10.2$ , 4.9, 2.4 Hz, 1H, H-5), 3.32 (s, 3H,  $\text{OCH}_3$  overlaps with  $\text{H}_2\text{O}$ ), 2.81 – 2.77 (m, 2H, triaz- $\text{CH}_2$ ), 2.46 – 2.42 (m, 2H,  $\text{CH}_2\text{CO}$ ), 2.04 (s, 3H,  $\text{CH}_3$  of OAc), 2.00 (s, 3H,  $\text{CH}_3$  of OAc), 1.75 (s, 3H,  $\text{CH}_3$  of OAc) ppm.

$^{13}\text{C}$  NMR (125 MHz, DMSO)  $\delta$  179.7 (CO), 170.1 (CO of OAc), 169.3 (CO of OAc), 169.2 (CO of OAc), 146.5 (triaz-C), 121.5 (triaz-CH), 97.1 (C-1), 69.1 (C-3), 68.5 (C-4), 67.1 (C-5), 61.8 (C-6), 60.9 (C-2), 55.0 (OCH<sub>3</sub>), 36.1 (CH<sub>2</sub>CO), 21.9 (triaz-CH<sub>2</sub>), 20.5 (CH<sub>3</sub> of OAc), 20.4 (CH<sub>3</sub> of OAc), 20.1 (CH<sub>3</sub> of OAc) ppm.

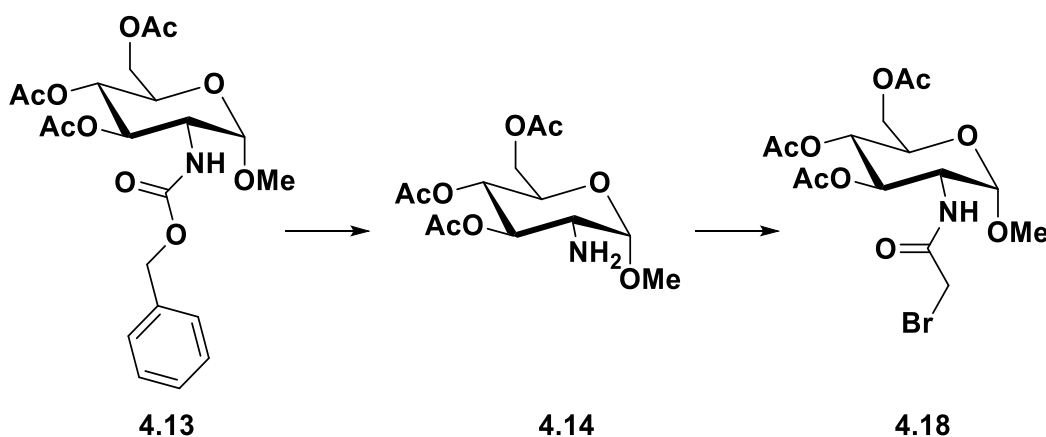
$^{195}\text{Pt}\{^1\text{H}\}$  NMR (108 MHz, DMSO)  $\delta$  1046.86 ppm.

IR (ATR) 3217.18, 1744.63, 1624.51, 1367.45, 1224.71, 1040.54, 928.27 cm<sup>-1</sup>.

HR-MS (+): m/z calcd for C<sub>18</sub>H<sub>31</sub>Cl<sub>2</sub>N<sub>5</sub>O<sub>11</sub>Pt + H<sup>+</sup> [M+H]<sup>+</sup> 759.1123, found 759.1141.

HR-MS (+): m/z calcd for C<sub>18</sub>H<sub>31</sub>Cl<sub>2</sub>N<sub>5</sub>O<sub>11</sub>Pt + Na<sup>+</sup> [M+Na]<sup>+</sup> 781.0943, found 781.0964.

**Methyl-2-(2-bromoacetamido)-2-deoxy-3,4,6-tri-O-acetyl- $\alpha$ -D-glucopyranoside (4.18)**



H<sub>2</sub> gas was bubbled through a suspension of **4.13** (3.826 g, 8.437 mmol) and Pd/C (0.382 g, 10 % w/w) in DCM (20 mL). It was left to stir for 18 hr at rt. The mixture was filtered through celite (washed with DCM); and dried in vacuo. The final product was reacted without further purification.

**4.14** (2.305 g, 7.21 mmol) was purged with N<sub>2</sub> and dissolved in dry DCM (19 mL). NEt<sub>3</sub> (1.2 mL, 8.66 mmol, 1.2 equiv) was added and the solution was allowed to stir over ice. Bromoacetyl bromide (0.75 mL, 8.66 mmol, 1.2 equiv.) was diluted with dry DCM (5 mL) and added to the flask *via* cannula. The reaction was stirred overnight, and the crude product was extracted with 1M HCl, aqueous NaHCO<sub>3</sub>, brine and dried with Na<sub>2</sub>SO<sub>4</sub>. Yielding a white solid (2.279 g, 5.176 mmol, 71%).

$R_f = 0.73$  (pet. ether: EtOAc 1:1).

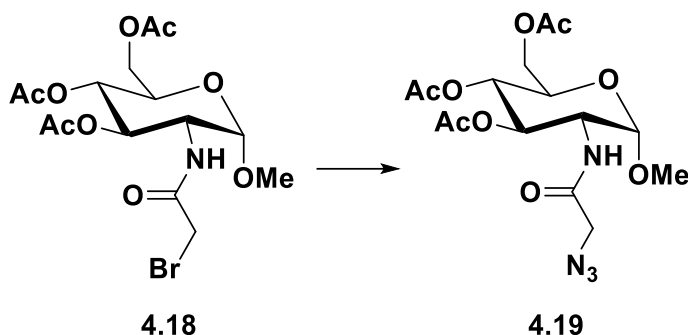
$^1\text{H NMR}$  (500 MHz,  $\text{CDCl}_3$ )  $\delta$  6.56 (d,  $J = 9.4$  Hz, 1H, NHCO), 5.25 (dd,  $J = 10.7, 9.5$  Hz, 1H, H-3), 5.09 (t,  $J = 10.2$  Hz, 1H, H-4), 4.74 (d,  $J = 3.6$  Hz, 1H, H-1), 4.31 – 4.20 (m, 2H, H-2, H-6), 4.09 (dd,  $J = 12.3, 2.4$  Hz, 1H, H-6'), 3.93 (ddd,  $J = 10.1, 4.7, 2.3$  Hz, 1H, H-5), 3.78 (d,  $J = 2.6$  Hz, 2H,  $\text{CH}_2\text{Br}$ ), 3.41 (s, 3H,  $\text{OCH}_3$ ), 2.08 (s, 3H,  $\text{CH}_3$  of OAc), 2.01 (s, 3H,  $\text{CH}_3$  of OAc), 1.99 (s, 3H,  $\text{CH}_3$  of OAc) ppm.

$^{13}\text{C NMR}$  (125 MHz,  $\text{CDCl}_3$ )  $\delta$  171.2 (CO of OAc), 170.8 (CO of OAc), 169.4 (CO of OAc), 166.0 (NHCO), 98.0 (C-1), 70.9 (C-3), 68.2 (C-4), 67.8 (C-5), 62.0 (C-6), 55.7 ( $\text{OCH}_3$ ), 52.6 (C-2), 28.5 ( $\text{CH}_2\text{Br}$ ), 20.8 (2x  $\text{CH}_3$  of OAc), 20.7 ( $\text{CH}_3$  of OAc) ppm.

**IR (ATR)** 3246.56, 1734.05, 1651.68, 1552.68, 1363.83, 1211.90, 1131.38, 1056.20, 1029.13, 924.95  $\text{cm}^{-1}$ .

**HR-MS (+):**  $m/z$  calcd for  $\text{C}_{15}\text{H}_{22}\text{BrNO}_9 + \text{Na}^+$   $[\text{M}+\text{Na}]^+$  462.0376, found 462.0319.

**Methyl-2-(2-azidoacetamido)-2-deoxy-3,4,6-tri-O-acetyl- $\alpha$ -D-glucopyranoside (4.19)**



**4.18** (1.818 g, 4.12 mmol) and  $\text{NaN}_3$  (0.536 g, 8.25 mmol, 2 equiv.) were dissolved in anhydrous DMF (24 mL) and refluxed at  $80^\circ\text{C}$  overnight. DMF was evaporated and the residue was redissolved in DCM and washed with cold water. The organic phase was dried with  $\text{Na}_2\text{SO}_4$ , filtered and dried *in vacuo* to yield a white solid (1.634 g, 4.06 mmol, 98%).

$R_f = 0.72$  (pet. ether: EtOAc 1:1).

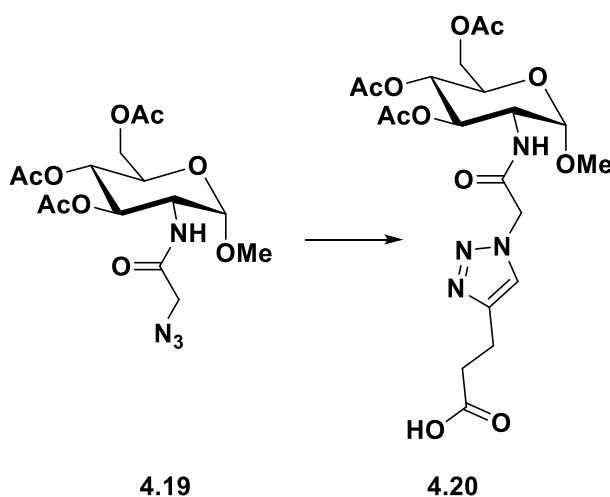
**<sup>1</sup>H NMR** (500 MHz, CDCl<sub>3</sub>) δ 6.50 (d, *J* = 9.5 Hz, 1H, NHCO), 5.25 (dd, *J* = 10.6, 9.5 Hz, 1H, H-3), 5.12 (t, *J* = 9.8 Hz, 1H, H-4), 4.74 (d, *J* = 3.6 Hz, 1H, H-1), 4.32 (ddd, *J* = 10.6, 9.5, 3.7 Hz, 1H, H-2), 4.25 (dd, *J* = 12.3, 4.6 Hz, 1H, H-6), 4.11 (dd, *J* = 12.3, 2.4 Hz, 1H, H-6'), 3.96 – 3.91 (m, 3H, H-5, CH<sub>2</sub>N<sub>3</sub>), 3.42 (s, 3H, OCH<sub>3</sub>), 2.10 (s, 3H, CH<sub>3</sub> of OAc), 2.03 (s, 3H, CH<sub>3</sub> of OAc), 2.01 (s, 3H, CH<sub>3</sub> of OAc) ppm.

**<sup>13</sup>C NMR** (125 MHz, CDCl<sub>3</sub>) δ 171.3 (CO of OAc), 170.8 (CO of OAc), 169.5 (CO of OAc), 166.8 (NHCO), 98.1 (C-1), 71.3 (C-3), 68.2 (C-4), 67.8 (C-5), 62.1 (C-6), 55.6 (OCH<sub>3</sub>), 52.7 (CH<sub>2</sub>N<sub>3</sub>), 52.1 (C-2), 20.9 (CH<sub>3</sub> of OAc), 20.8 (CH<sub>3</sub> of OAc), 20.7 (CH<sub>3</sub> of OAc) ppm.

**IR (ATR)** 3332.36, 2104.64, 1736.94, 1670.34, 1542.60, 1368.04, 1217.17, 1030.83, 923.96 cm<sup>-1</sup>.

**HR-MS (+):** *m/z* calcd for C<sub>15</sub>H<sub>22</sub>N<sub>4</sub>O<sub>9</sub> + H<sup>+</sup> [M+H]<sup>+</sup> 403.1465, found 403.1417. **HR-MS (+):** *m/z* calcd for C<sub>15</sub>H<sub>22</sub>N<sub>4</sub>O<sub>9</sub> + Na<sup>+</sup> [M+Na]<sup>+</sup> 425.1284, found 425.1237.

**Methyl-*N*-(2-deoxy-3,4,6-tri-*O*-acetyl- $\alpha$ -D-glucopyranosyl)-2-acetamido-1,2,3-triazol-4-yl]-propanoic acid (4.20)**



**4.19** (0.525 g, 1.304 mmol) and 4-Pentynoic acid (0.191 g, 1.956 mmol, 1.5 equiv.) were dissolved in 15 mL each of *t*-BuOH and H<sub>2</sub>O. Sodium ascorbate (0.183 g) and CuSO<sub>4</sub>·5H<sub>2</sub>O (0.140 g) were added to the solution. This was allowed to stir at room temperature overnight. The solvent was removed *in vacuo* and the residue was redissolved in DCM and washed with brine. The organic phase was dried with Na<sub>2</sub>SO<sub>4</sub>

and filtered. The crude product was purified with column chromatography (DCM:MeOH 9:1) to yield a white solid (0.267 g, 0.723 mmol, 41%)

$R_f = 0.78$  (90:10 DCM:MeOH).

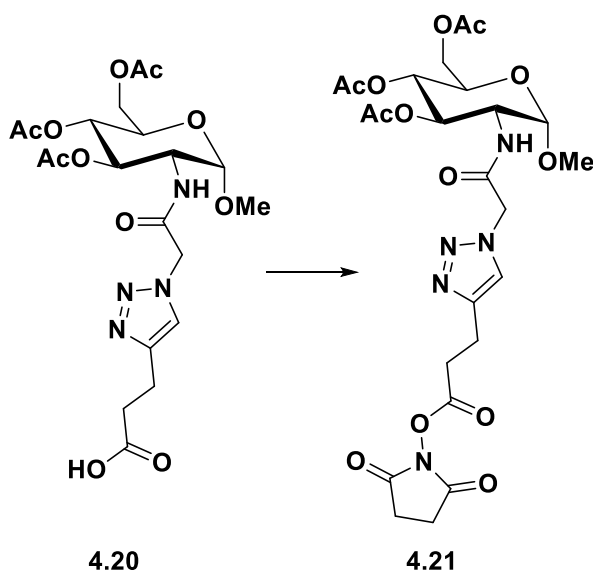
**$^1\text{H NMR}$**  (500 MHz,  $\text{CDCl}_3$ )  $\delta$  7.55 (s, 1H, triaz-CH), 6.72 (d,  $J = 9.0$  Hz, 1H, NHCO), 5.16 (t,  $J = 9.9$  Hz, 1H, H-3), 5.06 (t,  $J = 9.8$  Hz, 1H, H-4), 4.96 (q,  $J = 16.3$  Hz, 2H,  $\text{NHCOCH}_2$ ), 4.71 (d,  $J = 3.5$  Hz, 1H, H-1), 4.30 (td,  $J = 10.1, 3.6$  Hz, 1H, H-2), 4.24 (dd,  $J = 12.4, 4.7$  Hz, 1H, H-6), 4.07 (dd,  $J = 12.3, 2.2$  Hz, 1H, H-6'), 3.92 (ddd,  $J = 10.0, 4.5, 2.3$  Hz, 1H, H-5), 3.37 (s, 3H,  $\text{OCH}_3$ ), 3.01 (br s, 2H, triaz- $\text{CH}_2$ ), 2.73 (br s, 2H,  $\text{CH}_2\text{CO}$ ), 2.07 (s, 3H,  $\text{CH}_3$  of OAc), 2.00 (s, 3H,  $\text{CH}_3$  of OAc), 1.93 (s, 3H,  $\text{CH}_3$  of OAc) ppm.

**$^{13}\text{C NMR}$**  (125 MHz,  $\text{CDCl}_3$ )  $\delta$  176.2 (COOH), 171.5 (CO of OAc), 170.9 (CO of OAc), 169.5 (CO of OAc), 165.9 ( $\text{NHCOCH}_2$ ), 146.8 (triaz-C), 123.4 (triaz-CH), 98.0 (C-1), 71.3 (C-3), 68.2 (C-4), 67.7 (C-5), 62.1 (C-6), 55.7 ( $\text{OCH}_3$ ), 52.6 (C-2), 52.2 ( $\text{NHCOCH}_2$ ), 33.4 ( $\text{CH}_2\text{CO}$ ), 20.8 (2x  $\text{CH}_3$  of OAc), 20.72 (triaz- $\text{CH}_2$ ), 20.67 ( $\text{CH}_3$  of OAc) ppm.

**IR (ATR)** 2952.36, 1738.18, 1548.62, 1366.16, 1220.66, 1031.59, 732.92, 553.38  $\text{cm}^{-1}$ .

**HR-MS (+):**  $m/z$  calcd for  $\text{C}_{20}\text{H}_{28}\text{N}_4\text{O}_{11} + \text{H}^+$   $[\text{M}+\text{H}]^+$  501.1833, found 501.1783. **HR-MS (+):**  $m/z$  calcd for  $\text{C}_{20}\text{H}_{28}\text{N}_4\text{O}_{11} + \text{Na}^+$   $[\text{M}+\text{Na}]^+$  523.1652, found 523.1594.

**Methyl-*N*-(2-deoxy-3,4,6-tri-*O*-acetyl- $\alpha$ -D-glucopyranosyl)-2-acetamido-1,2,3-triazol-4-yl-(3-oxopropyl-(oxy(2,5-dioxopyrrolidin-1-yl))) (4.21)**



**4.20** (0.179 g, 0.357 mmol) was added to a flask with NHS (0.049 g, 0.429 mmol, 1.2 equiv.), purged with N<sub>2</sub> and dissolved in dry DCM. EDCI (0.082 g, 0.429 mmol, 1.2 equiv.) was dissolved in DCM and added *via* cannula. The reaction was stirred overnight at room temperature. The DCM was washed with 0.1M HCl, brine and dried with Na<sub>2</sub>SO<sub>4</sub>. The solvent was filtered and evaporated to yield a white solid which was used without further purification (0.176 g, 0.294 mmol, 82%).

R<sub>f</sub> = 0.64 (95:5 DCM:MeOH).

<sup>1</sup>H NMR (500 MHz, CDCl<sub>3</sub>) δ 7.59 (s, 1H, triaz-CH), 6.14 (d, *J* = 9.2 Hz, 1H, NHCO), 5.10 (dt, *J* = 26.2, 9.5 Hz, 2H, H-3, H-4), 4.98 (q, *J* = 16.4 Hz, 2H, NHCOCH<sub>2</sub>), 4.71 (d, *J* = 3.7 Hz, 1H, H-1), 4.29 (ddd, *J* = 10.3, 9.3, 3.7 Hz, 1H, H-2), 4.24 (dd, *J* = 12.4, 4.7 Hz, 1H, H-6), 4.08 (dd, *J* = 12.4, 2.4 Hz, 1H, H-6'), 3.90 (ddd, *J* = 9.8, 4.6, 2.3 Hz, 1H, H-5), 3.37 (s, 3H, OCH<sub>3</sub>), 3.21 (t, *J* = 7.1 Hz, 2H, triaz-CH<sub>2</sub>), 3.05 (dd, *J* = 10.6, 4.1 Hz, 2H, CH<sub>2</sub>CO), 2.84 (s, 4H, CH<sub>2</sub>CH<sub>2</sub>-succ), 2.09 (s, 3H, CH<sub>3</sub> of OAc), 2.01 (s, 3H, CH<sub>3</sub> of OAc), 1.98 (s, 3H, CH<sub>3</sub> of OAc) ppm.

<sup>13</sup>C NMR (125 MHz, CDCl<sub>3</sub>) δ 171.3 (CO of OAc), 170.8 (CO of OAc), 169.5 (CO of OAc), 169.2 (CO succ x2), 168.1 (CO), 165.4 (NHCOCH<sub>2</sub>), 145.7 (triaz-C), 123.4 (triaz-CH), 98.0 (C-1), 71.3 (C-3), 68.1 (C-4), 67.7 (C-5), 62.1 (C-6), 55.7 (OCH<sub>3</sub>), 52.9 (NHCOCH<sub>2</sub>),

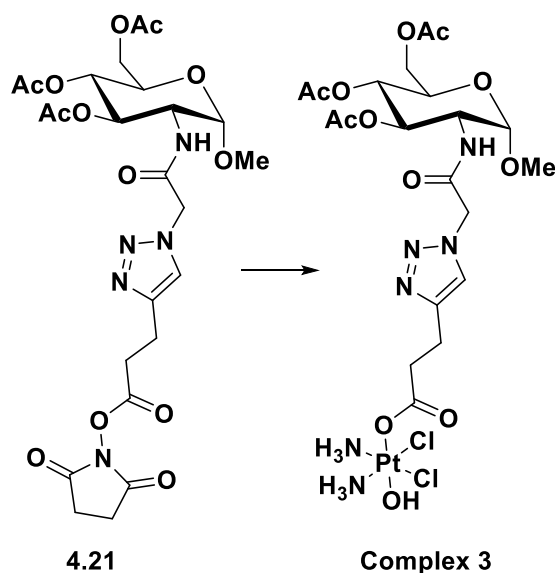
52.4 (C-2), 30.9 (CH<sub>2</sub>CO), 25.7 (CH<sub>2</sub>CH<sub>2</sub>-succ), 21.1 (triaz-CH<sub>2</sub>), 20.9 (CH<sub>3</sub> of OAc), 20.8 (CH<sub>3</sub> of OAc), 20.7 (CH<sub>3</sub> of OAc) ppm.

**IR (ATR)** 2960.39, 1731.85, 1542.01, 1366.05, 1208.29, 1031.45, 806.41, 647.24 cm<sup>-1</sup>.

**HR-MS (+):** m/z calcd for C<sub>24</sub>H<sub>31</sub>N<sub>5</sub>O<sub>13</sub> + H<sup>+</sup> [M+H]<sup>+</sup> 598.1997, found 598.2036. **HR-MS**

**(+):** m/z calcd for C<sub>24</sub>H<sub>31</sub>N<sub>5</sub>O<sub>13</sub> + Na<sup>+</sup> [M+Na]<sup>+</sup> 620.1816, found 620.1860.

***Cis,cis,trans*-[Pt<sup>IV</sup>(NH<sub>3</sub>)<sub>2</sub>(4.20)(OH)Cl<sub>2</sub>] (3)**



**4.21** (0.176 g, 0.294 mmol) was added to a suspension of oxoplatin (0.103 g, 0.309 mmol, 1.05 equiv.) in DMSO (10 mL) and stirred overnight at 60°C in the dark. The excess oxoplatin was filtered through cotton and the DMSO was lyophilised. The residue was redissolved in acetone and the product was precipitated with diethyl ether and dried with the schlenk line to yield a light yellow solid (0.197 g, 82%).

**<sup>1</sup>H NMR** (500 MHz, DMSO) δ 8.52 (d, *J* = 9.2 Hz, 1H, NHCO), 7.80 (s, 1H, triaz-CH), 5.97 (br t, *J* = 49.9 Hz, 6H), 5.15 (dd, *J* = 10.9, 9.4 Hz, 1H, H-3), 5.07 – 4.98 (m, 2H, NHCOCH<sub>2</sub>), 4.90 (t, *J* = 9.8 Hz, 1H, H-4), 4.75 (d, *J* = 3.4 Hz, 1H, H-1), 4.17 (dd, *J* = 12.4, 4.9 Hz, 1H, H-6), 4.14 – 4.09 (m, 1H, H-2), 4.04 (dd, *J* = 12.3, 2.3 Hz, 1H, H-6'), 3.93 (ddd, *J* = 10.1, 4.8, 2.4 Hz, 1H, H-5), 3.37 (s, 3H, OCH<sub>3</sub>), 2.81 (t, *J* = 7.5 Hz, 2H, triaz-



$CH_2$ ), 2.46 (t,  $J = 7.6$  Hz, 2H,  $CH_2CO$ ), 2.02 (s, 3H,  $CH_3$  of OAc), 1.97 (s, 3H,  $CH_3$  of OAc), 1.89 (s, 3H,  $CH_3$  of OAc) ppm.

$^{13}C$  NMR (125 MHz, DMSO)  $\delta$  179.9 (COO $^{Pt}$ ), 170.2 (CO of OAc), 169.9 (CO of OAc), 169.3 (CO of OAc), 166.2 (NHCO $CH_2$ ), 146.1 (triaz-C), 123.8 (triaz-CH), 97.6 (C-1), 70.4 (C-3), 68.6 (C-4), 67.0 (C-5), 61.9 (C-6), 55.0 (OCH $_3$ ), 51.3 (NHCO $CH_2$ ), 51.1 (C-2), 36.1 ( $CH_2CO$ ), 21.9 (triaz- $CH_2$ ), 20.6 ( $CH_3$  of OAc), 20.4 (2x  $CH_3$  of OAc) ppm.

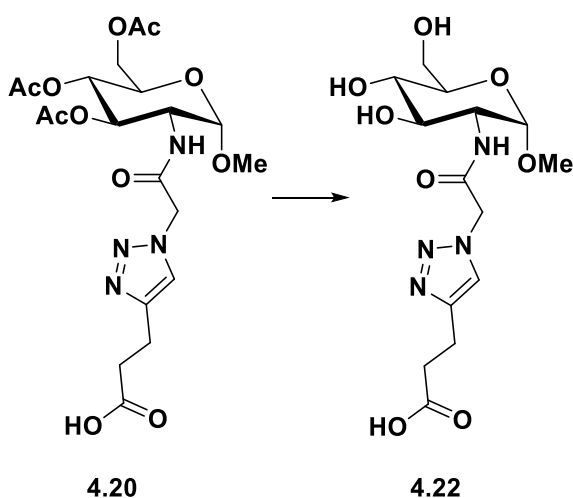
$^{195}Pt\{^1H\}$  NMR (108 MHz, DMSO)  $\delta$  1046.19 ppm.

IR (ATR) 3231.16, 1743.14, 1675.08, 1558.18, 1366.47, 1226.87, 1034.87  $cm^{-1}$ .

HR-MS (+):  $m/z$  calcd for  $C_{20}H_{34}Cl_2N_6O_{12}Pt + H^+$  [M+H] $^+$  817.5140, found 817.1320.

HR-MS (+):  $m/z$  calcd for  $C_{20}H_{34}Cl_2N_6O_{12}Pt + Na^+$  [M+Na] $^+$  839.4958, found 839.1130.

#### Methyl-*N*-(2-deoxy- $\alpha$ -D-glucopyranosyl-1,2,3-triazol-4-yl)-2-acetamido-propanoic acid (4.22)



**4.20** (0.297 g, 0.593 mmol) was dissolved in MeOH (6 mL) and H $_2$ O (3 mL). NEt $_3$  (0.1 mL) was added, and the reaction was stirred at 40°C overnight. The progress was monitored using TLC (90:10 DCM:MeOH). The solvent was dried, and the residue was redissolved in H $_2$ O and stirred with amberlite H $^+$  resin for 1 hour. The amberlite H $^+$  was filtered and the filtrate was dried by lyophilisation. Yielding a fluffy white solid (Yield 0.219 g, 0.585 mmol, 98%).

**<sup>1</sup>H NMR** (500 MHz, D<sub>2</sub>O) δ 7.80 (s, 1H, triaz-CH), 5.24 (s, 2H, NHCOCH<sub>2</sub>), 4.77 (d, *J* = 3.6 Hz, 1H, H-1), 3.96 (dd, *J* = 10.6, 3.6 Hz, 1H, H-2), 3.86 (dd, *J* = 12.3, 2.3 Hz, 1H, H-6), 3.74 (ddd, *J* = 16.1, 11.5, 7.3 Hz, 2H, H-3, H-6'), 3.67 (ddd, *J* = 10.0, 5.4, 2.3 Hz, 1H, H-5), 3.46 (t, *J* = 9.1 Hz, 1H, H-4), 3.38 (s, 3H, OCH<sub>3</sub>), 2.98 (t, *J* = 7.3 Hz, 2H, triaz-CH<sub>2</sub>), 2.66 (t, *J* = 7.3 Hz, 2H, CH<sub>2</sub>CO) ppm.

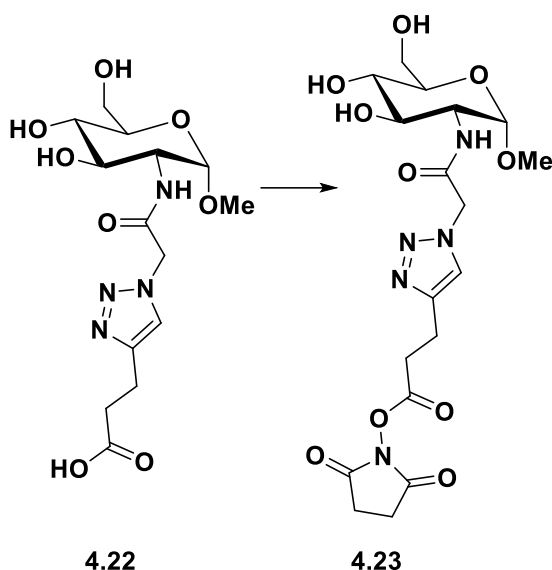
**<sup>13</sup>C NMR** (125 MHz, D<sub>2</sub>O) δ 179.0 (CO), 168.2 (NHCO), 147.2 (triaz-C), 124.5 (triaz-CH), 97.9 (C-1), 71.7 (C-5), 71.1 (C-3), 69.9 (C-4), 60.5 (C-6), 55.2 (OCH<sub>3</sub>), 53.8 (C-2), 51.8 (NHCOCH<sub>2</sub>), 34.5 (CH<sub>2</sub>CO), 20.7 (triaz-CH<sub>2</sub>) ppm.

**IR (ATR)** 3287.05, 1664.63, 1562.97, 1562.97, 1114.43, 1050.55, 1030.28 cm<sup>-1</sup>.

**HR-MS (+):** *m/z* calcd for C<sub>14</sub>H<sub>22</sub>N<sub>4</sub>O<sub>8</sub> + H<sup>+</sup> [M+H]<sup>+</sup> 375.1516, found 375.1510. **HR-MS**

**(+):** *m/z* calcd for C<sub>14</sub>H<sub>22</sub>N<sub>4</sub>O<sub>8</sub> + Na<sup>+</sup> [M+Na]<sup>+</sup> 397.1335, found 397.1327.

**Methyl-*N*-(2-deoxy- $\alpha$ -D-glucopyranosyl-1,2,3-triazol-4-yl)-2-acetamido-(3-oxopropyl-(oxy(2,5-dioxopyrrolidin-1-yl))) (4.23)**



**4.22** (0.05g, 0.1335 mmol) and TSTU (0.044 g, 0.1469 mmol, 1.1 equiv.) were added to a flask, flushed with  $N_2$  and dissolved in DMF (7 mL).  $NEt_3$  (0.02 mL, 0.1469 mmol, 1.1 equiv.) was added to the solution and the reaction was allowed to stir at room temperature for 20 minutes. Checking reaction progress by TLC (60:35:5 DCM:MeOH:H<sub>2</sub>O). The DMF was evaporated, and the residue was washed with DCM, collecting the precipitating product by centrifugation. The pink/white solid was washed with diethyl ether and dried *in vacuo* (Yield 0.049 g, 0.103 mmol, 79%).

$R_f$  = 0.83 (DCM:MeOH:H<sub>2</sub>O 60:35:5).

**<sup>1</sup>H NMR** (500 MHz, DMSO)  $\delta$  8.33 (d,  $J$  = 8.4 Hz, 1H, NHCO), 7.86 (s, 1H, triaz-CH), 5.13 – 5.05 (m, 2H, NHCOCH<sub>2</sub>), 5.04 (d,  $J$  = 5.7 Hz, 1H, OH of C-4), 4.90 (d,  $J$  = 5.6 Hz, 1H, OH of C-3), 4.56 (d,  $J$  = 3.5 Hz, 1H, H-1), 4.53 (t,  $J$  = 5.9 Hz, 1H, OH of C-6), 3.71 – 3.62 (m, 2H, H-2, H-6), 3.51 – 3.45 (m, 2H, H-6', H-3), 3.37 – 3.34 (m, 1H, overlaps with H<sub>2</sub>O, H-5), 3.27 (s, 3H, OCH<sub>3</sub>), 3.18 – 3.12 (m, 1H, H-4), 3.08 – 3.04 (m, 2H, CH<sub>2</sub>CO), 2.99 (dd,  $J$  = 11.3, 4.2 Hz, 2H, triaz-CH<sub>2</sub>), 2.81 (s, 4H, CH<sub>2</sub>CH<sub>2</sub>-succ) ppm.

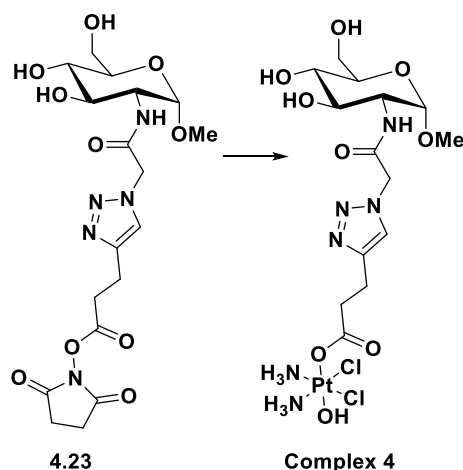
**<sup>13</sup>C NMR** (125 MHz, DMSO)  $\delta$  170.2 (CO succ x2), 168.4 (CO), 165.6 (CONH), 144.1 (triaz-C), 123.9 (triaz-CH), 97.7 (C-1), 72.8 (C-5), 70.8 (C-3), 70.7 (C-4), 60.8 (C-6), 54.3 (OCH<sub>3</sub>), 54.0 (C-2), 51.5 (NHCOCH<sub>2</sub>), 29.8 (CH<sub>2</sub>CO), 25.5 (CH<sub>2</sub>CH<sub>2</sub>-Succ), 20.3 (triaz-CH<sub>2</sub>) ppm.

**IR (ATR)** 3285.14, 1732.92, 1667.17, 1559.92, 1208.18, 1024.06, 646.62  $\text{cm}^{-1}$ .

**HR-MS (+):**  $m/z$  calcd for  $\text{C}_{18}\text{H}_{25}\text{N}_5\text{O}_{10} + \text{H}^+$   $[\text{M}+\text{H}]^+$  472.1680, found 472.1696. **HR-MS**

**(+):**  $m/z$  calcd for  $\text{C}_{18}\text{H}_{25}\text{N}_5\text{O}_{10} + \text{Na}^+$   $[\text{M}+\text{Na}]^+$  494.1499, found 494.1534.

***Cis,cis,trans*-[Pt<sup>IV</sup>(NH<sub>3</sub>)<sub>2</sub>(4.22)(OH)Cl<sub>2</sub>] (4)**



**4.23** (0.075 g, 0.159 mmol) dissolved in dry DMSO (5 mL) was added dropwise, over 24 hr, to a suspension of oxoplatin (0.106 g, 0.318 mmol, 2 equiv.) in dry DMSO (7 mL) at 40°C. The reaction flask was heated at 40°C for a further 5 days before filtration of excess oxoplatin and removal of solvent via lyophilisation. The resulting oil was rinsed with the minimum amount of MeOH, washed with diethyl ether and dried in vacuo to yield the product as a white-yellow powder (0.043g, 0.062 mmol, 39%)

**<sup>1</sup>H NMR** (500 MHz, DMSO)  $\delta$  8.34 (d,  $J = 8.5$  Hz, 1H, NHCO), 7.82 (s, 1H, triaz-CH), 5.97 (t, 6H, 2x NH<sub>3</sub>), 5.11 – 5.00 (m, 3H, NHCOCH<sub>2</sub>, OH of C-4), 4.94 (d,  $J = 5.2$  Hz, 1H, OH of C-3), 4.63 – 4.49 (m, 2H, H-1, OH of C-6), 3.72 – 3.62 (m, 2H, H-2, H-6), 3.51 – 3.32 (m, 3H, H-6', H-3, H-5), 3.27 (s, 3H, OCH<sub>3</sub>), 3.16 – 3.11 (m, 1H, H-4), 2.82 (t,  $J = 7.5$  Hz, 2H, triaz-CH<sub>2</sub>), 2.47 (t,  $J = 7.6$  Hz, 2H, CH<sub>2</sub>CO) ppm.

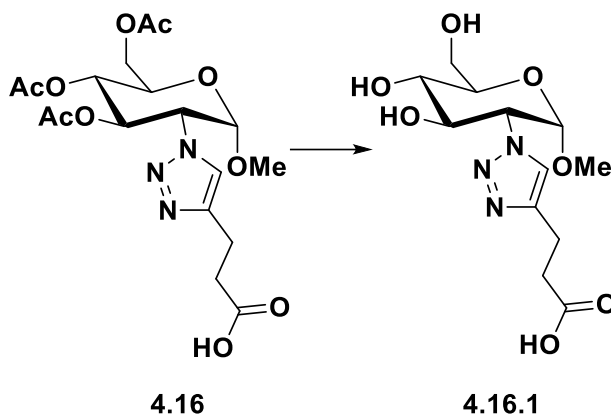
**<sup>13</sup>C NMR** (125 MHz, DMSO)  $\delta$  180.0 (COOPt), 165.8 (CONH), 146.1 (triaz-C), 123.8 (triaz-CH), 97.8 (C-1), 72.8 (C-5), 70.9 (C-3), 70.7 (C-4), 60.8 (C-6), 54.4 (OCH<sub>3</sub>), 54.1 (C-2), 51.5 (NHCOCH<sub>2</sub>), 36.2 (CH<sub>2</sub>CO), 22.0 (triaz-CH<sub>2</sub>) ppm.

$^{195}\text{Pt}\{^1\text{H}\}$  NMR (108 MHz, DMSO)  $\delta$  1044.47 ppm.

IR (ATR) 3256.68, 1676.10, 1559.39, 1021.64, 992.54  $\text{cm}^{-1}$ .

HR-MS (+):  $m/z$  calcd for  $\text{C}_{14}\text{H}_{28}\text{Cl}_2\text{N}_6\text{O}_9\text{Pt} + \text{H}^+$   $[\text{M}+\text{H}]^+$  690.1021, found 690.1102.

**Methyl-*N*-(2-deoxy- $\alpha$ -D-glucopyranosyl-1,2,3-triazol-4-yl)-propanoic acid (4.16.1)**



**4.16** (1.113 g, 2.510 mmol) was dissolved in MeOH (10 mL) and  $\text{H}_2\text{O}$  (5 mL).  $\text{NEt}_3$  (0.5 mL) was added, and the reaction was stirred at  $45^\circ\text{C}$  overnight. The progress was monitored using TLC (90:10 DCM:MeOH). The solvent was dried, and the residue was redissolved in  $\text{H}_2\text{O}$  and stirred with amberlite  $\text{H}^+$  resin for 1 hour. The amberlite  $\text{H}^+$  was filtered and the filtrate was dried by lyophilisation. Yielding a fluffy white solid (Yield 0.756 g, 2.38 mmol, 96%).

$^1\text{H}$  NMR (500 MHz, DMSO)  $\delta$  7.75 (s, 1H, triaz-CH), 4.81 (d,  $J = 3.5$  Hz, 1H, H-1), 4.47 (dd,  $J = 11.0, 3.5$  Hz, 1H, H-2), 3.99 (dd,  $J = 11.0, 8.5$  Hz, 1H, H-3), 3.70 (dd,  $J = 11.7, 1.9$  Hz, 1H, H-6), 3.54 (dd,  $J = 11.7, 5.7$  Hz, 1H, H-6'), 3.47 (ddd,  $J = 9.8, 5.6, 1.8$  Hz, 1H, H-5), 3.31 (dd,  $J = 9.8, 8.6$  Hz, 1H, H-4), 3.19 (s, 3H,  $\text{OCH}_3$ ), 2.83 (t,  $J = 7.6$  Hz, 2H, triaz- $\text{CH}_2$ ), 2.53 – 2.51 (m, 2H,  $\text{CH}_2\text{CO}$ ) ppm.

$^{13}\text{C}$  NMR (125 MHz, DMSO)  $\delta$  174.2 (COOH), 145.5 (triaz-C), 121.1 (triaz-CH), 97.8 (C-1), 73.1 (C-5), 70.7 (C-4), 70.1 (C-3), 64.2 (C-2), 60.6 (C-6), 54.4 ( $\text{OCH}_3$ ), 34.0 ( $\text{CH}_2\text{CO}$ ), 21.1 (triaz- $\text{CH}_2$ ) ppm.

IR (ATR) 3288.16, 2918.18, 1567.64, 1399.90, 1031.58, 848.57  $\text{cm}^{-1}$ .

**HR-MS (+):**  $m/z$  calcd for  $C_{12}H_{19}N_3O_7 + H^+$   $[M+H]^+$  318.1301, found 318.1317. **HR-MS**

**(+):**  $m/z$  calcd for  $C_{12}H_{19}N_3O_7 + Na^+$   $[M+Na]^+$  340.1121, found 340.1139.

# **Chapter 5: Multivalent Platinum(IV) Glycoconjugates**

## 5.1 Introduction

### 5.1.1 Hepatocellular carcinoma (HCC)

Primary liver cancer is the sixth most common form of cancer worldwide, with approximately 830,000 deaths in 2020. Hepatocellular carcinoma encompasses 75 – 85% of all primary liver cancer cases and is most common in East and Southeast Asia, North and West Africa [297]. Treatment options for this disease are determined using the Barcelona Clinic of Liver Cancer (BCLC) algorithm which divides patients with HCC into five clinical stages: very early stage (BCLC 0), early stage (BCLC A), intermediate stage (BCLC B), advanced stage (BCLC C) and terminal stage (BCLC D) [298]. Treatment for stages 0 and A typically include liver transplantation or radiofrequency ablation (RFA) to destroy the tumours and results in a five-year survival rate of 70 – 80%. Stage B is usually treated with a combination therapy composed of cisplatin, doxorubicin and epirubicin (**Figure 5.1**), accompanied by the embolisation of blood vessels which provide nutrients to the tumour. This therapeutic option is abbreviated to TACE or Trans Arterial Chemo-Embolisation. The treatment of stage C HCC is limited to the use of multi-kinase inhibitor such as sorafenib (**Figure 5.1**), while stage D patients can only rely on palliative care [299]. The survival rate for patients in stage B is only an average of 20 months and drops to 11 months for patients in stage C, whereas the treatment options for patients in stage D are practically non-existent, which highlights the need for further development and progress in producing drugs to treat this disease [300].

Much research has been carried out to identify specific therapeutic targets and to develop drugs selective for HCC. Tyrosine kinase inhibitors (TKIs) have played a pivotal role in the treatment of HCC. Sorafenib, as mentioned above, is a major therapeutic option which targets rapidly accelerated fibrosarcoma (RAF) kinase, epidermal growth factor receptor (EGFR), vascular endothelial growth factor receptor (VEGFR), platelet-derived growth factor receptor (PDGFR), FMS-like tyrosine kinase-3 and c-kit, which are all found to be overexpressed in HCC [299,301]. Due to the success of this TKI drug, a large body of research focused on the development and uses of different TKIs to treat HCC. In particular, the inclusion of apatinib (**Figure 5.1**) in TACE treatment has yielded better results than TACE alone



and a combination therapy of bevacizumab and erlotinib has also been extensively evaluated and has shown promising results [302].

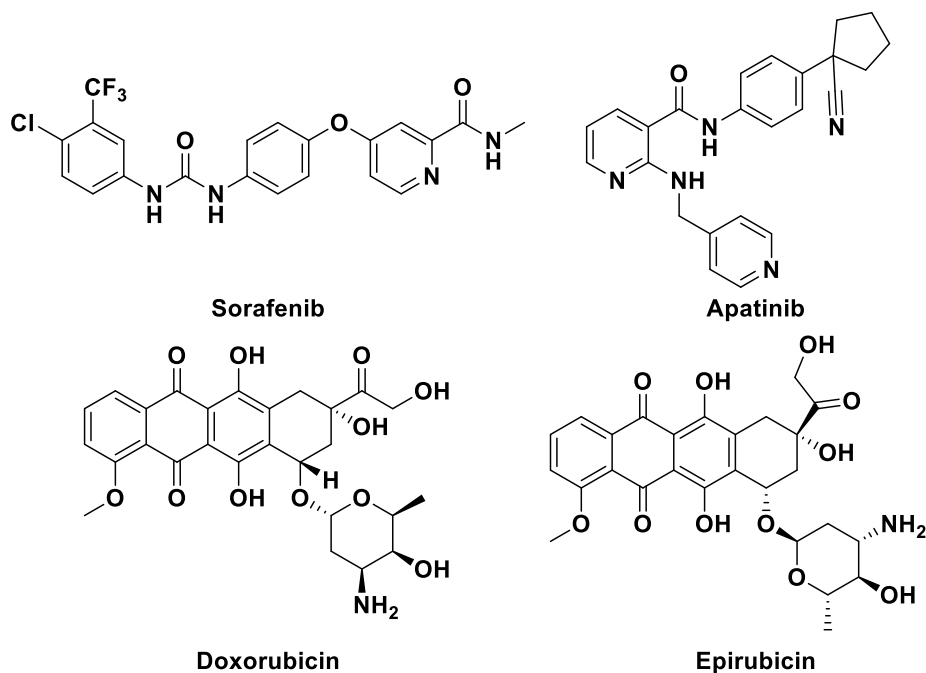


**Figure 5.1:** Structures of tyrosine kinase inhibitors (TKI) and anthracycline drugs for the treatment of HCC.

More recently, targeted delivery to HCC has been accomplished using carbohydrate ligands which target a major receptor found predominantly on hepatocytes and overexpressed in HCC cells, the asialoglycoprotein receptor (ASGPR) [303]. Some examples of carbohydrate-drug conjugates targeting HCC will be discussed in **Section 5.1.3.**

### 5.1.2 Asialoglycoprotein receptor (ASGPR)

In the previous three chapters we have discussed some methods used to target cancer cells through conjugation of bioactive ligands to the anticancer platinum drug core, cisplatin. The target of the ligands discussed so far were GLUTs, which are overexpressed on cancer cell membranes due to the Warburg effect [5]. The objective of this chapter is to target a different cellular protein, named asialoglycoprotein receptor (ASGPR), also known as the ‘Ashwell-Morell receptor’, a C-type lectin which is primarily found on hepatocytes and HCC cells but is minimally present on non-hepatic cells. This lectin is a hetero-oligomer which is composed of

two homologous transmembrane proteins, ASGPR1 (major) and ASGPR2 (minor) [304]. It plays a crucial role in serum glycoprotein homeostasis by mediating the endocytosis and lysosomal degradation of desialylated glycoproteins, which contain terminal galactose or *N*-acetylgalactosamine residues [305].

ASGPR selectively binds to galactose and *N*-acetylgalactosamine, with a weaker binding affinity for glucose [303]. Interestingly, the lectins affinity for galactose is increased when using multivalent ligands, with a 100- to 1000-fold increase when compared to monovalent ligands [306] and this enhanced affinity is due to the multivalent effect (discussed in **Section 5.1.3**). The specificity of ASGPR and its binding affinity is also dependent on the size of the ligand and spatial arrangement/clustering of the glycan chains [307]. Docking studies have shown that ASGPR binds galactose through calcium dependent carbohydrate recognition domains (CRD) and is stabilised through hydrogen bond interactions between various amino acids and the C1, C2 and C3 hydroxyl groups. Hydrophobic interactions between C3, C4, C5 and C6 of galactose to tryptophan 243 in the active site, as well as coordination of the C2 and C3 hydroxyl groups to the calcium ion can also be seen [308]. The docking diagram of this binding can be seen in **Figure 5.2** below.

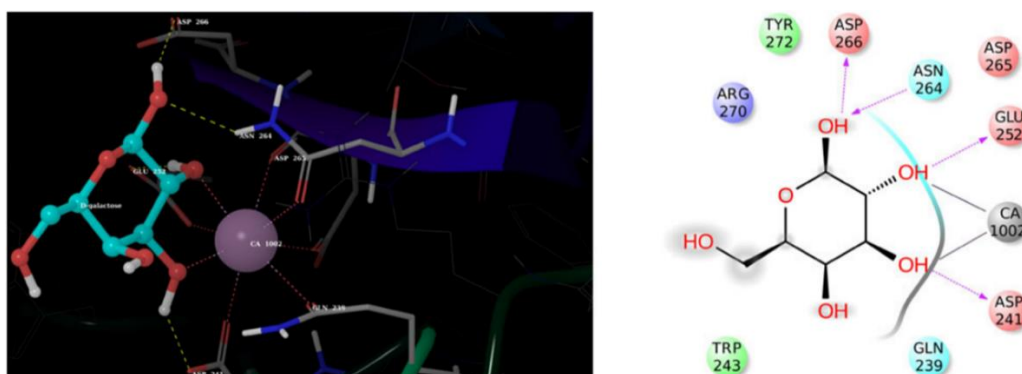


**Figure 5.2:** Glide docking diagram of galactose at the active site of ASGPR and its ligand interaction [308].

Once a ligand is bound in the CRD, it is internalised by clathrin-mediated endocytosis and the ligands are released to allow the receptor to cycle back to the cell membrane. Rapid recycling of the receptor is important for maintaining receptor concentration on the liver cell surfaces, which contain 100,000 – 500,000 binding sites per cell [309]. This high affinity binding is an extremely attractive route for targeted therapeutic

methods and has recently garnered much attention. In addition, the mammalian ASGPR is a hetero-oligomer composed of two subunits: H1 and one H2 subunit, with a geometrical disposition for the carbohydrate-binding sites as shown in **Figure 5.3**. For this reason, the use of multivalent ligands to target the ASGPR is a viable strategy due to the multivalent effect [310].

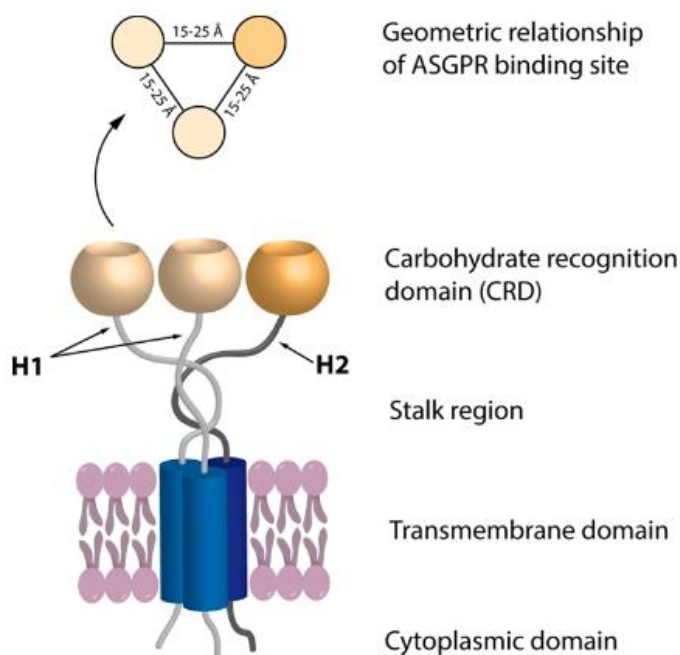


**Figure 5.3:** Schematic representation of ASGPR, showing the hetero-oligomer which is composed of two H1 and one H2 subunits. Adapted from [310].

### 5.1.3 Multivalent effect for the targeting of ASGPR

The multivalent effect is frequently observed in nature where univalent protein-ligand binding is weak, for example in the recognition of carbohydrate ligands by bacterial and mammalian lectins [311,312]. While the reasons for this enhanced binding affinity are not fully understood, there are three main mechanisms involved in this process:

(1) Intramolecular binding: the chelate effect [313], which is seen in many inorganic systems, where a bivalent ligand binding to a bivalent receptor has a greater affinity than its monovalent counterpart.

(2) Intermolecular binding: aggregation and precipitation [314] which occurs when ligands bind receptors causing them to precipitate from solution. These aggregates

are stabilised by different intermolecular forces, resulting in the formation of kinetically stable aggregates which can only occur through multivalent binding.

(3) Steric stabilisation: the binding of a large ligand near the surface of the receptor would prevent the approach of other macromolecules, thus stabilising the interaction [315].

Given the geometric relationship of the ASGPR depicted in **Figure 5.3**, drugs containing multivalent galactose and galactosamine units have been developed to target ASGPR. **Figure 5.4** shows two examples of anticancer drugs to target HCC using ASGPR. Compound **5.1** is a prodrug containing a derivative of  $\beta$ -elemene which acts as the anticancer agent through methods which have still not been fully elucidated [316]. This drug is functionalised with a trivalent display of galactose to target ASGPR and it is linked to the active therapeutic agent using a glutathione responsive disulfide bridge, which gives this compound its prodrug effect. It was also observed that mono- and divalent derivatives of this compound displayed reduced hepatocyte-targeting ability [317]. Compound **5.2** uses galactosamine to target hepatocytes through interaction with ASGPR; this drug is used to chelate copper(I) in patients with Wilson's disease and like **5.1**, the sugar is bound through disulfide bridges to act as a prodrug and release the copper chelator when inside hepatocytes [318].

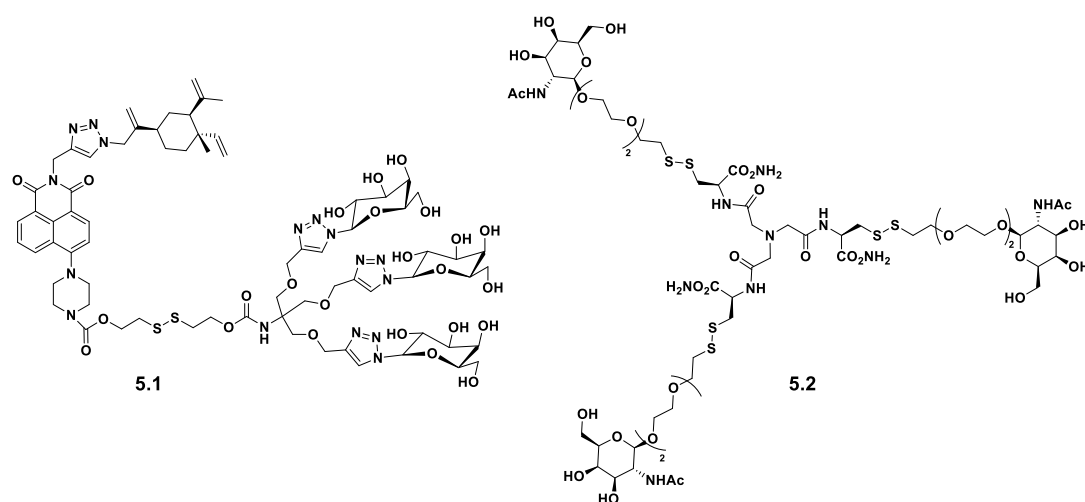
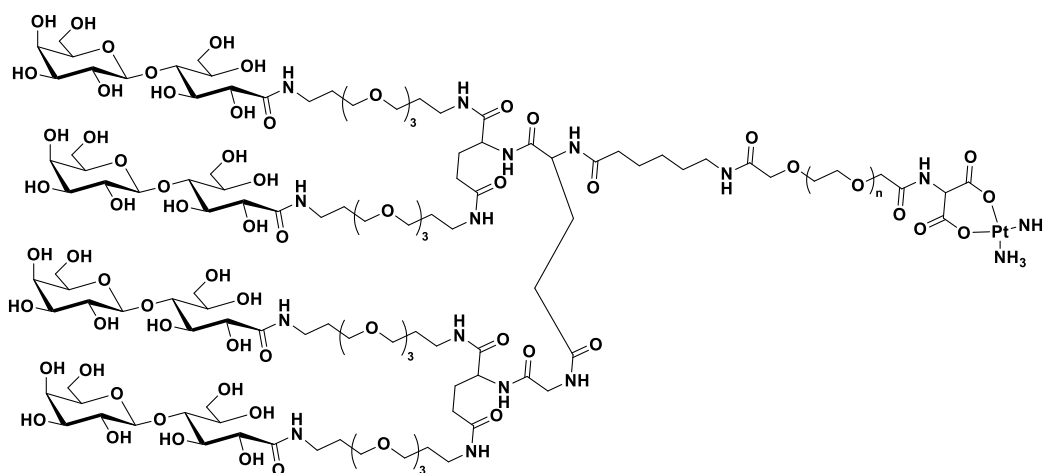


**Figure 5.4:** Structure of HCC selective drugs containing galactose (**5.1**) [317] and galactosamine (**5.2**) [318].

While the benefit of multivalency has been shown with a variety of glycoconjugates for diverse applications (such as anti-infection [319] or immunostimulant agents [320]), only few examples of metal multi-glycoconjugates (and even less platinum glycoconjugates [321,322]) have been designed. The one example to be found in the literature is a multivalent galactosylated-Pt(II) derivative which has four galactose presentations to target ASGPR (**Figure 5.5**). This group concluded that the presence of multiple galactose subunits improves the complexes *in vitro* cytotoxicity more than a complex with only one subunit [322].



5.3

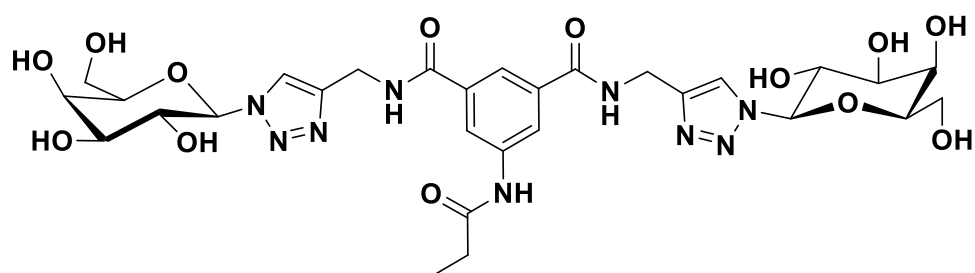
**Figure 5.5:** Structure of multivalent Pt(II) glycoconjugate for the treatment of HCC [322].

To date, there have been no multivalent Pt(IV) pro-drugs developed. The only attempts at multivalent carbohydrate complexes reported involve the bis-functionalisation of Pt(IV) complexes (as discussed in previous chapters), which was shown to be less efficient than their mono-functionalised derivatives, due to the difference in reduction potentials (**1.32 – 1.46**, **2.1 – 2.13**) [167,170,227]. Importantly, these complexes were not developed to target HCC, but to improve anticancer activity against cancers overexpressing GLUT. The following chapter discusses our attempt to synthesise the first multivalent Pt(IV) glycoconjugate.

## 5.2 Chapter objective

This chapter discusses the attempts to synthesise the first multivalent Pt(IV) pro-drug to target hepatocellular carcinoma using the ASGPR abundantly expressed in these

cells. The ligand we have focused is a derivative of compound **5.4** (**Figure 5.6**) which was previously shown to be a potent inhibitor of adherence of fungal pathogen *Candida albicans* to buccal epithelial cells [323]. Molecular modelling performed on **5.4** revealed that the distances between the anomeric carbon centres are typically in the range 6–15 Å. According to the estimated distances between the carbohydrate binding sites in the ASGPR hetero-oligomer (between 15 and 25 Å, **Figure 5.3**), it is plausible that **5.4** could recognise and bind two of the three galactose binding sites with high affinity given its divalent presentation of the galactose units [324].



5.4

**Figure 5.6:** Structure of *N,N'*-di-(β-D-galactopyranosyl-1,2,3-triazol-4-ylmethylamide)-*N''*-propyl-5-aminobenzene-1,3-dicarboxamide (**5.4**), divalent glycoconjugate previously reported as an inhibitor of the adherence of fungal pathogens to buccal epithelial cells [323].

The structure of **5.4** was modified by the introduction of a linker with a carboxylic acid to facilitate the binding to oxoplatin as shown below (**Figure 5.7**). The attempts to synthesise these complexes through different routes will be discussed in this chapter and we will offer some suggestions for future approaches towards the synthesis of these target compounds.

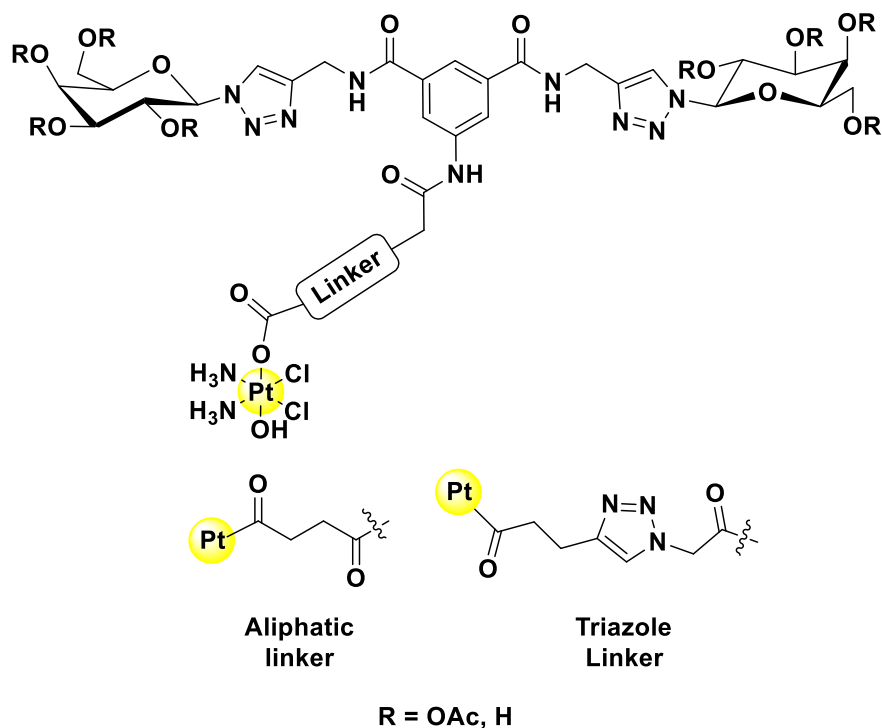
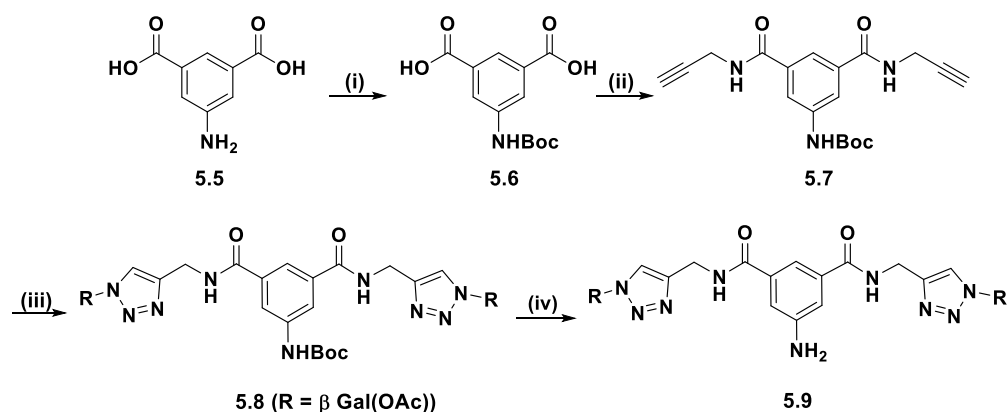


**Figure 5.7:** General structure of multivalent glycoconjugate Pt(IV) complexes based on the cisplatin scaffold, functionalised with galactose.

## 5.3 Results and Discussion

### 5.3.1 Synthesis of free amine scaffold (5.9)

The synthesis of the complexes shown in **Figure 5.7** required the introduction of a linker containing a carboxylic acid into the original structure of **5.4**. Initially, we needed to synthesise the compound **5.9**, the free amine precursor of **5.4**. The synthesis of this compound was originally developed in our group by Martin *et al.* [325]. Briefly, the amine of 5-aminoisophthalic acid was *N*-Boc protected and propargylamine was coupled to the carboxylic acid moieties using TBTU. Reaction of galactose azide (**2.17**) with **5.7** using CuAAC “click” conditions in a microwave reactor yielded **5.8** in very good yield. The *N*-Boc protecting group was removed with TFA and yielding the free amine (**5.9**).



**Scheme 5.1:** Synthetic route for **5.9**: (i) Di-*tert*-butyl dicarbonate, NaOH, 1,4-dioxane, 0°C to rt, 3 h, 80%; (ii) TBTU, NEt<sub>3</sub>, propargylamine, DMF, rt, 16 h, 76%; (iii) **2.17**, CuSO<sub>4</sub>·5H<sub>2</sub>O, NaAsc, acetonitrile, H<sub>2</sub>O, MW at 100°C, 30 mins, 65%; (v) TFA, DCM, 2 h, rt, 97%.

### 5.3.2 Cyclic derivatives through initial route to form multivalent Pt(IV) glycoconjugates

Initially, we planned to synthesise complexes **1** and **2** (Figure 5.8) through the introduction of an aliphatic linker. Our goal was to functionalise the resulting carboxylic acid with a succinimide ester and subsequently react this with oxoplatin to yield the complexes shown below. One complex where the galactose moieties are protected with acetyl groups and the other with free galactose. Unfortunately, upon esterification a ring closure reaction occurs forming the cyclic derivatives seen in Schemes 5.2 and 5.3.

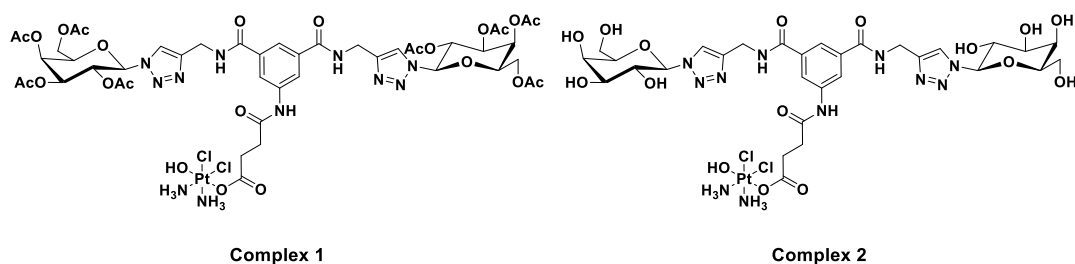
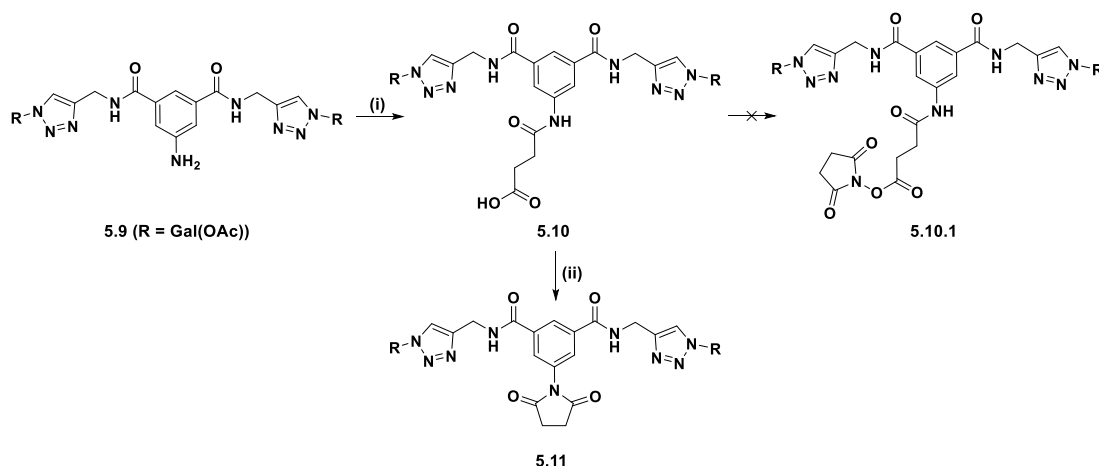


**Figure 5.8:** Proposed structures of multivalent glycoconjugated Pt(IV) complexes with shorter linkers.





**Scheme 5.2:** Proposed synthesis of multivalent Pt(IV) glycoconjugates, **1** and **2**: (i) succinic anhydride, DCM, rt, 16 h, 81%; (ii) EDCI, NHS, DCM, rt, 16 h, 81%.

In this approach, the free amine (**5.9**) was reacted at room temperature with succinic anhydride forming the carboxylic acid (**5.10**). The typical next step in this synthesis is the formation of the NHS active ester through a coupling reaction. In the case of the acetylated compounds, coupling of NHS to the carboxylic acids was performed using EDCI as a coupling reagent. However, it was found that during the reaction, intramolecular cyclisation takes place and yields the succinimide (**5.11**) instead. Using Baldwin's rules of ring closure [326], we determined this reaction could be classified as 5-exo-trig (**Figure 5.9**), which favours cyclisation.

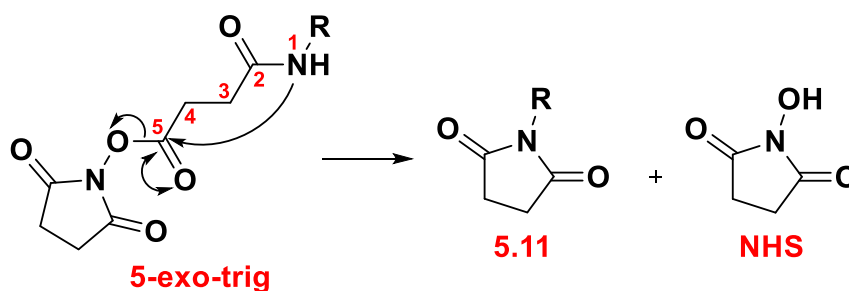


**Figure 5.9:** Mechanism of ring closure classified as 5-exo-trig using Baldwin's rules of ring closure.

A comparative  $^1\text{H}$  NMR spectra of **5.10** and **5.11** is shown in **Figure 5.10**, where the characteristic signals are highlighted. We expected to see a singlet corresponding to the NHS ester which integrates for four protons as well as a downfield shift in the methylene signals. However, the two methylene protons (red) appear as equivalent

protons in the spectra for **5.11** due to the symmetry of the molecule. In addition, **5.10** contains an amide proton (green) which is not present in **5.11**, indicating that a reaction took place at this nitrogen atom.

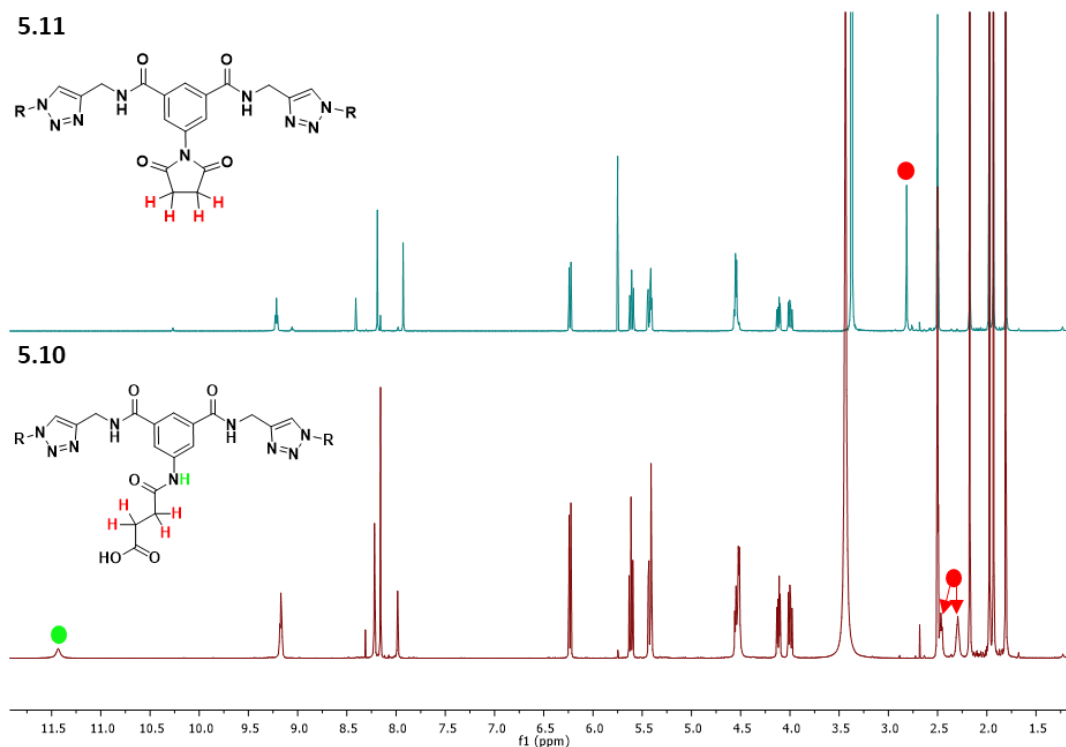
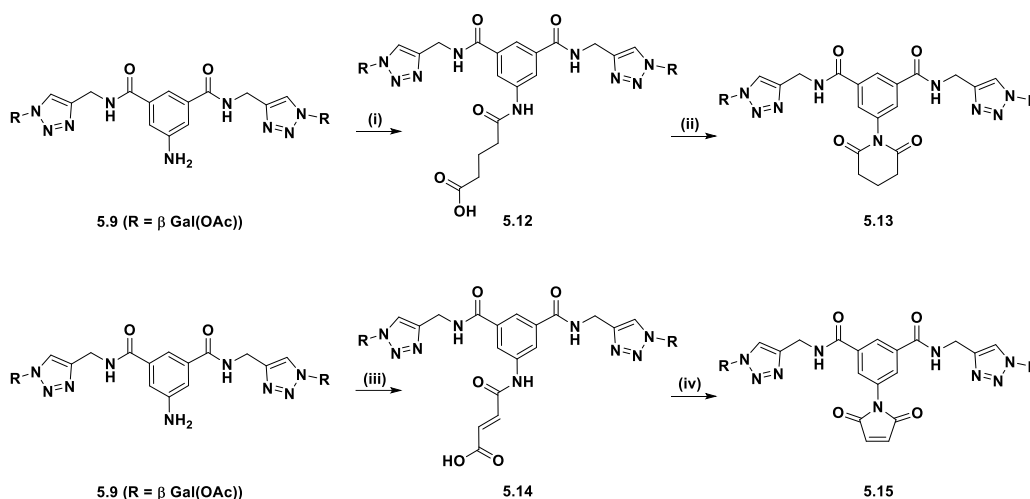


**Figure 5.10:** Stacked <sup>1</sup>H NMR spectrum of **5.10** and **5.11**, comparing the linker in its open and cyclised forms.

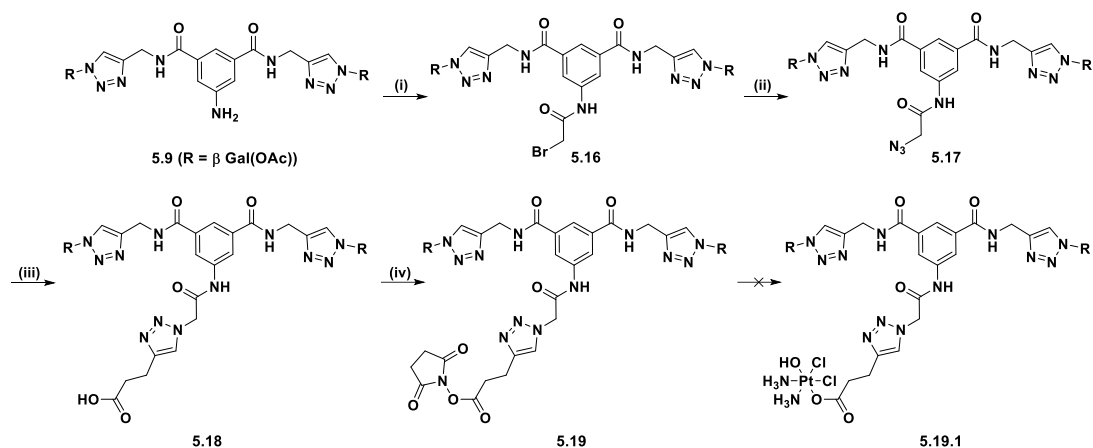
We also attempted this reaction using glutaric anhydride (a six membered cyclic anhydride), and maleic anhydride (five membered cyclic anhydride with increased rigidity) and encountered the same issues (**Scheme 5.3**). In the case of the **5.13** and **5.15**, they could not be isolated in high purity without the use of column chromatography. From the result of these reactions, we realised we needed to redesign the linker to avoid this ring closing reaction. To accomplish this, we used an approach which took advantage of CuAAC “click” chemistry.



**Scheme 5.3:** Structures of glutarimide and maleimide derivatives of **5.11**, synthesised using glutaric anhydride and maleic anhydride: (i) glutaric anhydride, DCM, rt, 16 h, 62%; (ii) NHS, EDCI, DCM, rt, 16 h, 43%; (iii) maleic anhydride, DCM, rt, 16 h, 76%; (iv) NHS, EDCI, DCM, rt, 16 h, 57%.

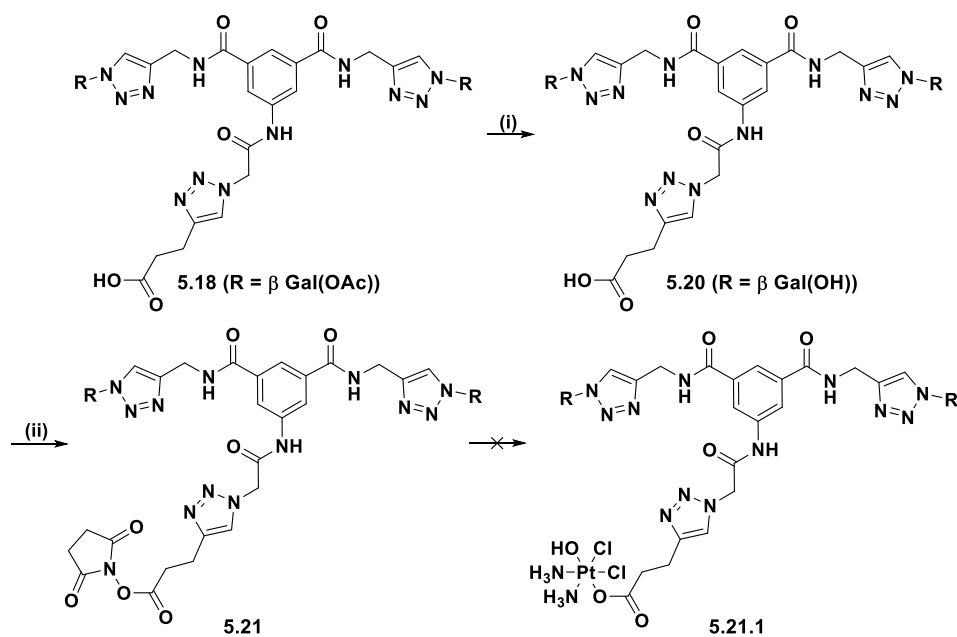
### 5.3.3 Synthesis of multivalent glycoconjugated Pt(IV) pro-drugs using alternative route

Our alternative synthetic route to form complexes **5.19.1** and **5.21.1** (Schemes **5.4** and **5.5**) containing a triazole linker (Click Chemistry) is depicted below. Our first approach involved the preparation of a synthetic intermediate azide (**5.17**). The synthesis of this compound was originally developed in our group by Martin *et al.* [325]. After the formation of the free amine (**5.9**) as discussed in section **5.3.1**, it was reacted with bromoacetyl bromide to give **5.16**. The bromide substituent was then replaced with an azido group using sodium azide, yielding **5.17** which was used without further purification. This azide (**5.17**) was reacted with 4-pentynoic acid to yield the carboxylic acid derivative (**5.18**) and esterified to form the NHS ester (**5.19**) which is discussed in later sections.



**Scheme 5.4:** Attempted synthetic route for Complex **5.19.1**: (i) bromoacetyl bromide,  $\text{NEt}_3$ , DCM, 16 h, 82%; (ii)  $\text{NaN}_3$ , DMF,  $80^\circ\text{C}$ , 16 h, 73%; (iii) 4-pentynoic acid,  $\text{CuSO}_4 \cdot 5\text{H}_2\text{O}$ , NaAsc, acetonitrile, *t*-BuOH,  $\text{H}_2\text{O}$ , rt, 16 h, 45%; (iv) TSTU,  $\text{NEt}_3$ , DMF, rt, 16 h, 81%.

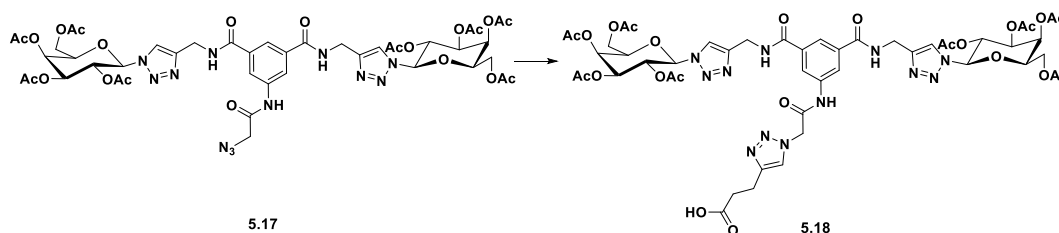
We also wanted to synthesise the free carbohydrate derivative of **5.19.1** to compare their anticancer activity and the protecting groups effects on the cellular uptake and selectivity (**Scheme 5.5**). To this end, we attempted to adapt the previously established procedures, discussed in earlier chapters. To synthesise Complex **5.21.1**, compound **5.20**, the free sugar derivative of **5.18**, was reacted with TSTU to yield **5.21**. We then attempted to coordinate this ligand to oxoplatin, which is discussed in later sections.



**Scheme 5.5:** Attempted synthetic route to Complex **5.21.1**: (i)  $\text{NEt}_3$ , MeOH,  $\text{H}_2\text{O}$ ,  $45^\circ\text{C}$ , 16 h, 99%; (ii) TSTU,  $\text{NEt}_3$ , DMF, rt, 20 mins, 76%.

### 5.3.4 Synthesis of acetylated multivalent ligand using CuAAC “Click” chemistry (5.18)

The acetylated carboxylic acid **5.18** was synthesised using CuAAC “click” chemistry reaction between the azide (**5.17**) and 4-pentynoic acid (**Scheme 5.6**), using a similar method discussed in **Chapter 4**, with a major difference being the solvent system used for the reaction.



**Scheme 5.6:** CuAAC “Click” reaction for the formation of acetylated ligand (**5.18**): 4-pentynoic acid, CuSO<sub>4</sub>·5H<sub>2</sub>O, NaAsc, acetonitrile, *t*-BuOH, H<sub>2</sub>O, rt, 16 h, 45%.

Compound **5.17** was insoluble in the reaction solvent mixture of *t*-BuOH and H<sub>2</sub>O used previously, so acetonitrile was added and the reaction was stirred at room temperature overnight. The product was purified by column chromatography, however, due to the high polarity of the ligand, a highly polar mobile phase (10-20% MeOH in DCM), accompanied by a very small amount of silica gel was used. Despite all these efforts, after the column we only achieved a 45% yield. It is likely the remaining product was left adhered to the silica and we were unable to recover it, even by flushing with 100% MeOH. Alternatively, the use of a flash chromatographic column (PuriFlash) could be employed to improve purification, where higher polarity solvent systems can be used. This ligand was characterised using NMR (<sup>1</sup>H, <sup>13</sup>C, COSY, HSQC and HMBC), IR spectroscopy and HR-MS.

The <sup>1</sup>H NMR spectrum of **5.18** is shown below where the characteristics peaks are highlighted (**Figure 5.11**). Importantly, the newly formed triazole,  $\delta = 7.80$  ppm (green) can be distinguished from the previous two triazoles,  $\delta = 8.20$  ppm (red) and the three aromatic protons through the HMBC (Appendix, pg. 346). The two methylene groups (purple and orange) can also be seen at  $\delta = 2.86$  ppm and  $\delta = 2.40$  ppm respectively, confirming the formation of **5.18**.

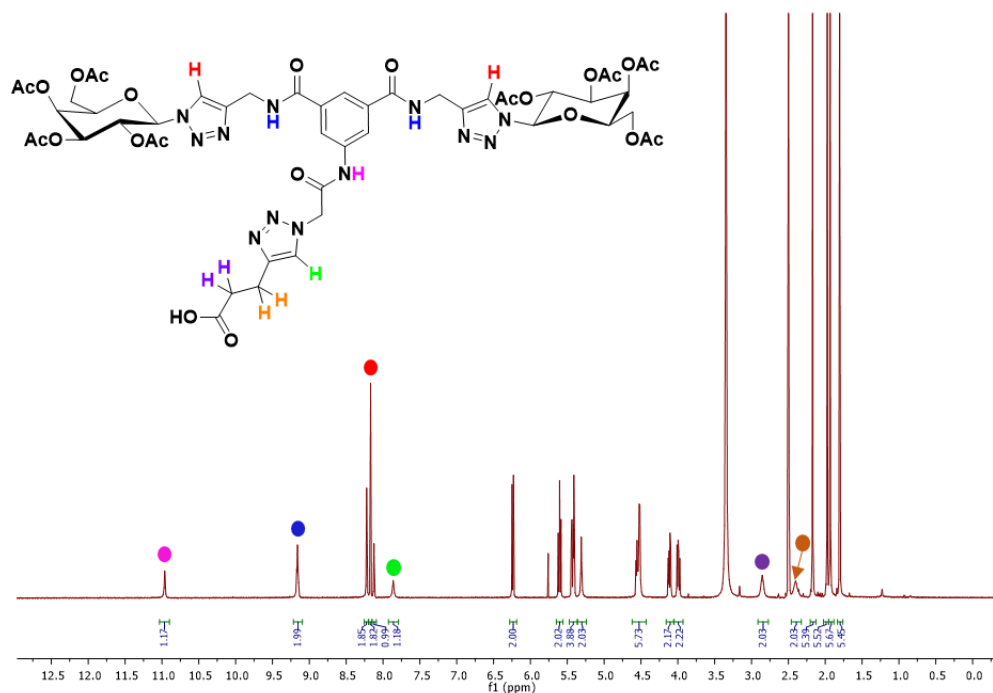
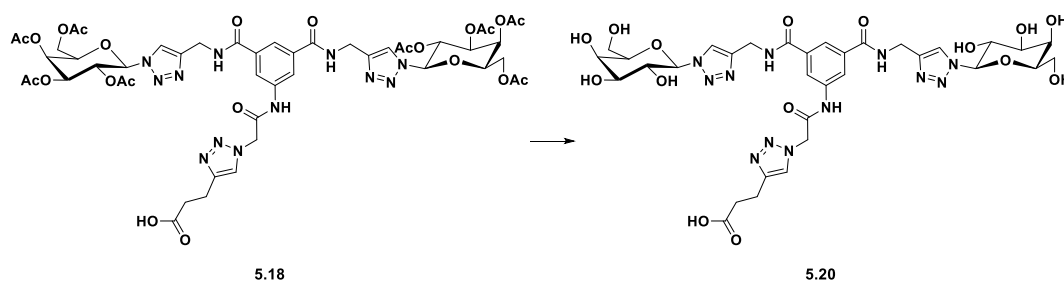


**Figure 5.11:**  $^1\text{H}$  NMR spectrum of acetylated ligand **5.18**, in  $\text{DMSO-d}_6$ .

### 5.3.4 Synthesis of free multivalent ligand (**5.20**)

The free sugar derivative (**5.20**) was synthesised through acetyl ester hydrolysis of **5.18** using the mild conditions previously discussed in **Chapter 3**. The product was isolated with a high yield (99%) and used in the next step without further purification.



**Scheme 5.7:** Deacetylation of **5.18** to form free ligand (**5.20**):  $\text{NEt}_3$ ,  $\text{MeOH}$ ,  $\text{H}_2\text{O}$ ,  $45^\circ\text{C}$ , 16 h, 99%.

The proton NMR spectrum of **5.20** is shown below (**Figure 5.12**) with its characteristic peaks highlighted. Importantly, the amide proton peaks are not visible due to the NMR solvent being  $\text{D}_2\text{O}$ . The presence of the methylene signals at  $\delta = 3.00$  ppm and  $\delta = 2.75$  ppm (pink and orange respectively) indicates that the linker is preserved throughout the reaction

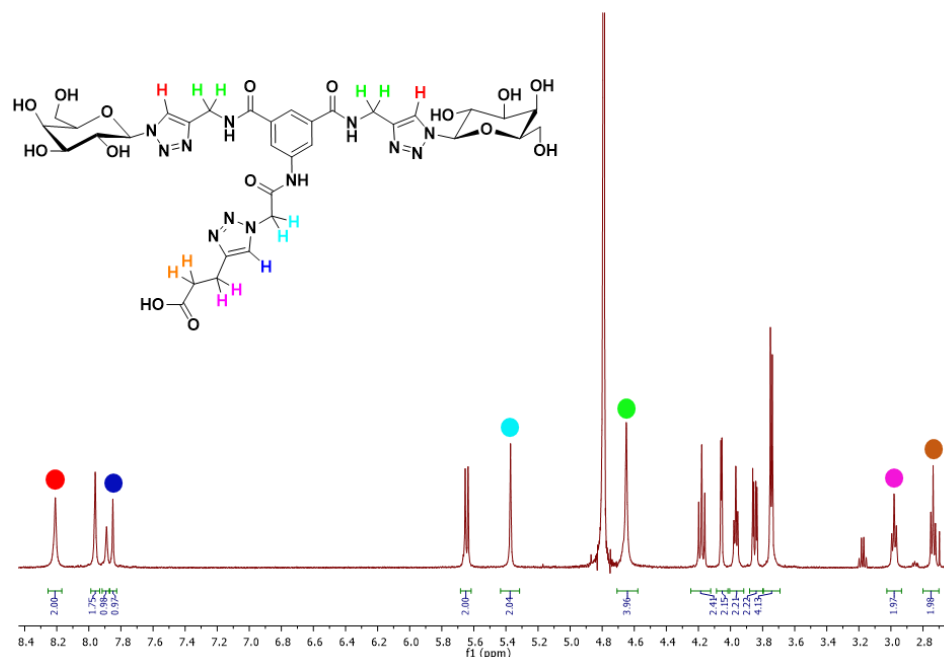
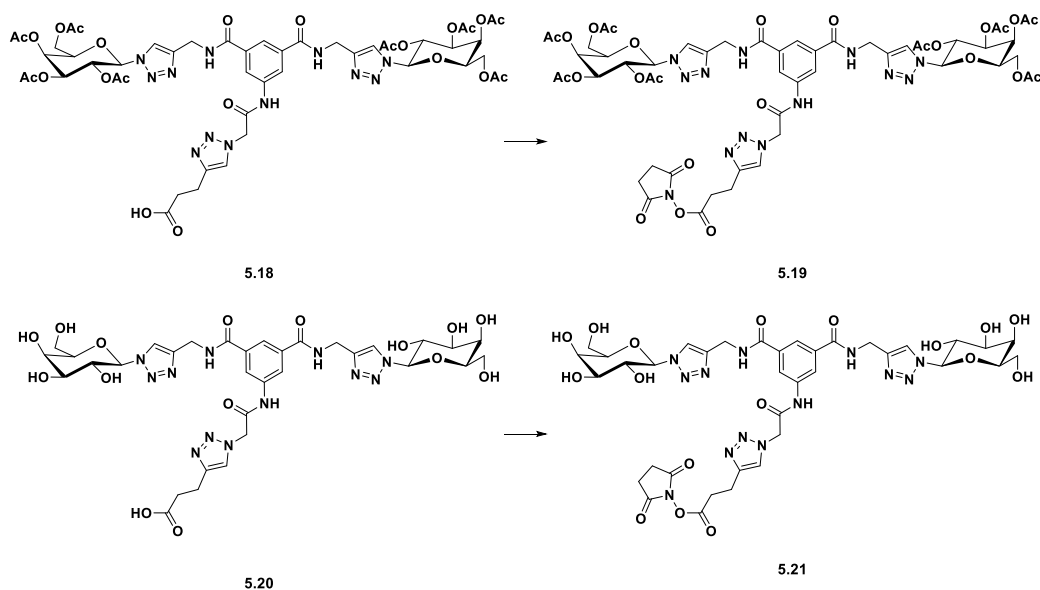


**Figure 5.12:**  $^1\text{H}$  NMR spectrum of **5.20** in  $\text{D}_2\text{O}$ .

### 5.3.5 Synthesis of multivalent active esters (**5.19** and **5.21**)

The active esters **5.19** and **5.21** were synthesised as shown in **Scheme 5.8**. The synthesis of **5.19** was much more difficult than expected. To synthesise the active NHS ester (**5.19**) we had initially planned to adapt the coupling reaction discussed in **Chapter 2**, where EDCI was used to activate the carboxylic acid and *N*-hydroxysuccinimide was added to form the corresponding NHS ester. However, the product recovered was impure, potentially containing the starting carboxylic acid (**5.18**).



**Scheme 5.8:** Activation of carboxylic acids (**5.18** and **5.20**) with the coupling agent TSTU to form active esters (**5.19** and **5.21**): TSTU,  $\text{NEt}_3$ , DMF, rt, 16 h, 81% (**5.19**); TSTU,  $\text{NEt}_3$ , DMF, rt, 20 mins, 76% (**5.21**).

Replacing NHS and EDCI in this reaction with TSTU, we succeeded to produce the active ester **5.19**. Originally, we had used this reagent for the synthesis of free sugar NHS esters described in **Chapter 3**, but it could also be used with organic soluble compounds due to the limited solubility of TSTU and its byproducts in organic solvents. This allows for the treatment the crude mixture with water, which removes the byproducts of the coupling reaction. **5.19** was characterised with NMR spectroscopy ( $^1\text{H}$ ,  $^{13}\text{C}$ , COSY, HSQC, HMBC), HR-MS and IR spectroscopy. **Figure 5.13** shows the  $^1\text{H}$  NMR spectrum of the active ester **5.19** with the characteristic peaks highlighted. In particular, the presence of the singlet (red) at  $\delta = 2.81$  ppm, which integrates for four protons confirms the formation of the active succinimide ester. Notably, the functionalisation of the carboxylic acid deshields the methylene protons (orange and purple), causing them to appear further downfield of  $\Delta\delta = 0.68$  and  $0.16$  ppm, respectively.



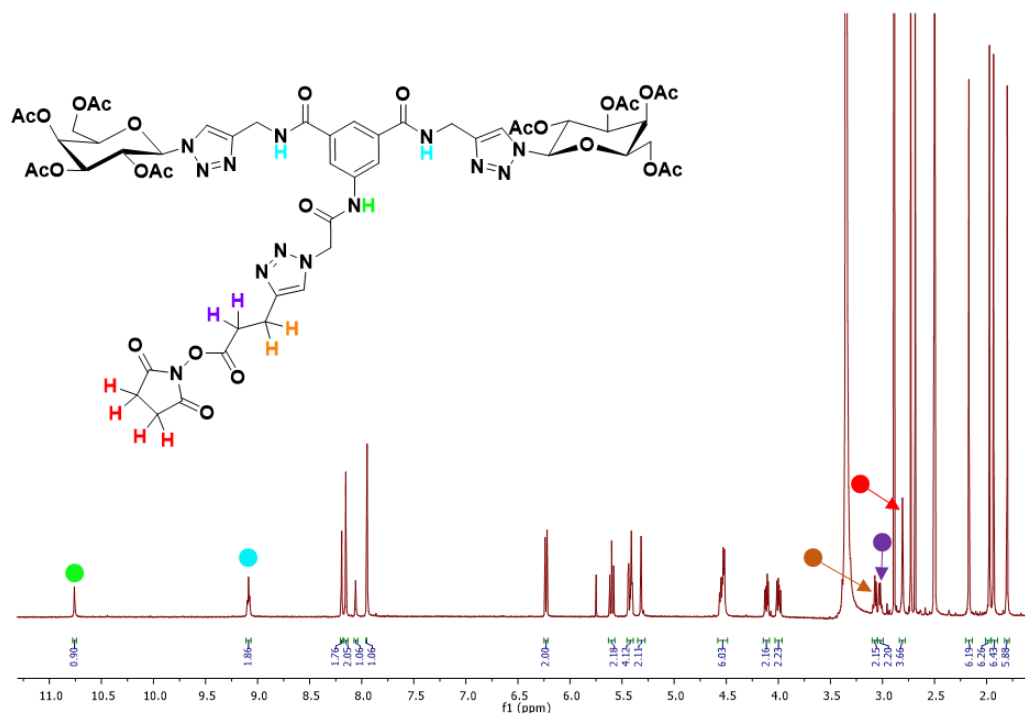


**Figure 5.13:**  $^1\text{H}$  NMR spectrum of **5.19** in  $\text{DMSO-d}_6$ , synthesised using TSTU.

The synthesis of free-sugar active ester **5.21** did not have the issues discussed for **5.19**. This compound was synthesised using TSTU according to the procedure previously discussed in **Chapter 3** and was used without further purification. The  $^1\text{H}$  NMR of **5.21** is shown below (**Figure 5.14**) with the characteristic peaks highlighted. Differently to the free carboxylic acid (**5.20**) this NMR was collected in  $\text{DMSO}$ , rather than  $\text{D}_2\text{O}$ . The amide protons (turquoise and green) can be seen at  $\delta = 9.12$  ppm and  $\delta = 10.79$  ppm respectively. The formation of the ester can be seen from the presence of the singlet at  $\delta = 2.81$  ppm (red) corresponding to the succinimide group.

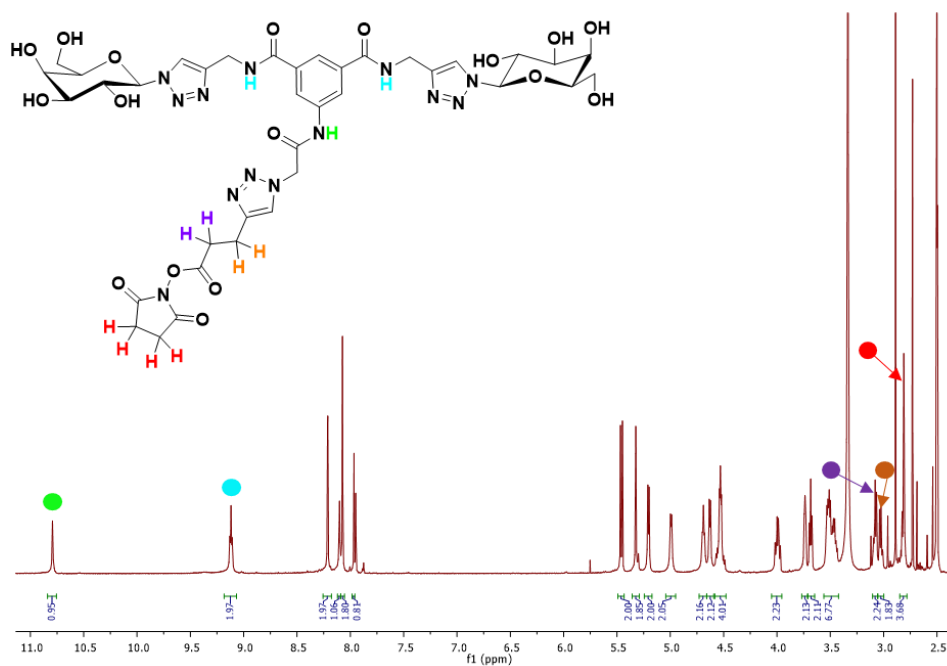


Figure 5.14:  $^1\text{H}$  NMR of active ester **5.21** in  $\text{DMSO-d}_6$ .

### 5.3.6 Attempted synthesis of multivalent Pt(IV) glycoconjugates (**5.19.1** and **5.21.1**)

Both the acetylated (**5.19**) and deacetylated (**5.21**) active esters were reacted with oxoplatin under a variety of conditions (Table 5.1 and 5.2), which had been viable methods in past chapters.

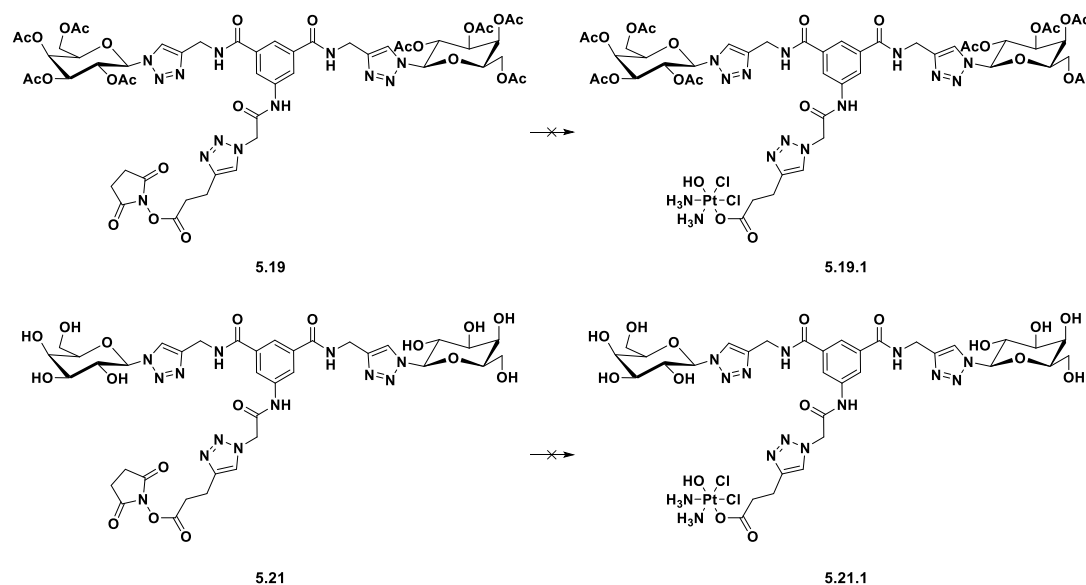
Table 5.1: Reaction conditions to form Complex **5.19.1**.

| Entry | Temperature ( $^{\circ}\text{C}$ ) | Reaction time (days) | Pt(equiv.) |
|-------|------------------------------------|----------------------|------------|
| 1     | 40                                 | 1                    | 1.05       |
| 2     | 40                                 | 2                    | 1.05       |
| 3     | 50                                 | 1                    | 1.05       |
| 4     | 60                                 | 1                    | 1.05       |
| 5     | 60                                 | 1                    | 2.00       |

Table 5.2: Reaction conditions to form Complex **5.21.1**.

| Entry | Temperature ( $^{\circ}\text{C}$ ) | Reaction time (days) | Pt(equiv.) |
|-------|------------------------------------|----------------------|------------|
| 1     | 40                                 | 1                    | 1.05       |
| 2     | 40                                 | 2                    | 1.05       |
| 3     | 40                                 | 5                    | 2.00       |

However, we were unable to isolate the complexes shown below (**Scheme 5.9**) in sufficient purity.



**Scheme 5.9:** Attempted synthesis of complexes (**5.19.1** and **5.21.1**).

**Figure 5.15** shows the stacked  $^1\text{H}$  NMR spectra of the different reactions attempted to form Complex **5.19.1**. It seems that conversion is temperature dependent, where lower temperatures result in higher proportions of product formation. This can be seen from **Figure 5.15**, where the broad triplet at  $\delta = 6.00$  ppm corresponding to the  $\text{NH}_3$  signal of Complex **5.19.1** is more prominent for the reactions carried out at lower temperatures. The best result was obtained when heating at  $40^\circ\text{C}$  for 1 day: the conversion was analysed through the comparison of the integral of the signal corresponding to the anomeric protons ( $\delta = 6.20$  ppm) and the triplet amine signal of the formed complex  $\delta = 6.00$  ppm. This ratio should be 2:6 (anomeric proton : amine), however when the reaction was carried out at  $40^\circ\text{C}$  for 1 day, we obtained 2:4, showing that the reaction had not proceeded to completion. When the reaction time was extended to two days, this ratio decreased slightly from 2:4 to 2:3. It is important to note that for the acetylated complexes discussed in **Chapters 2** and **4**, heating to  $60^\circ\text{C}$  overnight was sufficient for complex formation.

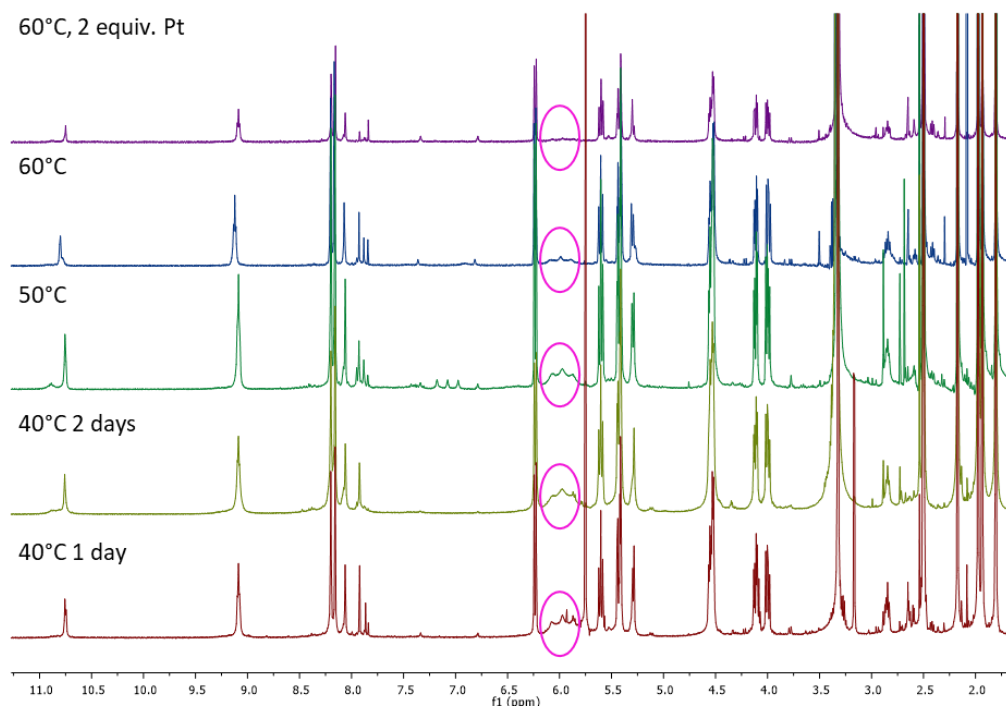


**Figure 5.15:** Stacked <sup>1</sup>H NMR spectra of reactions to form **5.19.1**, using different reaction conditions (temperature and equivalents). NMRs done in DMSO-d<sub>6</sub>.

We also attempted to form the free sugar Complex **5.21.1**, using some methods discussed in the previous chapters. We originally started with the procedure used for the free sugar complexes (**1 – 4**) in **chapter 3** (i.e. reaction at 40°C, over two days) and the procedure developed for the free sugar complex (**4**) in **Chapter 4**, (i.e. reaction at 40°C over 5 days and a large excess of oxoplatin to drive the reaction to completion). The reaction products were analysed by NMR. Unfortunately, these methods yielded similar results where the ratio of the anomeric protons to the amino ligand of the mono-functionalised complex was 2:2 instead of the expected 2:6. Importantly, the development of impurities over longer reaction periods was noticeable, as seen from the appearance of signals circled in pink and indicated with the red arrows in **Figure 5.16**.

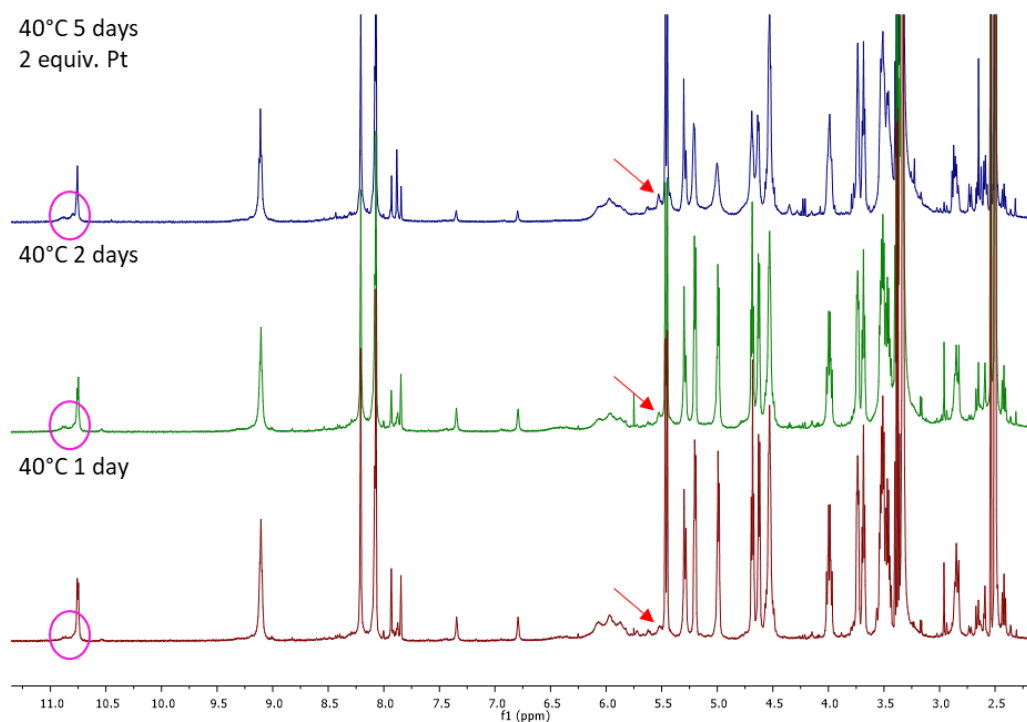


**Figure 5.16:** Stacked <sup>1</sup>H NMR spectra of reactions done to form **5.21.1**, using different conditions (reaction time and equivalents). NMRs done in DMSO-d<sub>6</sub>.

Based on the results obtained from the formation of complexes **5.19.1** and **5.21.1**, it is unclear whether these complexes can be formed in high purity using the methods described. Further purification was attempted through treatment of the products with various solvents, in particular methanol, where for both the ligands are soluble but the complexes are not. However, the resulting product never showed an improvement in purity. Interestingly, the typical reaction conditions for the formation of the acetylated Complex **5.19.1** (i.e. heating to 60°C with a small excess of oxoplatin) that yielded the successful formation of complexes (**1 – 4**) in **Chapter 2**, are so ineffective in this case. It is possible there are steric constraints associated with the proposed ligand that hinder the formation of complexes **5.19.1** and **5.21.1**.

The conformational analysis of **5.4** (previously reported by Martin *et al.* [324] (**Figure 5.17**) showed that **5.4** was found to adopt globular (e.g. conformer 40) and “semi-open” (e.g. conformer 99) structural motifs due to the intramolecular H-bond interactions between the OH groups of the terminal galactosyl units, triazolyl, amide carbonyl and NH groups.

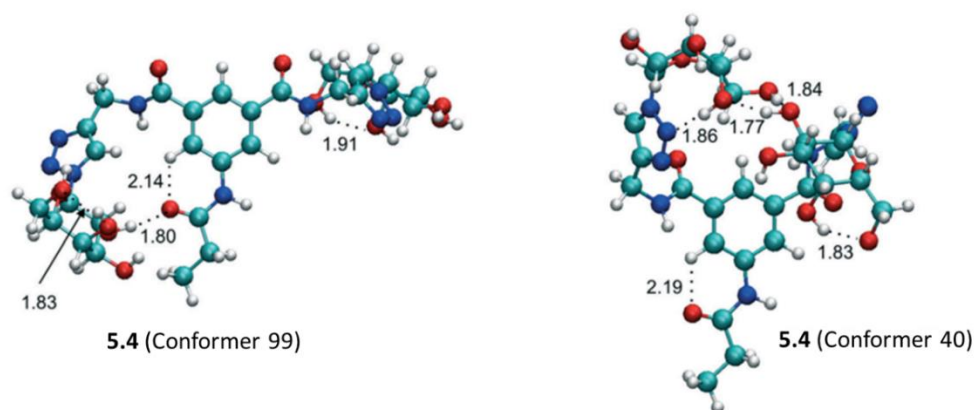


**Figure 5.17:** Geometries of low-energy conformers of **5.4** with hydrogen-bond distances (Å) [324].

Considering the structural similarities between our ligands (**5.18** and **5.20**) and the anti-adhesion glycoconjugate **5.4**, it is possible that “semi-open” conformation introduces significant steric hindrance which may inhibit product formation. Steric hindrance affecting the complexation step can be seen as an issue in the formation of imatinib and nilotinib Pt(IV) pro-drugs developed by D.F. Beirne in our group [327], which required the use of an extended linker to alleviate steric bulk around the metal centre. With this in mind, instead of using 4-pentynoic acid to click to the azide (**5.17**), a longer carbon chain derivative could be used, for example 6-heptynoic acid. Alternatively, the use of a PEGylated linker could also be used, which could overcome both of the issues discussed in this section, as well as **Section 5.3.2**.

## 5.4 Conclusions

The aim of this chapter was to synthesise two novel, multivalent glycoconjugated Pt(IV) pro-drugs for the treatment of hepatocellular carcinoma (HCC), a primary liver cancer which contains the asialoglycoprotein receptor (ASGPR), a lectin selective for galactose which is primarily found on cancer cells and not in healthy cells. Our goal was to synthesise both the acetylated and free galactose derivatives of this complex, to see if the presence of the galactose moieties would increase the cellular uptake through multivalent interaction with the ASGPR lectin.

Unfortunately, we were unable to synthesise these complexes in high purity and the conditions we have attempted have left us with the opinion that, based on the

conformational analysis put forward by Martin *et al.* [324], steric bulk associated with the divalent galactose ligand, hampers its reactivity with the axial hydroxyl group of oxoplatin. To overcome this issue, we recommend the use of a longer linker joining the platinum centre and the galactosylated ligand, possibly through the use of a polyethylene glycol-based linkage.

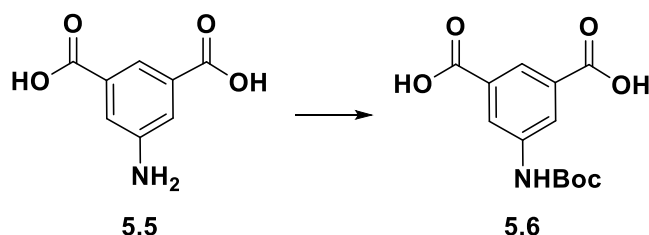
## 5.5 Materials and methods

All reagents and reactants were purchased from commercial sources. The two sources used were Sigma-Aldrich and Fluorochem. All solvents were used without further purification. Cisplatin and oxoplatin were synthesised as previously reported [262,263]. Starting materials (**5.5** – **5.9**) were synthesised according to previously reported procedures [325].

The elemental analysis studies (carbon, hydrogen, and nitrogen) were performed by means of a PerkinElmer 2400 series II analyzer. HR-Mass Spectra were recorded with a Waters LCT Premier XE Spectrometer. NMR:  $^1\text{H}$  and  $^{13}\text{C}$  NMR spectra were obtained in a solution of  $\text{D}_2\text{O}$  or  $\text{DMSO-}d_6$  at 300 K, in 5-mm sample tubes, with a premium shielded Agilent Varian 500 MHz (operating at 500.13 and 125.75 respectively). The  $^1\text{H}$  and  $^{13}\text{C}$  chemical shift was referenced to the residual impurity of the solvent. Infrared (IR) spectra were recorded in the region  $4000\text{--}400\text{ cm}^{-1}$  on a Perkin Elmer precisely spectrum 100 FT/IR spectrometer. The solid samples were run using ATR. An extensive biological evaluation of the activity of all the compounds was performed in human osteosarcoma cell line in vitro models as reported below.

## 5.6 Experimental procedures

### 5-[[1,1-Dimethylethoxy)carbonyl]amino]-1,3-benzenedicarboxylic acid (5.6)

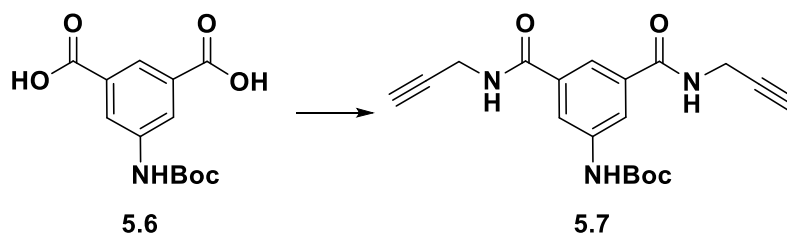


5-Aminoisophthalic acid (**5.5**) (1.0 g, 5.5 mmol) was dissolved in aqueous NaOH (1N, 10 mL) at 0 °C. Di-tert-butyl dicarbonate (1.32 g, 6.05 mmol, 1.1 equiv.) was dissolved in 1,4-dioxane (12 mL), which was added dropwise to the other solution over 2 h. The reaction mixture was stirred at 0-5 °C for 3 h, and then left to stir overnight at room temperature. The reaction mixture was evaporated to half its original volume *in vacuo* and then cooled in an ice-bath. The solution was acidified to pH 5 with a 20 % aqueous KHSO<sub>4</sub> (w/v, 20 g in 100 mL) solution. The precipitated was filtered and washed with water. The product was allowed to dry in the fumehood overnight to give the pure product (**5.6**) as an off-white solid (1.24 g, 80 %).

<sup>1</sup>H NMR (500 MHz, DMSO) δ 13.23 (s, 2H, COOH), 9.80 (s, 1H, NHBoc), 8.30 (d, *J* = 1.2 Hz, 2H, Ar-H), 8.07 (t, *J* = 1.5 Hz, 1H, Ar-H), 1.49 (s, 9H, C(CH<sub>3</sub>)<sub>3</sub>) ppm.

The NMR data is in agreement with data reported in the literature [325].

### *N,N'*-di(prop-2-yn-1-yl)-5-[[1,1-Dimethylethoxy)carbonyl]amino]isophthalamide (5.7)



**5.6** (1.12 g, 3.99 mmol) and TBTU (2.67 g, 8.31 mmol, 2.1 equiv.) were dissolved in anhydrous DMF (10 mL) under N<sub>2</sub> and NEt<sub>3</sub> (1.2 mL, 8.31 mmol, 2.1 equiv.) was added. After 10 mins, propargylamine (0.53 mL, 8.31 mmol, 2.1 equiv.) was added. The

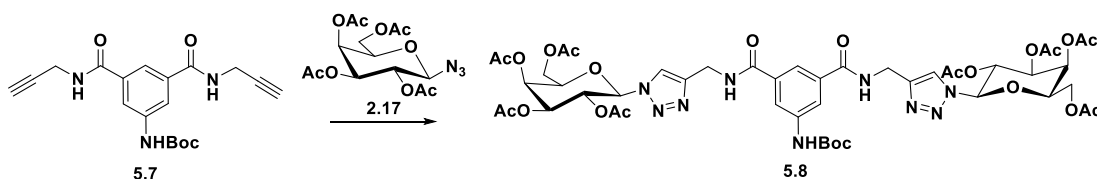


reaction mixture was allowed to stir for 24 h. The solution was then poured over ice (50 mL in 200 mL of water) and stirred for 20 minutes. The precipitated product was then collected by vacuum filtration and dried *in vacuo*. The product was isolated as an off white solid and used without further purification (1.07 g, 3.01 mmol, 76 %).

$^1\text{H NMR}$  (500 MHz, DMSO)  $\delta$  9.67 (s, 1H, *NHBoc*), 8.92 (t,  $J = 5.4$  Hz, 2H, *NHCH<sub>2</sub>CCH*), 8.04 (d,  $J = 1.3$  Hz, 2H, Ar-H), 7.85 (t,  $J = 1.5$  Hz, 1H, Ar-H), 4.04 (dd,  $J = 5.3, 2.4$  Hz, 4H, *CH<sub>2</sub>CCH*), 3.13 (t,  $J = 2.5$  Hz, 2H, *CH<sub>2</sub>CCH*), 1.49 (s, 9H, *C(CH<sub>3</sub>)<sub>3</sub>*) ppm.

The NMR data is in agreement with data reported in the literature [325].

***N,N'*-di-(2,3,4,6-tetra-*O*-acetyl- $\beta$ -D-galactopyranosyl-1,2,3-triazol-4-ylmethylamide)-*N''*-tert-butoxycarbonyl-5-aminobenzene-1,3-dicarboxamide (5.8)**



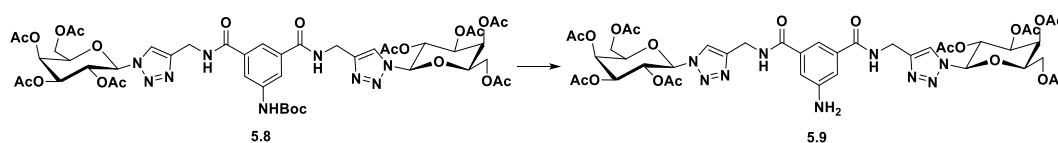
Copper sulphate pentahydrate (60 mg) and sodium ascorbate (120 mg) were added to a solution of **2.17** (1.267 g, 3.39 mmol, 2.1 equiv.) and **5.7** (0.574 g, 1.62 mmol) in acetonitrile/ $\text{H}_2\text{O}$  (4 mL/ 2mL). The reaction was allowed to stir at room temperature for 16 h. The solvent was removed *in vacuo*. The residue was dissolved in DCM (30 mL), washed with water (20 mL x 3), and dried ( $\text{MgSO}_4$ ). The mixture was filtered, and the solvent was removed *in vacuo* to yield the crude product, which was purified by silica gel column chromatography (DCM:MeOH 98:2-93:7) to give the pure product (**5.8**) as a white solid (1.15 g, 1.04 mmol, 65 %)

$^1\text{H NMR}$  (500 MHz, DMSO)  $\delta$  9.65 (s, 1H, *NHBoc*), 9.00 (t,  $J = 5.7$  Hz, 2H, 2x *NHCH<sub>2</sub>-triaz*), 8.14 (s, 2H, 2x triaz-*CH*), 8.05 (d,  $J = 1.2$  Hz, 2H, Ar-H), 7.90 (t,  $J = 1.4$  Hz, 1H, Ar-H), 6.24 (d,  $J = 9.3$  Hz, 2H, H-1), 5.60 (t, 2H, H-2), 5.46 – 5.40 (m, 4H, H-3, H-4), 4.56 (t,  $J = 7.3$  Hz, 2H, H-5), 4.51 (d,  $J = 5.7$  Hz, 4H, 2x *CH<sub>2</sub>-triaz*), 4.12 (dd,  $J = 11.6, 5.0$  Hz, 2H, H-6), 4.00 (dd,  $J = 11.6, 7.3$  Hz, 2H, H-6'), 2.18 (s, 6H, 2x *CH<sub>3</sub>* of OAc), 1.98 (s, 6H,

2x  $CH_3$  of OAc), 1.94 (s, 6H, 2x  $CH_3$  of OAc), 1.81 (s, 6H, 2x  $CH_3$  of OAc), 1.48 (s, 9H,  $C(CH_3)_3$ ) ppm.

The NMR data is in agreement with data reported in the literature [325].

***N,N'*-di-(2,3,4,6-tetra-*O*-acetyl- $\beta$ -D-galactopyranosyl-1,2,3-triazol-4-ylmethylamide)-5-aminobenzene-1,3-dicarboxamide (5.9)**

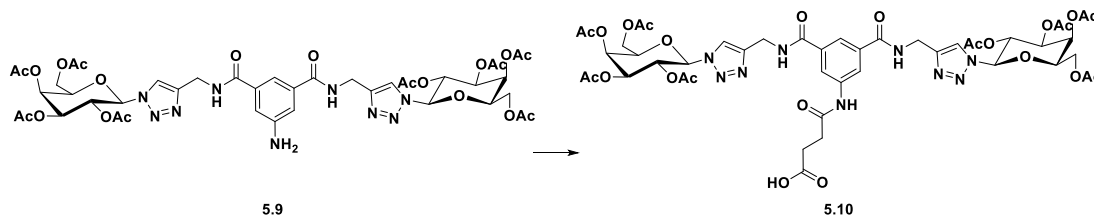


**5.8** (0.500 g, 0.453 mmol) was dissolved in DCM (5 mL) and was cooled to 0 °C in an ice-bath. TFA (1.5 mL) was added, and the reaction mixture was stirred at rt for 2 h. DCM (40 mL) was added to the reaction mixture, it was washed with sat.  $NaHCO_3$  (40 mL) and brine (40 mL), and dried ( $Na_2SO_4$ ). The mixture was filtered, and the solvent was removed *in vacuo* to yield the product (**5.9**) which was used without further purification as a pale-yellow solid (0.443 g, 0.442 mmol, 97 %).

**$^1H$  NMR** (500 MHz,  $CDCl_3$ )  $\delta$  7.98 (s, 2H, 2x triaz-H), 7.74 (t,  $J$  = 5.8 Hz, 2H, 2x  $NHCH_2$ -triaz), 7.47 (d,  $J$  = 1.3 Hz, 1H, Ar-H), 7.24 (d,  $J$  = 1.4 Hz, 2H, Ar-H), 5.95 (d,  $J$  = 9.2 Hz, 2H, H-1), 5.57 – 5.50 (m, 4H, H-2, H-4), 5.32 – 5.28 (m, 2H, H-3), 4.74 (dd,  $J$  = 15.2, 5.8 Hz, 2H, H-6), 4.60 (dd,  $J$  = 15.2, 5.7 Hz, 2H, H-6'), 4.34 – 4.29 (m, 2H, H-5), 4.17 (ddd,  $J$  = 27.2, 11.5, 6.5 Hz, 4H, 2x  $CH_2$ -triaz), 4.04 (s, 2H,  $NH_2$ ), 2.23 (s, 6H, 2x  $CH_3$  of OAc), 2.03 (s, 6H, 2x  $CH_3$  of OAc), 2.01 (s, 6H, 2x  $CH_3$  of OAc), 1.83 (s, 6H, 2x  $CH_3$  of OAc) ppm.

The NMR data is in agreement with data reported in the literature [325].

***N,N'*-di-(2,3,4,6-tetra-*O*-acetyl- $\beta$ -D-galactopyranosyl-1,2,3-triazol-4-ylmethylamide)-*N,N'*-(2-acetamido)-pentanoic acid-5-aminobenzene-1,3-dicarboxamide (5.10)**



**5.9** (0.513 g, 0.512 mmol) and succinic anhydride (0.102 g, 1.024 mmol, 2 equiv.) was dissolved in DCM (15 mL) and stirred at room temperature overnight. The organic phase was treated with 1M HCl, dried with Na<sub>2</sub>SO<sub>4</sub>, filtered and the DCM was evaporated *in vacuo*. The product was isolated as a white solid and used without further purification (0.457 g, 0.414 mmol, 81%)

$R_f = 0.65$  (DCM:MeOH 9:1)

**<sup>1</sup>H NMR** (500 MHz, DMSO)  $\delta$  11.43 (s, 1H, NHCOCH<sub>2</sub>), 9.17 (t,  $J = 5.6$  Hz, 2H, 2x NHCH<sub>2</sub>-triaz), 8.22 (s, 2H, Ar-H), 8.16 (s, 1H, 2x CH-triaz), 7.98 (s, 1H, Ar-H), 6.23 (d,  $J = 9.3$  Hz, 2H, H-1), 5.61 (t,  $J = 9.5$  Hz, 2H, H-2), 5.45 – 5.39 (m, 4H, H-3, H-4), 4.58 – 4.48 (m, 6H, H-5, 2x CH<sub>2</sub>-triaz), 4.12 (dd,  $J = 11.6, 5.0$  Hz, 2H, H-6), 4.00 (dd,  $J = 11.6, 7.3$  Hz, 2H, H-6'), 2.47 (t,  $J = 6.4$  Hz, 2H, CH<sub>2</sub>CO), 2.29 (s, 2H, NHCOCH<sub>2</sub>), 2.17 (s, 6H, 2x CH<sub>3</sub> of OAc), 1.97 (s, 6H, 2x CH<sub>3</sub> of OAc), 1.93 (s, 6H, 2x CH<sub>3</sub> of OAc), 1.81 (s, 6H, 2x CH<sub>3</sub> of OAc) ppm.

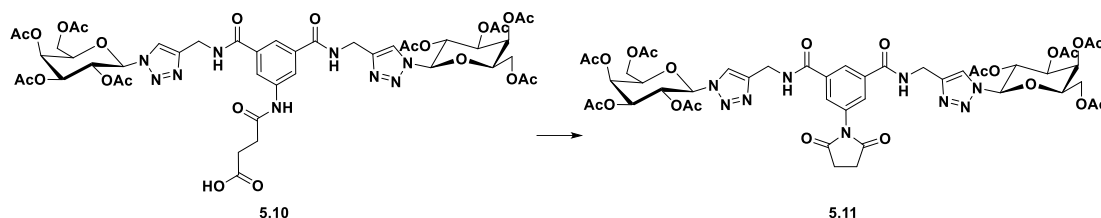
**<sup>13</sup>C NMR** (125 MHz, DMSO)  $\delta$  176.6 (NHCO), 172.4 (CH<sub>2</sub>CO), 170.1 (CO of OAc), 170.0 (CO of OAc), 169.5 (CO of OAc), 168.6 (CO of OAc), 166.1 (2x CONHCH<sub>2</sub>CCH), 145.5 (2x C-triaz), 139.9 (Ar-C), 134.9 (Ar-C), 122.6 (2x CH-triaz), 120.7 (Ar-CH), 120.2 (Ar-CH), 84.2 (C-1), 73.0 (C-5), 70.6 (C-3), 67.6 (C-2), 67.4 (C-4), 61.6 (C-6), 34.8 (2x CH<sub>2</sub>-triaz), 34.1 (CH<sub>2</sub>CO), 33.2 (NHCOCH<sub>2</sub>), 20.5 (2x CH<sub>3</sub> of OAc), 20.4 (2x CH<sub>3</sub> of OAc), 20.3 (2x CH<sub>3</sub> of OAc), 20.1 (2x CH<sub>3</sub> of OAc) ppm.

**IR(ATR)** 1743.22, 1368.10, 1211.41, 1045.48, 905.66 cm<sup>-1</sup>.

**HR-MS (+):**  $m/z$  calcd for C<sub>46</sub>H<sub>55</sub>N<sub>9</sub>O<sub>23</sub> + H<sup>+</sup> [M+H]<sup>+</sup> 1102.3489, found 1102.3477. **HR-**

**MS (+):**  $m/z$  calcd for C<sub>46</sub>H<sub>55</sub>N<sub>9</sub>O<sub>23</sub> + Na<sup>+</sup> [M+Na]<sup>+</sup> 1124.3308, found 1124.3295.

***N,N'*-di-(2,3,4,6-tetra-*O*-acetyl- $\beta$ -D-galactopyranosyl-1,2,3-triazol-4-ylmethylamide)-*N''*-(3-oxopropyl-(2,5-dioxypyrrolidin-1-yl))-5-aminobenzene-1,3-dicarboxamide (5.11)**



**5.10** (0.217 g, 0.196 mmol) and NHS (0.027 g, 0.236 mmol, 1.2 equiv.) were dissolved in DCM (9 mL) under  $N_2$  and in a separate flask, EDCI (0.045 g, 0.236 mmol, 1.2 equiv.) was also dissolved in DCM (3 mL) under  $N_2$  and added to the solution of **5.10** *via* cannula addition. This reaction was allowed to stir overnight. The organic phase was then treated with 0.1M HCl, and brine, dried with  $Na_2SO_4$  and filtered. The DCM was removed *in vacuo* and the product was isolated as a white solid (0.193 g, 0.178 mmol, 81%).

$R_f = 0.77$  (DCM:MeOH 9:1)

$^1H$  NMR (500 MHz, DMSO)  $\delta$  9.22 (t,  $J = 5.7$  Hz, 2H, 2x  $NHCH_2$ -triaz), 8.41 (t,  $J = 1.5$  Hz, 1H, Ar-H), 8.19 (s, 2H, 2x  $CH$ -triaz), 7.93 (d,  $J = 1.5$  Hz, 2H, Ar-H), 6.23 (d,  $J = 9.3$  Hz, 2H, H-1), 5.61 (t,  $J = 9.6$  Hz, 2H, H-2), 5.46 – 5.39 (m, 4H, H-3, H-4), 4.57 – 4.50 (m, 6H, H-5, 2x  $CH_2$ -triaz), 4.12 (dd,  $J = 11.6, 5.0$  Hz, 2H, H-6), 4.00 (dd,  $J = 11.6, 7.3$  Hz, 2H, H-6'), 2.82 (s, 4H,  $CH_2CH_2$ -succ), 2.17 (s, 6H, 2x  $CH_3$  of OAc), 1.98 (s, 6H, 2x  $CH_3$  of OAc), 1.93 (s, 6H, 2x  $CH_3$  of OAc), 1.81 (s, 6H, 2x  $CH_3$  of OAc) ppm.

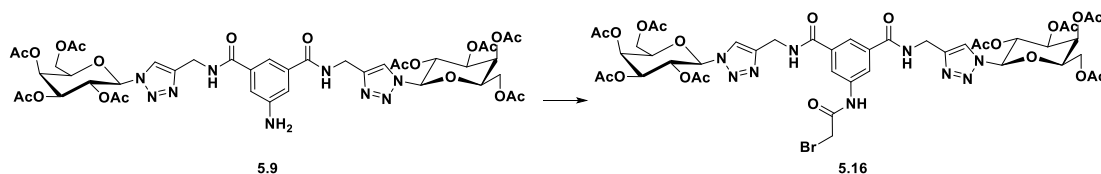
$^{13}C$  NMR (125 MHz, DMSO)  $\delta$  176.8 (2x CO-succ), 170.1 (CO of OAc), 170.0 (CO of OAc), 169.5 (CO of OAc), 168.6 (CO of OAc), 165.0 (2x CONHCH<sub>2</sub>CCH), 145.2 (2x C-triaz), 135.1 (Ar-C), 133.1 (Ar-C), 129.1 (Ar-CH), 125.8 (Ar-CH), 122.6 (2x CH-triaz), 84.2 (C-1), 73.0 (C-5), 70.5 (C-3), 67.7 (C-2), 67.4 (C-4), 61.6 (C-6), 34.9 (2x  $CH_2$ -triaz), 28.6 ( $CH_2CH_2$ -succ), 20.5 (2x  $CH_3$  of OAc), 20.5 (2x  $CH_3$  of OAc), 20.4 (2x  $CH_3$  of OAc), 20.1 (2x  $CH_3$  of OAc) ppm.

IR(ATR) 1743.99, 1709.30, 1368.49, 1211.23, 1046.24, 922.75  $cm^{-1}$ .

**HR-MS (+):**  $m/z$  calcd for  $C_{46}H_{53}N_9O_{22} + H^+$   $[M+H]^+$  1084.3383, found 1084.3383. **HR-**

**MS (+):**  $m/z$  calcd for  $C_{46}H_{53}N_9O_{22} + Na^+$   $[M+Na]^+$  1106.3203, found 1106.3207.

***N,N'*-di-(2,3,4,6-tetra-*O*-acetyl- $\beta$ -D-galactopyranosyl-1,2,3-triazol-4-ylmethylamide)-*N''*-(2-bromoacetamido)-5-aminobenzene-1,3-dicarboxamide (5.16)**

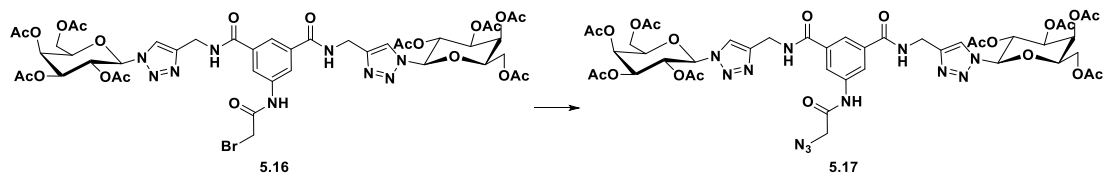


**5.9** (1.04 g, 1.03 mmol) was dissolved in dry DCM (20 mL).  $NEt_3$  (0.175 mL, 1.24 mmol) was added to this solution. Bromoacetyl bromide (0.11 mL, 1.25 mmol) was dissolved in dry DCM (5 mL) in a separate round-bottom flask. The first solution was added to the second dropwise via a cannula and the resulting reaction mixture was allowed to stir for 16 h. The reaction mixture was washed with water (20 mL), HCl (1M, 20 mL), sat.  $NaHCO_3$  solution (20 mL), followed by brine (20 mL). The organic phase was dried ( $Na_2SO_4$ ), and the solvent was removed *in vacuo* to obtain the pure product (**5.16**) without further purification as a white solid (0.951 g, 0.846 mmol, 82%).

$^1H$  NMR (500 MHz, DMSO)  $\delta$  10.68 (s, 1H,  $NHCOCH_2Br$ ), 9.11 (t,  $J = 5.7$  Hz, 2H, 2x  $NHCH_2$ -triaz), 8.19 (d,  $J = 1.4$  Hz, 2H, Ar-H), 8.17 (s, 2H, 2x  $CH$ -triaz), 8.05 (t,  $J = 1.4$  Hz, 1H, Ar-H), 6.24 (d,  $J = 9.3$  Hz, 2H, H-1), 5.61 (t,  $J = 9.3$  Hz, 2H, H-2), 5.48 – 5.38 (m, 4H, H-3, H-4), 4.60 – 4.47 (m, 6H, 2x  $CH_2$ -triaz, H-5), 4.12 (dd,  $J = 11.6, 5.0$  Hz, 2H, H-6), 4.06 (s, 2H,  $CH_2$ -Br), 4.00 (dd,  $J = 11.6, 7.3$  Hz, 2H, H-6'), 2.18 (s, 6H, 2x  $CH_3$  of OAc), 1.98 (s, 6H, 2x  $CH_3$  of OAc), 1.94 (s, 6H, 2x  $CH_3$  of OAc), 1.81 (s, 6H, 2x  $CH_3$  of OAc) ppm.

The NMR data is in agreement with data reported in the literature [325].

***N,N'*-di-(2,3,4,6-tetra-*O*-acetyl- $\beta$ -D-galactopyranosyl-1,2,3-triazol-4-ylmethylamide)-*N''*-(2-azidoacetamido)-5-aminobenzene-1,3-dicarboxamide (5.17)**

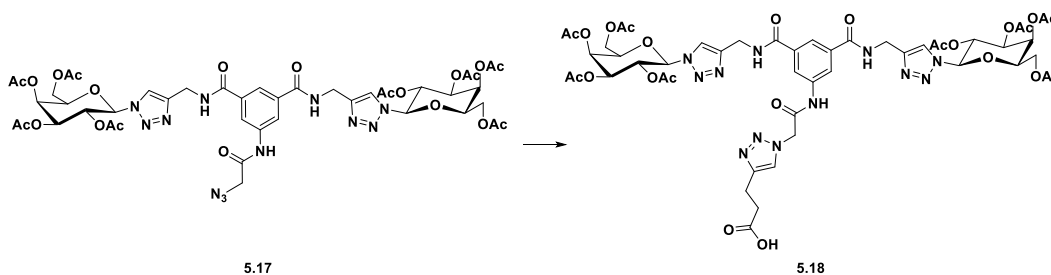


**5.16** (0.970 g, 0.8638 mmol) and  $\text{NaN}_3$  (0.112 g, 1.727 mmol, 2equiv.) were purged with  $\text{N}_2$  in a rbf and dissolved in anhydrous DMF (20 mL). The solution was refluxed at  $80^\circ\text{C}$  overnight and the solvent was removed *in vacuo*. The resulting residue was redissolved in DCM (20 mL) and washed with Brine (20 mL x 3). The organic phase was dried with  $\text{Na}_2\text{SO}_4$ , and the solvent was evaporated to yield the yellow solid product which was reacted without further purification (0.688 g, 0.634 mmol, 73%).

$^1\text{H NMR}$  (500 MHz, DMSO)  $\delta$  10.49 (s, 1H,  $\text{NHCOCH}_2\text{N}_3$ ), 9.12 (t,  $J = 5.7$  Hz, 2H, 2x  $\text{NHCH}_2$ -triaz), 8.21 (d,  $J = 1.4$  Hz, 2H, Ar-H), 8.18 (s, 2H, 2x  $\text{CH}$ -triaz), 8.06 (d,  $J = 1.3$  Hz, 1H, Ar-H), 6.25 (d,  $J = 9.3$  Hz, 2H, H-1), 5.61 (t,  $J = 9.8$  Hz, 2H, H-2), 5.46 – 5.39 (m, 4H, H-3, H-4), 4.58 – 4.50 (m, 6H, 2x  $\text{CH}_2$ -triaz, H-5), 4.12 (dd,  $J = 11.6, 5.0$  Hz, 2H, H-6), 4.08 (s, 2H,  $\text{CH}_2$ - $\text{N}_3$ ), 4.00 (dd,  $J = 11.6, 7.4$  Hz, 2H, H-6'), 2.18 (s, 6H, 2x  $\text{CH}_3$  of OAc), 1.98 (s, 6H, 2x  $\text{CH}_3$  of OAc), 1.94 (s, 6H, 2x  $\text{CH}_3$  of OAc), 1.81 (s, 6H, 2x  $\text{CH}_3$  of OAc) ppm.

The NMR data is in agreement with data reported in the literature [325].

***N,N'*-di-(2,3,4,6-tetra-*O*-acetyl- $\beta$ -D-galactopyranosyl-1,2,3-triazol-4-ylmethylamide)-*N,N'*-(2-acetamido-1,2,3-triazol-4-yl)-propanoic acid-5-aminobenzene-1,3-dicarboxamide (5.18)**



**5.17** (0.5 g, 0.46 mmol) and 4-pentynoic acid (0.067 g, 0.691 mmol, 1.5 equiv.) were dissolved in equal volumes of ACN, *t*-BuOH, and H<sub>2</sub>O (8:8:8 mL). CuSO<sub>4</sub>·5H<sub>2</sub>O (0.200 g) and sodium ascorbate (0.260 g) were added to the solution, and all were stirred at room temperature for 16 h. The solvent was evaporated, and the residue was redissolved in DCM, washed with brine, dried with Na<sub>2</sub>SO<sub>4</sub> and concentrated *in vacuo*. The crude product was purified using flash chromatography (9:1 DCM:MeOH) to yield the product as a white solid. (0.245 g, 0.207 mmol, 45%)

**R<sub>f</sub>** = 0.22 (9:1 DCM:MeOH)

**<sup>1</sup>H NMR** (500 MHz, DMSO)  $\delta$  10.96 (s, 1H, NHCOCH<sub>2</sub>-triaz), 9.16 (t, *J* = 5.5 Hz, 2H, 2x NHCH<sub>2</sub>-triaz), 8.22 (s, 2H, 2x Ar-H), 8.17 (s, 2H, 2x CH-triaz), 8.12 (s, 1H, Ar-H), 7.86 (s, 1H, CH-triaz), 6.24 (d, *J* = 9.3 Hz, 2H, H-1), 5.60 (t, *J* = 9.6 Hz, 2H, H-2), 5.45 – 5.39 (m, 4H, H-3, H-4), 5.31 (s, 2H, NHCOCH<sub>2</sub>-triaz), 4.58 – 4.49 (m, 6H, H-5, 2x CH<sub>2</sub>-triaz), 4.11 (dd, *J* = 11.6, 5.0 Hz, 2H, H-6), 3.99 (dd, *J* = 11.6, 7.3 Hz, 2H, H-6'), 2.86 (s, 2H, CH<sub>2</sub>CO), 2.40 (s, 2H, triaz-CH<sub>2</sub>), 2.17 (s, 6H, 2x CH<sub>3</sub> of OAc), 1.97 (s, 6H, 2x CH<sub>3</sub> of OAc), 1.93 (s, 6H, 2x CH<sub>3</sub> of OAc), 1.80 (s, 6H, 2x CH<sub>3</sub> of OAc) ppm.

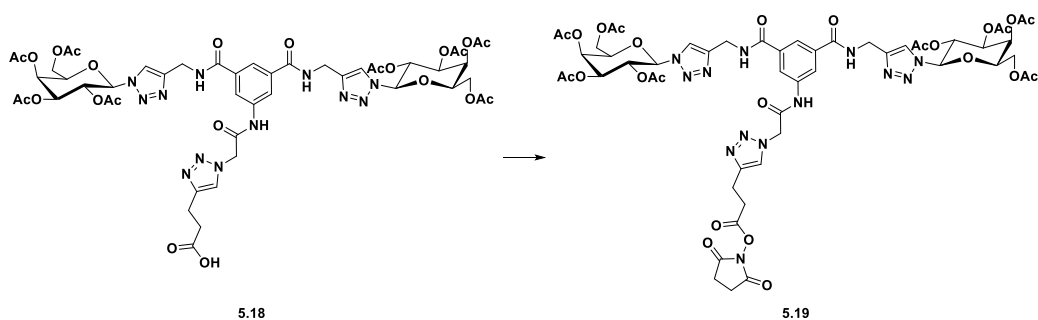
**<sup>13</sup>C NMR** (125 MHz, DMSO)  $\delta$  175.4 (CO), 170.0 (CO of OAc), 169.9 (CO of OAc), 169.4 (CO of OAc), 168.5 (CO of OAc), 165.6 (CONHCH<sub>2</sub>-triaz), 164.7 (NHCOCH<sub>2</sub>-triaz), 145.3 (2x C-triaz), 138.6 (Ar-C), 135.1 (Ar-C), 123.3 (CH-triaz), 122.4 (2x CH-triaz), 121.2 (Ar-CH), 121.1 (Ar-CH), 84.1 (C-1), 72.9 (C-5), 70.4 (C-3), 67.6 (C-2), 67.3 (C-4), 61.5 (C-6), 52.1 (NHCOCH<sub>2</sub>-triaz), 34.7 (2x CH<sub>2</sub>-triaz), 27.5 (CH<sub>2</sub>), 24.7 (CH<sub>2</sub>), 20.4 (2x CH<sub>3</sub> of OAc), 20.4 (2x CH<sub>3</sub> of OAc), 20.3 (2x CH<sub>3</sub> of OAc), 20.0 (2x CH<sub>3</sub> of OAc) ppm.

**IR(ATR)** 1744.06, 1651.74, 1538.48, 1368.01, 1211.40, 1048.83, 922.71  $\text{cm}^{-1}$ .

**HR-MS (+):**  $m/z$  calcd for  $\text{C}_{49}\text{H}_{58}\text{N}_{12}\text{O}_{23} + \text{H}^+$   $[\text{M}+\text{H}]^+$  1183.3816, found 1183.3804. **HR-**

**MS (+):**  $m/z$  calcd for  $\text{C}_{49}\text{H}_{58}\text{N}_{12}\text{O}_{23} + \text{Na}^+$   $[\text{M}+\text{Na}]^+$  1205.3635, found 1205.3609.

***N,N'*-di-(2,3,4,6-tetra-*O*-acetyl- $\beta$ -D-galactopyranosyl-1,2,3-triazol-4-ylmethylamide)-*N''*'-((2-acetamido-1,2,3-triazol-4-yl)-(3-oxopropyl-(oxy(2,5-dioxypyrrolidin-1-yl))))-5-aminobenzene-1,3-dicarboxamide (5.19)**



**5.18** (0.1 g, 0.0845 mmol) and TSTU (0.03 g, 0.101 mmol, 1.2 equiv.) were dissolved in DMF (5 mL) under  $\text{N}_2$ .  $\text{NEt}_3$  (0.014 mL, 0.101 mmol, 1.2 equiv.) was added and the solution was stirred overnight. DCM (100 mL) was added and treated with cold water (100 mL x 2), the organic phase was then dried with  $\text{Na}_2\text{SO}_4$ , filtered and the DCM was evaporated *in vacuo*. The final product was obtained as a brown solid and used without further purification. (0.087 g, 0.067 mmol, 81%).

$R_f = 0.35$  (9:1 DCM:MeOH)

$^1\text{H NMR}$  (500 MHz, DMSO)  $\delta$  10.76 (s, 1H,  $\text{NHCOCH}_2$ -triaz), 9.09 (t,  $J = 5.7$  Hz, 2H, 2x  $\text{NHCH}_2$ -triaz), 8.19 (d,  $J = 1.3$  Hz, 2H, Ar-H), 8.15 (s, 2H, 2x  $\text{CH}$ -triaz), 8.06 (s, 1H, Ar-H), 7.95 (s, 1H,  $\text{CH}$ -triaz), 6.23 (d,  $J = 9.3$  Hz, 2H, H-1), 5.60 (t,  $J = 9.6$  Hz, 2H, H-2), 5.42 (dt,  $J = 6.0, 3.5$  Hz, 4H, H-3, H-4), 5.32 (s, 2H,  $\text{NHCOCH}_2$ -triaz), 4.57 – 4.51 (m, 6H, H-5, 2x  $\text{CH}_2$ -triaz), 4.11 (dd,  $J = 11.6, 5.0$  Hz, 2H, H-6), 4.00 (dd,  $J = 11.6, 7.3$  Hz, 2H, H-6'), 3.08 (dd,  $J = 11.0, 4.1$  Hz, 2H,  $\text{CH}_2\text{CO}$ ), 3.04 – 3.00 (m, 2H, triaz- $\text{CH}_2$ ), 2.81 (s, 4H,  $\text{CH}_2\text{CH}_2$ -succ), 2.17 (s, 6H, 2x  $\text{CH}_3$  of OAc), 1.97 (s, 6H, 2x  $\text{CH}_3$  of OAc), 1.93 (s, 6H, 2x  $\text{CH}_3$  of OAc), 1.80 (s, 6H, 2x  $\text{CH}_3$  of OAc) ppm.



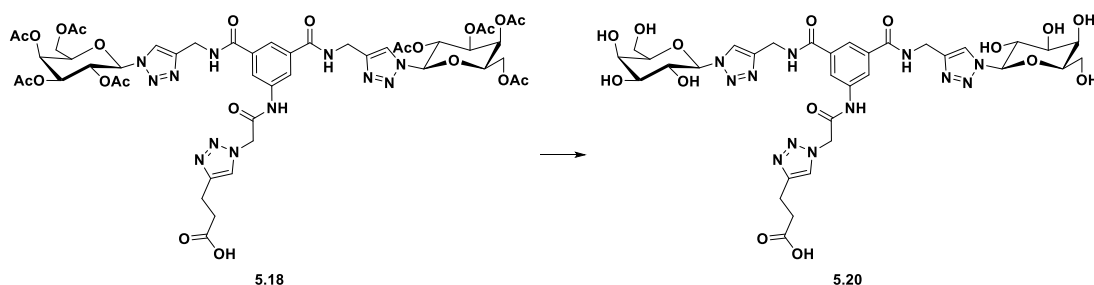
**<sup>13</sup>C NMR** (125 MHz, DMSO)  $\delta$  170.2 (CONCO-succ), 170.0 (CO of OAc), 169.9 (CO of OAc), 169.5 (CO of OAc), 168.5 (CO of OAc), 168.3 (CO-succ), 165.6 (CONHCH<sub>2</sub>-triaz), 164.6 (NHCOCH<sub>2</sub>), 145.3 (2x C-triaz), 144.3 (C-triaz), 138.5 (Ar-C), 135.1 (Ar-C), 124.0 (CH-triaz), 122.4 (2x CH-triaz), 121.3 (Ar-CH), 121.1 (Ar-CH), 84.1 (C-1), 72.9 (C-5), 70.5 (C-3), 67.6 (C-2), 67.3 (C-4), 61.5 (C-6), 52.2 (NHCOCH<sub>2</sub>-triaz), 34.7 (2x CH<sub>2</sub>-triaz), 29.8 (CH<sub>2</sub>CO), 25.4 (CH<sub>2</sub>CH<sub>2</sub>-succ), 20.5 (2x CH<sub>3</sub> of OAc), 20.4 (2x CH<sub>3</sub> of OAc), 20.3 (2x CH<sub>3</sub> of OAc), 20.2 (triaz-CH<sub>2</sub>), 20.0 (2x CH<sub>3</sub> of OAc) ppm.

**IR (ATR)** 3298.31, 2936.07, 1736.84, 1655.92, 1368.49, 1210.43, 1048.45, 922.32 cm<sup>-1</sup>.

**HR-MS (+):** m/z calcd for C<sub>53</sub>H<sub>61</sub>N<sub>13</sub>O<sub>25</sub> + H<sup>+</sup> [M+H]<sup>+</sup> 1280.3980, found 1280.3960. **HR-**

**MS (+):** m/z calcd for C<sub>53</sub>H<sub>61</sub>N<sub>13</sub>O<sub>25</sub> + Na<sup>+</sup> [M+Na]<sup>+</sup> 1302.3799, found 1302.3777.

***N,N'*-di-( $\beta$ -D-galactopyranosyl-1,2,3-triazol-4-ylmethylamide)-*N''*-(2-acetamido-1,2,3-triazol-4-yl)-propanoic acid-5-aminobenzene-1,3-dicarboxamide (5.20)**



**5.18** (0.503 g, 0.425 mmol) was dissolved in MeOH (5 mL) and H<sub>2</sub>O (3 mL). NEt<sub>3</sub> (0.3 mL) was added, and the solution was stirred at 45°C overnight. The MeOH was then evaporated and amberlite H<sup>+</sup> was added to the solution, which was stirred at room temperature for 40 minutes. The amberlite was filtered and the remaining water was removed by lyophilisation. The product was recovered as a white solid and was used without further purification. (0.355 g, 0.419 mmol, 99%).

**<sup>1</sup>H NMR** (500 MHz, D<sub>2</sub>O)  $\delta$  8.21 (s, 2H, 2x CH-triaz), 7.96 (s, 2H, Ar-H), 7.89 (s, 1H, Ar-H), 7.85 (s, 1H, CH-triaz), 5.65 (d, *J* = 9.2 Hz, 2H, H-1), 5.37 (s, 2H, NHCOCH<sub>2</sub>-triaz), 4.65 (s, 4H, 2x CH<sub>2</sub>-triaz), 4.18 (t, *J* = 9.5 Hz, 2H, H-2), 4.06 (d, *J* = 3.0 Hz, 2H, H-4), 3.97

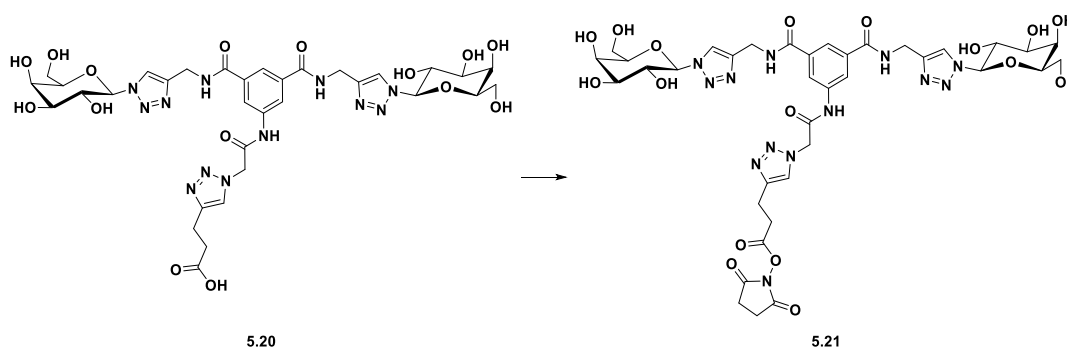
(t,  $J = 6.1$  Hz, 2H, H-5), 3.85 (dd,  $J = 9.8, 3.3$  Hz, 2H, H-3), 3.75 (d,  $J = 6.1$  Hz, 4H, H-6, H-6'), 2.98 (t,  $J = 7.2$  Hz, 2H, triaz-CH<sub>2</sub>), 2.74 (t,  $J = 7.2$  Hz, 2H, CH<sub>2</sub>CO) ppm.

<sup>13</sup>C NMR (125 MHz, D<sub>2</sub>O)  $\delta$  177.0 (CO), 168.6 (2x CONHCH<sub>2</sub>-triaz), 166.3 (NHCOCH<sub>2</sub>-triaz), 146.3 (C-triaz), 144.8 (2x C-triaz), 137.5 (Ar-C), 134.7 (Ar-C), 124.9 (CH-triaz), 122.9 (2x CH-triaz), 122.5 (Ar-CH), 122.4 (Ar-CH), 88.1 (C-1), 78.3 (C-5), 72.9 (C-3), 69.7 (C-2), 68.5 (C-4), 60.8 (C-6), 52.4 (NHCOCH<sub>2</sub>-triaz), 35.1 (2x CH<sub>2</sub>-triaz), 32.9 (CH<sub>2</sub>CO), 20.1 (triaz-CH<sub>2</sub>) ppm.

IR(ATR) 3261.88, 1641.32, 1541.50, 1219.11, 1091.17, 1053.88, 890.30 cm<sup>-1</sup>.

HR-MS (-):  $m/z$  calcd for C<sub>33</sub>H<sub>42</sub>N<sub>12</sub>O<sub>15</sub> - H<sup>+</sup> [M-H]<sup>+</sup> 845.2814, found 845.2815.

***N,N'*-di-( $\beta$ -D-galactopyranosyl-1,2,3-triazol-4-ylmethylamide)-*N''*-((2-acetamido-1,2,3-triazol-4-yl)-(3-oxopropyl-(oxy(2,5-dioxypyridin-1-yl))))-5-aminobenzene-1,3-dicarboxamide (5.21)**



**5.20** (0.1 g, 0.118 mmol) and TSTU (0.039 g, 0.129 mmol, 1.1 equiv.) were dissolved in DMF (10 mL) under N<sub>2</sub>. NEt<sub>3</sub> (0.017 mL, 0.129 mmol, 1.1 equiv.) was added and the solution was allowed to stir at room temperature for 20 minutes. The DMF was evaporated *in vacuo* and the product was precipitated using DCM and washed with diethyl ether. The light brown product was dried using a schlenk line and used without further purification. (0.084 g, 0.088 mmol, 76%)

$R_f = 0.47$  (60:35:5 DCM:MeOH:H<sub>2</sub>O)

<sup>1</sup>H NMR (500 MHz, DMSO)  $\delta$  10.79 (s, 1H, NHCOCH<sub>2</sub>-triaz), 9.12 (t,  $J = 5.6$  Hz, 2H, 2x NHCH<sub>2</sub>-triaz), 8.21 (s, 2H, Ar-H), 8.10 (s, 1H, Ar-H), 8.07 (s, 2H, 2x CH-triaz), 7.97 (s,

1H, *CH*-triaz), 5.46 (d,  $J = 9.2$  Hz, 2H, H-1), 5.32 (s, 2H,  $\text{NHCOCH}_2$ -triaz), 5.20 (d,  $J = 5.9$  Hz, 2H, *OH* of C-2), 4.99 (d,  $J = 5.3$  Hz, 2H, *OH* of C-3), 4.69 (t,  $J = 5.3$  Hz, 2H, *OH* of C-6), 4.63 (d,  $J = 5.5$  Hz, 2H, *OH* of C-4), 4.58 – 4.48 (m, 4H, 2x  $\text{CH}_2$ -triaz), 3.99 (td,  $J = 9.2, 5.8$  Hz, 2H, H-2), 3.74 (s, 2H, H-4), 3.68 (t,  $J = 6.1$  Hz, 2H, H-5), 3.54 – 3.43 (m, 6H, H-3, H-6, H-6'), 3.08 (dd,  $J = 10.9, 4.0$  Hz, 2H,  $\text{CH}_2\text{CO}$ ), 3.04 – 3.00 (m, 2H, triaz- $\text{CH}_2$ ), 2.81 (s, 4H,  $\text{CH}_2\text{CH}_2$ -succ) ppm.

$^{13}\text{C}$  NMR (125 MHz, DMSO)  $\delta$  170.2 (CONCO-succ), 168.3 (CO-succ), 165.6 (2x CONH $\text{CH}_2$ -triaz), 164.6 ( $\text{NHCOCH}_2$ -triaz), 144.9 (2x C-triaz), 144.3 (C-triaz), 138.6 (Ar-C), 135.1 (Ar-C), 124.0 (*CH*-triaz), 121.7 (2x CH-triaz), 121.18 (Ar-CH), 121.16 (Ar-CH), 88.0 (C-1), 78.4 (C-5), 73.7 (C-3), 69.4 (C-2), 68.5 (C-4), 60.4 (C-6), 52.2 ( $\text{NHCOCH}_2$ -triaz), 35.0 (2x  $\text{CH}_2$ -triaz), 29.8 ( $\text{CH}_2\text{CO}$ ), 25.5 ( $\text{CH}_2\text{CH}_2$ -succ), 20.3 (triaz- $\text{CH}_2$ ).

**IR(ATR)** 3323.40, 1731.87, 1647.83, 1541.47, 1212.10, 1091.07, 1061.64, 891.89  $\text{cm}^{-1}$ .

**HR-MS (+):**  $m/z$  calcd for  $\text{C}_{37}\text{H}_{45}\text{N}_{13}\text{O}_{17} + \text{H}^+$   $[\text{M}+\text{H}]^+$  944.3135, found 944.3128. **HR-MS (+):**  $m/z$  calcd for  $\text{C}_{37}\text{H}_{45}\text{N}_{13}\text{O}_{17} + \text{Na}^+$   $[\text{M}+\text{Na}]^+$  966.2954, found 966.2947.

## **Chapter 6: Conclusion**

## 6.1 Conclusion

The aim of the research described in this thesis was to develop novel glycosylated Pt(IV) pro-drugs using CuAAC “click” chemistry and to evaluate their potential as anticancer agents. As cancer cells overexpress the GLUTs receptors to increase the glucose uptake for ATP production (Warburg Effect), a series of glyco-functionalised Pt(IV) pro-drugs were developed with the aim to enhance the selectivity for tumoral tissues with respect to healthy cells.

In **Chapter 2**, four novel mono-functionalised Pt[IV]-glycosides based on the cisplatin scaffold were synthesised and fully characterised. The sugar moiety and the metal centre are connected through a triazole linker *via* ‘CuAAC’ click chemistry, which is used due to its versatility, mild reaction conditions and the triazoles ability to act as a bioisostere for amide bonds. The complexes were screened against a panel of different OS cell lines and showed very promising activity when compared to the reference cisplatin. The complexes were also particularly active towards CSCs (Cancer Stem Cells) with the most promising activity shown by Complex **4**, a galactose derivative. This preliminary study displayed that functionalisation with the sugar ligands, improved the anticancer activity as well as the drug internalisation compared to cisplatin (demonstrated by the uptake experiments in CSCs). The increased activity could be due to the protected acetyl sugar ligands, leading to an increase in lipophilicity and a higher cellular accumulation. This could mean that these acetylated complexes are internalised into the cell by passive diffusion rather than *via* the GLUTs transporters.

Based on the results obtained, in **Chapter 3** we synthesised the deprotected derivatives of these complexes. The complexes were tested on a panel of two 2D and 3D OS cell lines as well as on healthy OS cell. All the complexes showed very promising activity, comparable to the reference cisplatin, demonstrating that the presence of a monosaccharide does not hamper the anticancer effect. Notably, the complexes are much less active against the healthy line, showing a promising selectivity for these OS cell lines, with respect to cisplatin. The complexes were also particularly active on the 3D model, a more reliable system compared to 2D, with the

most promising activity shown by complexes **2** and **4** with galactose substituents. While the role of the free sugars as targeting vectors is not completely confirmed yet, the selectivity showed in 2D studies is a solid base to hypothesise that the carbohydrate moieties play an important role in targeted therapies. More specific biological studies should be conducted, but this selectivity was indeed not observed in the protected-Pt(IV) analogues reported in **Chapter 2**. While all the complexes showed very promising activity, the discrimination between the two linkers is not evident.

In **Chapter 4**, to improve the overall potency of our complexes, we functionalised the sugar at the C2 position. This had been previously shown to greatly increase cellular uptake in comparison to the other positions on the hexose ring [135]. In this series of complexes, the sugar targeting vector is linked to the platinum core at the C2 position always *via* CuAAC “click” chemistry. This series of Pt(IV) complexes contained both protected and deprotected sugar moieties, whose function was to improve drug selectivity, cellular uptake and cytotoxicity. This is the first time in literature that these kind of C2 glycol-conjugated Pt(IV) prodrugs containing carbohydrates conjugated at this C2 position have been reported. The complexes were tested against a panel of OS cells, a triple negative breast cancer cell line and a glioblastoma cell line, and they showed excellent activity in comparison to cisplatin. These complexes were particularly effective against OS cell lines, U-2 OS and MG63; and the triple negative breast cancer cell line, MDA-MB-468. In comparison to the complexes synthesised in previous chapters, it seems that the C2 functionalised sugars were more effective targeting vectors than the carbohydrates modified in the anomeric C1 position, in line with what was reported by Patra *et al.* [135]. While the results of the MTT assays show good cytotoxic activity from complexes **1 – 4**, it is important to note that healthy cell lines were not used yet in these assays and for the moment the selectivity of these drugs for cancer cells has not been assessed. At the time of writing, no cellular uptake or GLUT inhibition experiments have been conducted either, but all these studies are planned.

In addition to our original cellular target of glucose transporters, we attempted to synthesise two novel, multivalent glycoconjugated Pt(IV) pro-drugs (**Chapter 5**) for

the treatment of hepatocellular carcinoma (HCC). HCC is a primary liver cancer which overexpresses the asialoglycoprotein receptor (ASGPR), a lectin selective for galactose which is primarily found on cancer cells and to a lesser extent in healthy cells. Our goal was to synthesise both the acetylated and free divalent galactose derivatives of this complex, to see if the presence of the galactose moieties would increase the cellular uptake through multivalent interaction with the ASGPR lectin. Unfortunately, we were unable to synthesise these complexes in high purity and the conditions we have attempted have left us with the opinion that steric bulk associated with the divalent galactose ligand, hampers its reactivity with the axial hydroxyl group of oxoplatin. To overcome this issue, we recommend the use of a longer linker joining the platinum centre and the galactosylated ligand, possibly through the use of a polyethylene glycol-based linkage.

Future prospects for this research include conducting a more detailed uptake study, both to determine which of the discussed complexes are more preferentially taken into the cells; and also, to determine if drug uptake is facilitated by GLUTs, through the use of GLUT inhibition assays. Other than this, analysing these drugs against different cell lines might show superior activity when compared to the osteosarcoma cell lines that have been tested thus far. For instance, other platinum glycoconjugates have been tested against prostate and cervical cancer cell lines and have shown promising activity [91,135].

Other than biological tests, platinum scaffolds different to cisplatin could be employed (carboplatin/oxaliplatin) to take advantage of their different redox potentials and modes of activity. Platinum in the +2 oxidation state could also be used. For example, taking an oxaliplatin scaffold and functionalizing the bidentate dicarboxylic acid ligand with an azide or alkyne would provide a route to link a suitable carbohydrate moiety to the ligand. When coupled to oxaliplatin, this ligand can target cancer cells and is then hydrolysed to activate its anticancer activity.

Finally, mannose, a C2 epimer of glucose could be functionalised in the axial C2 position rather than equatorial to compare the activity of our complexes synthesised in **Chapter 4**. As discussed previously, the C2 position does not take part in the

binding of carbohydrates in the GLUT binding site, making it a suitable sugar for glycoconjugation to Pt anticancer drugs.



# Bibliography

1. Fares, J.; Fares, M.Y.; Khachfe, H.H.; Salhab, H.A.; Fares, Y. Molecular Principles of Metastasis: A Hallmark of Cancer Revisited. *Signal Transduct Target Ther* 2020, *5*.
2. World Health Organization Cancer. Available online: <https://www.who.int/news-room/fact-sheets/detail/cancer> (accessed on 24 January 2023).
3. Hanahan, D.; Weinberg, R.A. *The Hallmarks of Cancer Review Evolve Progressively from Normalcy via a Series of Pre*; 2000; Vol. 100;.
4. Pavlova, N.N.; Thompson, C.B. The Emerging Hallmarks of Cancer Metabolism. *Cell Metab* 2016, *23*, 27–47.
5. Otto Warburg, B.; Wind, F.; Negelein, N. THE METABOLISM OF TUMORS IN THE BODY. *J. Gen. Physiol.* **1927**, *8*, 519.
6. Liu, C.; Jin, Y.; Fan, Z. The Mechanism of Warburg Effect-Induced Chemoresistance in Cancer. *Front Oncol* 2021, *11*.
7. Yanagida, O.; Kanai, Y.; Chairoungdua, A.; Kim, K.; Segawa, H.; Nii, T.; Ho Cha, S.; Matsuo, H.; Fukushima, J.-I.; Fukasawa, Y.; et al. *Human L-Type Amino Acid Transporter 1 (LAT1): Characterization of Function and Expression in Tumor Cell Lines*; 2001; Vol. 1514;.
8. Nicklin, P.; Bergman, P.; Zhang, B.; Triantafellow, E.; Wang, H.; Nyfeler, B.; Yang, H.; Hild, M.; Kung, C.; Wilson, C.; et al. Bidirectional Transport of Amino Acids Regulates MTOR and Autophagy. *Cell* **2009**, *136*, 521–534, doi:10.1016/j.cell.2008.11.044.
9. 2022-Cancer-Facts-and-Figures. *American Cancer Society* **2022**.
10. Siegel, R.L.; Miller, K.D.; Fuchs, H.E.; Jemal, A. Cancer Statistics, 2022. *CA Cancer J Clin* **2022**, *72*, 7–33, doi:10.3322/caac.21708.
11. Rivlin, N.; Brosh, R.; Oren, M.; Rotter, V. Mutations in the P53 Tumor Suppressor Gene: Important Milestones at the Various Steps of Tumorigenesis. *Genes Cancer* 2011, *2*, 466–474.
12. Moore, P.S.; Chang, Y. Why Do Viruses Cause Cancer? Highlights of the First Century of Human Tumour Virology. *Nat Rev Cancer* 2010, *10*, 878–889.
13. White, M.K.; Pagano, J.S.; Khalili, K. Viruses and Human Cancers: A Long Road of Discovery of Molecular Paradigms. *Clin Microbiol Rev* **2014**, *27*, 463–481, doi:10.1128/CMR.00124-13.
14. Blackadar, C.B. Historical Review of the Causes of Cancer. *World J Clin Oncol* 2016, *7*, 54–86.
15. Arruebo, M.; Vilaboa, N.; Sáez-Gutierrez, B.; Lambea, J.; Tres, A.; Valladares, M.; González-Fernández, Á. Assessment of the Evolution of Cancer Treatment Therapies. *Cancers (Basel)* 2011, *3*, 3279–3330.
16. Baskar, R.; Lee, K.A.; Yeo, R.; Yeoh, K.W. Cancer and Radiation Therapy: Current Advances and Future Directions. *Int J Med Sci* 2012, *9*, 193–199.
17. Bernier, J.; Hall, E.J.; Giaccia, A. Radiation Oncology: A Century of Achievements. *Nat Rev Cancer* **2004**, *4*, 737–747.

18. Abbas, Z.; Rehman, S. An Overview of Cancer Treatment Modalities. In *Neoplasm*; InTech, 2018.
19. Debela, D.T.; Muzazu, S.G.; Heraro, K.D.; Ndalama, M.T.; Mesele, B.W.; Haile, D.C.; Kitui, S.K.; Manyazewal, T. New Approaches and Procedures for Cancer Treatment: Current Perspectives. *SAGE Open Med* **2021**, *9*, 205031212110343, doi:10.1177/20503121211034366.
20. Mokhtari, R.B.; Homayouni, T.S.; Baluch, N.; Morgatskaya, E.; Kumar, S.; Das, B.; Yeger, H. *Combination Therapy in Combating Cancer SYSTEMATIC REVIEW: COMBINATION THERAPY IN COMBATING CANCER BACKGROUND*; 2017; Vol. 8;.
21. Huaizhi, Z.; Yuantao, N. China's Ancient Gold Drugs. *Gold bull* **2001**, *34*, 24–29.
22. Hodgkinson, V.; Petris, M.J. Copper Homeostasis at the Host-Pathogen Interface. *Journal of Biological Chemistry* 2012, *287*, 13549–13555.
23. Ratia, C.; Cepas, V.; Soengas, R.; Navarro, Y.; Velasco-de Andrés, M.; Iglesias, M.J.; Lozano, F.; López-Ortiz, F.; Soto, S.M. A CAS-Cyclometallated Gold(III) Complex as a Novel Antibacterial Candidate Against Drug-Resistant Bacteria. *Front Microbiol* **2022**, *13*, doi:10.3389/fmicb.2022.815622.
24. Lloyd, N.C.; Morgan, H.W.; Nicholson, B.K.; Ronimus, R.S. The Composition of Ehrlich's Salvarsan: Resolution of a Century-Old Debate. *Angewandte Chemie - International Edition* **2005**, *44*, 941–944, doi:10.1002/anie.200461471.
25. Werner, A. Beitrag Zur Konstitution Anorganischer Verbindungen. *Zeiter Anorgan Chem* **1892**, *3*, 207–330.
26. Rosenberg, B.; VanCamp, L.; Trosko, J.E.; Mansour, V.H. Platinum Compounds: A New Class of Potent Antitumour Agents. *Nature* **1969**, *222*, 385–386.
27. Monneret, C. Platinum Anticancer Drugs. From Serendipity to Rational Design. *Ann Pharm Fr* 2011, *69*, 286–295.
28. Ho, G.Y.; Woodward, N.; Coward, J.I.G. Cisplatin versus Carboplatin: Comparative Review of Therapeutic Management in Solid Malignancies. *Crit Rev Oncol Hematol* 2016, *102*, 37–46.
29. Alcindor, T.; Beauger, N. Oxaliplatin: A Review in the Era of Molecularly Targeted Therapy. *Current Oncology* **2011**, *18*, doi:https://doi.org/10.3747%2Fco.v18i1.708.
30. Shimada, M.; Itamochi, H.; Kigawa, J. Nedaplatin: A Cisplatin Derivative in Cancer Chemotherapy. *Cancer Manag Res* 2013, *5*, 67–76.
31. Choi, C.H.; Cha, Y.J.; An, C.S.; Kim, K.J.; Kim, K.C.; Moon, S.P.; Lee, Z.H.; Min, Y.D. Molecular Mechanisms of Heptaplatin Effective against Cisplatin-Resistant Cancer Cell Lines: Less Involvement of Metallothionein. *Cancer Cell Int* **2004**, *4*, doi:10.1186/1475-2867-4-6.
32. Mckeage, M.J. Lobaplatin: A New Antitumour Platinum Drug. *Exp. Opin. Invest. Drugs* **2001**, *10*, 119–128, doi:https://doi.org/10.1517/13543784.10.1.119.

33. Johnstone, T.C.; Park, G.Y.; Lippard, S.J. Understanding and Improving Platinum Anticancer Drugs-Phenanthriplatin. *Anticancer Res.* **2014**, *34*, 471–476.
34. Carl, G.R.G.; Morris, R.; Atkins, L.M.; Smith, A.B. *Binding of an Antitumor Platinum Compound to Cells as Influenced by Physical Factors and Pharmacologically Active Agents*; 1973; Vol. 33;.
35. Ishida, S.; Lee, J.; Thiele, D.J.; Herskowitz, I. Uptake of the Anticancer Drug Cisplatin Mediated by the Copper Transporter Ctr1 in Yeast and Mammals. *Proceedings of the National Academy of Sciences* **2002**, *99*, 14298–14302.
36. Ciarimboli, G.; Ludwig, T.; Lang, D.; Pavenstä, H.; Koepsell, H.; Rgen Piechota, H.-J.; Rg Haier, J.; Jaehde, U.; Zisowsky, J.; Schlatter, E. *Cisplatin Nephrotoxicity Is Critically Mediated via the Human Organic Cation Transporter 2*; 2005; Vol. 167;.
37. Howell, S.B.; Safaei, R.; Larson, C.A.; Sailor, M.J. Copper Transporters and the Cellular Pharmacology of the Platinum-Containing Cancer Drugs. *Mol Pharmacol* 2010, *77*, 887–894.
38. Bompiani, K.M.; Tsai, C.Y.; Achatz, F.P.; Liebig, J.K.; Howell, S.B. Copper Transporters and Chaperones CTR1, CTR2, ATOX1, and CCS as Determinants of Cisplatin Sensitivity. *Metallomics* **2016**, *8*, 951–962, doi:10.1039/c6mt00076b.
39. Akerfeldt, M.C.; Tran, C.M.N.; Shen, C.; Hambley, T.W.; New, E.J. Interactions of Cisplatin and the Copper Transporter CTR1 in Human Colon Cancer Cells. *Journal of Biological Inorganic Chemistry* **2017**, *22*, 765–774, doi:10.1007/s00775-017-1467-y.
40. Zhou, J.; Kang, Y.; Chen, L.; Wang, H.; Liu, J.; Zeng, S.; Yu, L. The Drug-Resistance Mechanisms of Five Platinum-Based Antitumor Agents. *Front Pharmacol* 2020, *11*.
41. Ober, M.; Lippard, S.J. A 1,2-d(GpG) Cisplatin Intrastrand Cross-Link Influences the Rotational and Translational Setting of DNA in Nucleosomes. *J Am Chem Soc* **2008**, *130*, 2851–2861, doi:10.1021/ja710220x.
42. Dasari, S.; Bernard Tchounwou, P. Cisplatin in Cancer Therapy: Molecular Mechanisms of Action. *Eur J Pharmacol* 2014, *740*, 364–378.
43. Chaney, S.G.; Campbell, S.L.; Bassett, E.; Wu, Y. Recognition and Processing of Cisplatin- and Oxaliplatin-DNA Adducts. *Crit Rev Oncol Hematol* 2005, *53*, 3–11.
44. Browning, R.J.; Reardon, P.J.T.; Parhizkar, M.; Pedley, R.B.; Edirisinghe, M.; Knowles, J.C.; Stride, E. Drug Delivery Strategies for Platinum-Based Chemotherapy. *ACS Nano* **2017**, *11*, 8560–8578, doi:10.1021/acsnano.7b04092.
45. Arnesano, F.; Natile, G. Interference between Copper Transport Systems and Platinum Drugs. *Semin Cancer Biol* **2021**, *76*, 173–188, doi:10.1016/j.semcancer.2021.05.023.
46. Siddik, Z.H. Cisplatin: Mode of Cytotoxic Action and Molecular Basis of Resistance. *Oncogene* 2003, *22*, 7265–7279.
47. Fujii, R. -i; Mutoh, M.; Niwa, K.; Yamada, K.; Aikou, T.; Nakagawa, M.; Kuwano, M.; Akiyama, S. -i Active Efflux System for Cisplatin in Cisplatin-resistant Human KB Cells.

- Japanese Journal of Cancer Research* **1994**, *85*, 426–433, doi:10.1111/j.1349-7006.1994.tb02376.x.
48. Kuo, M.T.; Chen, H.H.W. Role of Glutathione in the Regulation of Cisplatin Resistance in Cancer Chemotherapy. *Met Based Drugs* 2010, *2010*.
  49. Chu, G. Cellular Responses to Cisplatin: The Roles Of DNA-Binding Proteins And DNA Repair. *Journal of Biological Chemistry* **1994**, *269*, 787–790.
  50. Lambert, I.H.; Sørensen, B.H. Facilitating the Cellular Accumulation of Pt-Based Chemotherapeutic Drugs. *Int J Mol Sci* 2018, *19*.
  51. Shen, D.W.; Pouliot, L.M.; Hall, M.D.; Gottesman, M.M. Cisplatin Resistance: A Cellular Self-Defense Mechanism Resulting from Multiple Epigenetic and Genetic Changes. *Pharmacol Rev* **2012**, *64*, 706–721, doi:10.1124/pr.111.005637.
  52. Florea, A.M.; Büsselberg, D. Cisplatin as an Anti-Tumor Drug: Cellular Mechanisms of Activity, Drug Resistance and Induced Side Effects. *Cancers (Basel)* 2011, *3*, 1351–1371.
  53. Miller, R.P.; Tadagavadi, R.K.; Ramesh, G.; Reeves, W.B. Mechanisms of Cisplatin Nephrotoxicity. *Toxins (Basel)* 2010, *2*, 2490–2518.
  54. Callejo, A.; Sedó-Cabezón, L.; Juan, I.D.; Llorens, J. Cisplatin-Induced Ototoxicity: Effects, Mechanisms and Protection Strategies. *Toxics* 2015, *3*, 268–293.
  55. Kanat, O.; Ertas, H.; Caner, B. Platinum-Induced Neurotoxicity: A Review of Possible Mechanisms. *World J Clin Oncol* 2017, *8*, 329–333.
  56. Hu, Y.; Sun, B.; Zhao, B.; Mei, D.; Gu, Q.; Tian, Z. Cisplatin-Induced Cardiotoxicity with Midrange Ejection Fraction: A Case Report and Review of the Literature. *Medicine (United States)* 2018, *97*.
  57. Ohno', S.; Strebel', F.R.; Stephens2, L.C.; Siddik3, Z.H.; Babal4, H.; Makino', M.; Khokhar3, A.R.; Bull', J.M.C. *Haematological Toxicity of Carboplatin and Cisplatin Combined with Whole Body Hyperthermia in Rats*; 1993;
  58. Taghizadeh, F.; Hosseinimehr, S.J.; Zargari, M.; Karimpour Malekshah, A.; Mirzaei, M.; Talebpour Amiri, F. Alleviation of Cisplatin-Induced Hepatotoxicity by Gliclazide: Involvement of Oxidative Stress and Caspase-3 Activity. *Pharmacol Res Perspect* **2021**, *9*, doi:10.1002/prp2.788.
  59. Shahid, F.; Farooqui, Z.; Khan, F. Cisplatin-Induced Gastrointestinal Toxicity: An Update on Possible Mechanisms and on Available Gastroprotective Strategies. *Eur J Pharmacol* 2018, *827*, 49–57.
  60. Oun, R.; Moussa, Y.E.; Wheate, N.J. The Side Effects of Platinum-Based Chemotherapy Drugs: A Review for Chemists. *Dalton Transactions* 2018, *47*, 6645–6653.
  61. Zhang, C.; Xu, C.; Gao, X.; Yao, Q. Platinum-Based Drugs for Cancer Therapy and Anti-Tumor Strategies. *Theranostics* 2022, *12*, 2115–2132.

62. Gustavsson, B.; Carlsson, G.; MacHover, D.; Petrelli, N.; Roth, A.; Schmoll, H.J.; Tveit, K.M.; Gibson, F. A Review of the Evolution of Systemic Chemotherapy in the Management of Colorectal Cancer. *Clin Colorectal Cancer* 2015, 14, 1–10.
63. Terenzi, A.; Pirker, C.; Keppler, B.K.; Berger, W. Anticancer Metal Drugs and Immunogenic Cell Death. *J Inorg Biochem* 2016, 165, 71–79, doi:10.1016/j.jinorgbio.2016.06.021.
64. Zhong, L.Z.; Xu, H.Y.; Zhao, Z.M.; Zhang, G.M.; Lin, F.W. Comparison of Efficacy and Toxicity between Nedaplatin and Cisplatin in Treating Malignant Pleural Effusion. *Onco Targets Ther* 2018, 11, 5509–5512, doi:10.2147/OTT.S168391.
65. Wang, Z.; Xu, L.; Wang, H.; Li, Z.; Lu, L.; Li, X.; Zhang, Q. Lobaplatin-Based Regimens Outperform Cisplatin for Metastatic Breast Cancer after Anthracyclines and Taxanes Treatment. *Saudi J Biol Sci* 2018, 25, 909–916, doi:10.1016/j.sjbs.2018.01.011.
66. Wu, Y.; Xu, X.Y.; Yan, F.; Sun, W.L.; Zhang, Y.; Liu, D.L.; Shen, B. Retrospective Study of the Efficacy and Toxicity of Lobaplatin in Combined Chemotherapy for Metastatic Breast Cancer. *Onco Targets Ther* 2019, 12, 4849–4857, doi:10.2147/OTT.S192373.
67. Zhou, N.N.; Zhao, Y.Y.; Zhai, L.Z.; Ruan, C.M.; Yang, Y.P.; Huang, Y.; Hou, X.; Chen, L.K.; Zhou, T.; Zhang, L. The Efficacy and Toxicity of Lobaplatin-Contained Chemotherapy in Extensive-Stage Small-Cell Lung Cancer. *J Cancer* 2018, 9, 2232–2236, doi:10.7150/jca.24557.
68. Li, H.; Gao, X.; Liu, R.; Wang, Y.; Zhang, M.; Fu, Z.; Mi, Y.; Wang, Y.; Yao, Z.; Gao, Q. *Glucose Conjugated Platinum(II) Complex: Antitumor Superiority to Oxaliplatin, Combination Effect and Mechanism of Action*; 2015; Vol. 101; ISBN 1351247913.
69. Gabano, E.; Cassino, C.; Bonetti, S.; Prandi, C.; Colangelo, D.; Ghiglia, A.; Osella, D. Synthesis and Characterisation of Estrogenic Carriers for Cytotoxic Pt(II) Fragments: Biological Activity of the Resulting Complexes. *Org Biomol Chem* 2005, 3, 3531–3539, doi:10.1039/b507716h.
70. Hall, M.D.; Dillon, C.T.; Zhang, M.; Beale, P.; Cai, Z.; Lai, B.; Stampfl, A.P.J.; Hambley, T.W. The Cellular Distribution and Oxidation State of Platinum(II) and Platinum(IV) Antitumour Complexes in Cancer Cells. *Journal of Biological Inorganic Chemistry* 2003, 8, 726–732, doi:10.1007/s00775-003-0471-6.
71. Ilangovan, G.; Li, H.; Zweier, J.L.; Kuppasamy, P. *In Vivo Measurement of Tumor Redox Environment Using EPR Spectroscopy*; 2002; Vol. 234;.
72. Kosthunova, H.; Petruzzella, E.; Gibson, D.; Kasparkova, J.; Brabec, V. An Anticancer Pt IV Prodrug That Acts by Mechanisms Involving DNA Damage and Different Epigenetic Effects. *Chemistry - A European Journal* 2019, 25, 5235–5245, doi:10.1002/chem.201805626.
73. Babu, T.; Ghareeb, H.; Basu, U.; Schueffl, H.; Theiner, S.; Heffeter, P.; Koellensperger, G.; Metanis, N.; Gandin, V.; Ott, I.; et al. Oral Anticancer Heterobimetallic PtIV–AuI Complexes Show High In Vivo Activity and Low Toxicity. *Angewandte Chemie - International Edition* 2023, 62, doi:10.1002/anie.202217233.

74. Spector, D.; Krasnovskaya, O.; Pavlov, K.; Erofeev, A.; Gorelkin, P.; Beloglazkina, E.; Majouga, A. Pt(IV) Prodrugs with Nsaids as Axial Ligands. *Int J Mol Sci* 2021, 22.
75. Cheng, Q.; Shi, H.; Wang, H.; Wang, J.; Liu, Y. Asplatin Enhances Drug Efficacy by Altering the Cellular Response. *Metallomics* 2016, 8, 672–678, doi:10.1039/c6mt00066e.
76. Johnstone, T.C.; Pil, P.M.; Lippard, S.J. Cisplatin and Related Drugs. In *Reference Module in Biomedical Sciences*; Elsevier, 2015.
77. Liu, X.; Barth, M.C.; Cseh, K.; Kowol, C.R.; Jakupec, M.A.; Keppler, B.K.; Gibson, D.; Weigand, W. Oxoplatin-Based Pt(IV) Lipoate Complexes and Their Biological Activity. *Chem Biodivers* 2022, 19, doi:10.1002/cbdv.202200695.
78. Liu, X.; Wenisch, D.; Barth, M.C.; Cseh, K.; Kowol, C.R.; Jakupec, M.A.; Gibson, D.; Keppler, B.K.; Weigand, W. Novel Oxaliplatin(IV) Complexes Conjugated with Ligands Bearing Pendant 1,2-Dithiolane/1,2-Diselenolane/Cyclopentyl Motifs. *Dalton Transactions* 2022, 51, 16824–16835, doi:10.1039/d2dt02217f.
79. Harrap, K.R.; Kelland, L.R.; Jones, M.; Goddard, P.M.; Orr, R.M.; Morgan, S.E.; Murrer, B.A.; Abrams, M.J.; Giandomenico, C.M.; Cobbleigh, T. *PLATINUM COORDINATION COMPLEXES WHICH CIRCUMVENT CISPLATIN RESISTANCE*;
80. Bhargava, A.; Vaishampayan, U.N. Satraplatin: Leading the New Generation of Oral Platinum Agents. *Expert Opin Investig Drugs* 2009, 18, 1787–1797.
81. Eastman, A. Glutathione-Mediated Activation of Anticancer Platinum(IV) Complexes. *Biochem Pharmacol* 1987, 36, 4177–4178.
82. Rischin, D.; Ling, V. *Ormaplatin Resistance Is Associated with Decreased Accumulation of Its Platinum (II) Analogue, Dichloro(D,L-Trans)1,2-Diaminocyclohexaneplatinum(II)*; 1996; Vol. 74;.
83. Johnstone, T.C.; Suntharalingam, K.; Lippard, S.J. The Next Generation of Platinum Drugs: Targeted Pt(II) Agents, Nanoparticle Delivery, and Pt(IV) Prodrugs. *Chem Rev* 2016, 116, 3436–3486.
84. Pendyala, L.; Krishnan, B.S.; Walsh, J.R.; Arakali, A. V; Cowens, J.W.; Creaven, P.J. *Studies on the Human Metabolism of Iproplatin*; 1989; Vol. 25;.
85. Hall, M.D.; Hambley, T.W. Platinum(IV) Antitumour Compounds: Their Bioinorganic Chemistry. *Coord Chem Rev* 2002, 232, 49–67.
86. Wheate, N.J.; Walker, S.; Craig, G.E.; Oun, R. The Status of Platinum Anticancer Drugs in the Clinic and in Clinical Trials. *Dalton Transactions* 2010, 39, 8113–8127, doi:10.1039/c0dt00292e.
87. Bouchal, P.; Jarkovsky, J.; Hrazdilova, K.; Dvorakova, M.; Struharova, I.; Hernychova, L.; Damborsky, J.; Sova, P.; Vojtesek, B. The New Platinum-Based Anticancer Agent LA-12 Induces Retinol Binding Protein 4 in Vivo. *Proteome Science* 2011, 9.
88. Kvardova, V.; Hrstka, R.; Walerych, D.; Muller, P.; Matoulkova, E.; Hruskova, V.; Stelcova, D.; Sova, P.; Vojtesek, B. The New Platinum(IV) Derivative LA-12 Shows

- Stronger Inhibitory Effect on Hsp90 Function Compared to Cisplatin. *Mol Cancer* **2010**, *9*, 147.
89. Kenny, R.G.; Marmion, C.J. Toward Multi-Targeted Platinum and Ruthenium Drugs—A New Paradigm in Cancer Drug Treatment Regimens? *Chem Rev* **2019**, *119*, 1058–1137, doi:10.1021/acs.chemrev.8b00271.
90. Ali, R.; Aouida, M.; Sulaiman, A.A.; Madhusudan, S.; Ramotar, D. Can Cisplatin Therapy Be Improved? Pathways That Can Be Targeted. *Int J Mol Sci* **2022**, *23*.
91. Ma, J.; Wang, Q.; Yang, X.; Hao, W.; Huang, Z.; Zhang, J.; Wang, X.; Wang, P.G. Glycosylated Platinum(IV) Prodrugs Demonstrated Significant Therapeutic Efficacy in Cancer Cells and Minimized Side-Effects. *Dalton Transactions* **2016**, *45*, 11830–11838, doi:10.1039/c6dt02207c.
92. Zhao, Z.; Ukidve, A.; Kim, J.; Mitragotri, S. Targeting Strategies for Tissue-Specific Drug Delivery. *Cell* **2020**, *181*, 151–167.
93. Ma, L.; Ma, R.; Wang, Y.; Zhu, X.; Zhang, J.; Chan, H.C.; Chen, X.; Zhang, W.; Chiu, S.-K.; Zhu, G. Chalcoplatin, a Dual-Targeting and P53 Activator-Containing Anticancer Platinum(IV) Prodrug with Unique Mode of Action. *Chemical Communications* **2015**, *51*, 6301–6304, doi:10.1039/C4CC10409A.
94. Ma, J.; Yang, X.; Hao, W.; Huang, Z.; Wang, X.; Wang, P.G. Mono-Functionalized Glycosylated Platinum(IV) Complexes Possessed Both PH and Redox Dual-Responsive Properties: Exhibited Enhanced Safety and Preferentially Accumulated in Cancer Cells in Vitro and in Vivo. *Eur J Med Chem* **2017**, *128*, 45–55, doi:10.1016/j.ejmech.2017.01.032.
95. Ma, J.; Wang, Q.; Huang, Z.; Yang, X.; Nie, Q.; Hao, W.; Wang, P.G.; Wang, X. Glycosylated Platinum(IV) Complexes as Substrates for Glucose Transporters (GLUTs) and Organic Cation Transporters (OCTs) Exhibited Cancer Targeting and Human Serum Albumin Binding Properties for Drug Delivery. *J Med Chem* **2017**, *60*, 5736–5748, doi:10.1021/acs.jmedchem.7b00433.
96. Ma, J.; Liu, H.; Xi, Z.; Hou, J.; Li, Y.; Niu, J.; Liu, T.; Bi, S.; Wang, X.; Wang, C.; et al. Protected and De-Protected Platinum(IV) Glycoconjugates With GLUT1 and OCT2-Mediated Selective Cancer Targeting: Demonstrated Enhanced Transporter-Mediated Cytotoxic Properties in Vitro and in Vivo. *Front Chem* **2018**, *6*, doi:10.3389/fchem.2018.00386.
97. Ndinguri, M.W.; Solipuram, R.; Gambrell, R.P.; Aggarwal, S.; Hammer, R.P. Peptide Targeting of Platinum Anti-Cancer Drugs. *Bioconjug Chem* **2009**, *20*, 1869–1878, doi:10.1021/bc900065r.
98. Kitteringham, E.; McKeon, A.M.; O'Dowd, P.; Devocelle, M.; Murphy, B.M.; Griffith, D.M. Synthesis and Characterisation of a Novel Mono Functionalisable Pt(IV) Oxaliplatin-Type Complex and Its Peptide Conjugate. *Inorganica Chim Acta* **2020**, *505*, doi:10.1016/j.ica.2020.119492.
99. Kitteringham, E.; Andriollo, E.; Gandin, V.; Montagner, D.; Griffith, D.M. Synthesis, Characterisation and in Vitro Antitumour Potential of Novel Pt(II) Estrogen Linked Complexes. *Inorganica Chim Acta* **2019**, *495*, doi:10.1016/j.ica.2019.05.043.



100. Fortin, S.; Brasseur, K.; Morin, N.; Asselin, É.; Bérubé, G. New Platinum(II) Complexes Conjugated at Position 7 $\alpha$  of 17 $\beta$ -Acetyl-Testosterone as New Combi-Molecules against Prostate Cancer: Design, Synthesis, Structure-Activity Relationships and Biological Evaluation. *Eur J Med Chem* **2013**, *68*, 433–443, doi:10.1016/j.ejmech.2013.08.011.
101. del Solar, V.; Contel, M. Metal-Based Antibody Drug Conjugates. Potential and Challenges in Their Application as Targeted Therapies in Cancer. *J Inorg Biochem* **2019**, *199*.
102. Beirne, D.F.; Dalla Via, M.; Velasco-Torrijos, T.; Montagner, D. Metal-Tyrosine Kinase Inhibitors: Targeted Metal-Drug Conjugates. *Coord Chem Rev* **2022**, *469*.
103. Mayer, M.P.; Bukau, B. Hsp70 Chaperones: Cellular Functions and Molecular Mechanism. *Cellular and Molecular Life Sciences* **2005**, *62*, 670–684, doi:10.1007/s00018-004-4464-6.
104. McKeon, A.M.; Noonan, J.; Devocelle, M.; Murphy, B.M.; Griffith, D.M. Platinum(IV) Oxaliplatin-Peptide Conjugates Targeting MemHsp70+ Phenotype in Colorectal Cancer Cells. *Chemical Communications* **2017**, *53*, 11318–11321, doi:10.1039/c7cc04764a.
105. Fronik, P.; Poetsch, I.; Kastner, A.; Mendrina, T.; Hager, S.; Hohenwallner, K.; Schueffl, H.; Herndler-Brandstetter, D.; Koellensperger, G.; Rampler, E.; et al. Structure-Activity Relationships of Triple-Action Platinum(IV) Prodrugs with Albumin-Binding Properties and Immunomodulating Ligands. *J Med Chem* **2021**, *64*, 12132–12151, doi:10.1021/acs.jmedchem.1c00770.
106. Hornyák, L.; Dobos, N.; Koncz, G.; Karányi, Z.; Páll, D.; Szabó, Z.; Halmos, G.; Székvölgyi, L. The Role of Indoleamine-2,3-Dioxygenase in Cancer Development, Diagnostics, and Therapy. *Front Immunol* **2018**, *9*.
107. Barnes, K.R.; Kutikov, A.; Lippard, S.J. Synthesis, Characterization, and Cytotoxicity of a Series of Estrogen-Tethered Platinum(IV) Complexes The Binding of These Proteins to Platinum-DNA Adducts Modulates the Cytotoxicity of Cisplatin [11-13] and Offers. *Chem Biol* **2004**, *11*, 557–564, doi:10.1016/j.
108. Vaidya, S.P.; Patra, M. Platinum Glycoconjugates: “Sweet Bullets” for Targeted Cancer Therapy? *Curr Opin Chem Biol* **2023**, *72*.
109. Fadaka, A.; Ajiboye, B.; Ojo, O.; Adewale, O.; Olayide, I.; Emuowhochere, R. Biology of Glucose Metabolization in Cancer Cells. *Journal of Oncological Sciences* **2017**, *3*, 45–51, doi:10.1016/j.jons.2017.06.002.
110. Crusio, W.E.; Radeke, H.H. The Heterogeneity of Cancer Metabolism. In *Advances in Experimental Medicine and Biology*; 2021; Vol. 1311, pp. 4–5.
111. Marie, S.K.N.; Shinjo, S.M.O. Metabolism and Brain Cancer. *Clinics* **2011**, *66*, 33–43, doi:10.1590/S1807-59322011001300005.
112. Yu, L.; Chen, X.; Sun, X.; Wang, L.; Chen, S. The Glycolytic Switch in Tumors: How Many Players Are Involved? *J Cancer* **2017**, *8*, 3430–3440.

113. Martínez-Reyes, I.; Chandel, N.S. Cancer Metabolism: Looking Forward. *Nat Rev Cancer* 2021, *21*, 669–680.
114. Diaz-Ruiz, R.; Rigoulet, M.; Devin, A. The Warburg and Crabtree Effects: On the Origin of Cancer Cell Energy Metabolism and of Yeast Glucose Repression. *Biochim Biophys Acta Bioenerg* 2011, *1807*, 568–576.
115. Diaz-Ruiz, R.; Uribe-Carvajal, S.; Devin, A.; Rigoulet, M. Tumor Cell Energy Metabolism and Its Common Features with Yeast Metabolism. *Biochim Biophys Acta Rev Cancer* 2009, *1796*, 252–265.
116. Infantino, V.; Santarsiero, A.; Convertini, P.; Todisco, S.; Iacobazzi, V. Cancer Cell Metabolism in Hypoxia: Role of HIF-1 as Key Regulator and Therapeutic Target. *Int J Mol Sci* 2021, *22*.
117. Xie, H.; Simon, M.C. Oxygen Availability and Metabolic Reprogramming in Cancer. *Journal of Biological Chemistry* 2017, *292*, 16825–16832.
118. Lin, S.Y.; Chang, H.H.; Lai, Y.H.; Lin, C.H.; Chen, M.H.; Chang, G.C.; Tsai, M.F.; Chen, J.J.W. Digoxin Suppresses Tumor Malignancy through Inhibiting Multiple Src-Related Signaling Pathways in Non-Small Cell Lung Cancer. *PLoS One* **2015**, *10*, doi:10.1371/journal.pone.0123305.
119. Wang, Y.; Ma, Q.; Zhang, S.; Liu, H.; Zhao, B.; Du, B.; Wang, W.; Lin, P.; Zhang, Z.; Zhong, Y.; et al. Digoxin Enhances the Anticancer Effect on Non-Small Cell Lung Cancer While Reducing the Cardiotoxicity of Adriamycin. *Front Pharmacol* **2020**, *11*, doi:10.3389/fphar.2020.00186.
120. Xiang, L.; Gilkes, D.M.; Chaturvedi, P.; Luo, W.; Hu, H.; Takano, N.; Liang, H.; Semenza, G.L. Ganetespib Blocks HIF-1 Activity and Inhibits Tumor Growth, Vascularization, Stem Cell Maintenance, Invasion, and Metastasis in Orthotopic Mouse Models of Triple-Negative Breast Cancer. *J Mol Med* **2014**, *92*, 151–164, doi:10.1007/s00109-013-1102-5.
121. Youssef, M.E.; Cavalu, S.; Hasan, A.M.; Yahya, G.; Abd-Eldayem, M.A.; Saber, S. Role of Ganetespib, an HSP90 Inhibitor, in Cancer Therapy: From Molecular Mechanisms to Clinical Practice. *Int J Mol Sci* 2023, *24*.
122. Cho, H.; Lee, H.Y.; Ahn, D.R.; Sang, Y.K.; Kim, S.; Keun, B.L.; You, M.L.; Park, H.; Eun, G.Y. Baicalein Induces Functional Hypoxia-Inducible Factor-1 $\alpha$  and Angiogenesis. *Mol Pharmacol* **2008**, *74*, 70–81, doi:10.1124/mol.107.040162.
123. Liu, Y.; Venna, C.K.; Morgan, J.B.; Mohammed, K.A.; Jekabsons, M.B.; Nagle, D.G.; Zhou, Y.D. Methylalpinumisoflavone Inhibits Hypoxia-Inducible Factor-1 (HIF-1) Activation by Simultaneously Targeting Multiple Pathways. *Journal of Biological Chemistry* **2009**, *284*, 5859–5868, doi:10.1074/jbc.M806744200.
124. Liu, Y.; Wang, X.; Li, W.; Xu, Y.; Zhuo, Y.; Li, M.; He, Y.; Wang, X.; Guo, Q.; Zhao, L.; et al. Oroxylin A Reverses Hypoxia-Induced Cisplatin Resistance through Inhibiting HIF-1 $\alpha$  Mediated XPC Transcription. *Oncogene* **2020**, *39*, 6893–6905, doi:10.1038/s41388-020-01474-x.

125. Thomas, R.; Kim, M.H. Epigallocatechin Gallate Inhibits HIF-1 $\alpha$  Degradation in Prostate Cancer Cells. *Biochem Biophys Res Commun* **2005**, *334*, 543–548, doi:10.1016/j.bbrc.2005.06.114.
126. Srivani, G.; Behera, S.K.; Dariya, B.; Aliya, S.; Alam, A.; Nagaraju, G.P. Resveratrol Binds and Inhibits Transcription Factor HIF-1 $\alpha$  in Pancreatic Cancer. *Exp Cell Res* **2020**, *394*, doi:10.1016/j.yexcr.2020.112126.
127. Sharma, A.; Sinha, S.; Shrivastava, N. Therapeutic Targeting Hypoxia-Inducible Factor (HIF-1) in Cancer: Cutting Gordian Knot of Cancer Cell Metabolism. *Front Genet* **2022**, *13*.
128. Mueckler, M.; Thorens, B. The SLC2 (GLUT) Family of Membrane Transporters. *Mol Aspects Med* **2013**, *34*, 121–138.
129. Deng, D.; Xu, C.; Sun, P.; Wu, J.; Yan, C.; Hu, M.; Yan, N. Crystal Structure of the Human Glucose Transporter GLUT1. *Nature* **2014**, *510*, 121–125, doi:10.1038/nature13306.
130. Custódio, T.F.; Paulsen, P.A.; Frain, K.M.; Pedersen, B.P. Structural Comparison of GLUT1 to GLUT3 Reveal Transport Regulation Mechanism in Sugar Porter Family. *Life Sci Alliance* **2021**, *4*, doi:10.26508/LSA.202000858.
131. Cura, A.J.; Carruthers, A. Role of Monosaccharide Transport Proteins in Carbohydrate Assimilation, Distribution, Metabolism, and Homeostasis. *Compr Physiol* **2012**, *2*, 863–914, doi:10.1002/cphy.c110024.
132. Holman, G.D. Structure, Function and Regulation of Mammalian Glucose Transporters of the SLC2 Family. *European Journal of Physiology* **2020**, *472*, 1155–1175, doi:10.1007/s00424-020-02411-3/Published.
133. Barnett, J.E.G.; Holman, G.D.; Munday, K.A. *Structural Requirements for Binding to the Sugar-Transport System of the Human Erythrocyte*; 1973; Vol. 131;.
134. Deng, D.; Sun, P.; Yan, C.; Ke, M.; Jiang, X.; Xiong, L.; Ren, W.; Hirata, K.; Yamamoto, M.; Fan, S.; et al. Molecular Basis of Ligand Recognition and Transport by Glucose Transporters. *Nature* **2015**, *526*, 391–396, doi:10.1038/nature14655.
135. Patra, M.; Awuah, S.G.; Lippard, S.J. Chemical Approach to Positional Isomers of Glucose-Platinum Conjugates Reveals Specific Cancer Targeting through Glucose-Transporter-Mediated Uptake in Vitro and in Vivo. *J Am Chem Soc* **2016**, *138*, 12541–12551, doi:10.1021/jacs.6b06937.
136. Calvaresi, E.C.; Hergenrother, P.J. Glucose Conjugation for the Specific Targeting and Treatment of Cancer. *Chem Sci* **2013**, *4*, 2319–2333, doi:10.1039/c3sc22205e.
137. Carbó, R.; Rodríguez, E. Relevance of Sugar Transport across the Cell Membrane. *Int J Mol Sci* **2023**, *24*.
138. Pauwels, E.K.J.; Sturm, E.J.C.; Bombardieri, E.; Cleton, F.J.; Stokkel, M.P.M. Positron-Emission Tomography with [ <sup>18</sup>F ]Fluorodeoxyglucose. *J Cancer Res Clin Oncol* **2000**, *126*, 549–559.

139. Sung, Y.; Tetrault, M.A.; Takahashi, K.; Ouyang, J.; Pratz, G.; Fakhri, G. El; Normandin, M.D. Dependence of Fluorodeoxyglucose (FDG) Uptake on Cell Cycle and Dry Mass: A Single-Cell Study Using a Multi-Modal Radiography Platform. *Sci Rep* **2020**, *10*, doi:10.1038/s41598-020-59515-0.
140. Hwang, J.; Yi, M.; Zhang, X.; Xu, Y.; Jung, J.H.; Kim, D.K. Cytochalasin B Induces Apoptosis through the Mitochondrial Apoptotic Pathway in HeLa Human Cervical Carcinoma Cells. *Oncol Rep* **2013**, *30*, 1929–1935, doi:10.3892/or.2013.2617.
141. Carter, S.B. Effects of Cytochalasins on Mammalian Cells. *Nature* **1967**, *213*, 261–264.
142. Malawista, S.E.; Gee, J.B.L.; Bensch, K.G. Cytochalasin B Reversibly Inhibits Phagocytosis: Functional, Metabolic, and Ultrastructural Effects in Human Blood Leukocytes and Rabbit Alveolar Macrophages. *Yale Journal of Biology and Medicine* **1971**, *44*, 286–300.
143. Klaus, G.G. Dissociation of Pinocytosis and Phagocytosis by Peritoneal Macrophages. *Exp Cell Res* **1973**, *79*, 73–78.
144. Schofield, J.G. Cytochalasin B and Release of Growth Hormone. *Nat New Biol* **1971**, *234*, 215–216.
145. Estensen, R.D.; Plagemann, P.G.W.; Davis, E.L.; Quie, R.D. & Immunol, J. Cytochalasin B: Inhibition of Glucose and Glucosamine Transport. *Proc. Nat. Acad. Sci.* **1972**, *69*, 1430–1434.
146. Kapoor, K.; Finer-Moore, J.S.; Pedersen, B.P.; Caboni, L.; Waight, A.; Hillig, R.C.; Bringmann, P.; Heisler, I.; Müller, T.; Siebeneicher, H.; et al. Mechanism of Inhibition of Human Glucose Transporter GLUT1 Is Conserved between Cytochalasin B and Phenylalanine Amides. *Proc Natl Acad Sci U S A* **2016**, *113*, 4711–4716, doi:10.1073/pnas.1603735113.
147. Gunnink, L.K.; Alabi, O.D.; Kuiper, B.D.; Gunnink, S.M.; Schuiteman, S.J.; Strohhenn, L.E.; Hamilton, K.E.; Wrobel, K.E.; Louters, L.L. Curcumin Directly Inhibits the Transport Activity of GLUT1. *Biochimie* **2016**, *125*, 179–185, doi:10.1016/j.biochi.2016.03.014.
148. Zhan, T.; Digel, M.; Küch, E.M.; Stremmel, W.; Füllekrug, J. Silybin and Dehydrosilybin Decrease Glucose Uptake by Inhibiting GLUT Proteins. *J Cell Biochem* **2011**, *112*, 849–859, doi:10.1002/jcb.22984.
149. Hytti, M.; Ruuth, J.; Kanerva, I.; Bhattarai, N.; Pedersen, M.L.; Nielsen, C.U.; Kauppinen, A. Phloretin Inhibits Glucose Transport and Reduces Inflammation in Human Retinal Pigment Epithelial Cells. *Mol Cell Biochem* **2023**, *478*, 215–227, doi:10.1007/s11010-022-04504-2.
150. Ehrenkranz, J.R.L.; Lewis, N.G.; Kahn, C.R.; Roth, J. Phlorizin: A Review. *Diabetes Metab Res Rev* **2005**, *21*, 31–38.
151. Amsler, K.; Cook, J.S.; COOK Development, J.S. Development of Na<sup>+</sup>-Dependent Hexose Transport in a Cultured Line of Porcine Kidney Cells. *J. Gen. Physiol* **1980**, *87*, 94–101.

152. Niu, W.Y.; Bilan, P.J.; Hayashi, M.; Da, Y.R.; Yao, Z. Insulin Sensitivity and Inhibition by Forskolin, Dipyrindamole and Pentobarbital of Glucose Transport in Three L6 Muscle Cell Lines. *Sci China C Life Sci* **2007**, *50*, 739–747, doi:10.1007/s11427-007-0088-z.
153. Pohl, J.; Bertram, • B; Hilgard, • P; Nowrousian, • M R; Stuben, J.; Wiel3ler, • M *D-19575-a Sugar-Linked Isophosphoramidate Mustard Derivative Exploiting Transmembrane Glucose Transport*; Springer-Verlag, 1995; Vol. 35;.
154. Calvaresi, E.C.; Hergenrother, P.J. Glucose Conjugation for the Specific Targeting and Treatment of Cancer. *Chem Sci* **2013**, *4*, 2319–2333, doi:10.1039/c3sc22205e.
155. Hartinger, C.G.; Nazarov, A.A.; Ashraf, S.M.; Dyson, P.J.; Keppler, B.-H.K. *Carbohydrate-Metal Complexes and Their Potential as Anticancer Agents*; 2008; Vol. 15;.
156. Liu, P.; Lu, Y.; Gao, X.; Liu, R.; Zhang-Negrerie, D.; Shi, Y.; Wang, Y.; Wang, S.; Gao, Q. Highly Water-Soluble Platinum(II) Complexes as GLUT Substrates for Targeted Therapy: Improved Anticancer Efficacy and Transporter-Mediated Cytotoxic Properties. *Chemical Communications* **2013**, *49*, 2421–2423, doi:10.1039/c3cc38589b.
157. Li, H.; Gao, X.; Liu, R.; Wang, Y.; Zhang, M.; Fu, Z.; Mi, Y.; Wang, Y.; Yao, Z.; Gao, Q. Glucose Conjugated Platinum(II) Complex: Antitumor Superiority to Oxaliplatin, Combination Effect and Mechanism of Action. *Eur J Med Chem* **2015**, *101*, 400–408, doi:10.1016/j.ejmech.2015.07.006.
158. Liu, R.; Fu, Z.; Zhao, M.; Gao, X.; Li, H.; Mi, Q.; Liu, P.; Yang, J.; Yao, Z.; Gao, Q. *GLUT1-Mediated Selective Tumor Targeting with Fluorine Containing Platinum(II) Glycoconjugates*; 2017;.
159. Mueckler, M.; Makepeace, C. Identification of an Amino Acid Residue That Lies between the Exofacial Vestibule and Exofacial Substrate-Binding Site of the Glut1 Sugar Permeation Pathway. *J Biol Chem* **1997**, *272*, 30141–30146.
160. Mi, Q.; Ma, Y.; Gao, X.; Liu, R.; Liu, P.; Mi, Y.; Fu, X.; Gao, Q. 2-Deoxyglucose Conjugated Platinum (II) Complexes for Targeted Therapy: Design, Synthesis, and Antitumor Activity. *J Biomol Struct Dyn* **2016**, *34*, 2339–2350, doi:10.1080/07391102.2015.1114972.
161. Patra, M.; Johnstone, T.C.; Suntharalingam, K.; Lippard, S.J. A Potent Glucose-Platinum Conjugate Exploits Glucose Transporters and Preferentially Accumulates in Cancer Cells. *Angewandte Chemie* **2016**, *128*, 2596–2600, doi:10.1002/ange.201510551.
162. Liu, R.; Li, H.; Gao, X.; Mi, Q.; Zhao, H.; Gao, Q. Mannose-Conjugated Platinum Complexes Reveals Effective Tumor Targeting Mediated by Glucose Transporter 1. *Biochem Biophys Res Commun* **2017**, *487*, 34–40, doi:10.1016/j.bbrc.2017.04.004.
163. Li, T.; Gao, X.; Yang, L.; Shi, Y.; Gao, Q. Methyl 6-Amino-6-Deoxy- d -Pyranoside-Conjugated Platinum(II) Complexes for Glucose Transporter (GLUT)-Mediated Tumor Targeting: Synthesis, Cytotoxicity, and Cellular Uptake Mechanism. *ChemMedChem* **2016**, *11*, 1069–1077, doi:10.1002/cmdc.201600079.

164. Han, J.; Gao, X.; Liu, R.; Yang, J.; Zhang, M.; Mi, Y.; Shi, Y.; Gao, Q. Design, Synthesis of Novel Platinum(II) Glycoconjugates, and Evaluation of Their Antitumor Effects. *Chem Biol Drug Des* **2016**, *87*, 867–877, doi:10.1111/cbdd.12718.
165. Gao, X.; Liu, S.; Shi, Y.; Huang, Z.; Mi, Y.; Mi, Q.; Yang, J.; Gao, Q. Mechanistic and Biological Characteristics of Different Sugar Conjugated 2-Methyl Malonatoplatinum(II) Complexes as New Tumor Targeting Agents. *Eur J Med Chem* **2017**, *125*, 372–384, doi:10.1016/j.ejmech.2016.09.047.
166. Gibson, D. The Mechanism of Action of Platinum Anticancer Agents - What Do We Really Know about It? *Dalton Transactions* **2009**, 10681–10689, doi:10.1039/b913896j.
167. Ma, J.; Wang, Q.; Yang, X.; Hao, W.; Huang, Z.; Zhang, J.; Wang, X.; Wang, P.G. Glycosylated Platinum(IV) Prodrugs Demonstrated Significant Therapeutic Efficacy in Cancer Cells and Minimized Side-Effects. *Dalton Transactions* **2016**, *45*, 11830–11838, doi:10.1039/c6dt02207c.
168. Zheng, Y.R.; Suntharalingam, K.; Johnstone, T.C.; Yoo, H.; Lin, W.; Brooks, J.G.; Lippard, S.J. Pt(IV) Prodrugs Designed to Bind Non-Covalently to Human Serum Albumin for Drug Delivery. *J Am Chem Soc* **2014**, *136*, 8790–8798, doi:10.1021/ja5038269.
169. Krishtalik, L.I. PH-Dependent Redox Potential: How to Use It Correctly in the activation Energy Analysis. *Biochemica et Biophysica acta* **2003**, *1604*, 13–21.
170. Ma, J.; Yang, X.; Hao, W.; Huang, Z.; Wang, X.; Wang, P.G. Mono-Functionalized Glycosylated Platinum(IV) Complexes Possessed Both PH and Redox Dual-Responsive Properties: Exhibited Enhanced Safety and Preferentially Accumulated in Cancer Cells in Vitro and in Vivo. *Eur J Med Chem* **2017**, *128*, 45–55, doi:10.1016/j.ejmech.2017.01.032.
171. Ma, J.; Liu, H.; Xi, Z.; Hou, J.; Li, Y.; Niu, J.; Liu, T.; Bi, S.; Wang, X.; Wang, C.; et al. Protected and De-Protected Platinum(IV) Glycoconjugates With GLUT1 and OCT2-Mediated Selective Cancer Targeting: Demonstrated Enhanced Transporter-Mediated Cytotoxic Properties in Vitro and in Vivo. *Front Chem* **2018**, *6*, doi:10.3389/fchem.2018.00386.
172. Bononi, G.; Iacopini, D.; Cicio, G.; Di Pietro, S.; Granchi, C.; Di Bussolo, V.; Minutolo, F. Glycoconjugated Metal Complexes as Cancer Diagnostic and Therapeutic Agents. *ChemMedChem* **2021**, *16*, 30–64.
173. Lee, S.Y.; Kim, C.Y.; Nam, T.G. Ruthenium Complexes as Anticancer Agents: A Brief History and Perspectives. *Drug Des Devel Ther* **2020**, *14*, 5375–5392, doi:10.2147/DDDT.S275007.
174. Dobrucki, J.W. *Interaction of Oxygen-Sensitive Luminescent Probes Ru(Phen) and Ru(Bipy) with Animal and Plant Cells in Vitro 3 Mechanism of Phototoxicity and Conditions for Non-Invasive Oxygen Measurements*; 2001; Vol. 65;.
175. Gottschaldt, M.; Schubert, U.S.; Rau, S.; Yano, S.; Vos, J.G.; Kroll, T.; Clement, J.; Hilger, I. Sugar-Selective Enrichment of a D-Glucose-Substituted Ruthenium

- Bipyridyl Complex inside HepG2 Cancer Cells. *ChemBioChem* **2010**, *11*, 649–652, doi:10.1002/cbic.200900769.
176. Godoy, A.; Ulloa, V.; Rodríguez, F.; Reinicke, K.; Yañez, A.J.; De Los Angeles García, M.; Medina, R.A.; Carrasco, M.; Barberis, S.; Castro, T.; et al. Differential Subcellular Distribution of Glucose Transporters GLUT1-6 and GLUT9 in Human Cancer: Ultrastructural Localization of GLUT1 and GLUT5 in Breast Tumor Tissues. *J Cell Physiol* **2006**, *207*, 614–627, doi:10.1002/jcp.20606.
177. Bairwa, K.; Grover, J.; Kania, M.; Jachak, S.M. Recent Developments in Chemistry and Biology of Curcumin Analogues. *RSC Adv* **2014**, *4*, 13946–13978.
178. Pröhl, M.; Bus, T.; Czaplowska, J.A.; Traeger, A.; Deicke, M.; Weiss, H.; Weigand, W.; Schubert, U.S.; Gottschaldt, M. Synthesis and in Vitro Toxicity of D-Glucose and d-Fructose Conjugated Curcumin–Ruthenium Complexes. *Eur J Inorg Chem* **2016**, *2016*, 5197–5204, doi:10.1002/ejic.201600801.
179. Butour, J.; Wimmer, S.; Wimmer, F.; Castan, P.; Bandar Seri Begawan, D. *Palladium(II) Compounds with Potential Antitumour Properties and Their Platinum Analogues: A Comparative Study of the Reaction of Some Orotic Acid Derivatives with DNA in Vitro*; 1997; Vol. 104;.
180. Hirohara, S.; Kawasaki, Y.; Funasako, R.; Yasui, N.; Totani, M.; Alitomo, H.; Yuasa, J.; Kawai, T.; Oka, C.; Kawaichi, M.; et al. Sugar and Heavy Atom Effects of Glycoconjugated Chlorin Palladium Complex on Photocytotoxicity. *Bioconjug Chem* **2012**, *23*, 1881–1890, doi:10.1021/bc300223j.
181. Pettenuzzo, A.; Pigot, R.; Ronconi, L. Metal-Based Glycoconjugates and Their Potential in Targeted Anticancer Chemotherapy. *MetalloDrugs* **2016**, *1*, doi:10.1515/medr-2015-0002.
182. Gamberi, T.; Chiappetta, G.; Fiaschi, T.; Modesti, A.; Sorbi, F.; Magherini, F. Upgrade of an Old Drug: Auranofin in Innovative Cancer Therapies to Overcome Drug Resistance and to Increase Drug Effectiveness. *Med Res Rev* **2022**, *42*, 1111–1146.
183. Marzano, C.; Gandin, V.; Folda, A.; Scutari, G.; Bindoli, A.; Rigobello, M.P. Inhibition of Thioredoxin Reductase by Auranofin Induces Apoptosis In-Resistant Human Ovarian Cancer Cells. *Free Radic Biol Med* **2007**, *42*, 872–881.
184. Tong, K.C.; Hu, D.; Wan, P.K.; Lok, C.N.; Che, C.M. Anticancer Gold(III) Compounds With Porphyrin or N-Heterocyclic Carbene Ligands. *Front Chem* **2020**, *8*.
185. Bertrand, B.; Casini, A. A Golden Future in Medicinal Inorganic Chemistry: The Promise of Anticancer Gold Organometallic Compounds. *Dalton Transactions* **2014**, *43*, 4209–4219.
186. Pettenuzzo, A.; Vezzù, K.; Di Paolo, M.L.; Fotopoulou, E.; Marchiò, L.; Via, L.D.; Ronconi, L. Design, Physico-Chemical Characterization And in Vitro Biological Activity of Organogold(III) Glycoconjugates. *Dalton Transactions* **2021**, *50*, 8963–8979, doi:10.1039/d1dt01100f.

187. Dondoni, A. Triazole: The Keystone in Glycosylated Molecular Architectures Constructed by a Click Reaction. *Chem Asian J* **2007**, *2*, 700–708, doi:10.1002/asia.200700015.
188. Rečnik, L.M.; Kandioller, W.; Mindt, T.L. 1,4-Disubstituted 1,2,3-Triazoles as Amide Bond Surrogates for the Stabilisation of Linear Peptides with Biological Activity. *Molecules* **2020**, *25*, doi:10.3390/molecules25163576.
189. Tiwari, V.K.; Mishra, B.B.; Mishra, K.B.; Mishra, N.; Singh, A.S.; Chen, X. Cu-Catalyzed Click Reaction in Carbohydrate Chemistry. *Chem Rev* **2016**, *116*, 3086–3240, doi:10.1021/acs.chemrev.5b00408.
190. Huisgen, R. 1,3-Dipolar Cycloadditions. Past and Future. *Angewandte Chemie International Edition in English* **1963**, *2*, 565–598, doi:10.1002/anie.196305651.
191. Hein, J.E.; Fokin, V. V. Copper-Catalyzed Azide-Alkyne Cycloaddition (CuAAC) and beyond: New Reactivity of Copper(I) Acetylides. *Chem Soc Rev* **2010**, *39*, 1302–1315, doi:10.1039/b904091a.
192. Tornøe, C.W.; Christensen, C.; Meldal, M. Peptidotriazoles on Solid Phase: [1,2,3]-Triazoles by Regiospecific Copper(I)-Catalyzed 1,3-Dipolar Cycloadditions of Terminal Alkynes to Azides. *Journal of Organic Chemistry* **2002**, *67*, 3057–3064, doi:10.1021/jo011148j.
193. Rostovtsev, V. V.; Green, L.G.; Fokin, V. V.; Sharpless, K.B. A Stepwise Huisgen Cycloaddition Process: Copper(I)-Catalyzed Regioselective “Ligation” of Azides and Terminal Alkynes. *Angewandte Chemie - International Edition* **2002**, *41*, 2596–2599, doi:10.1002/1521-3773(20020715)41:14<2596::AID-ANIE2596>3.0.CO;2-4.
194. Fantoni, N.Z.; El-Sagheer, A.H.; Brown, T. A Hitchhiker’s Guide to Click-Chemistry with Nucleic Acids. *Chem Rev* **2021**, *121*, 7122–7154.
195. Tron, G.C.; Pirali, T.; Billington, R.A.; Canonico, P.L.; Sorba, G.; Genazzani, A.A. Click Chemistry Reactions in Medicinal Chemistry: Applications of the 1,3-Dipolar Cycloaddition between Azides and Alkynes. *Med Res Rev* **2008**, *28*, 278–308.
196. Yang, L.; Chumsae, C.; Kaplan, J.B.; Moulton, K.R.; Wang, D.; Lee, D.H.; Zhou, Z.S. Detection of Alkynes via Click Chemistry with a Brominated Coumarin Azide by Simultaneous Fluorescence and Isotopic Signatures in Mass Spectrometry. *Bioconjug Chem* **2017**, *28*, 2302–2309, doi:10.1021/acs.bioconjchem.7b00354.
197. Kitteringham, E.; Andriollo, E.; Gandin, V.; Montagner, D.; Griffith, D.M. Synthesis, Characterisation and in Vitro Antitumour Potential of Novel Pt(II) Estrogen Linked Complexes. *Inorganica Chim Acta* **2019**, *495*.
198. Jewett, J.C.; Bertozzi, C.R. Cu-Free Click Cycloaddition Reactions in Chemical Biology. *Chem Soc Rev* **2010**, *39*, 1272–1279, doi:10.1039/b901970g.
199. Yao, K.; Bertran, A.; Howarth, A.; Goicoechea, J.M.; Hare, S.M.; Rees, N.H.; Foroozandeh, M.; Bowen, A.M.; Farrer, N.J. A Visible-Light Photoactivatable Di-Nuclear Pt(IV) Triazolato Azido Complex. *Chemical Communications* **2019**, *55*, 11287–11290, doi:10.1039/c9cc05310g.



200. Kitteringham, E.; Wu, D.; Cheung, S.; Twamley, B.; O'Shea, D.F.; Griffith, D.M. Development of a Novel Carboplatin like Cytoplasmic Trackable near Infrared Fluorophore Conjugate via Strain-Promoted Azide Alkyne Cycloaddition. *J Inorg Biochem* **2018**, *182*, 150–157.
201. Farrer, N.J.; Griffith, D.M. Exploiting Azide–Alkyne Click Chemistry in the Synthesis, Tracking and Targeting of Platinum Anticancer Complexes. *Curr Opin Chem Biol* **2020**, *55*, 59–68.
202. Misaghi, A.; Goldin, A.; Awad, M.; Kulidjian, A.A. Osteosarcoma: A Comprehensive Review. *SICOT J* **2018**, *4*.
203. Vasiliadis, H.S.; Arnaoutoglou, C.; Plakoutsis, S.; Doukas, M.; Batistatou, A.; Xenakis, T.A. Low-Grade Central Osteosarcoma of Distal Femur, Resembling Fibrous Dysplasia. *World J Orthop* **2013**, *4*, 327–332, doi:10.5312/wjo.v4.i4.327.
204. Kimura, Y.; Tomihara, K.; Tachinami, H.; Imaue, S.; Nakamori, K.; Fujiwara, K.; Suzuki, K.; Yasuda, T.; Miwa, S.; Nakayama, E.; et al. Conventional Osteosarcoma of the Mandible Successfully Treated with Radical Surgery and Adjuvant Chemotherapy after Responding Poorly to Neoadjuvant Chemotherapy: A Case Report. *J Med Case Rep* **2017**, *11*, doi:10.1186/s13256-017-1386-0.
205. Agrawal, M.; Patil, A.; James, T.; Kumar, N.; Premalata, C.S. Multifocal Osteosarcoma: Multiple Primaries or Metastases? A Report of Rare Case and Review of Literature. *J Orthop Case Rep* **2020**, *10*, 97–100, doi:10.13107/jocr.2020.v10.i08.1878.
206. Mahajan, A.; Vaish, R.; Desai, S.; Arya, S.; Sable, N.; D'cruz, A.K. Gnathic Osteosarcoma: Clinical, Radiologic, and Pathologic Review of Bone Beard Tumor. *J Glob Oncol* **2016**, *3*, 823–827.
207. Liu, X.-W.; Zi, Y.; Xiang, L.-B.; Han, T.-Y. Periosteal Osteosarcoma: A Review of Clinical Evidence. *Int J Clin Exp Med* **2015**, *8*, 37–44.
208. Prabowo, Y.; Kamal, A.F.; Kodrat, E.; Prasetyo, M.; Maruanaya, S.; Efar, T.S. Parosteal Osteosarcoma: A Benign-Looking Tumour, Amenable to a Variety of Surgical Reconstruction. *Int J Surg Oncol* **2020**, *2020*, doi:10.1155/2020/4807612.
209. Shimatani, A.; Aono, M.; Hoshi, M.; Oebisu, N.; Iwai, T.; Takada, N.; Hara, J.; Nitani, C.; Nakamura, H. Secondary Osteosarcoma in Patients Previously Treated for Childhood Cancer: Three Case Reports. *Mol Clin Oncol* **2018**, doi:10.3892/mco.2018.1752.
210. Zhao, X.; Wu, Q.; Gong, X.; Liu, J.; Ma, Y. Osteosarcoma: A Review of Current and Future Therapeutic Approaches. *Biomed Eng Online* **2021**, *20*.
211. Beird, H.C.; Bielack, S.S.; Flanagan, A.M.; Gill, J.; Heymann, D.; Janeway, K.A.; Livingston, J.A.; Roberts, R.D.; Strauss, S.J.; Gorlick, R. Osteosarcoma. *Nat Rev Dis Primers* **2022**, *8*, doi:10.1038/s41572-022-00409-y.
212. Han, X.; Wang, W.; He, J.; Jiang, L.; Li, X. Osteopontin as a Biomarker for Osteosarcoma Therapy and Prognosis (Review). *Oncol Lett* **2019**, *17*, 2592–2598, doi:10.3892/ol.2019.9905.

213. Hu, Z.; Wen, S.; Huo, Z.; Wang, Q.; Zhao, J.; Wang, Z.; Chen, Y.; Zhang, L.; Zhou, F.; Guo, Z.; et al. Current Status and Prospects of Targeted Therapy for Osteosarcoma. *Cells* **2022**, *11*, doi:10.3390/cells11213507.
214. Tan, G.; Xu, J.; Yu, Q.; Yang, Z.; Zhang, H. The Safety and Efficiency of Photodynamic Therapy for the Treatment of Osteosarcoma: A Systematic Review of in Vitro Experiment and Animal Model Reports. *Photodiagnosis Photodyn Ther* **2022**, *40*, doi:10.1016/j.pdpdt.2022.103093.
215. Desai, S.A.; Manjappa, A.; Khulbe, P. Drug Delivery Nanocarriers and Recent Advances Ventured to Improve Therapeutic Efficacy against Osteosarcoma: An Overview. *J Egypt Natl Canc Inst* **2021**, *33*, doi:10.1186/s43046-021-00059-3.
216. Fan, J.; Mei, J.; Zhang, M.Z.; Yuan, F.; Li, S.Z.; Yu, G.R.; Chen, L.H.; Tang, Q.; Xian, C.J. Clinicopathological Significance of Glucose Transporter Protein-1 Overexpression in Human Osteosarcoma. *Oncol Lett* **2017**, *14*, 2439–2445, doi:10.3892/ol.2017.6437.
217. Feng, Z.; Ou, Y.; Hao, L. The Roles of Glycolysis in Osteosarcoma. *Front Pharmacol* **2022**, *13*, doi:10.3389/fphar.2022.950886.
218. Zhang, Q.; Wu, J.; Zhang, X.; Cao, L.; Wu, Y.; Miao, X. Transcription Factor ELK1 Accelerates Aerobic Glycolysis to Enhance Osteosarcoma Chemoresistance through MiR-134/PTBP1 Signaling. *Aging* **2021**, *13*, 6804–6819.
219. Staehlke, S.; Rebl, H.; Nebe, B. Phenotypic Stability of the Human MG-63 Osteoblastic Cell Line at Different Passages. *Cell Biol Int* **2019**, *43*, 22–32, doi:10.1002/cbin.11073.
220. Hausser, H.-J.; Brenner, R.E. Phenotypic Instability of Saos-2 Cells in Long-Term Culture. *Biochem Biophys Res Commun* **2005**, *333*, 216–222.
221. Mohseny, A.B.; MacHado, I.; Cai, Y.; Schaefer, K.L.; Serra, M.; Hogendoorn, P.C.W.; Llombart-Bosch, A.; Cleton-Jansen, A.M. Functional Characterization of Osteosarcoma Cell Lines Provides Representative Models to Study the Human Disease. *Laboratory Investigation* **2011**, *91*, 1195–1205, doi:10.1038/labinvest.2011.72.
222. Czekanska, E.M.; Stoddart, M.J.; Ralphs, J.R.; Richards, R.G.; Hayes, J.S. A Phenotypic Comparison of Osteoblast Cell Lines versus Human Primary Osteoblasts for Biomaterials Testing. *J Biomed Mater Res A* **2014**, *102*, 2636–2643, doi:10.1002/jbm.a.34937.
223. Iaquinta, M.R.; Mazzoni, E.; Bononi, I.; Rotondo, J.C.; Mazziotta, C.; Montesi, M.; Sprio, S.; Tampieri, A.; Tognon, M.; Martini, F. Adult Stem Cells for Bone Regeneration and Repair. *Front Cell Dev Biol* **2019**, *7*.
224. Bassi, G.; Panseri, S.; Dozio, S.M.; Sandri, M.; Campodoni, E.; Dapporto, M.; Sprio, S.; Tampieri, A.; Montesi, M. Scaffold-Based 3D Cellular Models Mimicking the Heterogeneity of Osteosarcoma Stem Cell Niche. *Sci Rep* **2020**, *10*, doi:10.1038/s41598-020-79448-y.

225. Yang, L.; Shi, P.; Zhao, G.; Xu, J.; Peng, W.; Zhang, J.; Zhang, G.; Wang, X.; Dong, Z.; Chen, F.; et al. Targeting Cancer Stem Cell Pathways for Cancer Therapy. *Signal Transduct Target Ther* 2020, 5.
226. Siclari, V.A.; Qin, L. Targeting the Osteosarcoma Cancer Stem Cell. *J Orthop Surg Res* 2010, 5, doi:10.1186/1749-799X-5-78.
227. Wang, Q.; Huang, Z.; Ma, J.; Lu, X.; Zhang, L.; Wang, X.; George Wang, P. Design, Synthesis and Biological Evaluation of a Novel Series of Glycosylated Platinum(IV) Complexes as Antitumor Agents. *Dalton Transactions* 2016, 45, 10366–10374, doi:10.1039/c6dt01562j.
228. Upadhyaya, K.; Hamidullah; Singh, K.; Arun, A.; Shukla, M.; Srivastava, N.; Ashraf, R.; Sharma, A.; Mahar, R.; Shukla, S.K.; et al. Identification of Gallic Acid Based Glycoconjugates as a Novel Tubulin Polymerization Inhibitors. *Org Biomol Chem* 2016, 14, 1338–1358, doi:10.1039/c5ob02113h.
229. Rečnik, L.M.; Kandioller, W.; Mindt, T.L. 1,4-Disubstituted 1,2,3-Triazoles as Amide Bond Surrogates for the Stabilisation of Linear Peptides with Biological Activity. *Molecules* 2020, 25, doi:10.3390/molecules25163576.
230. Moynihan, E.; Bassi, G.; Ruffini, A.; Panseri, S.; Montesi, M.; Velasco-Torrijos, T.; Montagner, D. Click Pt(IV)-Carbohydrates Pro-Drugs for Treatment of Osteosarcoma. *Front Chem* 2021, 9, doi:10.3389/fchem.2021.795997.
231. Badáa, C.; Souard, F.; Vicent, C. Sugar-Oligoamides: Synthesis of DNA Minor Groove Binders. *Journal of Organic Chemistry* 2012, 77, 10870–10881, doi:10.1021/jo302238u.
232. Reddy, A.; Ramos-Ondono, J.; Abbey, L.; Velasco-Torrijos, T. 2-Chloroethyl and 2-Azidoethyl 2,3,4,6-Tetra-O-Acetyl- $\beta$ -D-Gluco- and  $\beta$ -D-Galactopyranosides. In *Carbohydrate Chemistry: Proven Synthetic Methods, Volume 4*; Murphy, P., Vogel, C., Eds.; 2017; pp. 201–208 ISBN 9781498726917.
233. Davis, B.G.; Fairbanks, A.J. *Carbohydrate Chemistry*; Oxford University Press, USA, 2002; ISBN 978-0-19-855833-0.
234. Haldón, E.; Nicasio, M.C.; Pérez, P.J. Copper-Catalysed Azide-Alkyne Cycloadditions (CuAAC): An Update. *Org Biomol Chem* 2015, 13, 9528–9550, doi:10.1039/c5ob01457c.
235. Bock, V.D.; Hiemstra, H.; Van Maarseveen, J.H. Cu I-Catalyzed Alkyne-Azide “Click” Cycloadditions from a Mechanistic and Synthetic Perspective. *European J Org Chem* 2006, 51–68, doi:10.1002/ejoc.200500483.
236. Rostovtsev, V. V.; Green, L.G.; Fokin, V. V.; Sharpless, K.B. A Stepwise Huisgen Cycloaddition Process: Copper(I)-Catalyzed Regioselective “Ligation” of Azides and Terminal Alkynes. *Angewandte Chemie - International Edition* 2002, 41, 2596–2599, doi:10.1002/1521-3773(20020715)41:14<2596::AID-ANIE2596>3.0.CO;2-4.
237. Zhu, L.; Brassard, C.J.; Zhang, X.; Guha, P.M.; Clark, R.J. On the Mechanism of Copper(I)-Catalyzed Azide–Alkyne Cycloaddition. *Chemical Record* 2016, 1501–1517, doi:10.1002/tcr.201600002.

238. Jin, L.; Tolentino, D.R.; Melaimi, M.; Bertrand, G. Isolation of Bis(Copper) Key Intermediates in Cu-Catalyzed Azide-Alkyne "click Reaction. *Sci Adv* **2015**, *1*, doi:10.1126/sciadv.1500304.
239. Nolte, C.; Mayer, P.; Straub, B.F. Isolation of a Copper(I) Triazolide: A "Click" Intermediate. *Angewandte Chemie - International Edition* **2007**, *46*, 2101–2103, doi:10.1002/anie.200604444.
240. Iacobucci, C.; Reale, S.; Gal, J.F.; De Angelis, F. Dinuclear Copper Intermediates in Copper(I)-Catalyzed Azide-Alkyne Cycloaddition Directly Observed by Electrospray Ionization Mass Spectrometry. *Angewandte Chemie - International Edition* **2015**, *54*, 3065–3068, doi:10.1002/anie.201410301.
241. Worrell, B.T.; Malik, J.A.; Folkin, V. V. Direct Evidence of a Dinuclear Copper Intermediate in Cu(I)-Catalyzed Azide-Alkyne Cycloadditions. *Science (1979)* **2013**, *340*, 457–460, doi:10.1126/science.1232139.
242. Mangunuru, H.P.R.; Yerabolu, J.R.; Liu, D.; Wang, G. Synthesis of a Series of Glucosyl Triazole Derivatives and Their Self-Assembling Properties. *Tetrahedron Lett* **2015**, *56*, 82–85, doi:10.1016/j.tetlet.2014.11.013.
243. Kinnory, D.S.; Takeda, Y.; Greenberg, D.M. Chromatography of Carboxylic Acids on a Silica Gel Column with a Benzene-Ether Solvent System. *Journal of Biological Chemistry* **1955**, *212*, 379–383.
244. Xu, Z.; Wang, Z.; Deng, S.; Zhu, G. Recent Advances in the Synthesis, Stability, and Activation of Platinum(IV) Anticancer Prodrugs. *Coord Chem Rev* **2021**, *442*, 213991.
245. Babu, T.; Sarkar, A.; Karmakar, S.; Schmidt, C.; Gibson, D. Multi-action Pt(IV) Carbamate Complexes Can Codeliver Pt(II) Drugs and Amine Containing Bioactive Molecules. *Inorg Chem* **2020**, *59*, 5182–5193, doi:10.1021/acs.inorgchem.0c00445.
246. Babu, T.; Ghareeb, H.; Basu, U.; Schueffl, H.; Theiner, S.; Heffeter, P.; Koellensperger, G.; Metanis, N.; Gandin, V.; Ott, I.; et al. Oral Anticancer Heterobimetallic PtIV–AuI Complexes Show High In Vivo Activity and Low Toxicity. *Angewandte Chemie - International Edition* **2023**, *62*, doi:10.1002/anie.202217233.
247. Chen, S.; Ng, K.Y.; Zhou, Q.; Yao, H.; Deng, Z.; Tse, M.K.; Zhu, G. The Influence of Different Carbonate Ligands on the Hydrolytic Stability and Reduction of Platinum(. *Dalton Transactions* **2022**, *51*, 885–897, doi:10.1039/d1dt03959h.
248. Yempala, T.; Babu, T.; Karmakar, S.; Nemirovski, A.; Ishan, M.; Gandin, V.; Gibson, D. Expanding the Arsenal of Pt IV Anticancer Agents: Multi-action Pt IV Anticancer Agents with Bioactive Ligands Possessing a Hydroxy Functional Group . *Angewandte Chemie* **2019**, *131*, 18386–18391, doi:10.1002/ange.201910014.
249. Klykov, O.; Weller, M.G. Quantification of N-Hydroxysuccinimide and N-Hydroxysulfosuccinimide by Hydrophilic Interaction Chromatography (HILIC). *Analytical Methods* **2015**, *7*, 6443–6448, doi:10.1039/c5ay00042d.
250. Lim, C.Y.; Owens, N.A.; Wampler, R.D.; Ying, Y.; Granger, J.H.; Porter, M.D.; Takahashi, M.; Shimazu, K. Succinimidyl Ester Surface Chemistry: Implications of the

- Competition between Aminolysis and Hydrolysis on Covalent Protein Immobilization. *Langmuir* **2014**, *30*, 12868–12878, doi:10.1021/la503439g.
251. Sheehan, J.C.; Cruickshank, P.A.; Boshart, G.L. A Convenient Synthesis of Water-Soluble Carbodiimides. *Org. Syntheses, Coll* **1961**, *26*, 2525–2528.
252. Ghosh, A.K.; Shahabi, D. Synthesis of Amide Derivatives for Electron Deficient Amines and Functionalized Carboxylic Acids Using EDC and DMAP and a Catalytic Amount of HOBt as the Coupling Reagents. *Tetrahedron Lett* **2021**, *63*, doi:10.1016/j.tetlet.2020.152719.
253. Drago, R.S. *Physical Methods for Chemists*; 2nd ed.; Saunders College Pub, 1992, 1992; ISBN 0030751764.
254. Still, B.M.; Kumar, P.G.A.; Aldrich-Wright, J.R.; Price, W.S. 195Pt NMR—Theory and Application. *Chem Soc Rev* **2007**, *36*, 665–686, doi:10.1039/b606190g.
255. Liu, Y.; Feng, X.; Zhang, Y.; Jiang, H.; Cai, X.; Yan, X.; Huang, Z.; Mo, F.; Yang, W.; Yang, C.; et al. Establishment and Characterization of a Novel Osteosarcoma Cell Line: CHOS. *Journal of Orthopaedic Research* **2016**, *34*, 2116–2125, doi:10.1002/jor.23245.
256. Lauvrak, S.U.; Munthe, E.; Kresse, S.H.; Stratford, E.W.; Namløs, H.M.; Meza-Zepeda, L.A.; Myklebost, O. Functional Characterisation of Osteosarcoma Cell Lines and Identification of MRNAs and MiRNAs Associated with Aggressive Cancer Phenotypes. *Br J Cancer* **2013**, *109*, 2228–2236, doi:10.1038/bjc.2013.549.
257. Brown, H.K.; Tellez-Gabriel, M.; Heymann, D. Cancer Stem Cells in Osteosarcoma. *Cancer Lett* **2017**, *386*, 189–195, doi:10.1016/j.canlet.2016.11.019.
258. Deshmukh, A.; Deshpande, K.; Arfuso, F.; Newsholme, P.; Dharmarajan, A. Cancer Stem Cell Metabolism: A Potential Target for Cancer Therapy. *Mol Cancer* **2016**, *15*, 69, doi:10.1186/s12943-016-0555-x.
259. Bouchet, B.P.; Akhmanova, A. Microtubules in 3D Cell Motility. *J Cell Sci* **2017**, *130*, 39–50, doi:10.1242/jcs.189431.
260. Valle, S.; Alcalá, S.; Martin-Hijano, L.; Cabezas-Sáinz, P.; Navarro, D.; Muñoz, E.R.; Yuste, L.; Tiwary, K.; Walter, K.; Ruiz-Cañas, L.; et al. Exploiting Oxidative Phosphorylation to Promote the Stem and Immuno-evasive Properties of Pancreatic Cancer Stem Cells. *Nat Commun* **2020**, *11*, doi:10.1038/s41467-020-18954-z.
261. Zheng, D.; Sussman, J.H.; Jeon, M.P.; Parrish, S.T.; MacMullan, M.A.; Delfarah, A.; Graham, N.A. AKT but Not MYC Promotes Reactive Oxygen Species-Mediated Cell Death in Oxidative Culture. *J Cell Sci* **2020**, *133*, doi:10.1242/jcs.239277.
262. Dhara, S.C. A Rapid Method for the Synthesis of Cis-[Pt(NH<sub>3</sub>)<sub>2</sub>Cl<sub>2</sub>]. *Indian J Chem* **1970**, *8*, 193–194.
263. Brandon, R.J.; Dabrowiak, J.C. Synthesis, Characterization, and Properties, of a Group of Platinum(IV) Complexes. *J Med Chem* **1984**, *27*, 861–865, doi:10.1021/jm00373a009.

264. Bassi, G.; Panseri, S.; Dozio, S.M.; Sandri, M.; Campodoni, E.; Dapporto, M.; Sprio, S.; Tampieri, A.; Montesi, M. Scaffold-Based 3D Cellular Models Mimicking the Heterogeneity of Osteosarcoma Stem Cell Niche. *Sci Rep* **2020**, *10*, 22294, doi:10.1038/s41598-020-79448-y.
265. Ma, J.; Wang, Q.; Huang, Z.; Yang, X.; Nie, Q.; Hao, W.; Wang, P.G.; Wang, X. Glycosylated Platinum(IV) Complexes as Substrates for Glucose Transporters (GLUTs) and Organic Cation Transporters (OCTs) Exhibited Cancer Targeting and Human Serum Albumin Binding Properties for Drug Delivery. *J Med Chem* **2017**, *60*, 5736–5748, doi:10.1021/acs.jmedchem.7b00433.
266. Zheng, Y.R.; Suntharalingam, K.; Johnstone, T.C.; Yoo, H.; Lin, W.; Brooks, J.G.; Lippard, S.J. Pt(IV) Prodrugs Designed to Bind Non-Covalently to Human Serum Albumin for Drug Delivery. *J Am Chem Soc* **2014**, *136*, 8790–8798, doi:10.1021/ja5038269.
267. Moynihan, E.; Panseri, S.; Bassi, G.; Rossi, A.; Campodoni, E.; Dempsey, E.; Montesi, M.; Velasco-Torrijos, T.; Montagner, D. Development of Novel Pt(IV)-Carbohydrate Derivatives as Targeted Anticancer Agents against Osteosarcoma. *Int J Mol Sci* **2023**, *24*, 6028, doi:10.3390/ijms24076028.
268. Meier, L.; Monteiro, G.C.; Baldissera, R.A.M.; Sá, M.M. *Simple Method for Fast Deprotection of Nucleosides by Triethylamine-Catalyzed Methanolysis of Acetates in Aqueous Medium*; 2010; Vol. 21;.
269. Bannwarth, W.; Knorr, R. Formation Of Carboxamides With N,N,N',N'-Tetramethyl (Succinimido) Uronium Tetrafluoroborate In Aqueous / Organic Solvent Systems. *Tetrahedron Lett* **1991**, *32*, 1157–1160.
270. Twibanire, J.D.A.K.; Grindley, T.B. Efficient and Controllably Selective Preparation of Esters Using Uronium-Based Coupling Agents. *Org Lett* **2011**, *13*, 2988–2991, doi:10.1021/ol201005s.
271. Liu, X.; Barth, M.C.; Cseh, K.; Kowol, C.R.; Jakupec, M.A.; Keppler, B.K.; Gibson, D.; Weigand, W. Oxoplatin-Based Pt(IV) Lipoate Complexes and Their Biological Activity. *Chem Biodivers* **2022**, *19*, doi:10.1002/cbdv.202200695.
272. Chen, C.K.J.; Kappen, P.; Gibson, D.; Hambley, T.W. Trans-Platinum(IV) pro-Drugs That Exhibit Unusual Resistance to Reduction by Endogenous Reductants and Blood Serum but Are Rapidly Activated inside Cells: 1H NMR and XANES Spectroscopy Study. *Dalton Transactions* **2020**, *49*, 7722–7736, doi:10.1039/d0dt01622e.
273. Visvader, J.E. Cells of Origin in Cancer. *Nature* **2011**, *469*, 314–322.
274. Cifuentes, M.; García, M.A.; Arrabal, P.M.; Martínez, F.; Yañez, M.J.; Jara, N.; Weil, B.; Domínguez, D.; Medina, R.A.; Nualart, F. Insulin Regulates GLUT1-Mediated Glucose Transport in MG-63 Human Osteosarcoma Cells. *J Cell Physiol* **2011**, *226*, 1425–1432, doi:10.1002/jcp.22668.
275. Arponen, M.; Jalava, N.; Widjaja, N.; Ivaska, K.K. Glucose Transporters GLUT1, GLUT3, and GLUT4 Have Different Effects on Osteoblast Proliferation and Metabolism. *Front Physiol* **2022**, *13*, doi:10.3389/fphys.2022.1035516.

276. Horvath, P.; Aulner, N.; Bickle, M.; Davies, A.M.; Nery, E. Del; Ebner, D.; Montoya, M.C.; Östling, P.; Pietiäinen, V.; Price, L.S.; et al. Screening out Irrelevant Cell-Based Models of Disease. *Nat Rev Drug Discov* 2016, 15, 751–769.
277. Edmondson, R.; Broglie, J.J.; Adcock, A.F.; Yang, L. Three-Dimensional Cell Culture Systems and Their Applications in Drug Discovery and Cell-Based Biosensors. *Assay Drug Dev Technol* 2014, 12, 207–218.
278. Krishnakumar, G.S.; Gostynska, N.; Dapporto, M.; Campodoni, E.; Montesi, M.; Panseri, S.; Tampieri, A.; Kon, E.; Marcacci, M.; Sprio, S.; et al. Evaluation of Different Crosslinking Agents on Hybrid Biomimetic Collagen-Hydroxyapatite Composites for Regenerative Medicine. *Int J Biol Macromol* 2018, 106, 739–748, doi:10.1016/j.ijbiomac.2017.08.076.
279. Bassi, G.; Panseri, S.; Dozio, S.M.; Sandri, M.; Campodoni, E.; Dapporto, M.; Sprio, S.; Tampieri, A.; Montesi, M. Scaffold-Based 3D Cellular Models Mimicking the Heterogeneity of Osteosarcoma Stem Cell Niche. *Sci Rep* 2020, 10, doi:10.1038/s41598-020-79448-y.
280. Dozio, S.M.; Montesi, M.; Campodoni, E.; Sandri, M.; Piattelli, A.; Tampieri, A.; Panseri, S. Differences in Osteogenic Induction of Human Mesenchymal Stem Cells between a Tailored 3D Hybrid Scaffold and a 2D Standard Culture. *J Mater Sci Mater Med* 2019, 30, doi:10.1007/s10856-019-6346-3.
281. Kim, W.H.; Lee, J.; Jung, D.W.; Williams, D.R. Visualizing Sweetness: Increasingly Diverse Applications for Fluorescent-Tagged Glucose Bioprobes and Their Recent Structural Modifications. *Sensors* 2012, 12, 5005–5027, doi:10.3390/s120405005.
282. Bononi, G.; Iacopini, D.; Cicio, G.; Di Pietro, S.; Granchi, C.; Di Bussolo, V.; Minutolo, F. Glycoconjugated Metal Complexes as Cancer Diagnostic and Therapeutic Agents. *ChemMedChem* 2021, 16, 30–64, doi:10.1002/cmdc.202000456.
283. Ahmad, M.G.; Balamurali, M.M.; Chanda, K. Click-Derived Multifunctional Metal Complexes for Diverse Applications. *Chem Soc Rev* 2023, doi:10.1039/d3cs00343d.
284. Pandiakumar, A.K.; Sarma, S.P.; Samuelson, A.G. Mechanistic Studies on the Diazo Transfer Reaction. *Tetrahedron Lett* 2014, 55, 2917–2920.
285. Cheng, J.; Zhao, W.; Yao, H.; Shen, Y.; Zhang, Y.; Li, Y.Z.; Qi, Q.; Wongprasert, K.; Tang, Y.J. Discovery of 4,6- O-Thenylidene-β- d -Glucopyranoside-(2''-Acetamido, 3''-Acetyl-Di- S-5-Fluorobenzothiazole/5-Fluorobenzoxazole)-4'-Demethylepipodophyllotoxin as Potential Less Toxic Antitumor Candidate Drugs by Reducing DNA Damage and Less Inhibition of PI3K. *J Med Chem* 2020, 63, 2877–2893, doi:10.1021/acs.jmedchem.9b01354.
286. Potter, G.T.; Jayson, G.C.; Miller, G.J.; Gardiner, J.M. An Updated Synthesis of the Diazo-Transfer Reagent Imidazole-1-Sulfonyl Azide Hydrogen Sulfate. *Journal of Organic Chemistry* 2016, 81, 3443–3446, doi:10.1021/acs.joc.6b00177.
287. Nyffeler, P.T.; Liang, C.H.; Koeller, K.M.; Wong, C.H. The Chemistry of Amine-Azide Interconversion: Catalytic Diazotransfer and Regioselective Azide Reduction. *J Am Chem Soc* 2002, 124, 10773–10778, doi:10.1021/ja0264605.

288. Nokami, T.; Shibuya, A.; Manabe, S.; Ito, Y.; Yoshida, J.I.  $\alpha$ - and  $\beta$ -Glycosyl Sulfonium Ions: Generation and Reactivity. *Chemistry - A European Journal* **2009**, *15*, 2252–2255, doi:10.1002/chem.200802293.
289. Miller, D.C.; Carbain, B.; Beale, G.S.; Alhasan, S.F.; Reeves, H.L.; Baisch, U.; Newell, D.R.; Golding, B.T.; Griffin, R.J. Regioselective Sulfamoylation at Low Temperature Enables Concise Syntheses of Putative Small Molecule Inhibitors of Sulfatases. *Org Biomol Chem* **2015**, *13*, 5279–5284, doi:10.1039/c5ob00211g.
290. Arimitsu, K.; Yagi, Y.; Koshino, K.; Nishito, Y.; Higuchi, T.; Yasui, H.; Kimura, H. Synthesis of <sup>18</sup>F-Labeled Streptozotocin Derivatives and an in-Vivo Kinetics Study Using Positron Emission Tomography. *Bioorg Med Chem Lett* **2020**, *30*, doi:10.1016/j.bmcl.2020.127400.
291. Martin, H.; Goyard, D.; Margalit, A.; Doherty, K.; Renaudet, O.; Kavanagh, K.; Velasco-Torrijos, T. Multivalent Presentations of Glycomimetic Inhibitor of the Adhesion of Fungal Pathogen *Candida Albicans* to Human Buccal Epithelial Cells. *Bioconjug Chem* **2021**, *32*, 971–982, doi:10.1021/acs.bioconjchem.1c00115.
292. Kolen, M.; Smith, W.A.; Mulder, F.M. Accelerating <sup>1</sup>H NMR Detection of Aqueous Ammonia. *ACS Omega* **2021**, *6*, 5698–5704, doi:10.1021/acsomega.0c06130.
293. Oh, S.; Kim, H.; Nam, K.S.; Shin, I. Glut1 Promotes Cell Proliferation, Migration and Invasion by Regulating Epidermal Growth Factor Receptor and Integrin Signaling in Triple-Negative Breast Cancer Cells. *BMB Rep* **2017**, *50*, 132–137, doi:10.5483/BMBRep.2017.50.3.189.
294. Cheng, J.; Zhao, W.; Yao, H.; Shen, Y.; Zhang, Y.; Li, Y.Z.; Qi, Q.; Wongprasert, K.; Tang, Y.J. Discovery of 4,6- O-Thenylidene- $\beta$ - d -Glucopyranoside-(2''-Acetamido, 3''-Acetyl-Di- S-5-Fluorobenzothiazole/5-Fluorobenzoxazole)-4'-Demethylepipodophyllotoxin as Potential Less Toxic Antitumor Candidate Drugs by Reducing DNA Damage and Less Inhibition of PI3K. *J Med Chem* **2020**, *63*, 2877–2893, doi:10.1021/acs.jmedchem.9b01354.
295. Miller, D.C.; Carbain, B.; Beale, G.S.; Alhasan, S.F.; Reeves, H.L.; Baisch, U.; Newell, D.R.; Golding, B.T.; Griffin, R.J. Regioselective Sulfamoylation at Low Temperature Enables Concise Syntheses of Putative Small Molecule Inhibitors of Sulfatases. *Org Biomol Chem* **2015**, *13*, 5279–5284, doi:10.1039/c5ob00211g.
296. Arimitsu, K.; Yagi, Y.; Koshino, K.; Nishito, Y.; Higuchi, T.; Yasui, H.; Kimura, H. Synthesis of <sup>18</sup>F-Labeled Streptozotocin Derivatives and an in-Vivo Kinetics Study Using Positron Emission Tomography. *Bioorg Med Chem Lett* **2020**, *30*, doi:10.1016/j.bmcl.2020.127400.
297. Sung, H.; Ferlay, J.; Siegel, R.L.; Laversanne, M.; Soerjomataram, I.; Jemal, A.; Bray, F. Global Cancer Statistics 2020: GLOBOCAN Estimates of Incidence and Mortality Worldwide for 36 Cancers in 185 Countries. *CA Cancer J Clin* **2021**, *71*, 209–249, doi:10.3322/caac.21660.
298. Vogel, A.; Meyer, T.; Sapisochin, G.; Salem, R.; Saborowski, A. Hepatocellular Carcinoma. *The Lancet* **2022**, *400*, 1345–1362, doi:10.1016/S0140-6736(22)01200-4.



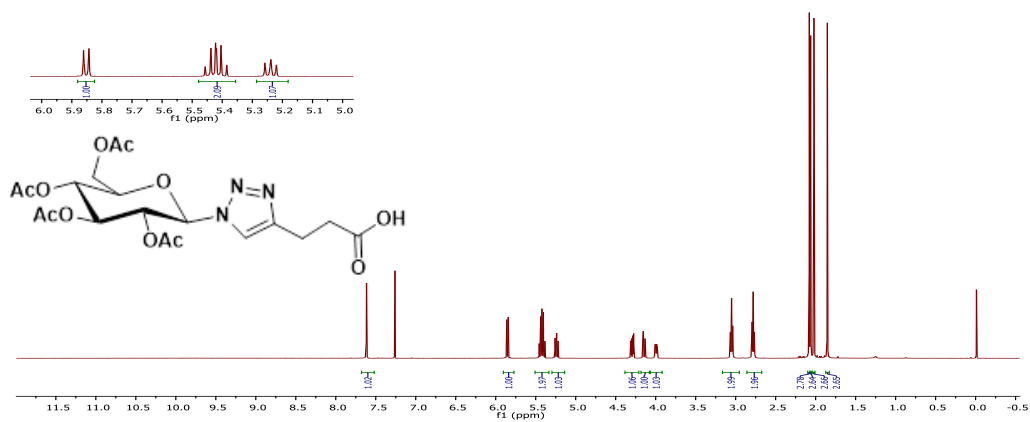
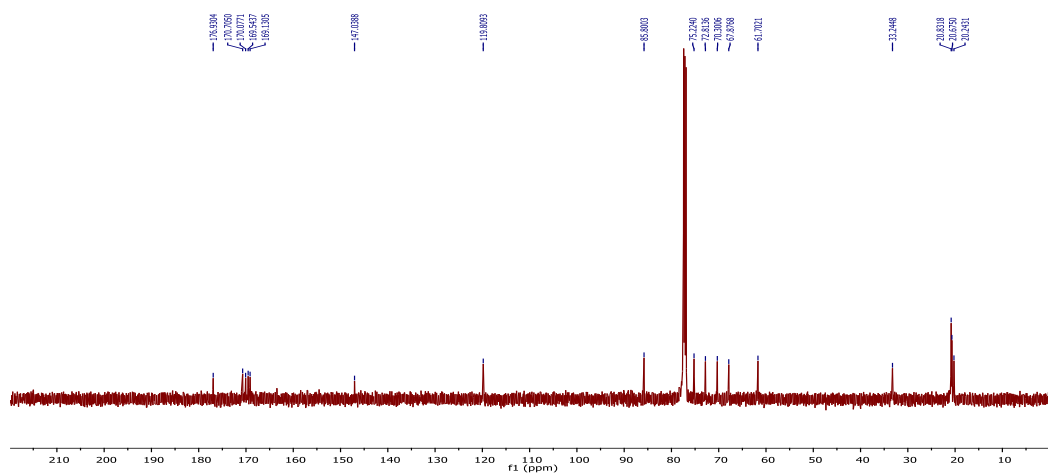
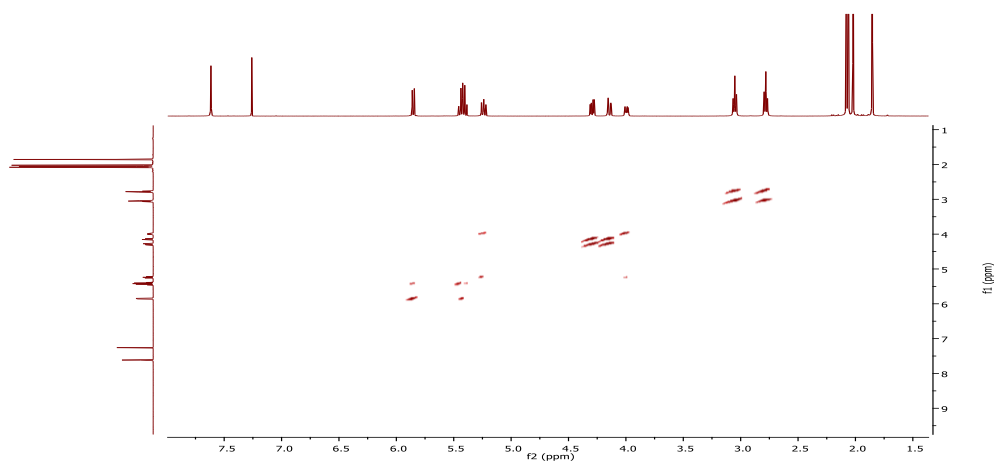
299. Raza, A.; Sood, G.K. Hepatocellular Carcinoma Review: Current Treatment, and Evidence-Based Medicine. *World J Gastroenterol* **2014**, *20*, 4115–4127, doi:10.3748/wjg.v20.i15.4115.
300. Saraswat, V.A.; Pandey, G.; Shetty, S. Treatment Algorithms for Managing Hepatocellular Carcinoma. *J Clin Exp Hepatol* **2014**, *4*, S80–S89, doi:10.1016/j.jceh.2014.05.004.
301. Chow, A.K.-M.; Yau, S.W.-L.; Ng, L. Novel Molecular Targets in Hepatocellular Carcinoma. *World J Clin Oncol* **2020**, *11*, 589–605, doi:10.5306/wjco.v11.i8.589.
302. Huang, A.; Yang, X.R.; Chung, W.Y.; Dennison, A.R.; Zhou, J. Targeted Therapy for Hepatocellular Carcinoma. *Signal Transduct Target Ther* **2020**, *5*, doi:10.1038/s41392-020-00264-x.
303. Huang, K.W.; Lai, Y.T.; Chern, G.J.; Huang, S.F.; Tsai, C.L.; Sung, Y.C.; Chiang, C.C.; Hwang, P.B.; Ho, T.L.; Huang, R.L.; et al. Galactose Derivative-Modified Nanoparticles for Efficient siRNA Delivery to Hepatocellular Carcinoma. *Biomacromolecules* **2018**, *19*, 2330–2339, doi:10.1021/acs.biomac.8b00358.
304. Monestier, M.; Charbonnier, P.; Gateau, C.; Cuillel, M.; Robert, F.; Lebrun, C.; Mintz, E.; Renaudet, O.; Delangle, P. ASGPR-Mediated Uptake of Multivalent Glycoconjugates for Drug Delivery in Hepatocytes. *ChemBioChem* **2016**, *17*, 590–594, doi:10.1002/cbic.201600023.
305. Susan-Resiga, D.; Girard, E.; Essalmani, R.; Roubtsova, A.; Marcinkiewicz, J.; Derbali, R.M.; Evagelidis, A.; Byun, J.H.; Lebeau, P.F.; Austin, R.C.; et al. Asialoglycoprotein Receptor 1 Is a Novel PCSK9-Independent Ligand of Liver LDLR Cleaved by Furin. *Journal of Biological Chemistry* **2021**, *297*, 101177.
306. D'Souza, A.A.; Devarajan, P. V. Asialoglycoprotein Receptor Mediated Hepatocyte Targeting — Strategies and Applications. *Journal of Controlled Release* **2015**, *203*, 126–139.
307. Grewal, P.K. The Ashwell-Morell Receptor. In *Methods in Enzymology*; Academic Press Inc., 2010; Vol. 479, pp. 223–241.
308. D'Souza, A.A.; Jain, P.; Galdhar, C.N.; Samad, A.; Degani, M.S.; Devarajan, P. V. Comparative in Silico-in Vivo Evaluation of ASGP-R Ligands for Hepatic Targeting of Curcumin Gantrez Nanoparticles. *AAPS Journal* **2013**, *15*, 696–706, doi:10.1208/s12248-013-9474-6.
309. Onizuka, T.; Shimizu, H.; Moriwaki, Y.; Nakano, T.; Kanai, S.; Shimada, I.; Takahashi, H. NMR Study of Ligand Release from Asialoglycoprotein Receptor under Solution Conditions in Early Endosomes. *FEBS Journal* **2012**, *279*, 2645–2656, doi:10.1111/j.1742-4658.2012.08643.x.
310. Huang, X.; Leroux, J.C.; Castagner, B. Well-Defined Multivalent Ligands for Hepatocytes Targeting via Asialoglycoprotein Receptor. *Bioconjug Chem* **2017**, *28*, 283–295.
311. Cecioni, S.; Imberty, A.; Vidal, S. Glycomimetics versus Multivalent Glycoconjugates for the Design of High Affinity Lectin Ligands. *Chem Rev* **2015**, *115*, 525–561.

312. Kitov, P.I.; Bundle, D.R. On the Nature of the Multivalency Effect: A Thermodynamic Model. *J Am Chem Soc* **2003**, *125*, 16271–16284, doi:10.1021/ja038223n.
313. Bowman, D.C. A Colorful Look at the Chelate Effect. *J Chem Educ* **2006**, *83*, 1158–1160, doi:10.1021/ed083p1158.
314. Schein, C.H. Protein Aggregation and Precipitation, Measurement and Control. *Encyclopedia of Industrial Biotechnology* **2010**, 1–29.
315. Lundquist, J.J.; Toone, E.J. The Cluster Glycoside Effect. *Chem Rev* **2002**, *102*, 555–578, doi:10.1021/cr000418f.
316. Bai, Z.; Yao, C.; Zhu, J.; Xie, Y.; Ye, X.Y.; Bai, R.; Xie, T. Anti-Tumor Drug Discovery Based on Natural Product  $\beta$ -Elemene: Anti-Tumor Mechanisms and Structural Modification. *Molecules* **2021**, *26*, doi:10.3390/molecules26061499.
317. Wang, M.; Li, Z.; Liu, F.; Yi, Q.; Pu, C.; Li, Y.; Luo, T.; Liang, J.; Wang, J. Development of Asialoglycoprotein-Mediated Hepatocyte-Targeting Antitumor Prodrugs Triggered by Glutathione. *J Med Chem* **2021**, *64*, 14793–14808, doi:10.1021/acs.jmedchem.1c01365.
318. Pujol, A.M.; Cuillel, M.; Jullien, A.S.; Lebrun, C.; Cassio, D.; Mintz, E.; Gateau, C.; Delangle, P. A Sulfur Tripod Glycoconjugate That Releases a High-Affinity Copper Chelator in Hepatocytes. *Angewandte Chemie - International Edition* **2012**, *51*, 7445–7448, doi:10.1002/anie.201203255.
319. Bernardi, A.; Jiménez-Barbero, J.; Casnati, A.; De Castro, C.; Darbre, T.; Fieschi, F.; Finne, J.; Funken, H.; Jaeger, K.E.; Lahmann, M.; et al. Multivalent Glycoconjugates as Anti-Pathogenic Agents. *Chem Soc Rev* **2013**, *42*, 4709–4727, doi:10.1039/c2cs35408j.
320. Anderluh, M.; Berti, F.; Bzducha-Wróbel, A.; Chiodo, F.; Colombo, C.; Compostella, F.; Durlík, K.; Ferhati, X.; Holmdahl, R.; Jovanovic, D.; et al. Recent Advances on Smart Glycoconjugate Vaccines in Infections and Cancer. *FEBS Journal* **2022**, *289*, 4251–4303, doi:10.1111/febs.15909.
321. Hartinger, C.G.; Nazarov, A.A.; Ashraf, S.M.; Dyson, P.J.; Keppler, B.-H.K. *Carbohydrate-Metal Complexes and Their Potential as Anticancer Agents*; 2008; Vol. 15;.
322. Ohya, Y.; Nagatomi, K.; Ouchi, T. Synthesis and Cytotoxic Activity of Macromolecular Prodrug of Cisplatin Using Poly(Ethylene Glycol) with Galactose Residues or Antennary Galactose Units. *Macromol Biosci* **2001**, *1*, 355–363, doi:10.1002/1616-5195(20011101)1:8<355::aid-mabi355>3.0.co;2-q.
323. Martin, H.; Govern, M.M.; Abbey, L.; Gilroy, A.; Mullins, S.; Howell, S.; Kavanagh, K.; Velasco-Torrijos, T. Inhibition of Adherence of the Yeast *Candida Albicans* to Buccal Epithelial Cells by Synthetic Aromatic Glycoconjugates. *Eur J Med Chem* **2018**, *160*, 82–93, doi:10.1016/j.ejmech.2018.10.011.
324. Martin, H.; Somers, T.; Dwyer, M.; Robson, R.; Pfeffer, F.M.; Bjornsson, R.; Krämer, T.; Kavanagh, K.; Velasco-Torrijos, T. Scaffold Diversity for Enhanced Activity of

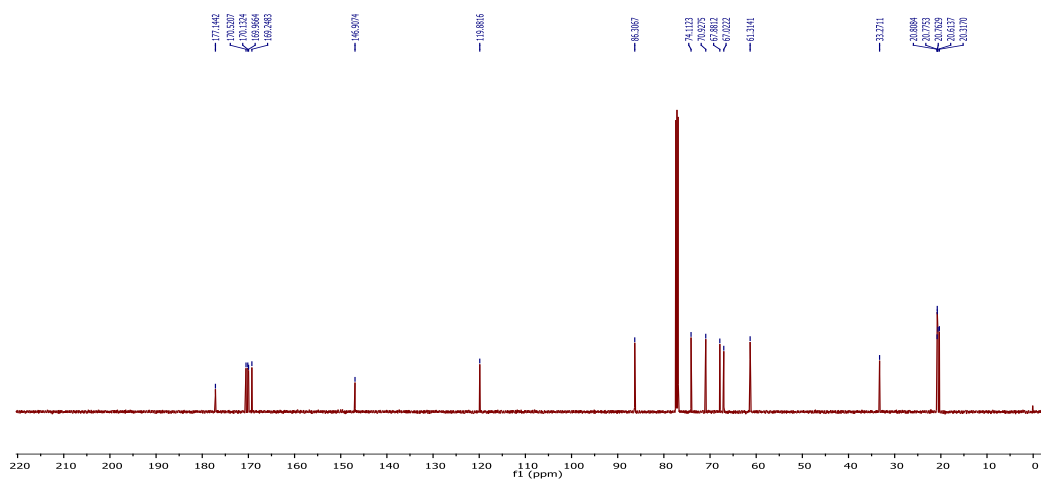
- Glycosylated Inhibitors of Fungal Adhesion. *RSC Med Chem* **2020**, *11*, 1386–1401, doi:10.1039/d0md00224k.
325. Martin, H.; Goyard, D.; Margalit, A.; Doherty, K.; Renaudet, O.; Kavanagh, K.; Velasco-Torrijos, T. Multivalent Presentations of Glycomimetic Inhibitor of the Adhesion of Fungal Pathogen *Candida Albicans* to Human Buccal Epithelial Cells. *Bioconj Chem* **2021**, *32*, 971–982, doi:10.1021/acs.bioconjchem.1c00115.
326. Gilmore, K.; Alabugin, I. V. Cyclizations of Alkynes: Revisiting Baldwin's Rules for Ring Closure. *Chem Rev* **2011**, *111*, 6513–6556, doi:10.1021/cr200164y.
327. Beirne, D.F.; Farkas, B.; Donati, C.; Gandin, V.; Rozas, I.; Velasco-Torrijos, T.; Montagner, D. Novel Design of Dual-Action Pt(IV) Anticancer pro-Drugs Based on Cisplatin and Derivatives of the Tyrosine Kinase Inhibitors Imatinib and Nilotinib. *Dalton Transactions* **2023**, doi:10.1039/D3DT02030D.

# Appendix

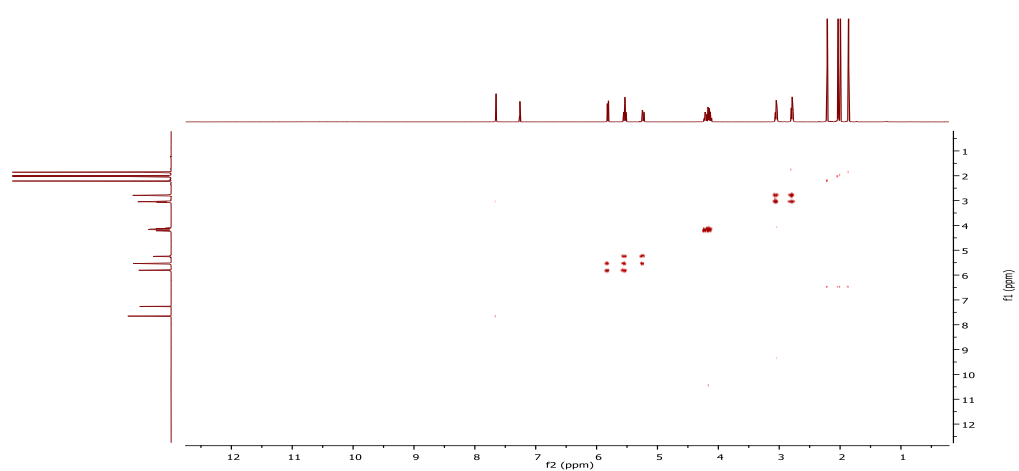
## Chapter 2

NMR spectra of **2.18**<sup>1</sup>H NMR spectrum of **2.18** in CDCl<sub>3</sub><sup>13</sup>C NMR spectrum of **2.18** in CDCl<sub>3</sub>COSY NMR spectrum of **2.18** in CDCl<sub>3</sub>

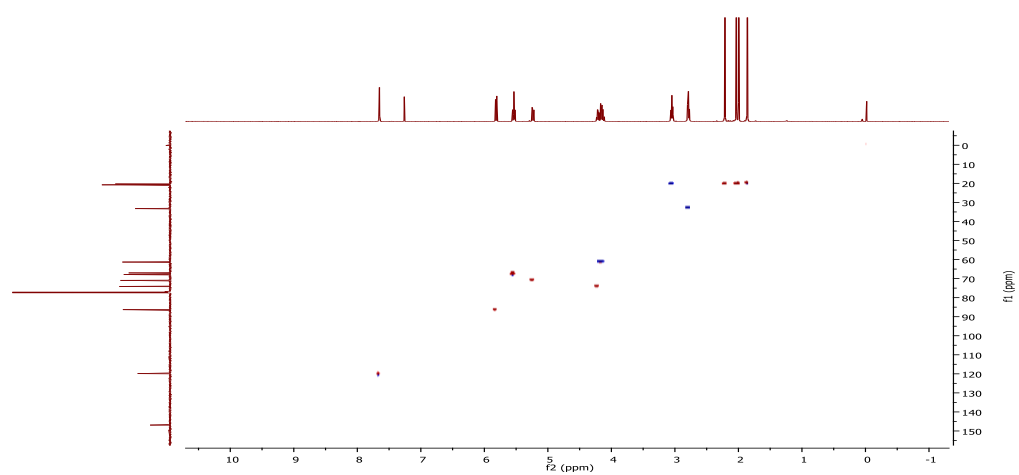




$^{13}\text{C}$  NMR spectrum of **2.19** in  $\text{CDCl}_3$



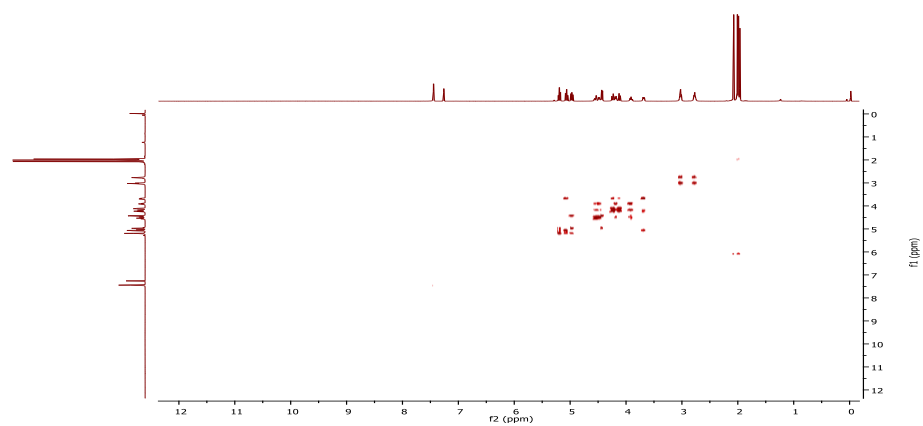
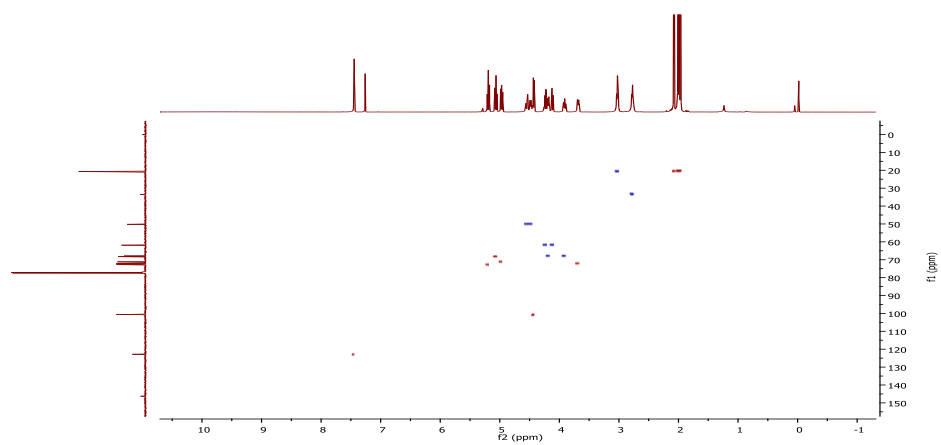
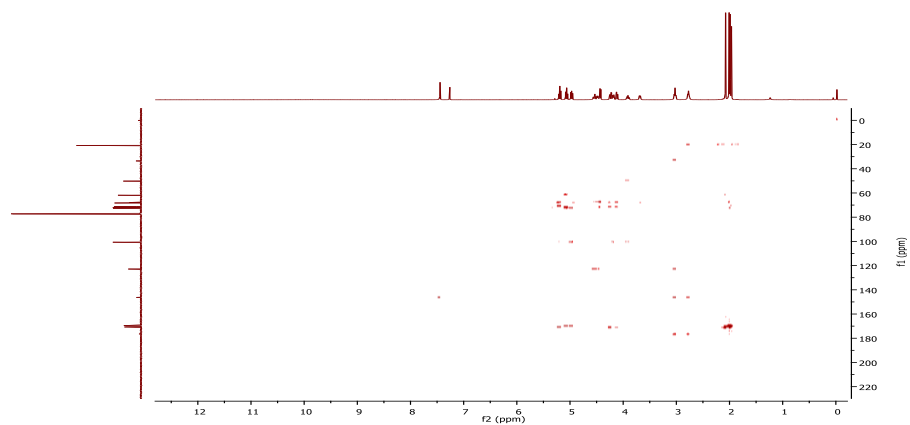
COSY NMR spectrum of **2.19** in  $\text{CDCl}_3$

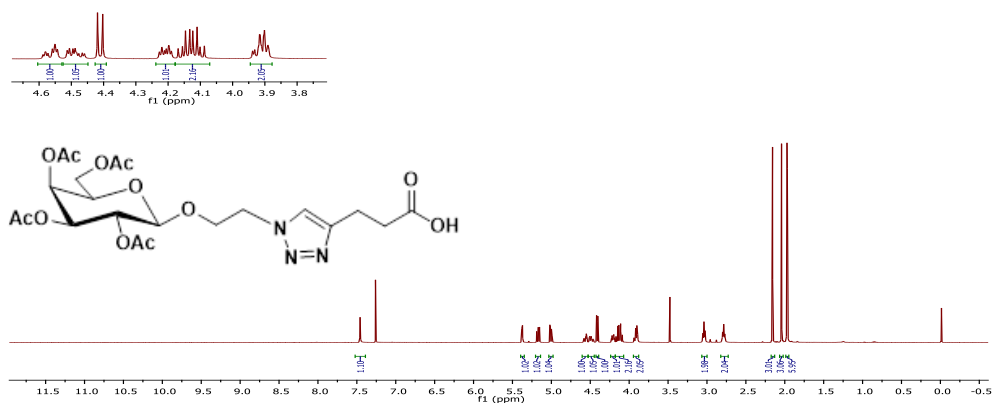
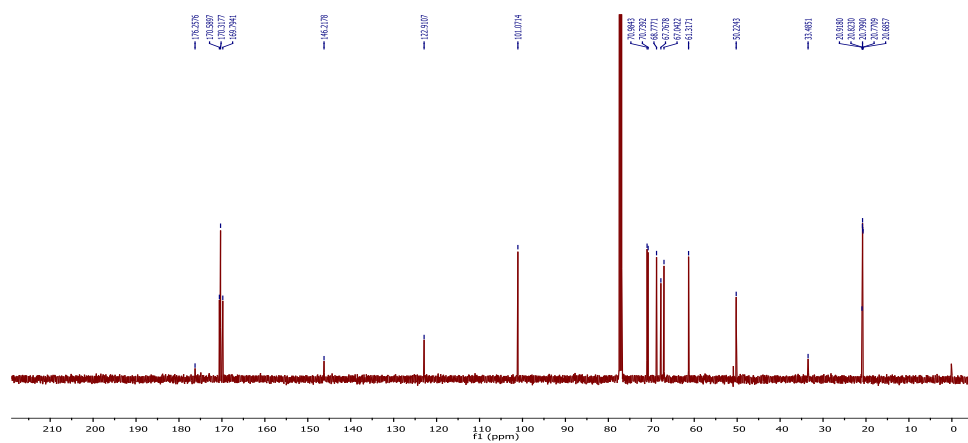
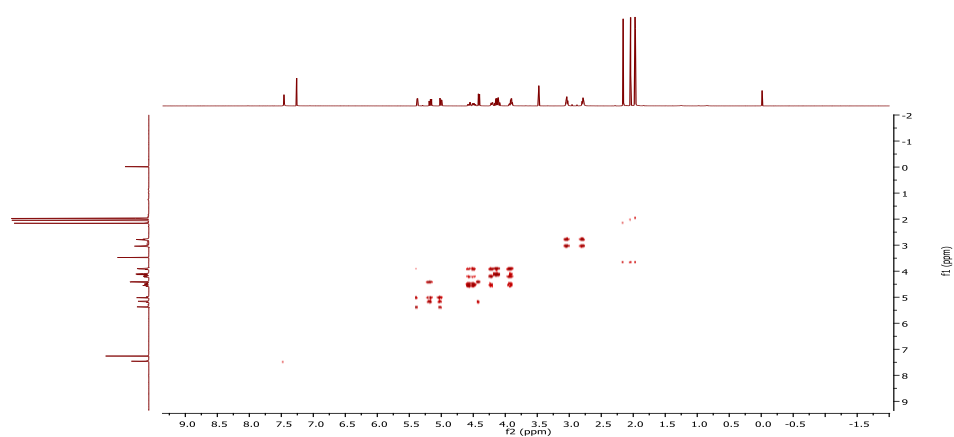


HSQC NMR spectrum of **2.19** in  $\text{CDCl}_3$

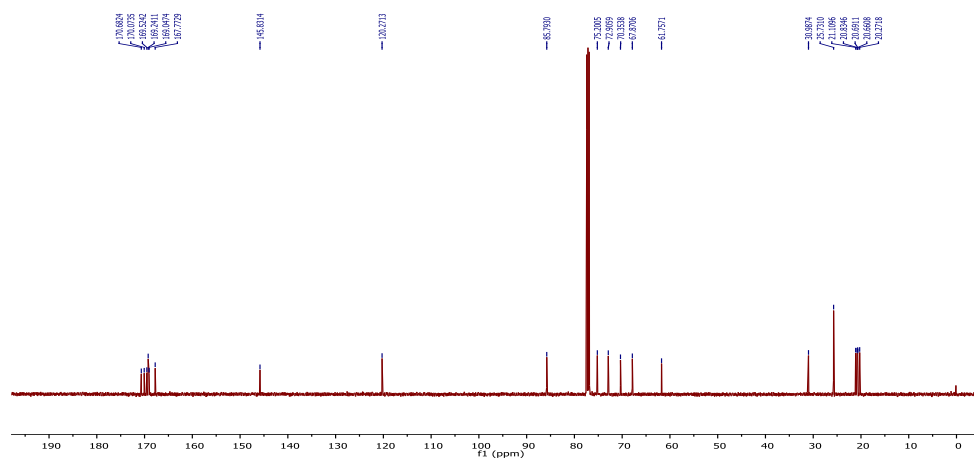




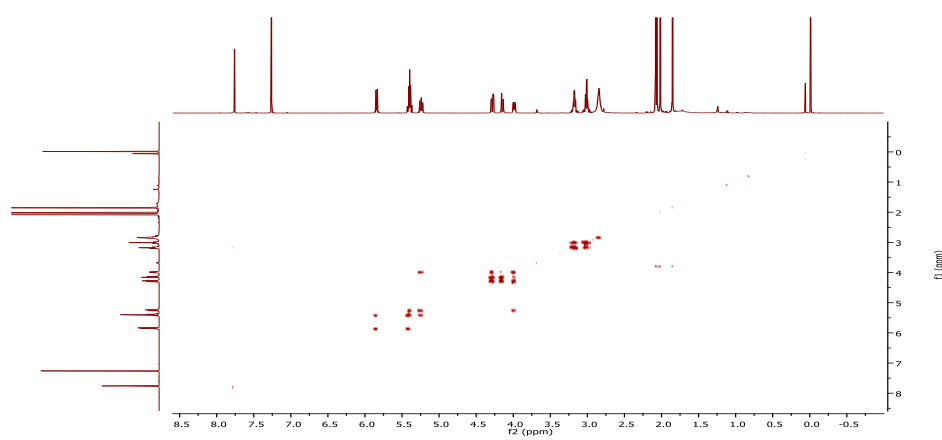
COSY NMR spectrum of **2.26** in CDCl<sub>3</sub>HSQC NMR spectrum of **2.26** in CDCl<sub>3</sub>HMBC NMR spectrum of **2.26** in CDCl<sub>3</sub>

NMR spectra of **2.27** $^1\text{H}$  NMR spectrum of **2.27** in  $\text{CDCl}_3$  $^{13}\text{C}$  NMR spectrum of **2.27** in  $\text{CDCl}_3$ COSY NMR spectrum of **2.27** in  $\text{CDCl}_3$

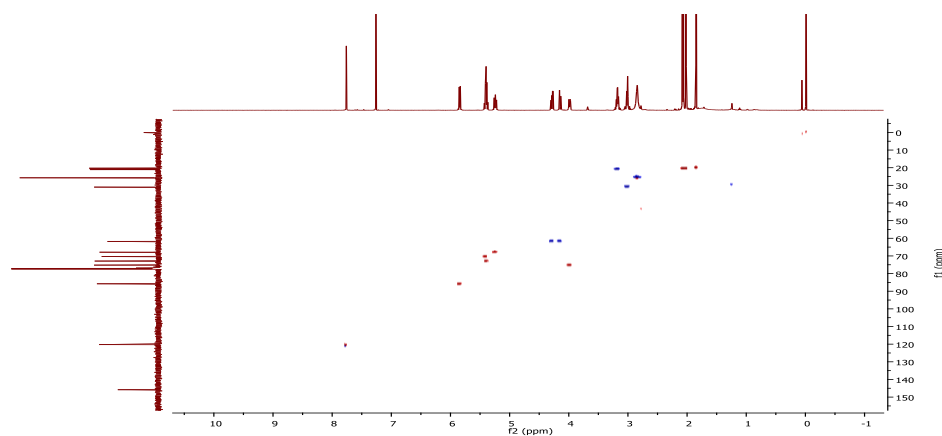




$^{13}\text{C}$  NMR spectrum of **2.20** in  $\text{CDCl}_3$

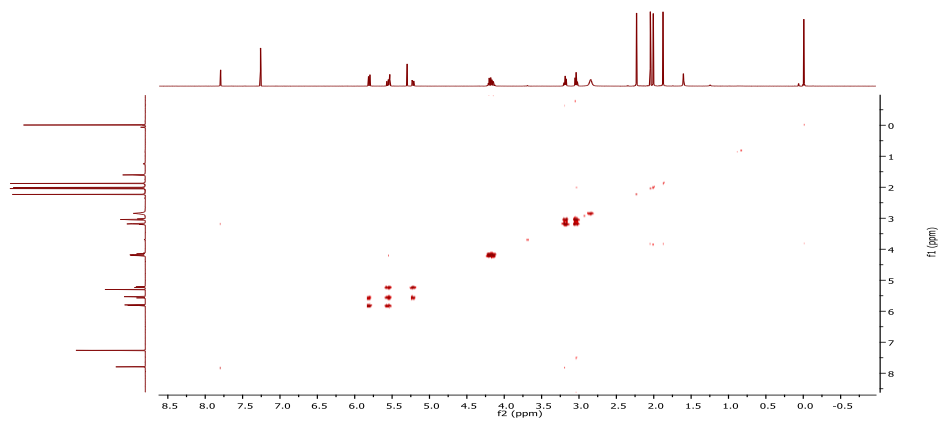
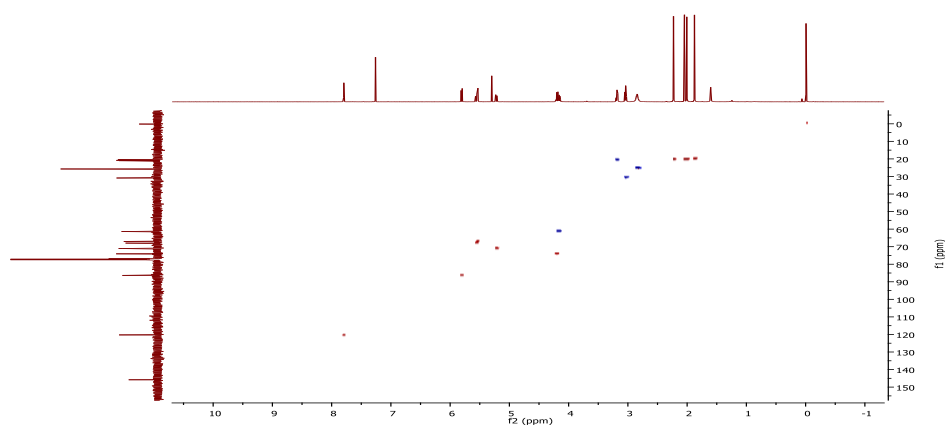
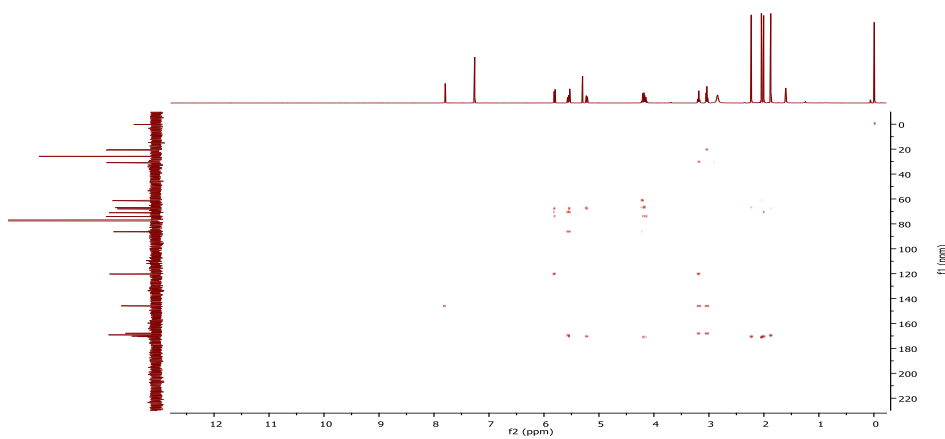


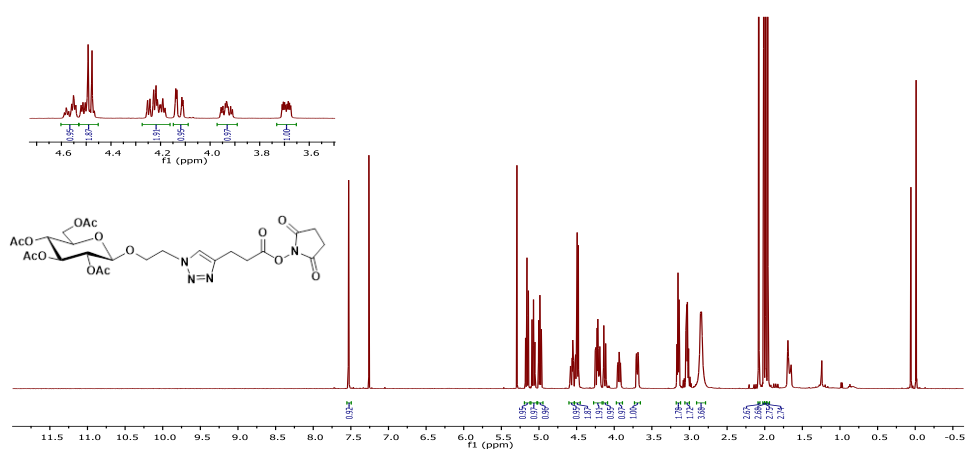
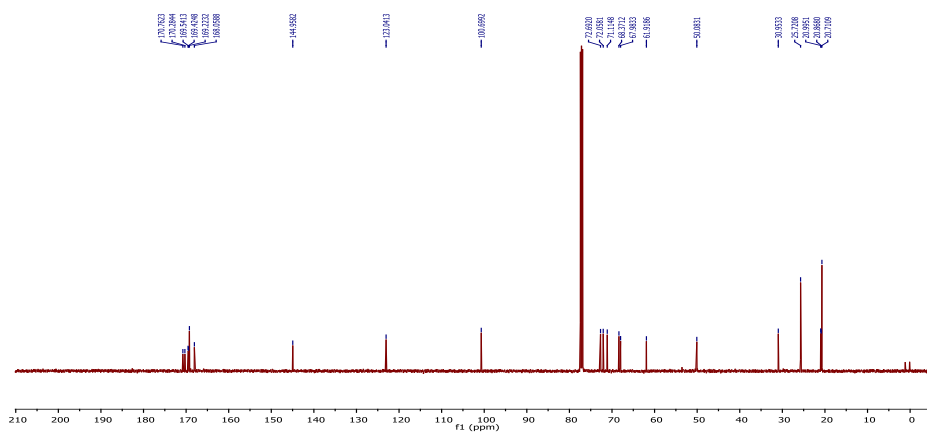
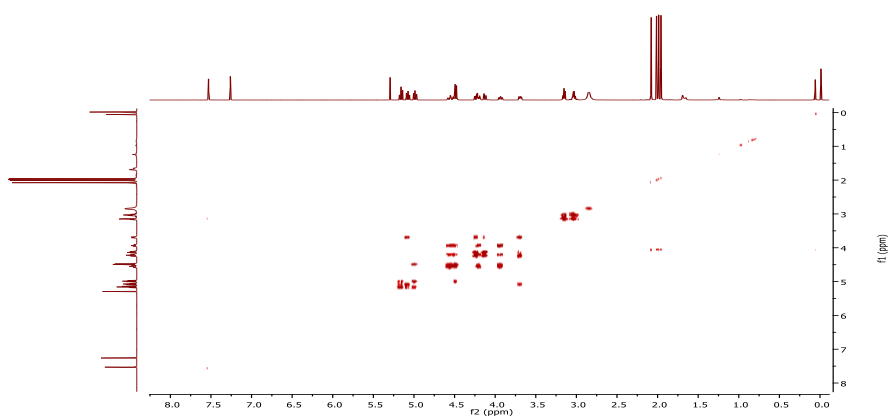
COSY NMR spectrum of **2.20** in  $\text{CDCl}_3$



HSQC NMR spectrum of **2.20** in  $\text{CDCl}_3$

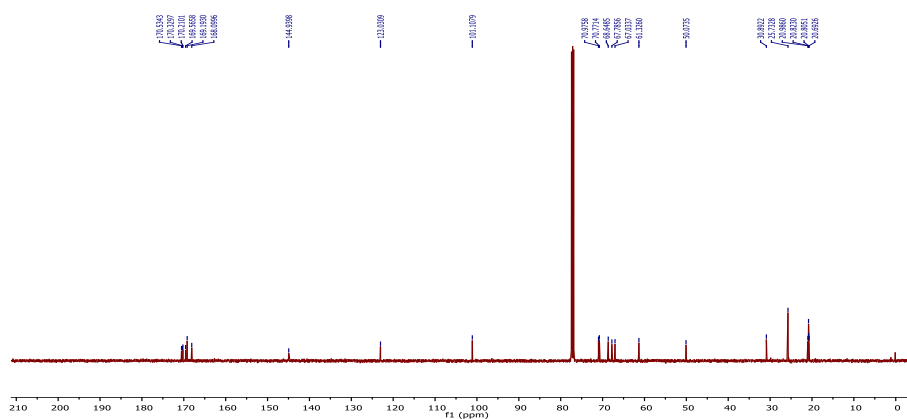


COSY NMR spectrum of **2.21** in CDCl<sub>3</sub>HSQC NMR spectrum of **2.21** in CDCl<sub>3</sub>HMBC NMR spectrum of **2.21** in CDCl<sub>3</sub>

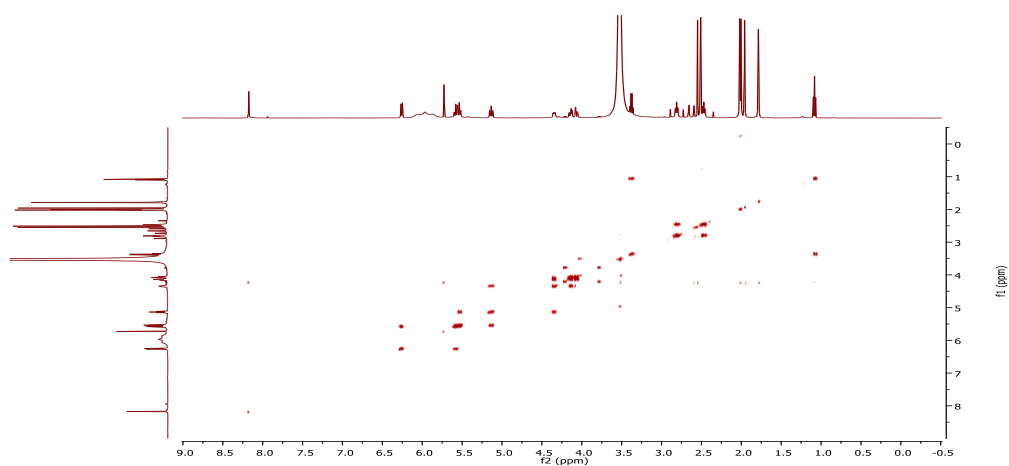
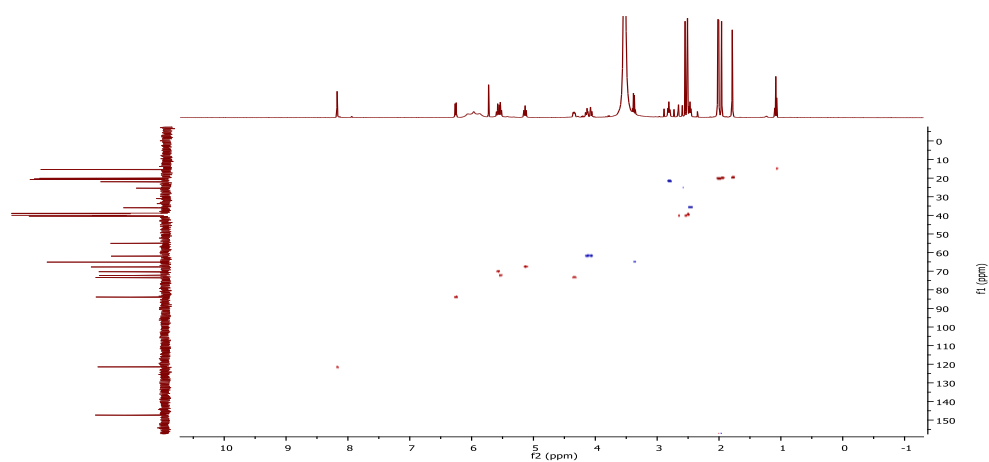
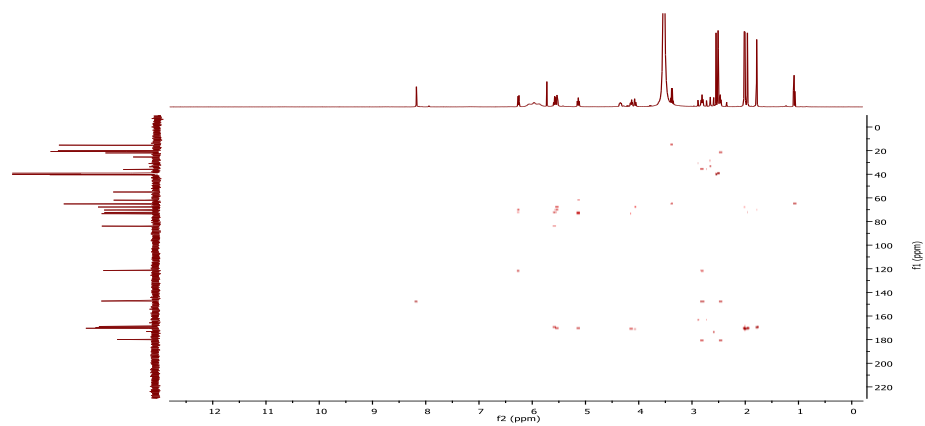
NMR spectra of **2.28**<sup>1</sup>H NMR spectrum of **2.28** in CDCl<sub>3</sub><sup>13</sup>C NMR spectrum of **2.28** in CDCl<sub>3</sub>COSY NMR spectrum of **2.28** in CDCl<sub>3</sub>

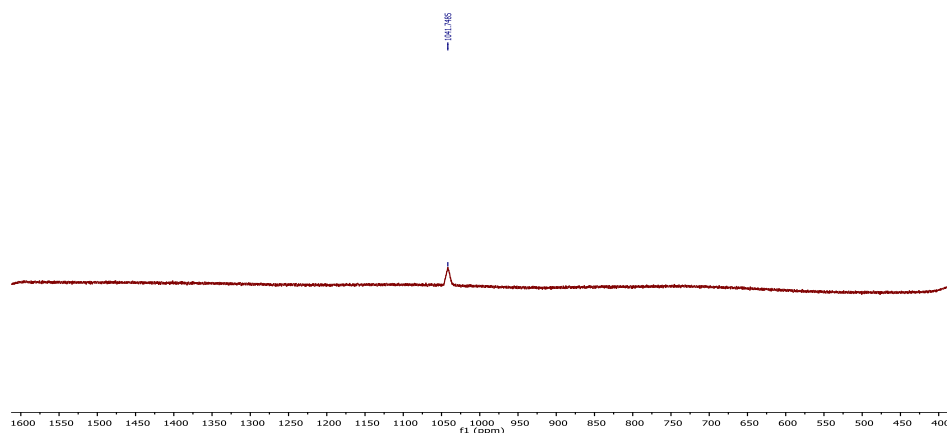
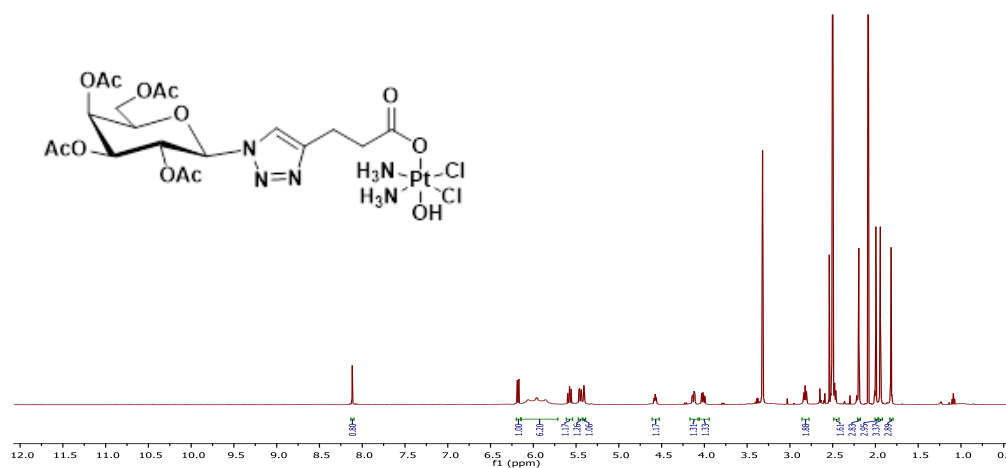
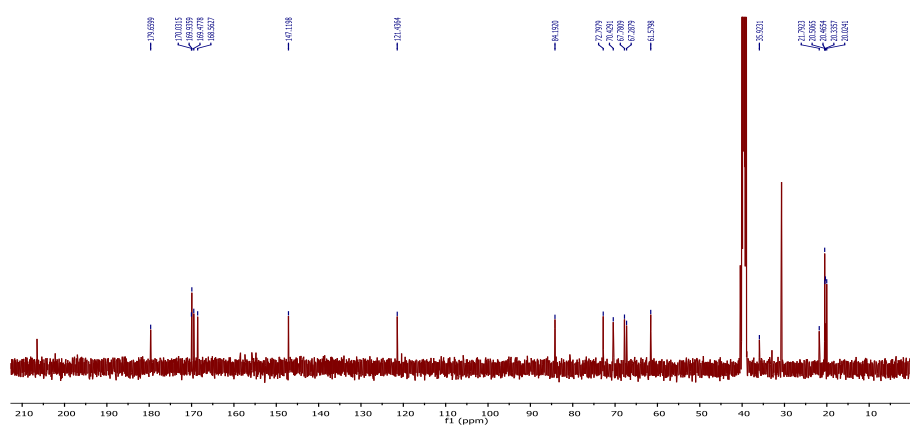


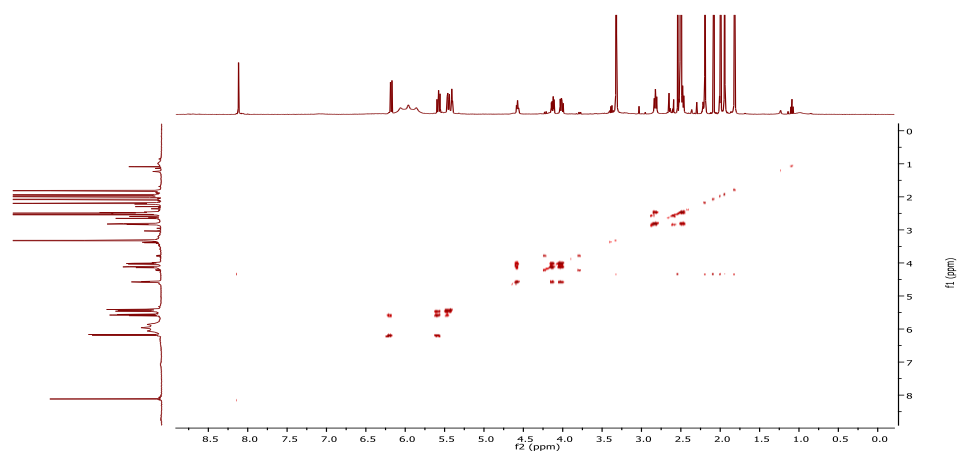
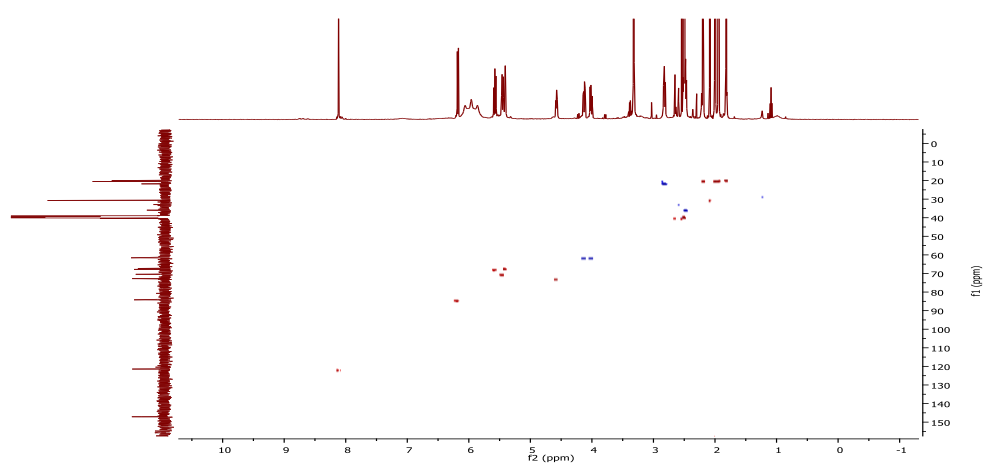
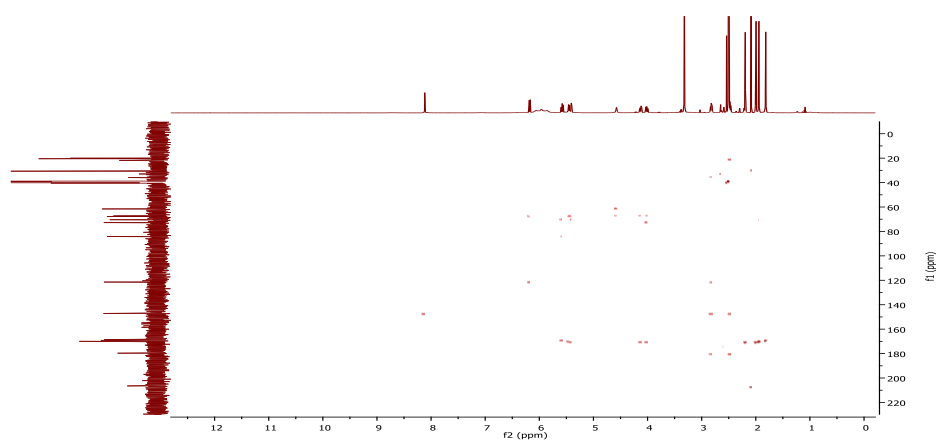


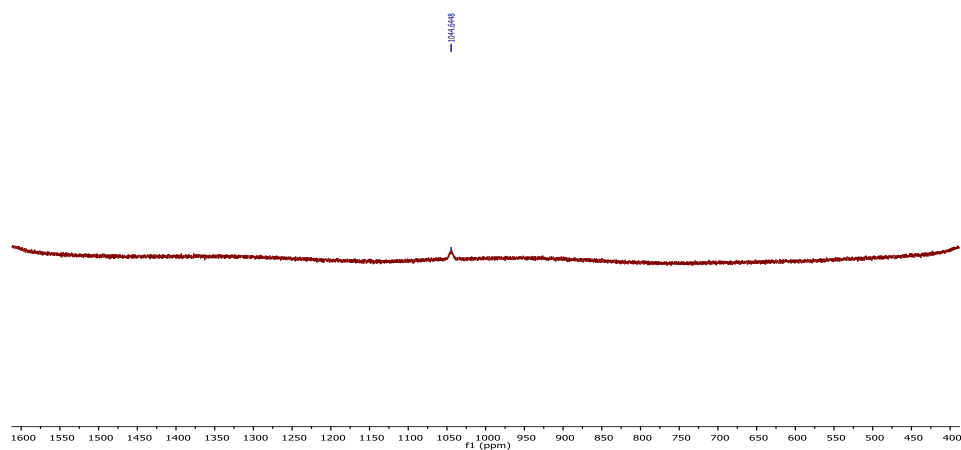
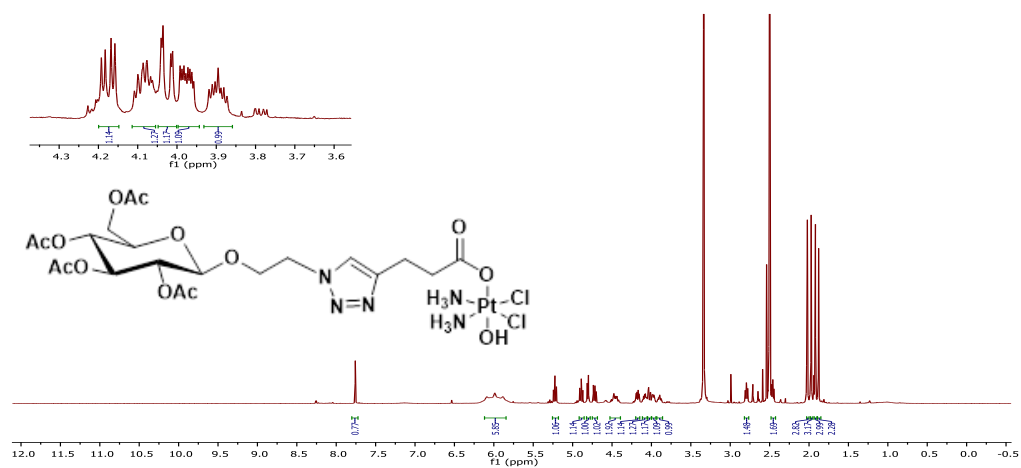
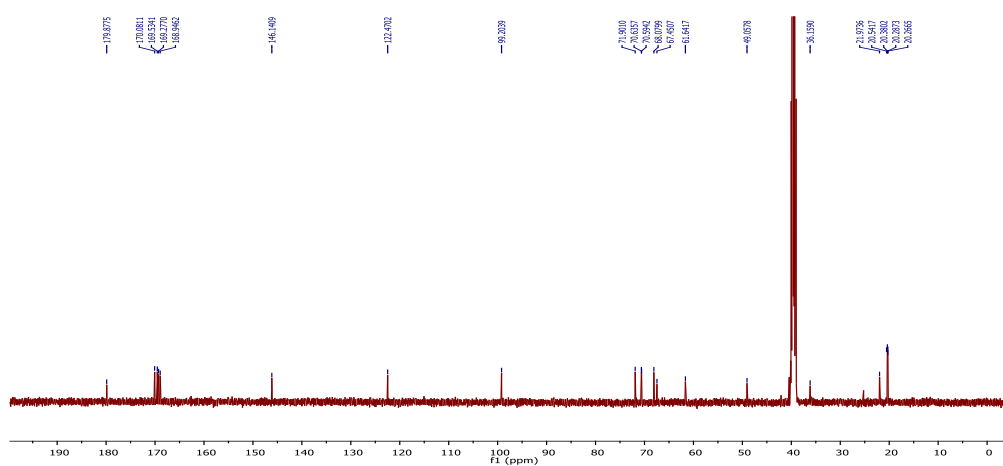




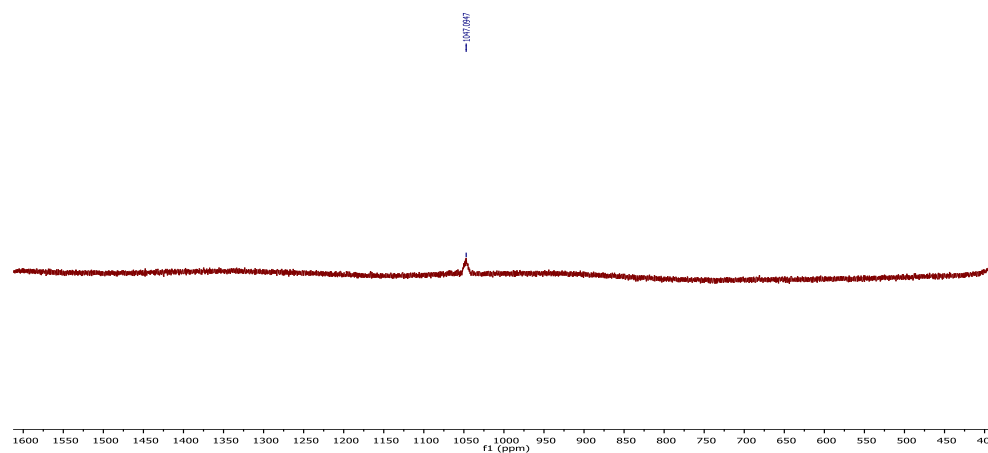
COSY NMR spectrum of **Complex 1** in DMSO-d<sub>6</sub>HSQC NMR spectrum of **Complex 1** in DMSO-d<sub>6</sub>HMBC NMR spectrum of **Complex 1** in DMSO-d<sub>6</sub>

 $^{195}\text{Pt}$  NMR spectrum of **Complex 1** in  $\text{DMSO-d}_6$ NMR spectra of **Complex 2** $^1\text{H}$  NMR spectrum of **Complex 2** in  $\text{DMSO-d}_6$  $^{13}\text{C}$  NMR spectrum of **Complex 2** in  $\text{DMSO-d}_6$

COSY NMR spectrum of **Complex 2** in DMSO-d<sub>6</sub>HSQC NMR spectrum of **Complex 2** in DMSO-d<sub>6</sub>HMBC NMR spectrum of **Complex 2** in DMSO-d<sub>6</sub>

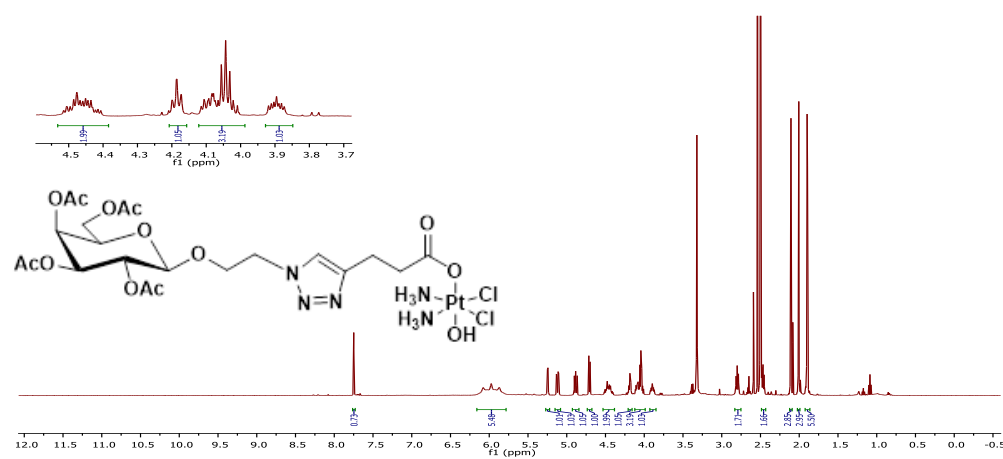
 $^{195}\text{Pt}$  NMR spectrum of **Complex 2** in  $\text{DMSO-d}_6$ NMR spectra of **Complex 3** $^1\text{H}$  NMR spectrum of **Complex 3** in  $\text{DMSO-d}_6$  $^{13}\text{C}$  NMR spectrum of **Complex 3** in  $\text{DMSO-d}_6$



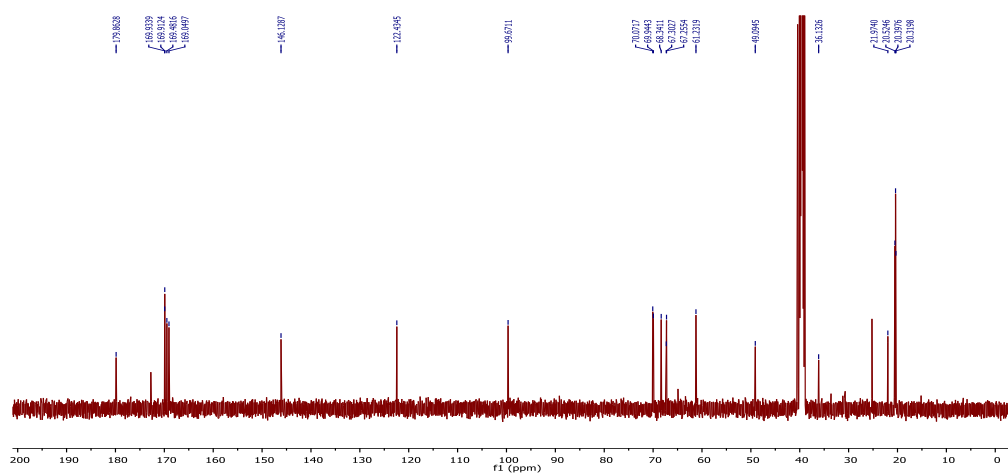


$^{195}\text{Pt}$  NMR spectrum of **Complex 3** in  $\text{DMSO-d}_6$

### NMR spectra of Complex 4

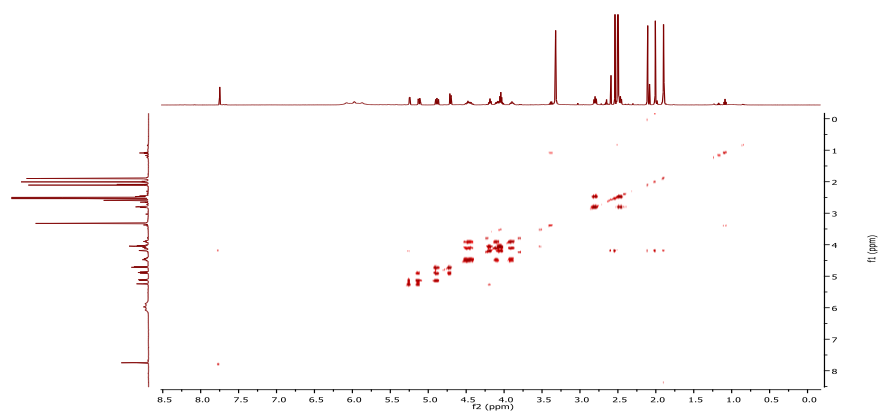
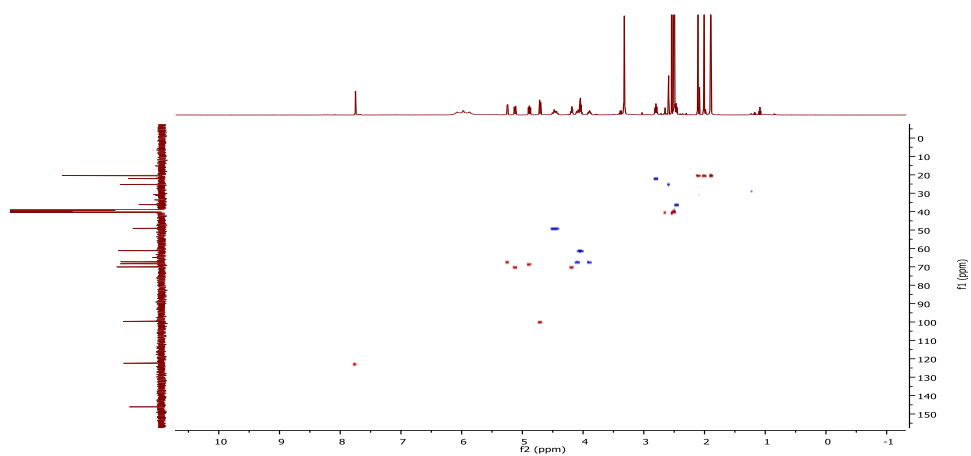
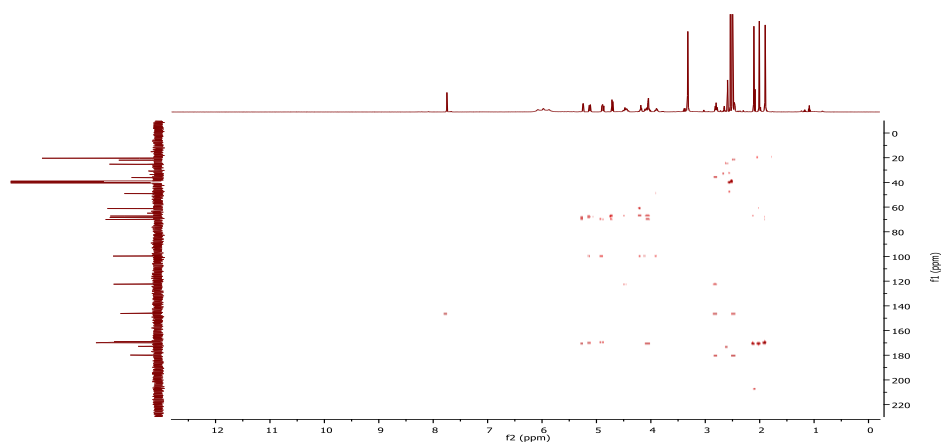


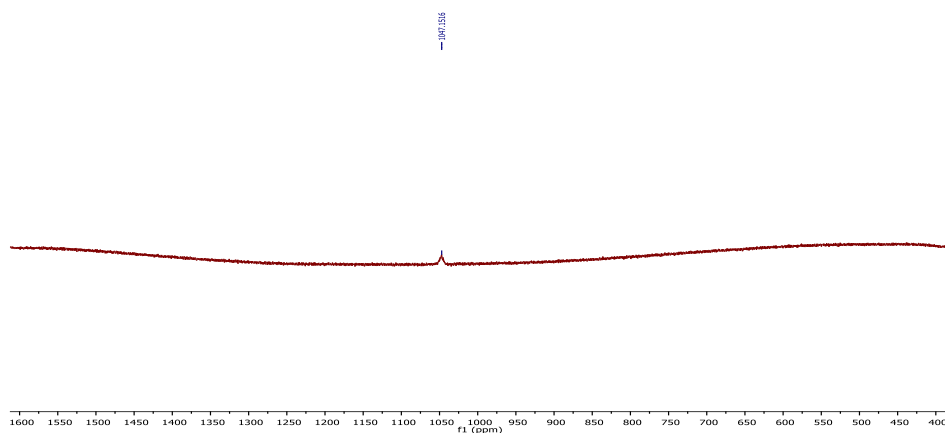
$^1\text{H}$  NMR spectrum of **Complex 4** in  $\text{DMSO-d}_6$



$^{13}\text{C}$  NMR spectrum of **Complex 4** in  $\text{DMSO-d}_6$

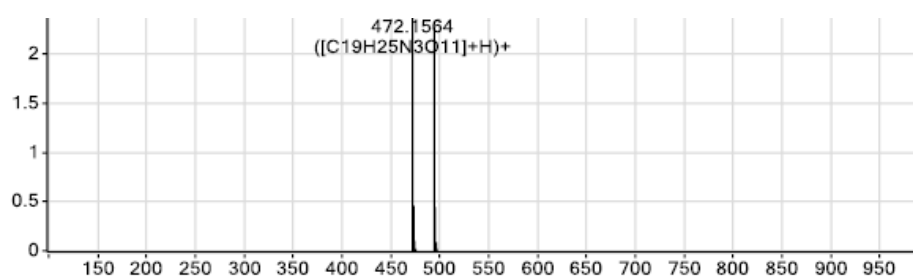


COSY NMR spectrum of **Complex 4** in DMSO-d<sub>6</sub>HSQC NMR spectrum of **Complex 4** in DMSO-d<sub>6</sub>HMBC NMR spectrum of **Complex 4** in DMSO-d<sub>6</sub>

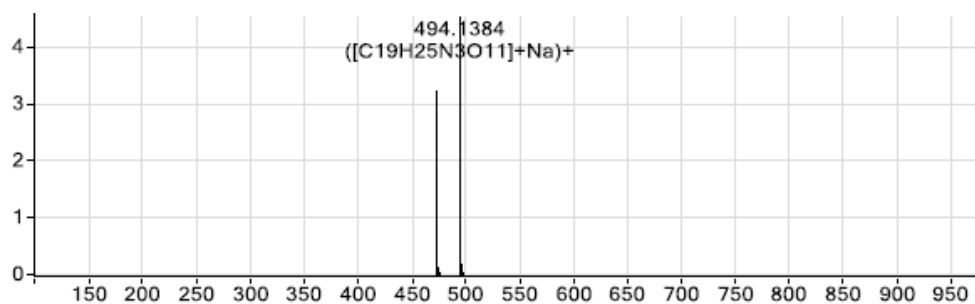


$^{195}\text{Pt}$  NMR spectrum of **Complex 4** in  $\text{DMSO-d}_6$

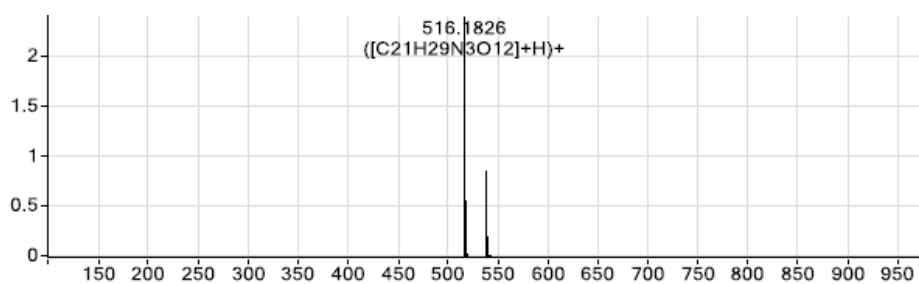
#### HR-MS



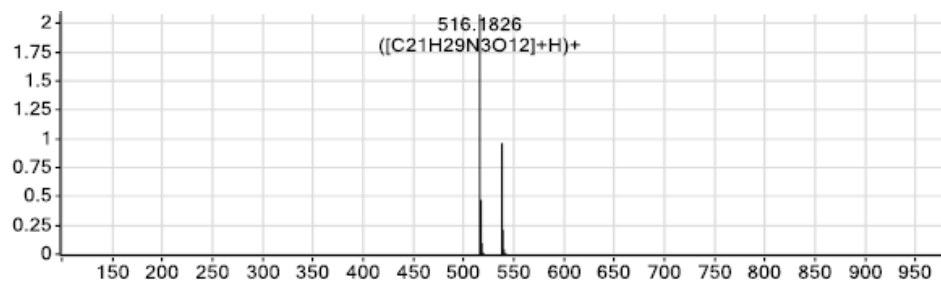
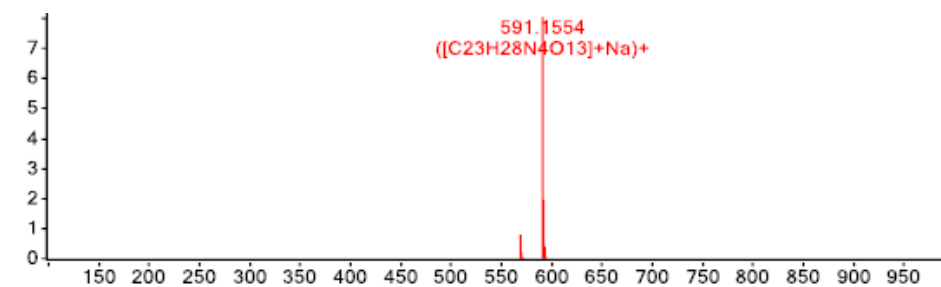
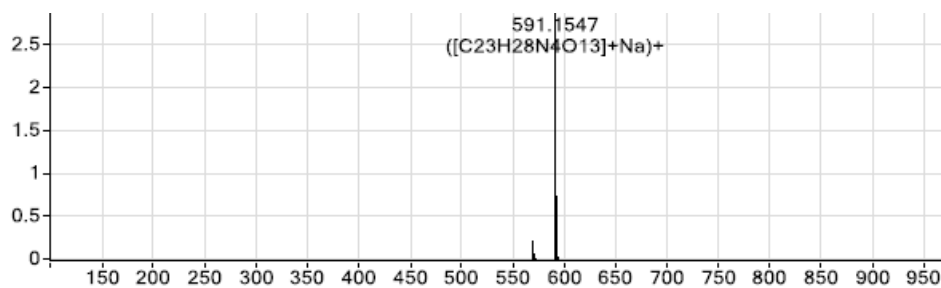
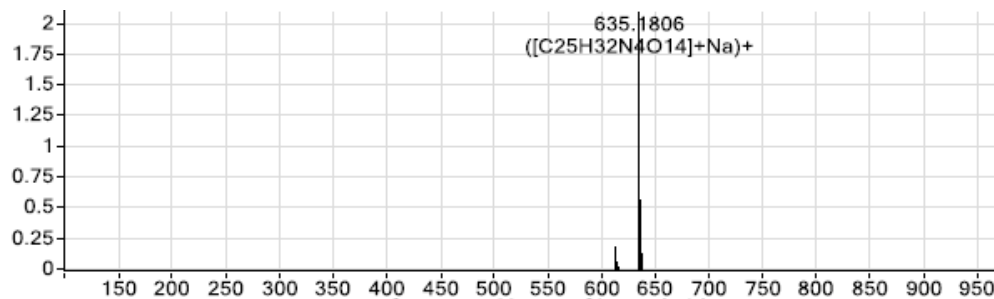
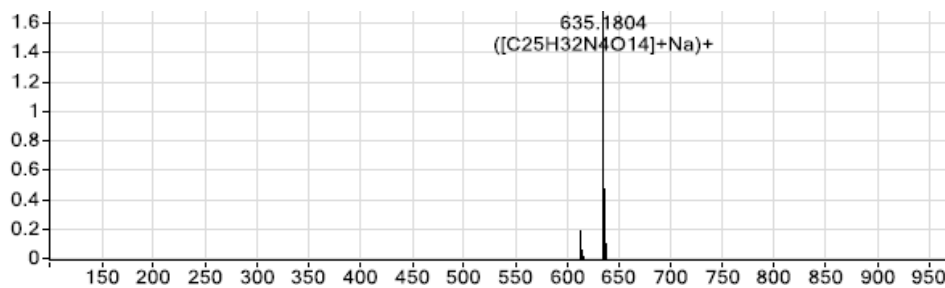
HR-MS spectrum of **2.18**

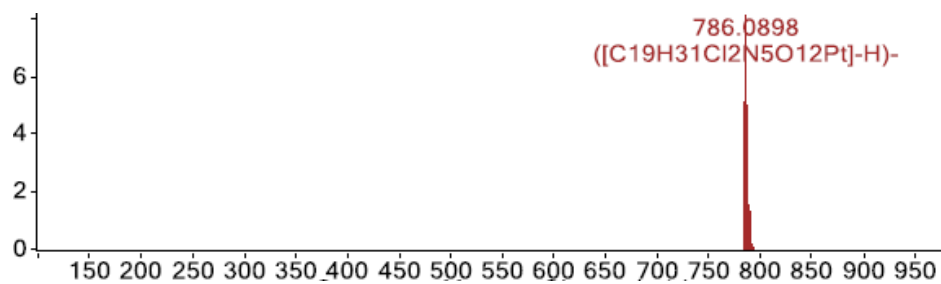
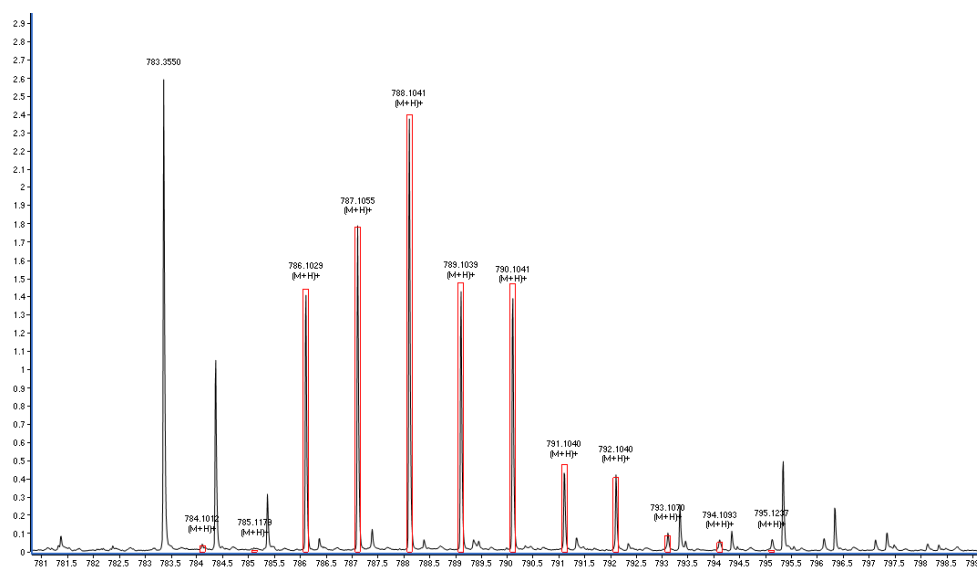
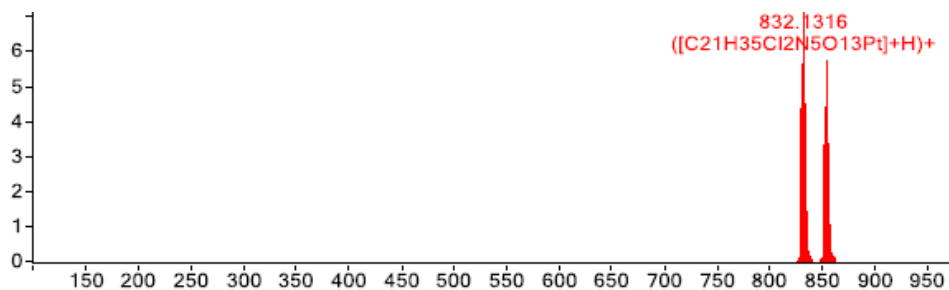
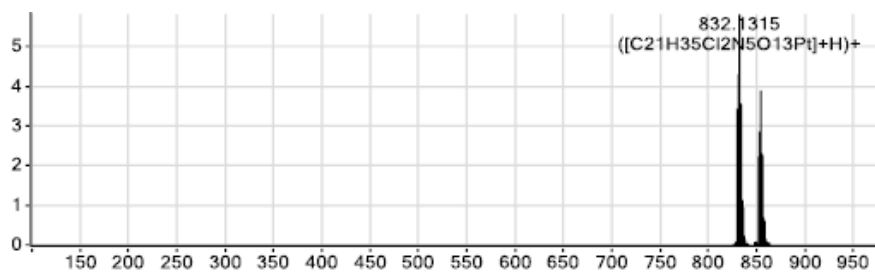


HR-MS spectrum of **2.19**

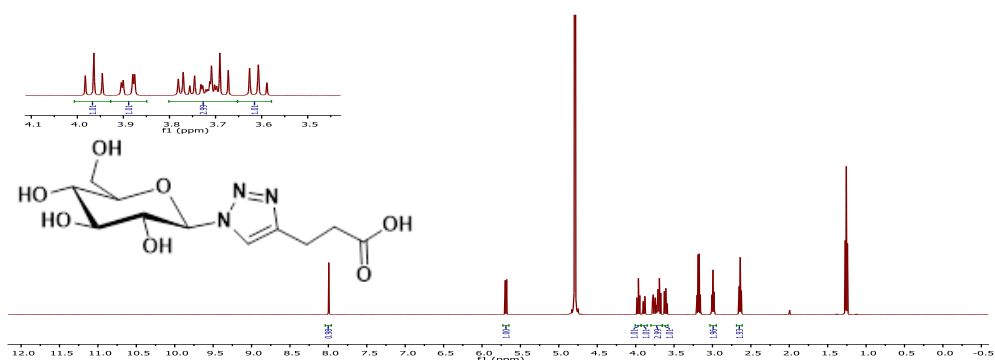
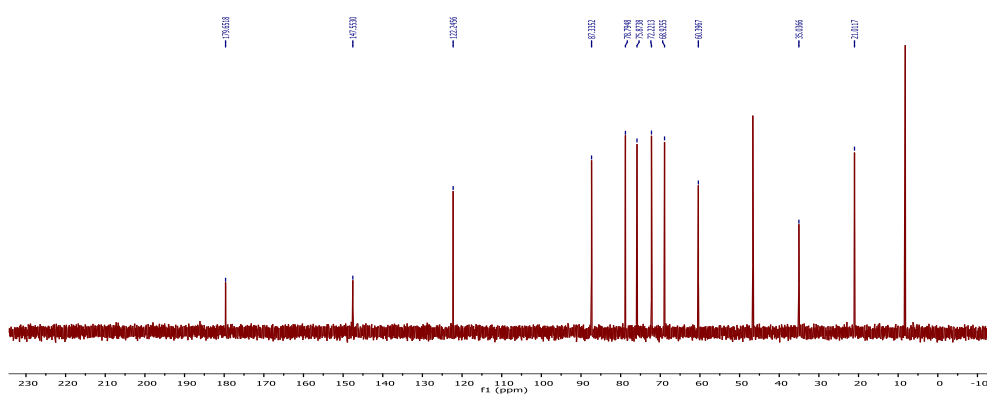
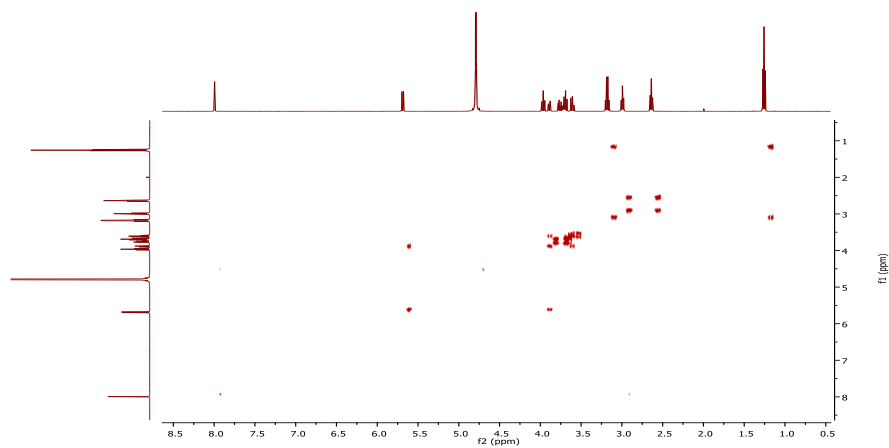


HR-MS spectrum of **2.26**

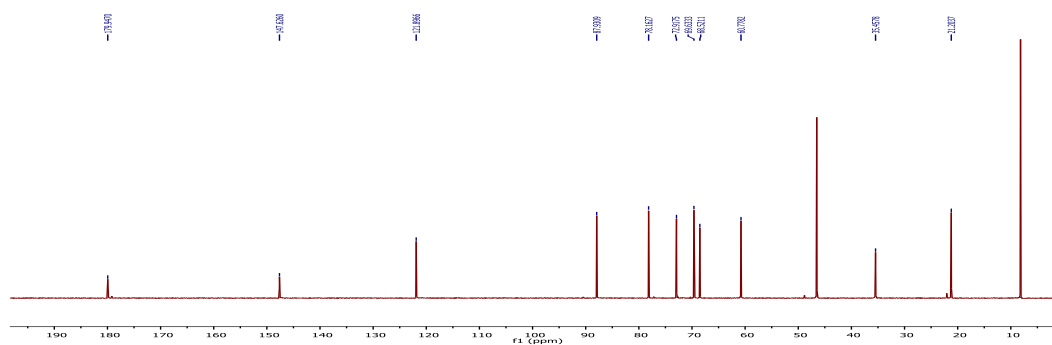
HR-MS spectrum of **2.27**HR-MS spectrum of **2.20**HR-MS spectrum of **2.21**HR-MS spectrum of **2.28**HR-MS spectrum of **2.29**

HR-MS spectrum of **Complex 1**HR-MS spectrum of **Complex 2**HR-MS spectrum of **Complex 3**HR-MS spectrum of **Complex 4**

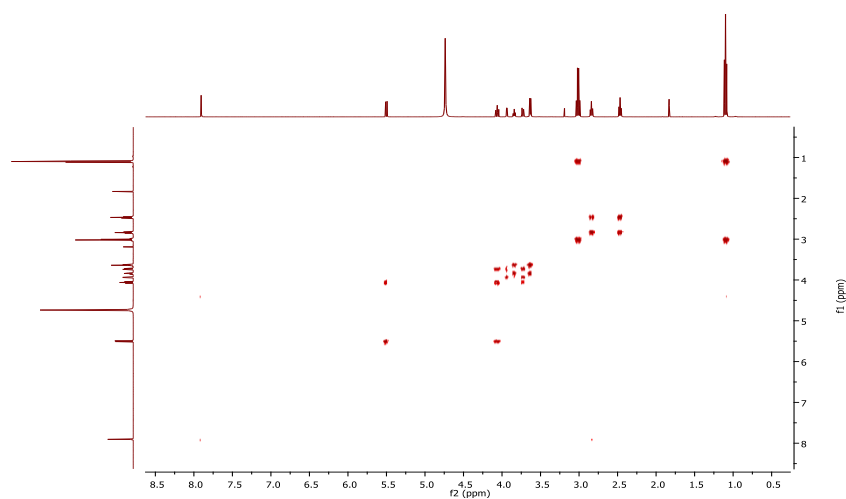
## Chapter 3

NMR spectra of **3.9** $^1\text{H}$  NMR spectrum of **3.9** in  $\text{D}_2\text{O}$  $^{13}\text{C}$  NMR spectrum of **3.9** in  $\text{D}_2\text{O}$ COSY NMR spectrum of **3.9** in  $\text{D}_2\text{O}$

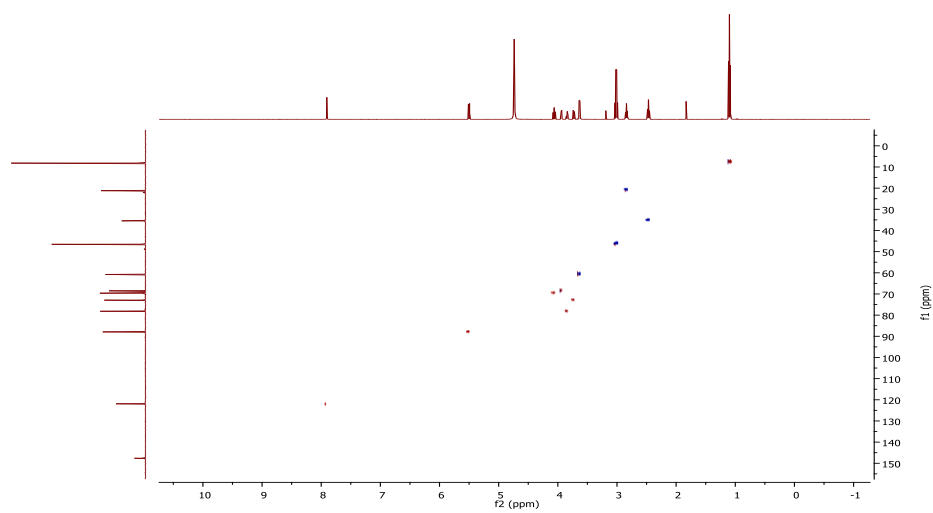




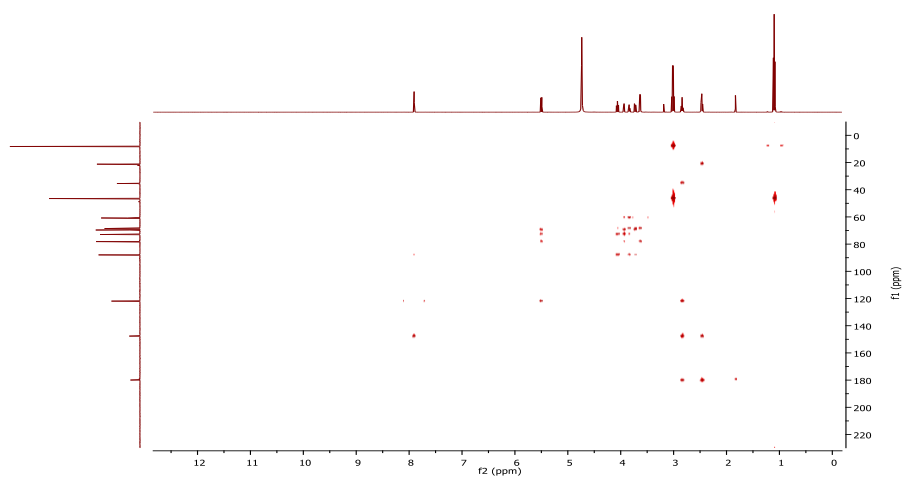
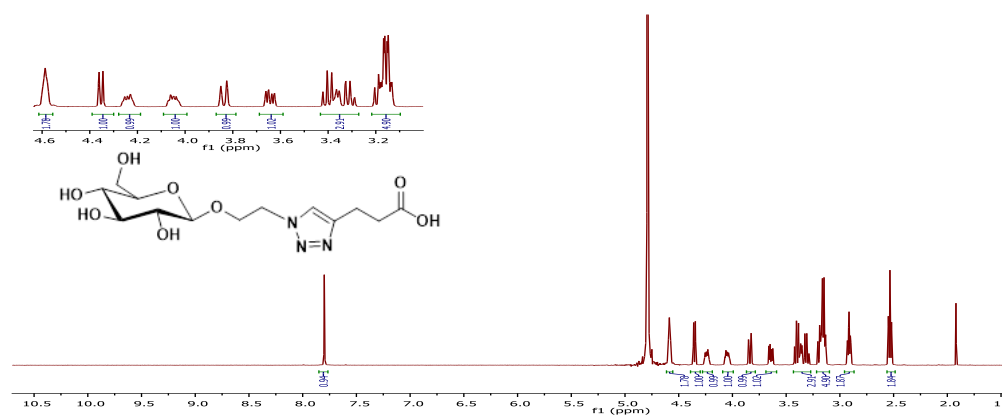
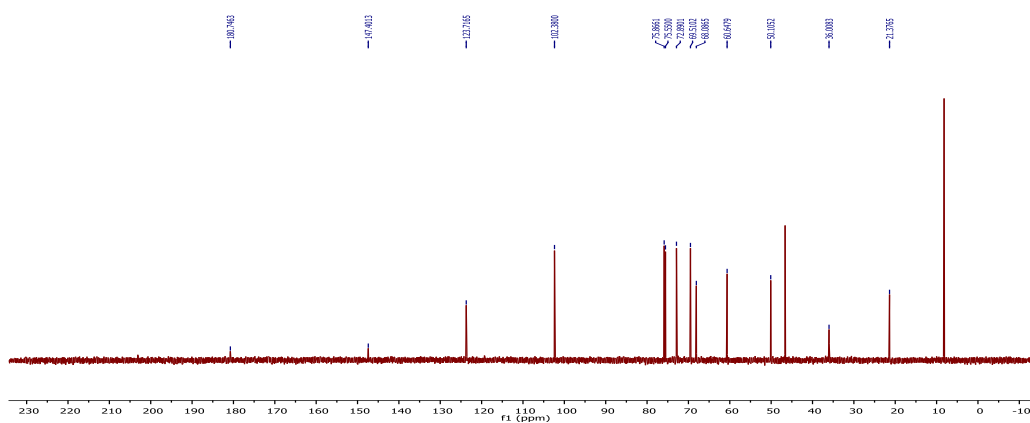
$^{13}\text{C}$  NMR spectrum of **3.10** in  $\text{D}_2\text{O}$



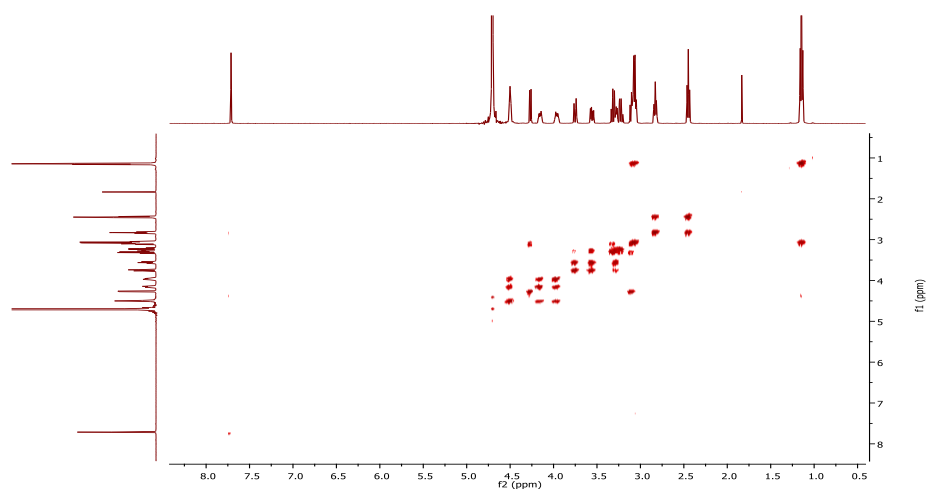
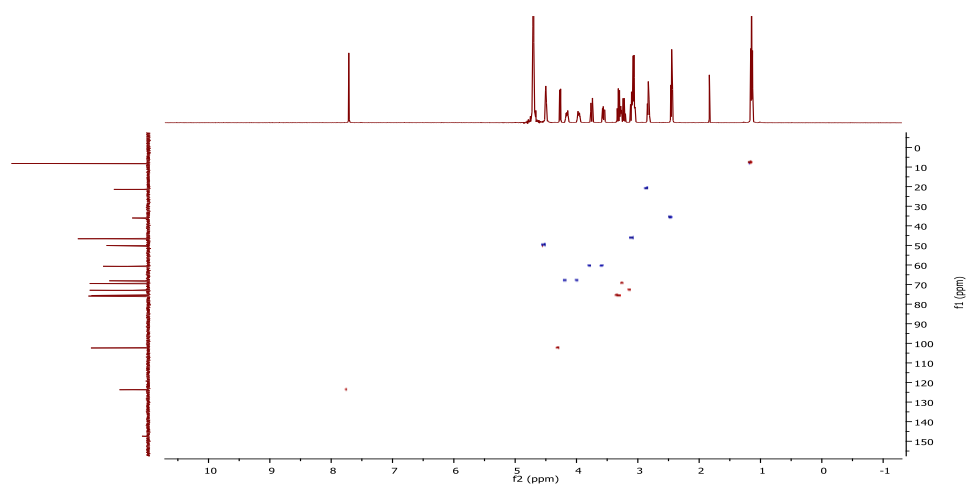
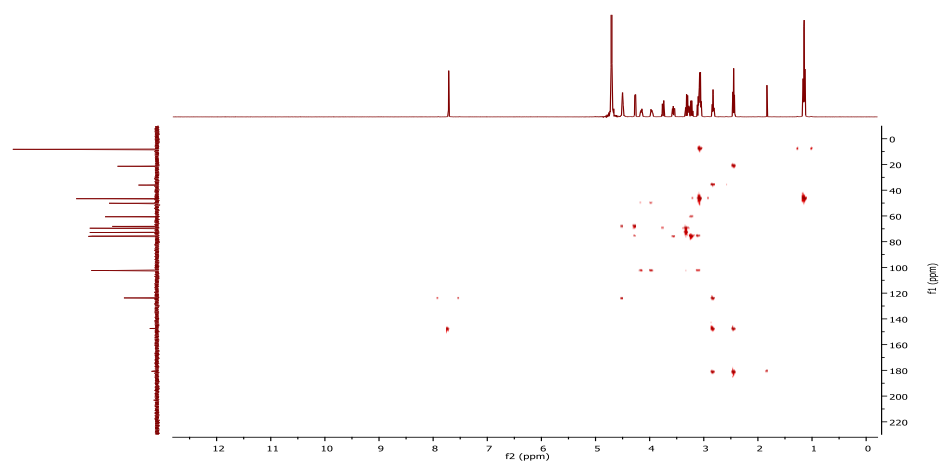
COSY NMR spectrum of **3.10** in  $\text{D}_2\text{O}$

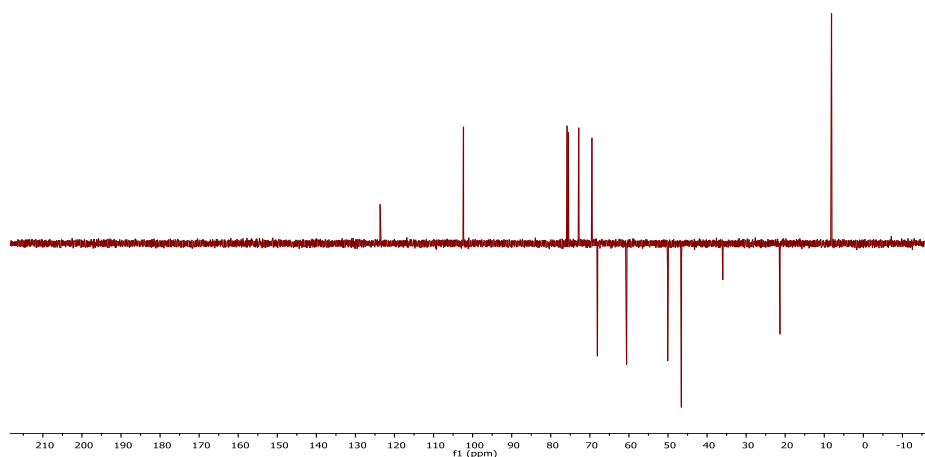
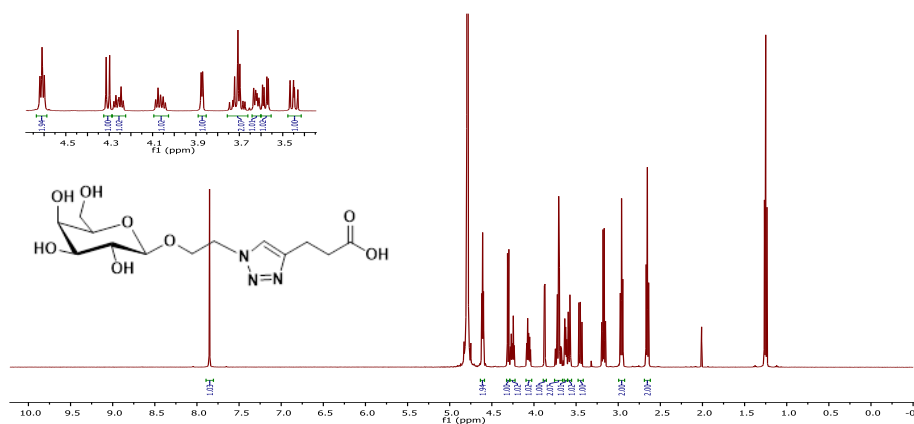
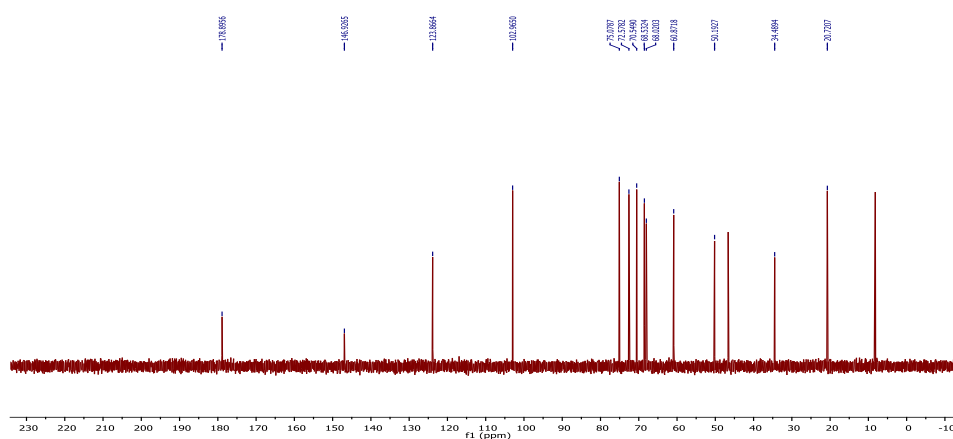


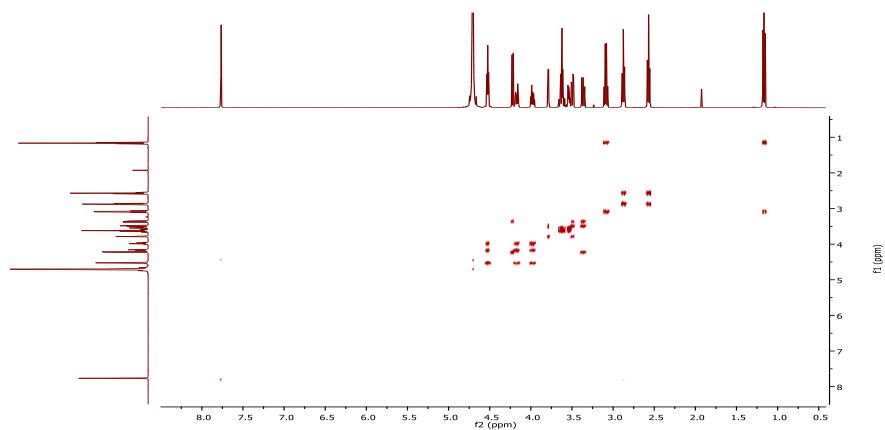
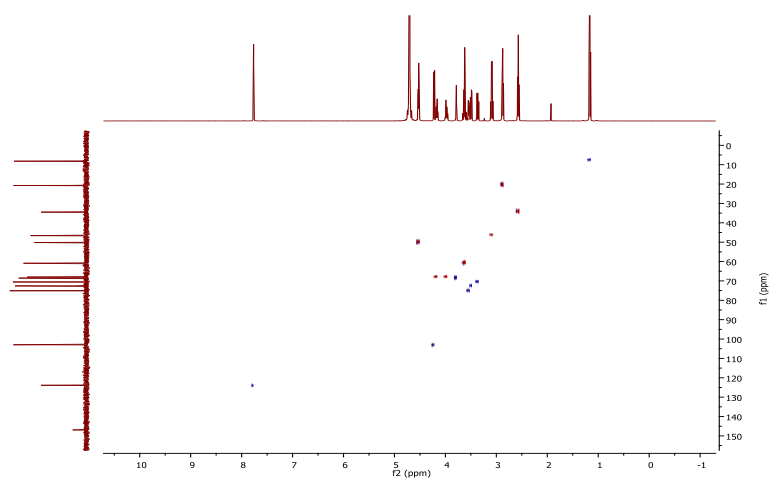
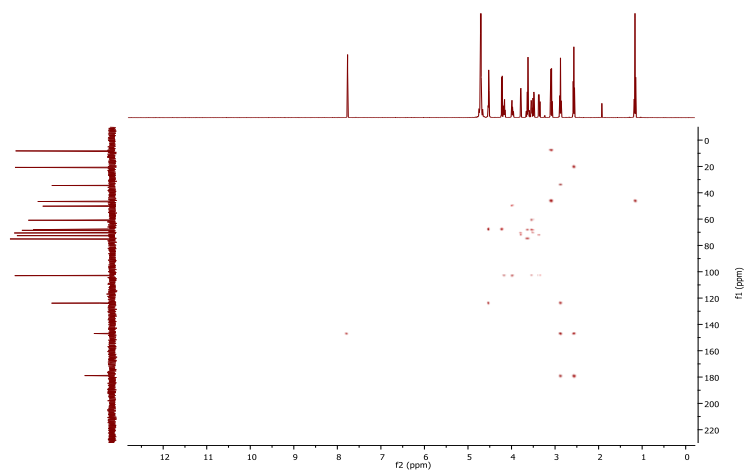
HSQC NMR spectrum of **3.10** in  $\text{D}_2\text{O}$

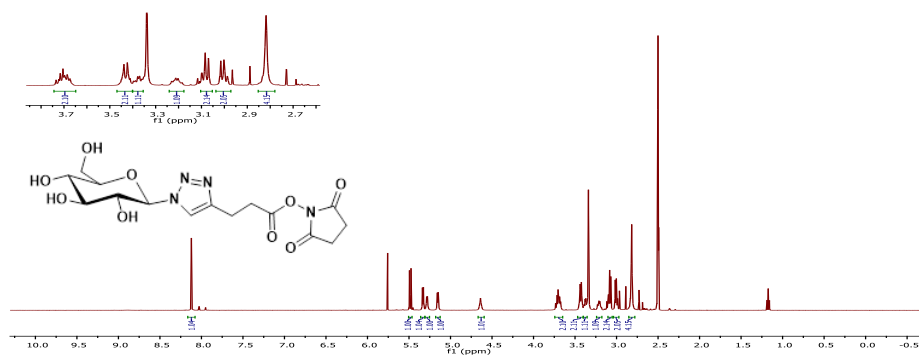
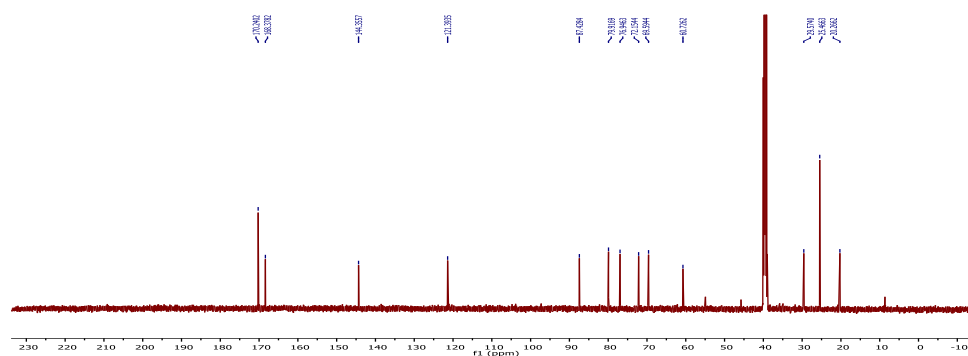
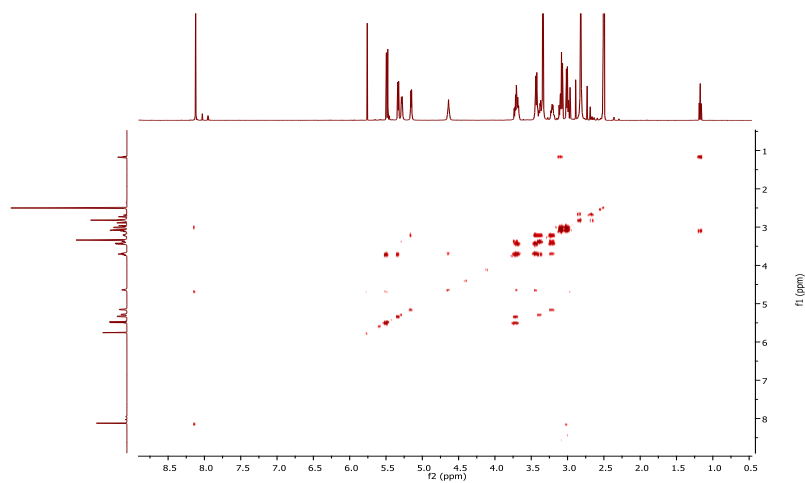
HMBC NMR spectrum of **3.10** in D<sub>2</sub>ONMR spectra of **3.13**<sup>1</sup>H NMR spectrum of **3.13** in D<sub>2</sub>O<sup>13</sup>C NMR spectrum of **3.13** in D<sub>2</sub>O



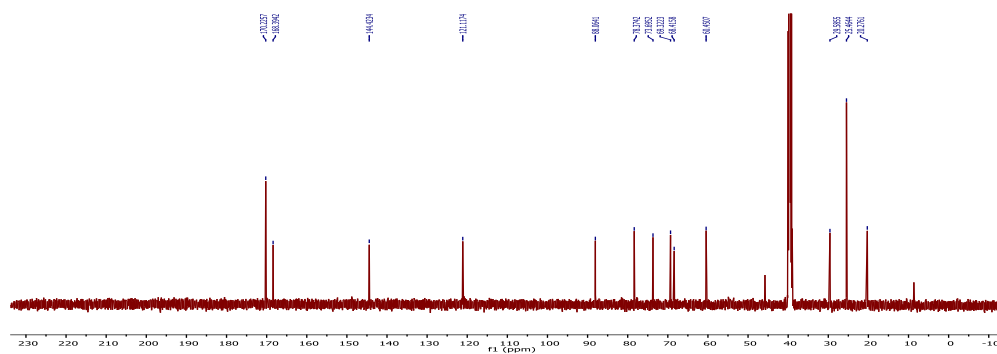
COSY NMR spectrum of **3.13** in D<sub>2</sub>OHSQC NMR spectrum of **3.13** in D<sub>2</sub>OHMBC NMR spectrum of **3.13** in D<sub>2</sub>O

DEPT-135 NMR spectrum of **3.13** in D<sub>2</sub>ONMR spectra of **3.14**<sup>1</sup>H NMR spectrum of **3.14** in D<sub>2</sub>O<sup>13</sup>C NMR spectrum of **3.14** in D<sub>2</sub>O

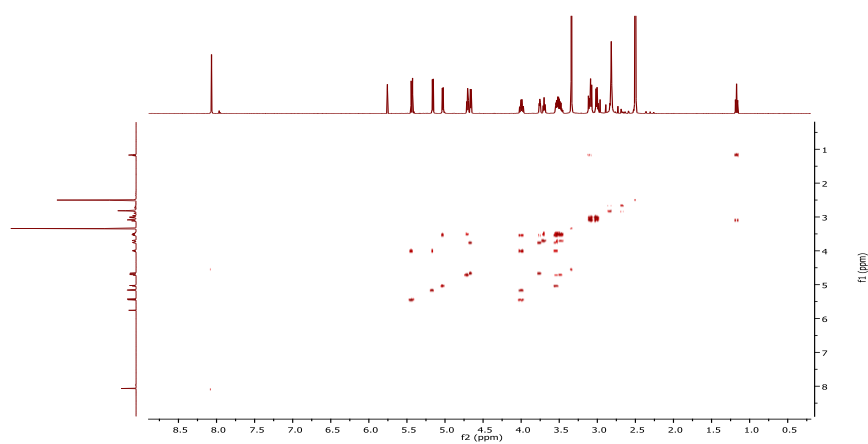
COSY NMR spectrum of **3.14** in D<sub>2</sub>OHSQC NMR spectrum of **3.14** in D<sub>2</sub>OHMBC NMR spectrum of **3.14** in D<sub>2</sub>O

NMR spectra of **3.11** $^1\text{H}$  NMR spectrum of **3.11** in  $\text{DMSO-d}_6$  $^{13}\text{C}$  NMR spectrum of **3.11** in  $\text{DMSO-d}_6$ COSY NMR spectrum of **3.11** in  $\text{DMSO-d}_6$

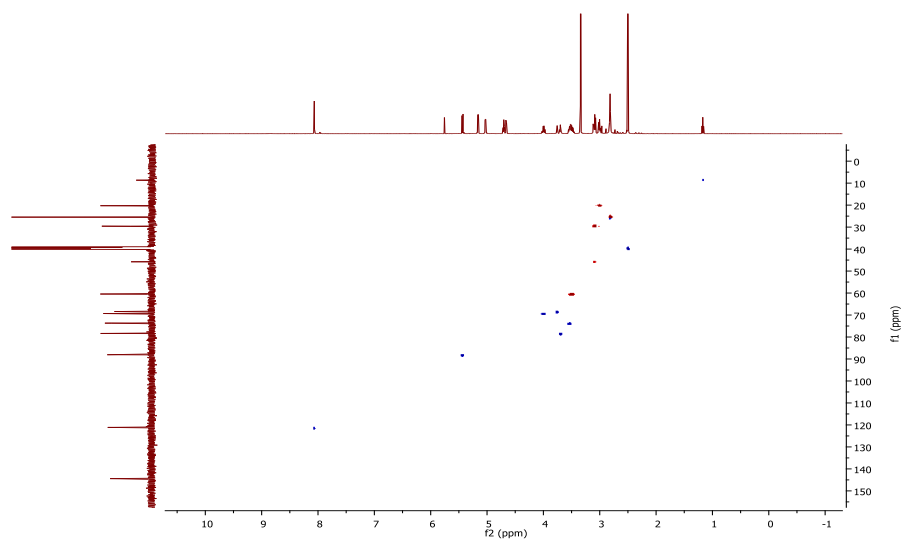




$^{13}\text{C}$  NMR spectrum of **3.12** in  $\text{DMSO-d}_6$

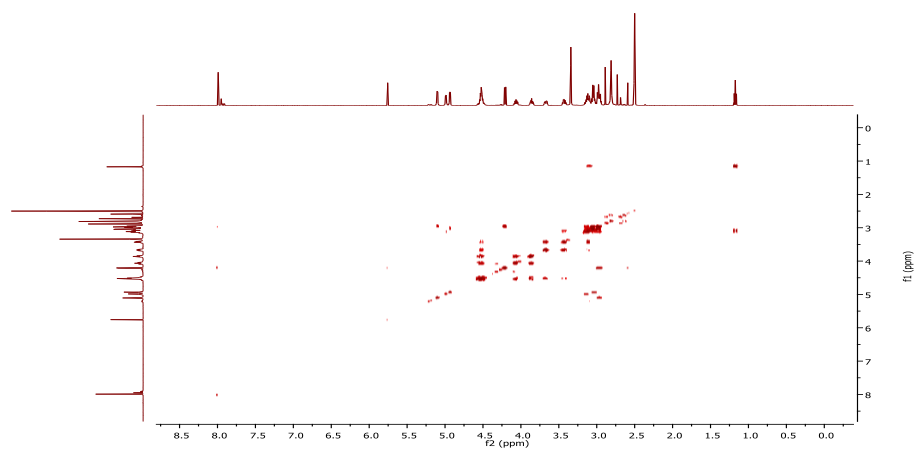
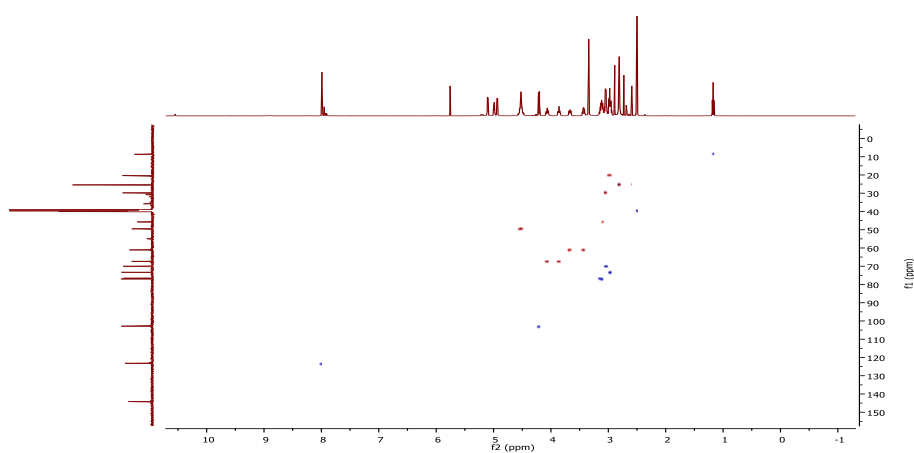
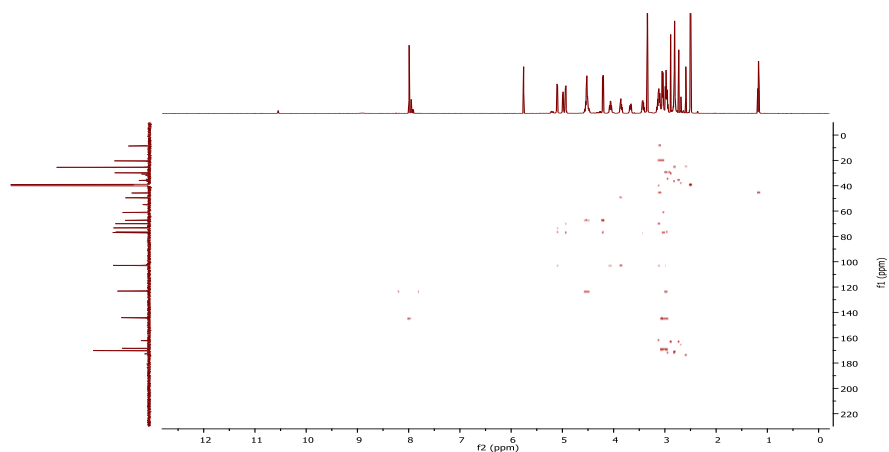


COSY NMR spectrum of **3.12** in  $\text{DMSO-d}_6$



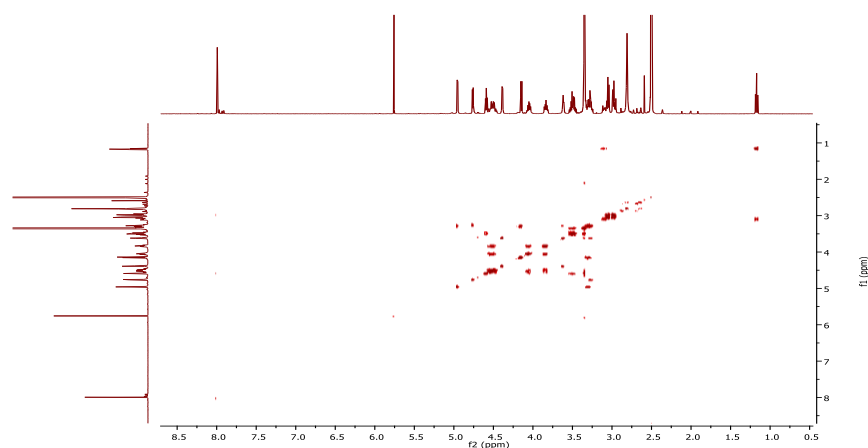
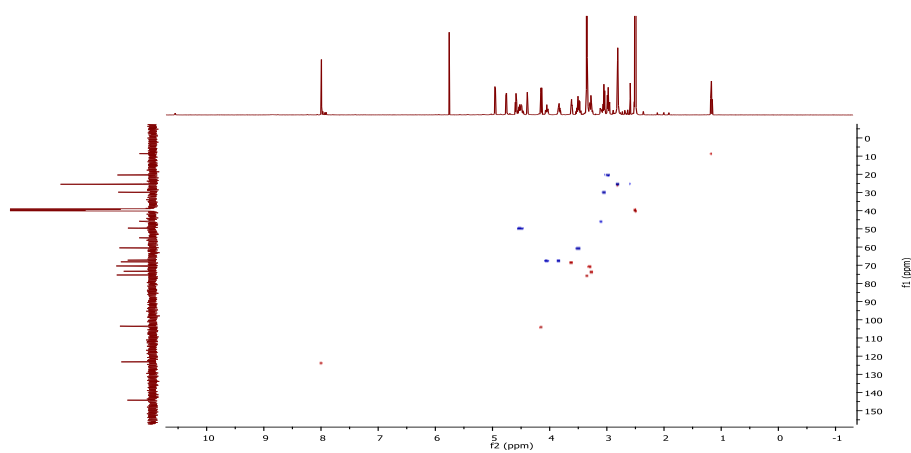
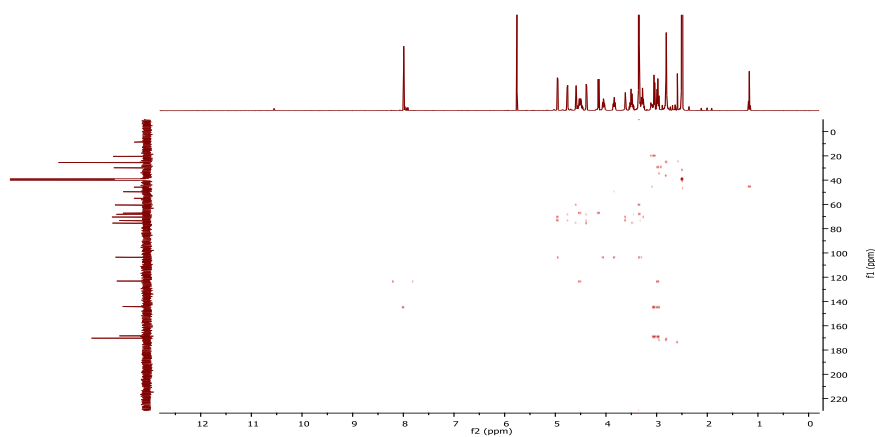
HSQC NMR spectrum of **3.12** in  $\text{DMSO-d}_6$

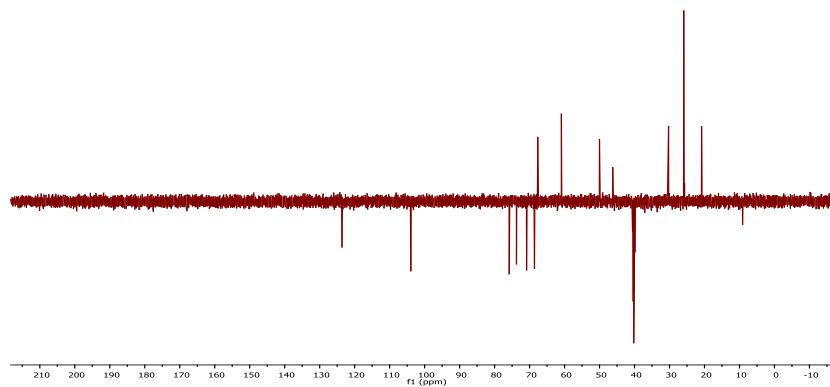


COSY NMR spectrum of **3.15** in DMSO-d<sub>6</sub>HSQC NMR spectrum of **3.15** in DMSO-d<sub>6</sub>HMBC NMR spectrum of **3.15** in DMSO-d<sub>6</sub>

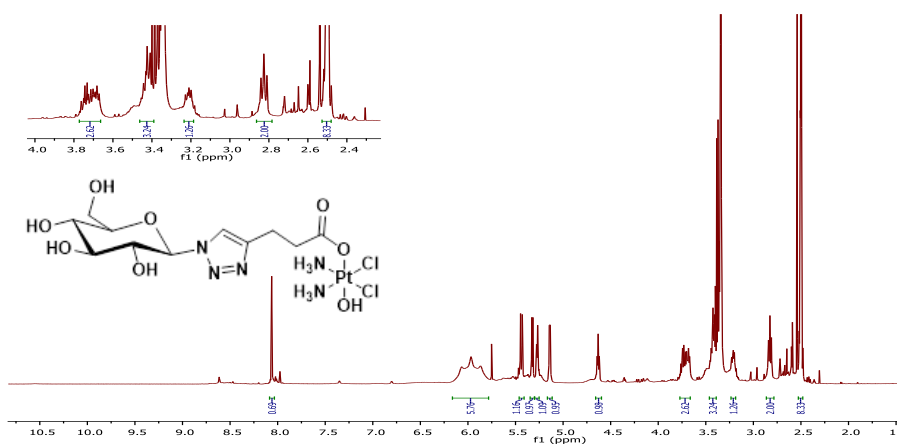
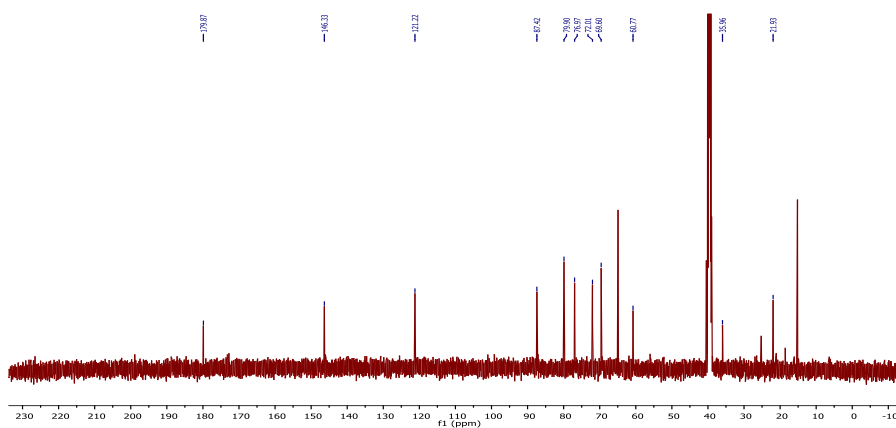


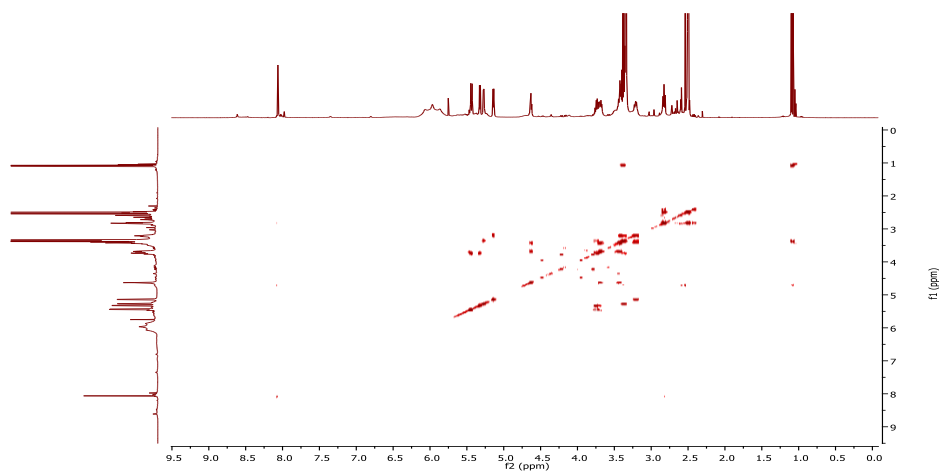
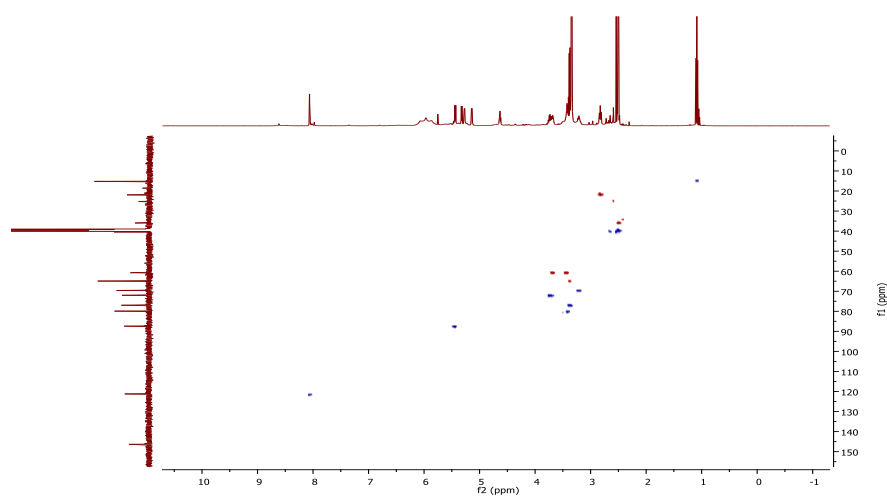
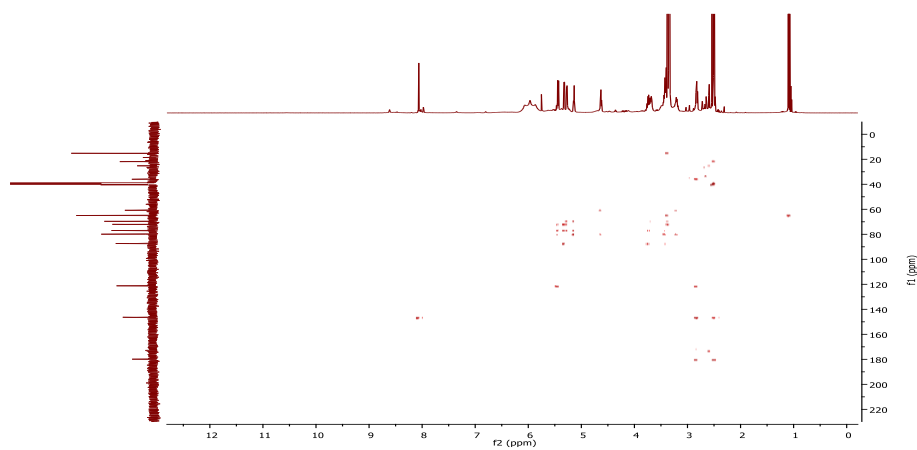


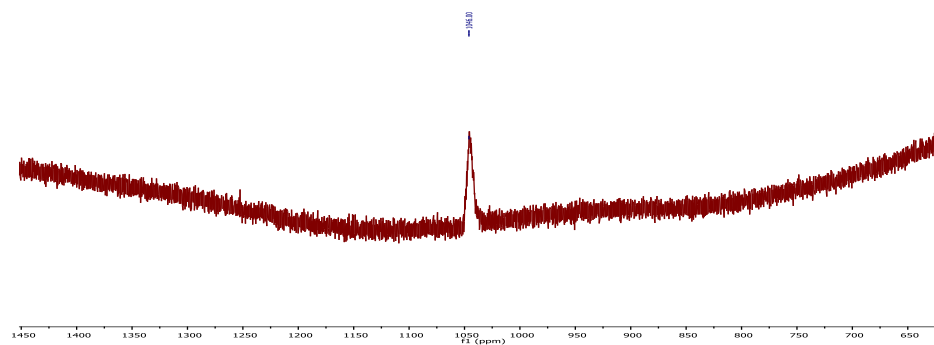
COSY NMR spectrum of **3.16** in DMSO-d<sub>6</sub>HSQC NMR spectrum of **3.16** in DMSO-d<sub>6</sub>HMBC NMR spectrum of **3.16** in DMSO-d<sub>6</sub>

DEPT-135 NMR spectrum of **3.16** in DMSO-d<sub>6</sub>

## NMR spectra of Complex 1

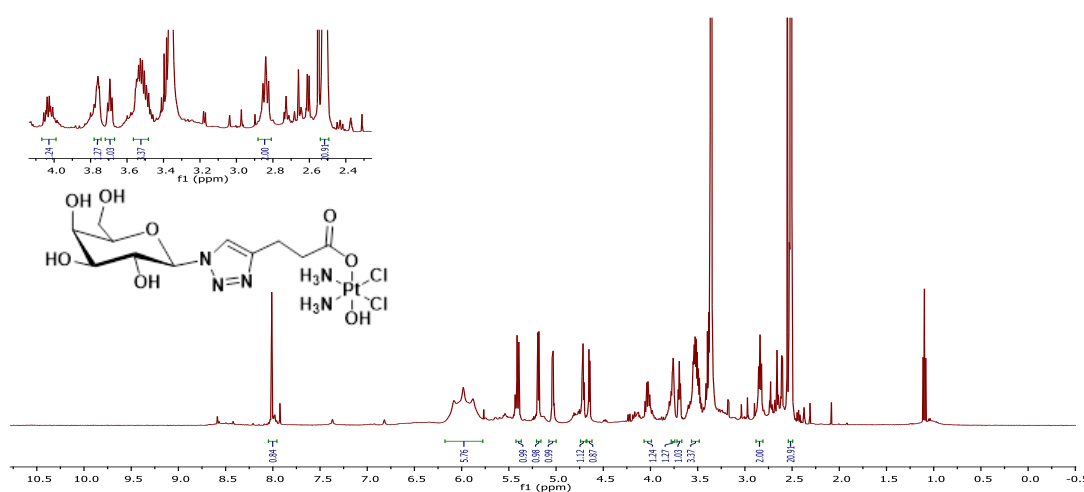
<sup>1</sup>H NMR spectrum of **Complex 1** in DMSO-d<sub>6</sub><sup>13</sup>C NMR spectrum of **Complex 1** in DMSO-d<sub>6</sub>

COSY NMR spectrum of **Complex 1** in DMSO-d<sub>6</sub>HSQC NMR spectrum of **Complex 1** in DMSO-d<sub>6</sub>HMBC NMR spectrum of **Complex 1** in DMSO-d<sub>6</sub>

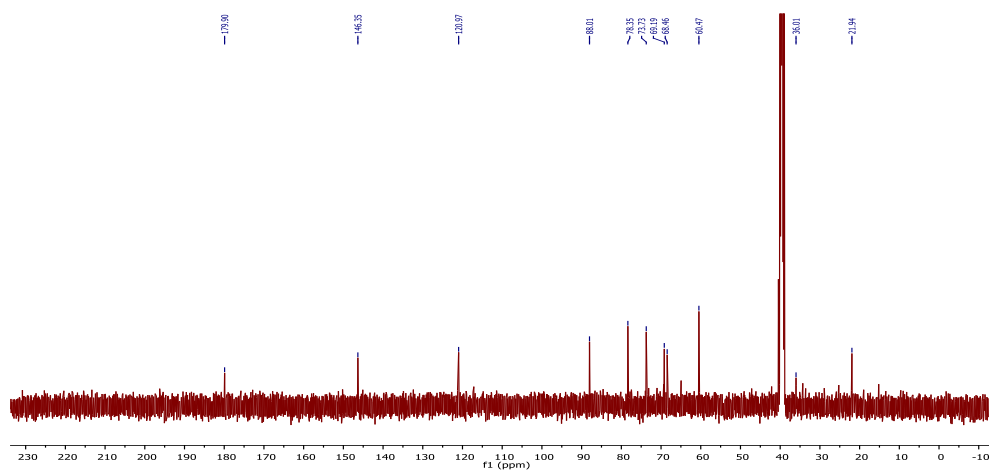


$^{195}\text{Pt}$  NMR spectrum of **Complex 1** in  $\text{DMSO-d}_6$

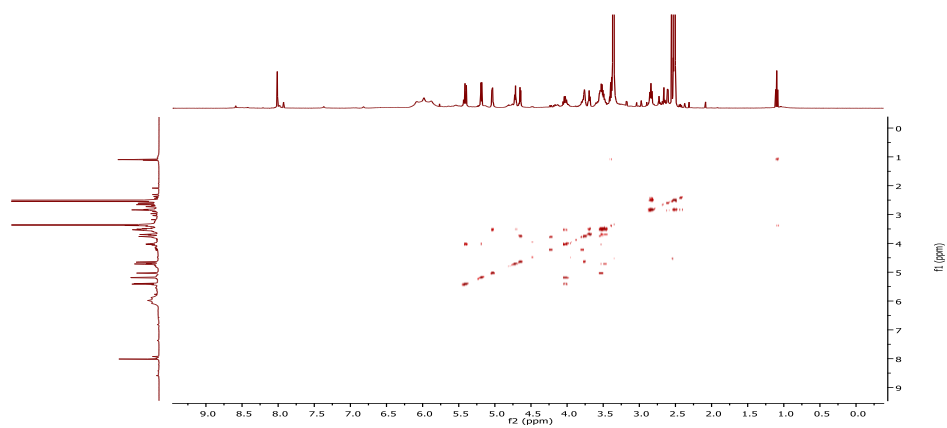
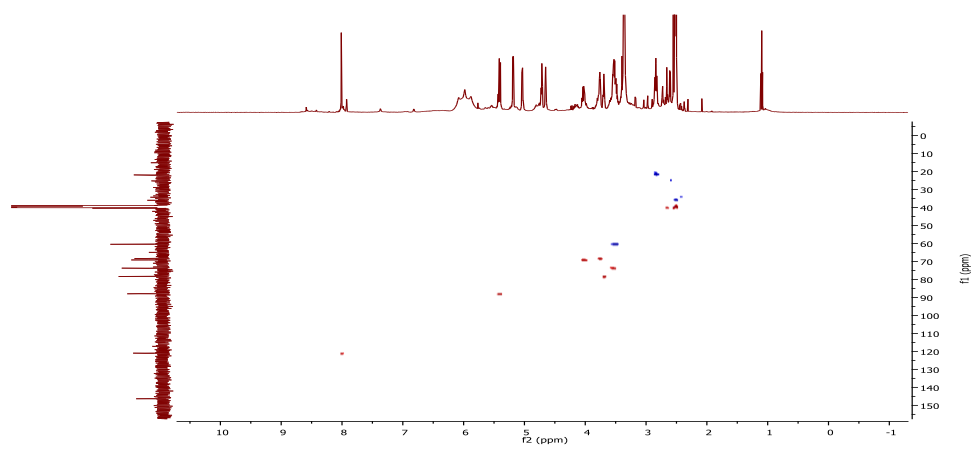
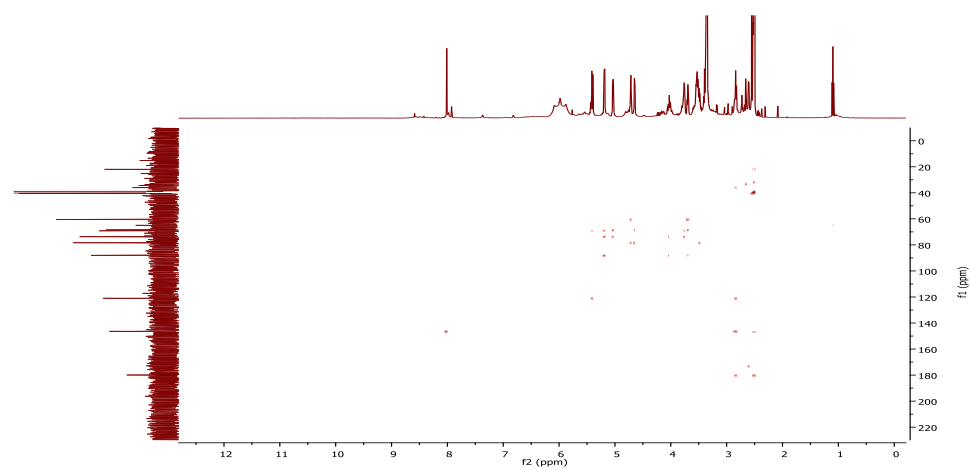
### NMR spectra of Complex 2

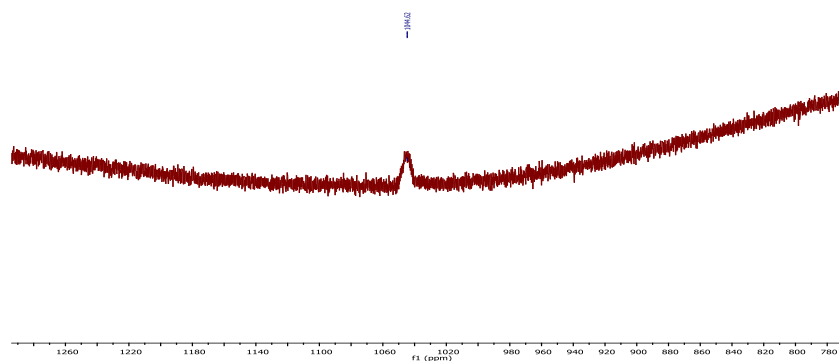


$^1\text{H}$  NMR spectrum of **Complex 2** in  $\text{DMSO-d}_6$



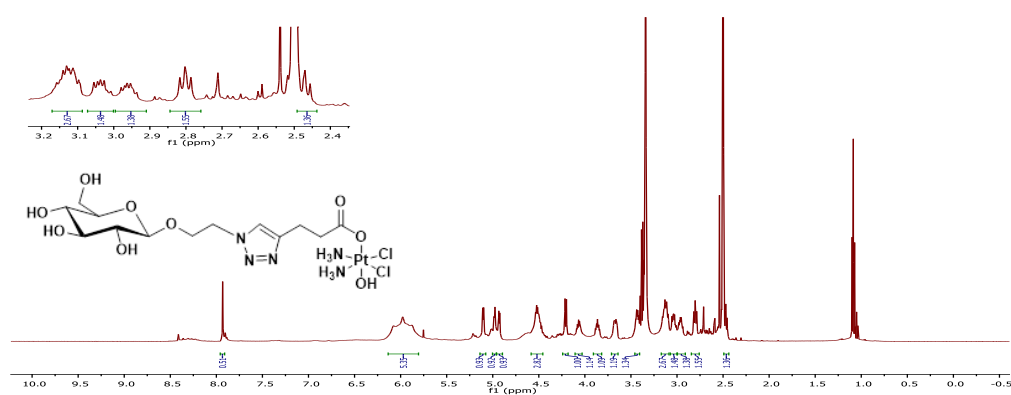
$^{13}\text{C}$  NMR spectrum of **Complex 2** in  $\text{DMSO-d}_6$

COSY NMR spectrum of **Complex 2** in DMSO-d<sub>6</sub>HSQC NMR spectrum of **Complex 2** in DMSO-d<sub>6</sub>HMBC NMR spectrum of **Complex 2** in DMSO-d<sub>6</sub>

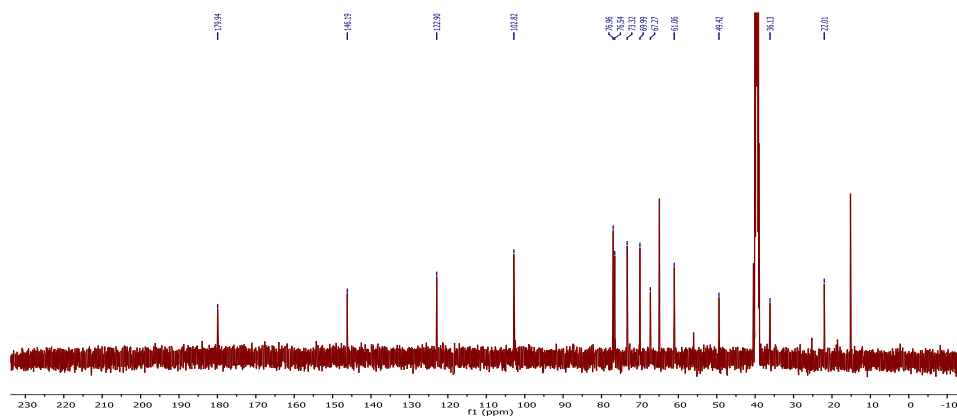


$^{195}\text{Pt}$  NMR spectrum of **Complex 2** in  $\text{DMSO-d}_6$

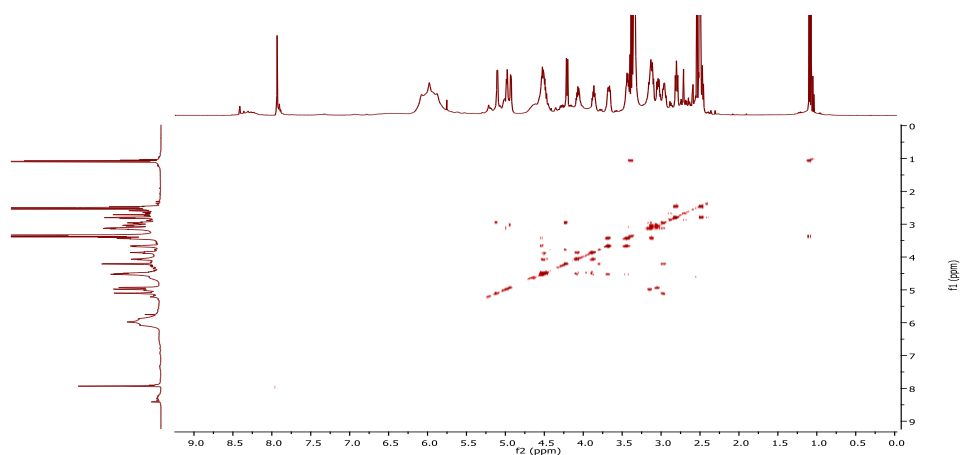
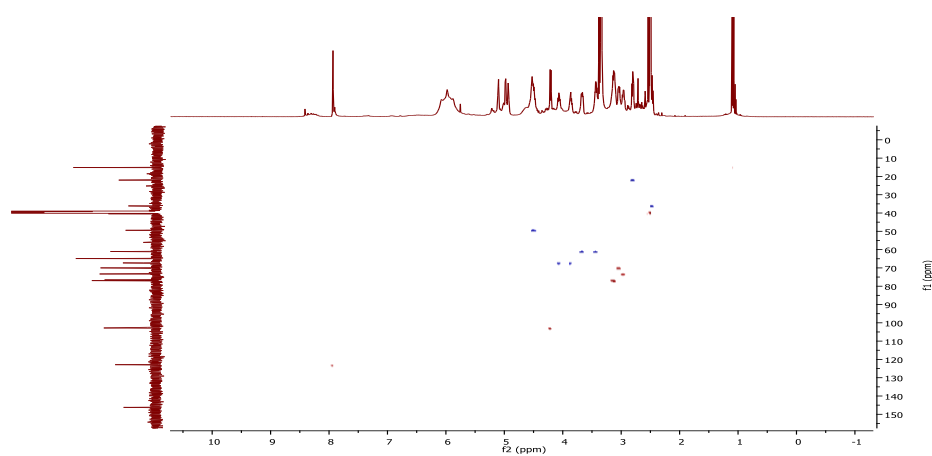
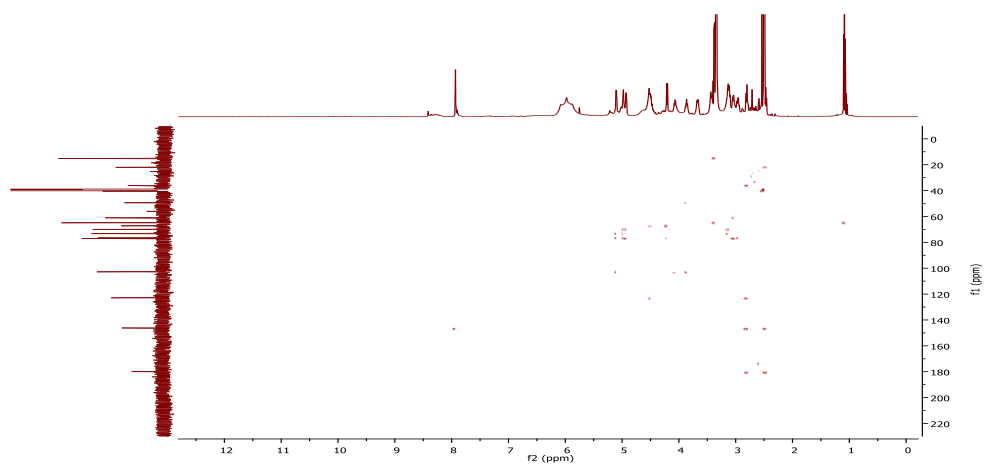
### NMR spectra of Complex 3



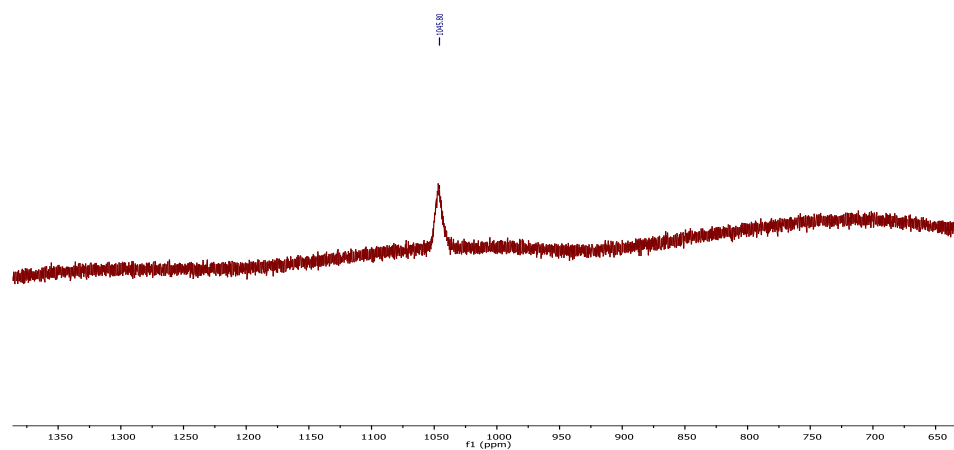
$^1\text{H}$  NMR spectrum of **Complex 3** in  $\text{DMSO-d}_6$



$^{13}\text{C}$  NMR spectrum of **Complex 3** in  $\text{DMSO-d}_6$

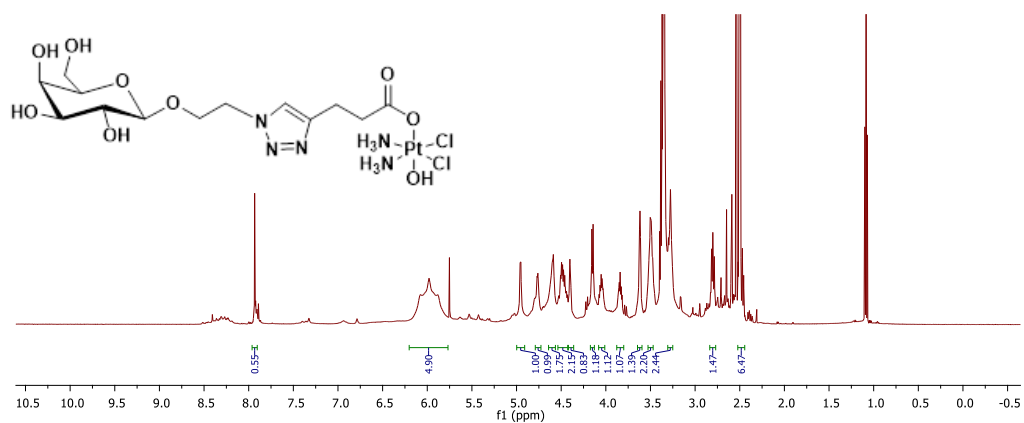
COSY NMR spectrum of **Complex 3** in DMSO-d<sub>6</sub>HSQC NMR spectrum of **Complex 3** in DMSO-d<sub>6</sub>HMBC NMR spectrum of **Complex 3** in DMSO-d<sub>6</sub>



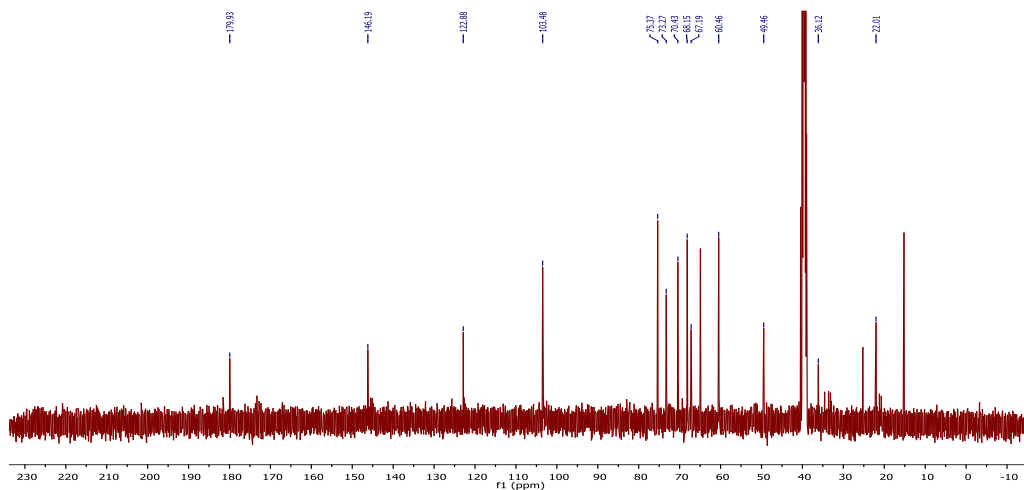


$^{195}\text{Pt}$  NMR spectrum of **Complex 3** in  $\text{DMSO-d}_6$

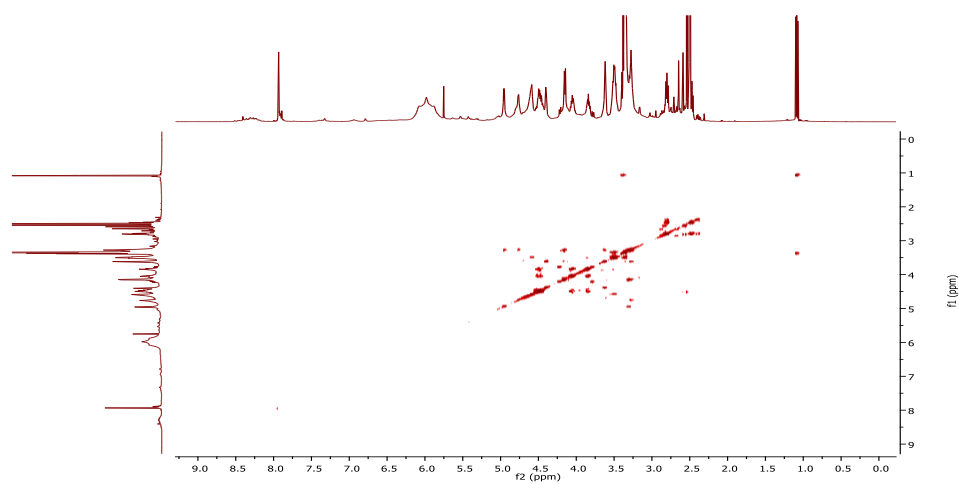
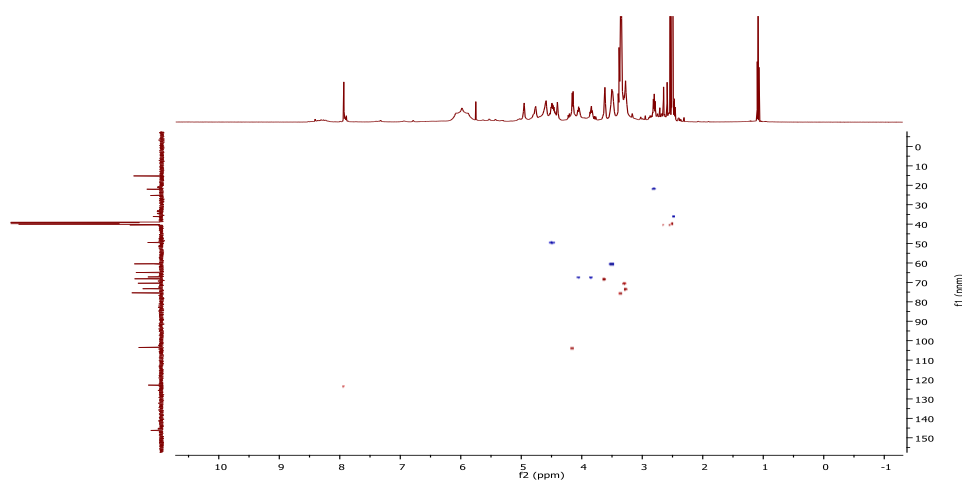
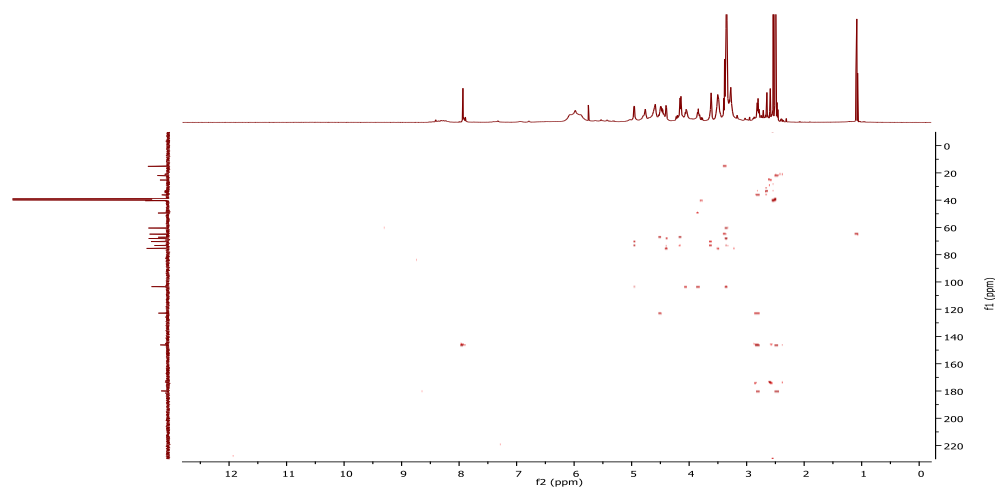
### NMR spectra of Complex 4

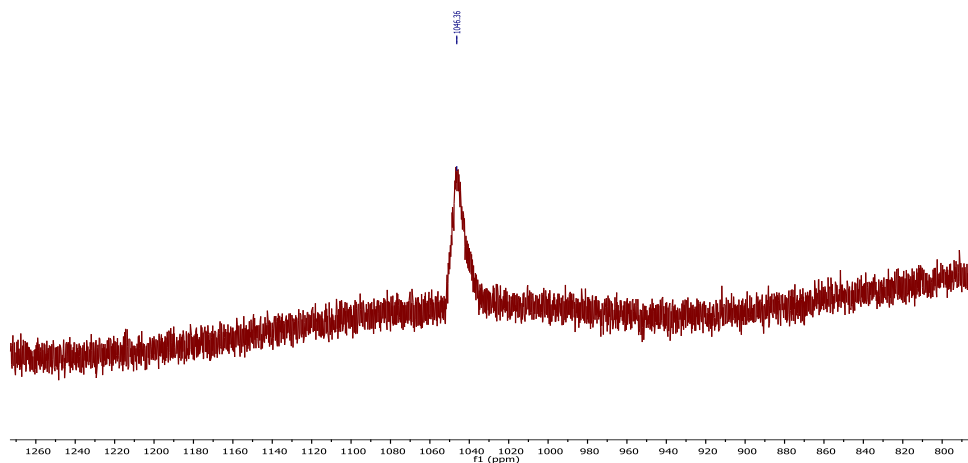


$^1\text{H}$  NMR spectrum of **Complex 4** in  $\text{DMSO-d}_6$



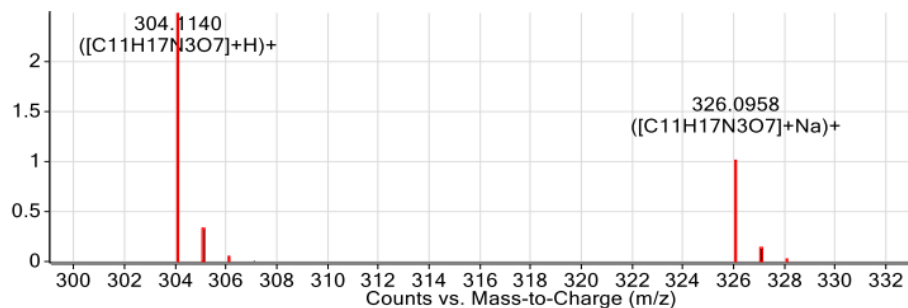
$^{13}\text{C}$  NMR spectrum of **Complex 4** in  $\text{DMSO-d}_6$

COSY NMR spectrum of **Complex 4** in DMSO-d<sub>6</sub>HSQC NMR spectrum of **Complex 4** in DMSO-d<sub>6</sub>HMBC NMR spectrum of **Complex 4** in DMSO-d<sub>6</sub>

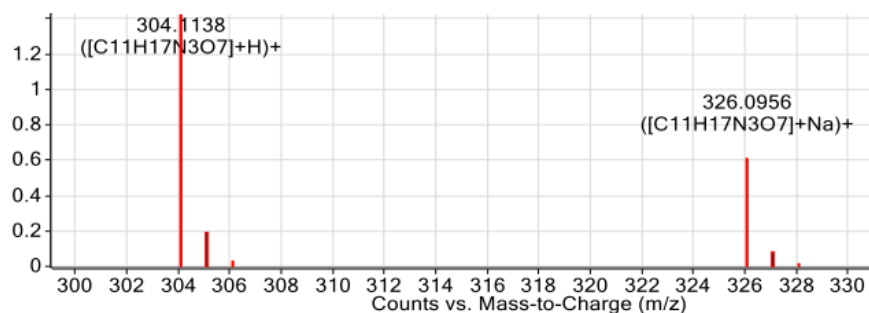


$^{195}\text{Pt}$  NMR spectrum of **Complex 4** in  $\text{DMSO-d}_6$

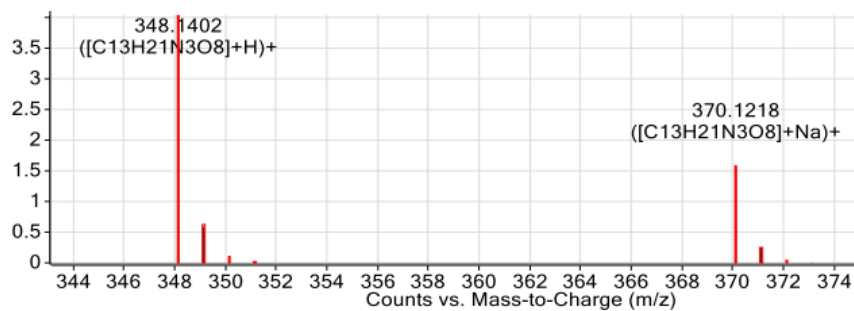
#### HR-MS



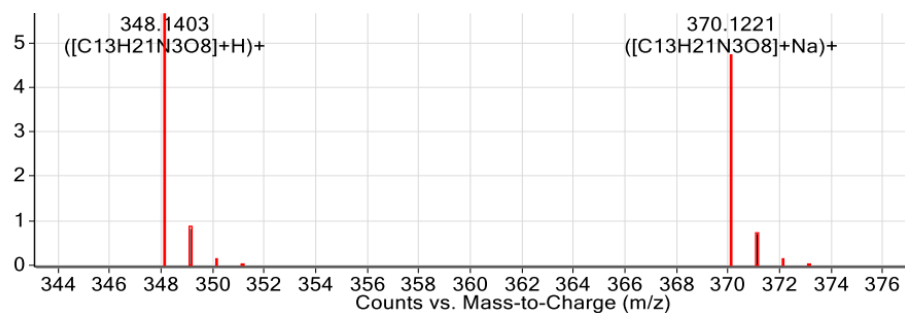
HR-MS spectrum of **3.9**



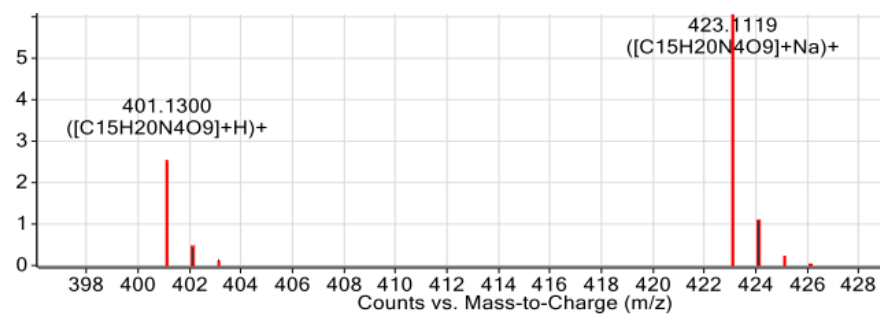
HR-MS spectrum of **3.10**



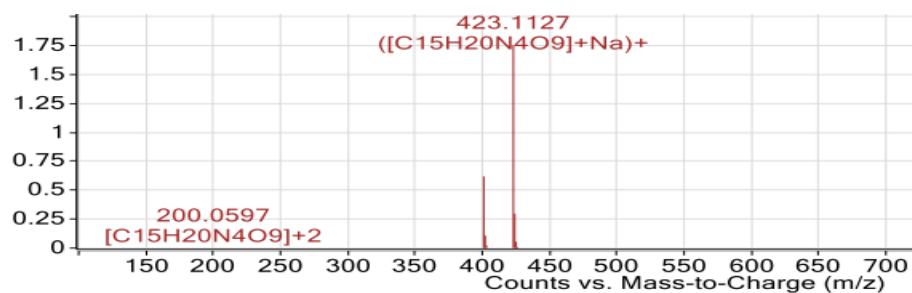
HR-MS spectrum of **3.13**



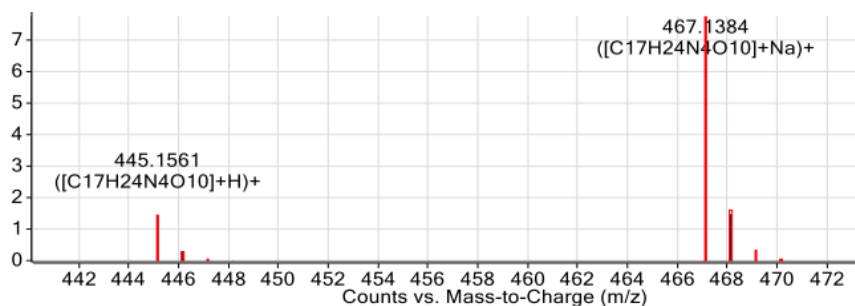
HR-MS spectrum of 3.14



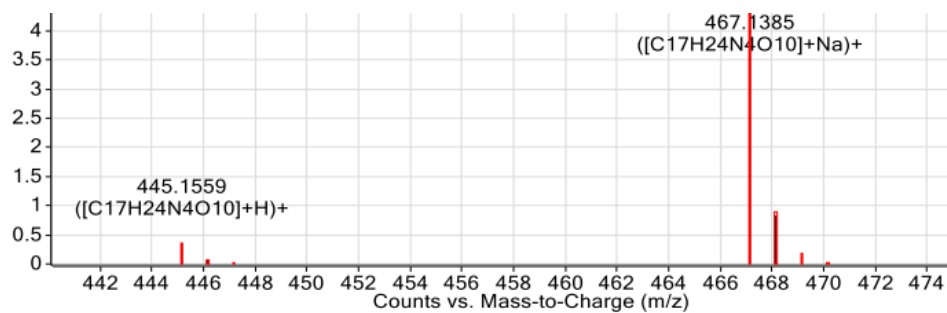
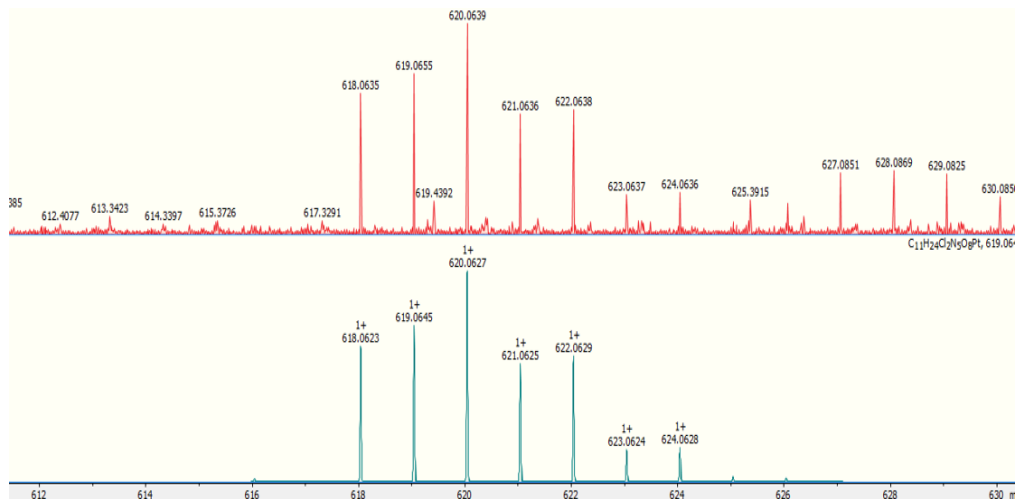
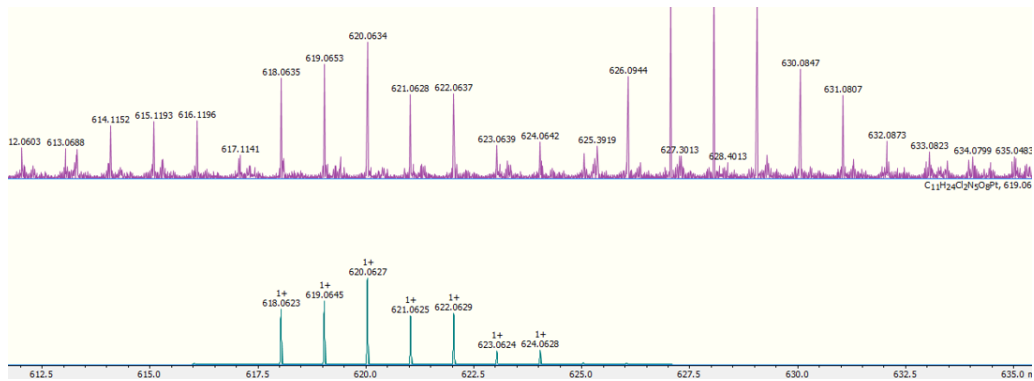
HR-MS spectrum of 3.11

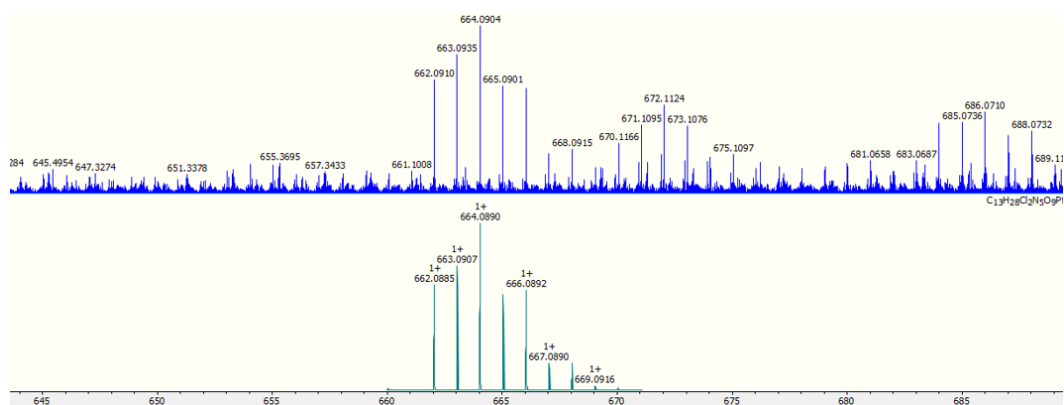
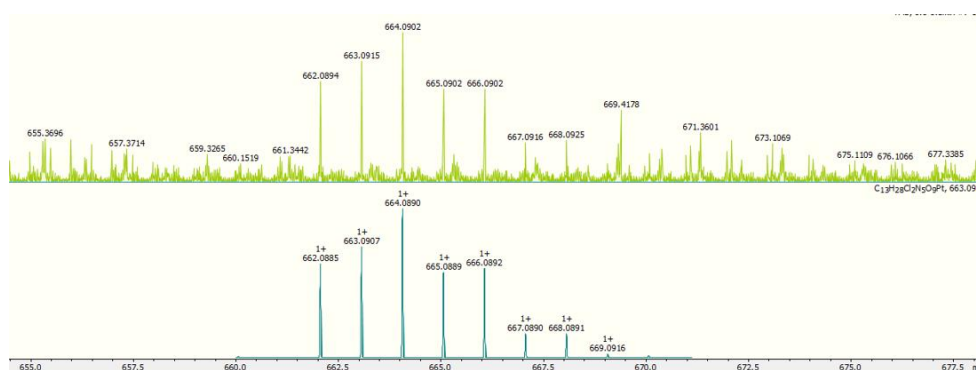


HR-MS spectrum of 3.12

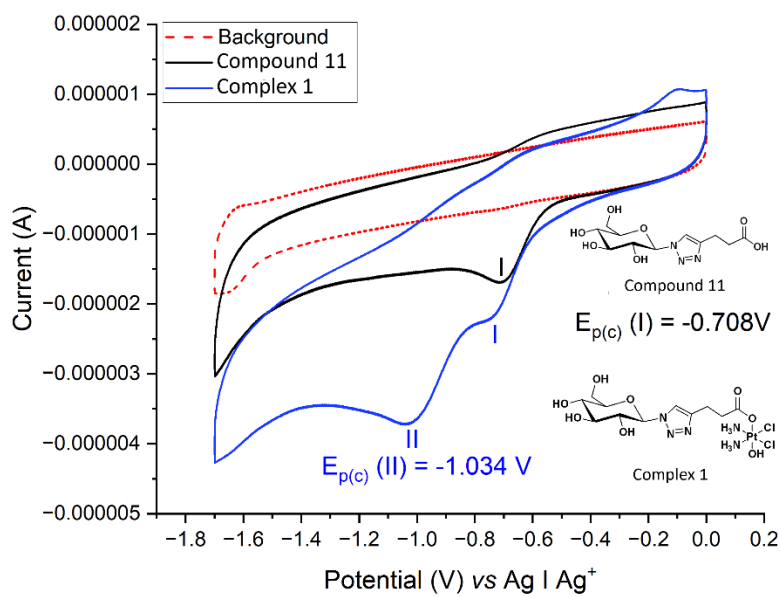


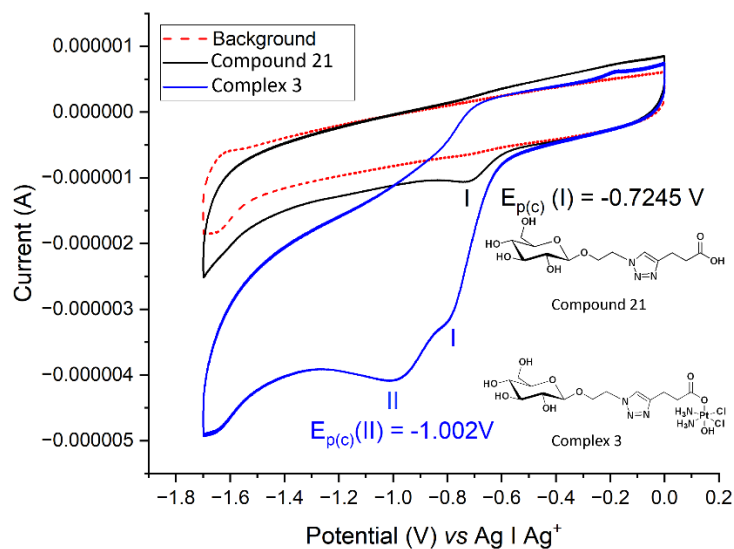
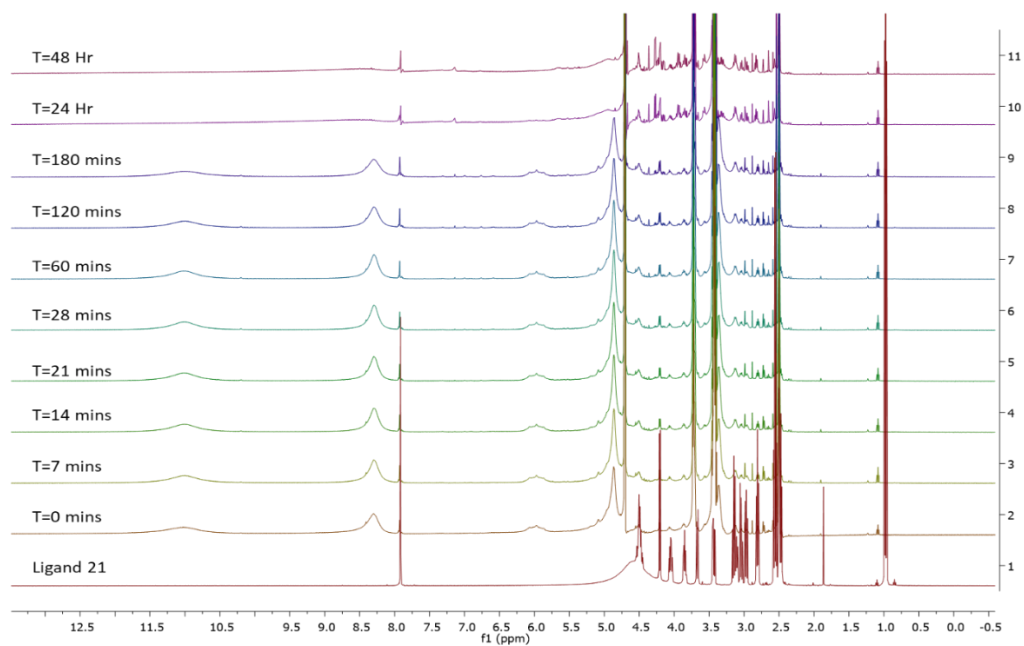
HR-MS spectrum of 3.15

HR-MS spectrum of **3.16**HR-MS spectrum of **Complex 1**HR-MS spectrum of **Complex 2**

HR-MS spectrum of **Complex 3**HR-MS spectrum of **Complex 4**

## Cyclic Voltammetry

Cyclic voltammogram of **Complex 1** and ligand **3.9**

Cyclic voltammogram of **Complex 3** and ligand **3.13****Reduction Study**

Complex 3: <sup>1</sup>H-NMR spectra of the **Complex 3** with addition of 10 eq. of ascorbic acid. NMR spectra were collected every 7 minutes for 30 minutes and then every hour for 3 hours and finally left to reduce for 2 days.

## Biological Figures

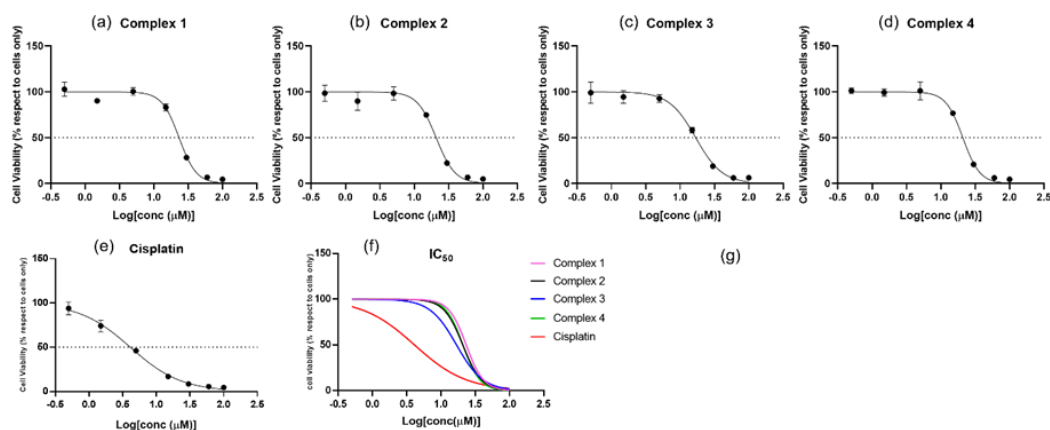


**Figure 1S.** 2D *in vitro* screening of complexes 1-4 on MG63 cell line by MTT assay and  $\text{IC}_{50}$  ( $\mu\text{M}$ ) values. Dose-response curves used to generate  $\text{IC}_{50}$  ( $\mu\text{M}$ ) for complexes 1 (a), 2 (b), 3 (c) and 4 (d), and for cisplatin (e) inhibitor activity on cell viability of MG63 cell line. The Log[concentration] in  $\mu\text{M}$  and the normalised response (%) of survival fraction of cells are reported on X and Y axes, respectively. For each complex, the curve interpolation with 50% survival cells is highlighted in Y dotted line and correspond to its  $\text{LogIC}_{50}$ . A comparison of all dose-response curves is reported (f).

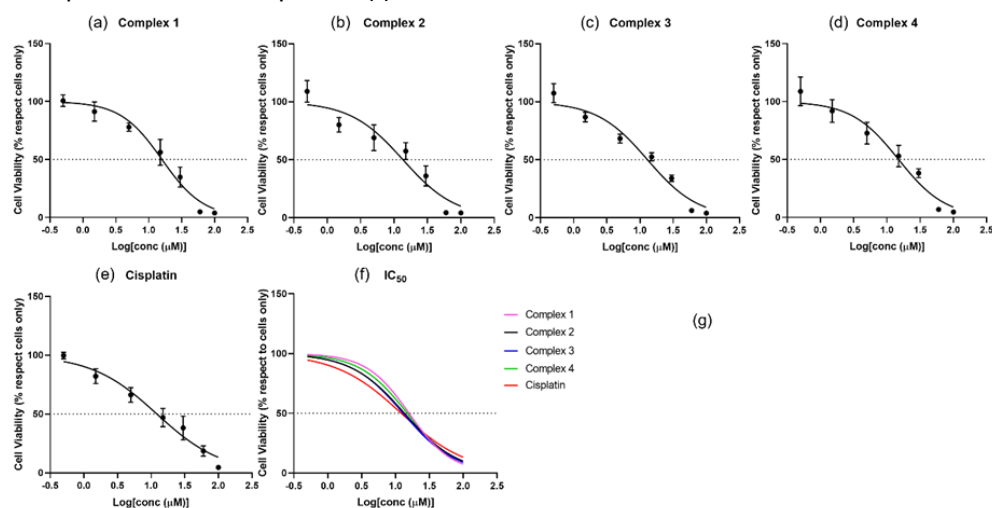


**Figure 2S.** 2D *in vitro* screening of complexes 1-4 on SAOS-2 cell line by MTT assay and  $\text{IC}_{50}$  ( $\mu\text{M}$ ) values. Dose-response curves used to generate  $\text{IC}_{50}$  ( $\mu\text{M}$ ) for complexes 1 (a), 2 (b), 3 (c) and 4 (d), and for cisplatin (e) inhibitor activity on cell viability of SAOS-2 cell line. The Log[concentration] in  $\mu\text{M}$  and the normalised response (%) of survival fraction of cells are reported on X and Y axes, respectively. For each complex, the curve interpolation with 50% survival cells is highlighted in Y dotted line and correspond to its  $\text{LogIC}_{50}$ . A comparison of all dose-response curves is reported (f).



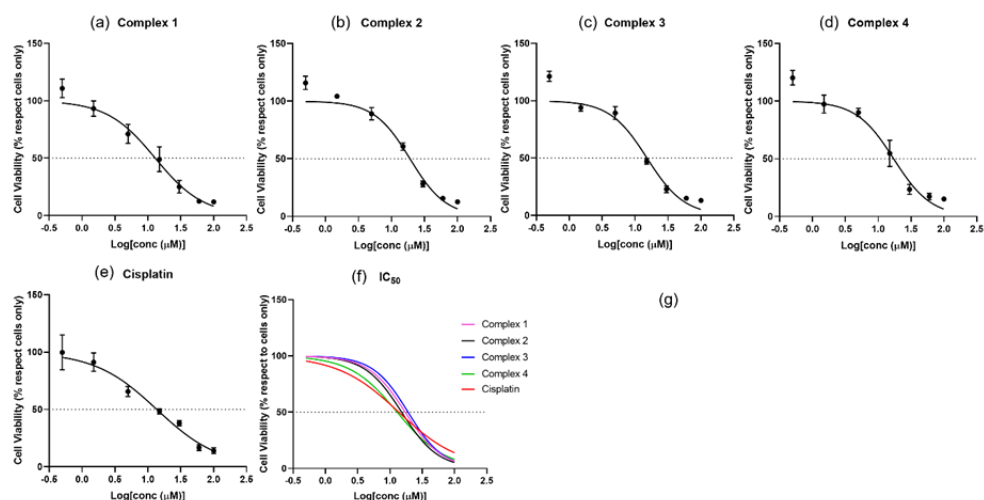


**Figure 3S.** 2D *in vitro* screening of complexes 1-4 on hFOB cells line by MTT assay and  $\text{IC}_{50}$  ( $\mu\text{M}$ ) values. Dose-response curves used to generate  $\text{IC}_{50}$  ( $\mu\text{M}$ ) for complexes 1 (a), 2 (b), 3 (c) and 4 (d), and for cisplatin (e) inhibitor activity on cell viability of hFOB cells line. The Log[concentration] in  $\mu\text{M}$  and the normalised response (%) of survival fraction of cells are reported on X and Y axes, respectively. For each complex, the curve interpolation with 50% survival cells is highlighted in Y dotted line and correspond to its  $\text{LogIC}_{50}$ . A comparison of all dose-response curves is reported (f).

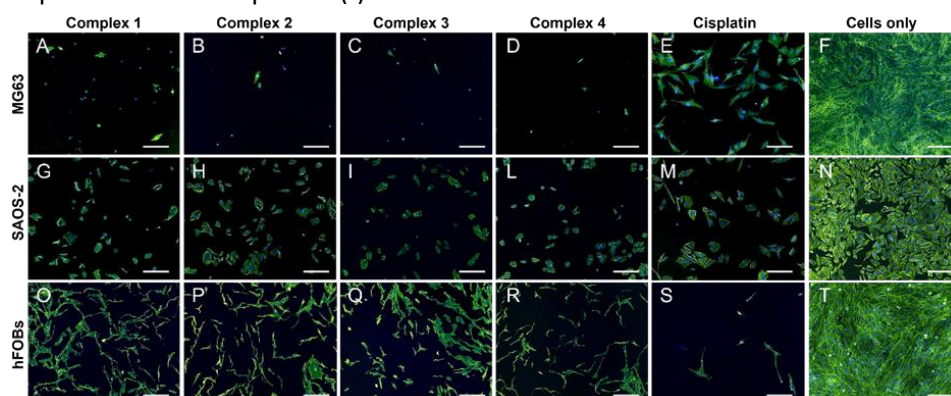


**Figure 4S.** Actin and DAPI staining of 2D *in vitro* screening of complexes 1-4. The cell morphology evaluation of MG63 (A – F), SAOS-2 (G – N) and hFOB (O – T) cell lines cultured with complexes 1-4 and cisplatin are reported in the figure. For SAOS-2 and hFOB 30  $\mu\text{M}$  concentration was selected for the analysis, while 60  $\mu\text{M}$  is reported for MG63 cells. F-actin filaments in Phalloidin (Green) and cell nuclei in DAPI (Blue). Scale bars 200  $\mu\text{m}$ .

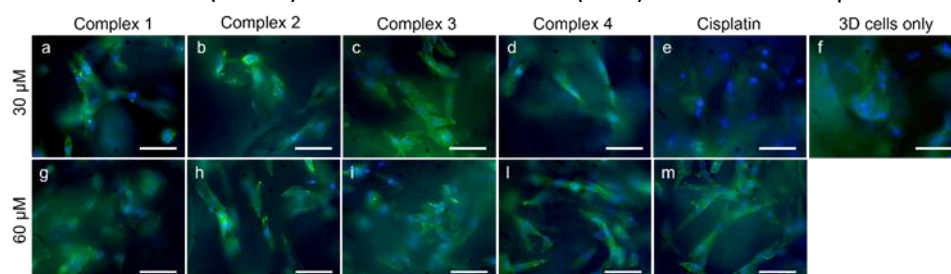
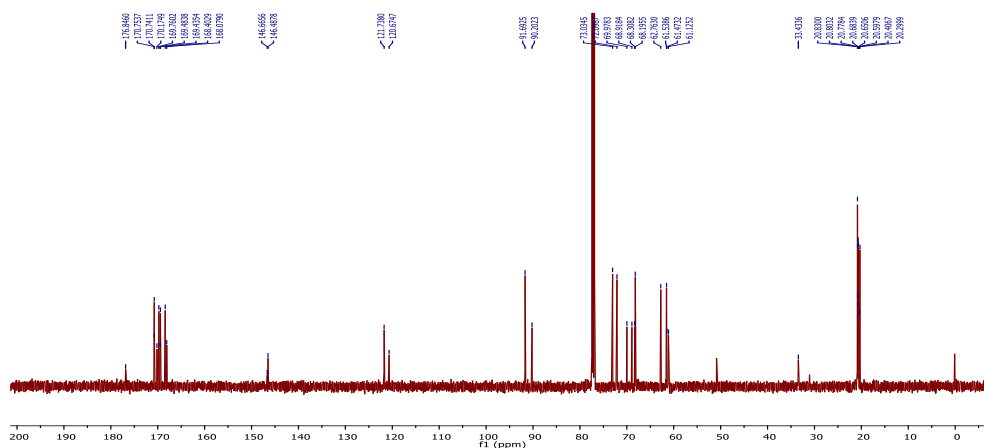
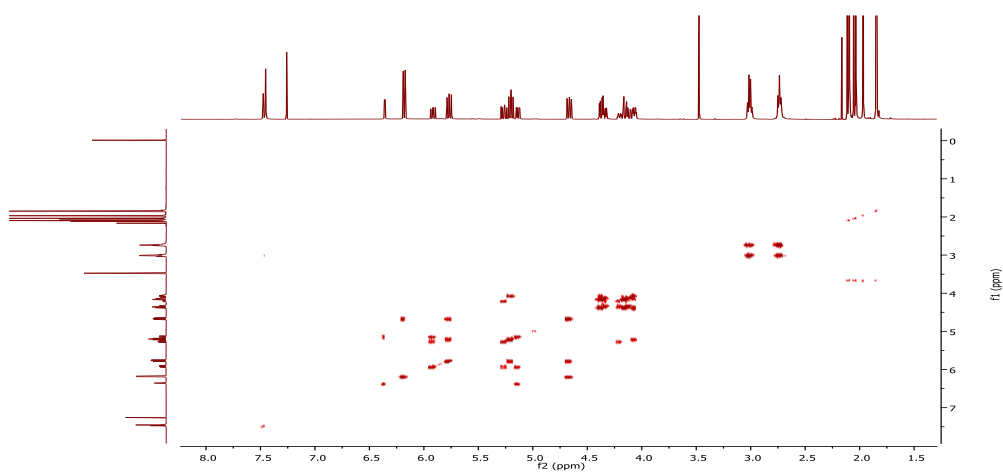


**Figure 5S.** Actin and DAPI staining of *in vitro* 3D OS model. Cell morphology evaluation 3D OS model of MG63 cells after 72 hours in the presence of Complex 1 (a;g), 2 (b;h), 3 (c;i), 4 (d;l) and cisplatin (e;m), and without any drug (f). F-Actin filaments in green (FITC) and cell nuclei in blue (DAPI). Scale bars 50  $\mu\text{m}$ .

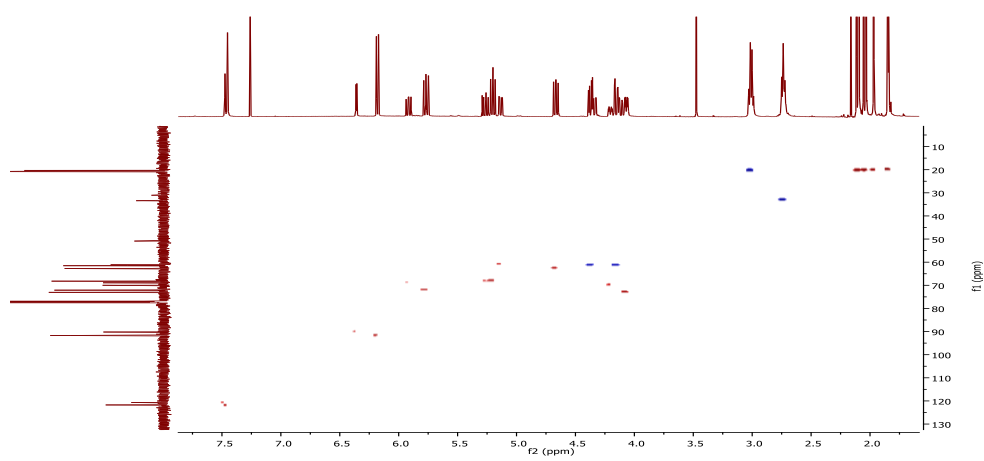




$^{13}\text{C}$  NMR spectrum of **4.9** in  $\text{CDCl}_3$

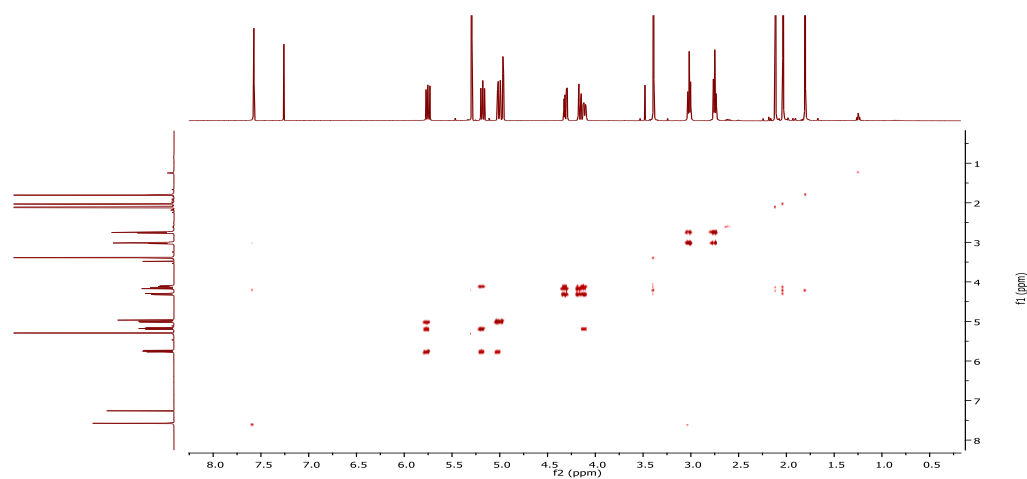
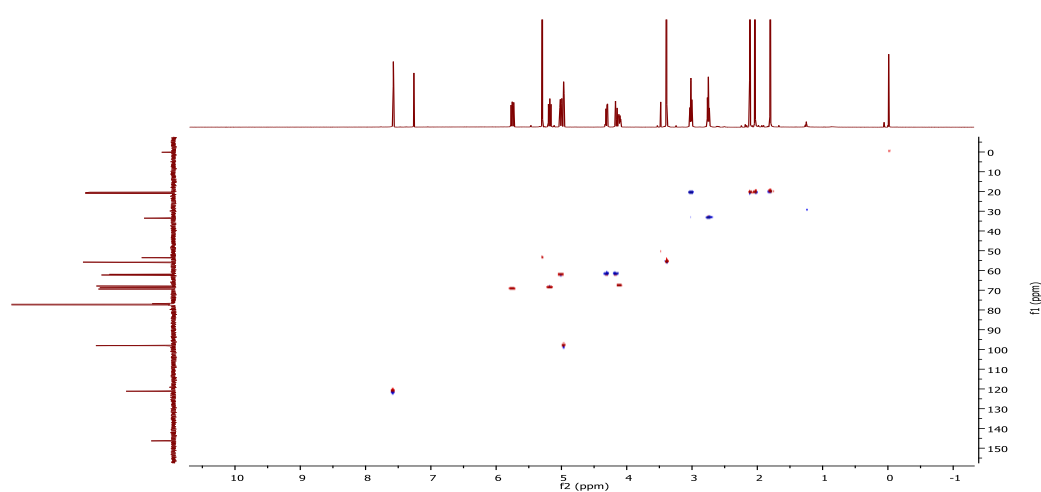
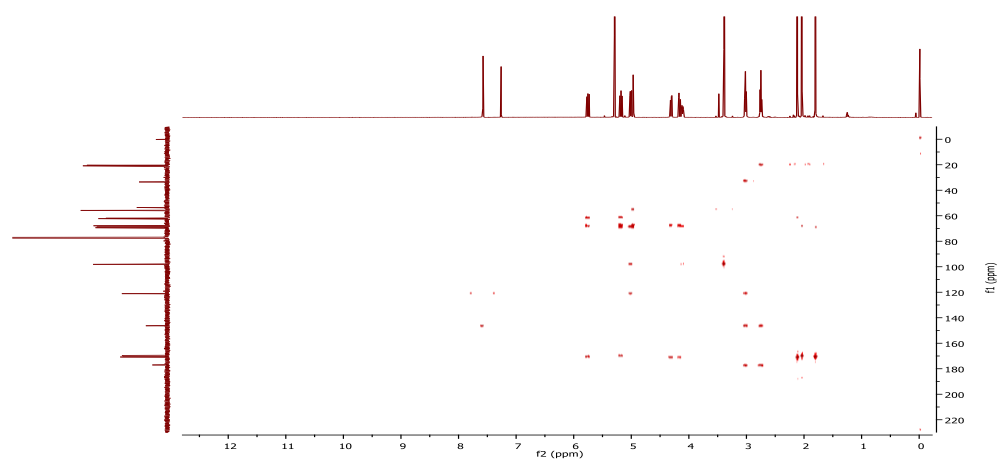


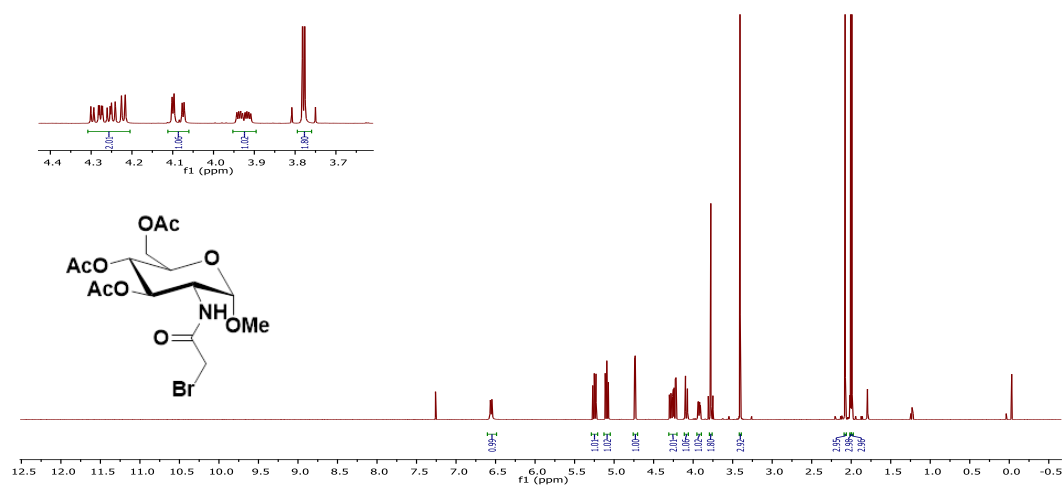
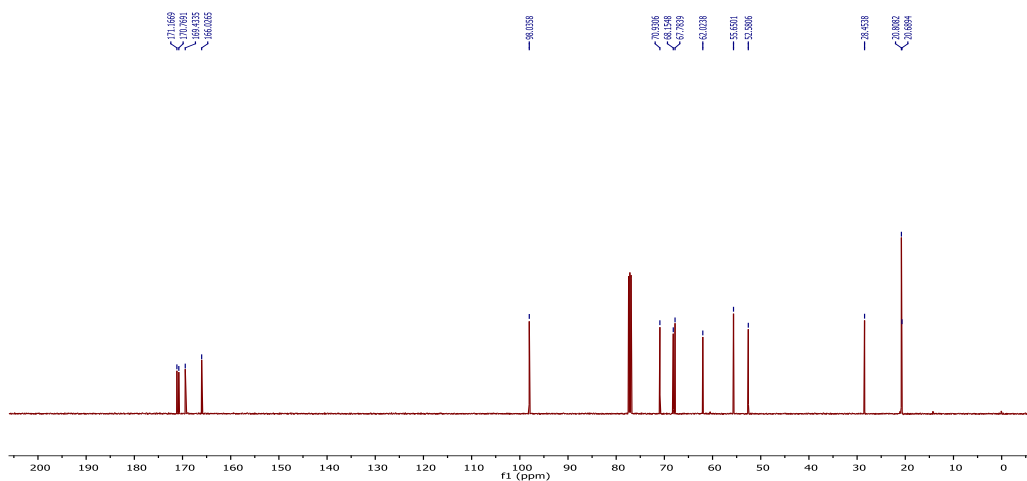
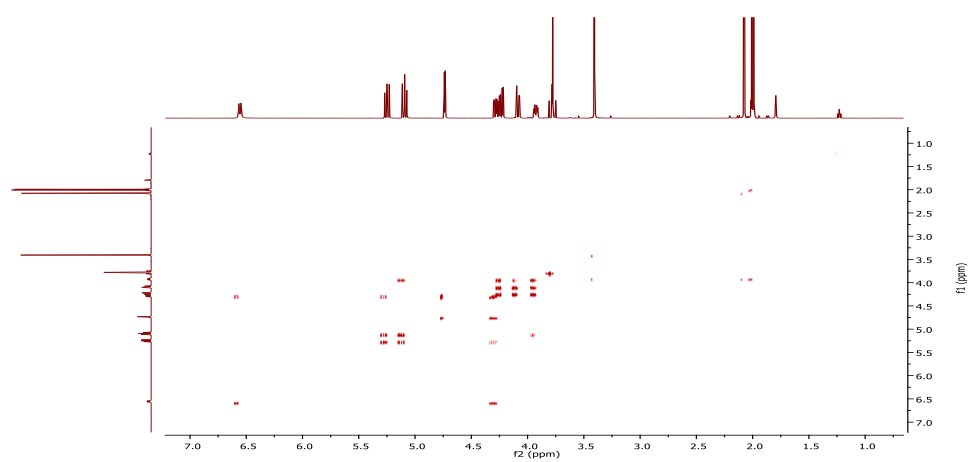
COSY NMR spectrum of **4.9** in  $\text{CDCl}_3$

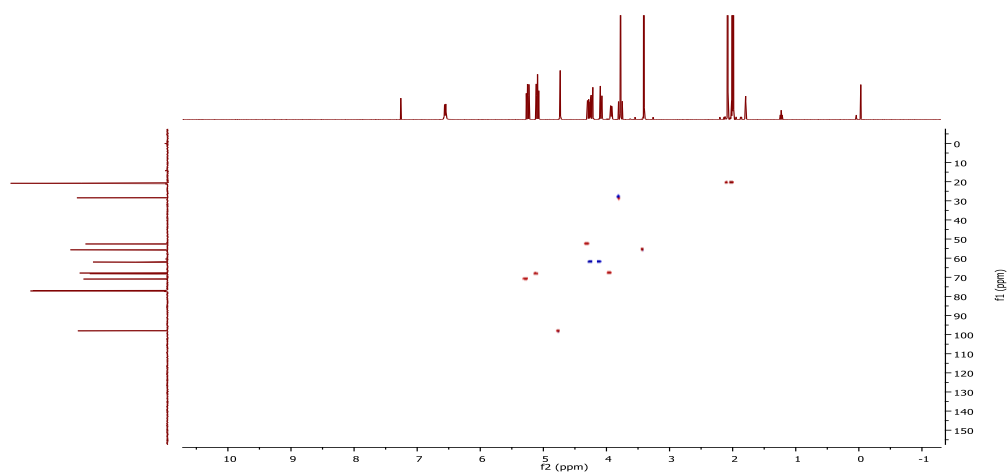
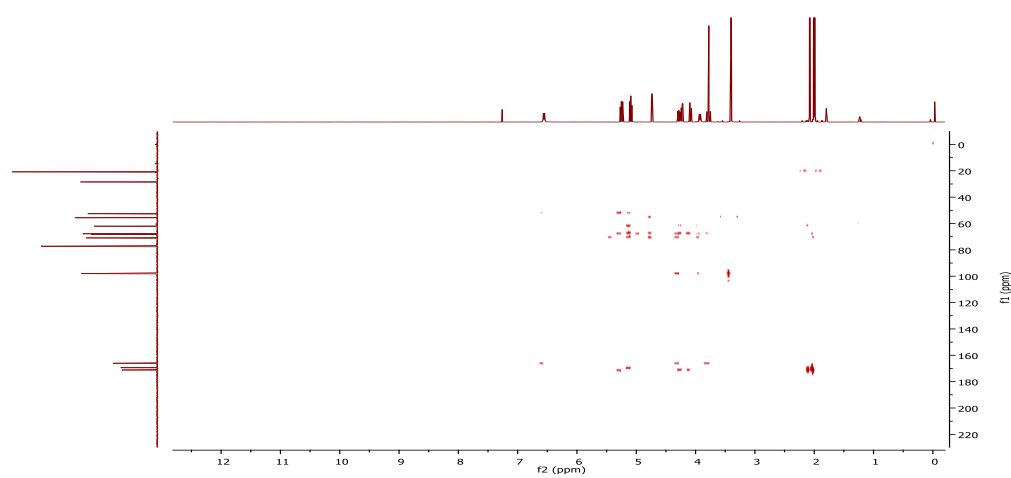
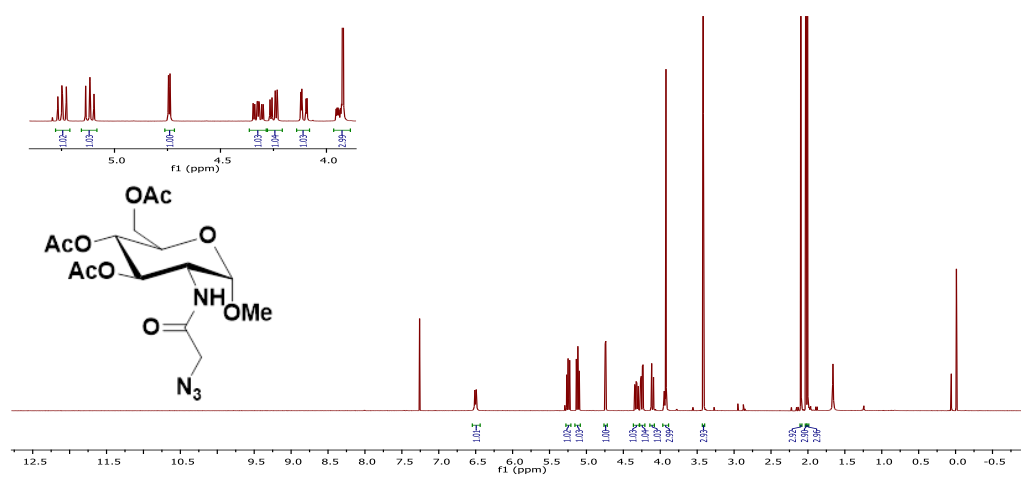


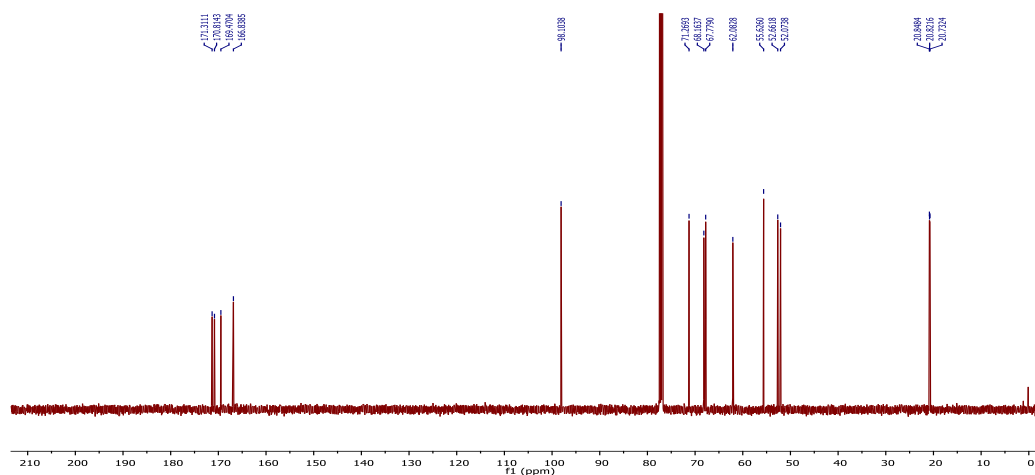
HSQC NMR spectrum of **4.9** in  $\text{CDCl}_3$



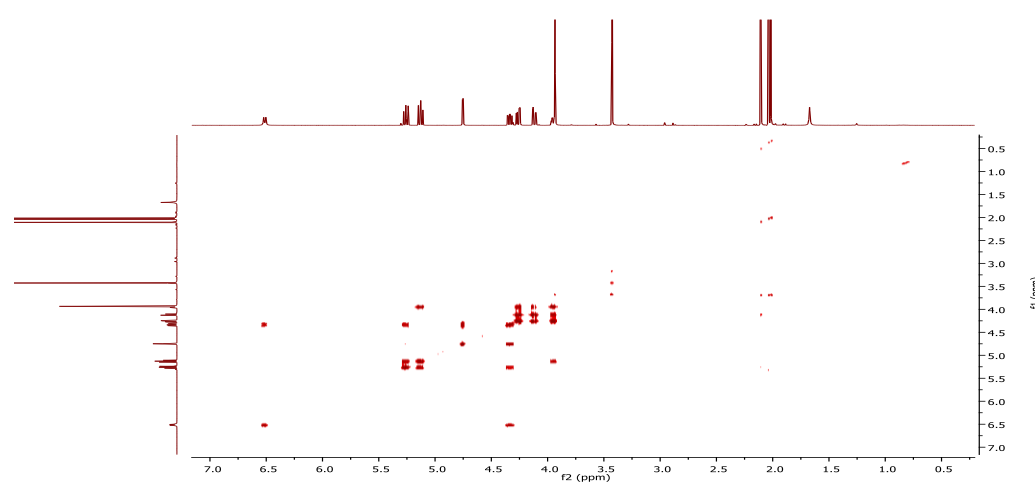
COSY NMR spectrum of **4.16** in CDCl<sub>3</sub>HSQC NMR spectrum of **4.16** in CDCl<sub>3</sub>HMBC NMR spectrum of **4.16** in CDCl<sub>3</sub>

NMR spectra of **4.18** $^1\text{H}$  NMR spectrum of **4.18** in  $\text{CDCl}_3$  $^{13}\text{C}$  NMR spectrum of **4.18** in  $\text{CDCl}_3$ COSY NMR spectrum of **4.18** in  $\text{CDCl}_3$

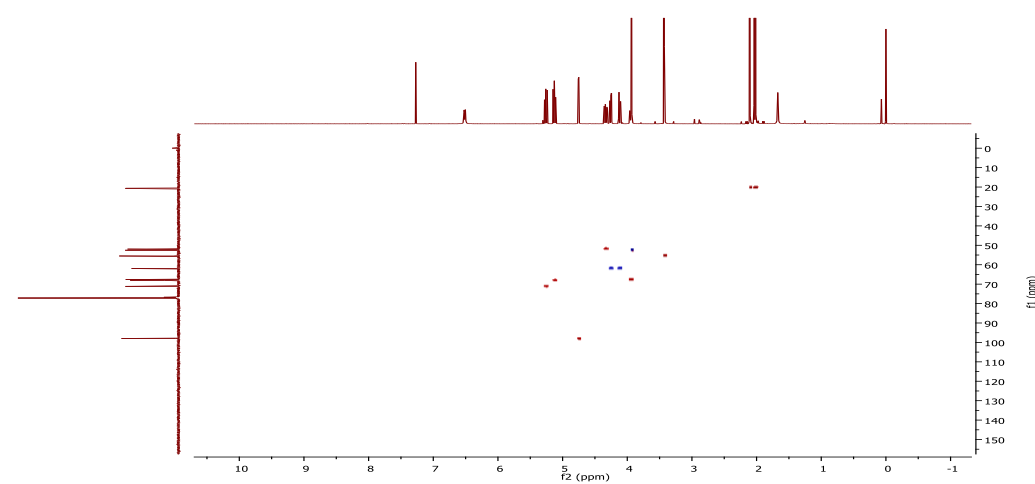
HSQC NMR spectrum of **4.18** in CDCl<sub>3</sub>HMBC NMR spectrum of **4.18** in CDCl<sub>3</sub>NMR spectra of **4.19**<sup>1</sup>H NMR spectrum of **4.19** in CDCl<sub>3</sub>



$^{13}\text{C}$  NMR spectrum of **4.19** in  $\text{CDCl}_3$

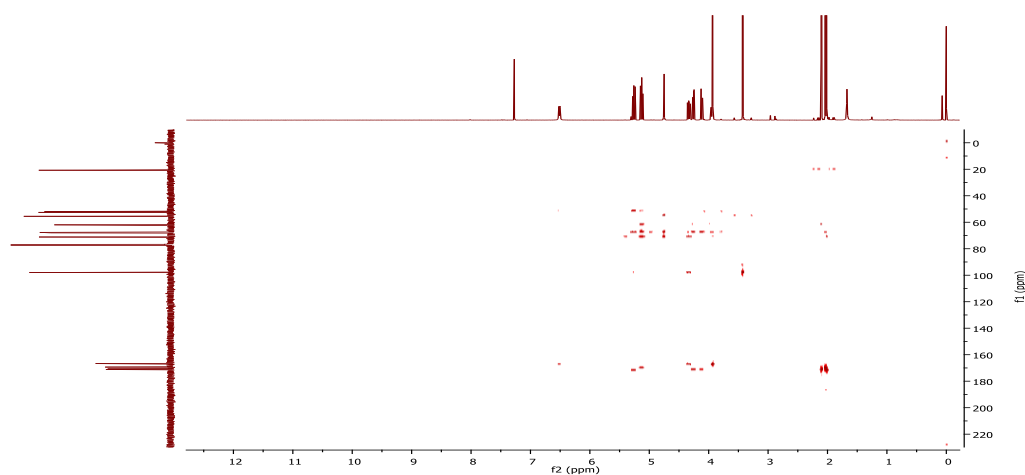
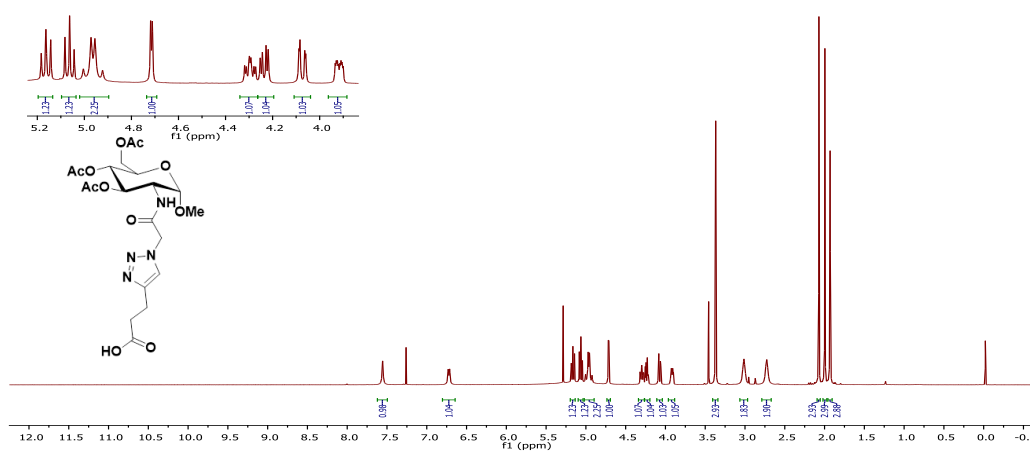
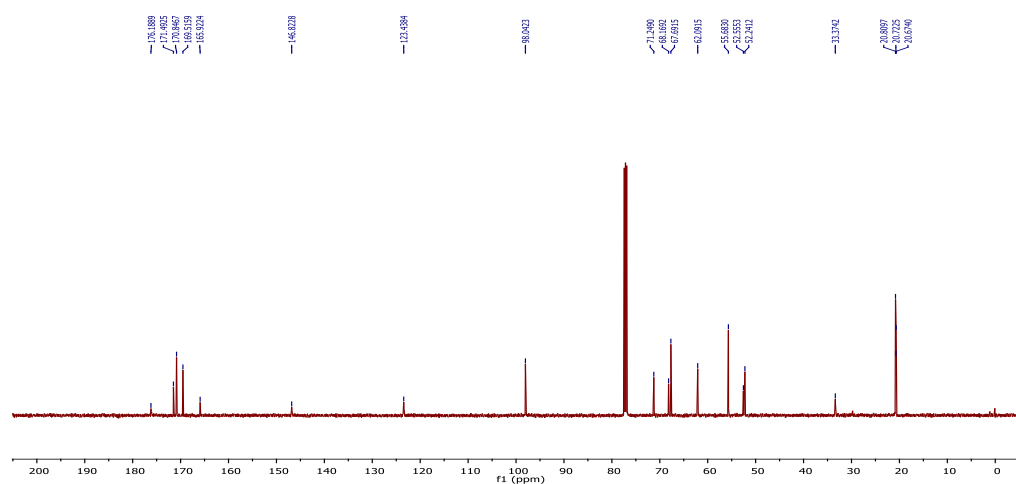


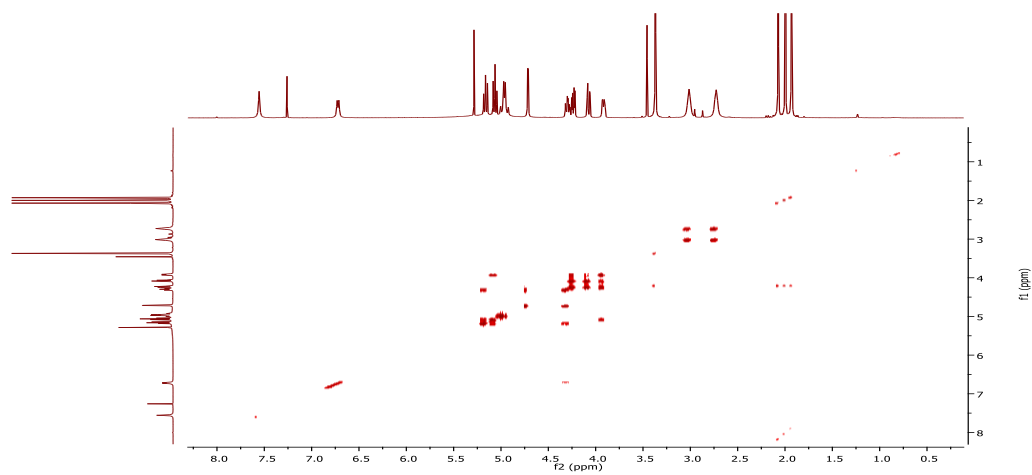
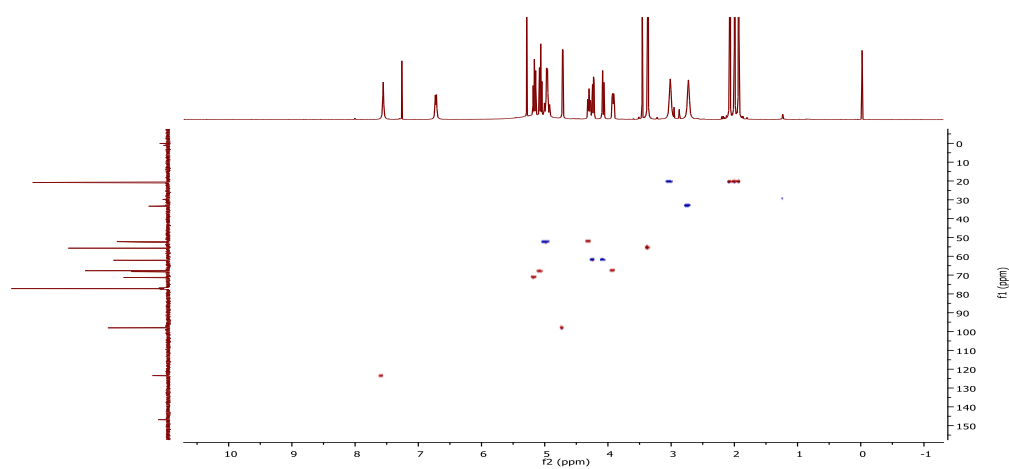
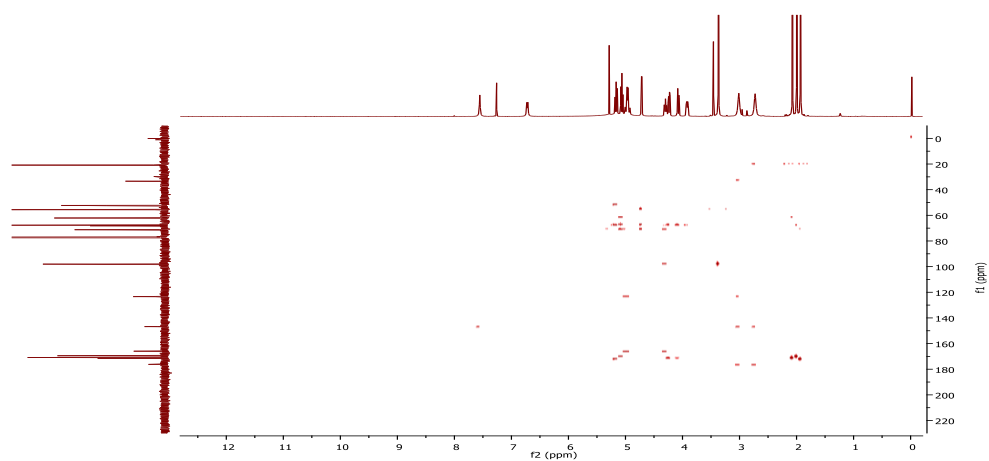
COSY NMR spectrum of **4.19** in  $\text{CDCl}_3$



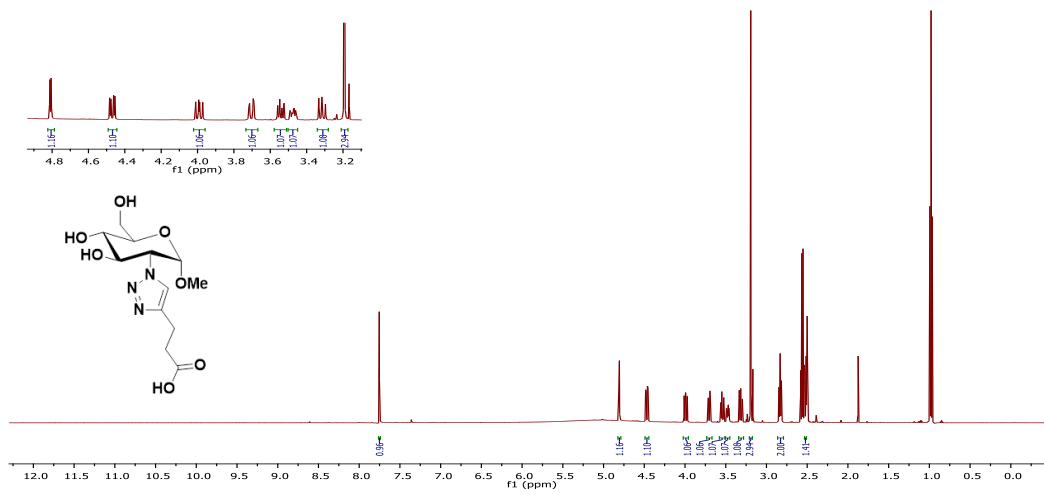
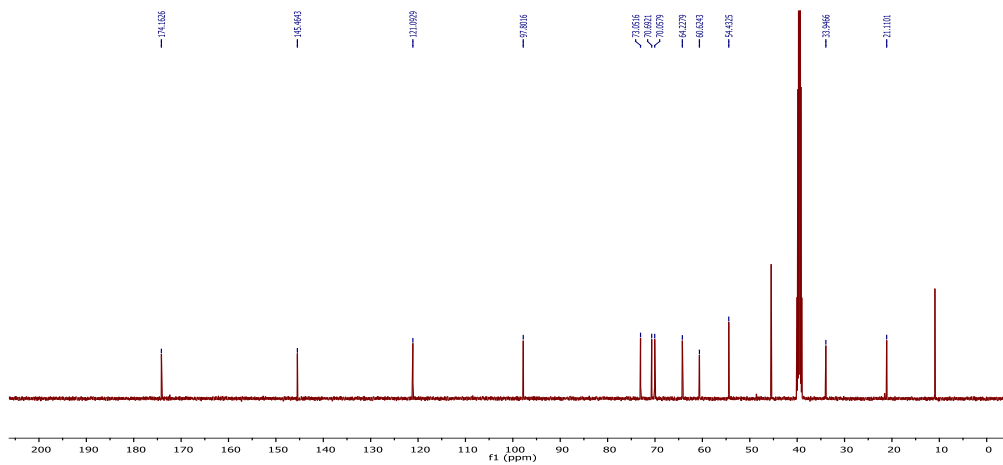
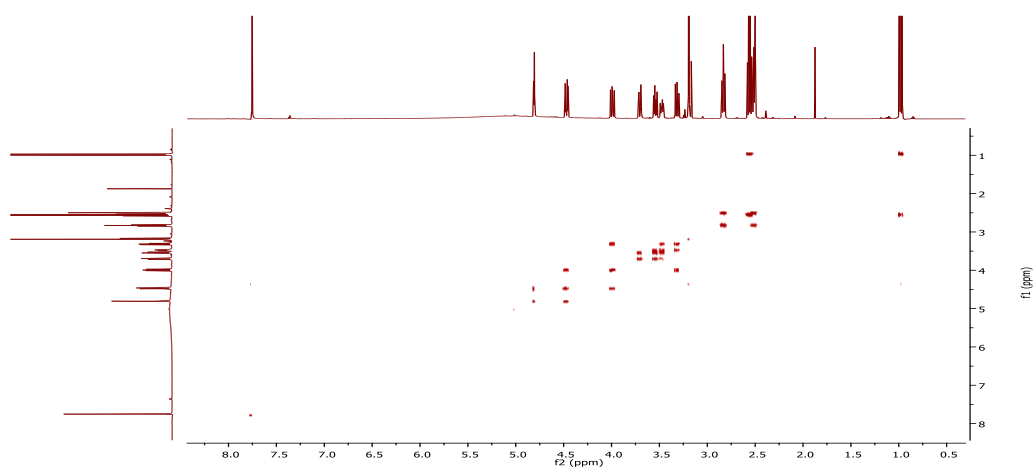
HSQC NMR spectrum of **4.19** in  $\text{CDCl}_3$

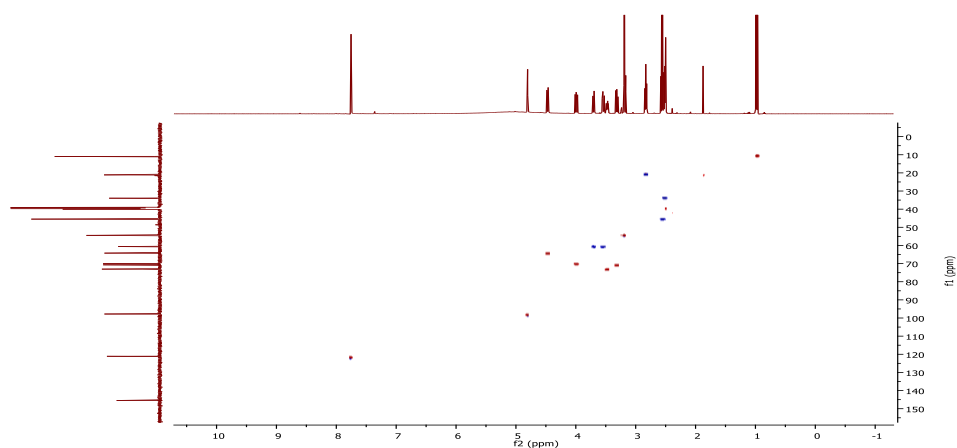
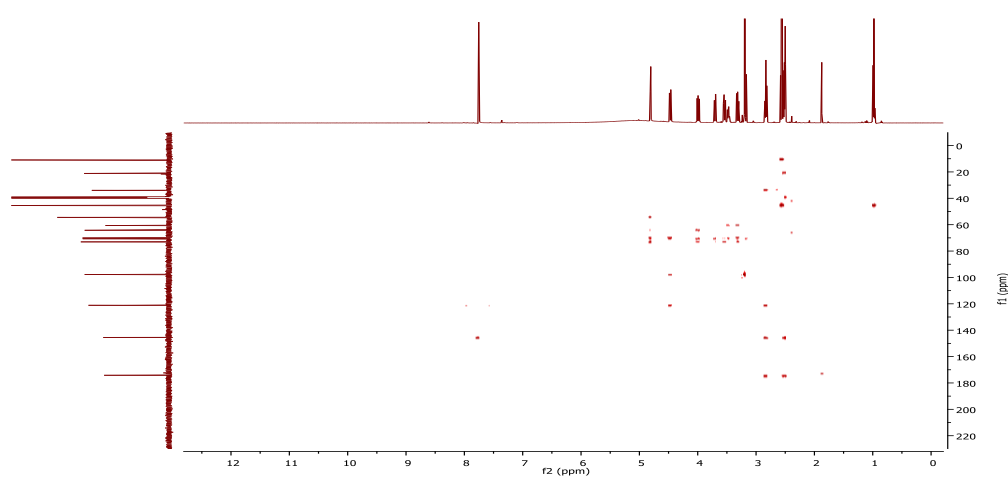
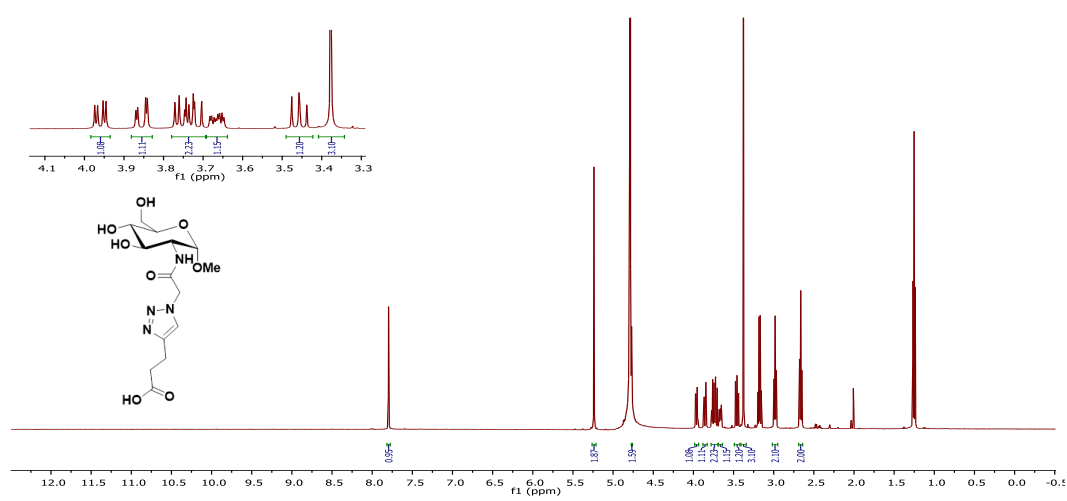


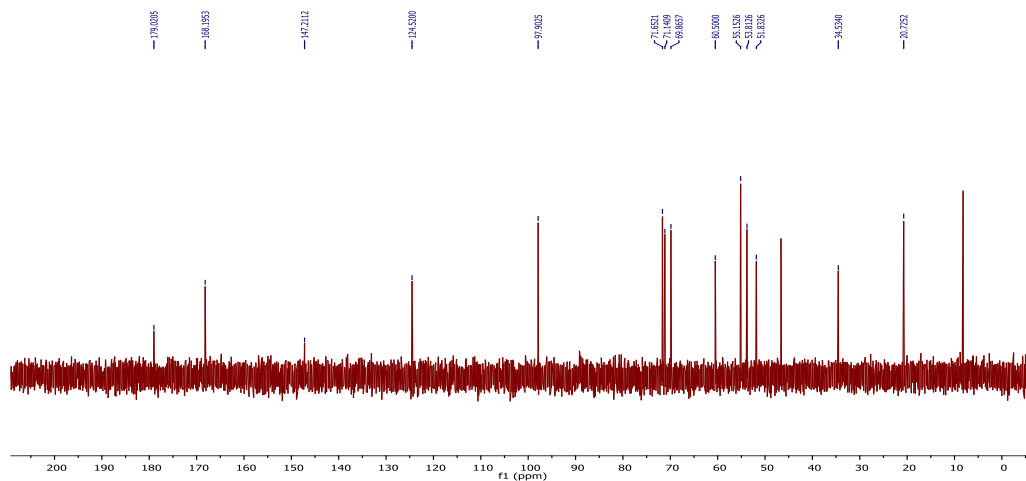
HMBC NMR spectrum of **4.19** in  $\text{CDCl}_3$ NMR spectra of **4.20** $^1\text{H}$  NMR spectrum of **4.20** in  $\text{CDCl}_3$  $^{13}\text{C}$  NMR spectrum of **4.20** in  $\text{CDCl}_3$

COSY NMR spectrum of **4.20** in CDCl<sub>3</sub>HSQC NMR spectrum of **4.20** in CDCl<sub>3</sub>HMBC NMR spectrum of **4.20** in CDCl<sub>3</sub>

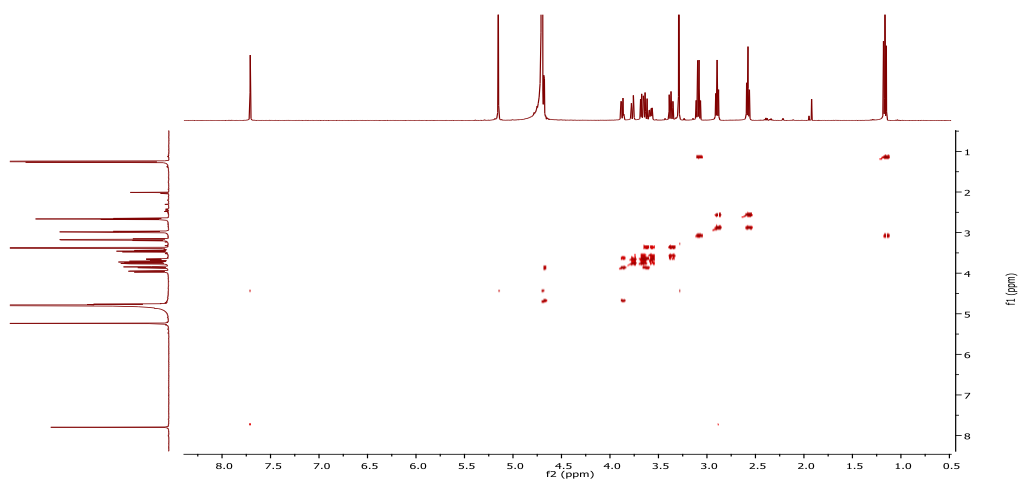
## NMR spectra of 4.16.1

<sup>1</sup>H NMR spectrum of 4.16.1 in DMSO-d<sub>6</sub><sup>13</sup>C NMR spectrum of 4.16.1 in DMSO-d<sub>6</sub>COSY NMR spectrum of 4.16.1 in DMSO-d<sub>6</sub>

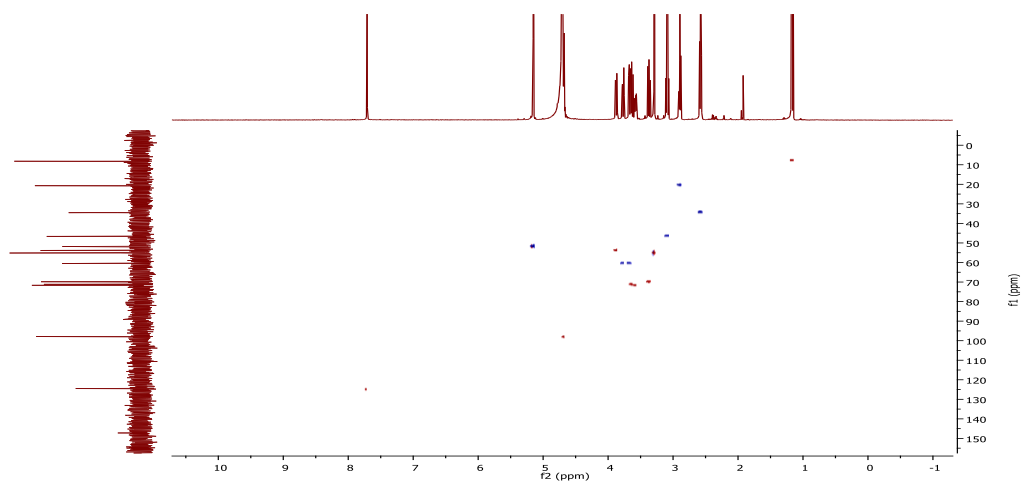
HSQC NMR spectrum of **4.16.1** in DMSO-d<sub>6</sub>HMBC NMR spectrum of **4.16.1** in DMSO-d<sub>6</sub>NMR spectra of **4.22**<sup>1</sup>H NMR spectrum of **4.22** in DMSO-d<sub>6</sub>



$^{13}\text{C}$  NMR spectrum of **4.22** in  $\text{DMSO-d}_6$

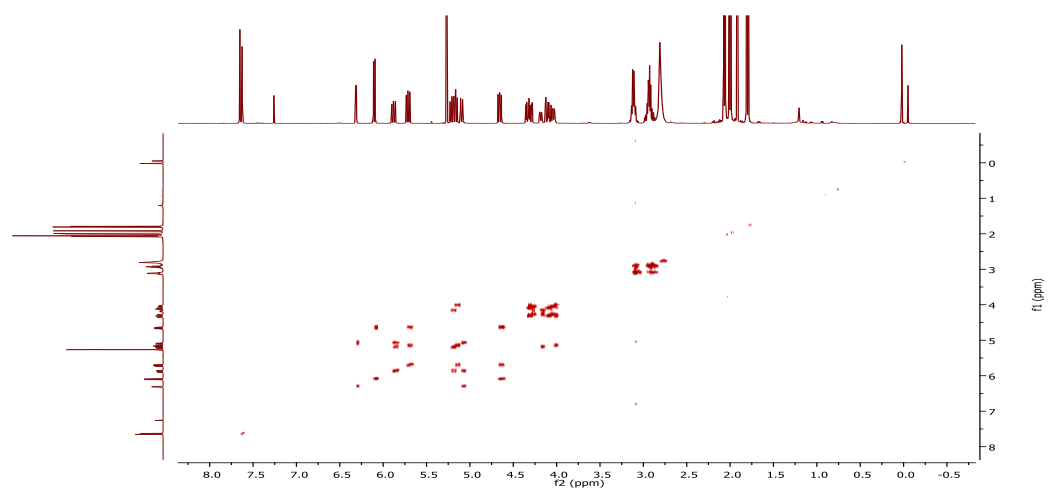
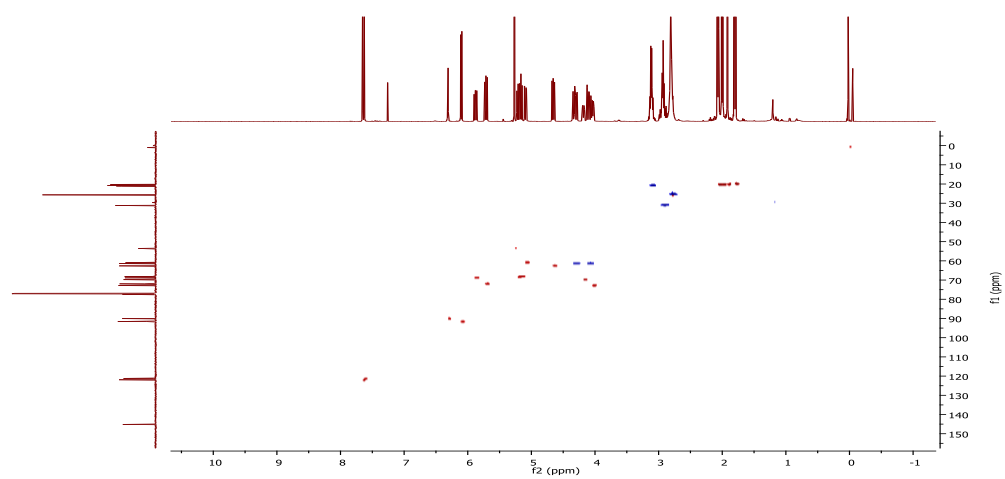
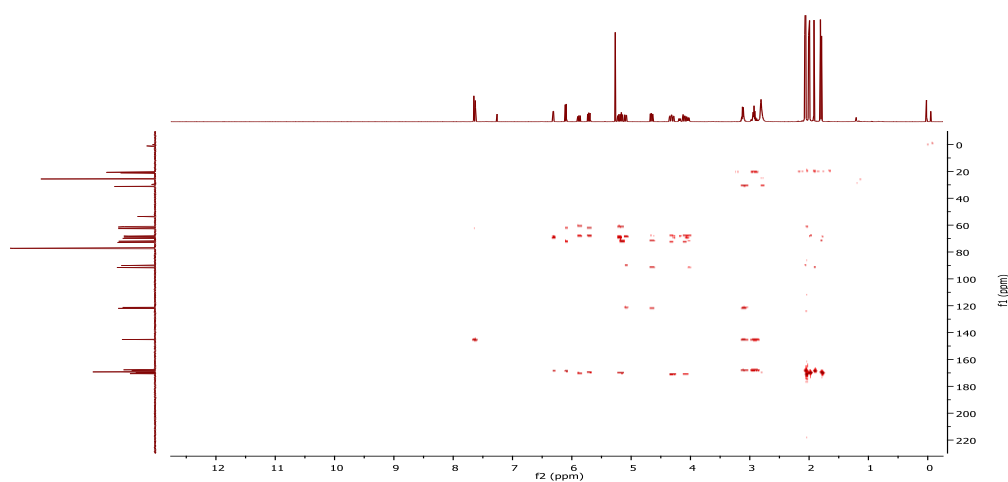


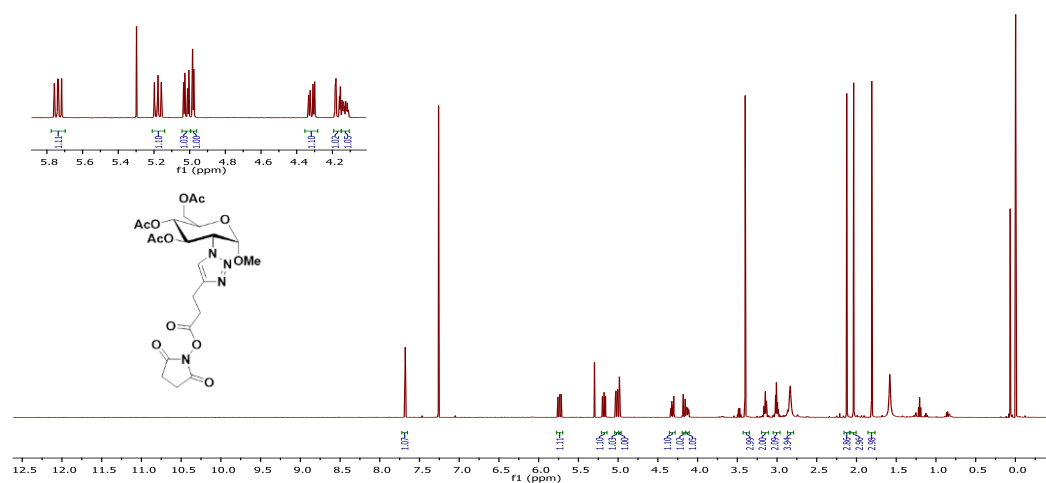
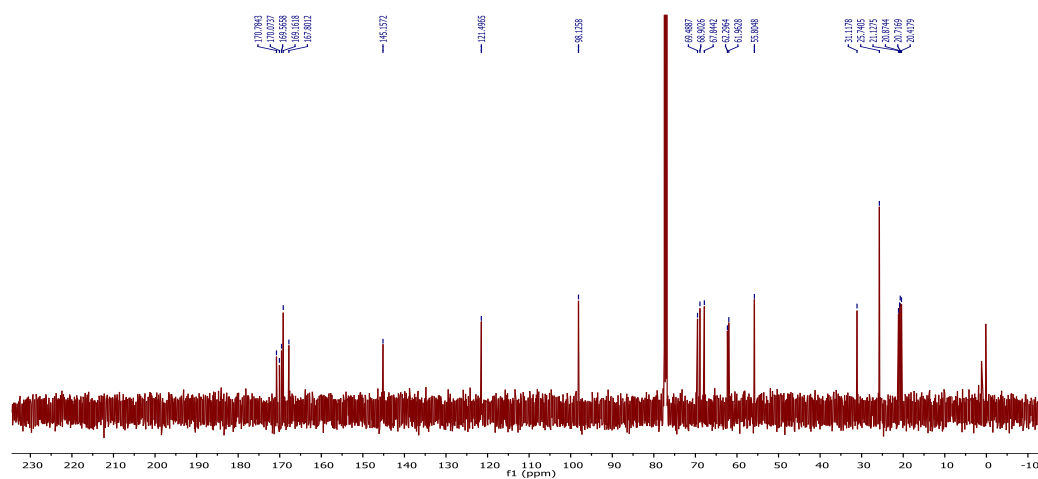
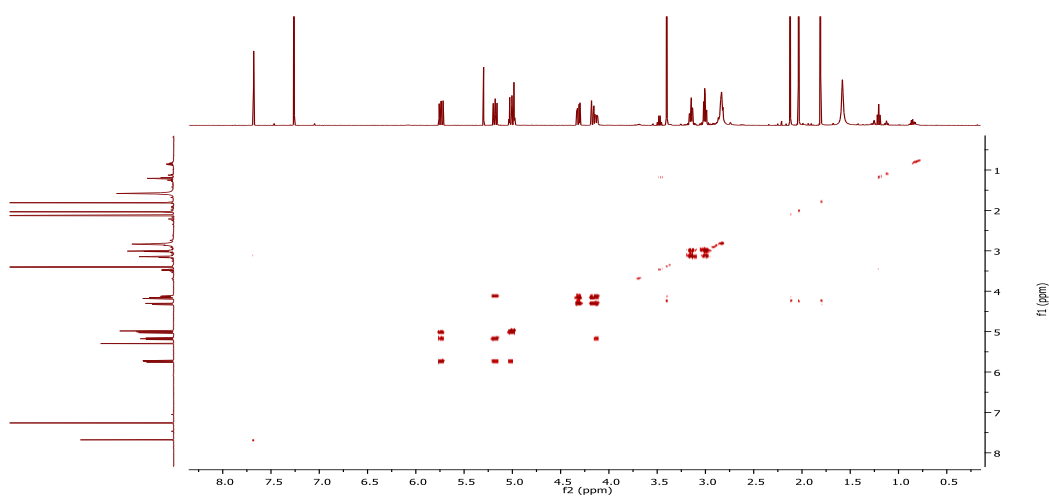
COSY NMR spectrum of **4.22** in  $\text{DMSO-d}_6$



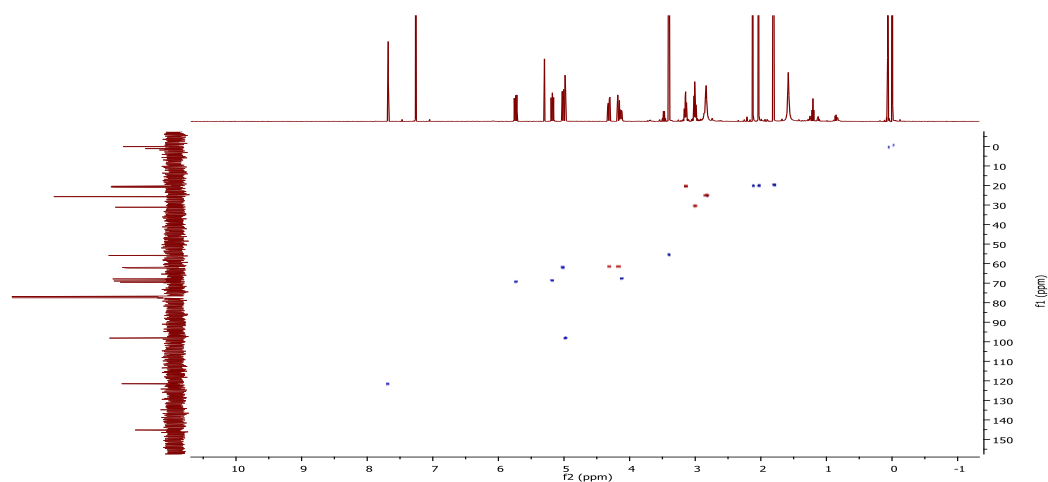
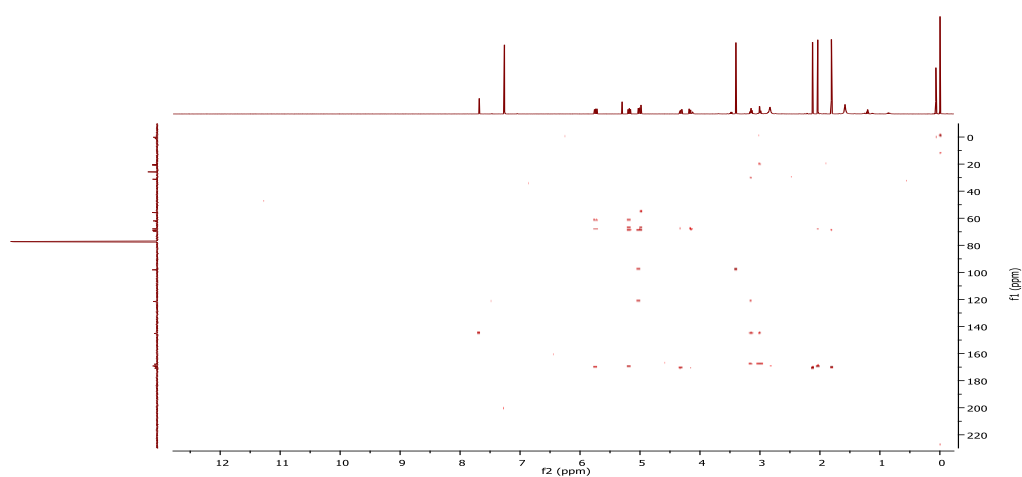
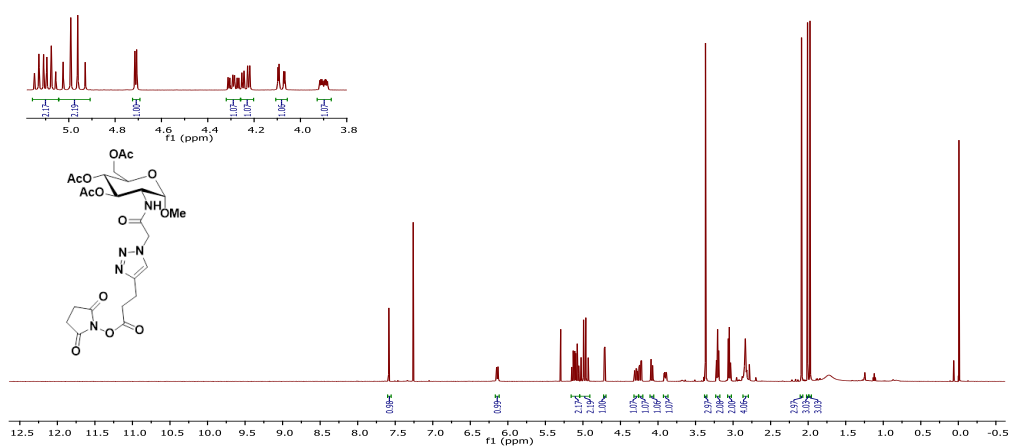
HSQC NMR spectrum of **4.22** in  $\text{DMSO-d}_6$

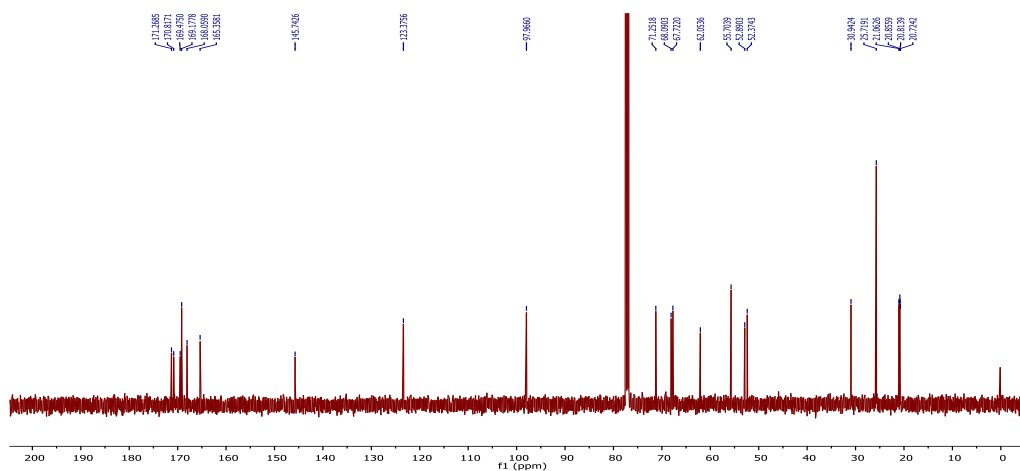


COSY NMR spectrum of **4.10** in CDCl<sub>3</sub>HSQC NMR spectrum of **4.10** in CDCl<sub>3</sub>HMBC NMR spectrum of **4.10** in CDCl<sub>3</sub>

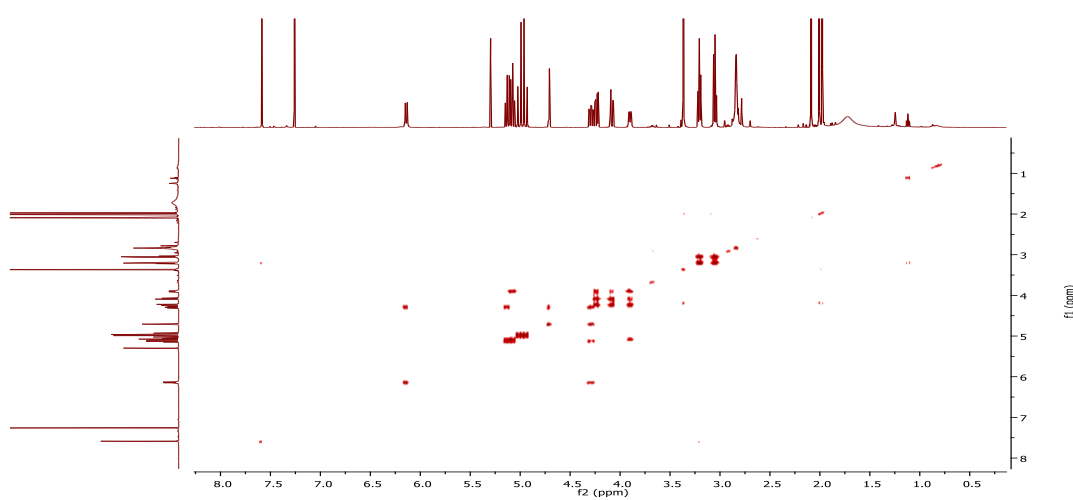
NMR spectra of **4.17** $^1\text{H}$  NMR spectrum of **4.17** in  $\text{CDCl}_3$  $^{13}\text{C}$  NMR spectrum of **4.17** in  $\text{CDCl}_3$ COSY NMR spectrum of **4.17** in  $\text{CDCl}_3$



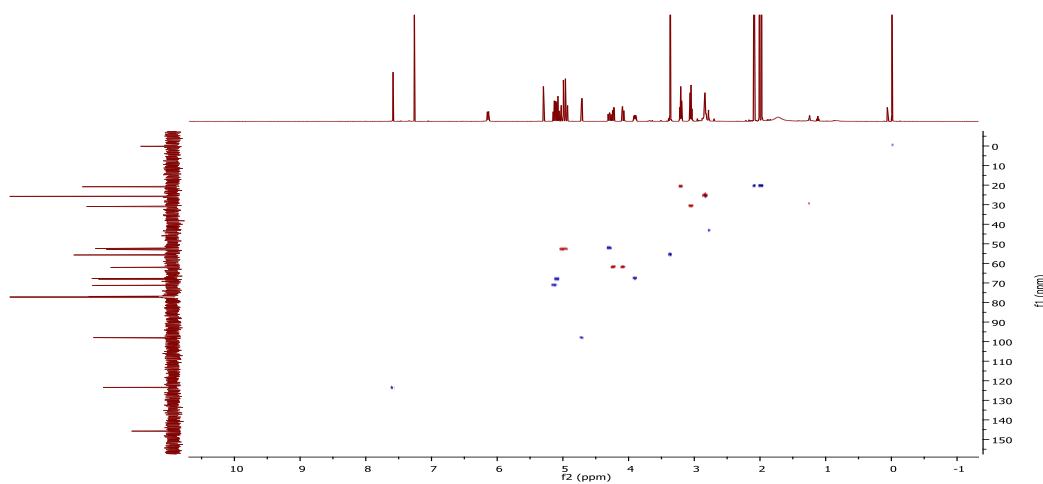
HSQC NMR spectrum of **4.17** in CDCl<sub>3</sub>HMBC NMR spectrum of **4.17** in CDCl<sub>3</sub>NMR spectra of **4.21**<sup>1</sup>H NMR spectrum of **4.21** in CDCl<sub>3</sub>



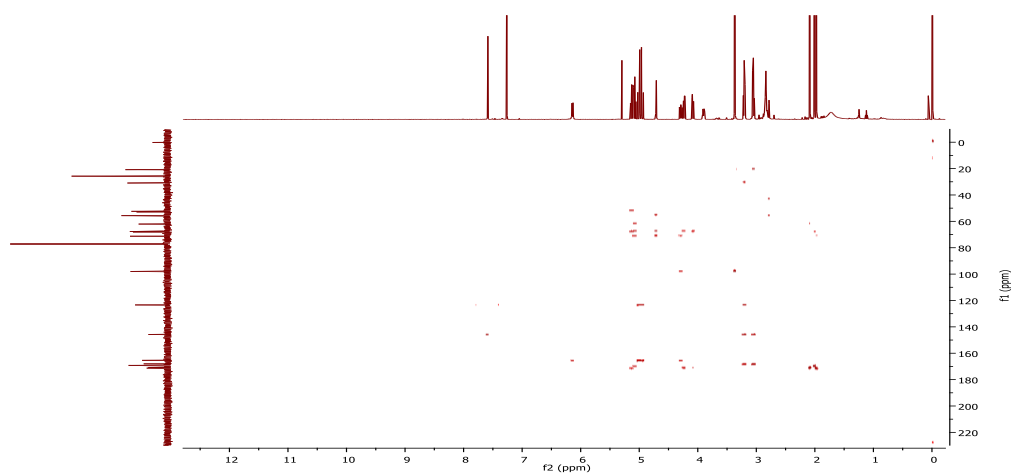
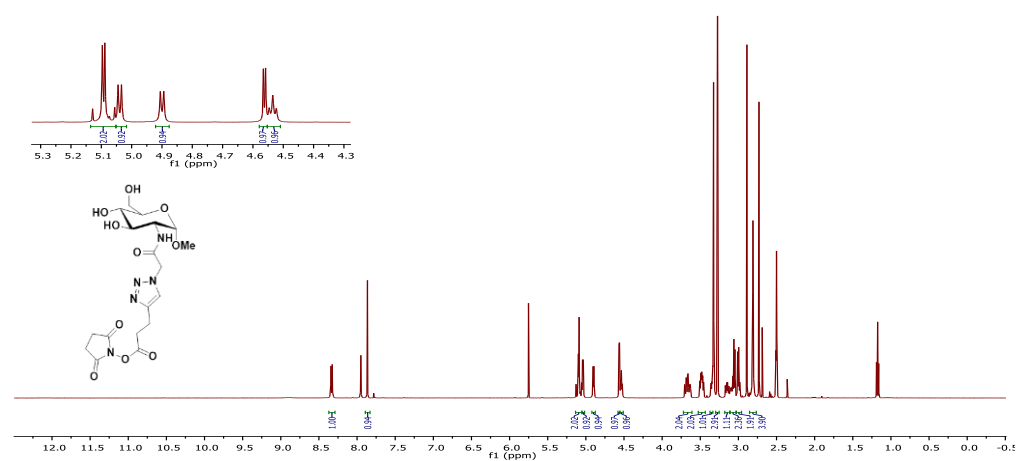
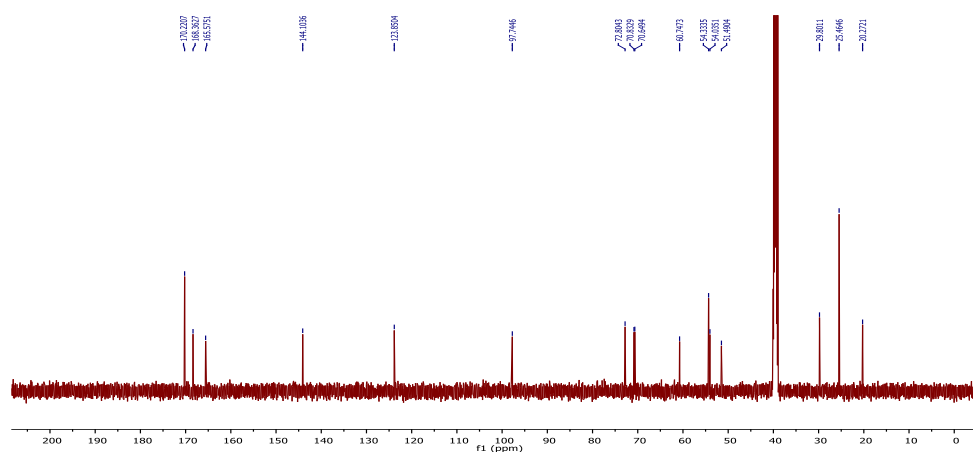
$^{13}\text{C}$  NMR spectrum of **4.21** in  $\text{CDCl}_3$

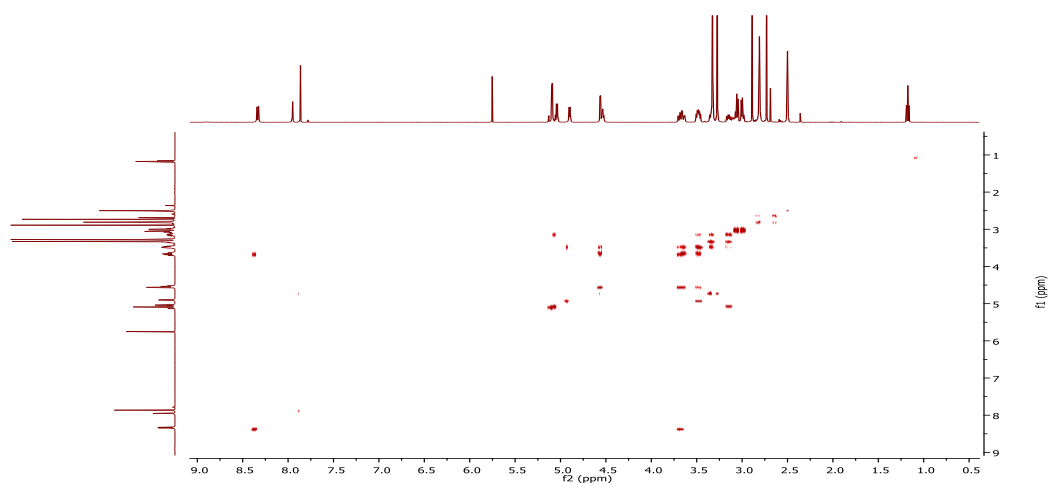
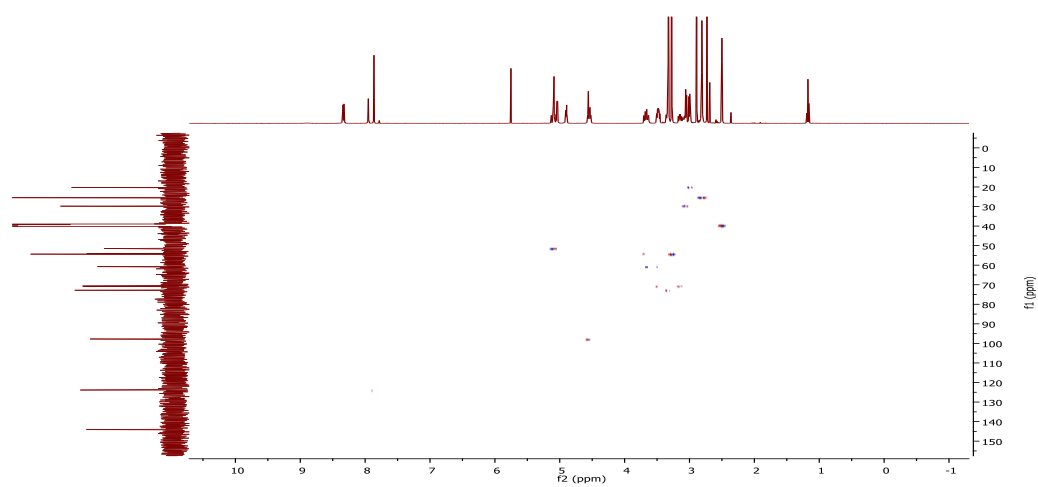
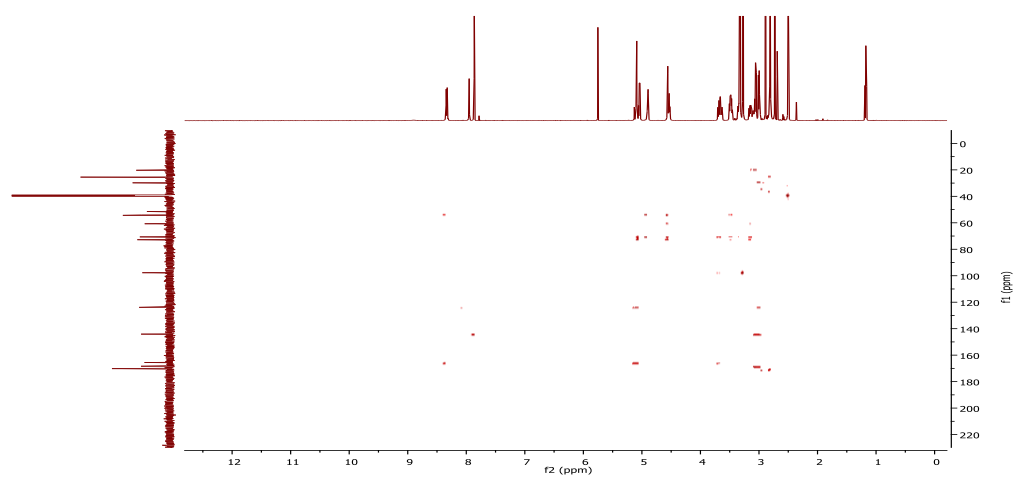


COSY NMR spectrum of **4.21** in  $\text{CDCl}_3$

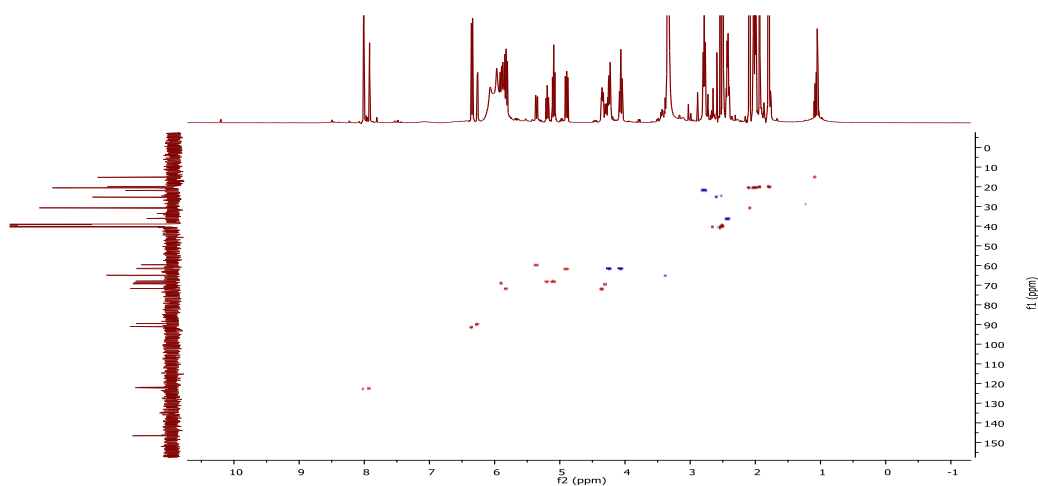
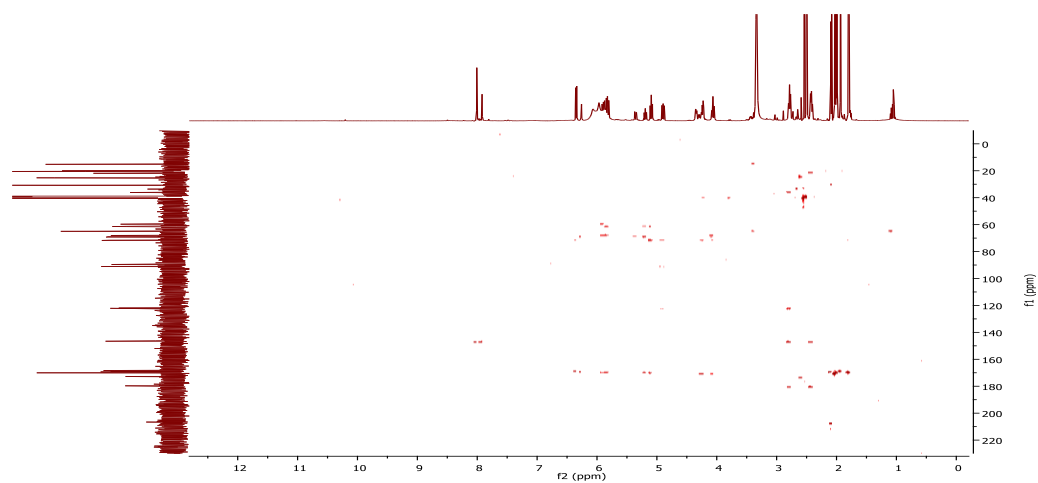
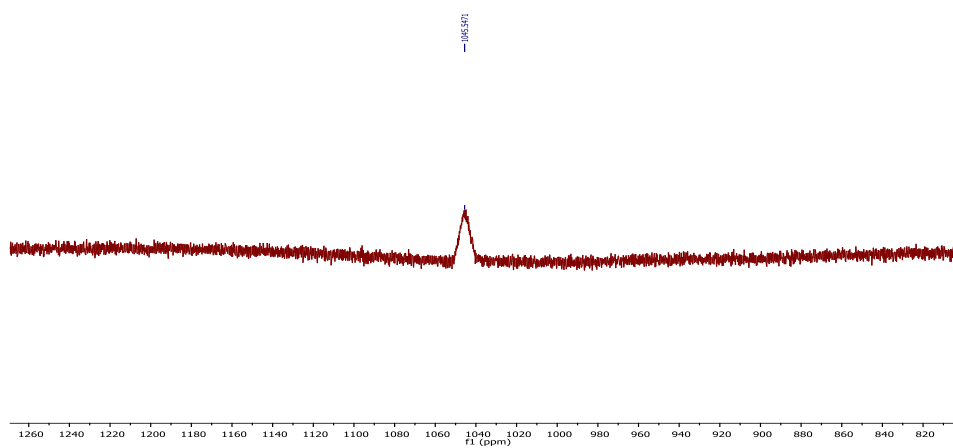


HSQC NMR spectrum of **4.21** in  $\text{CDCl}_3$

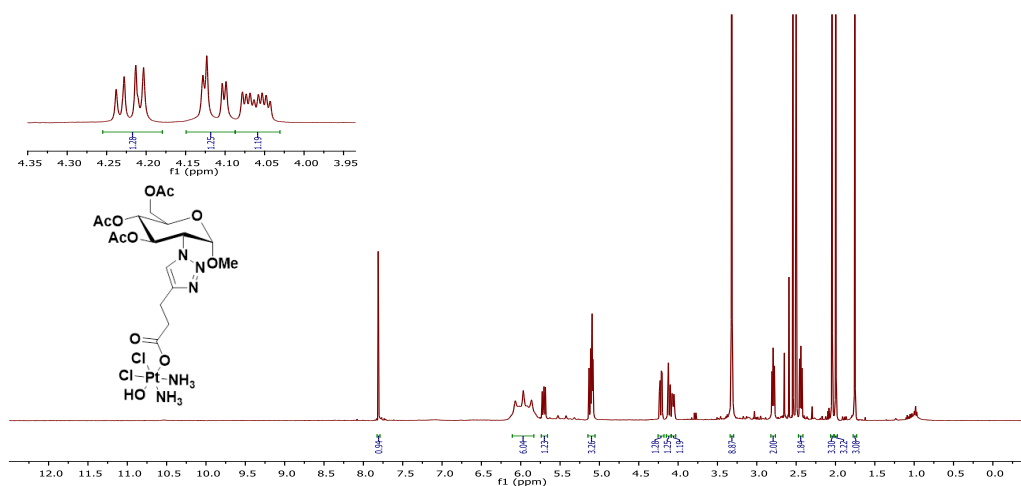
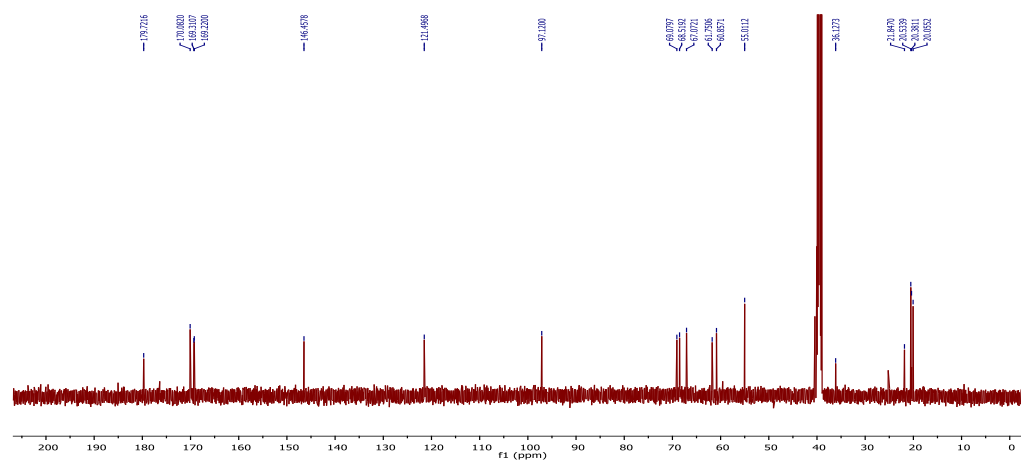
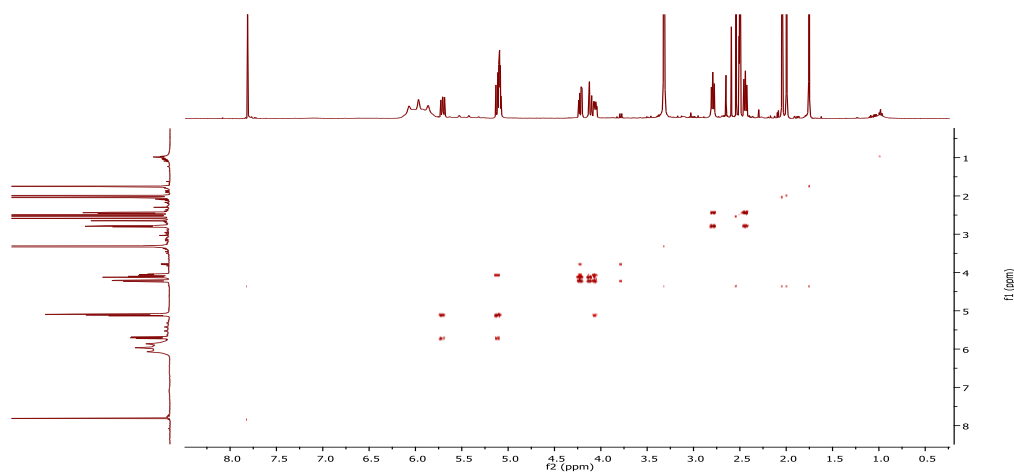
HMBC NMR spectrum of **4.21** in  $\text{CDCl}_3$ NMR spectra of **4.23** $^1\text{H}$  NMR spectrum of **4.23** in  $\text{DMSO-d}_6$  $^{13}\text{C}$  NMR spectrum of **4.23** in  $\text{DMSO-d}_6$

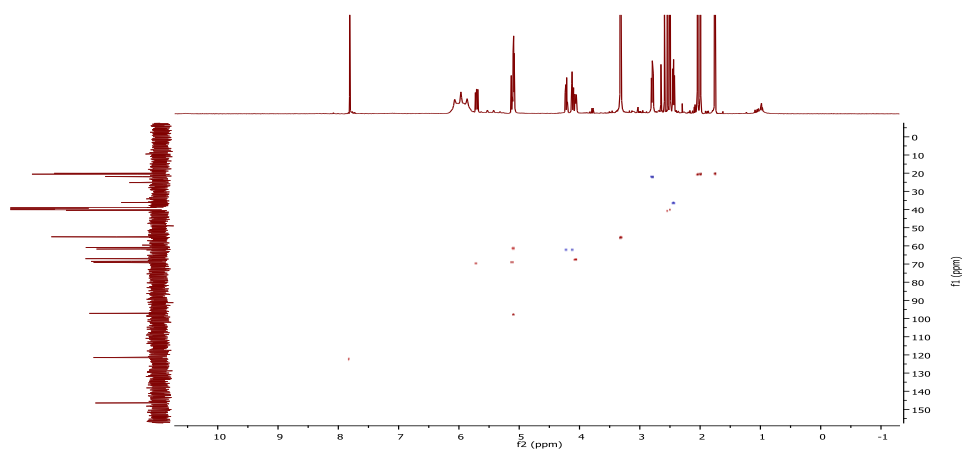
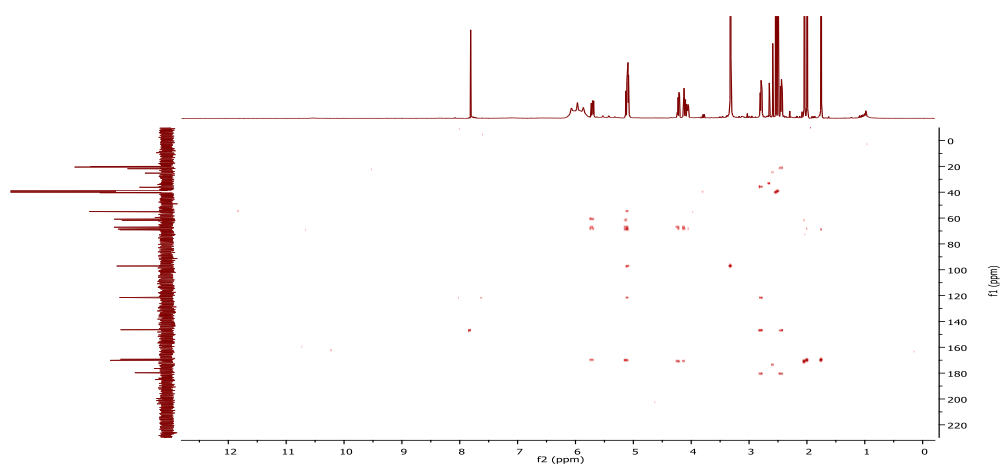
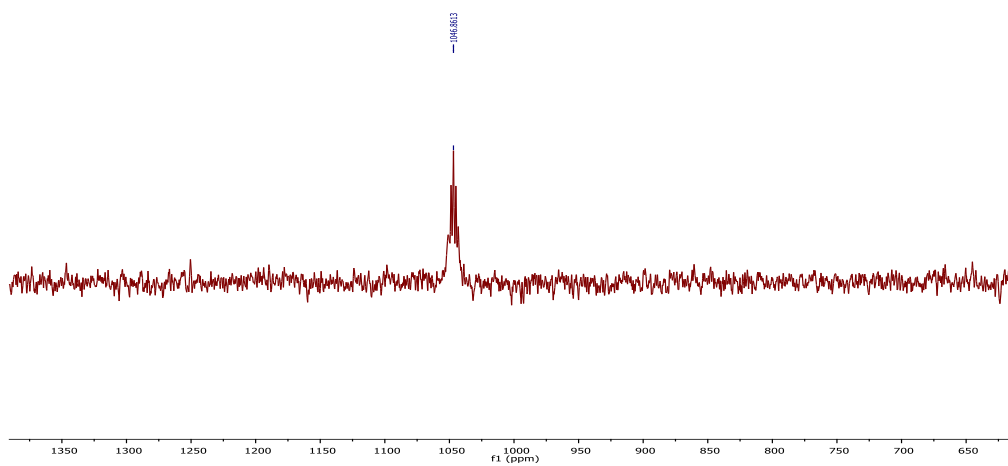
COSY NMR spectrum of **4.23** in DMSO-d<sub>6</sub>HSQC NMR spectrum of **4.23** in DMSO-d<sub>6</sub>HMBC NMR spectrum of **4.23** in DMSO-d<sub>6</sub>



HSQC NMR spectrum of **Complex 1** in DMSO-d<sub>6</sub>HMBC NMR spectrum of **Complex 1** in DMSO-d<sub>6</sub><sup>195</sup>Pt NMR spectrum of **Complex 1** in DMSO-d<sub>6</sub>

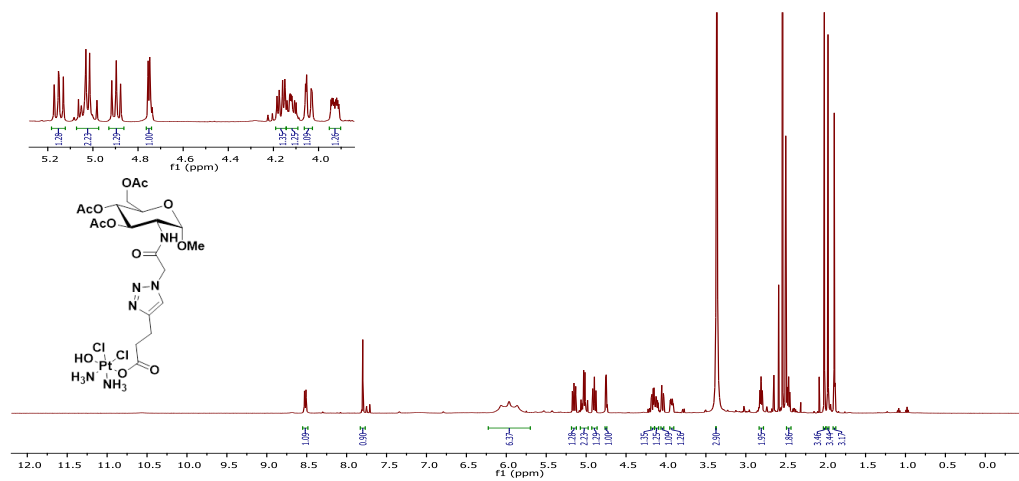
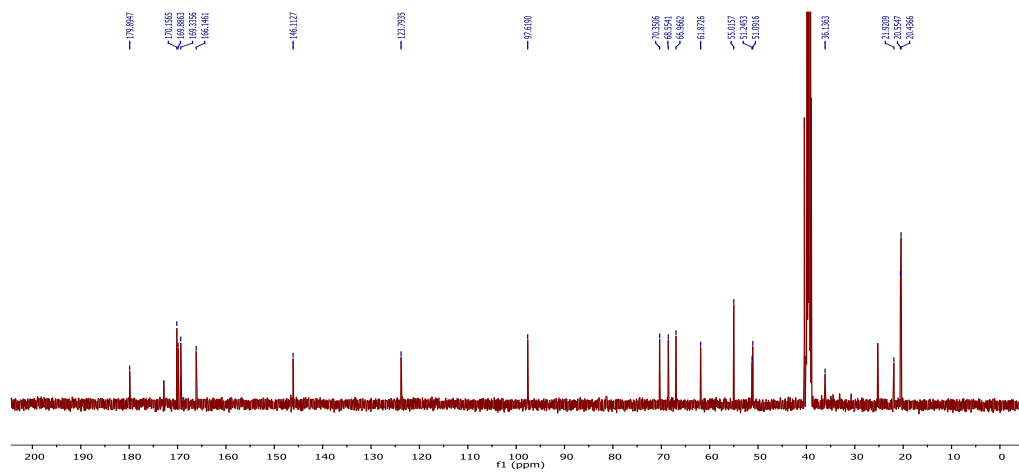
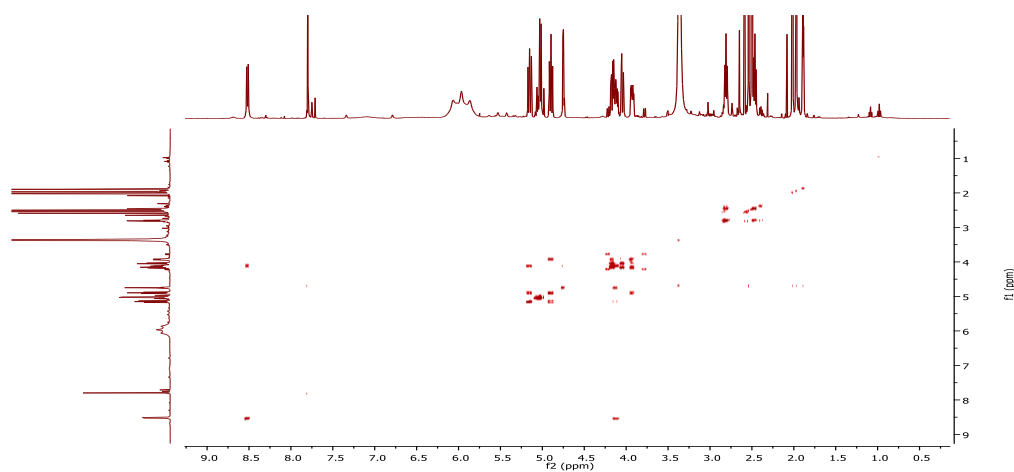
## NMR spectra of Complex 2

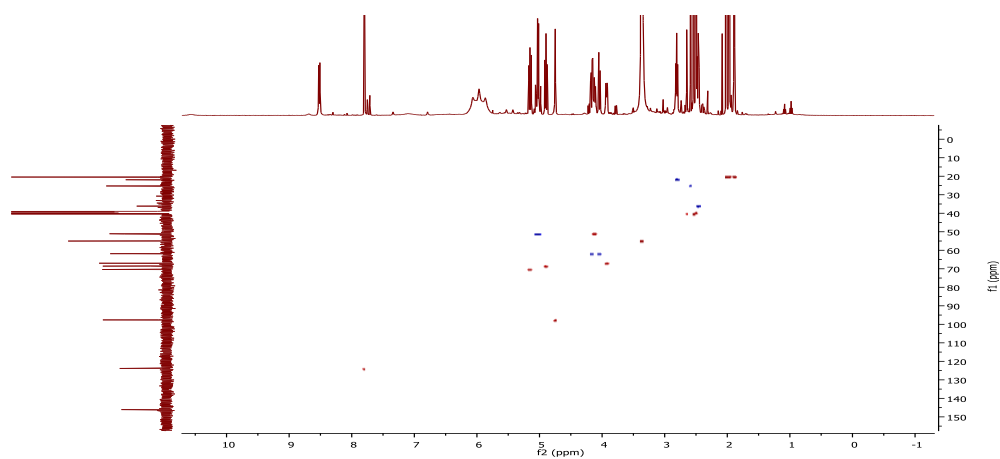
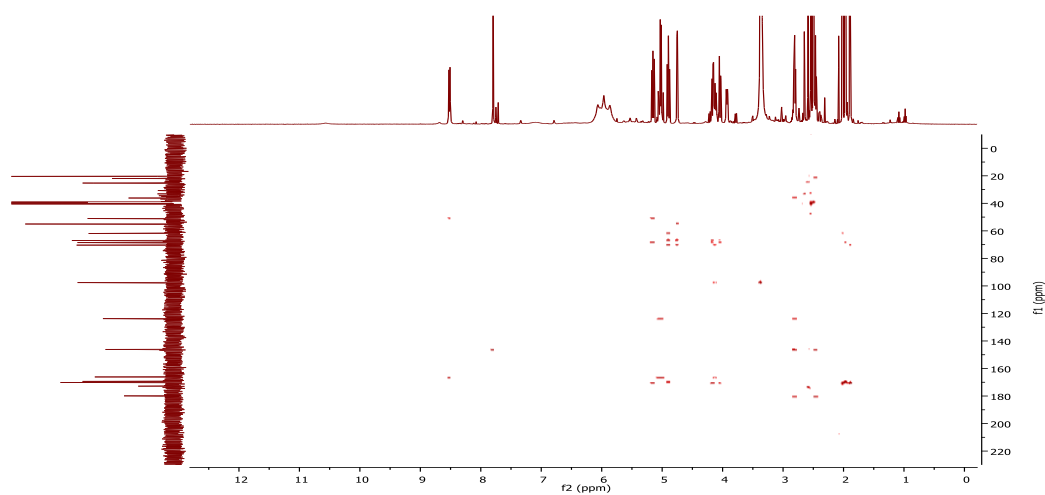
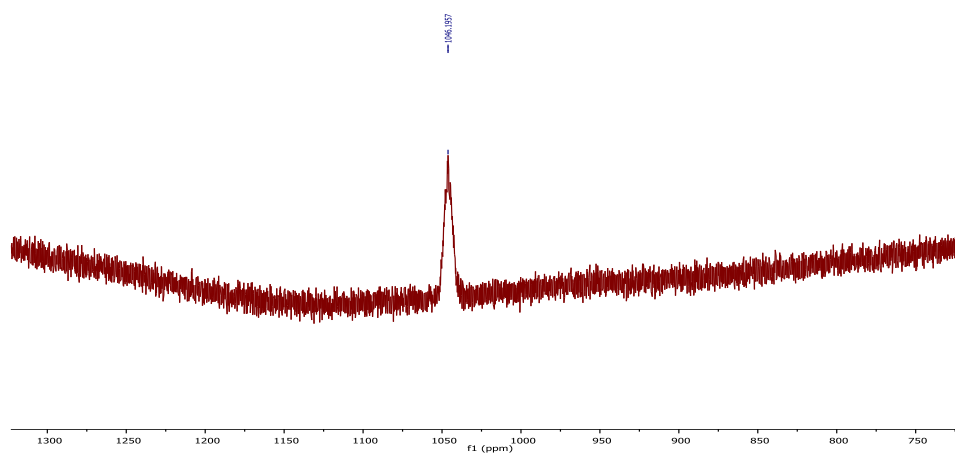
<sup>1</sup>H NMR spectrum of Complex 2 in DMSO-d<sub>6</sub><sup>13</sup>C NMR spectrum of Complex 2 in DMSO-d<sub>6</sub>COSY NMR spectrum of Complex 2 in DMSO-d<sub>6</sub>

HSQC NMR spectrum of **Complex 2** in DMSO-d<sub>6</sub>HMBC NMR spectrum of **Complex 2** in DMSO-d<sub>6</sub><sup>195</sup>Pt NMR spectrum of **Complex 2** in DMSO-d<sub>6</sub>

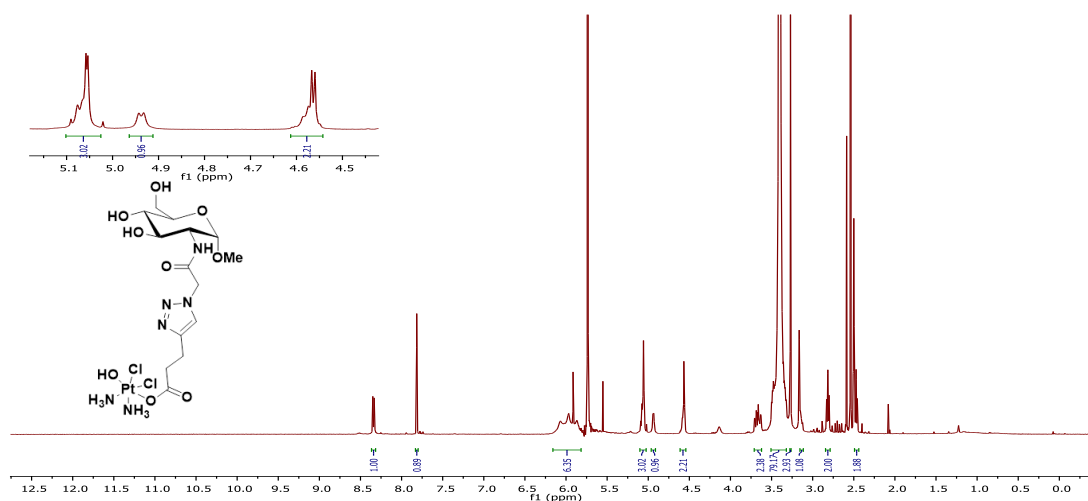
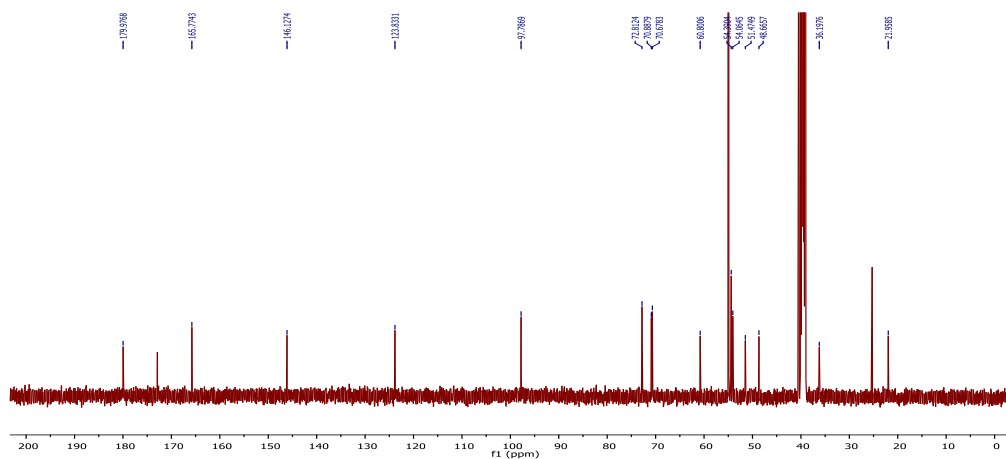
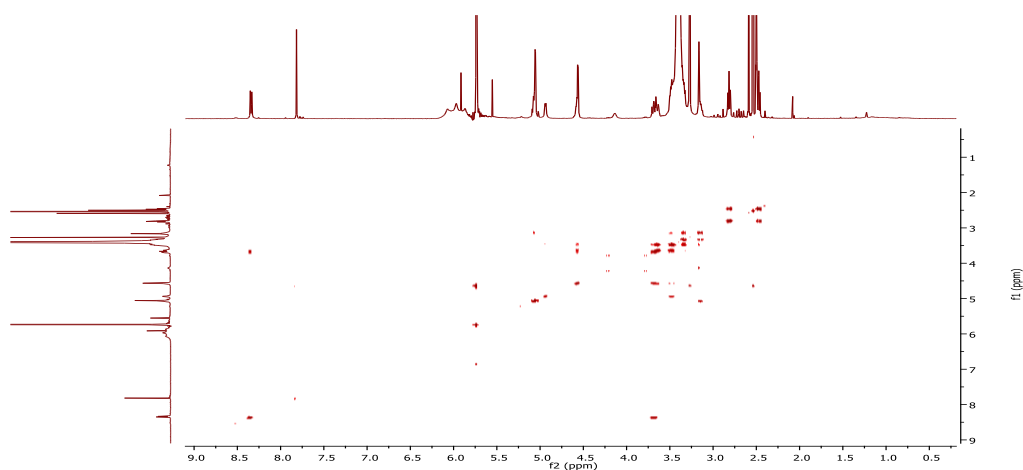


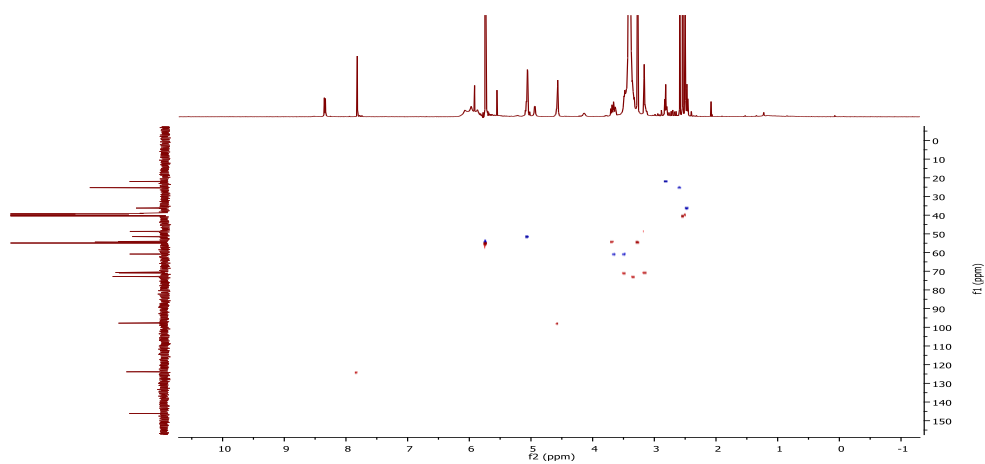
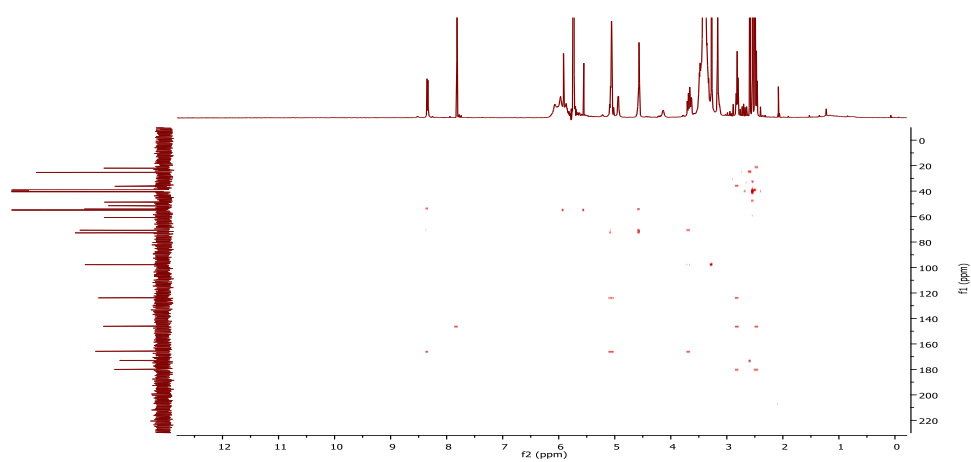
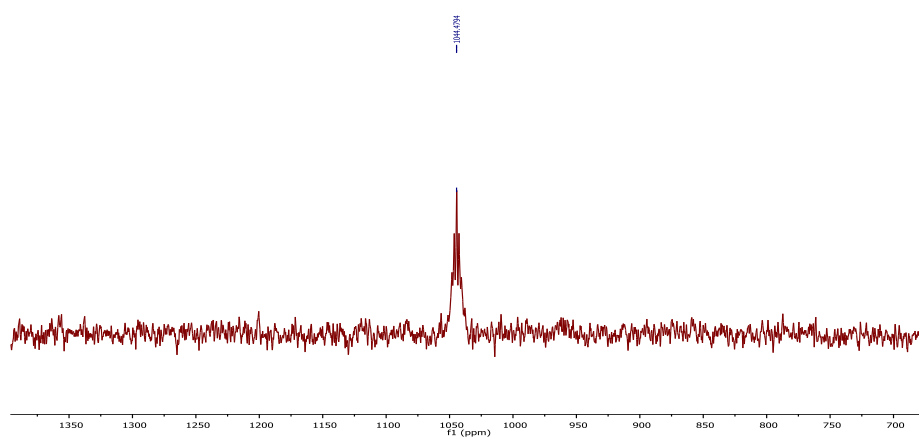
## NMR spectra of Complex 3

<sup>1</sup>H NMR spectrum of Complex 3 in DMSO-d<sub>6</sub><sup>13</sup>C NMR spectrum of Complex 3 in DMSO-d<sub>6</sub>COSY NMR spectrum of Complex 3 in DMSO-d<sub>6</sub>

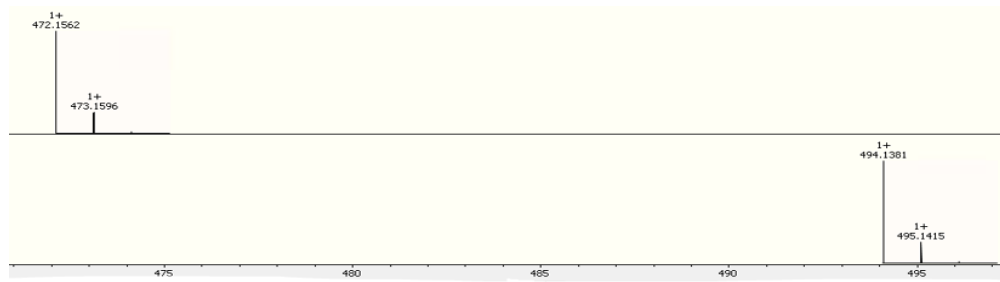
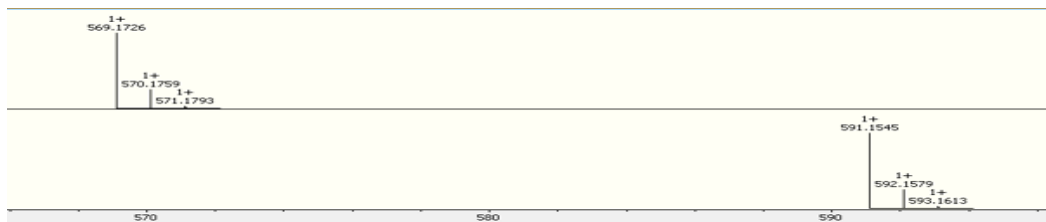
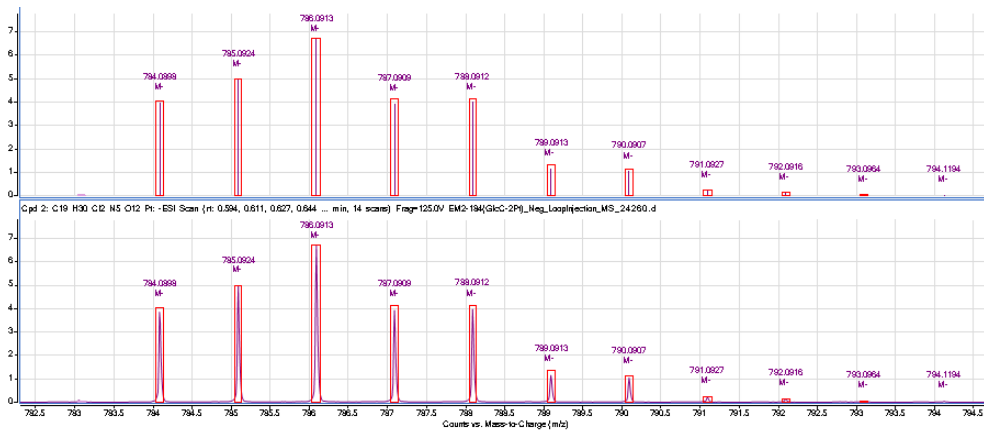
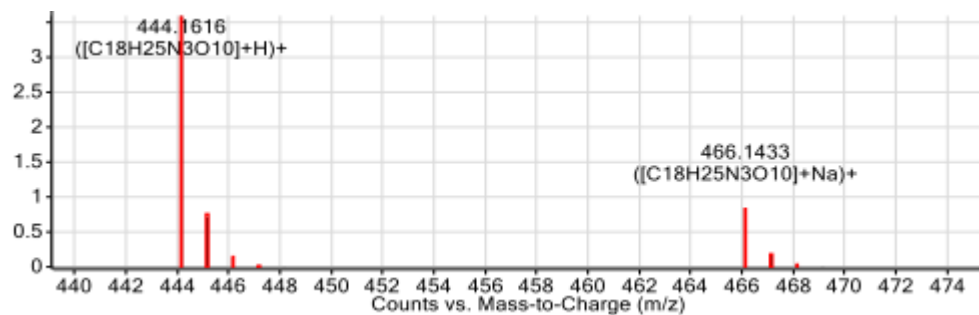
HSQC NMR spectrum of **Complex 3** in DMSO-d<sub>6</sub>HMBC NMR spectrum of **Complex 3** in DMSO-d<sub>6</sub><sup>195</sup>Pt NMR spectrum of **Complex 3** in DMSO-d<sub>6</sub>

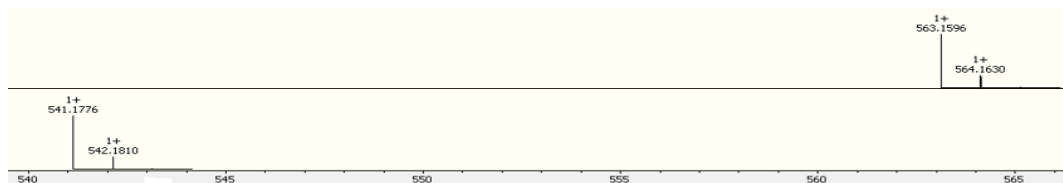
## NMR spectra of Complex 4

 $^1\text{H}$  NMR spectrum of Complex 4 in  $\text{DMSO-d}_6$  $^{13}\text{C}$  NMR spectrum of Complex 4 in  $\text{DMSO-d}_6$ COSY NMR spectrum of Complex 4 in  $\text{DMSO-d}_6$

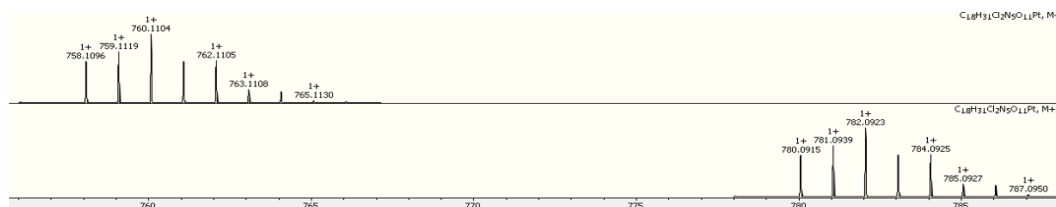
HSQC NMR spectrum of **Complex 4** in DMSO-d<sub>6</sub>HMBC NMR spectrum of **Complex 4** in DMSO-d<sub>6</sub><sup>195</sup>Pt NMR spectrum of **Complex 4** in DMSO-d<sub>6</sub>

## HR-MS

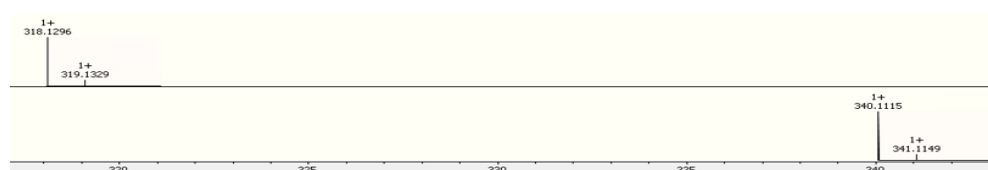
HR-MS spectrum of **4.9**HR-MS spectrum of **4.10**HR-MS spectrum of **Complex 1**HR-MS spectrum of **4.16**



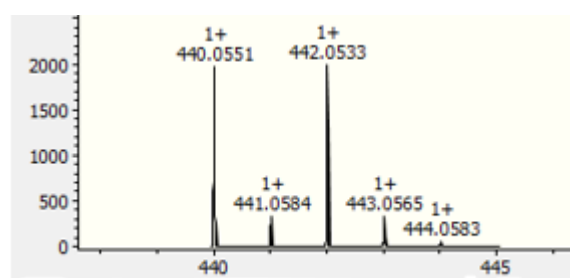
HR-MS spectrum of 4.17



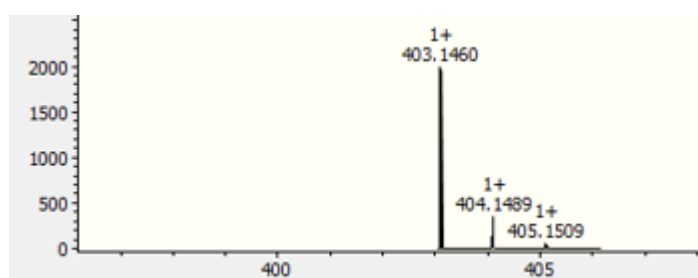
HR-MS spectrum of Complex 2



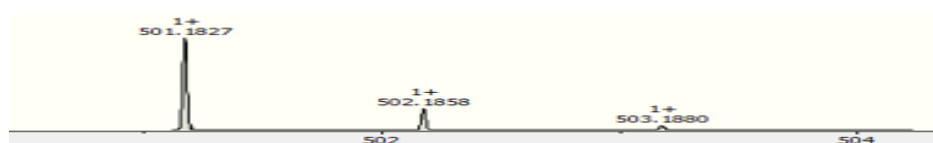
HR-MS spectrum of 4.16.1



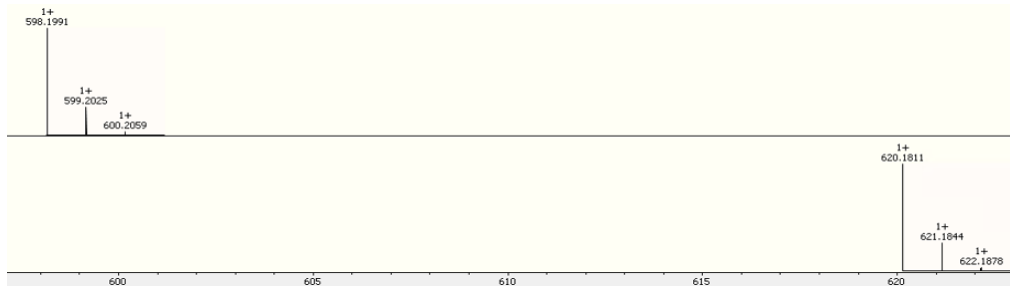
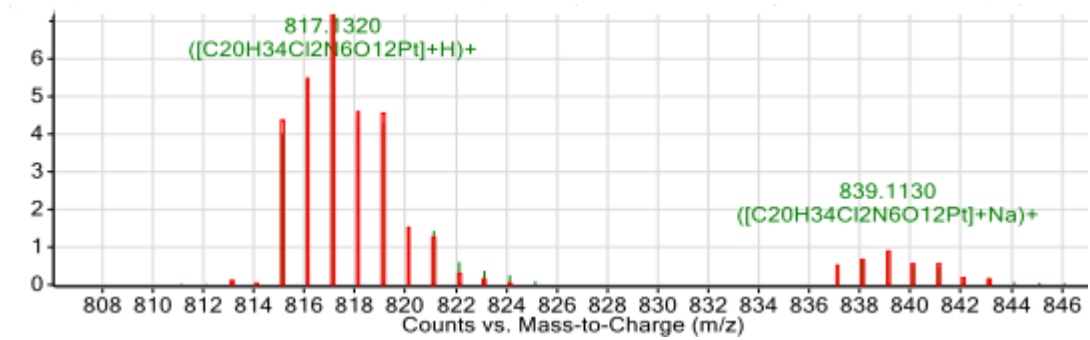
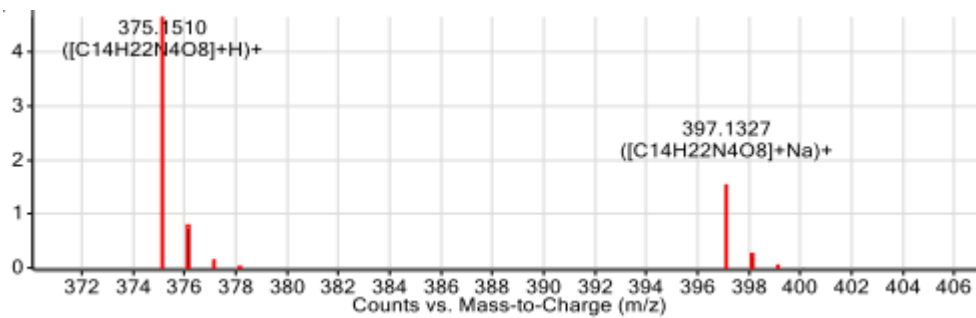
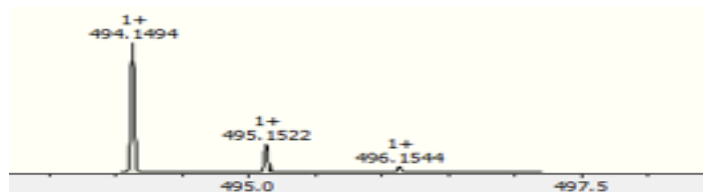
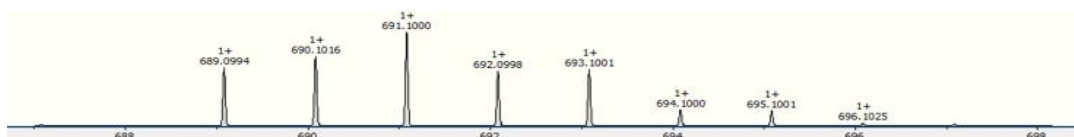
HR-MS spectrum of 4.18

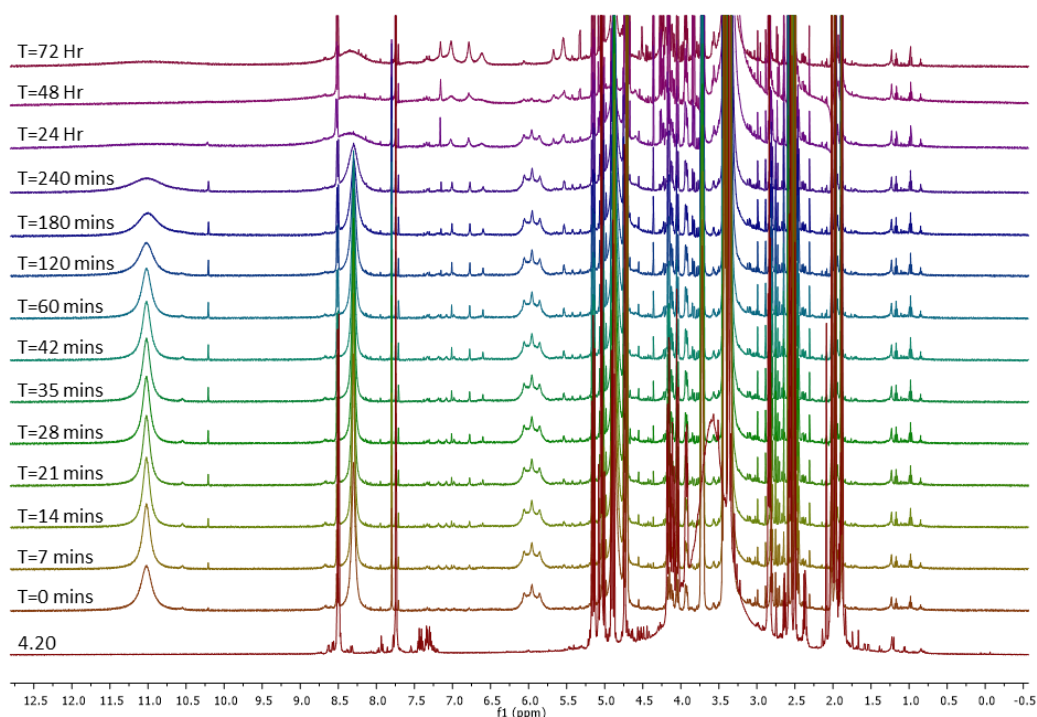


HR-MS spectrum of 4.19

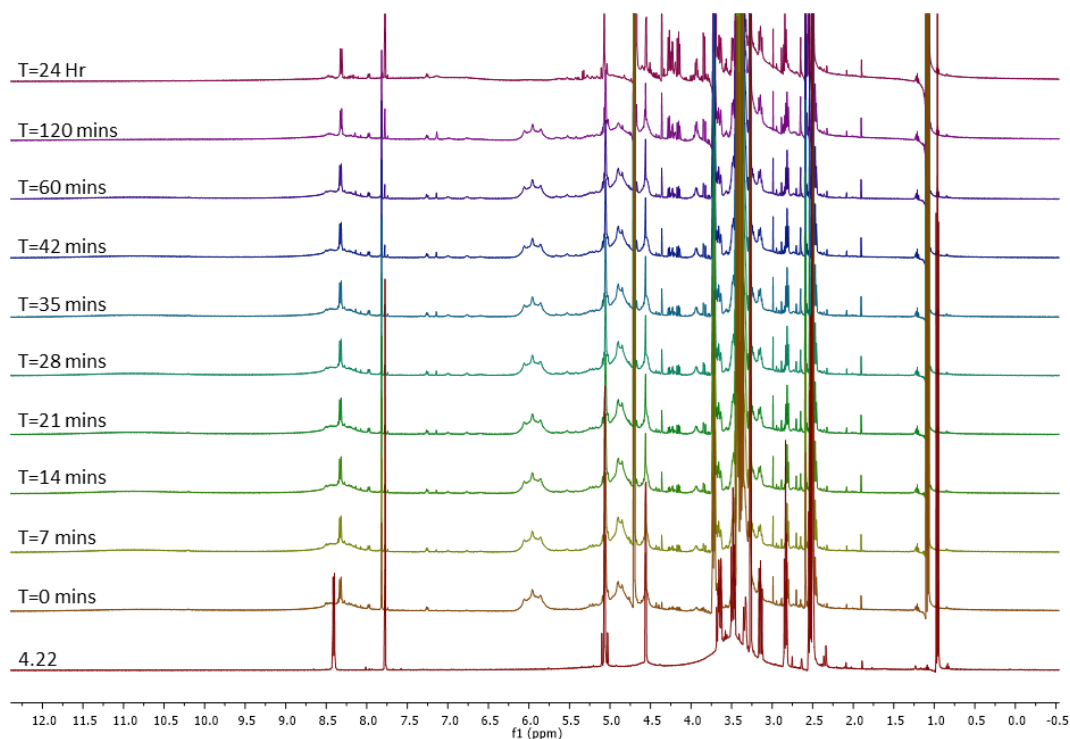


HR-MS spectrum of 4.20

HR-MS spectrum of **4.21**HR-MS spectrum of **Complex 3**HR-MS spectrum of **4.22**HR-MS spectrum of **4.23**HR-MS spectrum of **Complex 4**

**Reduction study**

**Complex 3:** <sup>1</sup>H-NMR spectra of the **Complex 3** with addition of 10 eq. of ascorbic acid. NMR spectra were collected every 7 minutes for 60 minutes and then every hour for 3 hours and finally left to reduce for 3 days.

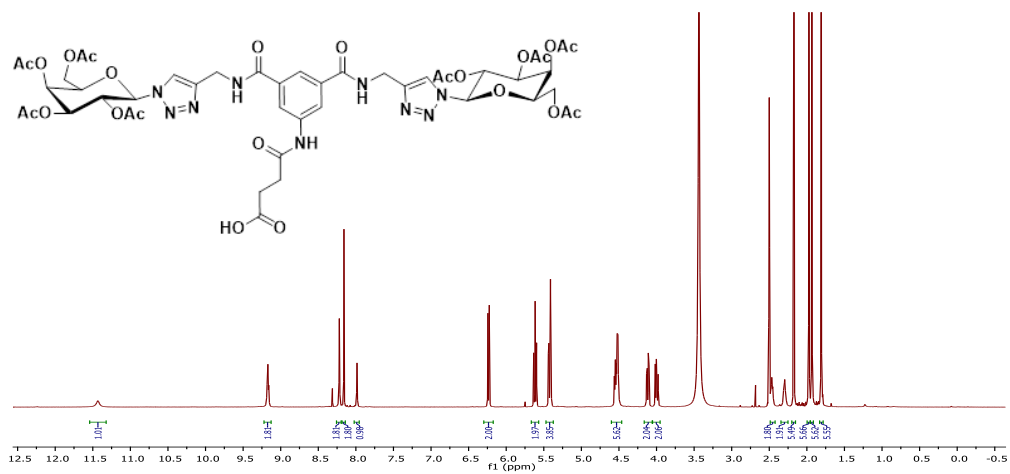
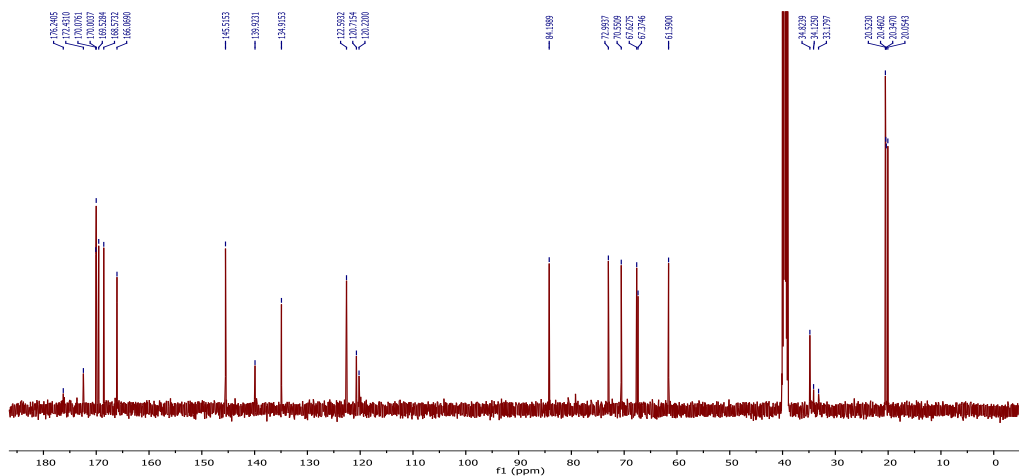
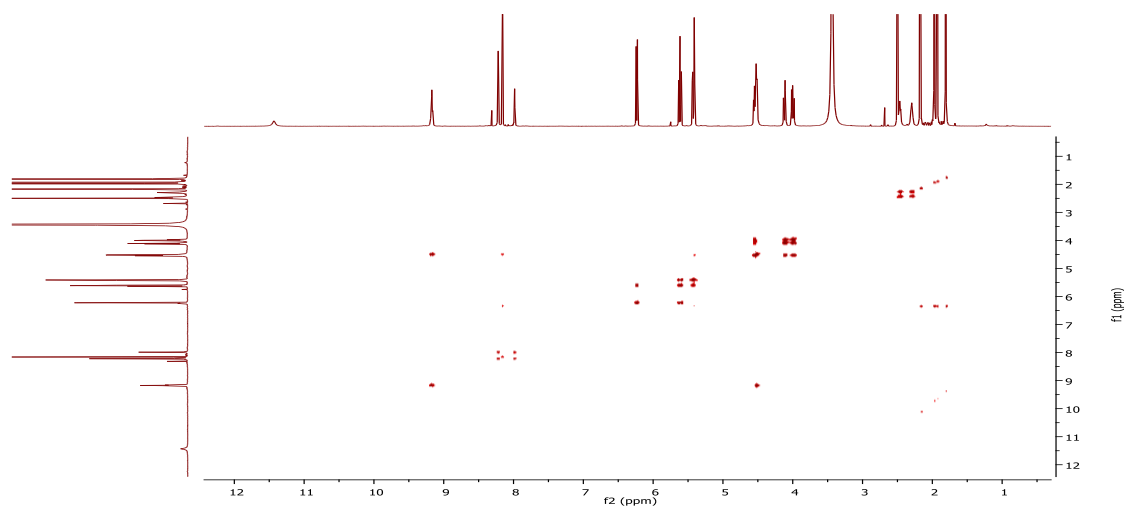


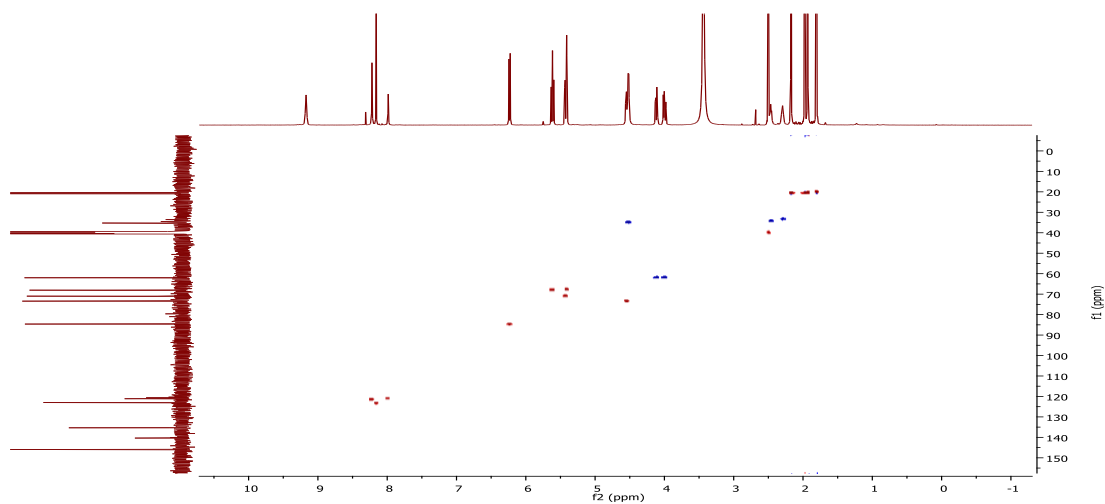
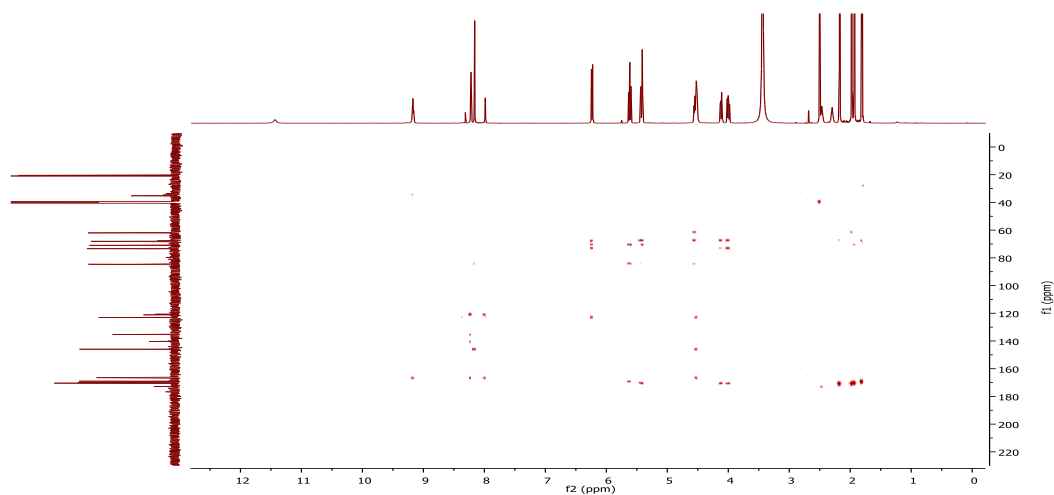
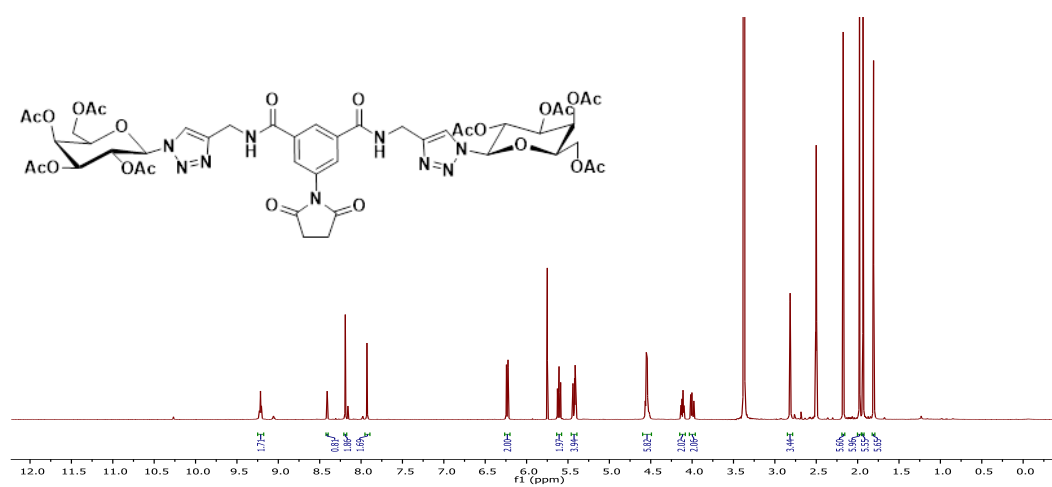
**Complex 4:** <sup>1</sup>H-NMR spectra of the **Complex 4** with addition of 10 eq. of ascorbic acid. NMR spectra were collected every 7 minutes for 60 minutes and then every hour for 2 hours and finally left to reduce for 1 day.

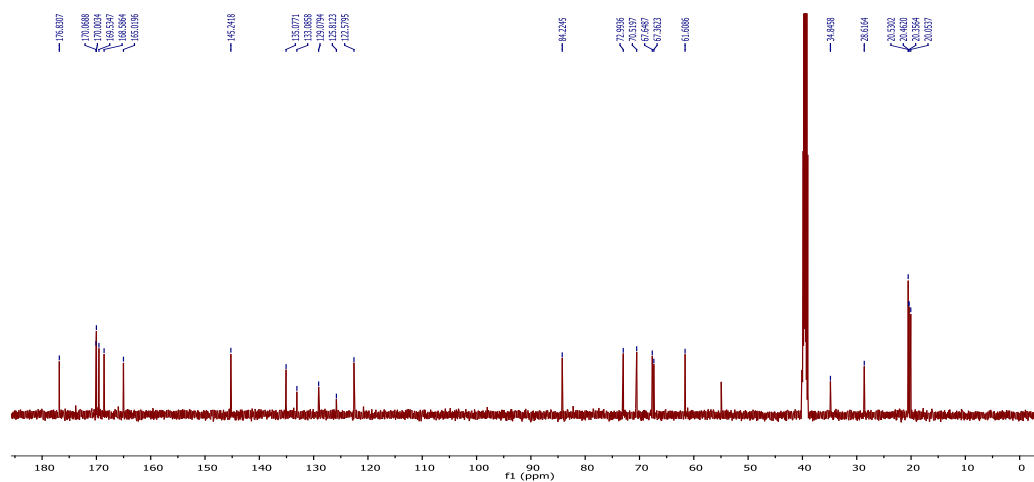


## Chapter 5

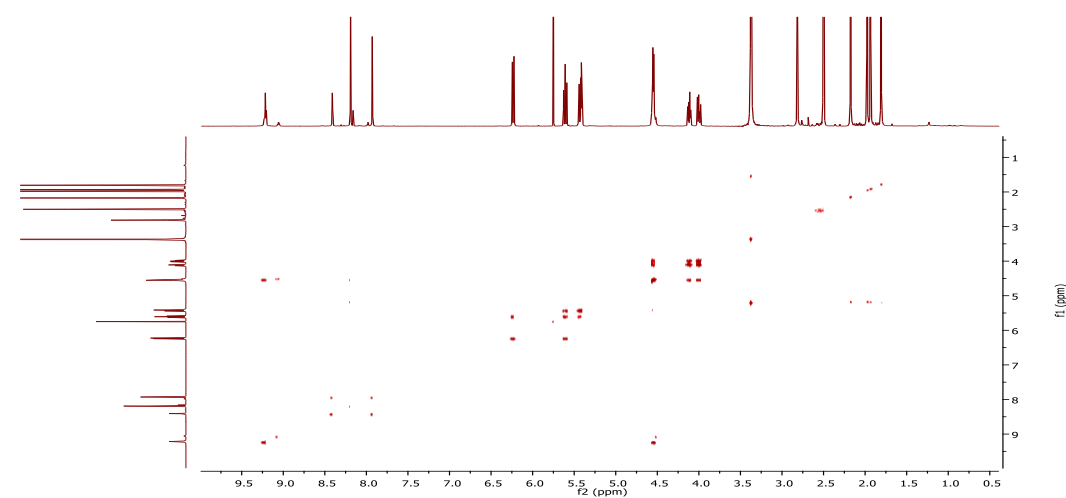
## NMR spectra of 5.10

 $^1\text{H}$  NMR spectrum of 5.10 in DMSO- $d_6$  $^{13}\text{C}$  NMR spectrum of 5.10 in DMSO- $d_6$ COSY NMR spectrum of 5.10 in DMSO- $d_6$

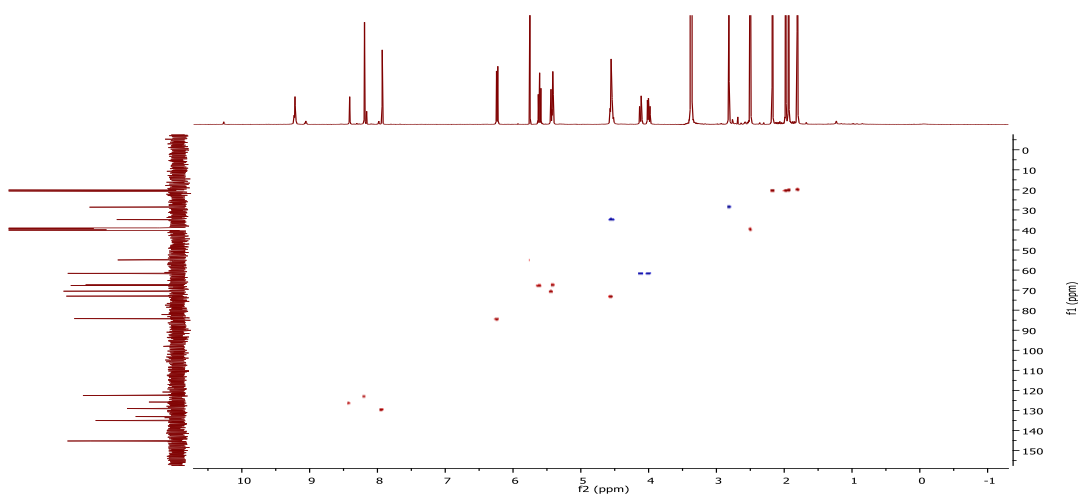
HSQC NMR spectrum of **5.10** in DMSO-d<sub>6</sub>HMBC NMR spectrum of **5.10** in DMSO-d<sub>6</sub>NMR spectra of **5.11**<sup>1</sup>H NMR spectrum of **5.11** in DMSO-d<sub>6</sub>



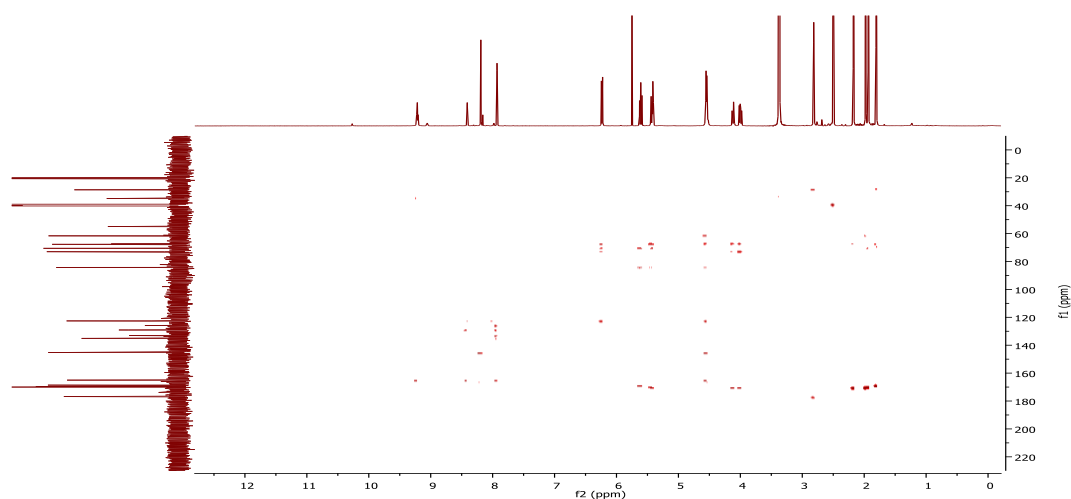
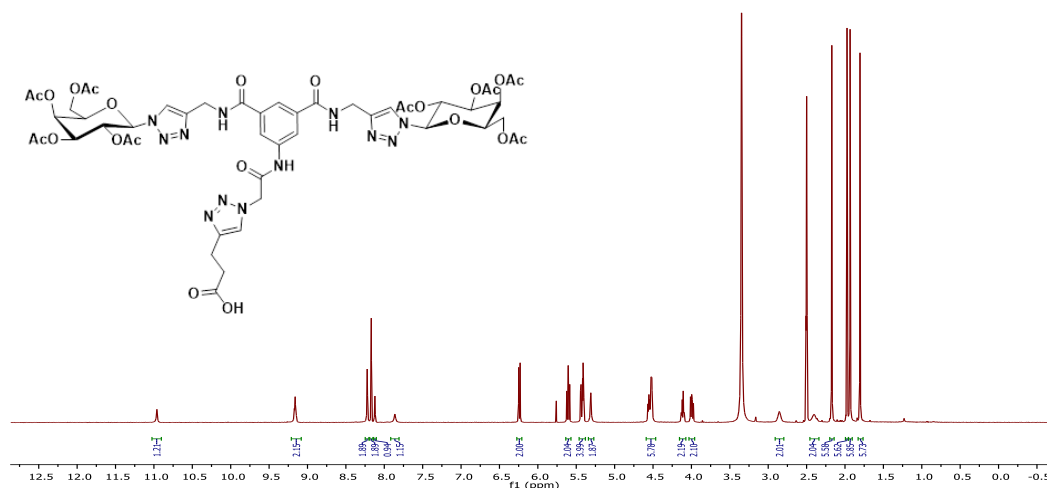
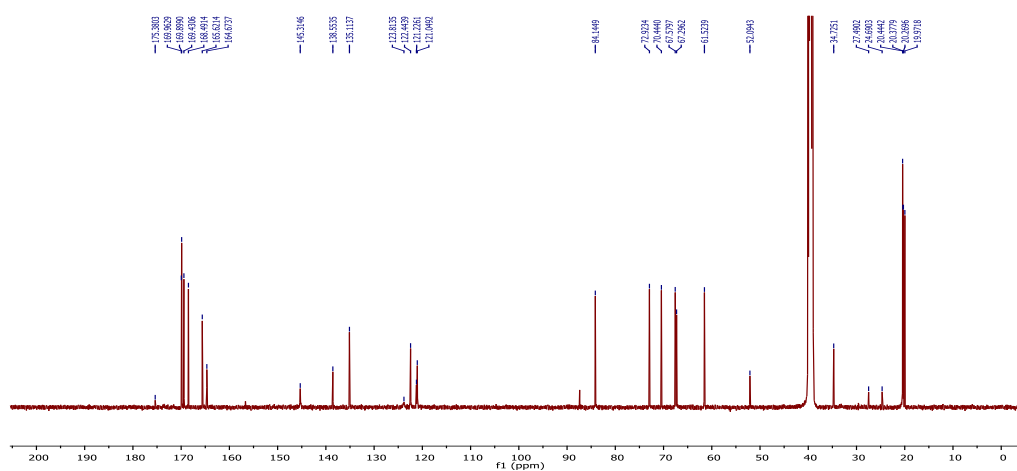
$^{13}\text{C}$  NMR spectrum of **5.11** in  $\text{DMSO-d}_6$

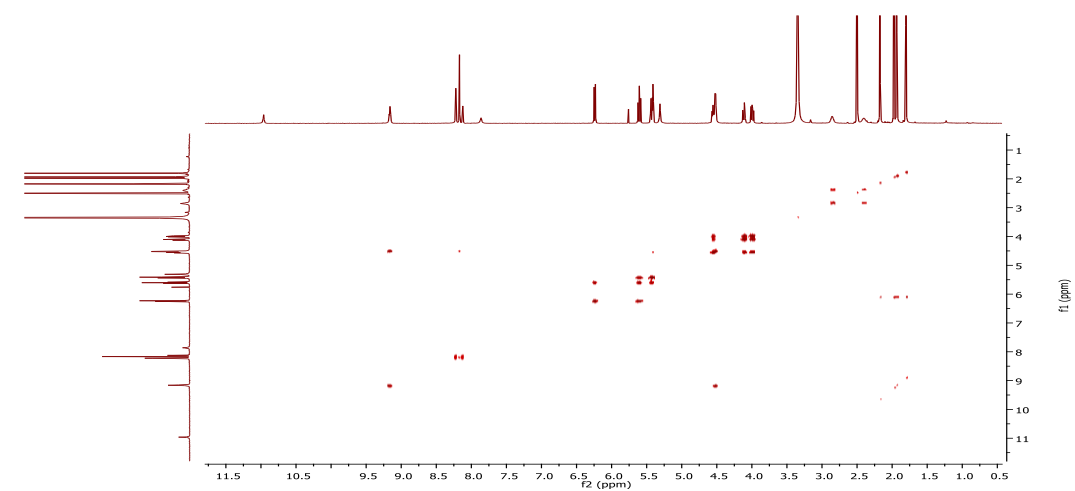
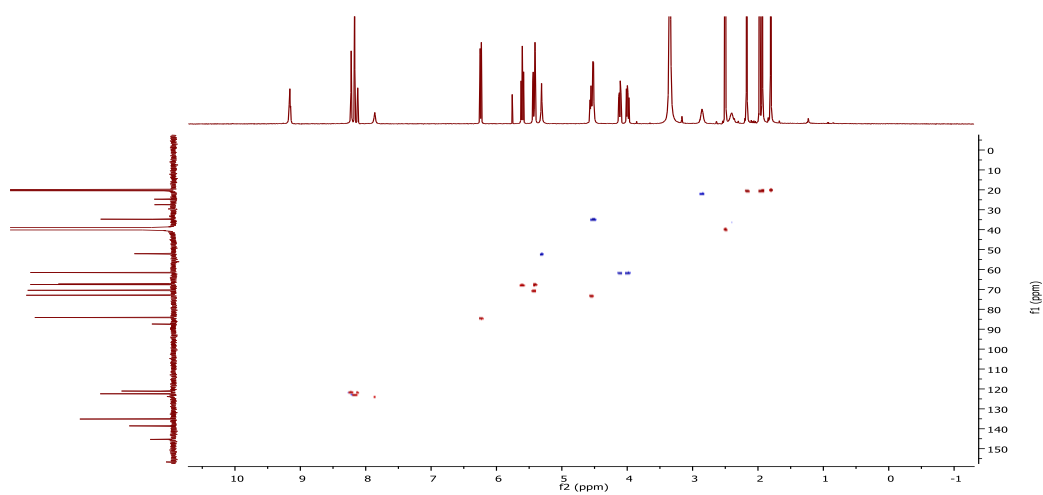
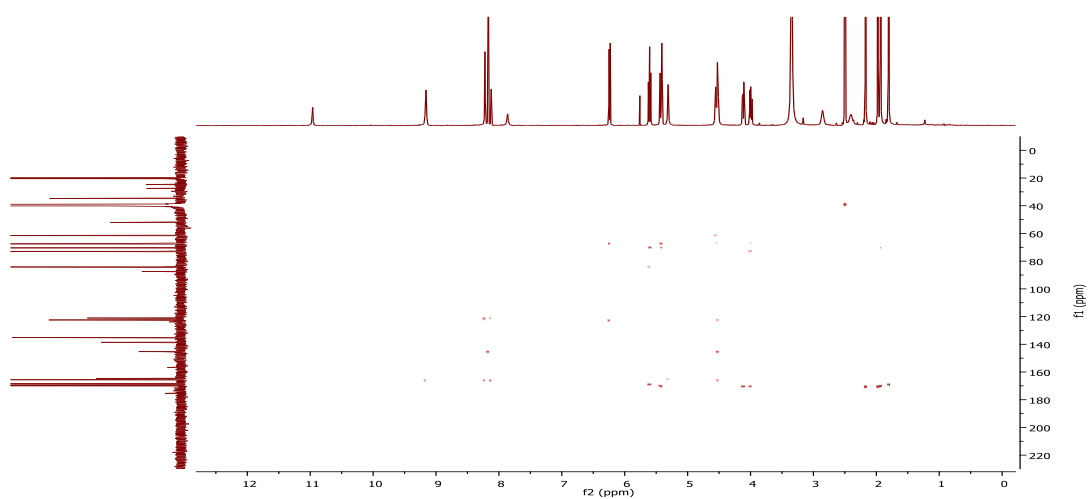


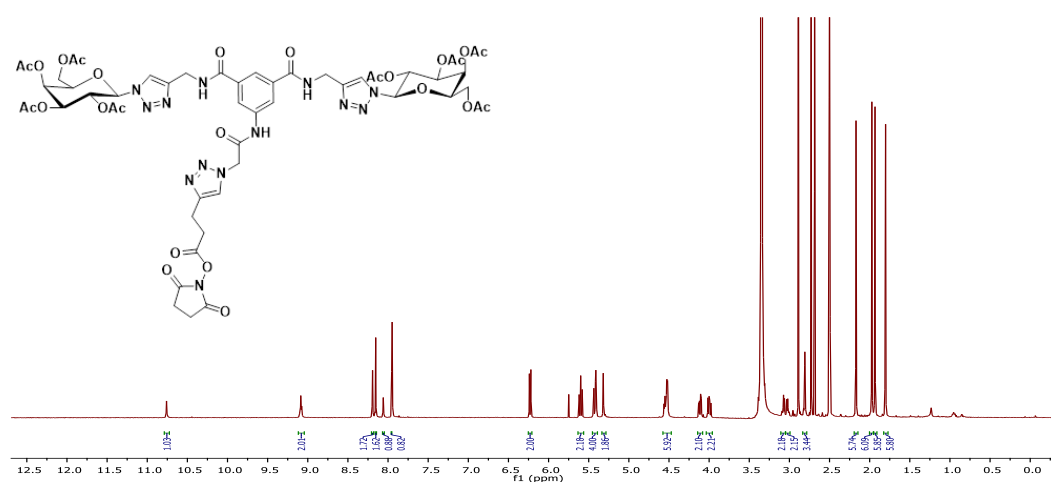
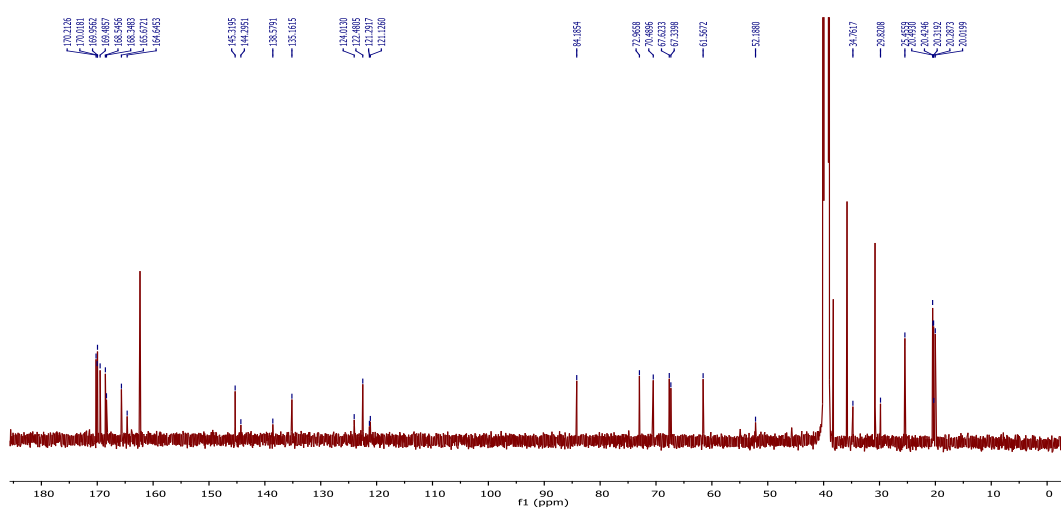
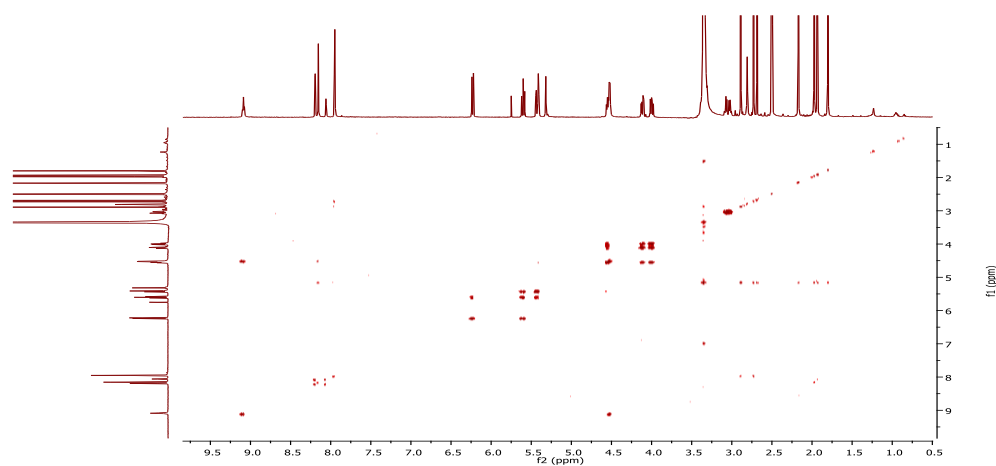
COSY NMR spectrum of **5.11** in  $\text{DMSO-d}_6$

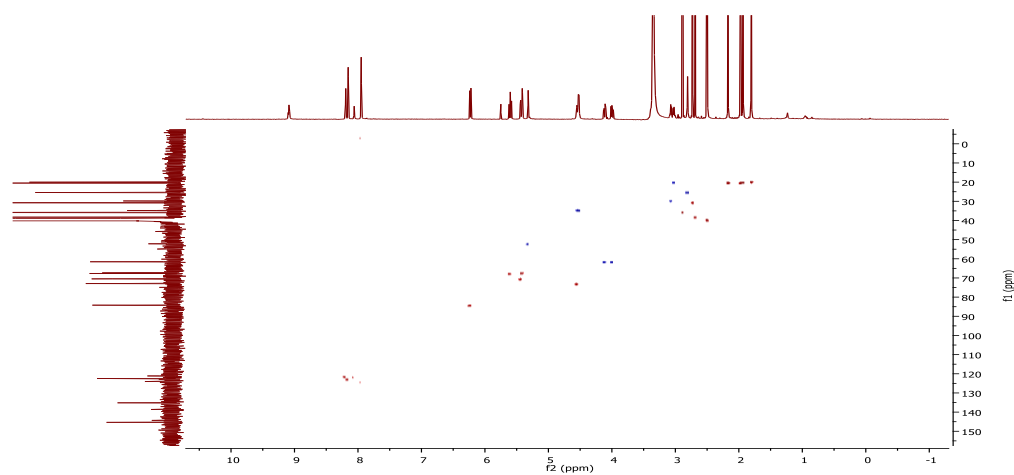
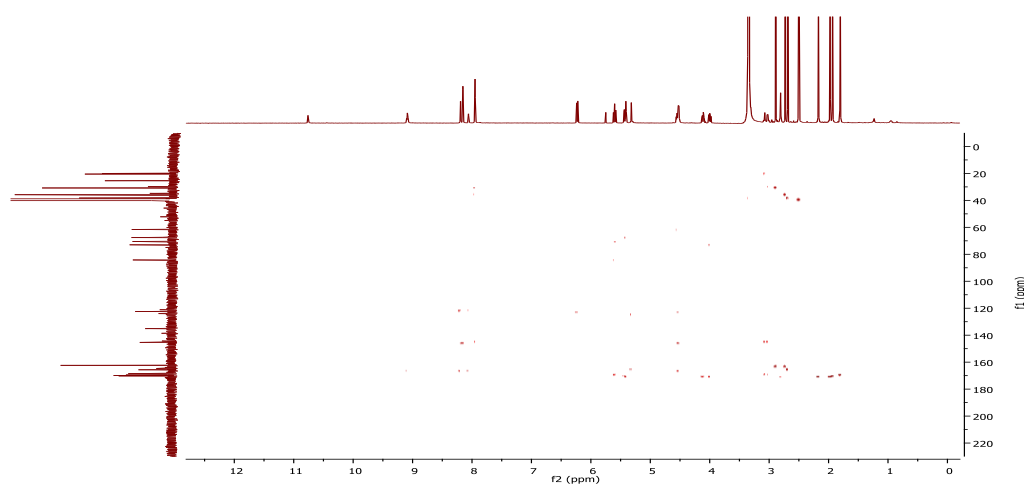
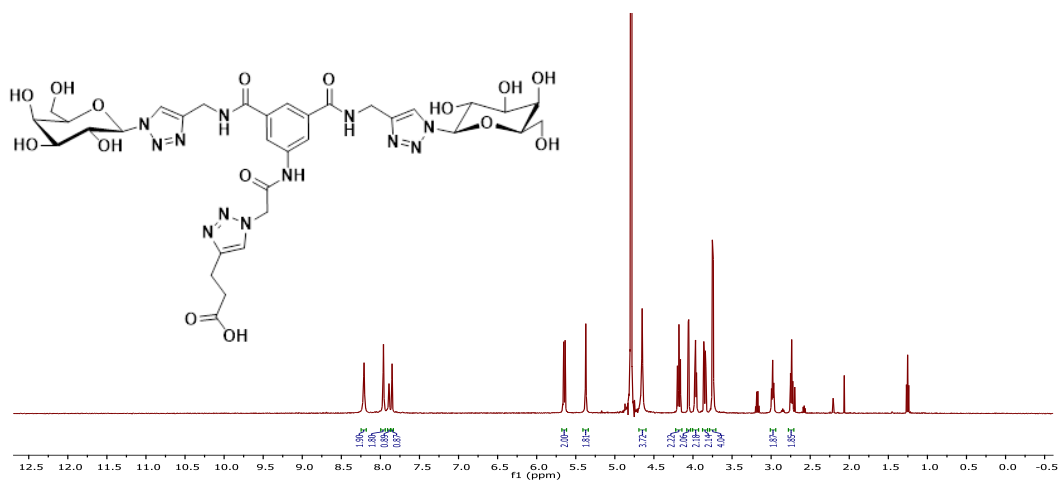


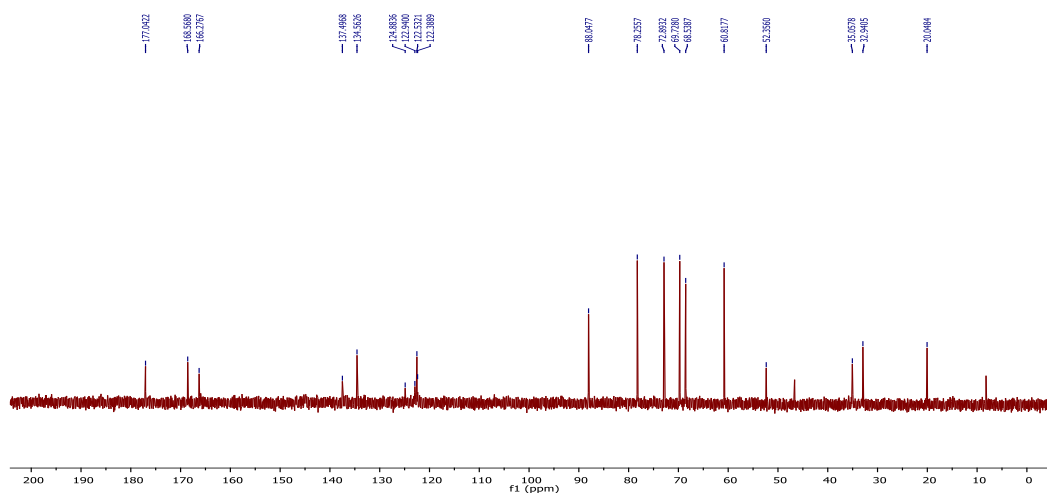
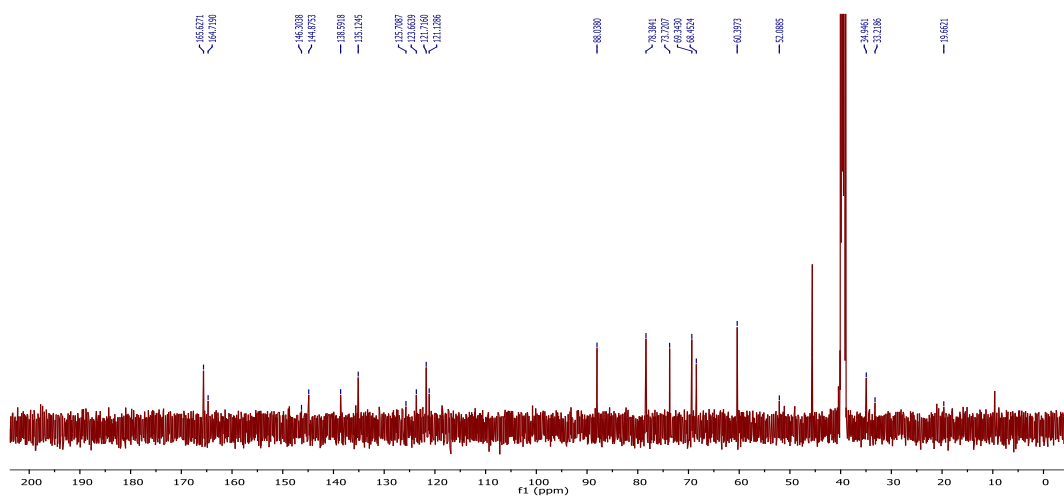
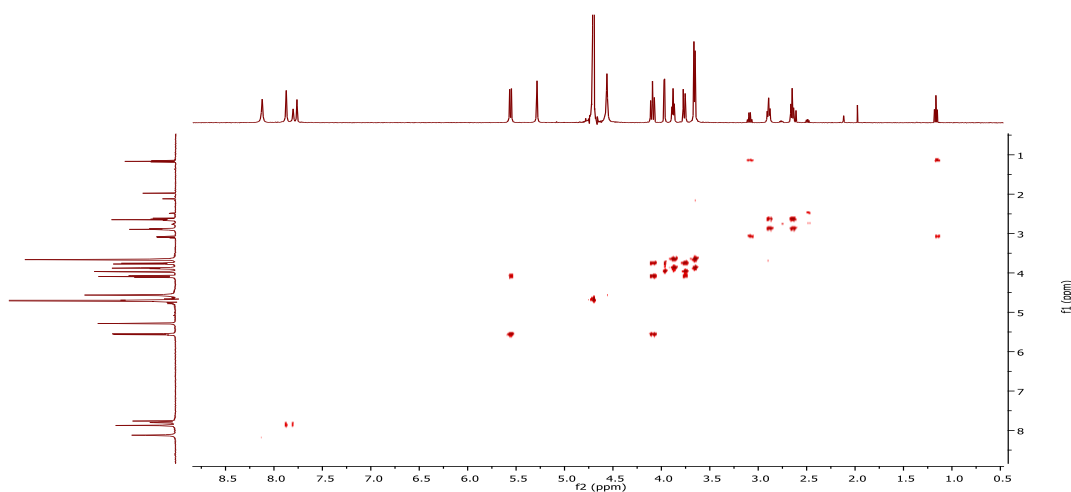
HSQC NMR spectrum of **5.11** in  $\text{DMSO-d}_6$

HMBC NMR spectrum of **5.11** in DMSO-d<sub>6</sub>NMR spectra of **5.18**<sup>1</sup>H NMR spectrum of **5.18** in DMSO-d<sub>6</sub><sup>13</sup>C NMR spectrum of **5.18** in DMSO-d<sub>6</sub>

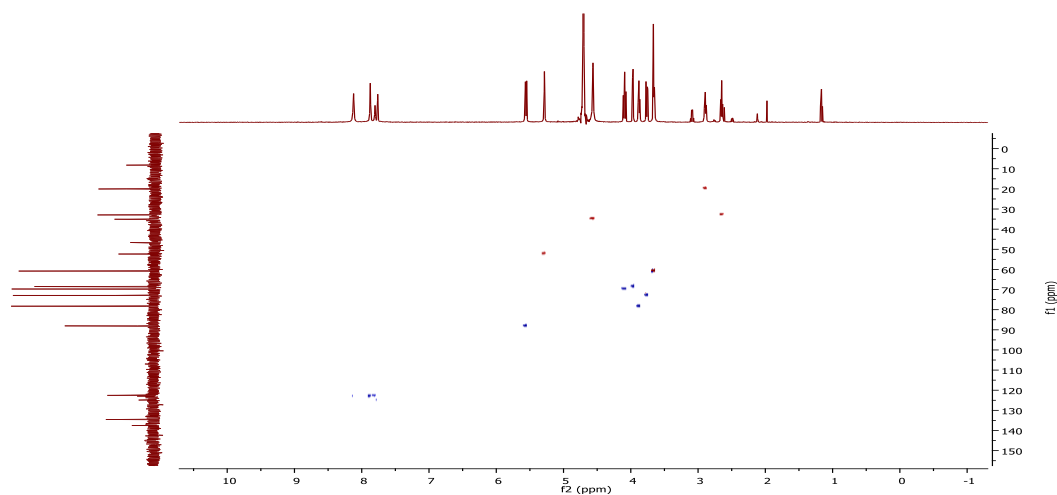
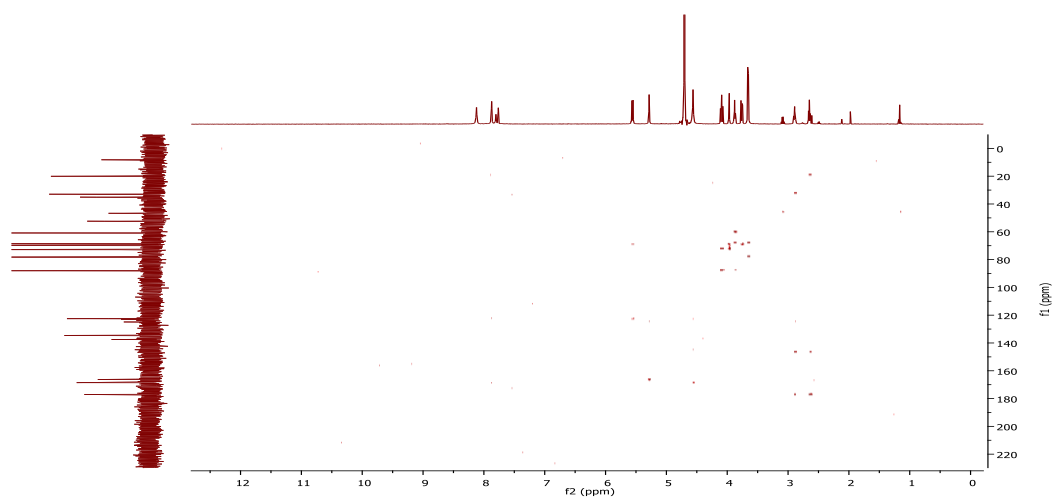
COSY NMR spectrum of **5.18** in DMSO-d<sub>6</sub>HSQC NMR spectrum of **5.18** in DMSO-d<sub>6</sub>HMBC NMR spectrum of **5.18** in DMSO-d<sub>6</sub>

NMR spectra of **5.19**<sup>1</sup>H NMR spectrum of **5.19** in DMSO-d<sub>6</sub><sup>13</sup>C NMR spectrum of **5.19** in DMSO-d<sub>6</sub>COSY NMR spectrum of **5.19** in DMSO-d<sub>6</sub>

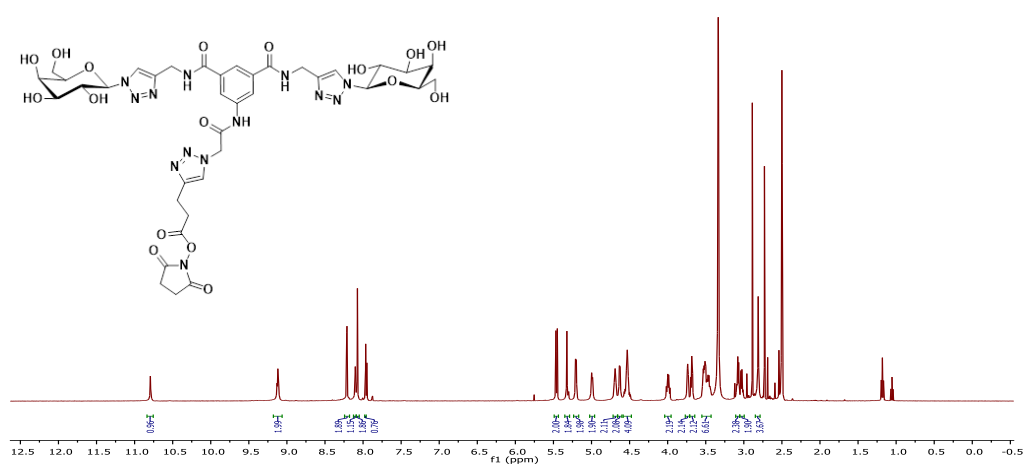
HSQC NMR spectrum of **5.19** in DMSO-d<sub>6</sub>HMBC NMR spectrum of **5.19** in DMSO-d<sub>6</sub>NMR spectra of **5.20**<sup>1</sup>H NMR spectrum of **5.20** in D<sub>2</sub>O

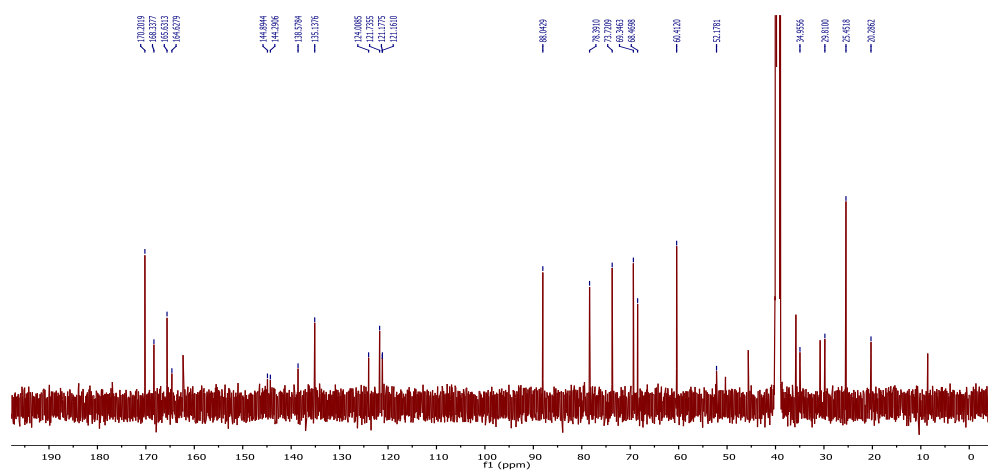
 $^{13}\text{C}$  NMR spectrum of **5.20** in  $\text{D}_2\text{O}$  $^{13}\text{C}$  NMR spectrum of **5.20** in  $\text{DMSO-d}_6$ COSY NMR spectrum of **5.20** in  $\text{D}_2\text{O}$



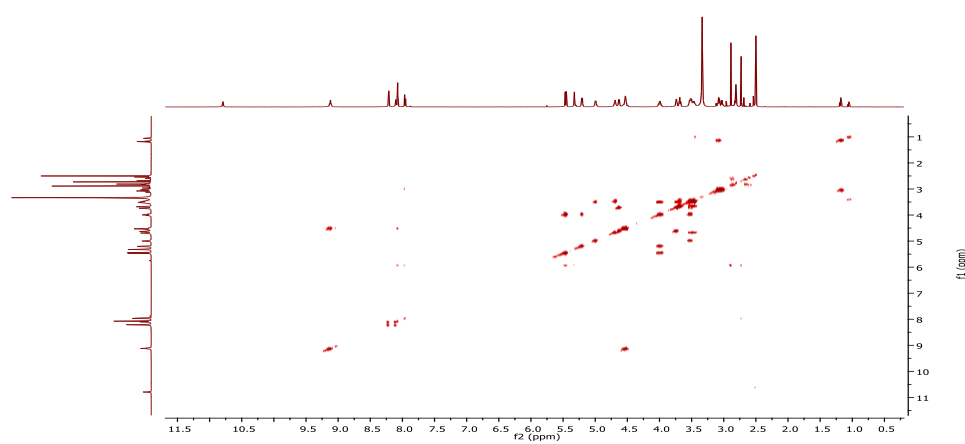
HSQC NMR spectrum of 5.20 in D<sub>2</sub>OHMBC NMR spectrum of 5.20 in D<sub>2</sub>O

## NMR spectra of 5.21

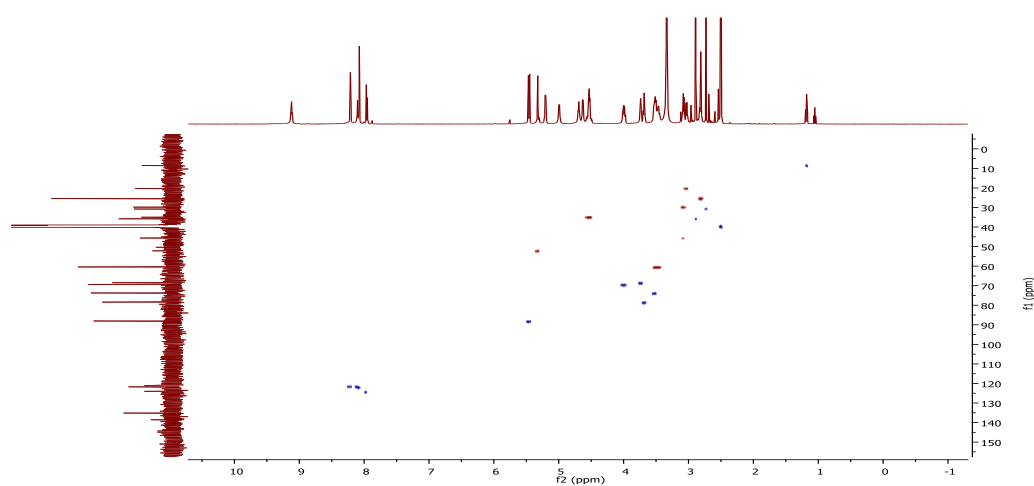
<sup>1</sup>H NMR spectrum of 5.21 in DMSO-d<sub>6</sub>



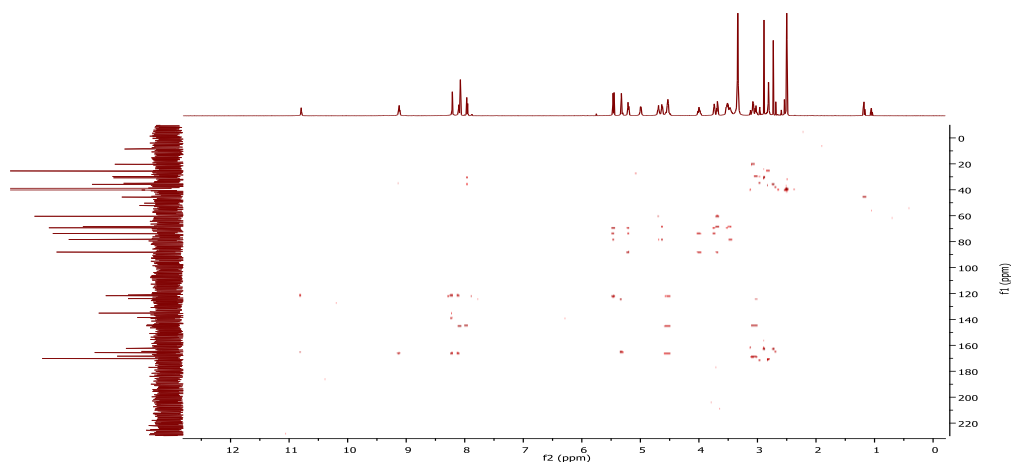
$^{13}\text{C}$  NMR spectrum of **5.21** in  $\text{DMSO-d}_6$



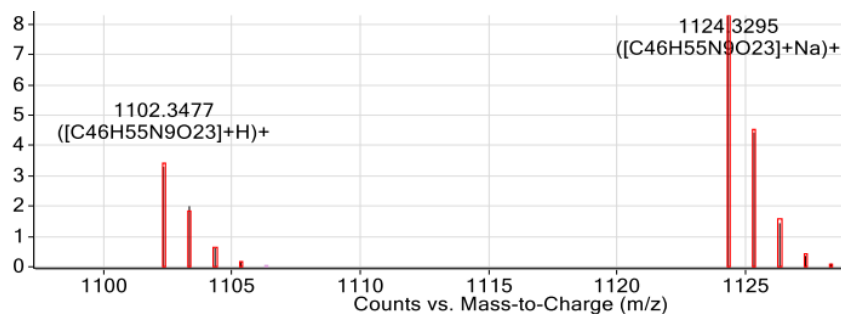
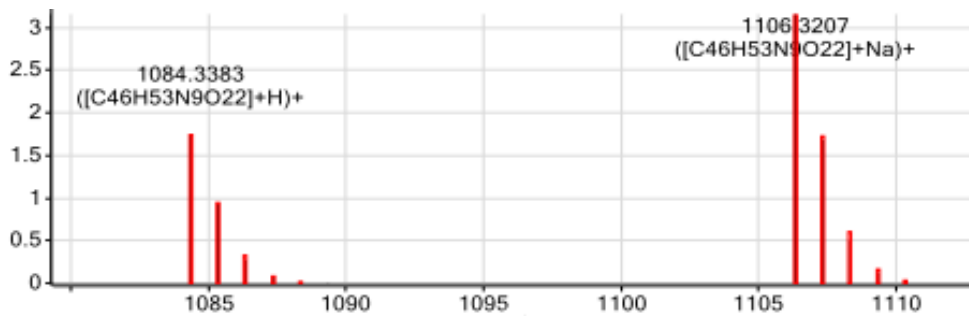
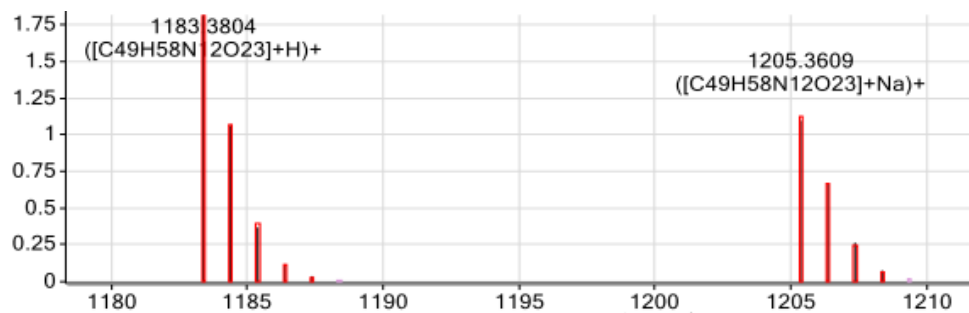
COSY NMR spectrum of **5.21** in  $\text{DMSO-d}_6$

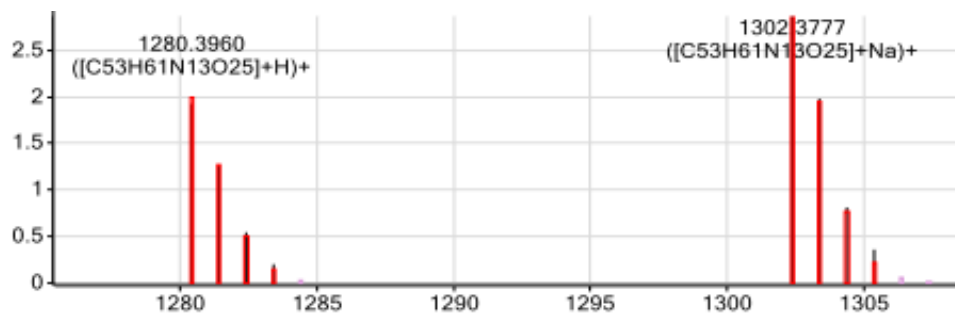


HSQC NMR spectrum of **5.21** in  $\text{DMSO-d}_6$

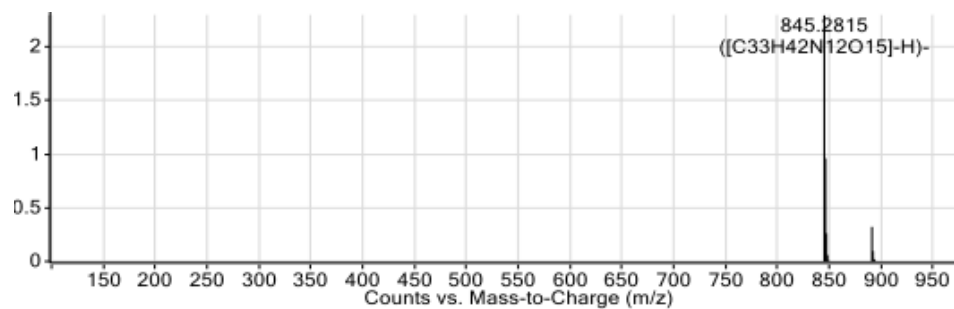
HMBC NMR spectrum of **5.21** in DMSO-d<sub>6</sub>

## HR-MS

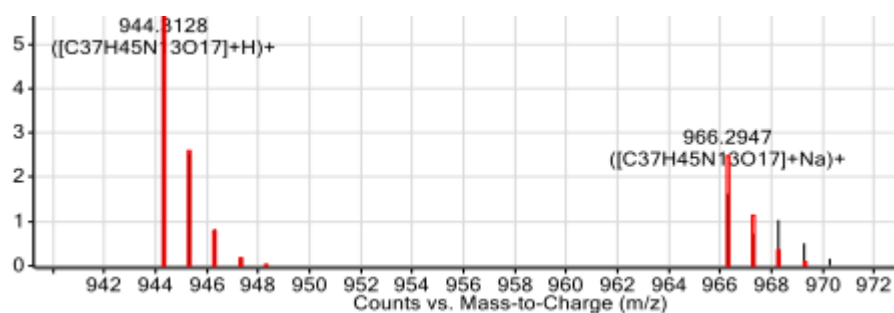
HR-MS spectrum of **5.10**HR-MS spectrum of **5.11**HR-MS spectrum of **5.18**



HR-MS spectrum of 5.19




HR-MS spectrum of 5.20




HR-MS spectrum of 5.21

## Author Publications:



ORIGINAL RESEARCH  
published: 07 December 2021  
doi: 10.3389/fchem.2021.795997



## Click Pt(IV)-Carbohydrates Pro-Drugs for Treatment of Osteosarcoma

Eoin Moynihan<sup>1</sup>, Giada Bassi<sup>2</sup>, Andrea Ruffini<sup>2</sup>, Silvia Panseri<sup>2</sup>, Monica Montesi<sup>2\*</sup>, Trinidad Velasco-Torrijos<sup>1,3\*</sup> and Diego Montagner<sup>1,3\*</sup>

<sup>1</sup>Department of Chemistry, Maynooth University, Maynooth, Ireland; <sup>2</sup>Institute of Science and Technology for Ceramics – National Research Council, Faenza, Italy; <sup>3</sup>Kathleen Lonsdale Institute for Human Health Research, Maynooth University, Maynooth, Ireland

The selectivity vs. cancer cells has always been a major challenge for chemotherapeutic agents and in particular for cisplatin, one of the most important anticancer drugs for the treatment of several types of tumors. One strategy to overcome this challenge is to modify the coordination sphere of the metallic center with specific vectors whose receptors are overexpressed in the tumoral cell membrane, such as monosaccharides. In this paper, we report the synthesis of four novel glyco-modified Pt(IV) pro-drugs, based on cisplatin scaffold, and their biological activity against osteosarcoma (OS), a malignant tumor affecting in particular adolescents and young adults. The sugar moiety and the Pt scaffold are linked exploiting the Copper Azide Alkyne Cycloaddition (CUAAC) reaction, which has become the flagship of click chemistry due to its versatility and mild conditions. Cytotoxicity and drug uptake on three different OS cell lines as well as CSCs (Cancer Stem Cell) are described.

**Keywords:** Pt(IV) prodrugs, cisplatin, sugars, osteosarcoma, cancer stem cells, click chemistry

**OPEN ACCESS**

**Edited by:**  
Mauro Ravera,  
Università del Piemonte Orientale, Italy

**Reviewed by:**  
Woo Han Ang,  
National University of Singapore,  
Singapore  
Xiao-Peng He,  
East China University of Science and  
Technology, China

**\*Correspondence:**  
Monica Montesi  
monica.montesi@istec.cnr.it  
Trinidad Velasco-Torrijos  
trinidad.velascotorrijos@mu.ie  
Diego Montagner  
diego.montagner@mu.ie

**Specialty section:**  
This article was submitted to  
Medicinal and Pharmaceutical  
Chemistry,  
a section of the journal  
Frontiers in Chemistry

**Received:** 15 October 2021  
**Accepted:** 08 November 2021  
**Published:** 07 December 2021

**Citation:**  
Moynihan E, Bassi G, Ruffini A,  
Panseri S, Montesi M,  
Velasco-Torrijos T and Montagner D  
(2021) Click Pt(IV)-Carbohydrates Pro-  
Drugs for Treatment of Osteosarcoma.  
Front. Chem. 9:795997.  
doi: 10.3389/fchem.2021.795997

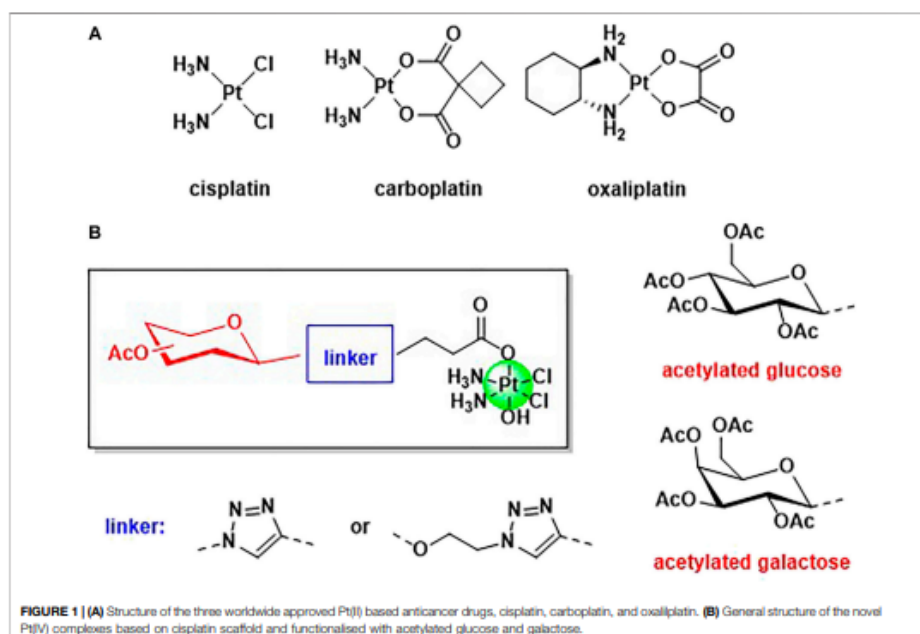
### INTRODUCTION

Despite the large success of cisplatin and of the second generation Pt(II) anticancer drugs (oxaliplatin and carboplatin) for the treatment of tumors, several drawbacks and side effects are limiting their use (Figure 1A) (Johnstone et al., 2013). The main concern is the lack of selectivity of Pt(II) based drugs, and in the last 2 decades a large interest has grown in the development of selective targeted metal-based anticancer drugs (Jung and Lippard, 2007).

A very promising strategy that has been successfully adopted is the use of carbohydrates, such as glucose and galactose, as targeting vectors, exploiting the Warburg effect (Koppenol et al., 2011; Wu et al., 2016). Tumoral tissues require a higher demand of nutrients, such as sugars, to maintain the fast proliferation rate, and many cancer cells are overexpressing glucose transporters (Jang et al., 2013). Several metal-based complexes have been modified with carbohydrates with the aim to increase selectivity versus cancer cells, including platinum, palladium, gold, ruthenium, copper, cobalt, and tin (Pettenuzzo et al., 2016). Many glyco-modified Pt(II) complexes are reported (Kenny and Marmion, 2019) but the literature on Pt(IV) functionalized with sugars mainly refers to the interesting works reported by Wang et al. (Ma et al., 2016; 2017a; 2017b, 2018). Pt(IV) complexes show several advantages with respect to Pt(II) counterparts, being more stable and less prone to substitution reactions (Harper et al., 2010). Pt(IV) species are also called pro-drugs because they must be activated by intracellular reduction with the release of the Pt(II) scaffold and the axial ligands (Harper et al., 2010), and dual-action Pt(IV) pro-drugs are obtained when the axial positions are occupied by another relevant biological molecule (another drug, an enzyme inhibitor, a vector, etc) (Neumann et al., 2014; Ma et al., 2015; Wexselblatt et al., 2015; Gibson, 2016; Lee et al., 2018; Lo Re

---

Frontiers in Chemistry | www.frontiersin.org
1
December 2021 | Volume 9 | Article 795997



et al., 2018; Montagner et al., 2018; Petruzzella et al., 2018; Savino et al., 2018; Almotairy et al., 2020; Gabano et al., 2021). In this work, we present a facile synthesis of mono glyco-functionalised Pt(IV) complexes based on cisplatin scaffold and their biological applications against osteosarcoma cell lines. Osteosarcoma (OS) is the main primary bone malignant entity affecting adolescents and young adults, and it is an aggressive tumor with a tendency to metastasize and invade para-carcinoma tissues (Heymann et al., 2019). The primary treatment for this tumor is a combination of surgery and chemotherapy but unfortunately, the prognosis remains poor due to chemoresistance and early metastasis (Han et al., 2019). The absence of specific and targeted strategies for the treatment of OS increased the scientific interest in designing and synthesizing new drugs able to selective target OS cancer cells. Cisplatin is a standard drug for osteosarcoma therapy but the effectiveness of the therapy is often limited by the chemoresistance and the absence of drug specificity (Li et al., 2018). As most of the tumoral tissues, also OS cancer cells exhibit increased glycolytic activity and accumulate greater quantities of sugars, compared to normal tissues (Cifuentes et al., 2011; Cura and Carruthers, 2012; Ogawa et al., 2021). It has been shown that the overexpression of sugar receptors in OS is predominantly associated with the likelihood of metastasis and poor patient prognosis (Medina and Owen, 2002).

For the first time, the carbohydrates and the platinum scaffold are linked, exploiting the Copper Azide Alkyne Cycloaddition (CUAAC) reaction, which has become the flagship of click chemistry. Click chemistry is becoming a very promising and emerging tool in synthetic medicinal chemistry because its versatility and mild conditions allow the conjugation of a plethora of functional groups (Pathak et al., 2014; Wirth et al., 2015; Lauria et al., 2020). Triazole linkers are very attractive bioisosteres that can often replace the amide bonds with increased metabolic stability (Valverde et al., 2013; Bonandi et al., 2017; Farrer and Griffith, 2020). Modification of the axial positions of a Pt(IV) scaffold with targeting vectors can be achieved using several synthetic strategies (reaction between the free carboxylic acid and oxaliplatin in the presence of a coupling reagent, or reaction of an activated acyl chloride with oxaliplatin) but often the final Pt(IV) compound requires purification (Zhang et al., 2013). In this paper, we will show how CUAAC chemistry can be used as a tool to link targeting carbohydrates to a Pt scaffold. We report the syntheses and characterization of four novel Pt(IV) complexes based on cisplatin and functionalized with acetylated glucose and galactose. Acetylated carbohydrate derivatives have been often found to have higher anti-cancer activity than their deprotected counterparts, likely due to an increase in lipophilicity that facilitates diffusion through cell



membranes (Morris et al., 2011; Upadhyaya et al., 2016; Wang et al., 2018). In addition, we investigated the effect of the linker connecting these structural moieties by the formation of anomeric *N*-triazolyl or *O*-ethylene glycosides (Figure 1B). Anomeric triazoles can offer additional sites of interaction for glucose transporters and hence enhance the activity of these types of derivatives compared to conventional glycosides (Brito et al., 2020; Ottoni et al., 2020). The anticancer activity and the cellular uptake of the complexes have been tested against three different osteosarcoma cell lines and in a model of enriched-cancer stem cells, in order to compare *in vitro* the effectiveness with standard cisplatin.

## EXPERIMENTAL

### Materials and Methods

All reagents and reactants (5 and 6) were purchased from commercial sources. The two sources used were Sigma-Aldrich and Fluorochem. All solvents were used without further purification. Cisplatin and oxoplatin were synthesized as previously reported (Dhara, 1970; Brandon and Dabrowiak, 1984).

The elemental analysis studies (carbon, hydrogen, and nitrogen) were performed by means of a PerkinElmer 2400 series II analyzer. ESI Mass Spectra were recorded with a Waters LCT Premier XE Spectrometer. NMR: <sup>1</sup>H, <sup>13</sup>C, and <sup>195</sup>Pt NMR spectra were obtained in a solution of CDCl<sub>3</sub> or DMSO-*d*<sub>6</sub> at 300 K, in 5-mm sample tubes, with a Bruker Advance 500 MHz spectrometer (operating at 500.13, 125.75, and 107.49 MHz, respectively). The <sup>1</sup>H and <sup>13</sup>C chemical shift was referenced to the residual impurity of the solvent. The external reference was Na<sub>2</sub>PtCl<sub>6</sub> in D<sub>2</sub>O (adjusted to δ = -1628 ppm from Na<sub>2</sub>PtCl<sub>6</sub>) for <sup>195</sup>Pt. The stability was followed using high-performance liquid chromatography (HPLC) with a Phenomenex Luna C18 (5 μm, 100 Å, 250 mm × 4.60 mm i.d.) column at room temperature at a flow rate of 1.0 ml/min with 254 nm UV detection. Mobile phase containing 80:20 acetonitrile (0.1% trifluoroacetic acid): water (0.1% trifluoroacetic acid): the complexes were dissolved in DMSO (0.5 ml) and diluted to a final concentration of 0.5 mM using acetonitrile and water solution (1/1) and 2 mM 4-(2-hydroxyethyl)piperazine-1-ethanesulfonic acid (HEPES) buffer (pH 6.8). Infrared (IR) spectra were recorded in the region 4,000–400 cm<sup>-1</sup> on a Perkin Elmer precisely spectrum 100 FT/IR spectrometer. The solid samples were run using ATR. Compounds 7, 8 (Tropper et al., 1992), 9 (Mangunuru et al., 2015), and 13–16 (Reddy et al., 2017) were prepared according to reported procedures. An extensive biological evaluation of the activity of all the compounds was performed in human osteosarcoma cell line *in vitro* models, as reported below.

### Synthesis

**Synthesis of N-(2,3,4,6-Tetra-O-Acetyl-β-D-Glucopyranosyl-1,2,3-Triazol-4-yl)-Propanoic Acid (9)**  
Compound 7 (0.98 g, 3.412 mmol) and 4-pentynoic acid (0.2 g, 2.038 mmol) were dissolved in a mixture of tetrahydrofuran

(6 ml), tert-Butanol (6 ml), and deionized water (4 ml). Separately, copper(II) sulphate pentahydrate (0.1 g, 0.08 mmol) and sodium ascorbate (0.161 g, 0.325 mmol) were dissolved in deionized water (2 ml), added to a reaction flask, and allowed to stir at r.t. overnight (16 h). The solvent was removed *in vacuo* and the residue was dissolved in DCM (15 ml) and washed with brine (2 ml × 20 ml). The organic phase was dried with MgSO<sub>4</sub>, filtered and the solvent was evaporated. The crude product was purified by column chromatography (1:1, petroleum ether: ethyl acetate) to yield a white solid (0.615 g, 1.304 mmol, 64%). R<sub>f</sub> = 0.92 (90:10 DCM: MeOH) [α]<sub>D</sub><sup>23</sup> -17.14 (c 0.7, MeOH). <sup>1</sup>H NMR (500 MHz, CDCl<sub>3</sub>) δ 7.62 (s, 1H, triaz-H), 5.85 (d, J = 9.0 Hz, 1H, H-1), 5.46–5.37 (m, 2H, H-2, H-3), 5.24 (t, J = 9.95 Hz, 1H, H-4), 4.29 (dd, J = 12.6, 5.0 Hz, 1H, H-6), 4.14 (dd, J = 12.6, 2.1 Hz, 1H, H-6'), 3.99 (ddd, J = 10.1, 5.0, 2.1 Hz, 1H, H-5), 3.05 (t, J = 7.3 Hz, 2H, triaz-CH<sub>2</sub>), 2.78 (t, J = 7.3 Hz, 2H, CH<sub>2</sub>CO), 2.08 (s, 3H, CH<sub>3</sub> of OAc), 2.06 (s, 3H, CH<sub>3</sub> of OAc), 2.02 (s, 3H, CH<sub>3</sub> of OAc), 1.85 (s, 3H, CH<sub>3</sub> of OAc) ppm. <sup>13</sup>C NMR (125 MHz, CDCl<sub>3</sub>) δ 176.93 (COOH), 170.70 (CO of OAc), 170.08 (CO of OAc), 169.54 (CO of OAc), 169.13 (CO of OAc), 147.04 (triaz-C), 119.81 (triaz-CH), 85.80 (C-1), 75.22 (C-5), 72.81 (C-3), 70.30 (C-2), 67.88 (C-4), 61.70 (C-6), 33.24 (CH<sub>2</sub>COOH), 20.83 (2 × CH<sub>3</sub> of OAc), 20.68 (2 × CH<sub>3</sub> of OAc), 20.24 (triaz-CH<sub>2</sub>) ppm. IR (ATR) 2966.47, 1738.08, 1701.08, 1429.63, 1369.28, 1218.46, 1096.44, 1037.86, 918.27, 838.17 cm<sup>-1</sup>. HR-MS (+): m/z calcd for C<sub>19</sub>H<sub>23</sub>N<sub>3</sub>O<sub>11</sub> + Na<sup>+</sup> (M + Na)<sup>+</sup> 494.1489, found 494.1383. HR-MS (+): m/z calcd for C<sub>19</sub>H<sub>23</sub>N<sub>3</sub>O<sub>11</sub> + H<sup>+</sup> (M + H)<sup>+</sup> 472.1489, found 472.1564.

### Synthesis of N-(2,3,4,6-Tetra-O-Acetyl-β-D-Galactopyranosyl-1,2,3-Triazol-4-yl)-Propanoic Acid (10)

Compound 10 was prepared according to the method reported for compound 9 (Yield 0.713 g, 1.512 mmol, 74%). R<sub>f</sub> = 0.33 (95:5 DCM: MeOH) [α]<sub>D</sub><sup>21.6</sup> -1.51 (c 0.66, MeOH). <sup>1</sup>H NMR (500 MHz, CDCl<sub>3</sub>) δ 7.65 (s, 1H, triaz-H), 5.81 (d, J = 9.4 Hz, 1H, H-1), 5.57–5.50 (m, 2H, H-2, H-3), 5.23 (dd, J = 10.3, 3.4 Hz, 1H, H-4), 4.24–4.10 (m, 3H, H-5, H-6, H-6'), 3.05 (t, J = 7.4 Hz, 2H, triaz-CH<sub>2</sub>), 2.79 (t, J = 7.4 Hz, 2H, CH<sub>2</sub>CO), 2.21 (s, 3H, CH<sub>3</sub> of OAc), 2.03 (s, 3H, CH<sub>3</sub> of OAc), 1.99 (s, 3H, CH<sub>3</sub> of OAc), 1.86 (s, 3H, CH<sub>3</sub> of OAc) ppm. <sup>13</sup>C NMR (125 MHz, CDCl<sub>3</sub>) δ 177.14 (COOH), 170.52 (CO of OAc), 170.13 (CO of OAc), 169.97 (CO of OAc), 169.25 (CO of OAc), 146.91 (triaz-C), 119.88 (triaz-CH), 86.31 (C-1), 74.11 (C-5), 70.93 (C-4), 67.88 (C-2), 67.02 (C-3), 61.31 (C-6), 33.27 (CH<sub>2</sub>COOH), 20.81 (triaz-CH<sub>2</sub>), 20.78 (CH<sub>3</sub> of OAc), 20.76 (CH<sub>3</sub> of OAc), 20.61 (CH<sub>3</sub> of OAc), 20.32 (CH<sub>3</sub> of OAc) ppm. IR (ATR) 3087.65, 1734.80, 1715.92, 1436.51, 1366.99, 1216.01, 1045.12, 923.00, 850.50, 717.78 cm<sup>-1</sup>. HR-MS (+): m/z calcd for C<sub>19</sub>H<sub>23</sub>N<sub>3</sub>O<sub>11</sub> + H<sup>+</sup> (M + H)<sup>+</sup> 472.1489, found 472.1564. HR-MS (+): m/z calcd for C<sub>19</sub>H<sub>23</sub>N<sub>3</sub>O<sub>11</sub> + Na<sup>+</sup> (M + Na)<sup>+</sup> 494.1489, found 494.1384.

### Synthesis of N-[2-O-(2,3,4,6-Tetra-O-Acetyl-β-D-Glucopyranosyl)-ethyl-1,2,3-Triazol-4-yl]-Propanoic Acid (17)

Compound 17 was prepared according to the method reported for compound 9 (Yield 0.147 g, 0.285 mmol, 44.24%). R<sub>f</sub> = 0.35 (DCM: MeOH 95:5) [α]<sub>D</sub><sup>21.6</sup> -8.57 (c 0.7, MeOH). <sup>1</sup>H NMR

(500 MHz, CDCl<sub>3</sub>) δ 7.44 (s, 1H, triaz-H), 5.19 (t, *J* = 9.5 Hz, 1H, H-3), 5.06 (t, *J* = 9.7 Hz, 1H, H-4), 4.97 (dd, *J* = 9.6, 8.0 Hz, 1H, H-2), 4.55 (dt, *J* = 14.4, 3.8 Hz, 1H, CH-triaz), 4.50–4.44 (m, 1H, CH'-triaz), 4.43 (d, *J* = 7.9 Hz, 1H, H-1), 4.24 (dd, *J* = 12.4, 4.7 Hz, 1H, H-6), 4.19 (dt, *J* = 10.6, 4.0 Hz, 1H, OCH), 4.11 (dd, *J* = 12.4, 2.2 Hz, 1H, H-6'), 3.95–3.87 (m, 1H, OCH'), 3.68 (ddd, *J* = 10.0, 4.6, 2.3 Hz, 1H, H-5), 3.02 (t, *J* = 7.0 Hz, 2H, triaz-CH<sub>2</sub>), 2.77 (t, *J* = 6.7 Hz, 2H, CH<sub>2</sub>CO), 2.07 (s, 3H, OAc), 2.01 (s, 3H, OAc), 1.99 (s, 3H, OAc), 1.96 (s, 3H, OAc) ppm. <sup>13</sup>C NMR (125 MHz, CDCl<sub>3</sub>) δ 176.42 (COOH), 170.78 (CO of OAc), 170.48 (CO of OAc), 169.59 (CO of OAc), 169.54 (CO of OAc), 146.25 (C-triaz), 122.83 (CH-triaz), 100.66 (C-1), 72.67 (C-3), 72.04 (C-5), 71.17 (C-2), 68.28 (C-4), 67.89 (OCH<sub>2</sub>), 61.85 (C-6), 50.20 (CH<sub>2</sub>-triaz), 33.54 (CH<sub>2</sub>COOH), 20.88 (triaz-CH<sub>2</sub>), 20.84 (CH<sub>3</sub> of OAc), 20.70 (2 × CH<sub>3</sub> of OAc), 20.68 (CH<sub>3</sub> of OAc) ppm. IR (ATR) 3136.33, 2954.03, 1753.42, 1742.06, 1720.47, 1428.59, 1367.14, 1251.30, 1221.16, 1167.23, 1046.93, 1031.50, 910.47, 826.13 cm<sup>-1</sup>. HR-MS (+): *m/z* calcd for C<sub>21</sub>H<sub>29</sub>N<sub>3</sub>O<sub>12</sub> + H<sup>+</sup> (M + H)<sup>+</sup> 516.1751, found 516.1826. HR-MS (+): *m/z* calcd for C<sub>21</sub>H<sub>29</sub>N<sub>3</sub>O<sub>12</sub> + Na<sup>+</sup> (M + Na)<sup>+</sup> 538.1781, found 538.1644.

#### Synthesis of N-[2-O-(2,3,4,6-Tetra-O-Acetyl-β-D-Galactopyranosyl)-ethyl-1,2,3-Triazol-4-yl]-Propanoic Acid (18)

Compound 18 was prepared according to the method reported for compound 9 (Yield 0.500 g, 0.969 mmol, 47%). *R<sub>f</sub>* = 0.41 (DCM: MeOH 95:5) [α]<sub>D</sub><sup>20</sup> -1.45 (c 0.68, MeOH). <sup>1</sup>H NMR (500 MHz, CDCl<sub>3</sub>) δ 7.46 (s, 1H, triaz-H), 5.38 (dd, *J* = 3.4, 0.9 Hz, 1H, H-4), 5.17 (dd, *J* = 10.5, 7.9 Hz, 1H, H-2), 5.01 (dd, *J* = 10.5, 3.4 Hz, 1H, H-3), 4.57 (dt, *J* = 7.7, 3.4 Hz, 1H, CH-triaz), 4.49 (ddd, *J* = 14.5, 8.8, 3.4 Hz, 1H, CH'-triaz), 4.41 (d, *J* = 7.9 Hz, 1H, H-1), 4.21 (dt, *J* = 10.6, 3.9 Hz, 1H, OCH), 4.13 (qd, *J* = 11.3, 6.7 Hz, 2H, H-6, H-6'), 3.95–3.87 (m, 2H, H-5, OCH'), 3.04 (t, *J* = 7.1 Hz, 2H, triaz-CH<sub>2</sub>), 2.79 (t, *J* = 7.1 Hz, 2H, CH<sub>2</sub>CO), 2.16 (s, 3H, CH<sub>3</sub> of OAc), 2.04 (s, *J* = 3.6 Hz, 3H, CH<sub>3</sub> of OAc), 1.97 (d, *J* = 2.1 Hz, 6H, 2 × CH<sub>3</sub> of OAc). <sup>13</sup>C NMR (125 MHz, CDCl<sub>3</sub>) δ 176.26 (COOH), 170.59 (CO of OAc), 170.32 (2 × CO of OAc), 169.79 (CO of OAc), 146.22 (C-triaz), 122.91 (CH-triaz), 101.07 (C-1), 70.98 (C-5), 70.74 (C-3), 68.78 (C-2), 67.77 (OCH<sub>2</sub>), 67.04 (C-4), 61.32 (C-6), 50.22 (CH<sub>2</sub>-triaz), 33.49 (CH<sub>2</sub>COOH), 20.92 (triaz-CH<sub>2</sub>), 20.82 (CH<sub>3</sub> of OAc), 20.80 (CH<sub>3</sub> of OAc), 20.77 (CH<sub>3</sub> of OAc), 20.69 (CH<sub>3</sub> of OAc). IR (ATR) 2940.25, 1739.44, 1430.24, 1367.99, 1214.32, 1043.51, 955.29, 916.32, 859.50, 827.84, 734.98 cm<sup>-1</sup>. HR-MS (+): *m/z* calcd for C<sub>21</sub>H<sub>29</sub>N<sub>3</sub>O<sub>12</sub> + H<sup>+</sup> (M + H)<sup>+</sup> 516.1751, found 516.1826. HR-MS (+): *m/z* calcd for C<sub>21</sub>H<sub>29</sub>N<sub>3</sub>O<sub>12</sub> + Na<sup>+</sup> (M + Na)<sup>+</sup> 538.1781, found 538.1664.

#### Synthesis of N-(2,3,4,6-Tetra-O-Acetyl-β-D-Glucopyranosyl)-ethyl-1,2,3-Triazol-4-yl]-[3-Oxopropyl-[oxy(2,5-Dioxopyrrolidin-1-yl)]] (11)

Compound 9 (0.2 g, 0.424 mmol) and N-hydroxysuccinimide (0.058 g, 0.604 mmol) were dissolved in anhydrous DCM (7 ml) and purged with N<sub>2</sub>. A solution of EDCl (0.097 g, 0.607 mmol) in anhydrous DCM (2 ml) was added *via* cannula over an ice bath and the solution was stirred for 45 min. The reaction was warmed to r.t. and stirred for a further 16 h. The organic layer was washed with 0.1 M HCl (2 × 10 ml) and dried

with MgSO<sub>4</sub>, filtered, and concentrated *in vacuo*. The product was obtained as a white solid which was reacted on without further purification (0.185 g, 0.325 mmol, 77%). *R<sub>f</sub>* = 0.72 (DCM: MeOH 95:5) [α]<sub>D</sub><sup>21.6</sup> -9.85 (c 0.71, CHCl<sub>3</sub>). <sup>1</sup>H NMR (500 MHz, CDCl<sub>3</sub>) δ 7.74 (s, 1H, CH-triaz), 5.83 (d, *J* = 9.2 Hz, 1H, H-1), 5.40–5.35 (m, 2H, H-2 and H-3), 5.24–5.18 (m, 1H, H-4), 4.25 (dd, *J* = 12.6, 5.1 Hz, 1H, H-6), 4.11 (dd, *J* = 12.6, 2.1 Hz, 1H, H-6'), 4.01–3.94 (m, 1H, H-5), 3.14 (td, *J* = 7.1, 3.2 Hz, 2H, triaz-CH<sub>2</sub>), 3.00–2.95 (m, 2H, CH<sub>2</sub>CO), 2.81 (s, 4H, CH<sub>2</sub>CH<sub>2</sub>-succ), 2.03 (s, 3H, OAc), 2.02 (s, 3H, OAc), 1.98 (s, 3H, OAc), 1.81 (s, 3H, OAc) ppm. <sup>13</sup>C NMR (125 MHz, CDCl<sub>3</sub>) δ 170.68 (CO of OAc), 170.07 (CO of OAc), 169.52 (CO of OAc), 169.24 (CO succ x2), 169.05 (CO of OAc), 167.77 (CO), 145.83 (C-triaz), 120.27 (CH-triaz), 85.79 (C-1), 75.20 (C-5), 72.91 (C-3), 70.35 (C-2), 67.87 (C-4), 61.76 (C-6), 30.99 (CH<sub>2</sub>CO), 25.73 (CH<sub>2</sub>CH<sub>2</sub>-succ), 21.11 (CH<sub>2</sub>-triaz), 20.83 (CH<sub>3</sub> of OAc), 20.69 (CH<sub>3</sub> of OAc), 20.66 (CH<sub>3</sub> of OAc), 20.27 (CH<sub>3</sub> of OAc) ppm. IR (ATR) 2945.90, 1732.16, 1430.40, 1367.42, 1203.35, 1064.13, 1035.83, 924.03, 813.55, 736.68 cm<sup>-1</sup>. HR-MS (+): *m/z* calcd for C<sub>23</sub>H<sub>28</sub>N<sub>4</sub>O<sub>13</sub> + H<sup>+</sup> (M + H)<sup>+</sup> 569.1653, found 569.1727. HR-MS (+): *m/z* calcd for C<sub>23</sub>H<sub>28</sub>N<sub>4</sub>O<sub>13</sub> + Na<sup>+</sup> (M + Na)<sup>+</sup> 591.1653, found 591.1554.

#### Synthesis of N-(2,3,4,6-Tetra-O-Acetyl-β-D-Galactopyranosyl-1,2,3-Triazol-4-yl)-[3-Oxopropyl-[oxy(2,5-Dioxopyrrolidin-1-yl)]] (12)

Compound 12 was prepared according to the method reported for compound 11 (Yield 0.131 g, 0.230 mmol, 54%). *R<sub>f</sub>* = 0.15 (pet. ether: EtOAc 1:1) [α]<sub>D</sub><sup>21.6</sup> +1.42 (c 0.7, DCM). <sup>1</sup>H NMR (500 MHz, CDCl<sub>3</sub>) δ 7.79 (s, 1H, CH-triaz), 5.81 (d, *J* = 9.3 Hz, 1H, H-1), 5.55 (dd, *J* = 12.5, 7.0 Hz, 2H, H-2 and H-4), 5.22 (dd, *J* = 10.3, 3.3 Hz, 1H, H-3), 4.23–4.12 (m, 3H, H-5, H-6 and H-6'), 3.18 (t, *J* = 7.1 Hz, 2H, triaz-CH<sub>2</sub>), 3.04 (t, *J* = 7.1 Hz, 2H, CH<sub>2</sub>CO), 2.84 (s, 4H, CH<sub>2</sub>CH<sub>2</sub>-succ), 2.23 (s, 3H, OAc), 2.05 (s, 3H, OAc), 2.01 (s, 3H, OAc), 1.88 (s, 3H, OAc) ppm. <sup>13</sup>C NMR (125 MHz, CDCl<sub>3</sub>) δ 170.52 (CO of OAc), 170.18 (CO of OAc), 170.00 (CO of OAc), 169.17 (CO of OAc), 169.14 (CO Succ x2), 167.84 (CO), 145.84 (C-triaz), 120.27 (CH-triaz), 86.35 (C-1), 74.08 (C-5), 71.07 (C-3), 67.95 (C-2), 67.01 (C-4), 61.38 (C-6), 30.87 (triaz-CH<sub>2</sub>), 25.73 (CH<sub>2</sub>CH<sub>2</sub>-succ), 21.01 (CH<sub>2</sub>CO), 20.81 (CH<sub>3</sub> of OAc), 20.78 (CH<sub>3</sub> of OAc), 20.66 (CH<sub>3</sub> of OAc), 20.38 (CH<sub>3</sub> of OAc) ppm. IR (ATR) 2944.04, 1731.92, 1430.13, 1368.12, 1205.23, 1045.44, 923.03, 812.54, 744.66 cm<sup>-1</sup>. HR-MS (+): *m/z* calcd for C<sub>23</sub>H<sub>28</sub>N<sub>4</sub>O<sub>13</sub> + H<sup>+</sup> (M + H)<sup>+</sup> 569.1653, found 569.1726. HR-MS (+): *m/z* calcd for C<sub>23</sub>H<sub>28</sub>N<sub>4</sub>O<sub>13</sub> + Na<sup>+</sup> (M + Na)<sup>+</sup> 591.1653, found 591.1547.

#### Synthesis of N-[2-O-(2,3,4,6-Tetra-O-Acetyl-β-D-Glucopyranosyl)-ethyl-1,2,3-Triazol-4-yl]-[3-Oxopropyl-[oxy(2,5-Dioxopyrrolidin-1-yl)]] (19)

Compound 19 was prepared according to the method discussed for compound 11 (0.126 g, 0.205 mmol, 87.5%). *R<sub>f</sub>* = 0.75 (DCM: MeOH 95:5) [α]<sub>D</sub><sup>21.6</sup> +1.42 (c 0.7, DCM). <sup>1</sup>H NMR (500 MHz, CDCl<sub>3</sub>) δ 7.49 (s, 1H, triaz-H), 5.11 (t, *J* = 9.5 Hz, 1H, H-3), 5.02 (t, *J* = 9.7 Hz, 1H, H-4), 4.92 (dd, *J* = 9.6, 7.9 Hz, 1H, H-2), 4.51 (ddd, *J* = 14.5, 4.6, 3.7 Hz, 1H, CH-triaz), 4.48–4.43 (m, 2H, H-1 and CH'-triaz), 4.21–4.11 (m, 2H, H-6' and OCH), 4.06 (dd, *J* = 12.3, 2.3 Hz, 1H, H-6), 3.88 (ddd, *J* = 10.7, 8.4, 3.6 Hz, 1H, OCH),



3.66 (ddd,  $J = 10.0, 4.8, 2.4$  Hz, 1H, H-5), 3.09 (dd,  $J = 10.7, 4.1$  Hz, 2H, triaz-CH<sub>2</sub>), 3.00–2.95 (m, 2H, CH<sub>2</sub>CO), 2.80 (d,  $J = 5.7$  Hz, 4H, CH<sub>2</sub>CH<sub>2</sub>-succ), 2.02 (s, 3H, OAc), 1.96 (s, 3H, OAc), 1.93 (s, 3H, OAc), 1.90 (s, 3H, OAc) ppm. <sup>13</sup>C NMR (125 MHz, CDCl<sub>3</sub>)  $\delta$  170.76 (CO of OAc), 170.28 (CO of OAc), 169.54 (CO of OAc), 169.42 (CO of OAc), 169.22 (CO succ x2), 168.06 (CO), 144.96 (C-triaz), 123.04 (CH-triaz), 100.70 (C-1), 72.69 (C-3), 72.06 (C-5), 71.11 (C-2), 68.37 (C-4), 67.98 (OCH<sub>2</sub>), 61.92 (C-6), 50.08 (CH<sub>2</sub>-triaz), 30.95 (CH<sub>2</sub>CO), 25.72 (CH<sub>2</sub>CH<sub>2</sub>-succ), 21.00 (triaz-CH<sub>2</sub>), 20.87 (CH<sub>3</sub> of OAc), 20.71 (3  $\times$  CH<sub>3</sub> of OAc) ppm. IR (ATR) 2955.80, 1733.40, 1430.16, 1366.33, 1208.17, 1033.60, 907.61, 812.61, 733.58, 700.28 cm<sup>-1</sup>. HR-MS (ESI<sup>+</sup>):  $m/z$  calcd for C<sub>25</sub>H<sub>32</sub>N<sub>4</sub>O<sub>14</sub> + H<sup>+</sup> (M + H)<sup>+</sup> 613.1915, found 613.1985. HR-MS (ESI<sup>+</sup>):  $m/z$  calcd for C<sub>25</sub>H<sub>32</sub>N<sub>4</sub>O<sub>14</sub> + Na<sup>+</sup> (M + Na)<sup>+</sup> 635.1915, found 635.1806.

**Synthesis of N-[2-O-(2,3,4,6-Tetra-O-Acetyl- $\beta$ -D-Galactopyranosyl)-ethyl-1,2,3-Triazol-4-yl]-[3-Oxopropyl-[oxy(2,5-Dioxopyrrolidin-1-yl)]] (20)**

Compound **20** was prepared according to the method reported for compound **11** (Yield 0.106 g, 0.173 mmol, 79%).  $R_f = 0.69$  (DCM: MeOH 95:5) [ $\alpha$ ]<sub>D</sub><sup>25</sup> -1.49 (c 0.67, DCM). <sup>1</sup>H NMR (500 MHz, CDCl<sub>3</sub>)  $\delta$  7.48 (s, 1H, triaz-H), 5.33 (d,  $J = 2.7$  Hz, 1H, H-4), 5.12 (dd,  $J = 10.5, 7.9$  Hz, 1H, H-2), 4.93 (dd,  $J = 10.5, 3.4$  Hz, 1H, H-3), 4.53 (dt,  $J = 14.4, 3.9$  Hz, 1H, CH-triaz), 4.49–4.42 (m, 1H, CH<sup>1</sup>-triaz), 4.40 (d,  $J = 7.9$  Hz, 1H, H-1), 4.19 (dt,  $J = 10.4, 4.1$  Hz, 1H, OCH<sup>1</sup>), 4.08 (ddd,  $J = 25.0, 11.3, 6.6$  Hz, 2H, H-6, H-6'), 3.93–3.85 (m, 2H, H-5, OCH), 3.11 (t,  $J = 6.8$  Hz, 2H, triaz-CH<sub>2</sub>), 3.03–2.97 (m, 2H, CH<sub>2</sub>CO), 2.80 (s,  $J = 12.2$  Hz, 4H, CH<sub>2</sub>CH<sub>2</sub>-succ), 2.11 (s, 3H, CH<sub>3</sub> of OAc), 2.00 (s, 3H, CH<sub>3</sub> of OAc), 1.92 (s, 3H, CH<sub>3</sub> of OAc), 1.91 (s, 3H, CH<sub>3</sub> of OAc). <sup>13</sup>C NMR (125 MHz, CDCl<sub>3</sub>)  $\delta$  170.53 (CO of OAc), 170.33 (CO of OAc), 170.21 (CO of OAc), 169.57 (CO of OAc), 169.19 (CO succ x2), 168.10 (CO), 144.95 (C-triaz), 123.03 (CH-triaz), 101.11 (C-1), 70.98 (C-5), 70.77 (C-3), 68.65 (C-2), 67.79 (OCH<sub>2</sub>), 67.03 (C-4), 61.32 (C-6), 50.07 (CH<sub>2</sub>-triaz), 30.89 (CH<sub>2</sub>CO), 25.73 (CH<sub>2</sub>H<sub>2</sub>-succ), 20.99 (triaz-CH<sub>2</sub>), 20.82 (2  $\times$  CH<sub>3</sub> of OAc), 20.81 (CH<sub>3</sub> of OAc), 20.69 (CH<sub>3</sub> of OAc). IR (ATR) 2959.63, 1732.72, 1429.93, 1367.59, 1211.91, 1045.63, 915.63, 812.19, 731.78 cm<sup>-1</sup>. HR-MS (+):  $m/z$  calcd for C<sub>25</sub>H<sub>32</sub>N<sub>4</sub>O<sub>14</sub> + H<sup>+</sup> (M + H)<sup>+</sup> 613.1915, found 613.1983. HR-MS (+):  $m/z$  calcd for C<sub>25</sub>H<sub>32</sub>N<sub>4</sub>O<sub>14</sub> + H<sup>+</sup> (M + H)<sup>+</sup> 635.1915, found 635.1804.

**Synthesis of Complex 1**

Compound **11** (0.140 g, 0.246 mmol) was added to a suspension of oxoplatin (0.086 g, 0.270 mmol) in DMSO (5 ml) and stirred at 60°C for 16 h. Residual oxoplatin was filtered through cotton wool and the solvent was removed by lyophilization. The oily residue was dissolved in acetone and the product was precipitated with diethyl ether and collected by centrifugation. The yellow-white solid was washed with diethyl ether and dried *in vacuo* (0.083 g, 0.105 mmol, 43%) [ $\alpha$ ]<sub>D</sub><sup>25</sup> -10.34 (c 0.58, DCM). <sup>1</sup>H NMR (500 MHz, DMSO)  $\delta$  8.16 (s, 1H, CH-triaz), 6.25 (d,  $J = 8.8$  Hz, 1H, H-1), 5.96 (br. t, 6H, 2  $\times$  NH<sub>3</sub>), 5.60–5.49 (m, 2H, H-2, H-3), 5.12 (t,  $J = 9.6$  Hz, 1H, H-4), 4.34 (ddd,  $J = 10.0, 5.2, 2.2$  Hz, 1H, H-5), 4.13 (dd,  $J = 12.5, 5.4$  Hz, 1H, H-6), 4.08–4.03 (m, 1H, H-6'), 2.80 (t,  $J = 7.6$  Hz, 2H, triaz-CH<sub>2</sub>), 2.46 (t,  $J = 7.7$  Hz, 2H, CH<sub>2</sub>CO), 2.01 (s, 3H, OAc), 1.99

(s, 3H, OAc), 1.95 (s, 3H, OAc), 1.78 (s, 3H, OAc) ppm. <sup>13</sup>C NMR (125 MHz, DMSO)  $\delta$  179.90 (COOPt), 170.34 (CO of OAc), 169.82 (CO of OAc), 169.61 (CO of OAc), 168.80 (CO of OAc), 147.32 (C-triaz), 121.44 (CH-triaz), 83.89 (C-1), 73.40 (C-5), 72.29 (C-3), 70.30 (C-2), 67.74 (H-4), 61.91 (C-6), 35.93 (CH<sub>2</sub>CO), 21.95 (triaz-CH<sub>2</sub>), 20.73 (CH<sub>3</sub> of OAc), 20.54 (CH<sub>3</sub> of OAc), 20.42 (CH<sub>3</sub> of OAc), 20.09 (CH<sub>3</sub> of OAc) ppm. <sup>195</sup>Pt(IV) NMR (108 MHz, DMSO)  $\delta$  1041.75 ppm. IR (ATR) 3212.46, 1746.40, 1627.32, 1367.46, 1215.23, 1035.51, 924.48, 822.96 cm<sup>-1</sup>. HR-MS (-):  $m/z$  calcd for C<sub>19</sub>H<sub>31</sub>Cl<sub>2</sub>N<sub>3</sub>O<sub>12</sub>Pt-H<sup>-</sup> (M-H)<sup>-</sup> 786.4640, found 786.0898. El. Anal. Calcd. for C<sub>19</sub>H<sub>31</sub>Cl<sub>2</sub>N<sub>3</sub>O<sub>12</sub>Pt: % C = 28.29; H = 3.97; N = 8.89; found: % C = 28.88; H = 4.18; N = 8.52.

**Synthesis of Complex 2**

Complex **2** was prepared according to the method reported for complex **1** (Yield 0.065 g, 0.082 mmol, 35.9%) [ $\alpha$ ]<sub>D</sub><sup>25</sup> -2.85 (c 0.7, DCM). <sup>1</sup>H NMR (500 MHz, DMSO)  $\delta$  8.12 (s, 1H, triaz-CH), 6.18 (d,  $J = 9.2$  Hz, 1H, H-1), 5.95 (br. t., 6H, 2  $\times$  NH<sub>3</sub>), 5.58 (t,  $J = 10.1$  Hz, 1H, H-2), 5.45 (dd,  $J = 10.1, 3.5$  Hz, 1H, H-3), 5.40 (dd,  $J = 3.4, 1.0$  Hz, 1H, H-4), 4.59–4.56 (t,  $J = 6.75$  Hz, 1H, H-5), 4.13 (dd,  $J = 11.6, 5.1$  Hz, 1H, H-6), 4.01 (dd,  $J = 11.5, 7.3$  Hz, 1H, H-6'), 2.82 (t,  $J = 7.25$  Hz, 2H, triaz-CH<sub>2</sub>), 2.47–2.46 (m, 2H, CH<sub>2</sub>CO), 2.19 (s, 3H, CH<sub>3</sub> of OAc), 1.99 (s, 3H, CH<sub>3</sub> of OAc), 1.94 (s, 3H, CH<sub>3</sub> of OAc), 1.82 (s, 3H, CH<sub>3</sub> of OAc) ppm. <sup>13</sup>C NMR (125 MHz, DMSO)  $\delta$  179.66 (COOPt), 170.03 (CO of OAc), 169.94 (CO of OAc), 169.48 (CO of OAc), 168.56 (CO of OAc), 147.12 (C-triaz), 121.44 (CH-triaz), 84.19 (C-1), 72.80 (C-5), 70.43 (C-3), 67.78 (C-2), 67.29 (C-4), 61.58 (C-6), 35.92 (CH<sub>2</sub>CO), 21.79 (triaz-CH<sub>2</sub>), 20.51 (CH<sub>3</sub> of OAc), 20.47 (CH<sub>3</sub> of OAc), 20.34 (CH<sub>3</sub> of OAc), 20.02 (CH<sub>3</sub> of OAc) ppm. <sup>195</sup>Pt(IV) NMR (108 MHz, DMSO)  $\delta$  1044.64 ppm. IR (ATR) 3207.92, 1746.25, 1625.63, 1368.09, 1214.56, 1050.93, 922.78 cm<sup>-1</sup>. HR-MS (+):  $m/z$  calcd for C<sub>19</sub>H<sub>31</sub>Cl<sub>2</sub>N<sub>3</sub>O<sub>12</sub>Pt + H<sup>+</sup> (M + H)<sup>+</sup> 786.4640, found 786.1041. El. Anal. Calcd. for C<sub>19</sub>H<sub>31</sub>Cl<sub>2</sub>N<sub>3</sub>O<sub>12</sub>Pt: % C = 28.98; H = 3.97; N = 8.89; found: % C = 28.48; H = 4.18; N = 8.52. 786.0994.

**Synthesis of Complex 3**

Complex **3** was prepared according to the method reported for complex **1** (0.05 g, 0.060 mmol, 29%) [ $\alpha$ ]<sub>D</sub><sup>25</sup> -1.66 (c 0.6, DCM). <sup>1</sup>H NMR (500 MHz, CDCl<sub>3</sub>)  $\delta$  7.76 (s, 1H, triaz-CH), 5.87 (br. t, 6H, 2  $\times$  NH<sub>3</sub>), 5.23 (t,  $J = 9.6$  Hz, 1H, H-3), 4.89 (t,  $J = 9.7$  Hz, 1H, H-4), 4.81 (d,  $J = 8.0$  Hz, 1H, H-1), 4.75–4.69 (m, 1H, H-2), 4.53–4.40 (m, 2H, CH<sub>2</sub>-triaz), 4.18 (dd,  $J = 12.3, 5.0$  Hz, 1H, H-6), 4.08 (dt,  $J = 8.9, 4.1$  Hz, 1H, OCH), 4.02 (dd,  $J = 12.2, 2.1$  Hz, 1H, H-6'), 3.98 (ddd,  $J = 9.9, 4.9, 2.4$  Hz, 1H, H-5), 3.89 (ddd,  $J = 11.4, 7.8, 4.0$  Hz, 1H, OCH<sup>1</sup>), 2.81–2.77 (m, 2H, triaz-CH<sub>2</sub>), 2.48–2.43 (m, 2H, CH<sub>2</sub>CO), 2.02 (s, 3H, CH<sub>3</sub> of OAc), 1.97 (s, 3H, CH<sub>3</sub> of OAc), 1.92 (s, 3H, CH<sub>3</sub> of OAc), 1.88 (s, 3H, CH<sub>3</sub> of OAc) ppm. <sup>13</sup>C NMR (125 MHz, CDCl<sub>3</sub>)  $\delta$  179.88 (COOPt), 170.08 (CO of OAc), 169.53 (CO of OAc), 169.28 (CO of OAc), 168.95 (CO of OAc), 146.14 (C-triaz), 122.47 (CH-triaz), 99.20 (C-1), 71.90 (C-3), 70.64 (C-2), 70.59 (C-5), 68.08 (C-4), 67.45 (OCH<sub>2</sub>), 61.64 (C-6), 49.06 (CH<sub>2</sub>-triaz), 36.16 (CH<sub>2</sub>CO), 21.97 (triaz-CH<sub>2</sub>), 20.54 (CH<sub>3</sub> of OAc), 20.38 (CH<sub>3</sub> of OAc), 20.29 (CH<sub>3</sub> of OAc), 20.27 (CH<sub>3</sub> of OAc) ppm. <sup>195</sup>Pt(IV) NMR (108 MHz, DMSO)  $\delta$  1047.09 ppm. IR (ATR) 3214.82, 1745.13, 1626.73, 1430.32,

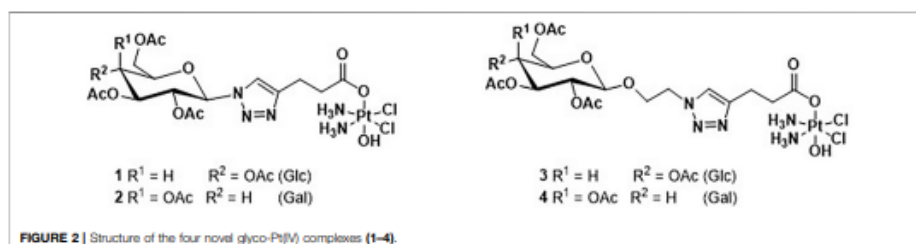


FIGURE 2 | Structure of the four novel glyco-Pt(IV) complexes (1–4).

1365.92, 1217.35, 1034.85, 908.82, 699.33  $\text{cm}^{-1}$ . HR-MS (+):  $m/z$  calcd for  $\text{C}_{21}\text{H}_{35}\text{Cl}_2\text{N}_5\text{O}_{13}\text{Pt} + \text{H}^+$  (M + H)<sup>+</sup> 832.5170, found 832.1316. HR-MS (+):  $m/z$  calcd for  $\text{C}_{21}\text{H}_{35}\text{Cl}_2\text{N}_5\text{O}_{13}\text{Pt} + \text{Na}^+$  (M + H)<sup>+</sup> 854.5170, found 854.1134. El. Anal. Calcd. for  $\text{C}_{21}\text{H}_{35}\text{Cl}_2\text{N}_5\text{O}_{13}\text{Pt}$ : % C = 30.33; H = 4.24; N = 8.42; found: % C = 30.79; H = 4.61; N = 8.90.

#### Synthesis of Complex 4

Complex 4 was prepared according to the method reported for complex 1 (0.07 g, 0.084 mmol, 38%)  $[\alpha]_D^{21.6} +43.1$  (c 0.58, DCM). <sup>1</sup>H NMR (500 MHz, DMSO)  $\delta$  7.75 (s, 1H, triaz-CH), 5.82 (br t, 6H, 2  $\times$  NH<sub>2</sub>), 5.24 (dd,  $J$  = 3.5, 0.8 Hz, 1H, H-4), 5.12 (dd,  $J$  = 10.4, 3.6 Hz, 1H, H-3), 4.88 (dd,  $J$  = 10.4, 8.0 Hz, 1H, H-2), 4.71 (d,  $J$  = 8.0 Hz, 1H, H-1), 4.52–4.40 (m, 2H, CH<sub>2</sub>-triaz), 4.19 (dd,  $J$  = 7.2, 6.3 Hz, 1H, H-5), 4.12–4.00 (m, 3H, H-6, H-6', OCH), 3.93–3.86 (m, 1H, OCH), 2.82–2.78 (t,  $J$  = 7.25 Hz, 2H, triaz-CH<sub>2</sub>), 2.47 (dd,  $J$  = 8.6, 6.9 Hz, 2H, CH<sub>2</sub>CO), 2.11 (s, 3H, CH<sub>3</sub> of OAc), 2.01 (s, 3H, CH<sub>3</sub> of OAc), 1.90 (s, 3H, CH<sub>3</sub> of OAc), 1.89 (s, 3H, CH<sub>3</sub> of OAc) ppm. <sup>13</sup>C NMR (125 MHz, DMSO)  $\delta$  179.86 (COO-Pt), 169.93 (CO of OAc), 169.91 (CO of OAc), 169.48 (CO of OAc), 169.05 (CO of OAc), 146.13 (C-triaz), 122.43 (CH-triaz), 99.67 (C-1), 70.07 (C-5), 69.94 (C-3), 68.34 (C-2), 67.30 (C-4), 67.26 (OCH<sub>2</sub>), 61.23 (C-6), 49.09 (CH<sub>2</sub>-triaz), 36.13 (CH<sub>2</sub>CO), 21.97 (triaz-CH<sub>2</sub>), 20.52 (CH<sub>3</sub> of OAc), 20.40 (CH<sub>3</sub> of OAc), 20.32 (2xCH<sub>3</sub> of OAc) ppm. <sup>195</sup>Pt{<sup>1</sup>H} NMR (108 MHz, DMSO)  $\delta$  1047.15 ppm. IR (ATR) 3214.92, 1740.41, 1631.39, 1429.52, 1367.30, 1217.81, 1173.03, 1045.52, 952.53  $\text{cm}^{-1}$ . HR-MS (+):  $m/z$  calcd for  $\text{C}_{21}\text{H}_{35}\text{Cl}_2\text{N}_5\text{O}_{13}\text{Pt} + \text{H}^+$  (M + H)<sup>+</sup> 832.5170, found 854.1139. HR-MS (+):  $m/z$  calcd for  $\text{C}_{21}\text{H}_{35}\text{Cl}_2\text{N}_5\text{O}_{13}\text{Pt} + \text{Na}^+$  (M + Na)<sup>+</sup> 854.5170, found 854.1315. El. Anal. Calcd. for  $\text{C}_{21}\text{H}_{35}\text{Cl}_2\text{N}_5\text{O}_{13}\text{Pt}$ : % C = 30.33; H = 4.24; N = 8.42; found: % C = 29.98; H = 4.69; N = 8.01.

#### In vitro Biological Evaluation

*In vitro* tests of cisplatin-based drugs were performed to evaluate the cellular behaviors in response to the different compounds (1–4) compared to cisplatin. All the drugs were reconstituted in Dimethyl Sulfoxide (DMSO) at 1 mg/ml final concentration, and then dissolved in the culture media at different concentrations: 15, 30, and 60  $\mu\text{M}$ . Three different osteosarcoma cells lines (MG63, SAOS-2, U-2OS) and an *in vitro* model of osteosarcoma stem cells (enriched-CSCs) were maintained in culture with and without the drugs for 72 h.

#### Cell Culture

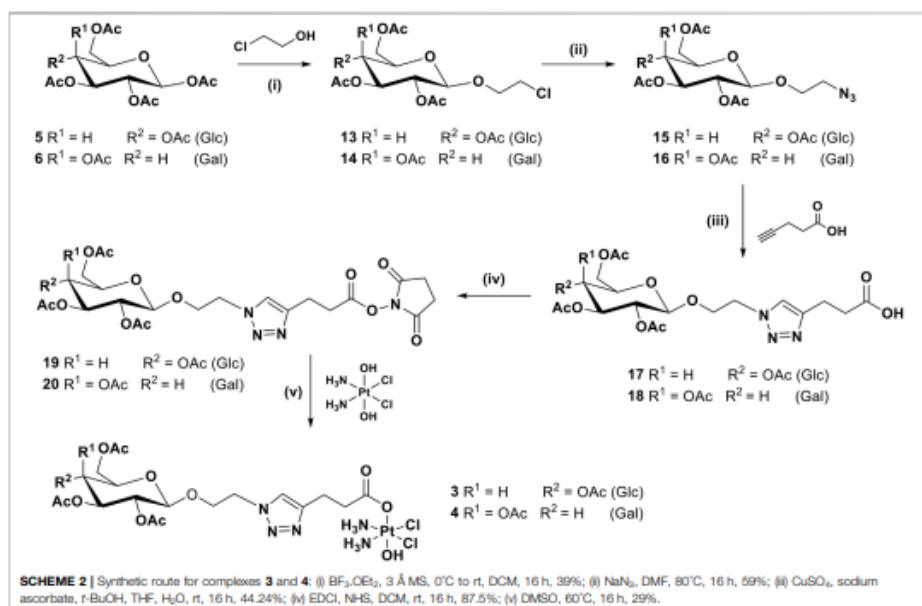
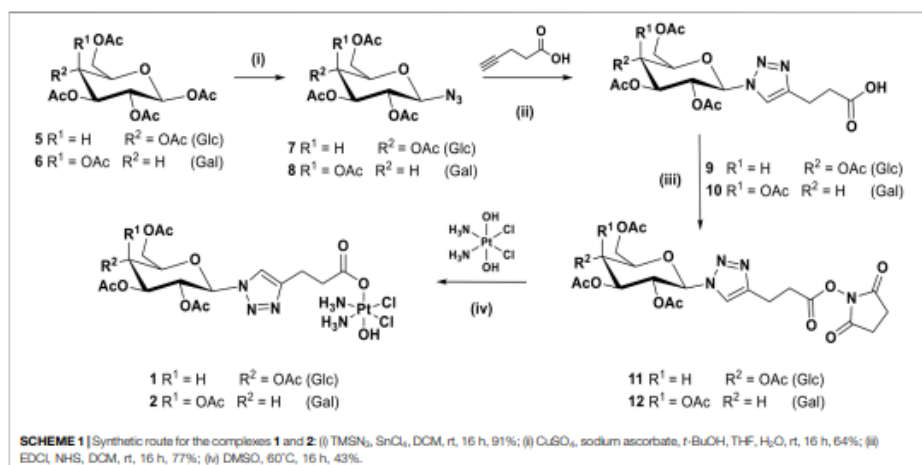
Human Osteosarcoma cell lines MG63 (ATCC<sup>®</sup> CRL1427<sup>™</sup>), U-2OS (ATCC<sup>®</sup> HTB-96<sup>™</sup>), and SAOS-2 (ATCC<sup>®</sup> HTB-85<sup>™</sup>), purchased from American Type Culture Collection (ATCC), were used. MG63 cell line was cultured in DMEM F12-GlutaMAX<sup>™</sup> Modified Medium (Gibco) supplemented with 10% Foetal Bovine Serum (FBS) (Gibco) and 1% of penicillin/streptomycin mixture (pen/strep) (100 U/ml–100  $\mu\text{g}/\text{ml}$ , Gibco). SAOS-2 and U-2OS cell lines were cultured in McCoy's 5A Modified Medium (Gibco) supplemented with 15 and 10% FBS, respectively, and 1% pen/strep. Cells were kept in an incubator at 37°C under controlled humidity and 5% CO<sub>2</sub> atmosphere conditions. Cells were detached from culture flasks by trypsinization and centrifuged. The cell number and viability were determined by Trypan Blue Dye Exclusion test and all cell handling procedures were performed under a laminar flow hood in sterility conditions. For the experiment, all cell lines were seeded  $5.0 \times 10^3$  cells/well in 96 well-plates and  $5.0 \times 10^4$  cells/well in 6 well-plates.

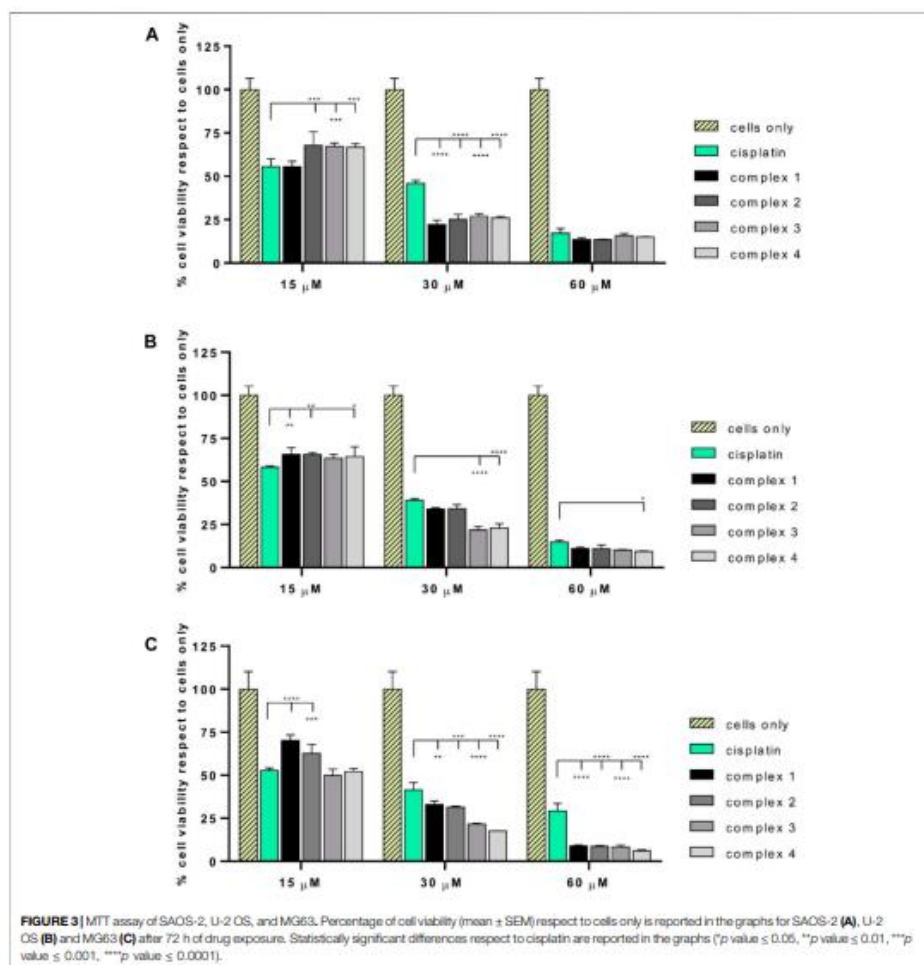
#### Enriched-CSCs Culture

Enriched-cancer stem cells (CSCs) were obtained under specific culture conditions as reported in the literature (Brown et al., 2017; Bassi et al., 2020) as a sarcosphere-forming method starting from a human MG63 osteosarcoma cell line. The MG63 cell line was seeded in Ultra-Low Attachment T25 flasks (Corning Inc., NY) with a density of  $2.0 \times 10^3$  cells/cm<sup>2</sup> in serum-free DMEM F12-GlutaMAX<sup>™</sup> Modified Medium supplemented with a specific cocktail of factors: 10  $\mu\text{L}/\text{ml}$  N2 (Gibco), 20  $\mu\text{L}/\text{ml}$  B27 (Gibco), 0.1  $\mu\text{L}/\text{ml}$  human Basic-Fibroblast Growth Factor (bFGF) (Invitrogen), and 0.01  $\mu\text{L}/\text{ml}$  human Epidermal Growth Factor (EGF) (PeproTech). The cocktail was added to each flask every 2/3 days for a total of 10 days of culture. After their formation, the CSCs were collected and centrifugated for 10 min at 130  $\times$  g; the pellet was resuspended in the same medium conditions, well mixed, and directly seeded in Ultra-Low Attachment 96 well-plate and Ultra-Low Attachment 6 well-plate with 200  $\mu\text{L}/\text{well}$  and 1.5 ml/well volume of cell culture medium, respectively. The factors' cocktail was added every 2/3 days during the experiment following the above-reported manufacturer's instructions.

#### MTT Cell Viability Assay

A quantitative analysis of cell viability and proliferation was carried out by MTT assay on cell cultures, by using the cells





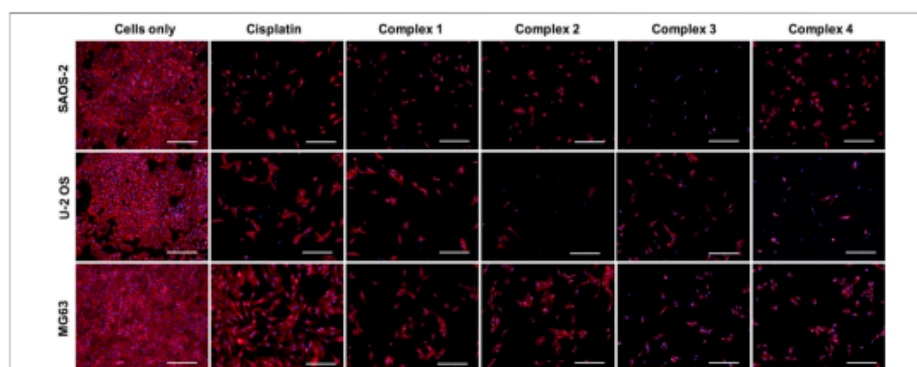
only as a negative control. At 72 h, the MTT assay was performed according to the manufacturer's instructions. Briefly, MTT reagent [3-(4,5-dimethylthiazol-2-yl)-2,5-diphenyltetrazolium bromide] (5 mg/ml) was dissolved in Phosphate Saline Buffer 1X (PBS 1X). At 72 h, the cells were incubated with 10% media volume MTT solution for 2 h at 37°C, 5% CO<sub>2</sub>, and controlled humidity conditions. The cell culture media was removed and substituted with DMSO (Sigma) dissolving formazan crystals derived from MTT conversion by

metabolically active cells. For CSCs, the total media was centrifugated and the deposited crystals were directly resuspended in DMSO. After 15-min of incubation under slight stirring conditions, the absorbance of formazan was read at 570 nm by using a Multiskan FC Microplate Photometer (Thermo Scientific). The values of absorbance are directly proportional to the number of metabolic active cells in each well. The experiment was carried out with three biological replicates for each condition.



**TABLE 1** | IC<sub>50</sub> (μM) values of Cisplatin and complexes 1–4 on OS cell lines.

| OS cancer cell | Cisplatin             |              | 1                     |              | 2                     |              | 3                     |              | 4                     |              |
|----------------|-----------------------|--------------|-----------------------|--------------|-----------------------|--------------|-----------------------|--------------|-----------------------|--------------|
|                | IC <sub>50</sub> (μM) | 95% CI       | IC <sub>50</sub> (μM) | 95% CI       | IC <sub>50</sub> (μM) | 95% CI       | IC <sub>50</sub> (μM) | 95% CI       | IC <sub>50</sub> (μM) | 95% CI       |
| SAOS-2         | 20.42                 | -4.13; +5.17 | 16.48                 | -1.84; +2.08 | 20.18                 | -2.38; +2.7  | 20.39                 | -2.12; +2.37 | 20.1                  | -1.99; +2.21 |
| U-2 OS         | 19.85                 | -1.64; +1.8  | 16.48                 | -0.98; +1.02 | 21.09                 | -0.86; +0.89 | 18.57                 | -1.3; +1.4   | 18.91                 | -1.5; +1.63  |
| MGR3           | 17.8                  | -3.34; +4.13 | 21.9                  | -0.86; +0.89 | 19.68                 | -1.27; +1.36 | 14.88                 | -0.91; +0.98 | 15.5                  | -0.54; +0.55 |

**FIGURE 4** | Cell morphology evaluation on SAOS-2, U-2 OS, and MGR3. Actin and DAPI staining of osteosarcoma cell lines treated with and without drugs (30 μM) for 72 h. F-actin filaments in red; cell nuclei in blue. Scale bars 200 μm.

#### Cell Morphology Evaluation

Cells treated with and without the drugs (30 μM) were fixed in 4% buffered Paraformaldehyde (PFA) following the manufacturer's instructions. The fixed cells were permeabilized in PBS 1X with 0.1% (v/v) Triton X-100 (Sigma) for 5 min at room temperature and F-actin filaments were highlighted with a red fluorescent solution of Rhodamine Phalloidin (Actin Red 555 Ready Probes™ Reagent, Invitrogen), following the company indications, for 30 min at room temperature. DAPI (600 nM) counterstaining was performed for cell nuclei identification, following the manufacturer's instructions. The images were acquired by using an Inverted Ti-E Fluorescent Microscope.

#### Inductively Coupled Plasma-Optical Emission Spectrometry

The ICP-OES (Agilent Technologies 5100 ICP-OES, Santa Clara, United States) was performed on Enriched-CSCs culture to quantify cellular internalization of drugs, following the manufacturer's instructions. At 72 h, cells were mechanically by 50–100 times p200 pipetting to disaggregate spheroid, counted by Trypan Blue Dye Exclusion Test, and collected in 400 μL PBS 1X. ICP-OES was used for the quantitative determination of platinum ions content per cell derived by cisplatin-based drugs, by using cells only as a negative control. Briefly, the samples were dissolved in 500 μL nitric acid (65 wt%) and 2.1 ml of milliQ water followed by 30 min of sonication in an

ultrasonic bath. The analytical wavelength of Pt was 265.945 nm. One experiment was carried out and for each condition, the amount of drug per cell was quantified in biological triplicate. The data are represented in the graph.

#### Statistical Analysis

Statistical analysis was performed by using GraphPad Prism Software (8.0.1 version). The results of the MTT assays are reported in the graphs as mean percentage of cell viability with respect to cells only ± standard deviation, and they were analyzed by Two-way analysis of variance (Two-way ANOVA) and Tukey's multiple comparisons test. IC<sub>50</sub> values were calculated as log(inhibitor) versus mean percentage of dead cells with respect to cells only, and the obtained values are reported in the graphs ± 95% confidence interval (CI) for each cell line. The results of MTT assays on CSCs are reported in the graph as mean percentage of cell viability with respect to cells only ± the standard error of the mean, and they were analyzed by Unpaired *t*-test setting the *p* value ≤ 0.05 to determine statistically significant differences. The ICP-OES data were elaborated as picograms of iron ions per cell and reported in the graph ± standard error of the mean. The results were analyzed by One-way analysis of variance (One-way ANOVA) and Dunnett's multiple comparisons test (\**p* value ≤ 0.05, \*\**p* value ≤ 0.01, \*\*\**p* value ≤ 0.001, \*\*\*\**p* value ≤ 0.0001).

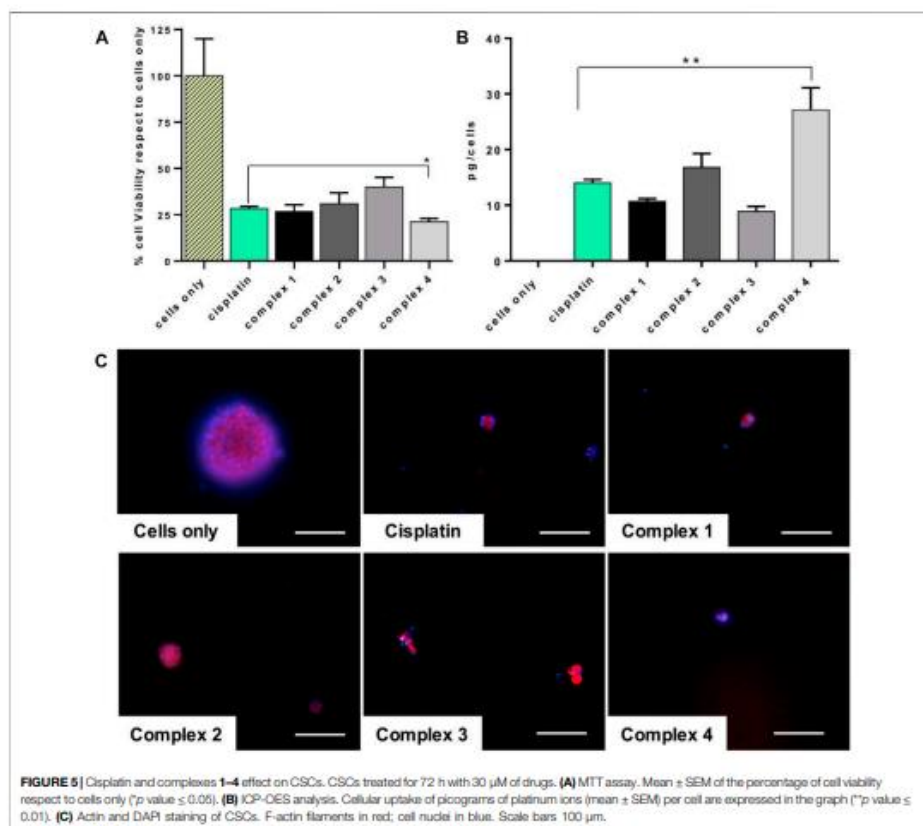


**FIGURE 5** | Cisplatin and complexes 1–4 effect on CSCs. CSCs treated for 72 h with 30 μM of drugs. **(A)** MTT assay. Mean ± SEM of the percentage of cell viability respect to cells only (\**p* value ≤ 0.05). **(B)** ICP-OES analysis. Cellular uptake of picograms of platinum ions (mean ± SEM) per cell are expressed in the graph (\*\**p* value ≤ 0.01). **(C)** Actin and DAPI staining of CSCs. F-actin filaments in red; cell nuclei in blue. Scale bars 100 μm.

## RESULTS AND DISCUSSION

The four novel glyco-Pt(IV) complexes are shown in **Figure 2**. Complexes **1** and **2** are β-anomeric triazolyl *N*-glycosides which have the triazole group directly attached to the anomeric carbon (**1**, glucose, and **2** galactose) while complexes **3** and **4** have an additional *O*-ethylene linker (**3**, glucose, and **4** galactose).

The synthetic route for complexes **1** and **2** can be seen in **Scheme 1**. Briefly, the per-acetylated glucose **5** and galactose **6** were transformed to the corresponding β-azides at the anomeric carbon, **7** and **8** respectively (Tropper et al., 1992), by reaction with azidotrimethylsilane and tin tetrachloride. Compounds **7** and **8** were then reacted with pentynoic acid, using CUAAC conditions at room temperature, to produce the carboxylic acids **9**

and **10** (Mangunuru et al., 2015). These latter carboxylic acids are activated, forming NHS esters **11** and **12**, respectively, that were reacted with oxoplatin to produce the final desired compounds **1** and **2**.

For complexes **3** and **4**, with an *O*-ethylene spacer between the anomeric carbon and the triazole ring, the synthetic route requires one more step, as shown in **Scheme 2**, whereby the per-acetylated sugars **5** and **6** were reacted with chloroethanol in the presence of boron trifluoride diethyl etherate to produce **13** and **14** (Reddy et al., 2017). They are then transformed to the corresponding azides **15** and **16** before being reacted with pentynoic acid under similar CUAAC conditions used previously, to give acids **17** and **18**. Activation to form NHS esters **19** and **20** followed by reaction with oxoplatin produced the final desired complexes **3** and **4**.

All the intermediate compounds (5–20) have been obtained with moderate to good yields and have been characterized with multinuclear NMR, IR, and LC(HR)-MS. The final complexes containing platinum (1–4) have been characterized with multinuclear NMR ( $^1\text{H}$ ,  $^{13}\text{C}$ , and  $^{193}\text{Pt}$ ), HR-MS, and Elemental Analyses to assess the purity. All the data and spectra can be found in the Experimental Section and the **Supplementary Material**.

The physiological stability has been evaluated with HPLC in DMSO/HEPES at pH 6.8 buffer and the complexes are stable (little decomposition of 8% observed after 1 week at r.t., see **Supplementary Material** for complex 4).

The biological effect of the complexes 1–4, in comparison with the effect of cisplatin has been evaluated on different osteosarcoma cell lines. All the drugs showed a dose-dependent anticancer effect (**Figure 3**) in all the tested cancer cell lines. A statistically significant decrease of cell viability induced by all the drug concentrations ( $p$  value  $\leq 0.0001$ ) has been reported with respect to the cells grown without drugs (cells only). Most excitingly, starting from 30  $\mu\text{M}$ , the complexes showed a significantly higher cytotoxicity with respect to cisplatin. Looking in detail at the single-cell lines, it was possible to observe phenotypic-dependent behaviors in response to the different complexes. In detail, the viability of SAOS-2 (**Figure 3A**) was significantly decreased in the presence of the four complexes with respect to cisplatin when supplied at 30  $\mu\text{M}$  ( $p$  value  $\leq 0.0001$ ); conversely the viability of U-2 OS (**Figure 3B**) was significantly reduced only in the presence of 3 and 4 compared to cisplatin at 30  $\mu\text{M}$  ( $p$  value  $\leq 0.0001$ ), and only in the presence of complex 4 at 60  $\mu\text{M}$  ( $p$  value  $\leq 0.05$ ). All the complexes seem to be more effective with respect to cisplatin in the MG63 cell line (**Figure 3C**), starting from 30  $\mu\text{M}$  and at higher concentrations, the anticancer effect greatly increases ( $p$  value  $\leq 0.0001$ ). The  $\text{IC}_{50}$  values ( $\mu\text{M}$ ) reported in **Table 1**, confirmed the phenotypic-dependent effect of the different complexes. In fact, in SAOS-2 the most effective drug is complex 1, showing a  $\text{IC}_{50}$  of 16.48 (–1.84; +2.08), while in U-2 OS and MG63 complex 3 has the best  $\text{IC}_{50}$  values of 18.57 (–1.3; +1.4) and 14.88 (–0.91; +0.98), respectively (see **Supplementary Material**).

The qualitative analysis of cell morphology confirmed the cytotoxicity results (**Figure 4**). As shown in the panel, the number of all the cells treated with cisplatin and complexes 1–4 drastically decreased compared to cells only which, on the contrary, showed a higher cell density. The different behaviors observed among the osteosarcoma cell lines, induced by the different drugs, are ascribable to the well-known different degrees of genetic complexity of each cell line, inducing cell-specific biological behaviors (e.g., tumorigenicity, colony-forming ability, invasive/migratory potential, metabolism, and proliferation capacity) (Lauvrak et al., 2013; Liu et al., 2016).

Furthermore, even cancer stem cells (CSCs), unipotent cell population presents within the tumor microenvironment, have the ability to alter their metabolism responding to specific bioenergetic and biosynthetic requirements (Deshmukh et al., 2016; Brown et al., 2017). CSCs are key tumor-initiating cells that play an integral role in the metastatic process, and tumor recurrence even after chemotherapy. It is easily understood why CSCs, in the last years, have gained intense interest as a specific target for new therapeutic strategies.

Based on this evidence, a preliminary *in vitro* study of the tested drug effect on the enriched osteosarcoma stem cell viability and on the drug uptake has been performed. Very promising outcomes indicated that the complex 4 has a statistically significant higher effect on CSCs,  $p$  value  $\leq 0.05$  (**Figure 5A**), strictly related to the observed increased quantity of platinum inside the cells (27.1 pg/cells,  $p$  value  $\leq 0.01$ ), compared to cisplatin (**Figure 5B**). The morphological evaluation showed a reduction of the dimension of the spheres, typical morphological markers of CSCs, confirming the cytotoxicity results (**Figure 5C**) (Bouchet and Akhmanova, 2017).

## CONCLUSION

Four novel glyco-modified Pt(IV) pro-drugs based on cisplatin scaffold were synthesized, linking the sugar moiety and the metal center via CUAAC click chemistry. The complexes were tested on a panel of different OS (Osteosarcoma) cell lines and showed very promising activity compared to the reference cisplatin, demonstrating that the presence of a monosaccharide strongly increased the anticancer effect. The complexes resulted also particularly active toward CSCs (Cancer Stem Cells) with the most promising activity shown by complex 4 with a galactose substituent. The interplay of galactose in the metabolism of cancer stem cells is attracting high attention because of potential diagnostic and therapeutic possibilities (Valle et al., 2020; Zheng et al., 2020). At the moment, it is not possible to affirm with certainty if the sugar in the complexes described herein is playing the role of active vector because more specific biological studies (beyond the scope of this work) should be conducted (i.e., inhibition of the GLUTs receptors), but it is clear that the presence of the sugar is increasing the anticancer activity and the drug internalization, as demonstrated with the uptake experiment in CSCs (this could be due to the higher lipophilicity). All the complexes showed very promising activity but the discrimination between glucose and galactose and between the two linkers is not evident yet and this could confirm the hypothesis that these species are internalized by passive diffusion. Ideally, the sugars should be deprotected in order to be better recognized by the receptors, and our group is working in this direction, even if the synthesis is not trivial. We are planning to speculate on the role of the sugar scaffold by developing analogous complexes where the carbohydrate is conjugated via the C2 carbon (not the anomeric carbon) that was demonstrated to be the best in terms of cellular recognition (Patra et al., 2016). Finally, we are conjugating these species, through specific linkers, to magnetic nanoparticles that will act as a delivery platform to increase the drug selectivity and cellular internalization.

## DATA AVAILABILITY STATEMENT

The original contributions presented in the study are included in the article/**Supplementary Material**, further inquiries can be directed to the corresponding authors.



## AUTHOR CONTRIBUTIONS

All authors listed have made a substantial, direct, and intellectual contribution to the work and approved it for publication.

## FUNDING

EM, SP, MM, and DM strongly acknowledge NANO4TARMED consortium H2020-WIDESPREAD-2020-5 project number 952063.

## REFERENCES

- Almotairy, A. R. Z., Montagner, D., Morrison, L., Devereux, M., Howe, O., and Erxleben, A. (2020). Pt(IV) Pro-drugs with an Axial HDAC Inhibitor Demonstrate Multimodal Mechanisms Involving DNA Damage and Apoptosis Independent of Cisplatin Resistance in A2780/A2780cis Cells. *J. Inorg. Biochem.* 210, 111125. doi:10.1016/j.jinorgbio.2020.111125
- Bassi, G., Panserri, S., Dozio, S. M., Sandri, M., Campodoni, E., Dapporto, M., et al. (2020). Scaffold-based 3D Cellular Models Mimicking the Heterogeneity of Osteosarcoma Stem Cell Niche. *Sci. Rep.* 10, 22294. doi:10.1038/s41598-020-79448-y
- Bonandi, E., Christodoulou, M. S., Fumagalli, G., Perdicchia, D., Rastelli, G., and Passarella, D. (2017). The 1,2,3-triazole Ring as a Bioisostere in Medicinal Chemistry. *Drug Discov. Today* 22, 1572–1581. doi:10.1016/j.drudis.2017.05.014
- Bouchet, B. P., and Akhmanova, A. (2017). Microtubules in 3D Cell Motility. *J. Cell Sci.* 130, 39–50. doi:10.1242/jcs.189431
- Brandon, R. J., and Dabrowski, J. C. (1984). Synthesis, Characterization, and Properties, of a Group of Platinum(IV) Complexes. *J. Med. Chem.* 27, 861–865. doi:10.1021/jm00373a009
- Brito, A., Pereira, P. M. R., Soares da Costa, D., Reis, R. L., Ulijn, R. V., Lewis, J. S., et al. (2020). Inhibiting Cancer Metabolism by Aromatic Carbohydrate Amphiphiles that Act as Antagonists of the Glucose Transporter GLUT1. *Chem. Sci.* 11, 3737–3744. doi:10.1039/D0SC00954G
- Brown, H. K., Tellez-Gabriel, M., and Heymann, D. (2017). Cancer Stem Cells in Osteosarcoma. *Cancer Lett.* 386, 189–195. doi:10.1016/j.canlet.2016.11.019
- Cifuentes, M., Garcia, M. A., Arrabal, P. M., Martinez, F., Yañez, M. J., Jara, N., et al. (2011). Insulin Regulates GLUT1-Mediated Glucose Transport in MG-63 Human Osteosarcoma Cells. *J. Cell. Physiol.* 226, 1425–1432. doi:10.1002/jcp.22668
- Curra, A. J., and Carruthers, A. (2012). "Role of Monosaccharide Transport Proteins in Carbohydrate Assimilation, Distribution, Metabolism, and Homeostasis," in *Comprehensive Physiology* (Wiley), 863–914. doi:10.1002/cphy.c110024
- Deshmukh, A., Deshpande, K., Arfuso, F., Newsholme, P., and Dharmarajan, A. (2016). Cancer Stem Cell Metabolism: a Potential Target for Cancer Therapy. *Mol. Cancer* 15, 69. doi:10.1186/s12943-016-0555-x
- Dhara, S. (1970). A Rapid Method for the Synthesis of cis-[Pt(NH<sub>3</sub>)<sub>2</sub>Cl<sub>2</sub>]. *Indian J. Chem.* 8, 193–194.
- Farrer, N. J., and Griffith, D. M. (2020). Exploiting Azide-Alkyne Click Chemistry in the Synthesis, Tracking and Targeting of Platinum Anticancer Complexes. *Curr. Opin. Chem. Biol.* 55, 59–68. doi:10.1016/j.cpbpa.2019.12.001
- Gabano, E., Rangone, B., Perin, E., Caron, G., Ermondi, G., Vallaro, M., et al. (2021). Pt(IV) Complexes Based on Cyclohexanediamines and the Histone Deacetylase Inhibitor 2-(2-propynyl)octanoic Acid: Synthesis, Characterization, Cell Penetration Properties and Antitumor Activity. *Dalton Trans.* 50, 4663–4672. doi:10.1039/D0DT04135A
- Gibson, D. (2016). Platinum(IV) Anticancer Prodrugs - Hypotheses and Facts. *Dalton Trans.* 45, 12983–12991. doi:10.1039/C6DT01414C
- Han, X., Wang, W., He, J., Jiang, L., and Li, X. (2019). Osteopontin as a Biomarker for Osteosarcoma Therapy and Prognosis (Review). *Oncol. Lett.* 17, 2592–2598. doi:10.3892/ol.2019.9905
- Harper, B. W., Krause-Heuer, A. M., Grant, M. P., Manohar, M., Garbutcheon-Singh, K. B., and Aldrich-Wright, J. R. (2010). Advances in Platinum

## ACKNOWLEDGMENTS

EM is grateful to Maynooth University for sponsoring his PhD with a Graduate Teaching Fellowship.

## SUPPLEMENTARY MATERIAL

The Supplementary Material for this article can be found online at: <https://www.frontiersin.org/articles/10.3389/fchem.2021.795997/full#supplementary-material>

- Chemotherapeutics. *Chem. - A Eur. J.* 16, 7064–7077. doi:10.1002/chem.201000148
- Heymann, M.-F., Lénot, F., and Heymann, D. (2019). The Contribution of Immune Infiltrates and the Local Microenvironment in the Pathogenesis of Osteosarcoma. *Cell Immunol.* 343, 103711. doi:10.1016/j.cellimm.2017.10.011
- Jang, M., Kim, S. S., and Lee, J. (2013). Cancer Cell Metabolism: Implications for Therapeutic Targets. *Exp. Mol. Med.* 45, e45. doi:10.1038/emmm.2013.85
- Johnstone, T. C., Wilson, J. J., and Lippard, S. J. (2013). Monofunctional and Higher-Valent Platinum Anticancer Agents. *Inorg. Chem.* 52, 12234–12249. doi:10.1021/ic400538c
- Jung, Y., and Lippard, S. J. (2007). Direct Cellular Responses to Platinum-Induced DNA Damage. *Chem. Rev.* 107, 1387–1407. doi:10.1021/cr068207j
- Kenny, R. G., and Marmion, C. J. (2019). Toward Multi-Targeted Platinum and Ruthenium Drugs-A New Paradigm in Cancer Drug Treatment Regimens? *Chem. Rev.* 119, 1058–1137. doi:10.1021/acs.chemrev.8b00271
- Koppenol, W. H., Bounds, P. L., and Dang, C. V. (2011). Otto Warburg's Contributions to Current Concepts of Cancer Metabolism. *Nat. Rev. Cancer* 11, 325–337. doi:10.1038/nrc3038
- Lauria, T., Slator, C., McKee, V., Müller, M., Stazzoni, S., Crisp, A. L., et al. (2020). A Click Chemistry Approach to Developing Molecularly Targeted DNA Scissors. *Chem. Eur. J.* 26, 16782–16792. doi:10.1002/chem.202002860
- Lauvrik, S. U., Muanthe, E., Kresse, S. H., Stratford, E. W., Namlos, H. M., Meza-Zepeda, I. A., et al. (2013). Functional Characterisation of Osteosarcoma Cell Lines and Identification of mRNAs and miRNAs Associated with Aggressive Cancer Phenotypes. *Br. J. Cancer* 109, 2228–2236. doi:10.1038/bjc.2013.549
- Lee, K. G. Z., Babak, M. V., Weiss, A., Dyson, P. J., Nowak-Silwinska, P., Montagner, D., et al. (2018). Development of an Efficient Dual-Action GST-Inhibiting Anticancer Platinum(IV) Prodrug. *ChemMedChem* 13, 1210–1217. doi:10.1002/cmdc.201800105
- Li, C., Cai, J., Ge, F., and Wang, G. (2018). TGM2 Knockdown Reverses Cisplatin Chemoresistance in Osteosarcoma. *Int. J. Mol. Med.* 42, 1799–1808. doi:10.3892/ijmm.2018.3753
- Liu, Y., Feng, X., Zhang, Y., Jiang, H., Cai, X., Yan, X., et al. (2016). Establishment and Characterization of a Novel Osteosarcoma Cell Line: CHOS. *J. Orthop. Res.* 34, 2116–2125. doi:10.1002/jor.23245
- Lo Be, D., Montagner, D., Ylan, D., Di Sanza, C., Iglesias, M., Calon, A., et al. (2018). Increased Immune Cell Infiltration in Patient-Derived Tumor Explants Treated with Tranilast: an Original Pt(IV) Pro-drug Based on Cisplatin and Tranilast. *Chem. Commun.* 54, 8324–8327. doi:10.1039/C8CC02071J
- Ma, J., Liu, H., Xi, Z., Hou, J., Li, Y., Niu, J., et al. (2018). Protected and De-protected Platinum(IV) Glycoconjugates with GLUT1 and OCT2-Mediated Selective Cancer Targeting: Demonstrated Enhanced Transporter-Mediated Cytotoxic Properties *In Vitro* and *In Vivo*. *Front. Chem.* 6, 1–15. doi:10.3389/fchem.2018.00386
- Ma, J., Wang, Q., Huang, Z., Yang, X., Nie, Q., Hao, W., et al. (2017a). Glycosylated Platinum(IV) Complexes as Substrates for Glucose Transporters (GLUTs) and Organic Cation Transporters (OCTs) Exhibited Cancer Targeting and Human Serum Albumin Binding Properties for Drug Delivery. *J. Med. Chem.* 60, 5736–5748. doi:10.1021/acs.jmedchem.7b00433
- Ma, J., Wang, Q., Yang, X., Hao, W., Huang, Z., Zhang, J., et al. (2016). Glycosylated Platinum(IV) Prodrugs Demonstrated Significant Therapeutic Efficacy in Cancer Cells and Minimized Side-Effects. *Dalton Trans.* 45, 11830–11838. doi:10.1039/c6dt02207c



- Ma, J., Yang, X., Hao, W., Huang, Z., Wang, X., and Wang, P. G. (2017b). Mono-functionalized Glycosylated Platinum(IV) Complexes Possessed Both pH and Redox Dual-Responsive Properties: Exhibited Enhanced Safety and Preferentially Accumulated in Cancer Cells *In Vitro* and *In Vivo*. *Eur. J. Med. Chem.* 128, 45–55. doi:10.1016/j.ejmech.2017.01.032
- Ma, L., Ma, R., Wang, Y., Zhu, X., Zhang, J., Chan, H. C., et al. (2015). Chalcoplatin, a Dual-Targeting and P53 Activator-Containing Anticancer Platinum(IV) Prodrug with Unique Mode of Action. *Chem. Commun.* 51, 6301–6304. doi:10.1039/C4CC10409A
- Mangunuru, H. P. R., Yerabolu, J. R., Liu, D., and Wang, G. (2015). Synthesis of a Series of Glycosyl Triazole Derivatives and Their Self-Assembling Properties. *Tetrahedron Lett.* 56, 82–85. doi:10.1016/j.tetlet.2014.11.013
- Medina, R. A., and Owen, G. I. (2002). Glucose Transporters: Expression, Regulation and Cancer. *Biol. Res.* 35, 9–26. doi:10.4067/s0716-97602002000100004
- Montagner, D., Tolan, D., Andriollo, E., Gandin, V., and Marzano, C. (2018). A Pt(IV) Prodrug Combining Chlorambucil and Cisplatin: a Dual-Acting Weapon for Targeting DNA in Cancer Cells. *Ijms* 19, 3775. doi:10.3390/ijms19123775
- Morris, J. C., Chiche, J., Grellier, C., Lopez, M., Bornaghi, L. F., Maresca, A., et al. (2011). Targeting Hypoxic Tumor Cell Viability with Carbohydrate-Based Carbonic Anhydrase IX and XII Inhibitors. *J. Med. Chem.* 54, 6905–6918. doi:10.1021/jm200892z
- Neumann, W., Crews, B. C., Marnett, L. J., and Hey-Hawkins, E. (2014). Conjugates of Cisplatin and Cyclooxygenase Inhibitors as Potent Antitumor Agents Overcoming Cisplatin Resistance. *ChemMedChem* 9, 1150–1153. doi:10.1002/cmdc.201402074
- Ogawa, T., Sasaki, A., Ono, K., Ohshika, S., Ishibashi, Y., and Yamada, K. (2021). Uptake of Fluorescent D- and L-Glucose Analogues, 2-NBDG and 2-NBDLG, into Human Osteosarcoma U2OS Cells in a Phloretin-Inhibitable Manner. *Hann. Cel* 34, 634–643. doi:10.1007/s13577-020-00483-y
- Ottoni, F. M., Gomes, E. R., Pádua, R. M., Oliveira, M. C., Silva, I. T., and Alves, R. J. (2020). Synthesis and Cytotoxicity Evaluation of Glycosidic Derivatives of Lawsonine against Breast Cancer Cell Lines. *Bioorg. Med. Chem. Lett.* 30, 126817. doi:10.1016/j.bmcl.2019.126817
- Pathak, R. K., McNitt, C. D., Popik, V. V., and Dhar, S. (2014). Copper-Free Click-Chemistry Platform to Functionalize Cisplatin Prodrugs. *Chem. Eur. J.* 20, 6861–6865. doi:10.1002/chem.201402573
- Patra, M., Awuah, S. G., and Lippard, S. J. (2016). Chemical Approach to Positional Isomers of Glucose-Platinum Conjugates Reveals Specific Cancer Targeting through Glucose-Transporter-Mediated Uptake *In Vitro* and *In Vivo*. *J. Am. Chem. Soc.* 138, 12541–12551. doi:10.1021/jacs.6b06937
- Petruzzella, E., Sirota, R., Solazzo, I., Gandin, V., and Gibson, D. (2018). Triple Action Pt(IV) Derivatives of Cisplatin: a New Class of Potent Anticancer Agents that Overcome Resistance. *Chem. Sci.* 9, 4299–4307. doi:10.1039/C8SC00428E
- Pettenuzzo, A., Pigot, R., and Ronconi, L. (2016). Metal-based Glycoconjugates and Their Potential in Targeted Anticancer Chemotherapy. *Metallodrugs* 1, 36–61. doi:10.1515/medr-2015-0002
- Reddy, A., Ramos-Ondono, J., Abbey, L., Velasco-Torrijos, T., and Ziegler, T. (2017). "2-Chloroethyl and 2-Azidoethyl 2,3,4,6-Tetra-O-Acetyl-β-D-Glucopyranosides," in *Carbohydrate Chemistry: Proven Synthetic Methods*. Edited P. Murphy and C. Vogel, 4, 201–208. doi:10.1201/9781315120300-25
- Savino, S., Gandin, V., Hoeschele, J. D., Marzano, C., Natile, G., and Margiotta, N. (2018). Dual-acting Antitumor Pt(IV) Prodrugs of Kiteplatin with Dichloroacetate Axial Ligands. *Dalton Trans.* 47, 7144–7158. doi:10.1039/C8DT00686E
- Tropper, F. D., Andersson, F. O., Braun, S., and Roy, R. (1992). Phase Transfer Catalysis as a General and Stereoselective Entry into Glycosyl Azides from Glycosyl Halides. *Synthesis* 1992, 618–620. doi:10.1055/s-1992-26175
- Upadhyaya, K., Hamidullah, H., Singh, K., Arun, A., Shukla, M., Srivastava, N., et al. (2016). Identification of Gallic Acid Based Glycoconjugates as a Novel Tubulin Polymerization Inhibitors. *Org. Biomol. Chem.* 14, 1338–1358. doi:10.1039/C5OB02113H
- Valle, S., Alcalá, S., Martín-Hijano, L., Cabezas-Sáinz, P., Navarro, D., Muñoz, E. R., et al. (2020). Exploiting Oxidative Phosphorylation to Promote the Stem and Immuno-evasive Properties of Pancreatic Cancer Stem Cells. *Nat. Commun.* 11, 5265–5284. doi:10.1038/s41467-020-18954-z
- Valverde, I. E., Bauman, A., Kluba, C. A., Vomstein, S., Walter, M. A., and Mindt, T. L. (2013). 1,2,3-Triazoles as Amide Bond Mimics: Triazole Scan Yields Protease-Resistant Peptidomimetics for Tumor Targeting. *Angew. Chem. Int. Ed.* 52, 8957–8960. doi:10.1002/anie.201303108
- Wang, G.-Q., Yan, L.-L., and Wang, Q.-A. (2018). Synthesis and Antiproliferative Activity of Flavonoid Triazolyl Glycosides. *Heterocycl. Commun.* 24, 119–124. doi:10.1515/hc-2017-0241
- Wesselblatt, E., Raveendran, R., Salameh, S., Friedman-Ezra, A., Yavin, E., and Gibson, D. (2015). On the Stability of Pt(IV) Pro-Drugs with Halooacetate Ligands in the Axial Positions. *Chem. Eur. J.* 21, 3108–3114. doi:10.1002/chem.201405467
- Wirth, R., White, J. D., Moghaddam, A. D., Ginzburg, A. L., Zakharov, I. N., Haley, M. M., et al. (2015). Azide vs Alkyne Functionalization in Pt(II) Complexes for Post-treatment Click Modification: Solid-State Structure, Fluorescent Labeling, and Cellular Fate. *J. Am. Chem. Soc.* 137, 15169–15175. doi:10.1021/jacs.5b09108
- Wu, M., Li, H., Liu, R., Gao, X., Zhang, M., Liu, P., et al. (2016). Galactose Conjugated Platinum(II) Complex Targeting the Warburg Effect for Treatment of Non-small Cell Lung Cancer and colon Cancer. *Eur. J. Med. Chem.* 110, 32–42. doi:10.1016/j.ejmech.2016.01.016
- Zhang, J. Z., Bonnitich, P., Wesselblatt, E., Klein, A. V., Najjeh, Y., Gibson, D., et al. (2013). Facile Preparation of Mono-, Di- and Mixed-Carboxylato Platinum(IV) Complexes for Versatile Anticancer Prodrug Design. *Chem. Eur. J.* 19, 1672–1676. doi:10.1002/chem.201203159
- Zheng, D., Sussman, J. H., Jeon, M. P., Farris, S. T., MacMullan, M. A., Delfarah, A., et al. (2020). AKT but Not MYC Promotes Reactive Oxygen Species-Mediated Cell Death in Oxidative Culture. *J. Cell Sci.* 133, jcs239277. doi:10.1242/jcs.239277

**Conflict of Interest:** The authors declare that the research was conducted in the absence of any commercial or financial relationships that could be construed as a potential conflict of interest.

**Publisher's Note:** All claims expressed in this article are solely those of the authors and do not necessarily represent those of their affiliated organizations, or those of the publisher, the editors and the reviewers. Any product that may be evaluated in this article, or claim that may be made by its manufacturer, is not guaranteed or endorsed by the publisher.

Copyright © 2021 Moynihan, Bassi, Ruffini, Panseri, Montesi, Velasco-Torrijos and Montagner. This is an open-access article distributed under the terms of the Creative Commons Attribution License (CC BY). The use, distribution or reproduction in other forums is permitted, provided the original author(s) and the copyright owner(s) are credited and that the original publication in this journal is cited, in accordance with accepted academic practice. No use, distribution or reproduction is permitted which does not comply with these terms.

## Article

# Development of Novel Pt(IV)-Carbohydrate Derivatives as Targeted Anticancer Agents against Osteosarcoma

Eoin Moynihan <sup>1</sup>, Silvia Panseri <sup>2</sup>, Giada Bassi <sup>2,3</sup>, Arianna Rossi <sup>2,4</sup>, Elisabetta Campodoni <sup>2</sup>, Eithne Dempsey <sup>1,5</sup>, Monica Montesi <sup>2,\*</sup>, Trinidad Velasco-Torrijos <sup>1,5</sup> and Diego Montagner <sup>1,5,\*</sup>

<sup>1</sup> Department of Chemistry, Maynooth University, W23 F2H6 Maynooth, Ireland

<sup>2</sup> Institute of Science, Technology and Sustainability for Ceramics, National Research Council (CNR), 48018 Faenza, Italy

<sup>3</sup> Department of Neuroscience, Imaging and Clinical Sciences, University of Studies "G. D'Annunzio", 66100 Chieti, Italy

<sup>4</sup> Department of Chemical, Biological, Pharmaceutical and Environmental Sciences, University of Messina, 98166 Messina, Italy

<sup>5</sup> Kathleen Lonsdale Institute for Human Health Research, Maynooth University, W23 F2H6 Maynooth, Ireland

\* Correspondence: monica.montesi@issmc.cnr.it (M.M.); diego.montagner@mu.ie (D.M.)

**Abstract:** Despite the enormous importance of cisplatin as a chemotherapeutic agent, its application is impacted by dose-limiting side effects and lack of selectivity for cancer cells. Researchers can overcome these issues by taking advantage of the pro-drug nature of the platinum(IV) oxidation state, and by modifying the coordination sphere of the metal centre with specific vectors whose receptors are overexpressed in tumour cell membranes (e.g., carbohydrates). In this paper we report the synthesis of four novel carbohydrate-modified Pt(IV) pro-drugs, based on the cisplatin scaffold, and their biological activity against osteosarcoma (OS), a malignant tumour which is most common in adolescents and young adults. The carbohydrate-targeting vectors and Pt scaffold are linked using copper-catalysed azide-alkyne cycloaddition (CuAAC) chemistry, which is synonymous with mild and robust reaction conditions. The novel complexes are characterised using multinuclear 1D-2D NMR (<sup>1</sup>H, <sup>13</sup>C and <sup>195</sup>Pt), IR, HR-MS, Elem. Analyses, and CV. Cytotoxicity on 2D and 3D and cell morphology studies on OS cell lines, as well as non-cancerous human foetal osteoblasts (hFOB), are discussed.

**Keywords:** Pt(IV) pro-drugs; cisplatin; carbohydrate; selective targeting; osteosarcoma; healthy cell; click chemistry



**Citation:** Moynihan, E.; Panseri, S.; Bassi, G.; Rossi, A.; Campodoni, E.; Dempsey, E.; Montesi, M.; Velasco-Torrijos, T.; Montagner, D. Development of Novel Pt(IV)-Carbohydrate Derivatives as Targeted Anticancer Agents against Osteosarcoma. *Int. J. Mol. Sci.* **2023**, *24*, 6028. <https://doi.org/10.3390/ijms24076028>

Academic Editors: Marialisa Piccolo and Claudia Riccardi

Received: 27 February 2023

Revised: 14 March 2023

Accepted: 17 March 2023

Published: 23 March 2023



**Copyright:** © 2023 by the authors. Licensee MDPI, Basel, Switzerland. This article is an open access article distributed under the terms and conditions of the Creative Commons Attribution (CC BY) license (<https://creativecommons.org/licenses/by/4.0/>).

## 1. Introduction

Cisplatin has been one of the most commonly used Platinum(II) chemotherapeutic drugs since its approval for clinical use over 40 years ago. However, issues associated with acquired or innate resistance, as well as dose-limiting side effects, have stymied its therapeutic potential [1]. Second and third generation Pt(II)-based chemotherapeutics, carboplatin and oxaliplatin, are used to combat resistance, by lowering hydration rates in the case of carboplatin, and by a different mechanism of action that avoids cross-resistance with cisplatin in the case of oxaliplatin [2]. While these drugs have helped to alleviate cisplatin resistance in a variety of cancers, the main problem is still a lack of targeted therapy to reduce the severe side effects associated with platinum-based drugs [3]. Platinum(IV) complexes have the potential to overcome some of the drawbacks of currently available Pt(II) drugs. They are more kinetically inert in comparison to their Pt(II) counterparts, which results in lower toxic side effects for the patient. These complexes are referred to as pro-drugs as they must be reduced from the inactive Pt(IV) complex to their active Pt(II) species by the reducing environment within cancer cells, which leads to a more

targeted approach of drug delivery to the cancer cells [4]. The most promising Pt(IV) drugs are satraplatin [5,6], ormaplatin [7,8] and iroplatin [9,10] but, despite promising results, none to date have been approved for widespread use in cancer treatments (Figure 1a) [3]. Promising strategies for imparting selectivity to Pt(IV) pro-drugs is the use of tumour-targeting ligands. Carbohydrates, such as glucose and galactose, can be used to exploit the Warburg effect [11], because cancer cells metabolise glucose differently from healthy cells. Rapid proliferation of cancer cells leads to the imbalance in the intake of oxygen and results in hypoxia, which drives cancer cells to choose anaerobic glycolysis to produce energy. This method of energy production is inefficient and leads to the overexpression of glucose transporters (GLUTs) on the cell membrane [12]. Several glyco-modified Pt(IV) complexes have been reported in literature, mainly from the group of Wang and co-workers [13–17], summarised excellently by Kenny and Marmion [3]. The most notable results were obtained when the Pt scaffold was cisplatin rather than carboplatin or oxaliplatin [18]. It was also determined that mono-functionalisation was more effective than bis-functionalised complexes [14]. Platinum-based complexes are extensively used to treat osteosarcoma (OS), the most common malignant primary bone tumour which affects adolescents and young adults, with a second spike of incidence in those over 50, and which tends to metastasize and invade para-carcinoma tissues [19]. Currently, treatment options incorporate surgery and combination chemotherapy, which cures 70% of patients. However, for patients with metastatic or relapsed OS, the modes of treatment have remained unchanged for over 30 years and result in a significantly lower survival rate among patients [20]. This reduction in survivability is partially because cisplatin is a standard drug in the treatment of OS and has limited effectiveness, stemming from chemoresistance and a lack of drug selectivity. This lack of selectivity and a need to overcome cisplatin resistance has led many to develop novel compounds to target specific molecular alterations in tumours, with the objective of restoring chemosensitivity [21]. Recently, our group reported the synthesis and biological evaluation against osteosarcoma of four acetylated glyco-modified Pt(IV) complexes, but, despite the promising results, the role of the sugars was not completely clarified [22]. The glycosylated complexes proved to have an enhanced cellular uptake, but this was probably due to the higher lipophilicity caused by the acetylated groups, rather than due to recognition by GLUTs. Indeed, these protecting groups are prone to enzymatic hydrolysis in the body, ultimately making them pro-drugs themselves [23]. The crystal structures of various GLUTs have enabled researchers to focus their work on the optimal presentation of their carbohydrates to target these transporters [24,25], and free sugars are employed as they more closely mimic the structure of the compounds recognised by various GLUTs that are overexpressed on cancer cell membranes. To try to clarify this aspect, we decided to synthesise four glyco-derivatives (two with glucose and two with galactose) for the previously reported complexes with the deprotected (free) sugars and evaluate their biological activity against two osteosarcoma cell lines and a non-cancerous human foetal osteoblast (hFOB), (Figure 1b). In this work we functionalise our carbohydrate-targeting vector in  $\beta$  configuration at the anomeric position, since an important factor for maintaining recognition is to conserve the sugars' ability to form hydrogen bonds with the GLUT binding site through the atom bound to the anomeric position acting as a H-bond acceptor [26]. To maintain this H-bonding ability, we take advantage of the copper-catalysed azide-alkyne cycloaddition (CuAAC) reaction due to its versatile nature and mild reaction conditions for the conjugation of our carbohydrates to the platinum core. The resulting 1,2,3-Triazole is recognised as a strong bio-isostere for many functionalities, including amide bonds, and has H-bonding acceptor properties [27]. Additionally, we wanted to investigate the use of both an anomeric *O*-ethylene linker (which resembles naturally occurring glycosides) and *N*-triazolyl glycomimetics, to analyse if there is a significant difference in the H-bond acceptor ability, and subsequent activity, of either group (Figure 1b).



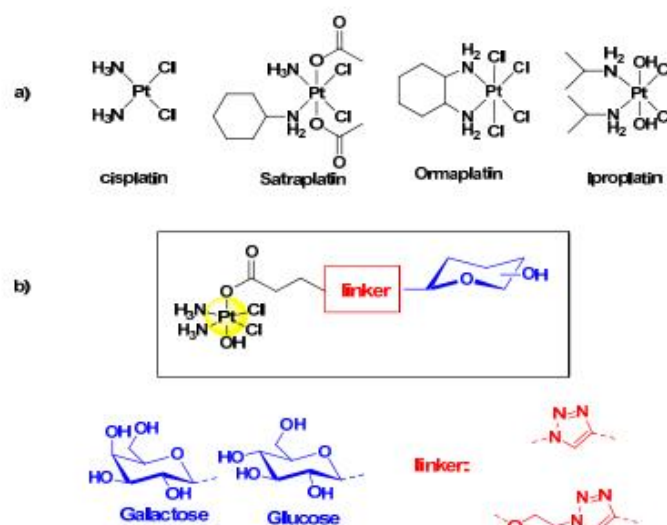


**Figure 1.** (a) Structures of cisplatin (*cis*-[(NH<sub>3</sub>)<sub>2</sub>PtCl<sub>2</sub>]) and of the three most promising Pt(IV) complexes, satraplatin (*cis,trans,cis*-[PtCl<sub>2</sub>(OAc)<sub>2</sub>(NH<sub>3</sub>)-cyclohexylamine]), ormaplatin ([PtCl<sub>4</sub>(cyclohexane-1,2-diamine)]), and iproplatin (*cis,trans,cis*-[PtCl<sub>2</sub>(OH)<sub>2</sub>(isopropylamine)<sub>2</sub>]). (b) General structure for the novel Pt(IV) complexes based on the cisplatin scaffold and functionalised with glucose and galactose.

The anticancer activity of the glyco-derivatives reported here have been investigated in both standard 2D and in 3D scaffold-based OS *in vitro* models, using two different OS cell lines (MG63 and SAOS-2) and osteoblast cells line (hFOB5) as healthy cells to compare the effectiveness against a standard of cisplatin.

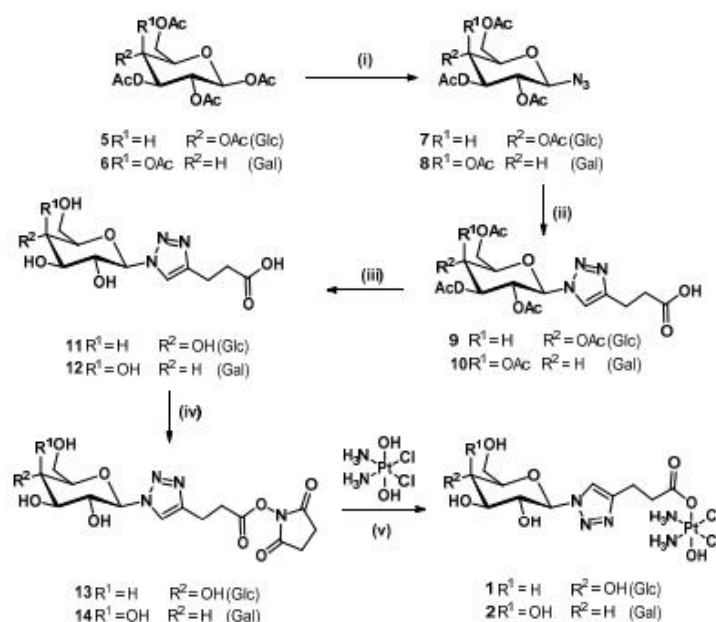
## 2. Results and Discussion

### 2.1. Synthesis and Characterisation

As described in the introduction, the aim of this work is to synthesise Pt(IV) anticancer pro-drugs based on a cisplatin scaffold modified with free sugars (glucose and galactose) that could act as delivery vectors to enhance selectivity for cancer cells, exploiting the Warburg effect. With respect to our recent work [22], the sugars here are de-acetylated to obtain a more reliable recognition by the GLUT receptors overexpressed on the cancer cell membrane, as discussed in the introduction. The sugar moieties are connected to the platinum centre via a triazolyl linker exploiting the versatility and mild conditions of click chemistry copper azide–alkyne cycloaddition (CuAAC) reactions, producing four novel complexes. The synthesis of the novel glycosylated Pt(IV) complexes proved to be rather challenging; in fact, the direct deprotection of the corresponding acetylated glycosylated precursor complexes, recently reported by us [22], did not produce the expected results. The use of standard deprotection methods (i.e., NEt<sub>3</sub> in MeOH) resulted in the decomposition of the complexes, forming a series of impurities and a complex mixture which was very difficult to purify and isolate. After several attempts and modifications, the final complexes were successfully synthesised, as shown in Schemes 1 and 2.

Scheme 1 represents the synthetic mechanism route to produce the N-glycoside (glucose and galactose) derivatives with shorter chains. The synthesis of compounds 5–10 has been reported by us previously [22]. To summarise briefly, the per-acetylated glucose

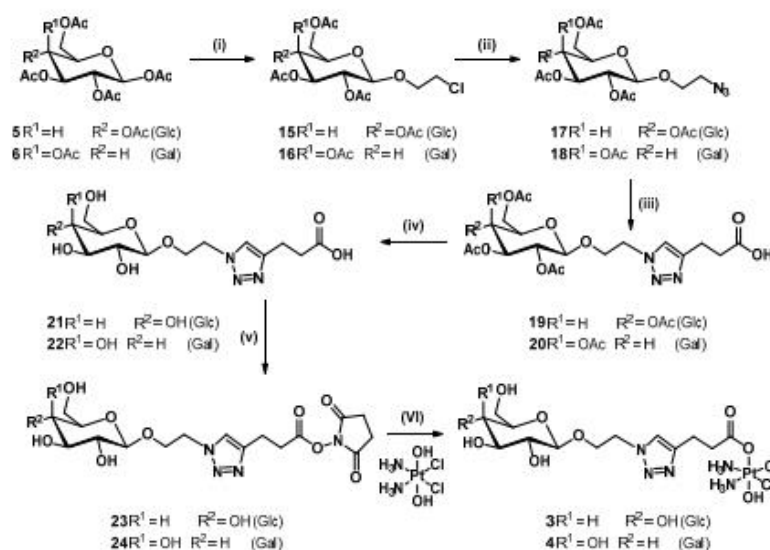
5 and galactose 6 are transformed to the corresponding  $\beta$ -azides, 7 and 8, through reaction with azidotrimethylsilane and tin tetrachloride. Following this, 7 and 8 are reacted with 4-pentynoic acid, using CuAAC conditions at room temperature, to produce the carboxylic acids 9 and 10. At this point, the acetylated sugars are deprotected with triethylamine in a mixture of MeOH/H<sub>2</sub>O at 45 °C to yield carboxylic acids 11 and 12. Many standard coupling reagents and conditions were screened in order to identify a suitable procedure that would allow for the synthesis of activated N-hydroxysuccinimide (NHS) esters 13 and 14 in the presence of the hydroxyl groups in the deprotected sugars. Initial attempts for the classic activation with NHS using EDCI or TBTU did not yield the desired products. Finally, optimised reaction conditions with TSTU (N,N,N',N'-Tetramethyl-O-(N-succinimidyl)uronium tetrafluoroborate) produced the activated NHS-esters 13 and 14 with good yield and purity. The advantage of using TSTU is that the reaction does not require the use of an additional coupling reagent and vastly reduces reaction time to a mere 20 min. The final complexes 1 and 2 were obtained through the dropwise addition of 13 and 14 to oxoplatin in DMSO over 2 days. The final complexes were characterised using <sup>1</sup>H, <sup>13</sup>C, <sup>195</sup>Pt-NMR, mass spectroscopy and cyclic voltammetry, and the purity was assessed with El. Anal. And HPLC (See Experimental Section and Supporting Information).



**Scheme 1.** Synthetic route for the complexes 1 and 2: (i) TMSN<sub>3</sub>, SnCl<sub>4</sub>, DCM, rt, 16 h, 91% (7), 89% (8); (ii) 4-pentynoic acid, CuSO<sub>4</sub>, sodium ascorbate, t-BuOH, THF, H<sub>2</sub>O, rt, 16 h, 64% (9), 74% (10); (iii) TEA, MeOH, H<sub>2</sub>O, 45 °C, 16 h, 95% (11), 97% (12); (iv) TSTU, TEA, DMF, rt, 20 min, 68% (13), 68% (14); (v) DMSO, 40 °C, 48 h, 59% (1), 35% (2).

Complexes 3 and 4, with a O-ethylene linker, were synthesised according to Scheme 2, in a manner similar to the synthesis of the N-triazolyl derivatives 1 and 2, described earlier. Compounds 19 and 20, recently reported by us [22], were hydrolysed under mild basic conditions to afford deacetylated carboxylic acids 21 and 22. The same challenges

described above remained for the synthesis of free sugar complexes **3** and **4** and consequently, the same strategies were applied. The successful formation of the NHS active esters **23** and **24** was achieved once again with the use of TSTU, and the final complexes **3** and **4** were obtained through the reaction of the activated deprotected sugar moieties **23** and **24** with oxoplatin in DMSO. These complexes were characterised using the same techniques as for complexes **1** and **2**. All the complexes show the typical features of Pt(IV) species based on a cisplatin scaffold, with a broad triplet around 6 ppm assigned to the NH<sub>3</sub> groups in the <sup>1</sup>H-NMR spectrum, the <sup>195</sup>Pt signal around 1600 ppm, typical of Pt in the oxidation state +4 and the typical Pt isotopic pattern in the mass spectra (Supplementary Materials Figures S1–S16).



**Scheme 2.** Synthetic route for complexes **3** and **4**: (i) 2-Chloroethanol, BF<sub>3</sub>·OEt<sub>2</sub>, 3 Å MS, 0 °C to rt, DCM, 16 h, 39% (**15**), 40% (**16**); (ii) NaN<sub>3</sub>, DME, 80 °C, 16 h, 59% (**17**), 57% (**18**); (iii) CuSO<sub>4</sub>, sodium ascorbate, t-BuOH, THE, H<sub>2</sub>O, rt, 16 h, 44% (**19**), 47% (**20**); (iv) TEA, MeOH, H<sub>2</sub>O, 45 °C, 16 h, 86% (**21**), 96% (**22**); (v) TSTU, TEA, DME, 20 min, rt, 60% (**23**), 75% (**24**); (vi) DMSO, 40 °C, 48 h, 47% (**3**), 61% (**4**).

The stability in physiological conditions of complexes **1** and **3**, taken as examples for the different substituents at the anomeric position) was analysed over a period of 96 h via <sup>1</sup>H, <sup>13</sup>C and <sup>195</sup>Pt-NMR in a solution of DMSO containing PBS buffer (pH = 6.8) and minimum decomposition was observed (Figure S17a–f in Supplementary Materials). The redox behaviour of complexes **1** and **3** (cathodic processes E<sub>p</sub><sup>c</sup> (I), E<sub>p</sub><sup>c</sup> (II), Figure 2) and of the corresponding axial glycol-ligands **11** and **21** (E<sub>p</sub><sup>c</sup> (I), Figure 2) was studied via Cyclic Voltammetry with E<sup>0</sup><sub>Pt(IV)/Pt(II)</sub> = −1.034 V and −1.002 V for **1** and **3**, respectively E<sub>p</sub><sup>c</sup> (II). The electrochemical reduction was irreversible, in line with previous reported Pt(IV) species based on cisplatin [28], and no major difference was observed according to the type of linker used to connect the carbohydrate moiety and the Pt centre (Figure 2, Figures S18 and S19 in Supplementary Materials).

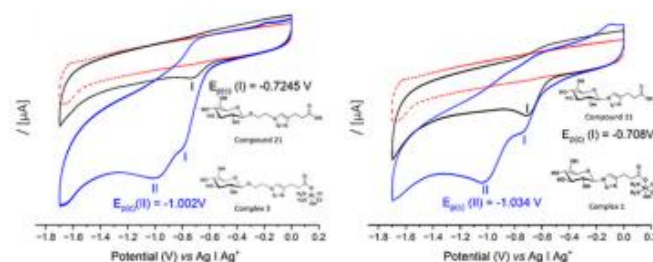


**Figure 2.** The cyclic voltammograms of the complexes **1** and **3** (blue), with evidence of irreversible cathodic processes I and II and of the axial ligands **11** and **21** (black), showing process I only, with background supporting electrolyte (red). All experiments were performed at the same concentration ([compound] = 2 mM) in deuterated 0.1 M DMSO- $[n\text{-Bu}_4\text{N}][\text{PF}_6]$  at a scan rate of  $0.1 \text{ V s}^{-1}$ .

For a confirmation of the activation through intracellular reduction that occurs in Pt(IV) species, the behaviour of the Pt(IV) pro-drugs was studied by means of the addition of an excess of ascorbic acid into a solution of complex **3** [29]. The reduction process was followed by  $^1\text{H-NMR}$  with complete release of the carbohydrate axial ligand after 48 h, as observed by the disappearance of the triazole proton at  $\delta = 7.93$  of complex **3** and the concomitant formation of the corresponding peak at  $\delta = 7.91$  of the free carboxylic acid **21** (Figure 3 and Figure S20 in Supplementary Materials).

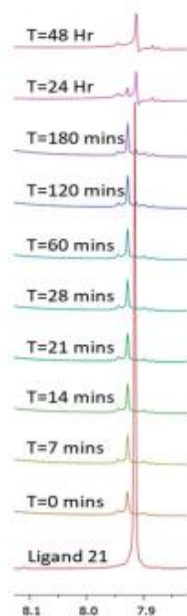


**Figure 3.** Reduction of complex **3** by a 10-fold excess of ascorbic acid.  $^1\text{H-NMR}$  spectra over 48 h in DMSO.



## 2.2. Biological Evaluation

The anticancer activity of the four complexes were tested in vitro in 2D and 3D against two osteosarcoma cancer cell lines (SAOS and MG63) and also in 2D against a healthy osteoblast cell line (hFOBs), to evaluate if the strategic use of glucose and galactose as vectors is enhancing the selectivity.

The evaluation of cell viability demonstrated a dose-dependent cancer cell toxicity exerted by all the drugs (Figure 4). Although no significant differences in the  $IC_{50}$  (Table 1, Figures S21–S23 in Supplementary Materials) were detected in the four complexes compared to cisplatin, at high concentrations the complexes showed better performance with respect to cisplatin. In MG63 cells, the mean effect of the complexes 1–4 showed a ~3-fold reduction of the cell viability with respect to cisplatin, and ~1.5-fold reduction for SAOS-2 (Figure 4). The higher anticancer activity of all the complexes 1–4, with respect to cisplatin, was statistically significant at 30  $\mu$ M for SAOS-2 and 60  $\mu$ M for MG63. The different cellular behaviour between the cell lines can be attributed to the intrinsic biological differences of the two osteosarcoma cell lines [30].

Most importantly, in the healthy cell hFOBs, the cisplatin began to be extremely toxic at very low concentration, 1.5  $\mu$ M ( $p \leq 0.001$  with respect to cells only), while complexes 1–4 showed a cytotoxic effect at much higher concentrations,  $\geq 15 \mu$ M (complex 1  $p \leq 0.05$ ; 2  $p \leq 0.001$ ; 3  $p \leq 0.0001$ ; 4  $p \leq 0.001$  respect to cells only). The evaluation of the  $IC_{50}$  values confirmed the cell viability results; in fact, in the hFOBs, the  $IC_{50}$  of the cisplatin (i.e., 4.1  $\mu$ M) was far lower compared to the  $IC_{50}$  values of complexes 1–4, which were  $> 16 \mu$ M (Table 1). Moreover, it was shown that the toxic effect of the complexes is statistically significantly lower, with respect to the effect of cisplatin, at 1.5  $\mu$ M, 5  $\mu$ M, 15  $\mu$ M, and 30  $\mu$ M (Figure 4). The cell behaviours observed in the cell viability assay were also confirmed using morphological analysis, where a reduction in cell density directly related to the increase in drug concentration was detected (Figure S24 in Supplementary Materials).

The results demonstrated that complexes 1–4 all have selectivity for these cancer cells and a lower toxic effect on healthy hFOBs. We believe that this selectivity could be ascribable to the overexpression of the GLUT family members, specifically GLUT-1, observed in cancer cells leading to an increased glycolytic activity [31,32]. The higher toxicity of all complexes with respect to the cisplatin, observed in both MG63 and SAOS-2 at 30  $\mu$ M and 60  $\mu$ M, strengthens the hypothesis of the role of the GLUT receptor overexpression in the uptake, induced by the presence of sugar moieties connected to the drug, and consequently in the increased anticancer effect.

In order to confirm these promising results, a proof of concept in vitro was performed using more relevant cancer models. In fact, it is well known that the use of conventional 2D approaches show some limitations because they fail to mimic a real tumour's complexity, leading to a low predictivity of preclinical results [33,34]. To overcome this limitation, and to strengthen the results obtained in the previous 2D study, an MG63 cell line was cultured on a 3D scaffold that mimics the feature of the bone extracellular matrix (Figure 5C) from a physical, chemical, and nanostructural point of view, as previously demonstrated [35,36].

After the seeding of the MG63 cell line, the cells were able to interact and colonise the scaffold, providing a more mimetic 3D scaffold-based osteosarcoma model (3D OS model) which was then used to test the effect of the proposed drugs. As shown in Figure 5A,B, MG63 cells easily adhered to the nanostructure of the biomimetic scaffolds and, 48 h after seeding, the scaffolds were nearly completely covered by the cells, exhibiting their characteristic morphology and a high level of cell/material interactions.

It is well known that the behaviour of the cells cultured in 3D condition is different respect to the standard 2D model [37]. For this reason, before testing the complexes in the 3D OS mode, a preliminary evaluation of the cisplatin effective concentration was performed by comparing the toxicity of cisplatin 15  $\mu$ M in 2D and in the 3D OS model. As shown in Figure S25 in Supplementary Materials, 15  $\mu$ M of cisplatin did not compromise the cell viability in 3D OS model, though it significantly reduced the viable cells grown in 2D standard culture conditions ( $p$ -value  $\leq 0.0001$ ).



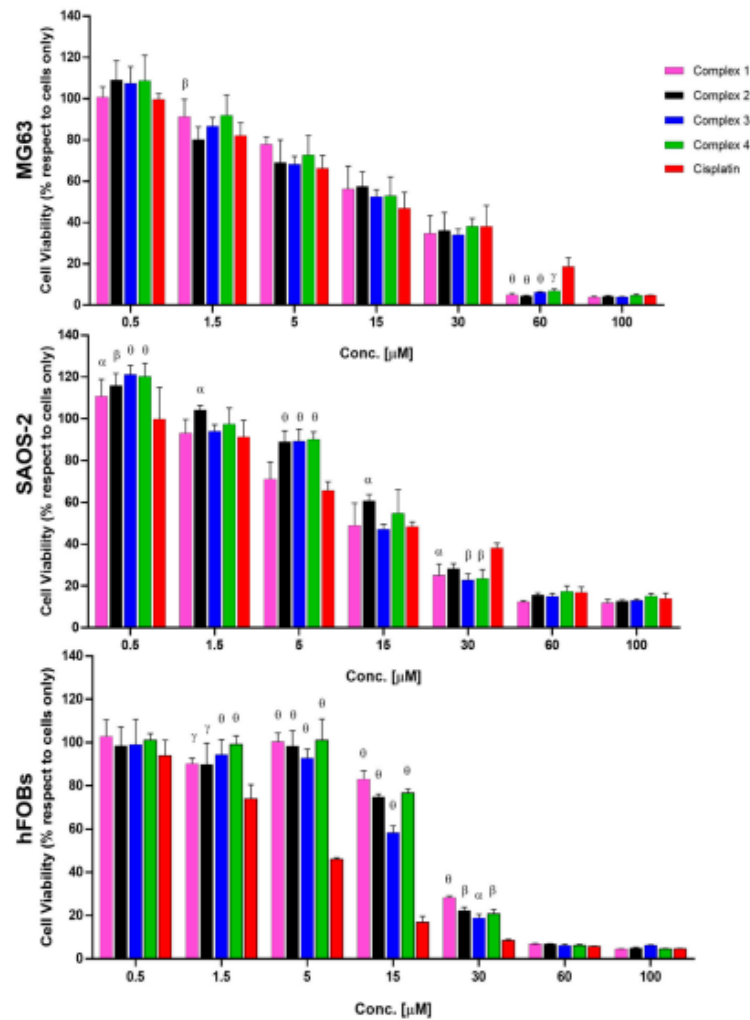


**Figure 4.** 2D drug screening of complexes 1–4 by MTT assay. Cell viability evaluation after 72 h incubation with complexes. Data are reported in the graph as percentage (%) mean  $\pm$  standard error of the mean. Statistical analyses with respect to cisplatin are reported in the graph,  $p$  value is  $\alpha \leq 0.05$ ,  $\beta \leq 0.01$ ,  $\gamma \leq 0.001$  and  $\theta \leq 0.0001$ .

**Table 1.** IC<sub>50</sub> (μM) values of the complexes 1–4 and cisplatin against MG63, SAOS-2 and hFOB3 cells.

|        | Cisplatin        |                 | Complex 1        |                 | Complex 2        |                 | Complex 3        |                | Complex 4        |                 |
|--------|------------------|-----------------|------------------|-----------------|------------------|-----------------|------------------|----------------|------------------|-----------------|
|        | IC <sub>50</sub> | 95% CI          | IC <sub>50</sub> | 95% CI          | IC <sub>50</sub> | 95% CI          | IC <sub>50</sub> | 95% CI         | IC <sub>50</sub> | 95% CI          |
| MG63   | 12.20            | +3.1;<br>−2.6   | 15.90            | +3.3;<br>−2.9   | 13.60            | +5.2;<br>−4.0   | 13.0             | +3.2;<br>−2.7  | 14.90            | +4.2;<br>−3.5   |
| SAOS-2 | 13.70            | +3.2;<br>−2.7   | 12.94            | +3.4;<br>−3.0   | 19.09            | +3.4;<br>−3.0   | 15.18            | +3.7;<br>−3.1  | 17.22            | +4.5;<br>−3.7   |
| hFOBs  | 4.109            | +0.42;<br>−0.47 | 23.36            | +1.72;<br>−1.82 | 20.85            | +1.92;<br>−2.11 | 16.88            | +1.7;<br>−1.75 | 20.91            | +0.42;<br>−0.47 |

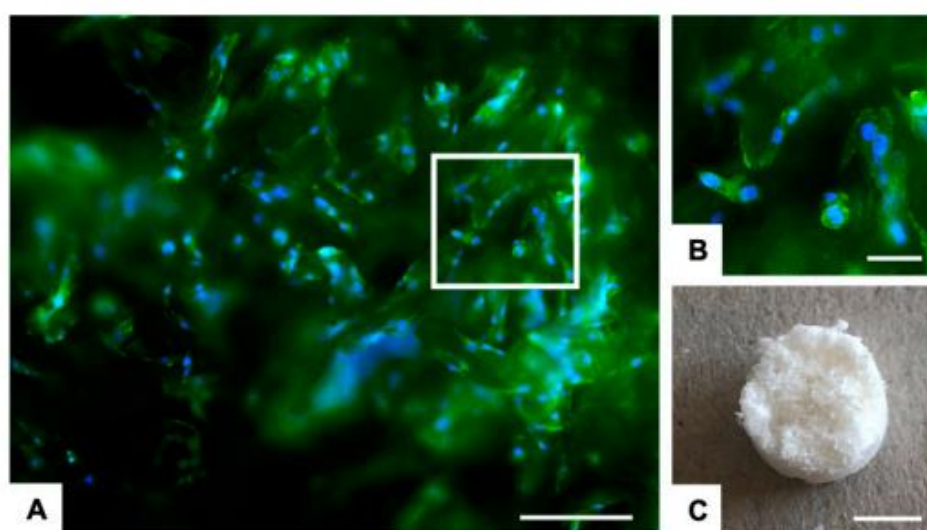


**Figure 5.** 3D scaffold-based osteosarcoma model (3D OS model). (A) Analysis of cell morphology of 3D MG63 culture on bone-mimetic scaffold 48 h after seeding. F-Actin filaments in green (FITC) and cell nuclei in blue (DAPI); scale bars 200 μm. (B) Image enlargement (white square) of the cell morphology details; scale bars 50 μm. (C) Representative image of the 3D bone-mimetic scaffold; scale bars 4 mm.

Based on these results, the complexes 1–4 and the cisplatin were tested at 30 and 60 μM in the 3D tumour model. At 60 μM, all the complexes showed higher toxic effect respect to the cisplatin, and these differences are statistically significant for complexes 2 and 4 with  $p$  value  $\leq 0.05$  (Figure 6). Morphological analysis (Figure S26 in Supplementary Materials) confirms the cell viability results.

This proof of concept highlights the cancer cells selectivity of the complexes for the considered OS cells, compared to the cisplatin action, and reinforces the data obtained in the 2D in vitro study, demonstrating better performances of the complexes 1–4 as anticancer drugs.

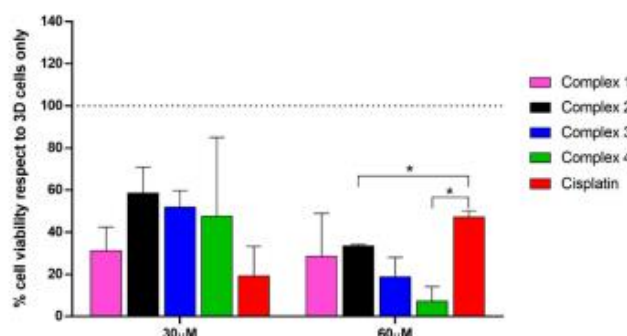


**Figure 6.** Anti-cancerous effect of 1–4 complexes on 3D OS model. Cell viability evaluation after 72 h of incubation with complexes using MTT assay. Data are reported in the graph as percentage (%) mean  $\pm$  standard error of the mean. Statistical analyses with respect to cisplatin are reported in the graph, \*  $p$  value  $\leq 0.05$ .

### 3. Materials and Methods

#### 3.1. General Methods

All reagents and reactants were purchased from commercial sources. The two sources used were Sigma-Aldrich (St.Louis, MO, USA) and Fluorochem (Graphite way, Hadfield, UK). All solvents were used without further purification. Cisplatin and oxoplatin were synthesised as previously reported [38,39]. Compounds 7–10 and 15–20 were synthesised as reported by us [22].

The elemental analysis studies (carbon, hydrogen, and nitrogen) were performed by means of a PerkinElmer 2400 series II analyser (Waltham, MA, USA). HR mass spectra were recorded with a Waters LCT Premier XE Spectrometer (Milford, MA, USA). NMR:  $^1\text{H}$ ,  $^{13}\text{C}$  and  $^{195}\text{Pt}$  NMR spectra were obtained in a solution of  $\text{D}_2\text{O}$  or  $\text{DMSO}-d_6$  at 300 K, in 5 mm sample tubes, with a premium shielded Agilent Varian 500 MHz (operating at 500.13, 125.75, and 107.49 MHz, respectively)(Santa Clara, CA, USA). The  $^1\text{H}$  and  $^{13}\text{C}$  chemical shift was referenced to the residual impurity of the solvent. The external reference was  $\text{Na}_2\text{PtCl}_4$  in  $\text{D}_2\text{O}$  (adjusted to  $\delta = -1628$  ppm from  $\text{Na}_2\text{PtCl}_6$ ) for  $^{195}\text{Pt}$ . The stability was followed using high-performance liquid chromatography (HPLC) with a Phenomenex Luna C18 (5  $\mu\text{M}$ , 100  $\text{\AA}$ , 250 mm  $\times$  4.60 mm i.d.) column (Torrance, CA, USA) at room temperature at a flow rate of 1.0 mL/min with 254 nm UV detection. Mobile phase containing 80:20 acetonitrile (0.1% trifluoroacetic acid): water (0.1% trifluoroacetic acid): the complexes were dissolved in DMF (0.5 mL) and diluted to a final concentration of 0.5 mM, using acetonitrile and water solution (1/1) and 2 mM 4-(2-hydroxyethyl)piperazine-1-ethanesulfonic acid (HEPES) buffer (pH 6.8). Infrared (IR) spectra were precisely recorded in the region 4000–400  $\text{cm}^{-1}$  on a Perkin Elmer spectrum 100 FT/IR spectrometer (Shelton, CT, USA). The solid samples were run using ATR. An extensive biological evaluation of the activity of all the compounds was performed in human osteosarcoma cell line in vitro models as reported below.

#### 3.2. Cyclic Voltammetry

Measurements were made using a Solartron SI2187 Electrochemical Potentiostat/Galvanostat (Berwyn, PA, USA) and a CHI Instruments 1200 Potentiostat (Austin, TX, USA). Non-aqueous voltammetry of 2 mM of each of 11, 21, 1 and 3 was carried out at a glassy carbon working electrode (0.07  $\text{cm}^2$ ) in a three-electrode configuration with Pt wire counter and non-aqueous  $\text{Ag} | \text{Ag}^+$  reference electrode in 0.1 M tetrabutylammonium hexafluorophosphate ( $\text{TBAPF}_6$ ) supporting electrolyte in DMSO as solvent. The working electrodes were prepared by polishing with 1  $\mu\text{m}$  microcrystalline diamond suspension on a micro-cloth,



followed by rinsing in deionised water. Voltammograms were generated over the range 0.2 to  $-1.7$  V vs. Ag/Ag<sup>+</sup> in a deaerated solution (N<sub>2</sub> bubbling 10 min), with a cathodic scan direction at  $100 \text{ mV}\cdot\text{s}^{-1}$  in all cases.

### 3.3. Stability and Reduction Studies

The stability was analysed via <sup>1</sup>H, <sup>13</sup>C and <sup>195</sup>Pt NMR. Complexes 1 and 3 (taken as examples for the different substituents at the anomeric position) were dissolved in a 1/1 mixture of DMSO and PBS (pH = 6.8), and the spectra were collected after 0 and 96 h. The reduction was followed by <sup>1</sup>H-NMR. Complex 3 (5 mg, 7.53  $\mu\text{mol}$ ) was dissolved in 500  $\mu\text{L}$  of DMSO-*d*<sub>6</sub> and ascorbic acid (13 mg, 10 Equiv.) was added. <sup>1</sup>H NMR spectrum was recorded every 7 min for 30 min, then every hour until 24 h and then after 48 h.

### 3.4. In Vitro Biological Evaluation

In vitro tests of the four Pt(IV)-Carbohydrate derivatives complexes (1–4) were performed to evaluate their biological activity towards two osteosarcoma cell lines (MG63 and SAOS-2) and a non-cancerous cell line of human foetal osteoblasts (hFOBs), compared to cisplatin. The drugs were reconstituted in dimethyl sulfoxide (DMSO) at 1 mg/mL concentration, before being diluted in culture media at the required concentration. A 2D in vitro screening of all the drugs was performed at 72 h in a wide concentration range (0.5; 1.5, 5, 15, 30, 60 and 100  $\mu\text{M}$ ) on the three different cell lines in terms of cell viability, and the IC<sub>50</sub> was calculated. The cell morphology in the presence of the complexes was evaluated at 15 and 30  $\mu\text{M}$  concentrations, for MG63 and SAOS-2 and hFOBs cells, respectively, according to the IC<sub>50</sub> at 72 h. Moreover, as more predictive in vitro cell culture systems, 3D tumour scaffold-based models of osteosarcoma were developed, and the anticancer activity of cisplatin and complexes 1–4 on MG63 cells, in terms of cell viability and morphology, was investigated at 30 and 60  $\mu\text{M}$  concentrations after 72 h of culture. For the models, a composite hydroxyapatite-based scaffold (MgHA/Coll), as a bone-like matrix, was used in combination with MG63 cells. For both the 2D and 3D in vitro cell cultures, cisplatin was used as a control group, and cells only were used as a negative control.

**Cell culture.** Human Osteosarcoma cell lines MG63 (ATCC<sup>®</sup> CRL1427<sup>TM</sup>), SAOS-2 (ATCC<sup>®</sup> HTB-85<sup>TM</sup>), and Human Foetal Osteoblasts (hFOBs 1.19) (ATCC<sup>®</sup> CRL-11372<sup>TM</sup>) were purchased from American Type Culture Collection (ATCC) and used for this study. The MG63 cell line was cultured in DMEM F12-GlutaMAX<sup>TM</sup> Modified Medium (Gibco), supplemented with 10% Foetal Bovine Serum (FBS) (Gibco) and 1% of penicillin/streptomycin mixture (pen/strep) (100 U/mL–100  $\mu\text{g}/\text{mL}$ , Gibco). The SAOS-2 cell line was cultured in McCoy's 5A Modified Medium (Gibco), supplemented with 15% and 10% FBS, respectively, and 1% pen/strep. The hFOBs cell line was cultured in DMEM F12 no phenol red, with L-glutamine supplemented with 10% FBS and 0.3 mg/mL Geneticin (G418, Gibco). Cells were kept in an incubator at 37 °C under controlled humidity and 5% CO<sub>2</sub> atmosphere conditions. Cells were detached from culture flasks via trypsinization and centrifuged. The cell number and viability were determined using the trypan blue dye exclusion test, and all cell handling procedures were performed under a laminar flow hood in sterility conditions.

**Synthesis of bone-mimetic scaffolds.** The Mg-doped hydroxyapatite collagen composite scaffolds were designed and synthesised at ISSMC of CNR of Italy [35]. In brief, 150 g of collagen gel (1 wt%, Opocrin SpA, MO, Italy) was diluted into a phosphoric acid solution (2.4 g in 500 mL; H<sub>3</sub>PO<sub>4</sub>, 85 wt.%, Sigma-Aldrich) at room temperature to obtain an acidic aqueous homogenous suspension. Separately, a basic aqueous suspension was obtained by mixing 2.7 g of calcium hydroxide (Ca(OH)<sub>2</sub>, 95 wt.%, Sigma) and 0.35 g of magnesium chloride (MgCl<sub>2</sub>·6H<sub>2</sub>O, 99 wt.%, Sigma) in 500 mL of milli-Q water at room temperature to obtain a basic aqueous homogenous suspension. The acidic suspension was dripped into the basic one at 25 ± 2 °C under continuous stirring condition and matured for 2 h. Later, the slurry solution was rinsed thrice in milli-Q water and filtered through metallic sieve (150 m) to exclude unreacted counter ions. The recovered slurry solution was cross-linked with 2 wt.% BDDGE (respect to Collagen) at 25 ± 2 °C for 24 h and at 4 °C for other

24 h. Later, the solution was rinsed thrice in milli-Q water to remove any residues and freeze-dried ( $-40\text{ }^{\circ}\text{C}$  and  $+25\text{ }^{\circ}\text{C}$ ) for 48 h under 0.086 mbar vacuum conditions (LIO 3000 PLT, SPASCAL, Italy). The obtained scaffolds ( $8 \times 4\text{ mm}$ ), named bone-mimetic scaffolds, were sterilised using 25 kGy  $\gamma$ -ray irradiation before use.

**3D scaffold-based osteosarcoma models (3D OS model).** For the development of the in vitro 3D scaffold-based osteosarcoma model, bone-mimetic scaffolds were used as bone-like matrix in combination with MG63 cells. The scaffolds were conditioned in culture media for 24 h before the cell seeding. MG63 cell line was seeded with a density of  $3.0 \times 10^4$  per scaffold by dropping the cellular suspension on the material upper surface followed by 30 min pre-adhesion at  $37\text{ }^{\circ}\text{C}$  before cell media addition. The 3D OS model has been grown in the incubator under standard culture medium condition for 48 h to allow cell colonization of the scaffold, then the medium was changed, and the drugs were added. The in vitro 3D OS models were cultured in the presence of the drugs for 72 h at  $37\text{ }^{\circ}\text{C}$  under controlled humidity and 5%  $\text{CO}_2$  atmosphere conditions; the cells grown in 3D in standard condition, without the drugs, were used as control group (3D cells only). All cell handling procedures were performed under a laminar flow hood in sterility conditions.

**MTT cell viability assay.** A quantitative analysis of cell viability was carried out by using MTT assay, following the manufacturer's instructions. For the in vitro 2D cell cultures, all cell lines were seeded at a density of  $5.0 \times 10^3$  cells/well in 96 well-plates. For in vitro 3D cell cultures, see at the "3D scaffold-based models of osteosarcoma" paragraph of Materials and Methods section. The MTT reagent [3-(4,5-dimethylthiazol-2-yl)-2,5-diphenyltetrazolium bromide] (5 mg/mL) was dissolved in phosphate saline buffer 1X (PBS 1X). At 72 h, the cells were incubated with 10% media volume MTT solution for 2 h at  $37\text{ }^{\circ}\text{C}$ , 5%  $\text{CO}_2$  and controlled humidity conditions. The cell culture media was removed and substituted with DMSO (Merck) dissolving formazan crystals, derived from MTT conversion by metabolically active cells. For the 3D scaffold-based models of osteosarcoma, each scaffold was transferred into a 2 mL Eppendorf, and completely broken using pestles after DMSO addition. After 15 min of incubation under slight stirring conditions, the absorbance of formazan was read at 570 nm by using a Multiskan FC Microplate Photometer (Thermo Fisher Scientific, Waltham, MA, USA). The values of absorbance are directly proportional to the number of metabolic active cells in each well. One experiment was carried out, and a biological triplicate for each condition was performed. For the 3D tumour models, one biological experiment was performed, and two scaffolds for each condition were used.

**Cell morphology evaluation.** For the in vitro 2D cell cultures, all cell lines were seeded at a density of  $5.0 \times 10^3$  cells/well in 96 well-plates, for the in vitro 3D cell cultures cells were treated as previously described. Both the 2D and 3D cell cultures were fixed in 4% buffered Paraformaldehyde (PFA) following the manufacturer's instructions. The fixed samples were permeabilised in PBS 1X with 0.1% (*v/v*) Triton X-100 (Merck) for 5 min at room temperature and F-actin filaments were highlighted with Alexa Fluor 488 Phalloidin (Invitrogen) for 20 min at room temperature in the dark. DAPI (600 nM) counterstaining was performed for cell nuclei identification, following the manufacturer's instructions. The images were acquired by using an Inverted Ti-E Fluorescent Microscope.

**Statistical Analysis.** Statistical analysis was performed using GraphPad Prism Software (8.0.1 version). The results of the MTT assay of the in vitro 2D drug screening are reported in the graphs as mean percentage of cell viability, with respect to cells only  $\pm$  standard deviation, and they were analysed using two-way analysis of variance (two-way ANOVA) and Dunnett's multiple comparisons test. The MTT results were further analysed using one-way analysis of variance (one-way ANOVA) and Dunnett's multiple comparisons test.  $\text{IC}_{50}$  values were calculated as  $\text{Log}(\text{inhibitor})$  versus mean percentage of dead cells, with respect to cells only, and the obtained values are reported in the graphs  $\pm 95\%$  confidence interval (CI) for each cell line. The MTT results for the 3D tumour engineered models of osteosarcoma were reported in the graph as percentage mean  $\pm$  standard error of the mean, and they were analysed with two-way ANOVA and Dunnett's multiple comparisons test. A further analysis was performed using the unpaired *t*-test on all drugs, with respect to cisplatin.



### 3.5. Synthetic Procedures

Compounds **7–10** and **15–20** were synthesised as reported by us [22].

#### *N*-(β-D-glucopyranosyl-1,2,3-triazol-4-yl)-propanoic acid (**11**)

**9** (0.612 g, 1.29 mmol) was suspended in a mixture of methanol (6 mL) and water (3 mL) and heated at 45 °C. NEt<sub>3</sub> (0.2 mL) was added, and the reaction was allowed to stir overnight. The progress was checked using TLC (95:5 DCM:MeOH). The solvent was removed under vacuum and the residue was redissolved in H<sub>2</sub>O and stirred with Amberlite H<sup>+</sup> resin for 40 min. The Amberlite was filtered, and the residue was dried via lyophilization and reacted in the following step without further purification (0.375 g, 1.04 mmol, 95%). *R*<sub>f</sub> = 0.40 (DCM:MeOH:H<sub>2</sub>O 60:35:5). [α]<sub>D</sub><sup>21.4</sup> +1.12 (c 0.825, MeOH). <sup>1</sup>H NMR (500 MHz, D<sub>2</sub>O) δ 7.97 (s, 1H, triaz-CH), 5.67 (d, *J* = 9.2 Hz, 1H, H-1), 3.95 (t, *J* = 9.2 Hz, 1H, H-2), 3.87 (dd, *J* = 12.4, 2.0 Hz, 1H, H-6), 3.77–3.64 (m, 3H, H-3, H-6', H-5), 3.62–3.56 (m, 1H, H-4), 2.96 (t, *J* = 7.4 Hz, 2H, triaz-CH<sub>2</sub>), 2.55 (t, *J* = 7.4 Hz, 2H, CH<sub>2</sub>CO). <sup>13</sup>C NMR (125 MHz, D<sub>2</sub>O) δ 180.90 (CO), 147.92 (triaz-C), 122.15 (triaz-CH), 87.35 (C-1), 78.79 (C-5), 75.87 (C-3), 72.22 (C-2), 68.92 (C-4), 60.40 (C-6), 36.18 (CH<sub>2</sub>CO), 21.49 (triaz-CH<sub>2</sub>). IR (ATR) 3256.84, 2915.58, 1567.38, 1396.39, 1042.54, 898.47, 599.49 cm<sup>-1</sup>. HR-MS (+): *m/z* calcd for C<sub>11</sub>H<sub>17</sub>N<sub>3</sub>O<sub>7</sub> + H<sup>+</sup> [M + H]<sup>+</sup> 304.1145, found 304.1140. HR-MS (+): *m/z* calcd for C<sub>11</sub>H<sub>17</sub>N<sub>3</sub>O<sub>7</sub> + Na<sup>+</sup> [M + Na]<sup>+</sup> 326.0964, found 326.0958.

#### *N*-(β-D-glucopyranosyl-1,2,3-triazol-4-yl)-(3-oxopropyl-(oxy(2,5-dioxopyrrolidin-1-yl))) (**13**)

**11** (0.2 g, 0.659 mmol) was added to a flask containing TSTU (0.218 g, 0.725 mmol, 1.1 equiv.) and placed under N<sub>2</sub>. Anhydrous DMF (10 mL) and anhydrous Triethylamine (0.101 mL, 0.725 mmol, 1.1 equiv.) were added. The reaction was stirred for 20 min, and reaction progress was monitored by TLC (60:35:5 DCM:MeOH:H<sub>2</sub>O). The solvent was removed in vacuo and the residue was washed with DCM. The precipitate was collected via centrifugation and dried, yielding a light pink powder (Yield 0.182 g, 0.454 mmol, 68%). *R*<sub>f</sub> = 0.92 (DCM:MeOH:H<sub>2</sub>O 60:35:5). [α]<sub>D</sub><sup>25.5</sup> + 3.75 (c 0.8, H<sub>2</sub>O). <sup>1</sup>H NMR (500 MHz, DMSO) δ 8.11 (s, 1H, triaz-CH), 5.48 (d, *J* = 9.3 Hz, 1H, H-1), 5.32 (d, *J* = 6.0 Hz, 1H, OH of C-2), 5.26 (d, *J* = 4.6 Hz, 1H, OH of C-3), 5.14 (d, *J* = 5.4 Hz, 1H, OH of C-4), 4.62 (s, 1H, OH of C-6), 3.74–3.66 (m, 2H, H-2, H-6), 3.43 (d, *J* = 7.6 Hz, 2H, H-6', H-5), 3.39 (dd, *J* = 8.9, 3.9 Hz, 1H, H-3), 3.21 (dt, *J* = 13.9, 7.0 Hz, 1H, H-4), 3.10–3.05 (m, 2H, CH<sub>2</sub>CO), 3.02–2.98 (m, 2H, triaz-CH<sub>2</sub>), 2.82 (s, 4H, CH<sub>2</sub>CH<sub>2</sub>-succ) ppm. <sup>13</sup>C NMR (125 MHz, DMSO) δ 170.25 (CO succ × 2), 168.38 (CO), 144.37 (triaz-C), 121.40 (triaz-CH), 87.44 (C-1), 79.92 (C-5), 76.95 (C-3), 72.16 (C-2), 69.60 (C-4), 60.74 (C-6), 29.58 (CH<sub>2</sub>CO), 25.47 (CH<sub>2</sub>CH<sub>2</sub>-succ), 20.27 (triaz-CH<sub>2</sub>) ppm. IR (ATR) 3298.62, 2917.68, 1731.73, 1708.88, 1406.06, 1367.70, 1206.78, 1019.20, 818.67, 647.68 cm<sup>-1</sup>. HR-MS (+): *m/z* calcd for C<sub>15</sub>H<sub>20</sub>N<sub>4</sub>O<sub>9</sub> + H<sup>+</sup> [M + H]<sup>+</sup> 401.1309, found 401.1300. HR-MS (+): *m/z* calcd for C<sub>15</sub>H<sub>20</sub>N<sub>4</sub>O<sub>9</sub> + Na<sup>+</sup> [M + Na]<sup>+</sup> 423.1128, found 423.1119.

#### [Pt<sup>IV</sup>(NH<sub>3</sub>)<sub>2</sub>(11)(OH)Cl<sub>2</sub>] (**1**)

**13** (0.321 g, 0.801 mmol) dissolved in DMSO (15 mL) was added dropwise overnight to a suspension of Oxoplatin (0.280 g, 0.841 mmol, 1.05 equiv.) in DMSO (5 mL) and stirred in the dark at 40 °C for 48 h. The yellow suspension was filtered and the DMSO was evaporated via lyophilization. The remaining oil was treated with methanol (10 mL) and the white/yellow precipitate that was formed was washed with DCM and diethyl ether. The product was dried under reduced pressure (Yield 0.293 g, 0.473 mmol, 59%). [α]<sub>D</sub><sup>22.5</sup> +2.22 (c 0.9, H<sub>2</sub>O). <sup>1</sup>H NMR (500 MHz, DMSO) δ 8.06 (s, 1H, triaz-CH), 6.17–5.79 (m, 6H, 2x NH<sub>3</sub>), 5.44 (d, *J* = 9.3 Hz, 1H, H-1), 5.32 (d, *J* = 6.0 Hz, 1H, OH of C-2), 5.27 (d, *J* = 4.8 Hz, 1H, OH of C-3), 5.14 (d, *J* = 5.4 Hz, 1H, OH of C-4), 4.63 (t, *J* = 5.6 Hz, 1H, OH of C-6), 3.77–3.65 (m, 2H, H-2, H-6), 3.43 (dt, *J* = 11.9, 4.9 Hz, 3H, H-6', H-3, H-5), 3.21 (dd, *J* = 8.9, 5.2 Hz, 1H, H-4), 2.83 (t, *J* = 7.6 Hz, 2H, triaz-CH<sub>2</sub>), 2.49 (m, 2H, CH<sub>2</sub>CO). <sup>13</sup>C NMR (125 MHz, DMSO) δ 179.89 (CO), 146.33 (triaz-C), 121.23 (triaz-CH), 87.42 (C-1), 79.90 (C-5), 76.97 (C-3), 72.01 (C-2), 69.60 (C-4), 60.77 (C-6), 35.96 (CH<sub>2</sub>CO), 21.93 (triaz-CH<sub>2</sub>). <sup>195</sup>Pt{<sup>1</sup>H} NMR (108 MHz, DMSO) δ 1047.07 ppm. IR (ATR) 3221.35, 1619.15, 1351.11, 1094.74, 579.32, 438.05 cm<sup>-1</sup>. HR-MS (+): *m/z* calcd for C<sub>11</sub>H<sub>23</sub>Cl<sub>2</sub>N<sub>5</sub>O<sub>8</sub>Pt + H<sup>+</sup> [M + H]<sup>+</sup> 619.0644, found

620.0639. El. Anal. Calcd. for  $C_{11}H_{23}Cl_2N_5O_8Pt$ : % C = 21.33; H = 3.74; N = 11.31; found: % C = 21.85; H = 3.39; N = 11.82.

***N*-(β-D-galactopyranosyl-1,2,3-triazol-4-yl)-propanoic acid (12)**

Compound 12 was synthesised according to the procedure reported for compound 11 (Yield 0.098 g, 0.323 mmol, 97%).  $R_f = 0.51$  (DCM:MeOH:H<sub>2</sub>O 60:35:5)  $[\alpha]_D^{23.7} + 16$  (c 0.625, MeOH). <sup>1</sup>H NMR (500 MHz, D<sub>2</sub>O) δ 7.96 (s, 1H, triaz-CH), 5.55 (d, *J* = 9.2 Hz, 1H, H-1), 4.11 (t, *J* = 9.5 Hz, 1H, H-2), 3.99 (dd, *J* = 3.3, 0.7 Hz, 1H, H-4), 3.89 (td, *J* = 6.0, 0.8 Hz, 1H, H-5), 3.78 (dd, *J* = 9.8, 3.3 Hz, 1H, H-3), 3.69 (d, *J* = 6.2 Hz, 2H, H-6, H-6'), 2.89 (t, *J* = 7.4 Hz, 2H, triaz-CH<sub>2</sub>), 2.52 (t, *J* = 7.4 Hz, 2H, CH<sub>2</sub>CO). <sup>13</sup>C NMR (125 MHz, D<sub>2</sub>O) δ 179.95 (CO), 147.63 (C-triaz), 121.90 (CH-triaz), 87.93 (C-1), 78.16 (C-5), 72.92 (C-3), 69.63 (C-2), 68.52 (C-4), 60.78 (C-6), 35.46 (CH<sub>2</sub>CO), 21.20 (triaz-CH<sub>2</sub>). IR (ATR) 3247.67, 1565.21, 1399.66, 1053.32, 883.22, 553.54 cm<sup>-1</sup>. HR-MS (+): *m/z* calcd for  $C_{11}H_{17}N_3O_7 + H^+$  [M + H]<sup>+</sup> 304.1145, found 304.1138. HR-MS (+): *m/z* calcd for  $C_{11}H_{17}N_3O_7 + Na^+$  [M + Na]<sup>+</sup> 326.0964, found 326.0956.

***N*-(β-D-galactopyranosyl-1,2,3-triazol-4-yl)-(3-oxopropyl-(oxy(2,5-dioxopyrrolidin-1-yl))) (14)**

Compound 14 was prepared according to the method reported for compound 13 (Yield 0.204 g, 0.509 mmol, 68%).  $R_f = 0.9$  (DCM:MeOH:H<sub>2</sub>O 60:35:5).  $[\alpha]_D^{23.5} - 4.28$  (c 0.7, H<sub>2</sub>O). <sup>1</sup>H NMR (500 MHz, DMSO) δ 8.07 (s, 1H, triaz-CH), 5.44 (d, *J* = 9.2 Hz, 1H, H-1), 5.16 (d, *J* = 6.0 Hz, 1H, OH of C-2), 5.03 (d, *J* = 5.7 Hz, 1H, OH of C-3), 4.70 (t, *J* = 5.7 Hz, 1H, OH of C-6), 4.66 (d, *J* = 4.9 Hz, 1H, OH of C-4), 4.03–3.96 (m, 1H, H-2), 3.76 (t, *J* = 3.75 Hz, 1H, H-4), 3.70 (t, *J* = 6.1 Hz, 1H, H-5), 3.56–3.44 (m, 3H, H-3, H-6, H-6'), 3.09 (t, *J* = 7.0 Hz, 2H, CH<sub>2</sub>CO), 3.02–2.99 (m, 2H, triaz-CH<sub>2</sub>), 2.82 (s, 2H, CH<sub>2</sub>CH<sub>2</sub>-succ). <sup>13</sup>C NMR (125 MHz, DMSO) δ 170.23 (CO succ ×2), 168.39 (CO), 144.42 (triaz-C), 121.12 (triaz-CH), 88.06 (C-1), 78.37 (C-5), 73.670 (C-3), 69.32 (C-2), 68.42 (C-4), 60.45 (C-6), 29.59 (CH<sub>2</sub>CO), 25.46 (CH<sub>2</sub>CH<sub>2</sub>-succ), 20.28 (triaz-CH<sub>2</sub>) ppm. IR (ATR) 3309.24, 2917.95, 1731.99, 1368.41, 1205.61, 1020.46, 891.00, 820.54, 647.48 cm<sup>-1</sup>. HR-MS (+): *m/z* calcd for  $C_{15}H_{20}N_4O_9 + H^+$  [M + H]<sup>+</sup> 401.1309, found 401.1305. HR-MS (+): *m/z* calcd for  $C_{15}H_{20}N_4O_9 + Na^+$  [M + Na]<sup>+</sup> 423.1128, found 423.1127.

**[Pt<sup>IV</sup>(NH<sub>3</sub>)<sub>2</sub>(12)(OH)Cl<sub>2</sub>] (2)**

Complex 2 was synthesised according to the method reported for complex 1 (Yield 0.111 g, 0.179 mmol, 35%).  $[\alpha]_D^{23.5} + 10$  (c 0.9, H<sub>2</sub>O). <sup>1</sup>H NMR (500 MHz, DMSO) δ 8.00 (s, 1H, triaz-CH), 6.11–5.80 (br t, 6H, 2x NH<sub>3</sub>), 5.39 (d, *J* = 9.2 Hz, 1H, H-1), 5.18 (d, *J* = 5.9 Hz, 1H, OH of C-2), 5.03 (d, *J* = 5.6 Hz, 1H, OH of C-3), 4.70 (t, *J* = 5.6 Hz, 1H, OH of C-6), 4.64 (d, *J* = 5.1 Hz, 1H, OH of C-4), 4.05–3.98 (m, 1H, H-2), 3.75 (t, *J* = 3.6 Hz, 1H, H-4), 3.68 (t, *J* = 5.9 Hz, 1H, H-5), 3.56–3.47 (m, 3H, H-3, H-6, H-6'), 2.83 (t, *J* = 7.45 Hz, 2H, triaz-CH<sub>2</sub>), 2.53–2.51 (m, 2H, CH<sub>2</sub>CO, overlaps with DMSO). <sup>13</sup>C NMR (125 MHz, DMSO) δ 179.90 (CO), 146.35 (triaz-C), 120.97 (triaz-CH), 88.01 (C-1), 78.35 (C-5), 73.73 (C-3), 69.19 (C-2), 68.46 (C-4), 60.47 (C-6), 36.01 (CH<sub>2</sub>CO), 21.94 (triaz-CH<sub>2</sub>). <sup>195</sup>Pt(<sup>1</sup>H) NMR (108 MHz, DMSO) δ 1045.09 ppm. IR (ATR) 3224.69, 1617.95, 1352.08, 1090.21, 890.51, 563.88, 437.95 cm<sup>-1</sup>. HR-MS (+): *m/z* calcd for  $C_{11}H_{23}Cl_2N_5O_8Pt + H^+$  [M + H]<sup>+</sup> 619.0644, found 620.0634. El. Anal. Calcd. for  $C_{11}H_{23}Cl_2N_5O_8Pt$ : % C = 21.33; H = 3.74; N = 11.31; found: % C = 21.64; H = 3.82; N = 11.72.

***N*-(2-O-(β-D-glucopyranosyl)-ethyl-1,2,3-triazol-4-yl)-propanoic acid (21)**

Compound 21 was synthesised according to the procedure used for compound 11 (Yield 0.053 g, 0.152 mmol, 89%).  $R_f = 0.56$  (DCM:MeOH:H<sub>2</sub>O 60:35:5).  $[\alpha]_D^{24.4} + 4.18$  (c 0.716, MeOH). <sup>1</sup>H NMR (500 MHz, D<sub>2</sub>O) δ 7.80 (s, 1H, triaz-CH), 4.57 (dd, *J* = 14.3, 3.5 Hz, 2H, CH<sub>2</sub>-triaz), 4.35 (d, *J* = 6.8 Hz, 1H, H-1), 4.27–4.20 (m, 1H, OCH), 4.05 (dt, *J* = 6.2, 4.1 Hz, 1H, OCH'), 3.84 (d, *J* = 12.3 Hz, 1H, H-6), 3.67–3.60 (m, 1H, H-6'), 3.43–3.27 (m, 3H, H-3, H-4, H-5), 3.21–3.18 (m, 5H, H-2), 2.92 (td, *J* = 7.3, 1.3 Hz, 2H, triaz-CH<sub>2</sub>), 2.53 (t, *J* = 7.4 Hz, 2H, CH<sub>2</sub>CO). <sup>13</sup>C NMR (125 MHz, D<sub>2</sub>O) δ 180.75 (CO), 147.40 (triaz-C), 123.72 (triaz-CH), 102.38 (C-1), 75.87 (C-3), 75.55 (C-5), 72.89 (C-2), 69.51 (C-4), 68.09 (OCH<sub>2</sub>), 60.65 (C-6), 50.11 (CH<sub>2</sub>-triaz), 36.01 (CH<sub>2</sub>CO), 21.38 (triaz-CH<sub>2</sub>). IR (ATR) 3334.48, 2885.68, 1711.54, 1553.96, 1358.20, 1219.58, 1030.84, 828.66, 494.93 cm<sup>-1</sup>. HR-MS (+): *m/z* calcd for  $C_{13}H_{21}N_3O_8 + H^+$  [M + H]<sup>+</sup> 348.1407, found 348.1402. HR-MS (+): *m/z* calcd for  $C_{13}H_{21}N_3O_8 + Na^+$  [M + Na]<sup>+</sup> 370.1226, found 370.1218.



**N-[2-O-(β-D-glucopyranosyl)-ethyl-1,2,3-triazol-4-yl]-[3-oxopropyl-(oxy(2,5-dioxopyrrolidin-1-yl))] (23)**

Compound 23 was synthesised according to the procedure for compound 13. (Yield 0.380 g, 0.855 mmol, 80%).  $R_f = 0.86$  (DCM:MeOH:H<sub>2</sub>O 60:35:5).  $[\alpha]_D^{23} + 1.07$  (c 0.93, MeOH). <sup>1</sup>H NMR (500 MHz, DMSO) δ 7.99 (s, 1H, triaz-CH), 5.10 (d, *J* = 5.0 Hz, 1H, OH of C-2), 4.99 (d, *J* = 4.8 Hz, 1H, OH of C-3), 4.94 (d, *J* = 5.3 Hz, 1H, OH of C-4), 4.52 (dt, *J* = 6.8, 4.2 Hz, 3H, CH<sub>2</sub>-triaz, OH of C-6), 4.21 (d, *J* = 7.8 Hz, 1H, H-1), 4.06 (ddd, *J* = 10.6, 5.9, 4.4 Hz, 1H, OCH), 3.86 (ddd, *J* = 11.2, 6.7, 4.4 Hz, 1H, OCH'), 3.67 (ddd, *J* = 11.5, 5.9, 1.8 Hz, 1H, H-6), 3.43 (dt, *J* = 11.7, 5.9 Hz, 1H, H-6'), 3.16–3.08 (m, 2H, H-3, H-5), 3.08–3.01 (m, 3H, CH<sub>2</sub>CO, H-4), 3.00–2.93 (m, 3H, H-2, triaz-CH<sub>2</sub>), 2.81 (s, 4H, CH<sub>2</sub>CH<sub>2</sub>-succ). <sup>13</sup>C NMR (125 MHz, DMSO) δ 170.20 (CO succ x2), 168.33 (CO), 144.17 (triaz-C), 123.18 (triaz-CH), 102.86 (C-1), 76.97 (C-3), 76.57 (C-5), 73.31 (C-2), 70.01 (C-4), 67.31 (OCH<sub>2</sub>), 61.08 (C-6), 49.54 (CH<sub>2</sub>-triaz), 29.81 (CH<sub>2</sub>CO), 25.45 (CH<sub>2</sub>CH<sub>2</sub>-succ), 20.37 (triaz-CH<sub>2</sub>). IR (ATR) 3369.66, 2886.72, 1728.66, 1366.57, 1206.12, 1033.96, 813.22, 645.50 cm<sup>-1</sup>. HR-MS (+): *m/z* calcd for C<sub>17</sub>H<sub>24</sub>N<sub>4</sub>O<sub>10</sub> + H<sup>+</sup> [M + H]<sup>+</sup> 445.1571, found 445.1561. HR-MS (+): *m/z* calcd for C<sub>17</sub>H<sub>24</sub>N<sub>4</sub>O<sub>10</sub> + Na<sup>+</sup> [M + Na]<sup>+</sup> 467.1390, found 467.1384.

**[Pt<sup>IV</sup>(NH<sub>3</sub>)<sub>2</sub>(21)(OH)Cl<sub>2</sub>] (3)**

Complex 3 prepared according to the method reported for complex 1. (Yield 0.218 g, 0.328 mmol, 47%).  $[\alpha]_D^{21.8} + 15$  (c 0.4, H<sub>2</sub>O). <sup>1</sup>H NMR (500 MHz, DMSO) δ 7.93 (s, 1H, triaz-CH), 5.98 (t, *J* = 48.2 Hz, 6H, 2x NH<sub>3</sub>), 5.10 (d, *J* = 4.9 Hz, 1H, OH of C-2), 4.98 (d, *J* = 4.7 Hz, 1H, OH of C-3), 4.93 (d, *J* = 5.2 Hz, 1H, OH of C-4), 4.57–4.46 (m, 3H, CH<sub>2</sub>-triaz, OH of C-6), 4.21 (d, *J* = 7.8 Hz, 1H, H-1), 4.10–4.03 (m, 1H, OCH), 3.89–3.83 (m, 1H, OCH'), 3.67 (dd, *J* = 10.7, 4.4 Hz, 1H, H-6), 3.43 (dd, *J* = 11.4, 5.6 Hz, 1H, H-6'), 3.16–3.09 (m, 2H, H-3, H-5), 3.03 (dd, *J* = 9.0, 4.0 Hz, 1H, H-4), 2.98–2.93 (m, 1H, H-2), 2.80 (t, *J* = 7.2 Hz, 2H, triaz-CH<sub>2</sub>), 2.46 (d, *J* = 7.3 Hz, 2H, CH<sub>2</sub>CO). <sup>13</sup>C NMR (125 MHz, DMSO) δ 179.94 (CO), 146.18 (triaz-C), 122.90 (triaz-CH), 102.82 (C-1), 76.95 (C-3), 76.54 (C-5), 73.32 (C-2), 69.99 (C-4), 67.27 (OCH<sub>2</sub>), 61.06 (C-6), 49.42 (CH<sub>2</sub>-triaz), 36.12 (CH<sub>2</sub>CO), 22.01 (triaz-CH<sub>2</sub>). <sup>195</sup>Pt{<sup>1</sup>H} NMR (108 MHz, DMSO) δ 1047.34 ppm. IR (ATR) 3247.15, 1623.71, 1356.54, 1035.26, 578.92, 426.46 cm<sup>-1</sup>. HR-MS (+): *m/z* calcd for C<sub>13</sub>H<sub>27</sub>Cl<sub>2</sub>N<sub>5</sub>O<sub>9</sub>Pt + H<sup>+</sup> [M + H]<sup>+</sup> 663.0907, found 664.0904. EL Anal. Calcd. for C<sub>13</sub>H<sub>27</sub>Cl<sub>2</sub>N<sub>5</sub>O<sub>9</sub>Pt: % C = 23.54; H = 4.10; N = 10.56; found: % C = 23.27; H = 4.91; N = 10.11.

**N-[2-O-(β-D-galactopyranosyl)-ethyl-1,2,3-triazol-4-yl]-propanoic acid(22)**

Compound 22 was prepared according to the procedure reported for compound 11 (Yield 0.231 g, 0.665 mmol, 96%).  $R_f = 0.30$  (DCM:MeOH:H<sub>2</sub>O 60:35:5).  $[\alpha]_D^{23} + 4.24$  (c 0.707, MeOH). <sup>1</sup>H NMR (500 MHz, D<sub>2</sub>O) δ 7.85 (s, 1H, triaz-CH), 4.61 (t, *J* = 5.1 Hz, 2H, CH<sub>2</sub>-triaz), 4.31 (d, *J* = 7.9 Hz, 1H, H-1), 4.26 (dt, *J* = 11.5, 4.7 Hz, 1H, OCH), 4.09–4.04 (m, 1H, OCH'), 3.87 (d, *J* = 3.4 Hz, 1H, H-4), 3.75–3.67 (m, 2H, H-6, H-6'), 3.62 (dd, *J* = 7.7, 4.6 Hz, 1H, H-5), 3.58 (dd, *J* = 9.9, 3.5 Hz, 1H, H-3), 3.45 (dd, *J* = 9.9, 7.9 Hz, 1H, H-2), 2.96 (t, *J* = 7.3 Hz, 2H, triaz-CH<sub>2</sub>), 2.65 (t, *J* = 7.3 Hz, 2H, CH<sub>2</sub>CO). <sup>13</sup>C NMR (125 MHz, D<sub>2</sub>O) δ 178.90 (CO), 146.93 (C-triaz), 123.87 (CH-triaz), 102.97 (C-1), 75.08 (C-5), 72.58 (C-3), 70.55 (C-2), 68.53 (C-4), 68.02 (OCH<sub>2</sub>), 60.87 (C-6), 50.19 (CH<sub>2</sub>-triaz), 34.49 (CH<sub>2</sub>CO), 20.72 (triaz-CH<sub>2</sub>). IR (ATR) 3282.63, 2926.54, 1568.45, 1398.02, 1044.17, 781.51, 533.03 cm<sup>-1</sup>. HR-MS (+): *m/z* calcd for C<sub>13</sub>H<sub>21</sub>N<sub>3</sub>O<sub>8</sub> + H<sup>+</sup> [M + H]<sup>+</sup> 348.1407, found 348.1403. HR-MS (+): *m/z* calcd for C<sub>13</sub>H<sub>21</sub>N<sub>3</sub>O<sub>8</sub> + Na<sup>+</sup> [M + Na]<sup>+</sup> 370.1226, found 370.1221.

**N-[2-O-(β-D-galactopyranosyl)-ethyl-1,2,3-triazol-4-yl]-[3-oxopropyl-(oxy(2,5-dioxopyrrolidin-1-yl))] (24)**

Compound 24 was prepared according to the procedure reported for compound 13 (Yield 0.360 g, 0.810 mmol, 75%).  $R_f = 0.84$  (DCM:MeOH:H<sub>2</sub>O 60:35:5).  $[\alpha]_D^{28} + 5.5$  (c 0.366, MeOH). <sup>1</sup>H NMR (500 MHz, DMSO) δ 7.99 (s, 1H, triaz-CH), 4.95 (d, *J* = 4.6 Hz, 1H, OH of C-2), 4.76 (d, *J* = 5.3 Hz, 1H, OH of C-3), 4.59 (t, *J* = 5.7 Hz, 1H, OH of C-6), 4.51 (qdd, *J* = 14.3, 6.4, 4.2 Hz, 2H, CH<sub>2</sub>-triaz), 4.39 (d, *J* = 4.6 Hz, 1H, OH of C-4), 4.15 (d, *J* = 7.3 Hz, 1H, H-1), 4.05 (ddd, *J* = 10.7, 6.2, 4.3 Hz, 1H, OCH), 3.83 (ddd, *J* = 11.1, 6.7, 4.3 Hz, 1H, OCH'), 3.63–3.60 (m, 1H, H-4), 3.55–3.44 (m, 2H, H-6, H-6'), 3.34–3.24 (m, 3H, H-2, H-5, H-3), 3.07–3.03 (m, 2H, CH<sub>2</sub>CO), 3.00–2.95 (m, 2H, triaz-CH<sub>2</sub>), 2.81 (s, 4H, CH<sub>2</sub>CH<sub>2</sub>-succ).



$^{13}\text{C}$  NMR (125 MHz, DMSO)  $\delta$  170.22 (CO succ x2), 168.35 (CO), 144.19 (triaz-C), 123.16 (triaz-CH), 103.48 (C-1), 75.37 (C-5), 73.30 (C-3), 70.41 (C-2), 68.15 (C-4), 67.20 (OCH<sub>2</sub>), 60.46 (C-6), 49.56 (CH<sub>2</sub>-triaz), 29.82 (CH<sub>2</sub>CO), 25.46 (CH<sub>2</sub>CH<sub>2</sub>-succ), 20.38 (triaz-CH<sub>2</sub>). IR (ATR) 3378.02, 2939.53, 1728.86, 1366.45, 1206.01, 1046.41, 648.73 cm<sup>-1</sup>. HR-MS (+):  $m/z$  calcd for C<sub>17</sub>H<sub>24</sub>N<sub>4</sub>O<sub>10</sub> + H<sup>+</sup> [M + H]<sup>+</sup> 445.1571, found 445.1559. HR-MS (+):  $m/z$  calcd for C<sub>17</sub>H<sub>24</sub>N<sub>4</sub>O<sub>10</sub> + Na<sup>+</sup> [M + Na]<sup>+</sup> 467.1390, found 467.1385.

**[Pt<sup>IV</sup>(NH<sub>3</sub>)<sub>2</sub>(22)(OH)Cl<sub>2</sub>] (4)**

Complex 4 was prepared according to the procedure reported for complex 1 (Yield 0.296 g, 0.446 mmol, 61%).  $[\alpha]_D^{22} + 3.36$  (c 0.9, H<sub>2</sub>O).  $^1\text{H}$  NMR (500 MHz, DMSO)  $\delta$  7.93 (s, 1H, triaz-CH), 5.98 (t,  $J = 48.4$  Hz, 6H, 2 × NH<sub>3</sub>), 4.96 (d,  $J = 4.3$  Hz, 1H, OH of C-3), 4.77 (d,  $J = 4.4$  Hz, 1H, OH of C-2), 4.59 (d,  $J = 5.1$  Hz, 1H, OH of C-6), 4.55–4.41 (m, 2H, CH<sub>2</sub>-triaz), 4.40 (d,  $J = 4.4$  Hz, 1H, OH of C-4), 4.15 (d,  $J = 7.1$  Hz, 1H, H-1), 4.05 (ddd,  $J = 14.4, 9.4, 6.4$  Hz, 1H, OCH), 3.84 (ddd,  $J = 11.0, 6.5, 4.6$  Hz, 1H, OCH'), 3.62 (s, 1H, H-4), 3.50 (dd,  $J = 12.2, 6.4$  Hz, 2H, H-6, H-6'), 3.35 (s, 1H, H-5 overlaps with H<sub>2</sub>O), 3.30–3.27 (m, 2H, H-2, H-3), 2.82–2.77 (m, 2H, triaz-CH<sub>2</sub>), 2.46 (d,  $J = 7.3$  Hz, 2H, CH<sub>2</sub>CO).  $^{13}\text{C}$  NMR (125 MHz, DMSO)  $\delta$  179.93 (CO), 146.19 (triaz-C), 122.88 (triaz-CH), 103.48 (C-1), 75.37 (C-5), 73.27 (C-3), 70.43 (C-2), 68.15 (C-4), 67.19 (OCH<sub>2</sub>), 60.46 (C-6), 49.46 (CH<sub>2</sub>-triaz), 36.12 (CH<sub>2</sub>CO), 22.01 (triaz-CH<sub>2</sub>).  $^{195}\text{Pt}$  NMR (108 MHz, DMSO)  $\delta$  1046.82 ppm. IR (ATR) 3215.30, 1618.19, 1358.28, 1061.49, 575.94 cm<sup>-1</sup>. HR-MS (+):  $m/z$  calcd for C<sub>13</sub>H<sub>27</sub>Cl<sub>2</sub>N<sub>5</sub>O<sub>9</sub>Pt + H<sup>+</sup> [M + H]<sup>+</sup> 663.0907, found 664.0902. El. Anal. Calcd. for C<sub>13</sub>H<sub>27</sub>Cl<sub>2</sub>N<sub>5</sub>O<sub>9</sub>Pt: % C = 23.54; H = 4.10; N = 10.56; found: % C = 23.18; H = 4.75; N = 10.06.

#### 4. Conclusions

Four novel Pt(IV) pro-drugs, based on a cisplatin scaffold with carbohydrate vectors in axial positions, were synthesised, linking the sugar moiety and the metal centre via CuAAC click chemistry. These pro-drugs were functionalised with deprotected glyco-moieties that act as real vectors to selectively target cancer cells. Most of the carbohydrate-functionalised Pt-based complexes reported in literature contain protected acetylated sugars, due to an easy synthesis and purification procedure. The complexes were tested on a panel of two 2D and 3D OS (Osteosarcoma) cell lines, as well as on healthy OS cells. All the complexes showed very promising activity, comparable to the reference cisplatin, demonstrating that the presence of a monosaccharide does not hamper the anticancer effect. Notably, the complexes are much less active against the healthy line, showing a promising selectivity for these OS cell lines, with respect to cisplatin. The complexes were also particularly active in the 3D model, a more reliable system compared to 2D, with the most promising activity shown by complexes 2 and 4 with a galactose substituent. The role of galactose in the metabolism of cancer cells is attracting significant attention because of potential diagnostic and therapeutic possibilities [40,41]. While the role of the free sugars as targeting vectors is not completely confirmed, the selectivity shown in 2D studies is a solid base to hypothesise that the carbohydrate moieties play an important role in targeted therapies. More specific biological studies (beyond the scope of this work) should be conducted (i.e., inhibition of the GLUTs receptors), but this selectivity was not observed in the analogue protected-Pt(IV) pro-drugs, recently reported by us. While all the complexes showed very promising activity, the discrimination between the two linkers is not observed. These complexes have been conjugated to graphene oxide nanoparticles that act as delivering agents, to further enhance the selectivity. The next step in our studies is the synthesis and characterisation of analogous complexes, where the carbohydrate is conjugated via the C2 carbon (not the anomeric carbon) that was demonstrated to be the best in term of cellular recognition [42].

**Supplementary Materials:** The following supporting information can be downloaded at: <https://www.mdpi.com/article/10.3390/ijms24076028/s1>.

**Author Contributions:** Conceptualization, D.M., T.V.-T., M.M. and E.M.; methodology, D.M., E.M. and M.M.; formal analysis, E.M., G.B., A.R., E.C. and E.D.; investigation, E.M., G.B. and A.R.; curation, D.M., S.P. and M.M.; writing—original draft preparation, D.M., T.V.-T., E.M., M.M. and G.B.; supervision, D.M., T.V.-T. and M.M.; funding acquisition, D.M. and S.P. All authors have read and agreed to the published version of the manuscript.

**Funding:** This work was funded by the European Project Horizon 2020 NANO4TARMED (H2020-WIDESPREAD-2020-5; GA number 952063).

**Data Availability Statement:** The data presented in this study are available in the article and in the Supplementary Material.

**Acknowledgments:** E.M. is grateful to Maynooth University for sponsoring postgrad scholarship with a Graduate Teaching Fellowship. Science Foundation Ireland 2012 Strategic Opportunity Fund (Infrastructure award 12/RI/2346/SOF) for NMR facilities.

**Conflicts of Interest:** The authors declare that the research was conducted in the absence of any commercial or financial relationships that could be construed as a potential conflict of interest.

## References

- Mortensen, A.C.L.; Mohajershojai, T.; Hariri, M.; Pettersson, M.; Spiegelberg, D. Overcoming Limitations of Cisplatin Therapy by Additional Treatment With the HSP90 Inhibitor Onalespib. *Front. Oncol.* **2020**, *10*, 532285. [CrossRef] [PubMed]
- Zhang, C.; Xu, C.; Gao, X.; Yao, Q. Platinum-based drugs for cancer therapy and anti-tumor strategies. *Theranostics* **2022**, *12*, 2115–2132. [CrossRef] [PubMed]
- Kenny, R.G.; Marmion, C.J. Toward Multi-Targeted Platinum and Ruthenium Drugs—A New Paradigm in Cancer Drug Treatment Regimens? *Chem. Rev.* **2019**, *119*, 1058–1137. [CrossRef] [PubMed]
- Fronik, P.; Gutmann, M.; Vician, P.; Stojanovic, M.; Kastner, A.; Heffeter, P.; Pirker, C.; Keppler, B.K.; Berger, W.; Kowol, C.R. A platinum(IV) prodrug strategy to overcome glutathione-based oxaliplatin resistance. *Commun. Chem.* **2022**, *5*, 46. [CrossRef] [PubMed]
- Harrap, K.R.; Kelland, L.R.; Jones, M.; Goddard, P.M.; Orr, R.M.; Morgan, S.E.; Murrer, B.A.; Abrams, M.J.; Giandomenico, C.M.; Cobbleigh, T. Platinum coordination complexes which circumvent cisplatin resistance. *Adv. Enzym. Regul.* **1991**, *31*, 31–43. [CrossRef]
- Bhargava, A.; Vaishampayan, U.N. Satraplatin: Leading the new generation of oral platinum agents. *Expert Opin. Investig. Drugs* **2009**, *18*, 1787–1797. [CrossRef]
- Eastman, A. Glutathione-mediated activation of anticancer platinum(IV) complexes. *Biochem. Pharmacol.* **1987**, *36*, 4177–4178. [CrossRef]
- Rischin, D.; Ling, V. Ormaplatin resistance is associated with decreased accumulation of its platinum (II) analogue, dichloro(D,L-trans)1,2-diaminocyclohexaneplatinum (II). *Br. J. Cancer* **1996**, *74*, 590–596. [CrossRef]
- Pendyala, L.; Krishnan, B.S.; Walsh, J.R.; Arakali, A.V.; Cowens, J.W.; Creaven, P.J. Studies on the Human Metabolism of Iproplatin. *Cancer Chemother. Pharmacol.* **1989**, *25*, 10–14. [CrossRef]
- Wheate, N.J.; Walker, S.; Craig, G.E.; Oun, R. The status of platinum anticancer drugs in the clinic and in clinical trials. *Dalton Trans.* **2010**, *39*, 8113–8127. [CrossRef]
- Warburg, O.; Wind, F.; Negelein, E. The metabolism of tumors in the body. *J. Gen. Physiol.* **1927**, *8*, 519. [CrossRef] [PubMed]
- Liu, C.; Jin, Y.; Fan, Z. The Mechanism of Warburg Effect-Induced Chemoresistance in Cancer. *Front. Oncol.* **2021**, *11*, 698023. [CrossRef] [PubMed]
- Ma, L.; Ma, R.; Wang, Y.; Zhu, X.; Zhang, J.; Chan, H.C.; Chen, X.; Zhang, W.; Chiu, S.-K.; Zhu, G. Chalcoplatin, a dual-targeting and p53 activator-containing anticancer platinum(IV) prodrug with unique mode of action. *Chem. Commun.* **2015**, *51*, 6301–6304. [CrossRef] [PubMed]
- Ma, J.; Yang, X.; Hao, W.; Huang, Z.; Wang, X.; Wang, P.G. Mono-functionalized glycosylated platinum(IV) complexes possessed both pH and redox dual-responsive properties: Exhibited enhanced safety and preferentially accumulated in cancer cells in vitro and in vivo. *Eur. J. Med. Chem.* **2017**, *128*, 45–55. [CrossRef] [PubMed]
- Ma, J.; Wang, Q.; Huang, Z.; Yang, X.; Nie, Q.; Hao, W.; Wang, P.G.; Wang, X. Glycosylated Platinum(IV) Complexes as Substrates for Glucose Transporters (GLUTs) and Organic Cation Transporters (OCTs) Exhibited Cancer Targeting and Human Serum Albumin Binding Properties for Drug Delivery. *J. Med. Chem.* **2017**, *60*, 5736–5748. [CrossRef]
- Ma, J.; Wang, Q.; Yang, X.; Hao, W.; Huang, Z.; Zhang, J.; Wang, X.; Wang, P.G. Glycosylated platinum(IV) prodrugs demonstrated significant therapeutic efficacy in cancer cells and minimized side-effects. *Dalton Trans.* **2016**, *45*, 11830–11838. [CrossRef]
- Ma, J.; Liu, H.; Xi, Z.; Hou, J.; Li, Y.; Niu, J.; Liu, T.; Bi, S.; Wang, X.; Wang, C.; et al. Protected and De-protected Platinum(IV) Glycoconjugates With GLUT1 and OCT2-Mediated Selective Cancer Targeting: Demonstrated Enhanced Transporter-Mediated Cytotoxic Properties in vitro and in vivo. *Front. Chem.* **2018**, *6*, 386. [CrossRef]
- Wang, Q.; Huang, Z.; Ma, J.; Lu, X.; Zhang, L.; Wang, X.; Wang, P.G. Design, synthesis and biological evaluation of a novel series of glycosylated platinum(IV) complexes as antitumor agents. *Dalton Trans.* **2016**, *45*, 10366–10374. [CrossRef]



19. Heymann, M.-F.; Lézot, F.; Heymann, D. The contribution of immune infiltrates and the local microenvironment in the pathogenesis of osteosarcoma. *Cell. Immunol.* **2019**, *343*, 103711. [[CrossRef](#)]
20. Kansara, M.; Teng, M.W.; Smyth, M.J.; Thomas, D.M. Translational biology of osteosarcoma. *Nat. Rev. Cancer* **2014**, *14*, 722–735. [[CrossRef](#)]
21. Li, C.; Cai, J.; Ge, F.; Wang, G. TGM2 knockdown reverses cisplatin chemoresistance in osteosarcoma. *Int. J. Mol. Med.* **2018**, *42*, 1799–1808. [[CrossRef](#)] [[PubMed](#)]
22. Moynihan, E.; Bassi, G.; Ruffini, A.; Panseri, S.; Montesi, M.; Velasco-Torrijos, T.; Montagner, D. Click Pt(IV)-Carbohydrates Pro-Drugs for Treatment of Osteosarcoma. *Front. Chem.* **2021**, *9*, 795997. [[CrossRef](#)] [[PubMed](#)]
23. Upadhyaya, K.; Hamidullah, H.; Singh, K.; Arun, A.; Shukla, M.; Srivastava, N.; Ashraf, R.; Sharma, A.; Mahar, R.; Shukla, S.K.; et al. Identification of gallic acid based glycoconjugates as a novel tubulin polymerization inhibitors. *Org. Biomol. Chem.* **2015**, *14*, 1338–1358. [[CrossRef](#)] [[PubMed](#)]
24. Sun, L.; Zeng, X.; Yan, C.; Sun, X.; Gong, X.; Rao, Y.; Yan, N. Crystal structure of a bacterial homologue of glucose transporters GLUT1–4. *Nature* **2012**, *490*, 361–366. [[CrossRef](#)] [[PubMed](#)]
25. Deng, D.; Xu, C.; Sun, P.; Wu, J.; Yan, C.; Hu, M.; Yan, N. Crystal structure of the human glucose transporter GLUT1. *Nature* **2014**, *510*, 121–125. [[CrossRef](#)] [[PubMed](#)]
26. Holman, G.D. Structure, function and regulation of mammalian glucose transporters of the SLC2 family. *Pflug. Arch.-Eur. J. Physiol.* **2020**, *472*, 1155–1175. [[CrossRef](#)] [[PubMed](#)]
27. Malik, M.S.; Ahmed, S.A.; Althagafi, I.I.; Ansari, M.A.; Kamal, A. Application of triazoles as bioisosteres and linkers in the development of microtubule targeting agents. *RSC Med. Chem.* **2020**, *11*, 327–348. [[CrossRef](#)]
28. Liu, X.; Barth, M.; Cseh, K.; Kowol, C.R.; Jakupec, M.A.; Keppler, B.K.; Gibson, D.; Weigand, W. Oxoplatin-Based Pt(IV) Lipocate Complexes and Their Biological Activity. *Chem. Biodivers.* **2022**, *19*, e202200695. [[CrossRef](#)]
29. Chen, C.K.J.; Kappen, P.; Gibson, D.; Hambley, T.W. *trans*-Platinum(IV) pro-drugs that exhibit unusual resistance to reduction by endogenous reductants and blood serum but are rapidly activated inside cells: <sup>1</sup>H NMR and XANES spectroscopy study. *Dalton Trans.* **2020**, *49*, 7722–7736. [[CrossRef](#)]
30. Visvader, J.E. Cells of origin in cancer. *Nature* **2011**, *469*, 314–322. [[CrossRef](#)]
31. Cifuentes, M.; García, M.A.; Arrabal, P.M.; Martínez, F.; Yañez, M.J.; Jara, N.; Weil, B.; Domínguez, D.; Medina, R.A.; Nualart, F. Insulin regulates GLUT1-mediated glucose transport in MG-63 human osteosarcoma cells. *J. Cell. Physiol.* **2011**, *226*, 1425–1432. [[CrossRef](#)]
32. Arponen, M.; Jalava, N.; Widjaja, N.; Ivaska, K.K. Glucose transporters GLUT1, GLUT3, and GLUT4 have different effects on osteoblast proliferation and metabolism. *Front. Physiol.* **2022**, *13*, 1035516. [[CrossRef](#)]
33. Horvath, P.; Aulner, N.; Bickle, M.; Davies, A.M.; Del Nery, E.; Ebner, D.; Montoya, M.C.; Östling, P.; Pietiäinen, V.; Price, L.S.; et al. Screening out irrelevant cell-based models of disease. *Nat. Rev. Drug Discov.* **2016**, *15*, 751–769. [[CrossRef](#)] [[PubMed](#)]
34. Edmondson, R.; Broglie, J.J.; Adcock, A.F.; Yang, L. Three-Dimensional Cell Culture Systems and Their Applications in Drug Discovery and Cell-Based Biosensors. *ASSAY Drug Dev. Technol.* **2014**, *12*, 207–218. [[CrossRef](#)]
35. Krishnakumar, G.S.; Gostyrnska, N.; Dapporto, M.; Campodoni, E.; Montesi, M.; Panseri, S.; Tampieri, A.; Kon, E.; Marcacci, M.; Sprio, S.; et al. Evaluation of different crosslinking agents on hybrid biomimetic collagen-hydroxyapatite composites for regenerative medicine. *Int. J. Biol. Macromol.* **2018**, *106*, 739–748. [[CrossRef](#)] [[PubMed](#)]
36. Bassi, G.; Panseri, S.; Dozio, S.M.; Sandri, M.; Campodoni, E.; Dapporto, M.; Sprio, S.; Tampieri, A.; Montesi, M. Scaffold-based 3D cellular models mimicking the heterogeneity of osteosarcoma stem cell niche. *Sci. Rep.* **2020**, *10*, 22294. [[CrossRef](#)] [[PubMed](#)]
37. Dozio, S.M.; Montesi, M.; Campodoni, E.; Sandri, M.; Piattelli, A.; Tampieri, A.; Panseri, S. Differences in osteogenic induction of human mesenchymal stem cells between a tailored 3D hybrid scaffold and a 2D standard culture. *J. Mater. Sci. Mater. Med.* **2019**, *30*, 136. [[CrossRef](#)]
38. Dhara, S.C. A Rapid Method for the Synthesis of Cis-[Pt(NH<sub>3</sub>)<sub>2</sub>Cl<sub>2</sub>]. *Indian J. Chem.* **1970**, *8*, 193–194.
39. Brandon, R.J.; Dabrowiak, J.C. Synthesis, characterization, and properties, of a group of platinum(IV) complexes. *J. Med. Chem.* **1984**, *27*, 861–865. [[CrossRef](#)]
40. Valle, S.; Alcalá, S.; Martín-Hijano, L.; Cabezas-Sáinz, P.; Navarro, D.; Muñoz, E.R.; Yuste, L.; Tiwary, K.; Walter, K.; Ruiz-Cañas, L.; et al. Exploiting oxidative phosphorylation to promote the stem and immunoevasive properties of pancreatic cancer stem cells. *Nat. Commun.* **2020**, *11*, 5265. [[CrossRef](#)]
41. Zheng, D.; Sussman, J.H.; Jeon, M.P.; Parrish, S.T.; MacMullan, M.A.; Delfarah, A.; Graham, N.A. AKT but not MYC promotes reactive oxygen species-mediated cell death in oxidative culture. *J. Cell Sci.* **2020**, *133*, jcs239277. [[CrossRef](#)] [[PubMed](#)]
42. Patra, M.; Awuah, S.G.; Lippard, S.J. Chemical Approach to Positional Isomers of Glucose–Platinum Conjugates Reveals Specific Cancer Targeting through Glucose-Transporter-Mediated Uptake in Vitro and in Vivo. *J. Am. Chem. Soc.* **2016**, *138*, 12541–12551. [[CrossRef](#)] [[PubMed](#)]

**Disclaimer/Publisher's Note:** The statements, opinions and data contained in all publications are solely those of the individual author(s) and contributor(s) and not of MDPI and/or the editor(s). MDPI and/or the editor(s) disclaim responsibility for any injury to people or property resulting from any ideas, methods, instructions or products referred to in the content.